DESIGN, SYNTHESIS AND CHARACTERIZATION OF MOLECULAR AND POLYMERIC CYCLOSILANES

by
Qifeng Jiang

A dissertation submitted to Johns Hopkins University in conformity with the requirements for the degree of Doctor of Philosophy

Baltimore, Maryland
January 2023

Abstract

The structural complexity of crystalline silicon has inspired synthetic chemists to design cyclosilane building blocks for well-defined novel silicon materials with tunable optical properties. This dissertation describes synthetic strategies of constructing novel molecular and polymeric cyclosilane materials and their structure-property-relationships. Polycyclosilanes exhibit microstructure-dependent thermal properties and connectivity-dependent UV-vis absorption features. Novel hybrid σ,π-conjugated cyclosilane building blocks with pre-defined stereochemistry allow access to stereoregular polysilanes. Constitutional isomers of sulfur-incorporated π,n,σ-conjugated cyclosilanes can exhibit distinct conformations and delocalization patterns. Theoretical investigations through density functional theory calculations contribute to understanding the optical and electronic properties of these molecular and polymeric cyclosilane materials.

Advisor: Professor Rebekka S. Klausen

Reader: Professor J.D. Tovar

Reader: Professor Howard Fairbrother

Acknowledgements

First, I would like to thank my advisor, Professor Rebekka S. Klausen for her mentorship. Bekka welcomed me as a visiting undergraduate student purchasing summer research and then as a graduate student joining the group. She has not only led me to grow as a synthetic chemist but encouraged me to always explore more throughout graduate school. I could not get through the hard time during the pandemic without her care and support. What I learnt from Bekka, with no doubt, will be a priceless treasure of my life.

I want to thank my thesis committee members, Prof. J.D. Tovar and Prof. Howard Fairbrother, and my GBO committee member, Prof V. Sara Thoi, for their guidance of research and thoughtful advice on career development.

I would also like to thank all the staff in the chemistry department who supported my research in the past 5 years. I want to express my appreciation to Dr. Jonathan Catazaro, the NMR manager of the chemistry department. He has been a great mentor and a heartwarming friend during my time working with him as NMR TA.

Next, I would like to thank all the former and current members of the Klausen lab. I enjoyed the welcoming and inclusive lab culture in the Klausen group and will always miss the lab after graduation. They are already more than colleagues but personal friends of mine. In particular, I would like to thank Dr. Heidi van de Wouw and Dr Eric A. Marro for their mentorship which helped me develop experimental skills and grow as a scientific researcher. I would also like to thank my fantastic undergraduate, Ms. Sydnee Wong. I grew a lot as a mentor while working together with her for almost 3 years. I wish Sydnee the best for the future!

Then I would like to thank all my friends at Hopkins. Together we have been through a wonderful journey. I want to thank Dr. Yuyang Ji, my lab mate and also a friend from my first year. He is more than a close friend, a great collaborator, but a model polymer scientist to me. I learnt a lot about polymer science from him. I would also like to thank Bing Xu, my friend from undergraduate and roommate for 5 years. I will miss all these research discussions when I talk to you about material science and you try to convince me biochemistry is fun.

Last but not least, I would like to express my deepest appreciation to my family. They always encouraged me to chase my dreams. Even on the other side of the world, they supported me with their generous love for years. Without my family, none of my accomplishments can ever be possible. This dissertation is a gift to my family.

Table of Content

List of Tables

List of Figures

List of Schemes

Chapter 1: Introduction

1.1 Forward

Silicon is the center of the modern world for its extensive usage in electronic devices. It is such a dominant material that the current period can be defined as the silicon age.[1] Its high abundance in the earth's crust[1] ensures silicon a relatively affordable and sustainable material for electronics industry and energy-relative technology. Nanoscale silicon materials are particularly attractive for their optical and electronic properties with dimensional tunability.[2] They have found applications in high-speed transistors[3], light-emitting devices[4], lithium-ion battery anode[5] and bioimaging.[6]

Top-down synthetic approaches are mostly employed in these applications mentioned above. However, to achieve a precise control of hierarchical structures and therefore understand the structure-property relationships, the bottom-up strategy is necessary. Design, synthesis and characterization of molecular silicon-based materials (e.g., silanes) lead towards unique electronic properties arising from silicon scaffolds. Their capability as molecular building blocks further motivates exploration of synthesizing polymeric materials with well-defined structures and tailored properties.

1.2 σ-Conjugation in silanes

Silanes exhibit unique optical properties compared to their group 14 relatives, saturated hydrocarbons.[7] In 1964 when Sakurai and Kumada studied the ultraviolet spectra of oligosilanes, they found oligosilanes had strong absorption in the near ultraviolet region (210 to 260 nm) and the introduction of pentamethyldisilyl group into benzene caused an obvious red shift.[8] This evidence suggests delocalization though Si-Si σ bonds, later known

as σ-conjugation. σ-Conjugation is extended across the oilgosilanes with the increasing chain length similar to π-conjugated systems[8,9], but also found to be strongly dependent on the silane conformations.[10–13]

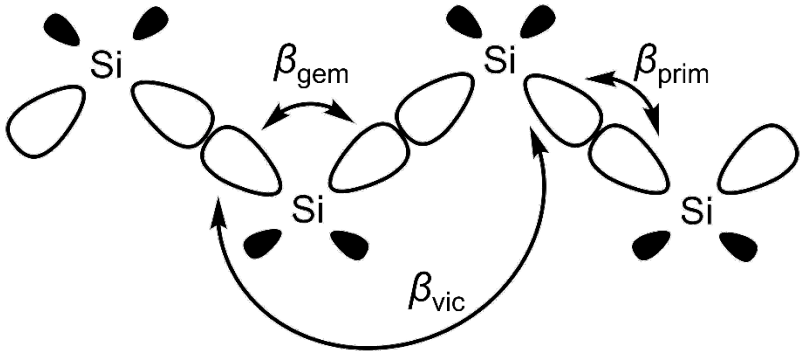

Figure 1.2.1 Ladder C model of σ-conjugation.

The Sandorfy C and H approximations were first applied to understand the delocalization across oligosilanes. However, they failed to interpret conformational effects of σ-conjugation.[7] The ladder C model, developed and optimized by Michl[14,15], then was proved to fit experimental observation of linear oligosilanes better.

Three major types of orbital interactions are considered in oligosilanes: primary interaction – overlap of sp^3 orbitals on Si atoms oriented towards each other; geminal interaction – hyperconjugation between geminal σ orbitals on the same silicon atom; vicinal interaction - σ orbitals on the neighboring silicon atoms which are not oriented towards each other (Figure 1.2.1). The strength of these orbital interactions can be evaluated by the resonance integral β based on the degrees of orbital overlap.

While β_{prim} and β_{gem} are not sensitive to orbital geometries, β_{vic} is a function of the Si-Si-Si-Si dihedral angle ω of the silane chain (Figure 1.2.2a). During the free rotation of the Si-Si bond and change of dihedral angle ω, the strength of vicinal interaction increases significantly when the silane adopts to the *anti*-conformation (ω = 180˚). Meanwhile, the

syn-conformation[16] (ω = 0°) is not favored to maximize the vicinal interaction: β_{vic} is calculated to decrease by 1.4 eV.[17] This dependence of β_{vic} on the dihedral angle ω results in the conformational effects on molecular orbital (MO) energies (Figure 1.2.2b). The HOMO energy increases and the LUMO energy decreases with larger β_{vic}, so that the all-*anti* conformation reduces the HOMO-LUMO gap allowing the most effective σ-conjugation (Figure 1.2.2b left). On the contrary the all-*cis* conformation minimizes β_{vic}, resulting in a larger HOMO-LUMO gap (Figure 1.2.2b right).

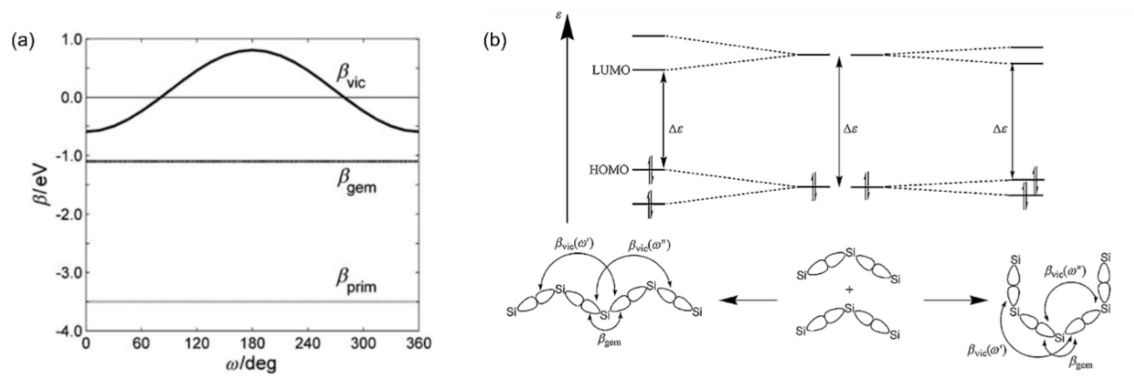

Figure 1.2.2 a) The resonance integrals β_{prim}, β_{gem}, and β_{vic} as a function of the dihedral angle ω. b) MO diagram describing schematically the effect of chain length doubling for the case of strong (left) and weak (right) σ-conjugation. Reprinted with permission from reference.[17] Copyright 2009 Wiley.

These predictions on MO energy tendency are supported by experimental studies on photoelectron spectra of oligosilanes.[10,11,18,19] West reported thermochromism of poly(di-*n*-hexylsilane) (PDHS) in hexane, where multiple absorption bands showed in the UV spectrum upon cooling of the fresh solution of PDHS (Figure 1.2.3).[10] It indicated that PDHS existed in three different conformational forms in the solution, which was observed the first time in a polysilane. Band III was assigned as the absorption of *anti*- or near *anti*-conformation of the polysilane for its red shift from Band II (*transoid*-conformation)

(Figure 1.2.3c). Tamao is one of the pioneers of confirming the conformational dependence of σ-conjugation by conformationally constrained oligosilanes.[11,18] *Syn*- and *anti*-disilane units were designed to construct tetrasilanes in which the dihedral angles are controlled to *syn(S)*, *anti(A)*, and *eclipsed (E)*. When ω increases from 7.1˚→117.5˚→180˚ (conformation: *syn*→ *eclipsed*→ *anti*), λ_{max} of UV absorption change from 210 nm to 238 nm[18] (Figure 1.2.4a). Similar trend was also found in hexasilane compounds[18] (Figure 1.2.4b). With more sterically constrained silane units, Tamao prepared *anti,cisoid*-alternating hexa- to decasilanes and obtained the first clear-cut experimental evidence that a small dihedral angle such as *cisoid* turn suppresses the σ-conjugation in polysilanes.[11] λ_{max} remain around 240 nm regardless of the silicon chain length in all the *anti,cisoid*-alternating oligosilanes (Figure 1.2.5a), but increase with the chain length in *transoid*-oligosilanes (Figure 1.2.5b). More recently, Nuckolls designed bicyclo[2.2.2]octasilane, which has *cisoid* Si–Si–Si–Si dihedral angles ranging from 15° to 20° for its three silane bridges.[19] These silanes were found to be of extremely low conductance due to destructive σ-interference using a scanning tunnelling microscope break junction (STM-BJ) technique.

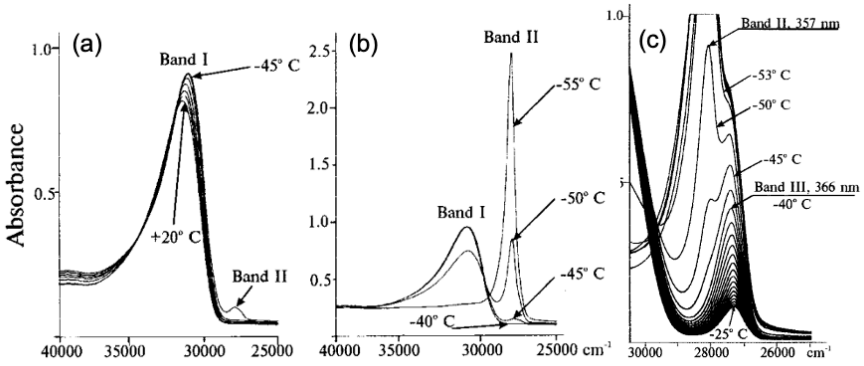

Figure 1.2.3 Temperature evolution of the UV spectrum of PDHS upon cooling of the fresh solution. Rapid cooling (a) from +20 to -45 °C and (b) from -40 to -55 °C. (c) Slow

cooling from -20 to -60 °C. Reprinted with permission from reference.[10] Copyright 2001 ACS.

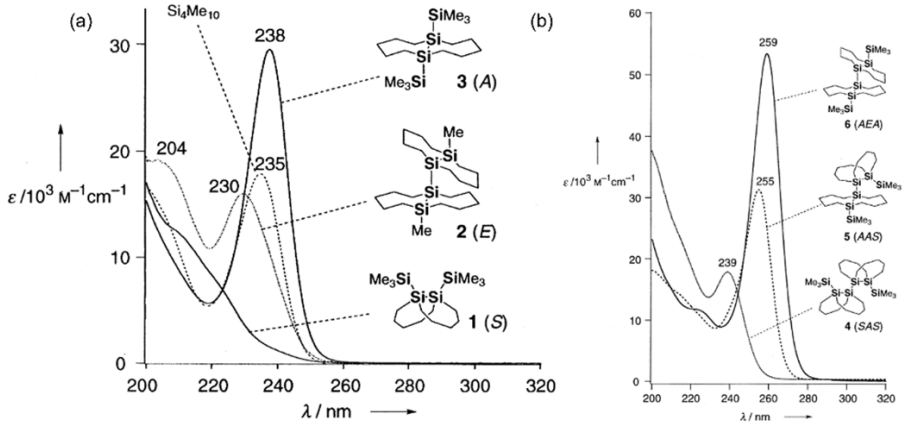

Figure 1.2.4 UV absorption spectra of the (a) tetrasilane and (b) hexasilane compounds. Reprinted with permission from reference.[18] Copyright 2000 Wiley.

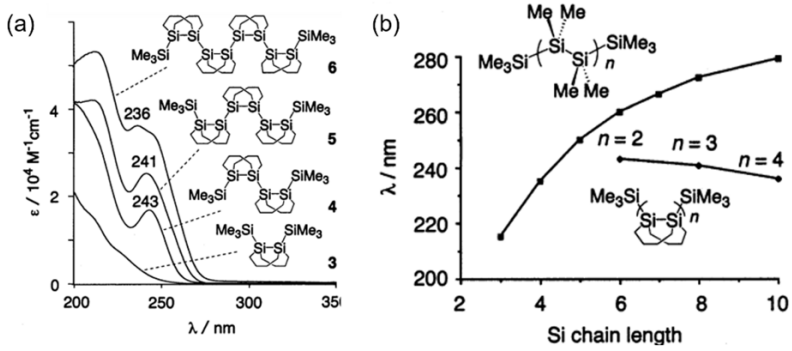

Figure 1.2.5 (a) UV absorption spectra of *anti,cisoid*-alternating oligosilanes. (b) Absorption maximum wavelength of constrained and unconstrained oligosilanes. Reprinted with permission from reference.[11] Copyright 2003 ACS.

1.3 Cyclosilanes inspired by crystalline silicon

Cyclosilanes have been widely studied for their unusual properties due to electron delocalization in the σ-frameworks and their reactivity pattern in the past 100 years.[20] The first synthesis of cyclosilanes can be dated back to 1921, when Kipping reported series of "saturated and unsaturated Si_4Ph_8".[21] Though some structure assignments were not

accurate initially, Gilman confirmed these compounds as perphenylated tetra, penta and hexacyclosilanes (Scheme 1.3.1).[22,23] 30 years later, the first permethylated cyclosilane dodecamethylhexacyclosilane (Si_6Me_{12}) was discovered as a minor product (2% yield) in the synthesis of polydimethylsilane.[24] The synthesis was optimized by West using lithium in tetrahydrofuran as the reducing agent and the yield was increased to about 80%.[25]

West, Hengge and Marschner contributed tremendously to this field for their efforts including mechanistic studies of cyclosilane reactivities, precise control of ring sizes and development of polycyclic silanes.[26–30] Recently more examples are discovered on enriching functionality on the silicon scaffolds and the resulting unique properties.[19,31]

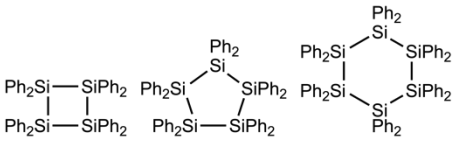

Kipping 1921[21], Gilman 1963[22],1965[23]

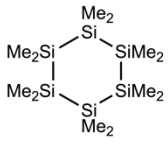

Burkhard 1949[24], West 1985[25]

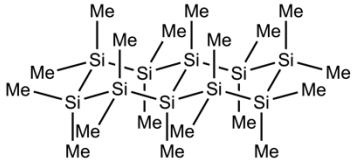

West 1972[26], Hengge 1993[27], Klausen 2019[35]

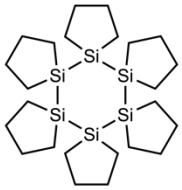

West 1984[28]

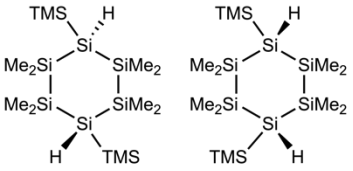

Marschner 2003[29]

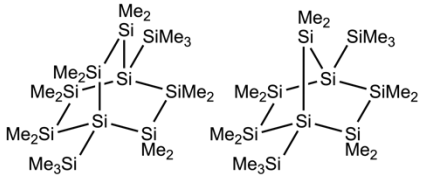

Marschner 2003[29]

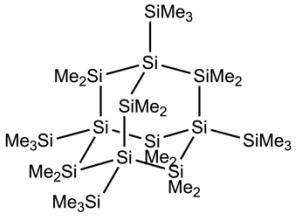

Marschner 2005[30]

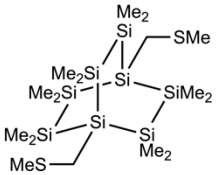

Nuckolls 2018[19]

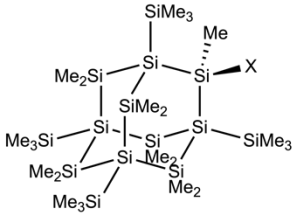

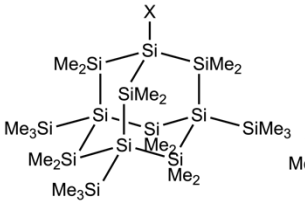

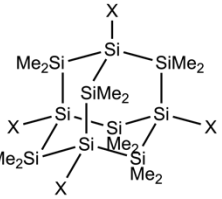

Su 2022[31]

Scheme 1.3.1 Cyclosilane structures.

In addition to the important electronic and optical properties of crystalline silicon, its structural complexity is also tempting and inspiring to synthetic chemists. Polycyclic fragments of chair cyclosilanes can be found in the structure of crystalline silicon lattice (Figure 1.3.1a), which brings a revealing insight on designing novel silicon materials with tunable optical properties.[32] The Klausen lab has been extensively exploring the target-oriented synthesis of cyclosilanes inspired by crystalline silicon in the past few years (Figure 1.3.1b).[32–36] The chemically inert Si-Me groups and reactive Si-H groups allow selective functionalization and polymerization of these cyclosilanes.

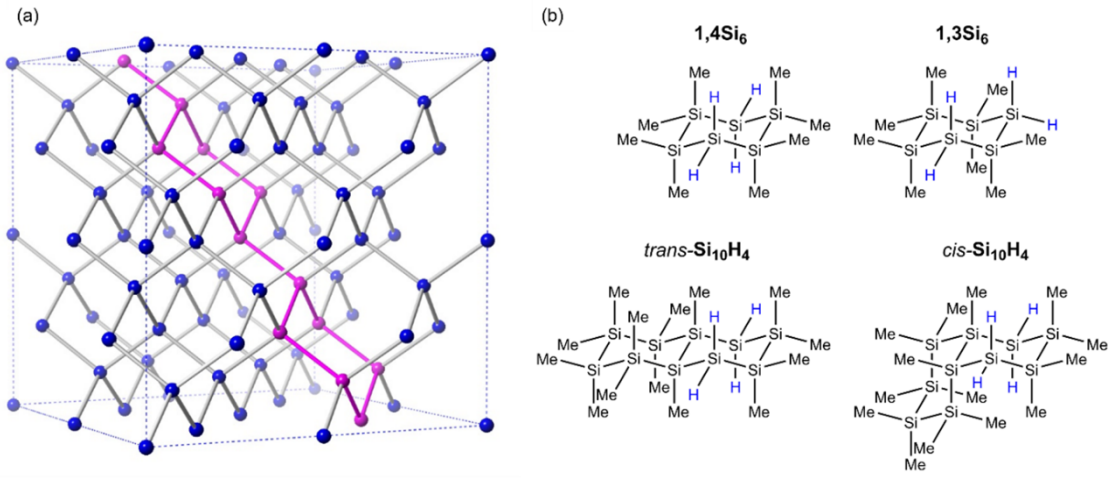

Figure 1.3.1 a) Polycyclic fragments highlighted in the crystalline silicon lattice. b) Cyclosilanes synthesized by the Klausen group.

The synthetic routes of cyclosilanes inspired by crystalline silicon are summarized in Scheme 1.3.2. The key intermediates for the synthesis of Si-H functionalized cyclosilanes are a class of oligosilyl dianions (Scheme 1.3.2a). Starting from di(TMS)diphenylsilane (**1.1**), TMS terminated oligosilanes (**1.2a-b**) were synthesized through salt metathesis as precursors, and treated with *tert*-butoxide/crown ether yielding

α,ω-dipotassiodisilanides (**1.3a-b**).[36] The chain length is tunable by using different dichlorooligosilanes. The cyclization of diaions and dichlorosilanes results in the isomeric tetraphenyl-functionalized cyclohexasilanes (**1.4** and **1.5,** Scheme 1.3.2b-c). The phenyl groups can be removed by treatment of trifluoromethanesulfonic acid (TfOH) giving silyl triflate intermediates, which are thereupon reduced by lithium aluminum hydride (LAH) leading to tetrahydrocyclohexasilanes, **1,4Si$_6$**[33] and **1,3Si$_6$**[34], which are of isomeric structures but different Si-H functional patterns. **1,4Si$_6$** is a white crystalline solid and the crystal structure suggests its chair-like conformation and high symmetry.[33] Meanwhile, **1,3Si$_6$** is a colorless oil at room temperature, but its precursor **1.5** is found to adapt a chair-like conformation in the solid state.[34]

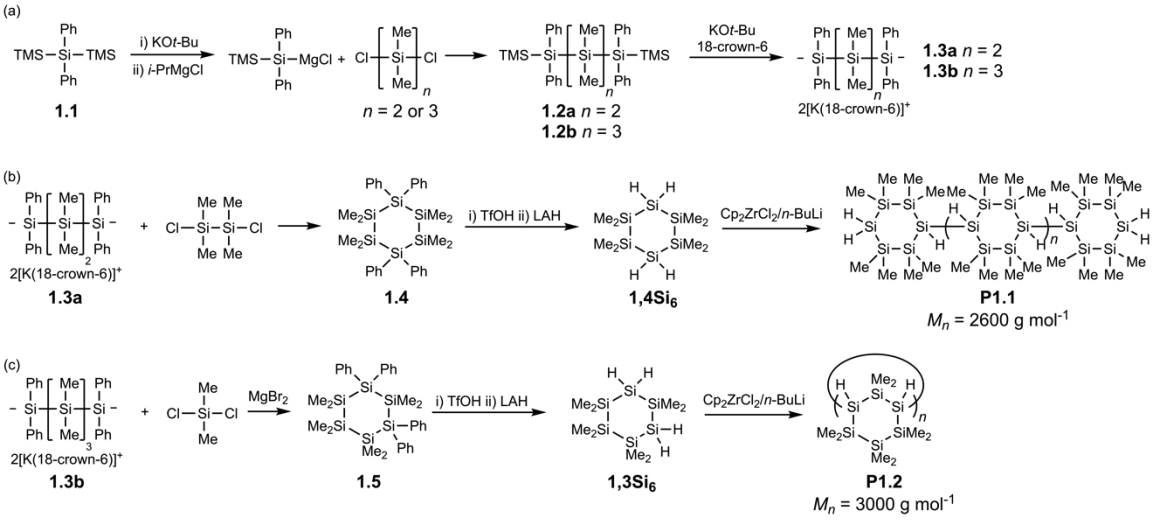

Scheme 1.3.2 Synthesis and polymerization of cyclohexasilanes.[33,34,36]

Polycyclosilanes feature a structural pattern of a periodic alternation of methylated and hydrogenated silicon atoms. Cp_2ZrCl_2/*n*-BuLi mediated dehydrocoupling polymerizations were performed on the bifunctional cyclosilane building blocks **1,4Si$_6$** and **1,3Si$_6$** yielding poly(cyclosilane)s of comparable molecular weights but different

microstructures (Scheme 1.3.2b-c). Polymerization of **1,4Si$_6$** resulted in a linear polymer **P1.1**, whereas **1,3Si$_6$** templated a macrocyclic architecture **P1.2**.

The cyclic polymer is distinct from the linear one by its high symmetry and the absence of SiH_2 end groups. This makes Si-H bonds diagnostic for spectroscopic characterization such as NMR spectroscopy and infrared spectroscopy. Comparison of experimental NMR spectra of the cyclosilane building blocks and their polymers reveals poly(cyclosilane) microstructures (Figure 1.3.2a).[33,34] In the ^{1}H NMR spectrum of **P1.1**, several broad resonances are observed in the typical region of Si-H groups (3.5-3.0 ppm).[33] These signals are assigned as internal SiH groups and SiH_2 end groups arising from a linear structure. On the other hand, a broad singlet corresponding to internal SiH groups at 3.25 ppm dominates the Si-H region in the ^{1}H NMR spectrum of **P1.2**.[34] This indicates the high symmetry macrocyclic structure rather than a linear polymer structure.

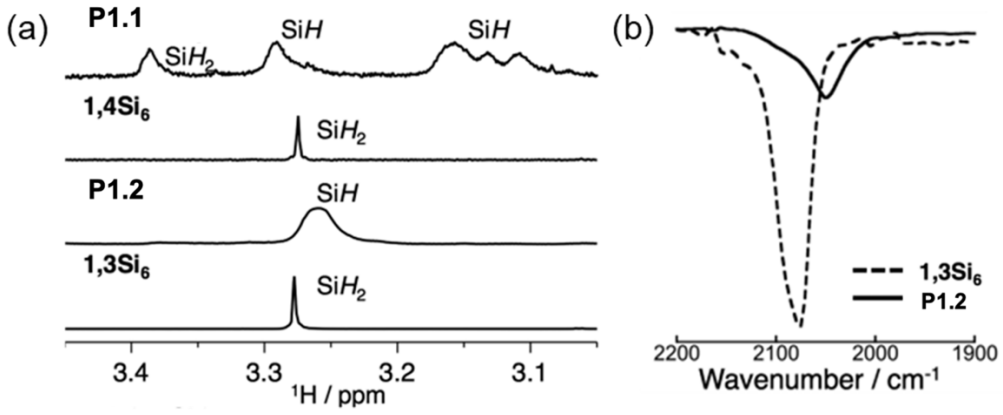

Figure 1.3.2 Characterization of poly(cyclosilane) microstructures. (a) Cropped ^{1}H NMR spectra of (top to bottom) poly(**1,4Si$_6$**), **1,4Si$_6$**, poly(**1,3Si$_6$**), and **1,3Si$_6$**. Only the SiH region is shown. (b) Cropped ATR-FTIR spectra of **1,3Si$_6$** (dashed line) and poly(**1,3Si$_6$**) (solid line). Only the Si−H stretching frequencies are shown. Reprinted with permission from reference.[34] Copyright 2018 ACS.

The microstructure assignment can be further confirmed by IR spectroscopy (Figure 1.3.2b). Si-H bonds have characteristic stretching frequencies at ~2100 cm^{-1} in IR spectroscopy and their exact values depend on the degree of silyl- substitution. The stretching frequency shifts towards lower wavenumber with silyl-substitution increasing.[37] The IR spectrum of polymerized **1,3Si$_6$** has a symmetric band in the Si-H region centered at lower frequency than before polymerization (Figure 1.3.2b).[34] This observation indicates a macrocyclic structure lacking SiH_2 end group.

Synthesis of siladecalin, the silicon analog of decalin, has been a long-standing challenge to synthetic chemists for decades. Although in 1972 West reported first reported its synthesis as a minor product (4 % yield) of dimethyldichlorosilane and trimethylchlorosilane reductive coupling[26], the structure was finally assigned via X-ray crystallography by Hengge in 1993.[27] Recently, Klausen reported stereocontrolled syntheses of functionalized *cis*- and *trans*-siladecalins via coupling of **Si$_4$** dianion and 1,2-dichlorohexacyclosilane (Scheme 1.3.3).[38] This approach allows control of relative stereochemistry and functional group interconversion.

Under optimized conditions, *cis*-**Si$_{10}$Ph$_4$** was synthesized with high diastereoselectivity (dr 10:90 *trans:cis*), and converted to *cis*-**Si$_{10}$H$_4$** (dr 15:85 *trans:cis*) in 65% yield via dearylation with TfOH and reduction with LAH. *cis*-**Si$_{10}$Ph$_4$** underwent epimerization when heated with excess **Si$_4$** dianion in toluene, yielding *trans*-**Si$_{10}$Ph$_4$** (dr 97:3 *trans:cis*) as the thermodynamically favorable product. Similar reaction conditions with *trans*-**Si$_{10}$Ph$_4$** (dr 97:3 *trans:cis*) provided 95:5 *trans*-**Si$_{10}$H$_4$** in 68% yield. Their structures were fully characterized and assigned by IR spectroscopy, NMR spectroscopies and X-ray crystallography. Si-H functional groups enable capabilities for future

functionalization and therefore make *trans*- and *cis*-$\mathbf{Si_{10}H_4}$ potential bicyclic silane building blocks for novel conjugated structures.

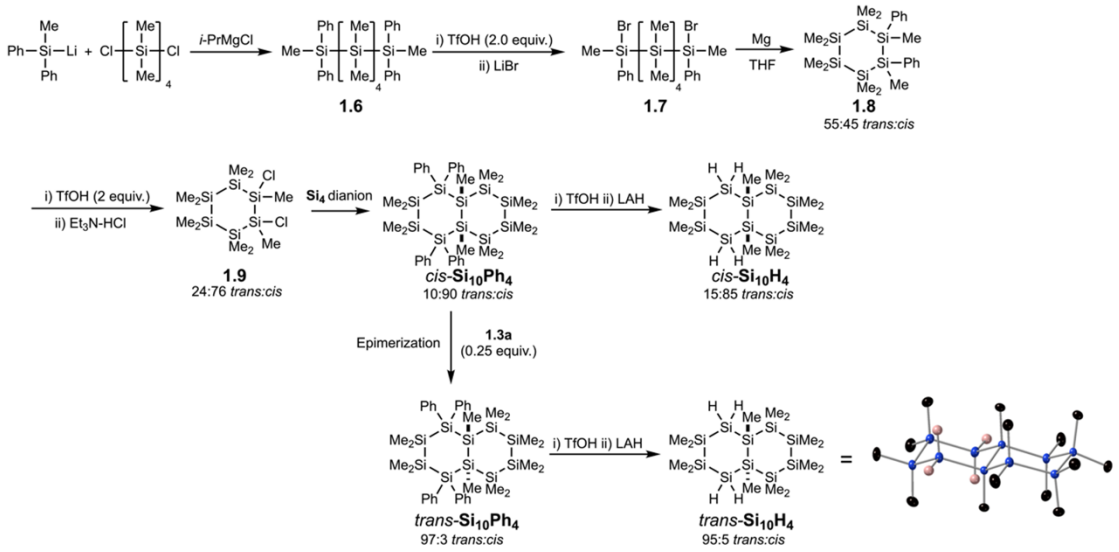

Scheme 1.3.3 Selective synthesis of functionalized *trans*- and *cis*-siladecalin.

1.4 Hydrosilylation reactions

Hydrosilylation, the addition of hydrosilanes across unsaturated bonds (Scheme 1.4.1a), serves as an essential method to synthesize and functionalize organosilicon materials. The study of hydrosilylation reactions can be dated to 1947 when Sommer reported the first hydrosilylation of 1-octene using trichlorosilane catalyzed by peroxide.[39] Later in 1957, Speier reported H_2PtCl_6-catalyzed hydrosilylation of 1-pentene and cyclohexene leading to the industrial usage of transition metal catalysts in this field.[40] In 1973 Karstedt developed a platinum(0) catalyst (also known Karstedt's catalyst, Scheme 1.4.1b) showing high reactivity under ambient condition and it has been widely used in the industrial preparation of various silicone polymers.[41] Nowadays, the collection of catalysts has been extended from Pt to other group VIII to X transition metals including Pd[42], Co[43], Fe[44,45], Ni[46], Rh[47–49] and Ru.[50,51]

Chalk and Harrod proposed the first widely accepted mechanism of group VIII metal-catalyzed hydrosilylation of olefins[52], which was then modified based on quantum chemical investigation.[53] The reaction typically undergoes the following catalytic pathway: oxidative addition of a hydrosilane to a transition metal center, olefin coordination, migratory insertion of the olefin forming a Si-C bond and reductive elimination through C-H bond formation (Scheme 1.4.1c).

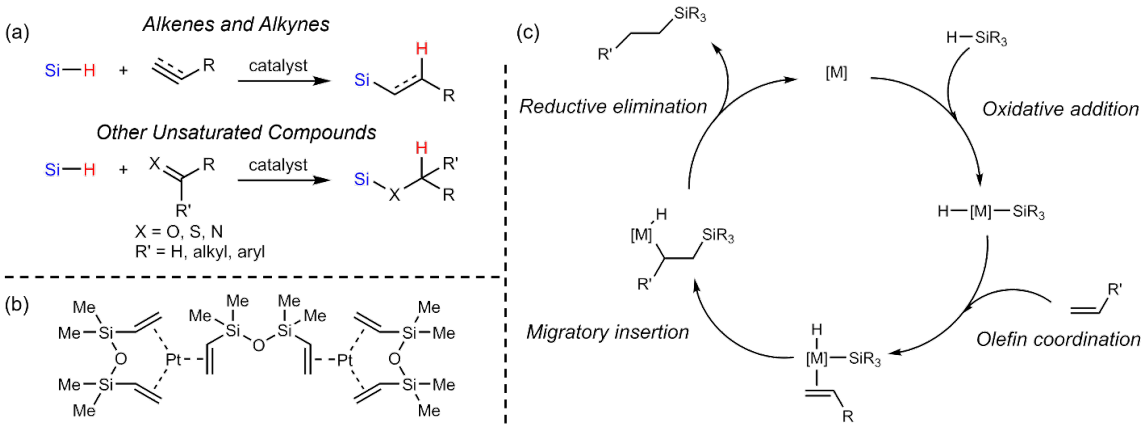

Scheme 1.4.1 a) Generic scheme of hydrosilylation. b) Structure of Karstedt's catalyst. c) Modified Chalk-Harrod mechanism of hydrosilylation.

1.5 Polycarbosilane synthesis via hydrosilylation

Interest in synthesizing saturated polycarbosilanes has been greatly motivated since Yajima first reported polysilane and polycarbosilane pyrolysis to silicon carbide fibers at >1000 °C in the 1970's (Scheme 1.5.1).[54–56]

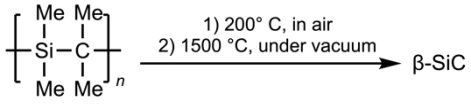

Scheme 1.5.1 SiC fibers synthesized from polycarbosilane.

Copolymerization of hydromonosilanes with alkenes through transition metal-catalyzed hydrosilylations has been extensively explored as a feasible synthetic approach

to saturated polycarbosilanes. Corriu reported the polymerization of dimethylvinylsilane catalyzed by H_2PtCl_6 yielding poly(dimethylsilylethylene) of low molecular weight (M_n = 2740 g/mol) (Scheme 1.5.2a).[57] The reaction exhibits a low selectivity towards α addition (yielding *n* units) and β addition (yielding *m* units) on alkenes. Similar selectivity is also seen in the polymerization of dichlorovinylsilane catalyzed by Pt/C.[58] Increasing the steric hinderance on starting hydrosilanes and utilizing Karstedt's catalyst results in high ratio of β-addition units. Optically active (S)-1-phenyl-1-naphthyl-1-vinyl-3,3-dimethyl-1,3-disiloxane was polymerized in the presence of Karstedt's catalyst to yield an optically pure and highly stereoregular polycarbosiloxane with all β-addition units (Scheme 1.5.2b).[59] More recently, He reported the construction of polymers featuring Si-stereogenic heteroarylsilanes (Scheme 1.5.2c).[60] The Si steric centers are preserved in the hydrosilylation, opening up a new approach towards tailormade chiral polymers with a wide range of applications. To obtain polycarbosilanes of high molecular weights, Rh-based catalysts were used for intermolecular hydrosilylation of the vinylhydrosilane (Scheme 1.5.2d).[47] The resulting polymers exhibit wide molecular weight distribution featuring *Mw* up to 102000 g/mol in gel permeation chromatography.

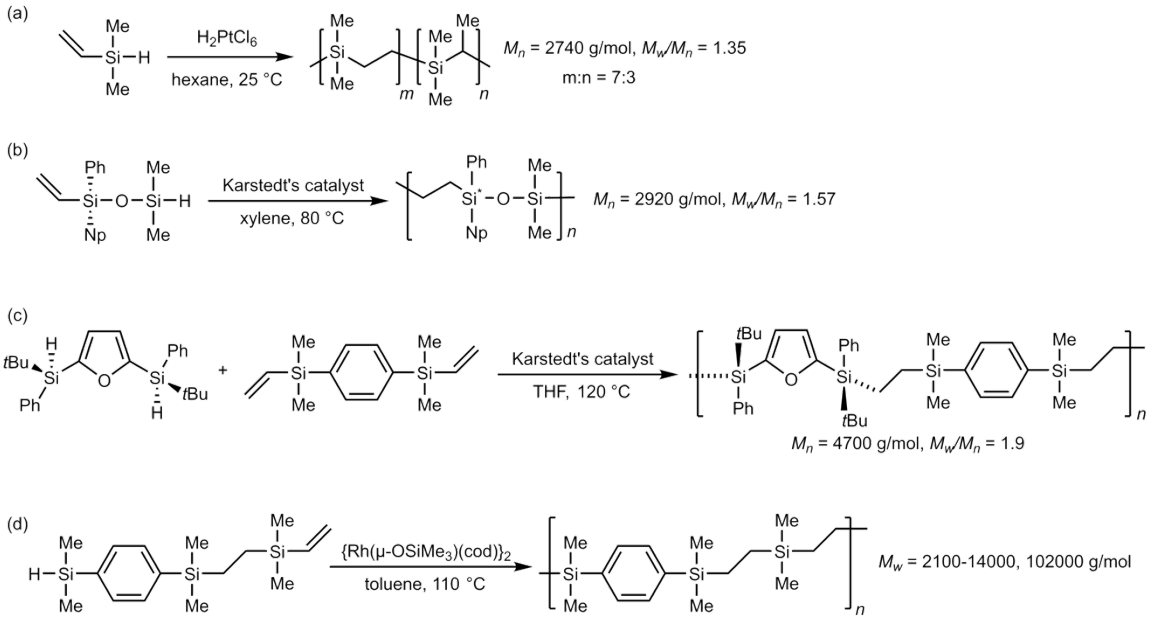

Scheme 1.5.2 Synthesis of saturated polycarbosilanes through transition metal-catalyzed hydrosilylation.

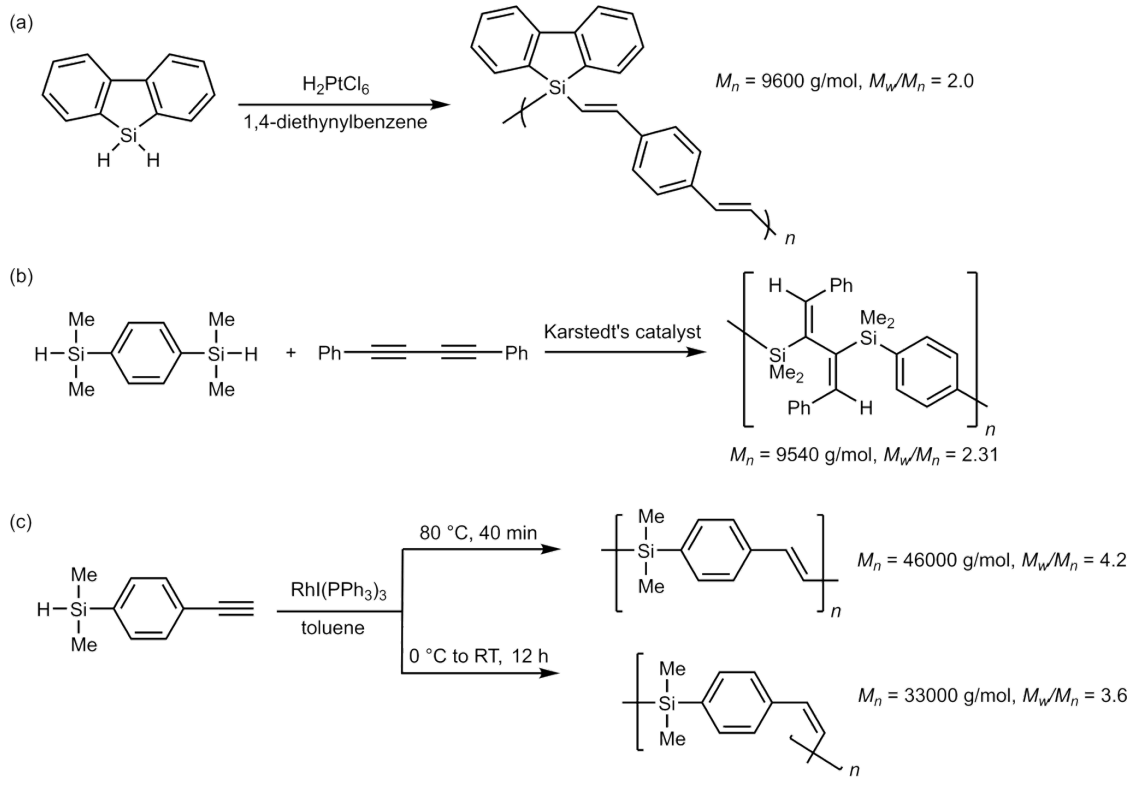

Scheme 1.5.3 Synthesis of unsaturated polycarbosilanes through transition metal catalyzed hydrosilylation.

On the other hand, hydrosilylation between hydrosilane and alkynes leads to hybrid conjugated polymers with unique optical properties arising from mixing of σ and π orbitals (Scheme 1.5.3). Poly(silafluorene-phenylene-divinylene) was synthesized through hydrosilylation between 1,1-silafluorene and 1,4-diethynylbenzene (Scheme 1.5.3a).[61] The photoluminescent polymer maintains a regioregular *(E)*-vinylene Si-C backbone allowing σ^*-π/π^* conjugation. Serial photoluminescent silylene-arylene-vinylene polymers were obtained via addition of bis(silylhydrides) to 1,3-diynes (Scheme 1.5.3b).[62] Although H_2PtCl_6 and Karstedt's catalyst find their ways in synthesizing novel σ, π-conjugated polymers, Rh-based catalysts have been attracting more attention to achieve better selectivity, higher efficiency and high molecular weights. $RhI(PPh_3)_3$ allows a highly selective synthesis of *(E)*- and *(Z)*-poly(silylene-1,4-phenylenevinylene)s controlled by temperature (Scheme 1.5.3c).[48] The formation of *trans* polymers favors reaction conditions at high temperature (up to 160 ˚C), whereas the ambient condition leads to the *cis* products.

1.6 Functionalization of oligo- and polysilanes via hydrosilylation

Despite the numerous achievements on polycarbonsilane synthesis through hydrosilylation between hydromonosilane and alkenes/alkynes, the application of hydrosilylation to oligo- and polysilanes is very challenging due to the extensive Si-Si cleavage with the presence of transition metal catalysts.[63–65] The mechanism was studied experimentally by the synthesis of bis(silylene)ruthenium complex from hydrodisilane.[64] The same as hydromonosilanes, hydrodisilanes react with the catalyst starting from transition metal insertion between the Si-H bond (oxidative addition). However, with existence of the weak Si-Si bonds the transition metal center prefers to further migrate

between Si atoms yielding metal-silylene complexes, which react with alkynes forming Si-Si bond cleaved products (Scheme 1.6.1).

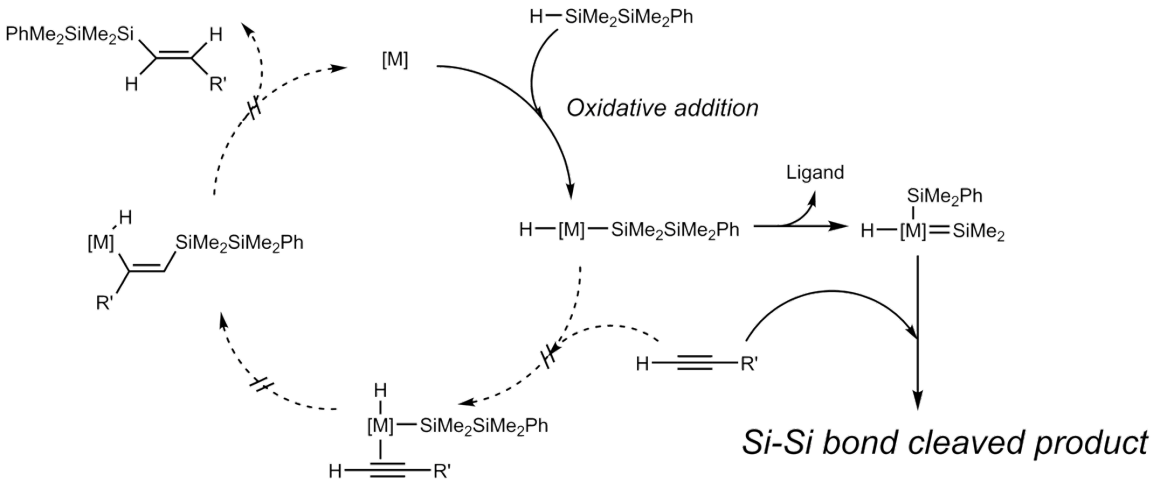

Scheme 1.6.1 Mechanism of Si-Si bond cleavage in hydrosilylation of alkynes with hydrodisilane.

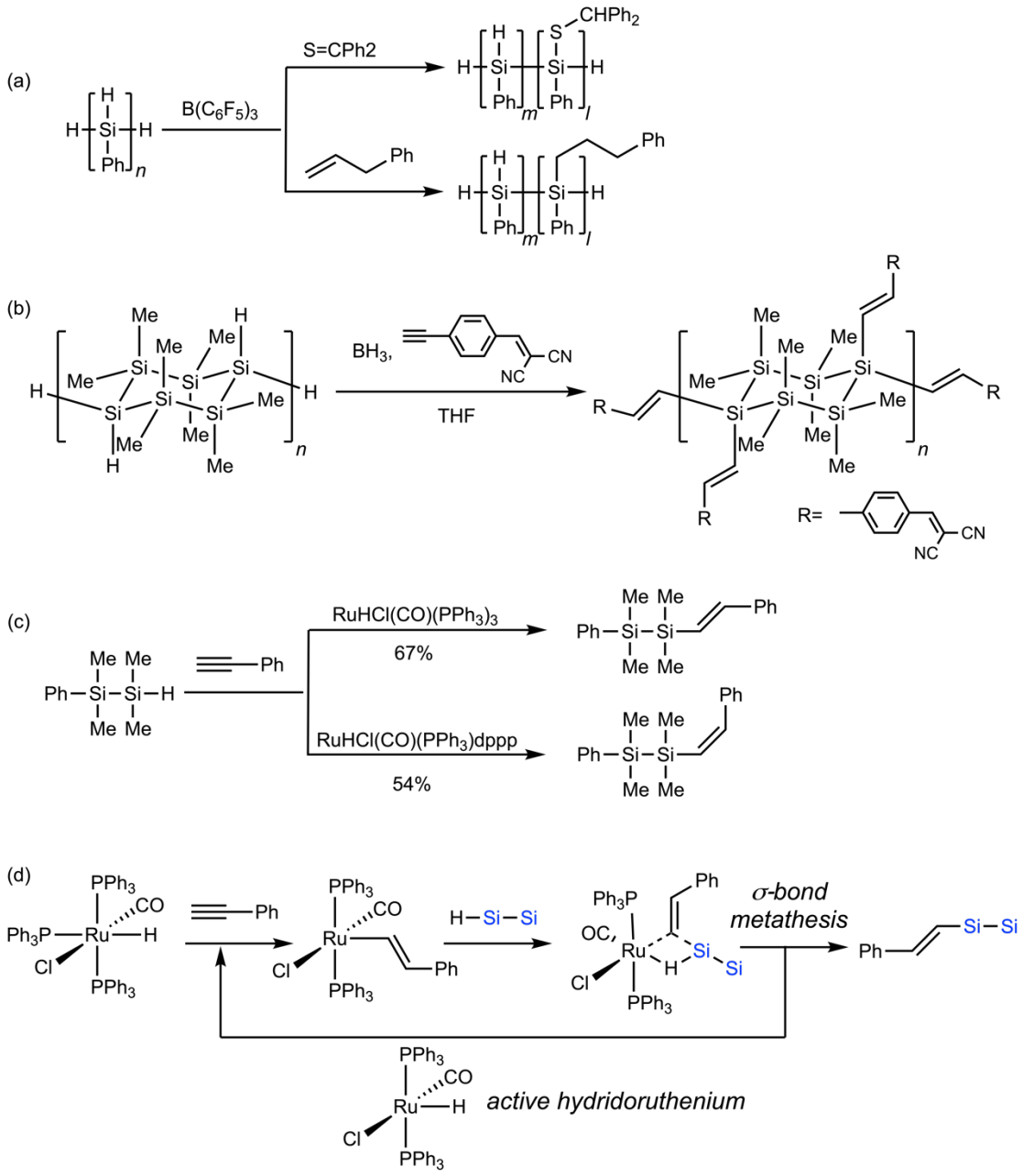

Scheme 1.6.2 a) $B(C_6F_5)_3$ catalyzed hydrosilylation of poly(phenylsilane). b) BH_3 catalyzed hydrosilylation of poly(cyclosilane). c) Ru-catalyzed hydrosilylation of hydrodisilane. d) Reaction mechanisms of hydrosilylation in the presence of $RuHCl(CO)(PPh_3)_3$.

Borane Lewis acids were used for hydrosilylation on polysilanes without skeletal fragmentation. Rosenberg reported functionalization of poly(phenylsilane) with X=C

groups catalyzed by tris(pentafluorophenyl)borane ($B(C_6H_5)_3$) (Scheme 1.6.2a).[66,67] Klausen performed BH_3 catalyzed functionalization of poly(cyclosilane)s with electron-poor aryl alkynes (Scheme 1.6.2b).[33] Introduction of organic side chains containing dicyanovinyl electron acceptors results in novel well-defined silane donor−acceptor compounds.

Recently, Kyushin reported Ru catalyzed *(E)- and (Z)-* selective hydrosilylation of alkynes and hydrooligosilanes without Si–Si bond cleavage (Scheme 1.6.2c).[50,51] The Si-Si bonds survive the reaction by avoiding formation of reactive metal-silylene intermediates (Scheme 1.6.2d). These studies enable the functionalization of oligo- and polysilanes to maintain diverse Si skeletons and give arise to novel organosilicon materials with desired thermal performance and unique optical properties.

1.7 Conclusion

The discussions above highlighted the progress of designing novel cyclosilanes building blocks and their polymerization. Investigating the effect of microstructures (linear vs cyclic) and connectivity patterns (1,3-linking vs 1,4 linking) on the thermal and optical properties of poly(cyclosilane)s led to further understanding the structure-property relationship of poly(cyclosilane)s as a new class of polymeric materials (Chapter 2&3). Hydrosilylation enabled novel cyclosilanes building blocks for constructing σ,π-conjugated hybrid polymers with stereoregularity (Chapter 4&6). Dehydrocoupling of hydrocyclosilanes and thiols allows access to σ-n-π conjugated molecules and density functional theory calculations bring insights to understand electron transition behaviors (Chapter 5).

1.8 Reference

(1) Emsley, J. *In The Elements*; Oxford: Clarendron, 1998.
(2) Teo, B. K.; Sun, X. H. *Chem. Rev.* **2007**, *107*, 1454–1532.
(3) Bohr, M. T. *IEEE Trans. Nanotechnol.* **2002**, *1*, 56–62.
(4) Daldosso, N.; Pavesi, L. *Laser Photonics Rev.* **2009**, *3*, 508–534.
(5) Xu, Z.-L.; Liu, X.; Luo, Y.; Zhou, L.; Kim, J.-K. *Prog. Mater. Sci.* **2017**, *90*, 1–44.
(6) Peng, F.; Su, Y.; Zhong, Y.; Fan, C.; Lee, S.-T.; He, Y. *Acc. Chem. Res.* **2014**, *47*, 612–623.
(7) Miller, R. D.; Michl, J. *Chem. Rev.* **1989**, *89*, 1359–1410.
(8) Sakurai, H.; Kumada, M. *Bull. Chem. Soc. Jpn.* **1964**, *37*, 1894–1895.
(9) Gillam, A. E.; Hey, D. H. *J. Chem. Soc.* **1939**, 1170–1177.
(10) Bukalov, S. S.; Leites, L. A.; West, R. *Macromolecules* **2001**, *34*, 6003–6004.
(11) Tsuji, H.; Terada, M.; Toshimitsu, A.; Tamao, K. *J. Am. Chem. Soc.* **2003**, *125*, 7486–7487.
(12) Fukazawa, A.; Tsuji, H.; Tamao, K. *J. Am. Chem. Soc.* **2006**, *128*, 6800–6801.
(13) Tsuji, H.; Michl, J.; Tamao, K. *J. Organomet. Chem.* **2003**, *685*, 9–14.
(14) Plitt, H. S.; Michl, J. *Chem. Phys. Lett.* **1992**, *198*, 400–405.
(15) Schepers, T.; Michl, J. *J. Phys. Org. Chem.* **2002**, *15*, 490–498.
(16) Michl, J.; West, R. *Acc. Chem. Res.* **2000**, *33*, 821–823.
(17) Bande, A.; Michl, J. *Chem. - A Eur. J.* **2009**, *15*, 8504–8517.
(18) Tamao, K.; Tsuji, H.; Terada, M.; Asahara, M.; Yamaguchi, S.; Toshimitsu, A. *Angew. Chemie - Int. Ed.* **2000**, *39*, 3287–3290.
(19) Garner, M. H.; Li, H.; Chen, Y.; Su, T. A.; Shangguan, Z.; Paley, D. W.; Liu, T.; Ng, F.; Li, H.; Xiao, S.; Nuckolls, C.; Venkataraman, L.; Solomon, G. C. *Nature* **2018**, *558*, 416–419.
(20) Hengge, E.; Janoschek, R. *Chem. Rev.* **1995**, *95*, 1495–1526.
(21) Kipping, F. S.; Sands, J. E. *J. Chem. Soc. Trans.* **1921**, *119*, 830–847.
(22) Gilman, H.; Schwebke, G. L. *J. Am. Chem. Soc.* **1963**, *85*, 1016.
(23) Gilman, H.; Peterson, D. J.; Tomasi, R. A.; Harrell, R. L. *J. Organomet. Chem.* **1965**, *4*, 167–171.
(24) Burkhard, C. A. *J. Am. Chem. Soc.* **1949**, *71*, 963–964.
(25) Chen, S. M.; Katti, A.; Blinka, T. A.; West, R. *Synth.* **1985**, *1985*, 684–686.
(26) West, R.; Indriksons, A. *J. Am. Chem. Soc.* **1972**, *94*, 6110–6115.
(27) Jenkner, P. K.; Hengge, E.; Czaputa, R.; Kratky, C. *J. Organomet. Chem.* **1993**, *446*, 83–90.
(28) Carlson, C. W.; Haller, K. J.; Zhang, X. H.; West, R. *J. Am. Chem. Soc.* **1984**, *106*, 5521–5531.
(29) Fischer, R.; Konopa, T.; Ully, S.; Baumgartner, J.; Marschner, C. *J. Organomet. Chem.* **2003**, *685*, 79–92.
(30) Fischer, J.; Baumgartner, J.; Marschner, C. *Science (80-.).* **2005**, *310*, 825.
(31) Siu, T. C.; Imex Aguirre Cardenas, M.; Seo, J.; Boctor, K.; Shimono, M. G.; Tran, I. T.; Carta, V.; Su, T. A. *Angew. Chemie - Int. Ed.* **2022**, *61*.
(32) Marro, E. A.; Klausen, R. S. *Chem. Mater.* **2019**, *31*, 2202–2211.
(33) Press, E. M.; Marro, E. A.; Surampudi, S. K.; Siegler, M. A.; Tang, J. A.; Klausen, R. S. *Angew. Chemie Int. Ed.* **2017**, *56*, 568–572.

(34) Marro, E. A.; Press, E. M.; Siegler, M. A.; Klausen, R. S. *J. Am. Chem. Soc.* **2018**, *140*, 5976–5986.
(35) Marro, E. A.; Folster, C. P.; Press, E. M.; Im, H.; Ferguson, J. T.; Siegler, M. A.; Klausen, R. S. *J. Am. Chem. Soc.* **2019**, *141*, 17926–17936.
(36) Marro, E. A.; Press, E. M.; Purkait, T. K.; Jimenez, D.; Siegler, M. A.; Klausen, R. S. *Chem. - A Eur. J.* **2017**, *23*, 15633–15637.
(37) Kanabus-kaminska, J. M.; Hawari, J. A.; Griller, D.; Chatgilialoglu, C. *J. Am. Chem. Soc.* **1987**, *109*, 5267–5268.
(38) Marro, E. A.; Folster, C. P.; Press, E. M.; Im, H.; Ferguson, J. T.; Siegler, M. A.; Klausen, R. S. *J. Am. Chem. Soc.* **2019**, *141*, 17926–17936.
(39) Sommer, L. H.; Pietrusza, E. W.; Whitmore, F. C. *J. Am. Chem. Soc.* **1947**, *69*, 188.
(40) Speier, J. L.; Webster, J. A.; Barnes, G. H. *J. Am. Chem. Soc.* **1957**, *79*, 974–979.
(41) Troegel, D.; Stohrer, J. *Coord. Chem. Rev.* **2011**, *255*, 1440–1459.
(42) Miller, Z. D.; Montgomery, J. *Org. Lett.* **2014**, *16*, 5486–5489.
(43) Wen, H.; Wan, X.; Huang, Z. *Angew. Chemie - Int. Ed.* **2018**, *57*, 6319–6323.
(44) Zhang, M.; Zhang, A. *Applied Organometallic Chemistry*. November 2010, pp 751–757.
(45) Tondreau, A. M.; Atienza, C. C. H.; Weller, K. J.; Nye, S. A.; Lewis, K. M.; Delis, J. G. P. P.; Chirik, P. J. *Science (80-.).* **2012**, *335*, 567–570.
(46) Chang, A. S. M.; Kawamura, K. E.; Henness, H. S.; Salpino, V. M.; Greene, J. C.; Zakharov, L. N.; Cook, A. K. *ACS Catal.* **2022**, *12*, 11002–11014.
(47) Pawluc, P.; Marciniec, B.; Kownacki, I.; Maciejewski, H. *Appl. Organomet. Chem.* **2005**, *19*, 49–54.
(48) Kwak, G.; Masuda, T. *Macromol. Rapid Commun.* **2002**, *23*, 68–72.
(49) Onopchenko, A.; Sabourin, E. T.; Beach, D. L. *J. Org. Chem.* **1983**, *48*, 5101–5105.
(50) Kanno, K. ichiro; Aikawa, Y.; Kyushin, S. *Tetrahedron Lett.* **2020**, *61*, 152274.
(51) Kanno, K. ichiro; Noguchi, S.; Ono, Y.; Egawa, S.; Otsuka, N.; Mita, M.; Kyushin, S. *J. Organomet. Chem.* **2022**, *961*, 122234.
(52) Chalk, A. J.; Harrod, J. F. *J. Am. Chem. Soc.* **1965**, *87*, 16–21.
(53) Sakaki, S.; Mizoe, N.; Sugimoto, M. *Organometallics* **1998**, *17*, 2510–2523.
(54) Yajima, S.; Hayashi, J.; Omori, M. *Chem. Lett.* **1975**, *4*, 931–934.
(55) Yajima, S.; Hasegawa, Y.; Okamura, K.; Matsuzawa, T. *Nature* **1978**, *273*, 525–527.
(56) Yajima, S.; Hayashi, J.; Omori, J.; Okamura, K. *Nature* **1976**, *261*, 683–685.
(57) Corriu, R. J. P.; Leclercq, D.; Mutin, P. H.; Planeix, J. M.; Vioux, A. *Organometallics* **1993**, *12*, 454–462.
(58) Boury, B.; Carpenter, L.; Corriu, R. J. P. *Angew. Chemie Int. Ed. English* **1990**, *29*, 785–787.
(59) Li, Y.; Kawakami, Y. *Macromolecules* **1998**, *31*, 5592–5597.
(60) Chen, S.; Zhu, J.; Ke, J.; Li, Y.; He, C. *Angew. Chemie Int. Ed.* **2022**, *61*.
(61) Sanchez, J. C.; Urbas, S. A.; Toal, S. J.; Dipasquale, A. G.; Rheingold, A. L.; Trogler, W. C. *Macromolecules* **2008**, *41*, 1237–1245.
(62) Perry, R. J.; Karageorgis, M.; Hensler, J. *Macromolecules* **2007**, *40*, 3929–3938.
(63) Yamamoto, K.; Kumada, M.; Nakajima, I.; Maeda, K.; Imaki, N. *J. Organomet. Chem.* **1968**, *13*, 329–341.
(64) Tobita, H.; Wada, H.; Ueno, K.; Ogino, H. *Organometallics* **1994**, *13*, 2545–2547.

(65) Sharma, H. K.; Pannell, K. H. *Chem. Rev.* **1995**, *95*, 1351–1374.
(66) Lee, P. T. K.; Rosenberg, L. *Dalt. Trans.* **2017**, *46*, 8818–8826.
(67) Lee, P. T. K. K.; Skjel, M. K.; Rosenberg, L. *Organometallics* **2013**, *32*, 1575–1578.

Chapter 2: Effect of poly(cyclosilane) microstructure on thermal properties

The work presented in this chapter has been published as: Jiang, Q.; Wong, S.; Klausen, R. S. *Polym. Chem.* **2021**, *12*, 4785–4794.

2.1 Introduction

Hydrocarbon-based elastomers, thermoplastics, and thermosets are distinguished by their thermal properties, such as the operating temperature (above or below the glass transition temperature, T_g) and physical behaviour above the phase transition (e.g. flow).[1] Models can quantitatively relate polymer T_g to structural phenomena (e.g. the Flory–Fox equation[1,2] and the number-average molecular weight). In addition to reversible phenomena that occur at relatively low temperature like the phase transitions T_g or T_m, there is interest in the chemical reactivity of polymers at high temperature (pyrolysis).[3] In contrast to hydrocarbon polymers, structure-based understanding of polysilane thermal property relationships[4,5] is more limited and has focused on the influence of organic side chains.[6,7] Two possible reasons for this issue are (1) the synthetic challenge of creating a structurally well-defined homologous series of polysilanes and (2) the propensity of some polysilanes to undergo skeletal rearrangement to polycarbosilanes at elevated temperatures.[8,9] The polysilane to polycarbosilane rearrangement precedes the ultimate formation of silicon carbide (SiC) fibers.[10–12]

We recently described the synthesis and Cp_2ZrCl_2/*n*-BuLi-mediated[13,14] dehydrocoupling polymerization of the bifunctional cyclosilane monomers **1,4Si$_6$** and **1,3Si$_6$** (Figure 2.1.1a).[15–20] These directional building blocks template distinct linear or cyclic polymeric architectures: polymers *lin*-poly(**1,4Si$_6$**) and *cyc*-poly(**1,3Si$_6$**) were

obtained in comparable molecular weights (M_n ca. 3000 g mol^{-1}), but *cyc*-poly(**1,3Si$_6$**) lacked spectroscopic signatures consistent with end groups. We considered these materials an opportunity to investigate the effect of polysilane backbone on thermal properties without variation of the side chain, which in all cases were methyl or hydro groups.

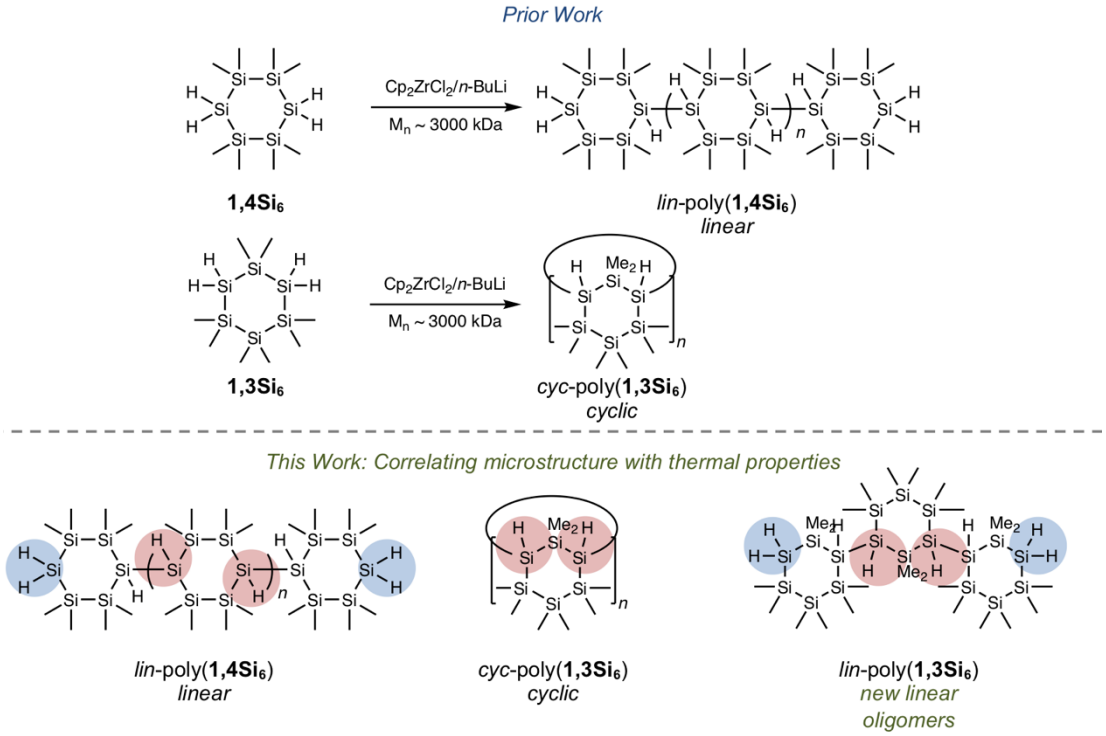

Figure 2.1.1 a) Prior work: Cp_2ZrCl_2/*n*-BuLi-mediated dehydrocoupling polymerization of directional building blocks **1,4Si$_6$** and **1,3Si$_6$**. b) This work: Synthesis of new linear *lin*-poly(**1,3Si$_6$**) and analysis of relationships between microstructure and thermal decomposition.

We hypothesized that *lin*-poly(**1,4Si$_6$**) and *cyc*-poly(**1,3Si$_6$**) would exhibit distinct thermal behaviour and reactivity. Cyclic polymers, both experimentally and computationally, show markedly different properties from linear variants despite similar chemical compositions.[21–28] For example, Roovers *et al*. reported that low molecular weight cyclic polystyrene (M_w = 4,700 g mol^{-1}) has a glass transition temperature 21 °C

higher than linear polystyrene of the same molecular weight.[27] In addition, the SiH_2 end groups present in *lin*-poly(**1,4Si$_6$**) are significantly stronger than SiH internal groups (Figure 2.1.1b) due to the weakening effect of silyl substitution on Si–H bonds,[29] which may perturb the sequence of chemical steps during thermolysis. To probe these differences, we also sought the synthesis of a linear polymer of **1,3Si$_6$** (*lin*-poly(**1,3Si$_6$**)) which would have the same relative connectivity of *cyc*-poly(**1,3Si$_6$**) but would possess SiH_2 end groups.

Herein, we report that replacement of the standard Cp_2ZrCl_2/*n*BuLi catalyst with Cp_2ZrMe_2 provided *lin*-poly(**1,3Si$_6$**), the desired linear polymer of **1,3Si$_6$**, a structural assignment supported by ^1H and ^{29}Si NMR spectroscopy. We investigate the influence of poly(cyclosilane) microstructure on thermal behavior and decomposition using a combined theoretical and experimental study. Thermal stability was investigated by differential scanning calorimetry (DSC) and thermogravimetric analysis (TGA) complemented by density functional theory (DFT) calculations. All three samples were glassy solids at room temperature. A glass transition was observed at 108 °C in *cyc*-poly(**1,3Si$_6$**), but no reversible phase transitions were found below 200 °C in *lin*-poly(**1,4Si$_6$**) and *lin*-poly(**1,3Si$_6$**). Above 250 °C, all three poly(cyclosilane)s showed significant thermal decomposition that proceeded in two phases. A generic thermolysis process of poly(cyclosilane)s is proposed based on this combined theoretical and experimental study. As a polymeric material combining cyclic subunits and mixed H- and Me- termination, poly(cyclosilane)s may find utility as ceramic precursors.

2.2 Dehydrocoupling of hydrosilanes catalyzed by Group 4 metallocene

Reductive Wurtz coupling of dichlorosilanes mediated by alkali metal has been the most popular method to access high molecular weight polysilanes (Scehme 2.2.1).[30] Alkyl

and aryl groups are mostly seen as side chains in the yielding polysilanes, such as poly($SiMe_2$), poly(di-*n*-hexylsilane) and polymethylphenylsilane. However, strong reductive conditions and intolerance to functional groups limit its utilization of synthesizing more diverse polysilane structures.[19]

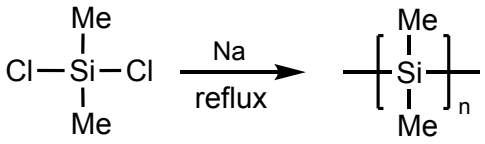

Scheme 2.2.1 Polymerization of dichlorodimethylsilane via Wurtz coupling.

Dehydrogenative polymerization of primary silanes (e.g. $PhSiH_3$) catalyzed by Group 4 metallocenes (Cp_2MX_2, M = Ti, Zr and Hf) serves as an intriguing alternative to Wurtz coupling polymerization. Harrod reported the first example of dehydrogenative polymerization making polyphenylsilane using Cp_2TiMe_2 in 1985 (Scheme 2.2.2a).[31] A long induction period (hours to days) was observed in such reactions. Corey later reported Group 4 metallocene chlorides (Cp_2MCl_2, M = Ti, Zr and Hf) *in situ* activated by 2 equivalents of *n*-BuLi were also able to catalyze the polymerization of primary silanes (Scheme 2.2.2b).[32] Once metallocene chlorides activated, no induction period was required for the polymerization. Notably, the same catalytic system led to dehydrocoupling of secondary silanes rather than polymerization, and showed no reactivity to tertiary silanes.[33]

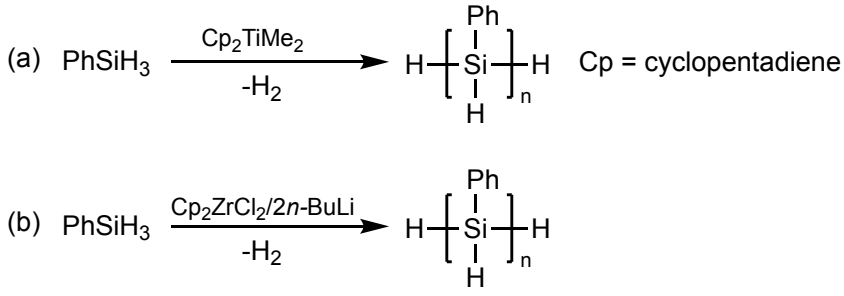

Scheme 2.2.2 Dehydrogenative polymerization of primary silanes.

Corey also proposed the mechanism of dehydrogenative coupling of hydrosilanes catalyzed by the Cp_2ZrCl_2/*n*-BuLi system (Scheme 2.2.3).[13] Although the mechanism of catalyst activation remained unclear, Corey hypothesized a highly reactive intermediate [Cp_2Zr] was generated by treating Cp_2ZrCl_2 with 2 equivalents of *n*-BuLi. Through σ-bond metathesis first proposed by Tilley[34], the coupled silane product was formed and zirconocene hydride later turned to the initial reactive [Cp_2Zr].

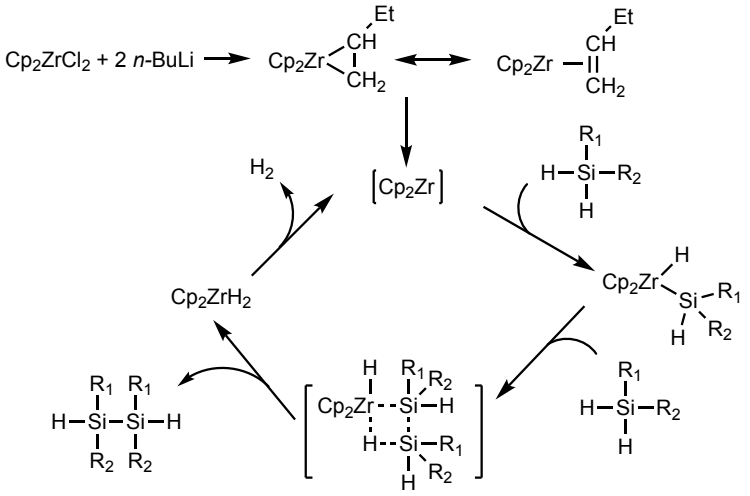

Scheme 2.2.3 Mechanism of dehydrogenative polymerization of primary silanes catalyzed by the Cp_2ZrCl_2/*n*-BuLi, proposed by Corey.[33]

The Klausen group carried out a mechanistic study of dehydrocoupling polymerization of cyclosilane **1,4Si$_6$**.[35] The polymerization is sensitive to the bulkiness of metallocene ligands. With Cp groups replaced by bulkier Cp* (permethylated cyclopentadiene), the reactivity of zirconocene catalysts decreased. Incomplete conversion and a modest decrease of molecular weight were observed with Cp*CpZrCl$_2$/*n*-BuLi system. The bulkiest Cp*$_2$ZrCl$_2$/*n*-BuLi did not catalyzed the polymerization.

Poly(**1,4Si$_6$**) molecular weight characteristics were also affected by transition metal center. Cp_2ZrCl_2/*n*-BuLi turned out to be the most effective system yielding polysilanes

with full consumption of starting **1,4Si$_6$**, highest molecular weight and best molecular weight distribution. Cp_2HfCl_2/*n*-BuLi exhibited lower reactivity for observation of starting cyclosilane after 24 hours and lower molecular weight of resulting poly(**1,4Si$_6$**). Although Cp_2TiCl_2/*n*-BuLi also gave full conversion of **1,4Si$_6$**, low molecular weight and dispersed molecular weight distribution were observed.

^{29}Si NMRs showed Cp_2TiCl_2/*n*-BuLi resulted in a significant structural rearrangement of the poly(cyclosilane) (Figure 2.2.1a). Identical SiH and SiH_2 resonances were found in ^{29}Si NMRs of Cp_2ZrCl_2/*n*-BuLi and Cp_2HfCl_2/*n*-BuLi catalyzed polymers. Such observation of internal tertiary silanes (SiH) and external secondary silane end groups (SiH_2) indicated a typical linear microstructure of poly(**1,4Si$_6$**). However, Cp_2TiCl_2/*n*-BuLi catalysis led to a significant structural difference: diminished intensity of SiH and SiH_2 resonances in ^{29}Si NMRs (Figure 2.2.1a). This suggests alkyl redistribution on poly(cyclosilane) yielding highly substituted species.[32,35] The structural change of Ti-catalysis is also supported by UV-Vis spectroscopy (Figure 2.2.1b). An broader and less-well defined absorption band of Ti-derived poly(**1,4Si$_6$**) is consistent with the structural assignments above.

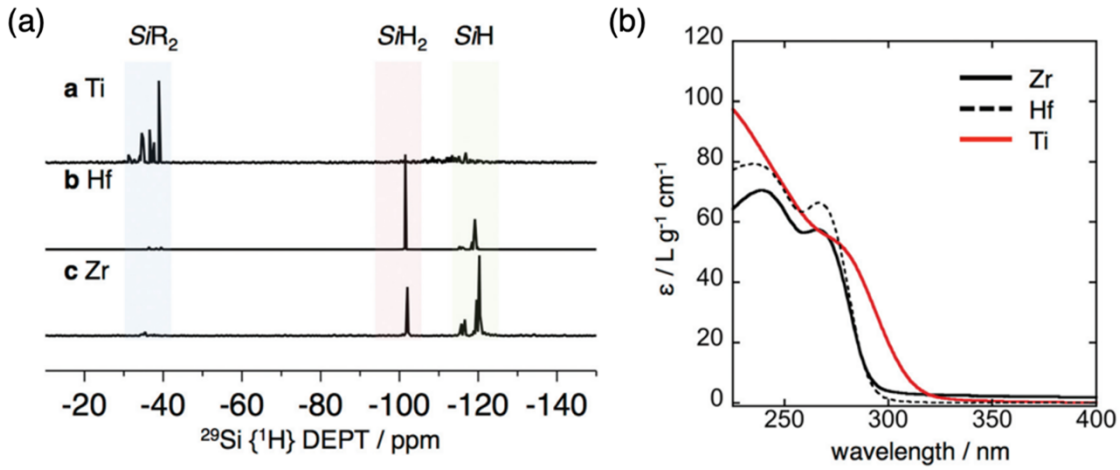

Figure 2.2.1 a) Cropped ^{29}Si {^{1}H} DEPT NMR spectra of poly(**1,4Si$_6$**) in benzene-d_6 b) UV-vis spectra of poly(**1,4Si$_6$**) samples. Spectra recorded in THF at room temperature. Reprinted with permission from reference.[35] Copyright 2018 RSC.

2.3 Synthesis of *lin*-poly(1,3Si$_6$)

During our initial work on **1,3Si$_6$** polymerization with Cp_2ZrCl_2/*n*-BuLi, we identified two fractions by gel permeation chromatography (GPC): a dominant higher molecular weight fraction corresponding to *cyc*-poly(**1,3Si$_6$**) and a minor low molecular weight fraction attributed to linear oligomers too short to cyclize (Figure 2.3.1, dashed line).[17] Spectroscopic support for this hypothesis arose from observation of minor signals consistent with SiH_2 end groups in ^{1}H NMR and ^{29}Si DEPT spectra.

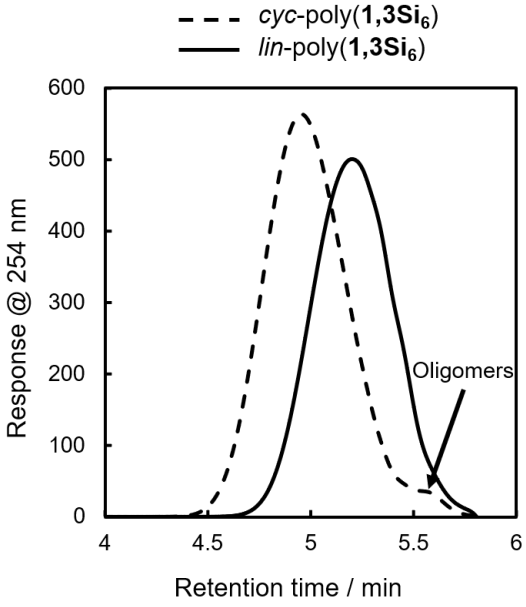

Figure 2.3.1 GPC of *cyc*-poly(**1,3Si$_6$**) (dotted line) and *lin*-poly(**1,3Si$_6$**) (solid line). Determined relative to polystyrene standards at 254 nm (THF, [polymer] = 1 mg mL^{-1}, 40 °C, 0.35 mL min^{-1},10 μL injection).

Hypothesizing that at a lower average degree of polymerization, poly(**1,3Si$_6$**) might exist exclusively of linear oligomers we reinvestigated catalysis of **1,3Si$_6$** polymerization.

We found that Cp_2ZrMe_2-polymerization could provide either linear or cyclic samples depending on solvent. Bulk polymerization of **1,3Si$_6$** with Cp_2ZrMe_2 (Scheme 2.3.1) provided *lin*-poly(**1,3Si$_6$**) in 87% yield that subsequent NMR analysis indicated was consistent with structural assignment to a predominantly linear structure (*vide infra*). GPC analysis indicated *lin*-poly(**1,3Si$_6$**) consisted of a single fraction (Figure 2.3.1). Dilution of the **1,3Si$_6$**/Cp_2ZrMe_2 polymerization with toluene resulted in *cyc*-poly(**1,3Si$_6$**)**,** which NMR characterization suggested was consistent with a predominantly cyclic architecture (Table 2.3.1). A 7-day reaction time was required for Cp_2ZrMe_2 catalysis in toluene, as this catalyst requires a 4-day induction period.[36,37] Heating the reaction at 65 °C shortened the induction period to 24 hours.

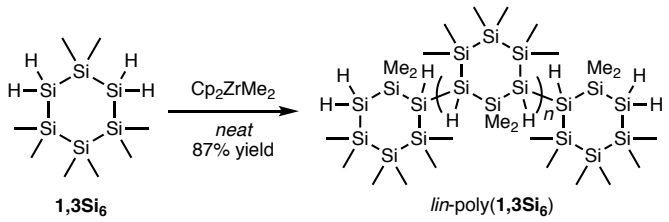

Scheme 2.3.1 Synthesis of *lin*-poly(**1,3Si$_6$**), a linear polymer of **1,3Si$_6$**.

GPC analysis also indicated that *cyc*-poly(**1,3Si$_6$**) was obtained in higher molecular weight (ca. 3000 g mol^{-1}) than *lin*-poly(**1,3Si$_6$**) (ca. 1700 g mol^{-1}) which supports the hypothesis that cyclization is inhibited at lower degrees of polymerization presumably due to strain in forming smaller cycles. However, the known tendency of cyclic polymers to adopt more compact conformations that can lead to anomalous elution on GPC affects confidence in the GPC-estimated molecular weight characteristics of *cyc*-poly(**1,3Si$_6$**) and *lin*-poly(**1,3Si$_6$**). For example, Veige *et al.* showed that GPC overestimated the molecular weight of cyclic polystyrene by 10,000 g mol^{-1}, or approximately 100 degrees of polymerization.[26] For the cyclosilane system, however, GPC is unlikely to significantly

misestimate poly(cyclosilane) molecular weight as silane dehydropolymerization rarely exceeds 20 degrees of polymerization.[38]

We suggest that linear oligomers were formed during bulk polymerization due to a change in physical properties. In the absence of solvent, the mixture of monomer and Cp_2ZrMe_2 gradually changes from a liquid to a glass. This may sequester oligomers from further reaction, providing a single fraction of low molecular weight oligomers too short to cyclize. This hypothesis is consistent with the observation that dilution with toluene actually increased molecular weight and lead to cyclized polymer. Dilution typically inhibits intermolecular reactions, such as chain extension.

Table 2.3.1 Molecular weight characteristics for metallocene-initiated dehydrocoupling polymerization of cyclosilane building blocks and resultant polymers.

Polymer	Monomer	Catalyst	Solvent	Reaction time	Structure	$M_{n,\,GPC}$ (kg mol^{-1})	$M_{w,\,GPC}$ (kg mol^{-1})	**Đ**[B]	$\overline{DP}^{c}$
lin-poly(**1,4Si$_6$**)	**1,4Si$_6$**	Cp_2ZrCl_2/*n*-BuLi	Toluene	24 h	Linear	2.59	3.29	1.27	9
cyc-poly(**1,3Si$_6$**)	**1,3Si$_6$**	Cp_2ZrCl_2/*n*-BuLi	Toluene	24 h	Cyclic	3.07	4.52	1.48	10
lin-poly(**1,3Si$_6$**)	**1,3Si$_6$**	Cp_2ZrMe_2	none	24 h	Linear	1.77	2.39	1.35	6
cyc-poly(**1,3Si$_6$**)	**1,3Si$_6$**	Cp_2ZrMe_2	Toluene	7 d	Cyclic	3.84	7.27	1.90	13

Mechanistic differences between the Cp_2ZrMe_2 and Cp_2ZrCl_2/*n*-BuLi catalysts may also play a role in the results. Group 4 metallocene derivatives are among the best-studied catalysts for hydrosilane dehydropolymerization and have long served an important role in understanding novel inorganic mechanisms.[38,39] Corey *et al*. first reported that *in situ* activation of Cp_2ZrCl_2 in toluene with two equivalents of *n*-butyllithium yielded an effective catalyst for secondary silane polymerization.[13,14] Chloride substitution by the alkyllithium yields an intermediate dialkyl zirconocene, which further reacts via β-hydrogen abstraction to yield the active, undercoordinated catalyst, although the exact

catalyst structure remains ambiguous.[40] In contrast, dimethyl zirconocene (Cp_2ZrMe_2), first reported by Harrod *et al*., does not require activation by an exogenous agent and can therefore be used either neat or with added solvent.[36,41,42] However, reactions with Cp_2ZrMe_2 can show an induction period,[41] presumably due to slow formation of the active undercoordinated catalyst in the absence of β-hydrogens.

2.4 Poly(cyclosilane) microstructure

Poly(cyclosilane)s feature a well-defined, periodic alternation of methylated and hydrogenated silicon atoms (Figure 2.1.1b). This structural pattern provides diagnostic features for spectroscopic characterization based on the unique signatures of tertiary (Si_3Si-*H*), secondary (Si_2Si*H*$_2$), and primary ($SiSi$*H*$_3$) bonds. Variable silyl- and hydro-substitution strongly influences chemical shift in ^{29}Si NMR spectroscopy.[43,44] The degree of silyl substitution has a marked weakening effect on Si–H bond strength,[29] which is reflected in a significant shift to lower-frequency FTIR resonances for the weaker Si_3Si*H* internal groups relative to stronger Si_2Si*H*$_2$ end groups.[17]

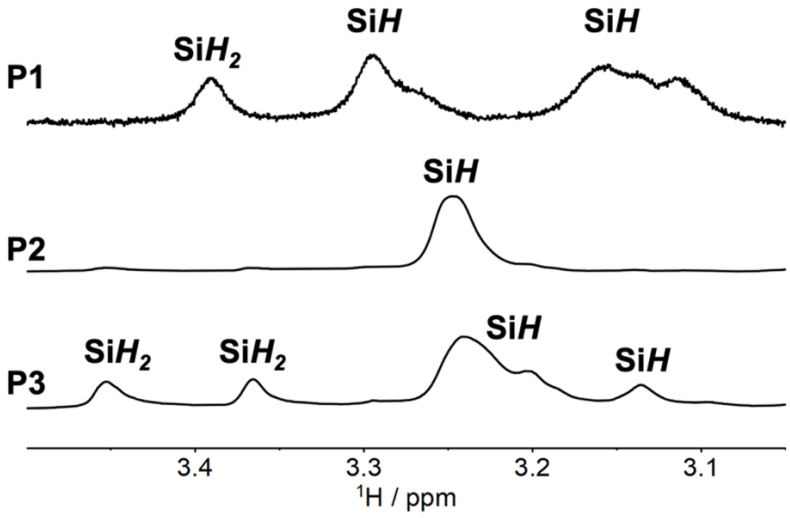

Figure 2.4.1 Cropped ^{1}H NMR spectra of *lin*-poly(**1,4Si$_6$**), *cyc*-poly(**1,3Si$_6$**) and *lin*-poly(**1,3Si$_6$**). Only the SiH region is shown.

^{1}H NMR spectra are shown in Figure 2.3.1. The spectrum of *cyc*-poly(**1,3Si$_6$**) is dominated by a single broad resonance at δ 3.25, consistent with its high symmetry macrocyclic structure.[17] *lin*-Poly(**1,4Si$_6$**) has a series of resonances in the SiH_x region (δ 3.5-3.0), which were assigned to SiH_2 end groups or SiH internal sites by ^{1}H-^{29}Si HSQC.[17] The ^{1}H NMR spectrum of *lin*-poly(**1,3Si$_6$**) is strikingly similar to *lin*-poly(**1,4Si$_6$**) with several broad resonances from δ 3.45 to 3.10, even though each is a polymer of an isomeric cyclosilane. These spectral data are consistent with assignment of *lin*-poly(**1,3Si$_6$**) to a lower-symmetry linear structure rather than a macrocycle.

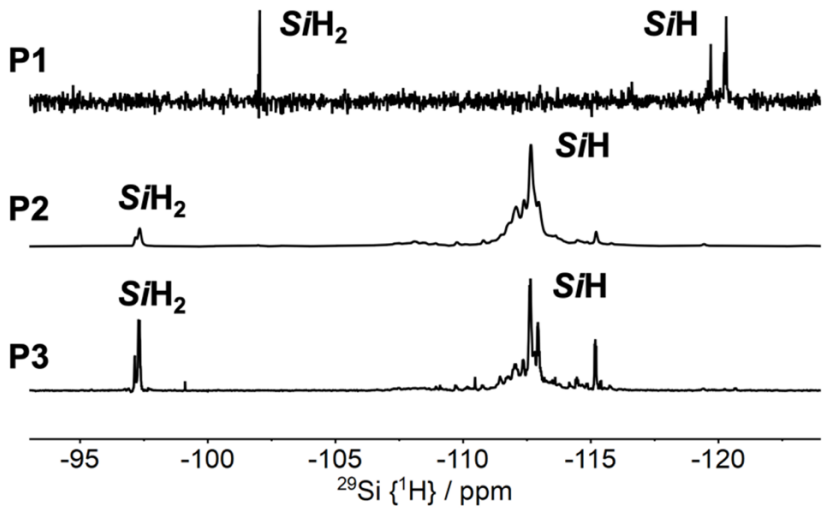

Figure 2.4.2 Cropped ^{29}Si{^{1}H} DEPT spectra of *lin*-poly(**1,4Si$_6$**), *cyc*-poly(**1,3Si$_6$**) and *lin*-poly(**1,3Si$_6$**). Only the SiH region is shown. DEPT = distortionless enhancement by polarization transfer.

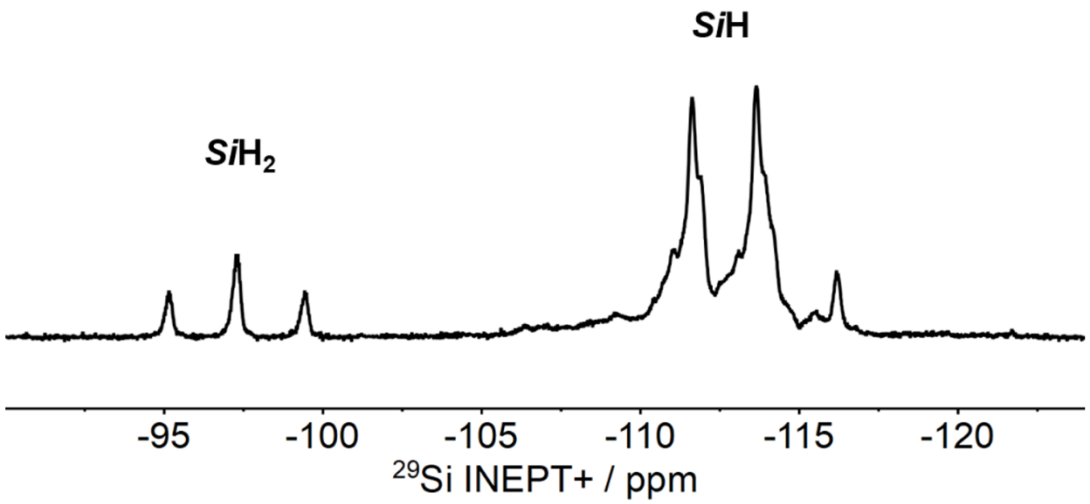

Figure 2.4.3. ^{29}Si INEPT+ NMR spectrum (79 MHz, Benzene-d_6) of *lin*-poly(**1,3Si$_6$**).

Further support for assignment of *lin*-poly(**1,3Si$_6$**) to a predominantly linear structure comes from the ^{29}Si {^{1}H} DEPT (Figure 2.3.2), ^{29}Si {^{1}H} INEPT+ (Figure 2.3.3) and ^{1}H-^{29}Si HSQC (Figure 2.3.4) spectra. Like *lin*-poly(**1,4Si$_6$**), the ^{29}Si {^{1}H} DEPT spectrum of *lin*-poly(**1,3Si$_6$**) possesses two sets of strong resonances consistent with Si_3SiH tertiary silanes (internal sites, δ -115.3) and Si_2SiH_2 secondary silanes (end groups, δ -97.46). A proton-coupled ^{29}Si INEPT+ spectrum showed the expected multiplicities for the number of attached protons, confirming these assignments (Figure 2.3.3). The family of doublets (δ -109.8 to -117.0, $^1J_{SiH}$ = 160.1 Hz) were assigned to *Si*H internal resonances. The triplet (δ -97.3, $^1J_{SiH}$ = 172.3 Hz) was assigned to SiH_2 end groups, consistent with assignment of *lin*-poly(**1,3Si$_6$**) to a linear polymer of **1,3Si$_6$**. The experimentally measured coupling constants were consistent with typical one-bond coupling constants between silicon and proton.

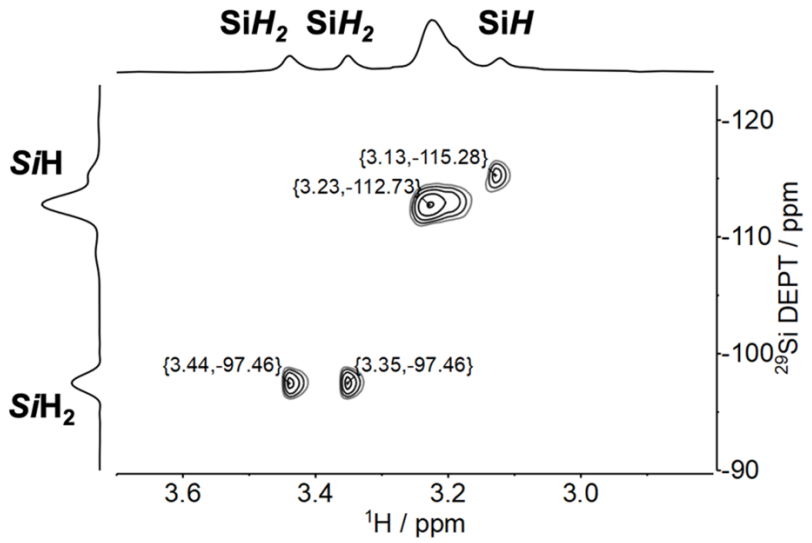

Figure 2.4.4 ^{1}H-^{29}Si HSQC NMR spectrum of *lin*-poly(**1,3Si$_6$**). Crosspeaks are labelled. HSQC = heteronuclear single quantum coherence; DEPT = distortionless enhancement by polarization transfer.

In the ^{1}H-^{29}Si HSQC spectrum of *lin*-poly(**1,3Si$_6$**), crosspeaks were observed between the ^{1}H resonances at δ 3.25 to 3.10 and ^{29}Si NMR resonances centered at δ -112 assigned to $Si_3\mathit{Si}H$ sites (Figure 2.3.4). Meanwhile, ^{1}H resonances at δ 3.44 to 3.28 correlated with the ^{29}Si NMR resonances centered at δ -97 assigned to $Si_2\mathit{Si}H_2$ sites. The 2-D spectral correlations confirm the assignment of the *lin*-poly(**1,3Si$_6$**) structure to a linear structure containing both tertiary silane internal sites and secondary silane end groups.

Finally, *lin*-poly(**1,3Si$_6$**)'s Fourier transform infrared (FTIR) spectrum showed two resonances in the SiH_x region consistent with stronger Si_2SiH_2 and weaker Si_3SiH bonds (Figure 2.3.5). *cyc*-Poly(**1,3Si$_6$**) lacking Si_2SiH_2 end groups has a more symmetric band in this region centered at a lower frequency. The spectroscopic studies described here support assignment of *lin*-poly(**1,3Si$_6$**) to a largely linear structure.

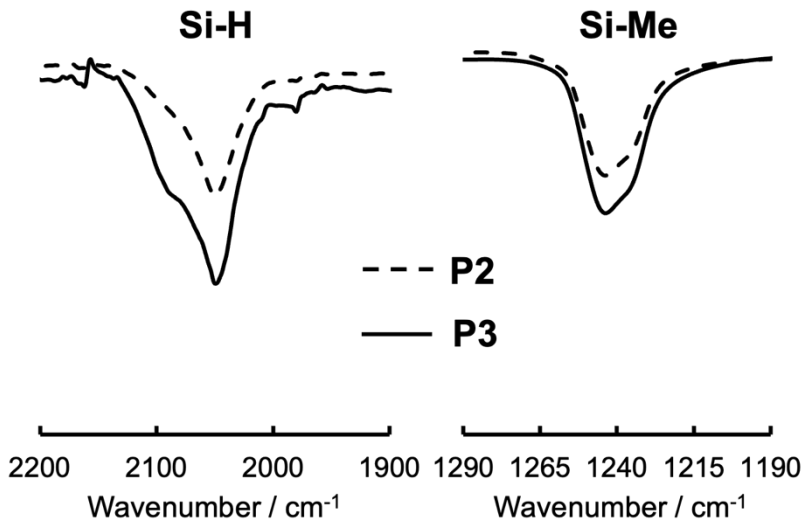

Figure 2.4.5 Cropped ATR-FTIR spectra of *cyc*-poly(**1,3Si$_6$**) and *lin*-poly(**1,3Si$_6$**) highlighting the Si–H and Si–Me regions.

2.5 Differential Scanning Calorimetry

While the thermal properties of Si-O polymers are well-characterized, and cyclic and linear polydimethylsiloxane (PDMS) were foundational models for understanding the effect of architecture on the T_g,[23] systematic investigation of polysilane thermal properties has been largely limited to understanding the role of organic side chains in influencing backbone conformation and optical properties. Polysilanes with longer side chains (hexyl, heptyl, octyl) exhibit solid-state thermochromism,[45,46] while polysilanes with shorter side chains (butyl, pentyl) do not.[47] Significant experimentation supports the following model: (1) Polysilanes with short side chains adopt a helical Si-Si conformation at room temperature that absorbs higher energy light (λ = 317 nm). (2) In contrast, polysilanes with longer side chains adopt an all-*anti* conformation at room temperature that maximizes σ-conjugation and results in a bathochromically shifted absorption band (λ = 375 nm). This is attributed to side chain crystallization that locks the Si-Si backbone into the *anti*-

conformation. At elevated temperatures, side chain melting results in a backbone disordering that shifts the absorption band back to higher energies (λ = 317 nm).

Rabolt *et al*. found by differential scanning calorimetry (DSC) a reversible first-order transition at ca. 40 °C in poly(di-*n*-hexylsilane) that was assigned to the side-chain melting.[46] Schilling *et al.* reported that DSC analysis of poly(di-*n*-butylsilane) and poly(di-*n*-pentylsilane) yielded significantly different results, including the lack of a transition comparable to side-chain melting (a weaker transition to a more disordered phase was found above ca. 80 °C).[47] In addition, Schilling *et al.* reported a very weak second-order transition at 36 °C (only apparent in poly(di-*n*-butylsilane) during slow DSC runs) and an intense second-order transition at –40 °C. On the basis of solid-state NMR experiments (^{13}C CP-MAS), all phase transitions were attributed to side chains.

The poly(di-*n*-alkylsilanes) studied by Miller,[46] Schilling,[47] and others were prepared by Wurtz polymerization of the corresponding dichlorodialkylsilane. Wurtz polymerization typically results in higher molecular weight materials than those prepared by dehydropolymerization and the products also differ in possessing two alkyl side chains rather than one (e.g. poly(SiR_2) vs. poly(SiHR)). While monoalkyl polysilanes surely possess different thermal properties than dialkyl, we have identified only one report of thermal analysis of a polysilane prepared by dehydropolymerization. Corey *et al.* reported dehydropolymerization of *p*-tolylsilane and that DSC analysis of poly(SiH(*p*-tol)) (degree of polymerization ca. 20) revealed no phase transitions over the temperature range 25 to 200 °C.[48] Some insight into the influence of hydro side chains arises from comparison of the copolymer poly($SiPh_2$-*co*-SiMeH) to poly(SiMePh).[49] Both poly(SiMePh) and poly($SiPh_2$-co-SiMeH) exhibited a single glass transition, but the poly($SiPh_2$-co-SiMeH)

T_g decreased with increasing methylhydro composition (T_g = 64 to 85 °C vs. 88 °C for poly(SiMePh)). These data were interpreted as showing greater flexibility and mobility in hydro-substituted polysilanes.

While prior work has provided insight into side chain effects, little is understood about how the silane architecture might influence thermal properties. We therefore performed DSC analysis of the three poly(cyclosilane)s in the temperature range 35 to 200 °C as thermogravimetric analysis (TGA, vide infra) indicated polymer decomposition above 200 °C. Heating rates between 3 and 20 °C min^{-1} were tested.

For the two linear systems *lin*-poly(**1,4Si$_6$**) and *lin*-poly(**1,3Si$_6$**), no reversible phase transition was observed below 200 °C at any heating rate (Figure 2.4.1a,c). In contrast, for *cyc*-poly(**1,3Si$_6$**) we observed an apparent second-order phase transition at 108 °C (Figure 2.4.1b). The transition was only observed with a heating rate of 20 °C min^{-1} and a cooling rate of 3 °C min^{-1}; no transition was apparent at slower heating rates. The reversibility of the 108 °C transition is unclear: no transition is seen on cooling (Figure 2.4.2) but the transition observed on heating is reproducible (second and third heating cycles overlay, Figure 2.4.3), which is inconsistent with a change in chemical structure. The 108 °C transition was apparent in all samples of *cyc*-poly(**1,3Si$_6$**) evaluated, regardless of preparative method.

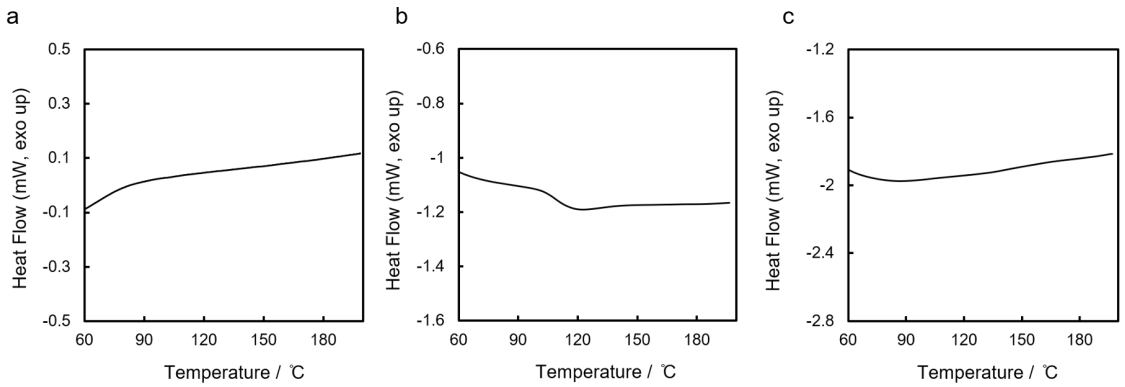

Figure 2.5.1 DSC curves of a) *lin*-poly(**1,4Si$_6$**), b) *cyc*-poly(**1,3Si$_6$**), and c) and *lin*-poly(**1,3Si$_6$**). The second cycle is shown. Heating rate: 3 °C min^{-1} for *lin*-poly(**1,4Si$_6$**), 20 °C min^{-1} for *cyc*-poly(**1,3Si$_6$**) and *lin*-poly(**1,3Si$_6$**).

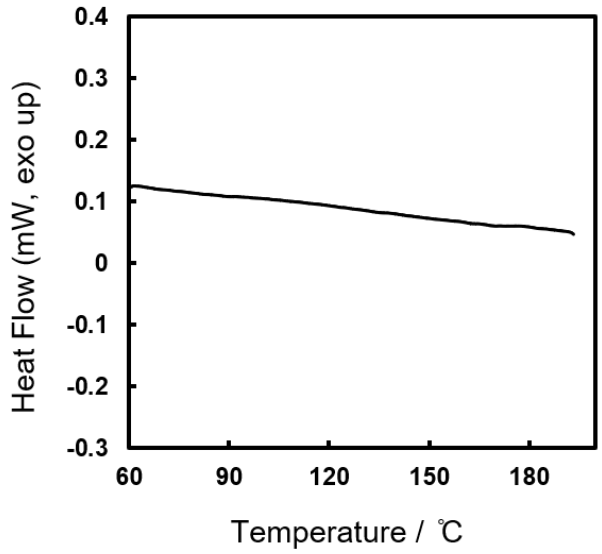

Figure 2.5.2. The second cooling cycle of DSC measurement of *lin*-poly(**1,3Si$_6$**). Cooling rate: 3 °C min^{-1}. No phase transition was observed.

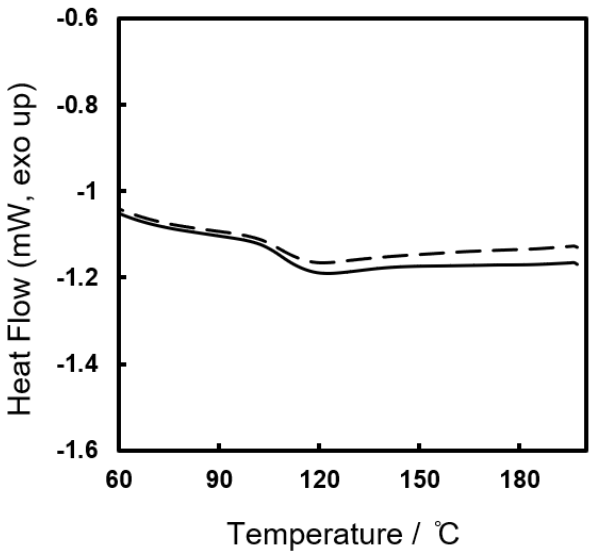

Figure 2.5.3. The overlay of the second (solid line) and third (dotted line) heating cycle of DSC measurement of *lin*-poly(**1,3Si$_6$**). Heating rate: 20 °C min^{-1}.

The DSC analysis of *lin*-poly(**1,4Si$_6$**) and *lin*-poly(**1,3Si$_6$**) is similar to that reported by Corey *et al.* for linear poly(SiH(*p*-tol)).[48] The comparatively high mobility of monoalkyl segments in linear polysilanes may complicate observation of the T_g in polymers with the general formula poly(SiHR). The observation of a 108 °C phase transition is unprecedented. We suggest assignment to a glass transition. While the T_g is not apparent on cooling, this may arise from crystallization during the heating phase. Assignment to a glass transition is also consistent with the known tendency of cyclic polymers to exhibit anomalous glass transitions relative to linear polymers.

2.6 Thermal stability of poly(cyclosilane)s

Polymers based on main group elements find application as solution-processable precursors to ceramics (polymer-derived ceramics, PDCs).[8,11] Yajima *et al.* discovered pyrolysis of polydimethylsilane ($[SiMe_2]_n$) yielding silicon carbide (SiC) fibers.[50,51] Polysilazane pyrolysis yields silicon nitride (Si_3N_4) or Si/C/N ceramics depending on the

precursor and thermolysis conditions.[8,52,53] Several studies have demonstrated the influence of precursor structure on PDC structure and properties. Schilling *et al*. demonstrated the positive influence of backbone branching on SiC ceramic yield using polycarbosilanes prepared by potassium reduction of vinylmethyldichlorosilane.[54] Polysilanes bearing both hydrogen and alkyl substituents[55] are particularly attractive to circumvent carbon formation during pyrolysis, as shown by Laine *et al*. in the decomposition of polymethylsilane (–$[MeSiH]_x$–).[56]

The thermal decomposition of poly(cyclosilane)s was studied by thermogravimetric analysis (Figure 2.5.1). The three polymers showed overall similar thermal decomposition behavior. A minor mass loss at 65 °C in *lin*-poly(**1,4Si$_6$**) was attributed to residual catalyst (Figure 2.5.1a), which was easier to remove from the more soluble *cyc*-poly(**1,3Si$_6$**) and *lin*-poly(**1,3Si$_6$**) samples. TGA curves of derivative weight change reveal two main phases of weight loss when samples are heated from 40 to 600 ˚C in argon flow. When the temperature increased to 500 °C, about 50% weight loss is observed in all three samples. Then, the weight became constant above 550 ˚C. A black solid residue remained in the sample pan after the TGA measurement. These observations are consistent with ceramization,[8] although the product was not characterized in this study.

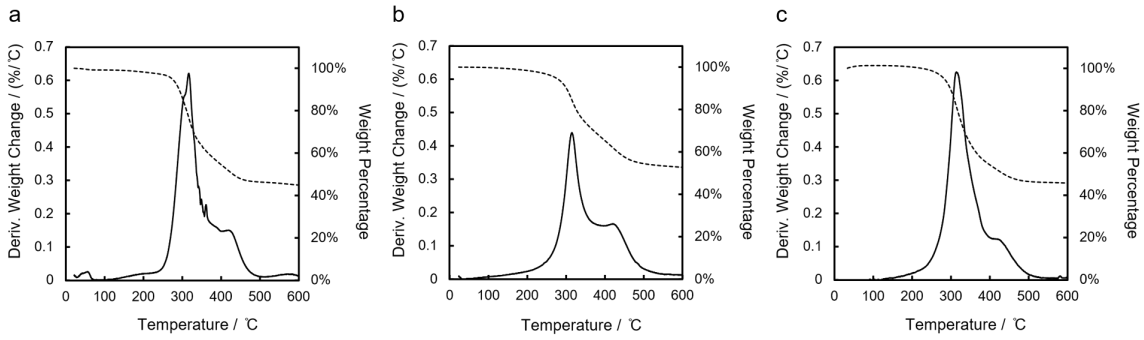

Figure 2.6.1 TGA curves of a) *lin*-poly(**1,4Si$_6$**), b) *cyc*-poly(**1,3Si$_6$**) and c) *lin*-poly(**1,3Si$_6$**). Solid lines: derivative weight change; dotted lines: percentage weight change.

Some differences between the polymer systems were also apparent between 200 to 400 °C. The linear polymers both showed similar derivative weight change in this region, with a peak value greater than 0.6, while for *cyc*-poly(**1,3Si$_6$**) the peak value was lower than 0.5 (Figure 2.5.1b). Both linear polymers lost approximately 45% of their weight in this phase, while only 33% for *cyc*-poly(**1,3Si$_6$**). This indicates that linear poly(cyclosilane)s decomposed more rapidly than *cyc*-poly(**1,3Si$_6$**) in this temperature range. In addition, multiple features (e.g. peaks and shoulders) appeared in the derivative weight change curve of *lin*-poly(**1,4Si$_6$**), while smoother curves were obtained in the measurements of *cyc*-poly(**1,3Si$_6$**) and *lin*-poly(**1,3Si$_6$**).

These observations point to microstructure-dependent differences in early stage poly(cyclosilane) pyrolysis. The first phase of polysilane pyrolysis to SiC is skeletal rearrangement from a polysilane to a polycarbosilane;[57] in poly(SiMeH) pyrolysis, this rearrangement occurs at 400 °C.[56] The pyrolysis of hexamethyldisilane is a model system for polysilane thermolysis and several reactive intermediates have been proposed, including radical,[57,58] silylene (R_2Si),[59] and silene (C=Si) species.[58] In all cases, homolysis of a weak bond (e.g. $Me_3Si–SiMe_3$ to $2Me_3Si\bullet$) initiates skeletal rearrangement. The different poly(cyclosilane) microstructures, especially with respect to Si–H bond strengths, may influence the relative rates of processes implicated in poly(cyclosilane) thermolysis.

2.7 Bond dissociation energy calculations

To understand the influence of poly(cyclosilane) microstructure on thermolysis, we carried out density functional theory (DFT) calculations of bond dissociation energy on monomers and model molecules. As a compromise between computational ease and experimental relevance, the monomer **1,4Si$_6$** and its linear trimer were selected for study.

Geometries were fully optimized without symmetry restrictions using B3LYP hybrid exchange-correlation functional with the 6-31G(d) basis set. The basis set was utilized to investigate structures and expected characteristics of linear and cyclic forms of poly(**1,3Si$_6$**).[17] To ensure optimized geometries were local minima on their potential energy surfaces, the same level of theory was utilized to perform frequency calculations and showed no imaginary frequencies. The optimized geometry of **1,4Si$_6$** is a chair conformation (consistent with a prior X-ray crystallographic study),[16] whereas in the linear trimer rings were slightly twisted. Table 2.6.1 summarizes calculated homolytic bond dissociation energies (BDEs) of **1,4Si$_6$** and its trimer.

Table 2.7.1. Calculated bond dissociation energy of **1,4Si$_6$** and *lin*-(**1,4Si$_6$**)$_3$.

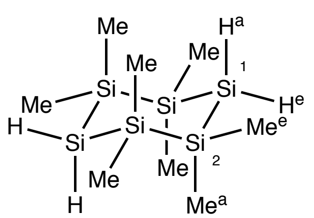

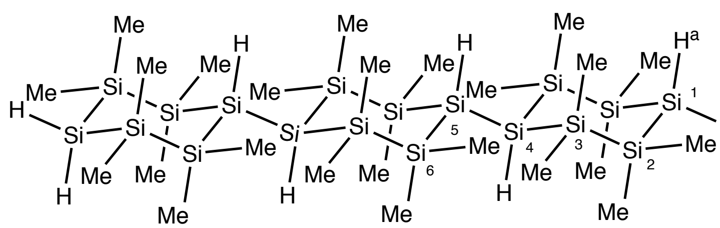

1,4Si$_6$		*lin*-(**1,4Si$_6$**)$_3$	
Bond	BDE (kcal mol^{-1})	Bond	BDE (kcal mol^{-1})
Si(1)-H^a	88.0	Si(1)-H^a	88.4
Si(1)-H^e	86.5	Si(1)-H^e	86.7
Si(2)-Me^a	80.0	Si(4)-H	85.6
Si(2)-Me^e	78.9	Si(6)-Me^a	73.4
Si(1)-Si(2)	68.1	Si(6)-Me^e	73.3
Si(2)-Si(2)	68.4	Si(2)-Si(3)	63.0
		Si(3)-Si(4)	59.6
		Si(4)-Si(5)	54.9

In **1,4Si$_6$**, Si–Si bonds were significantly weaker than Si–Me and Si–H bonds by 12-18 kcal mol^{-1}. A similar trend in relative bond strengths (from high to low: Si-H, Si-Me, and Si-Si) was observed in *lin*-(**1,4Si$_6$**)$_3$. The Si-Si bond between repeat units was notably weaker than endocyclic Si–Si bonds by 5 to 8 kcal mol^{-1}. These data suggest that the Si-Si bonds between monomers are most likely to homolyse first in poly(cyclosilane) thermolysis. Small, volatile silanes generated from homolysis near an end group in linear poly(cyclosilane)s would result in a significant weight decrease, which is consistent with the major weight loss observed between 200 to 400 ˚C in TGA measurements. In *cyc*-poly(**1,3Si$_6$**), fewer volatile products may form as at least two Si–Si bond rupture events would be required to form a volatile byproduct. This may account for the slower mass loss observed in *cyc*-poly(**1,3Si$_6$**) relative to linear poly(cyclosilane)s.

At higher temperatures, organic side groups and hydrogen atoms start to detach from silicon leading to the second phase of weight loss. Combining experimental measurements and BDE calculations, the thermolysis process of poly(cyclosilane)s is proposed as shown in Figure 2.6.1.

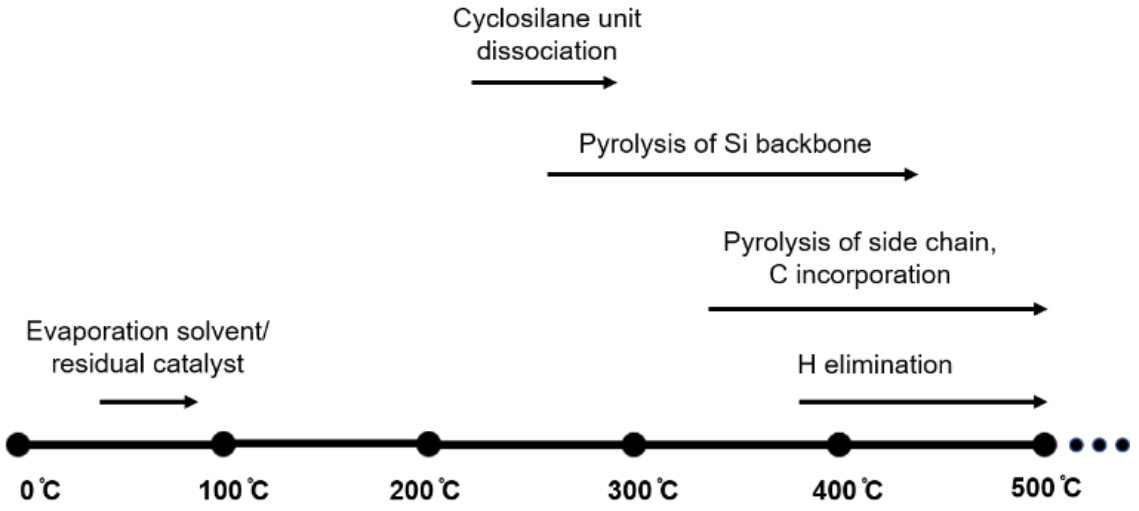

Figure 2.7.1 Proposed poly(cyclosilane) pyrolysis.

2.8 Conclusion

Herein, we investigated the microstructure-dependent thermal properties of poly(cyclosilane)s. We prepared a known linear polymer of **1,4Si$_6$** (*lin*-poly(**1,4Si$_6$**)) and a predominantly cyclic polymer of **1,3Si$_6$** (*cyc*-poly(**1,3Si$_6$**)). In the course of these efforts, we also synthesized a new, linear oligomer of cyclosilane **1,3Si$_6$** (*lin*-poly(**1,3Si$_6$**)). Thermal analysis by DSC found no phase transitions for linear poly(cyclosilane)s below the decomposition temperature, but a phase transition at 108 ℃ was found for *cyc*-poly(**1,3Si$_6$**). We suggested assignment to a glass transition temperature. Poly(cyclosilane) thermolysis was investigated by TGA and investigated by density functional theory calculations. Lower rates of mass loss were found for *cyc*-poly(**1,3Si$_6$**), which was attributed to the need for two bond homolysis events to form volatile byproducts. These studies provide insights into how synthetic control of polysilane microstructure can predictably influence thermal properties.

2.9 Reference

(1) Odian, G. *Principles of Polymerization*; John Wiley & Sons, 2004.
(2) Fox, T. G.; Flory, P. J. *J. Appl. Phys.* **1950**, *21*, 581–591.
(3) Anuar Sharuddin, S. D.; Abnisa, F.; Wan Daud, W. M. A.; Aroua, M. K. *Energy Convers. Manag.* **2016**, *115*, 308–326.
(4) Zeigler, J. M. *Synth. Met.* **1989**, *28*, 581–591.
(5) Miller, R. D.; Michl, J. *Chem. Rev.* **1989**, *89*, 1359–1410.
(6) Demoustier-Champagne, S.; Cordier, S.; Devaux, J. *Polymer (Guildf).* **1995**, *36*, 1003–1007.
(7) Asuke, T.; West, R. *Macromolecules* **1991**, *24*, 343–344.
(8) Birot, M.; Pillot, J. P.; Dunoguès, J. *Chem. Rev.* **1995**, *95*, 1443–1477.
(9) Shiina, K.; Kumada, M. *J. Org. Chem.* **1958**, *23*, 139.
(10) Yajima, S.; Hayashi, J.; Omori, J.; Okamura, K. *Nature* **1976**, *261*, 683–685.
(11) Colombo, P.; Mera, G.; Riedel, R.; Sorarù, G. D. *J. Am. Ceram. Soc.* **2010**, *93*, 1805–1837.
(12) Barroso, G.; Li, Q.; Bordia, R. K.; Motz, G. *J. Mater. Chem. A* **2019**, *7*, 1936–1963.
(13) Corey, J. Y.; Zhu, X. H.; Bedard, T. C.; Lange, L. D. *Organometallics* **1991**, *10*, 924–930.
(14) Corey, J. Y.; Chang, L. S.; Corey, E. R. *Organometallics* **1987**, *6*, 1595–1596.

(15) Marro, E. A.; Folster, C. P.; Press, E. M.; Im, H.; Ferguson, J. T.; Siegler, M. A.; Klausen, R. S. *J. Am. Chem. Soc.* **2019**, *141*, 17926–17936.
(16) Press, E. M.; Marro, E. A.; Surampudi, S. K.; Siegler, M. A.; Tang, J. A.; Klausen, R. S. *Angew. Chemie Int. Ed.* **2017**, *56*, 568–572.
(17) Marro, E. A.; Press, E. M.; Siegler, M. A.; Klausen, R. S. *J. Am. Chem. Soc.* **2018**, *140*, 5976–5986.
(18) Folster, C. P.; Klausen, R. S. *Polym. Chem.* **2018**, *9*, 1938–1941.
(19) Marro, E. A.; Klausen, R. S. *Chem. Mater.* **2019**, *31*, 2202–2211.
(20) Dorn, R. W.; Marro, E. A.; Hanrahan, M. P.; Klausen, R. S.; Rossini, A. J. *Chem. Mater.* **2019**, *31*, 9168–9178.
(21) Jia, Z.; Monteiro, M. J. *J. Polym. Sci. Part A Polym. Chem.* **2012**, *50*, 2085–2097.
(22) Bannister, D. J.; Semlyen, J. A. *Polymer (Guildf).* **1981**, *22*, 377–381.
(23) Clarson, S. J.; Dodgson, K.; Semlyen, J. A. *Polymer (Guildf).* **1985**, *26*, 930–934.
(24) Orrah, D. J.; Semlyen, J. A.; Ross-Murphy, S. B. *Polymer (Guildf).* **1988**, *29*, 1452–1454.
(25) Roovers, J.; Toporowski, P. M. *Macromolecules* **1983**, *16*, 843–849.
(26) Roland, C. D.; Li, H.; Abboud, K. A.; Wagener, K. B.; Veige, A. S. *Nat. Chem.* **2016**, *8*, 791–796.
(27) Santangelo, P. G.; Roland, C. M.; Chang, T.; Cho, D.; Roovers, J. *Macromolecules* **2001**, *34*, 9002–9005.
(28) Gao, L.; Oh, J.; Tu, Y.; Chang, T.; Li, C. Y. *Polymer (Guildf).* **2019**, *170*, 198–203.
(29) Kanabus-kaminska, J. M.; Hawari, J. A.; Griller, D.; Chatgilialoglu, C. *J. Am. Chem. Soc.* **1987**, *109*, 5267–5268.
(30) Kipping, F. S. *J. Chem. Soc., Trans.* **1924**, *125*, 2291–2297.
(31) Aitken, C.; Harrod, J. F.; Samuel, E. *J. Organomet. Chem.* **1985**, *279*, C11–C13.
(32) Corey, J. Y.; Xiao-Hong, Z. *J. Organomet. Chem.* **1992**, *439*, 1–17.
(33) Corey, J. Y.; Zhu, X. H.; Bedard, T. C.; Lange, L. D. *Organometallics* **1991**, *10*, 924–930.
(34) Woo, H. G.; Walzer, J. F.; Tilley, T. D. *J. Am. Chem. Soc.* **1992**, *114*, 7047–7055.
(35) Folster, C. P.; Klausen, R. S. *Polym. Chem.* **2018**, *9*, 1938–1941.
(36) Aitken, C.; Harrod, J. F.; Gill, U. S. *Can. J. Chem.* **1987**, *65*, 1804–1809.
(37) Mu, Y.; Aitken, C.; Cote, B.; Harrod, J. F.; Samuel, E. *Can. J. Chem.* **1991**, *69*, 264–276.
(38) Tilley, T. D. *Acc. Chem. Res.* **1993**, *26*, 22–29.
(39) Waterman, R. *Chem. Soc. Rev.* **2013**, *42*, 5629–5641.
(40) Dioumaev, V. K.; Harrod, J. F. *Organometallics* **1997**, *16*, 1452–1464.
(41) Aitken, C.; Harrod, J. F.; Samuel, E. *Can. J. Chem.* **1986**, *64*, 1677–1679.
(42) Campbell, W. H.; Hilty, T. K.; Yurga, L. *Organometallics* **1989**, *8*, 2615–2618.
(43) Blinka, T. A.; Helmer, B. J.; West, R. *Adv. Organomet. Chem.* **1984**, *23*, 193–218.
(44) Hanrahan, M. P.; Fought, E. L.; Windus, T. L.; Wheeler, L. M.; Anderson, N. C.; Neale, N. R.; Rossini, A. J. *Chem. Mater.* **2017**, *29*, 10339–10351.
(45) Miller, R. D.; Hofer, D.; Rabolt, J.; Fickes, G. N. *J. Am. Chem. Soc.* **1985**, *107*, 2172–2174.
(46) Rabolt, J. F.; Hofer, D.; Miller, R. D.; Fickes, G. N. *Macromolecules* **1986**, *19*, 611–616.
(47) Schilling, F. C.; Lovinger, A. J.; Zeigler, J. M.; Davis, D. D.; Bovey, F. A.

Macromolecules **1989**, *22*, 3055–3063.
(48) Grimmond, B. J.; Corey, J. Y. *Organometallics* **2000**, *19*, 3776–3783.
(49) Sacarescu, L.; Siokou, A.; Sacarescu, G.; Simionescu, M.; Mangalagiu, I. *Macromolecules* **2008**, *41*, 1019–1024.
(50) Yajima, S.; Hayashi, J.; Omori, M. *Chem. Lett.* **1975**, *4*, 931–934.
(51) Yajima, S.; Hasegawa, Y.; Okamura, K.; Matsuzawa, T. *Nature* **1978**, *273*, 525–527.
(52) Han, H. N.; Lindquist, D. A.; Haggerty, J. S.; Seyferth, D. *Chem. Mater.* **1992**, *4*, 705–711.
(53) SEYFERTH, D.; WISEMAN, G. H. *J. Am. Ceram. Soc.* **1984**, *67*, C-132-C-133.
(54) Schilling, C. L.; Wesson, J. P.; Williams, T. C. *J. Polym. Sci. Polym. Symp.* **1983**, *70*, 121–128.
(55) Seyferth, D.; Wood, T. G.; Tracy, H. J.; Robison, J. L. *J. Am. Ceram. Soc.* **1992**, *75*, 1300–1302.
(56) Zhang, Z. -F; Babonneau, F.; Laine, R. M.; Mu, Y.; Harrod, J. F.; Rahn, J. A. *J. Am. Ceram. Soc.* **1991**, *74*, 670–673.
(57) Yajima, S.; Hasegawa, Y.; Hayashi, J.; Iimura, M. *J. Mater. Sci.* **1978**, *13*, 2569–2576.
(58) Davidson, I. M. T.; Howard, A. V. *J. Chem. Soc. Faraday Trans. 1 Phys. Chem. Condens. Phases* **1975**, *71*, 69–77.
(59) Davidson, I. M. T. *J. Organomet. Chem.* **1988**, *341*, 255–265.

Chapter 3: Poly(cyclosilane) connectivity tunes optical absorbance

The work presented in this chapter has been published as: Fang, F.; Jiang, Q.; Klausen, R. S. *J. Am. Chem. Soc.* **2022**, 144, 17, 7834–7843

3.1 Introduction

Polysilanes are a class of organometallic polymers with a backbone comprised of Si–Si atoms[1–5] that have long attracted interest for their longer-wavelength optical transitions relative to organic polyolefins.[6] Polysilane absorption spectra are conformation-dependent,[7,8] giving rise to thermochromism in the solid- and solution-state[9–11] and conformation-dependent molecular conductance.[12–16] Efforts to control conformation, with corresponding bathochromic shifts in absorption spectra, have focused on modifying the organic backbone of the molecular[17–20] or polymeric silane.[9,10]

We now demonstrate tailoring of polysilane optical properties via changes in the silicon skeleton. The connectivity of isomeric cyclosilanes introduces distinct conformations and σ-conjugated pathways: 1,3-linkages achieve extended zigzag pathways not available to 1,4-linked cyclosilanes, resulting in a 20-nm difference in λ_{max} (Figure 1). Critically, this insight enables a connection between structural design and tunable absorption spectra. We show that copolymerization of the cyclosilane monomers **1,3Si$_6$** and **1,4Si$_6$**, results in systematic increases in λ_{max} with higher compositions of **1,3Si$_6$**.

Skeletal control of polysilane optical absorbance requires complex monomers. The earliest polysilanes were prepared by sodium-mediated Wurtz polymerization, which is limited to simple diorganodichlorosilanes (e.g. Cl_2SiMe_2)[21] due to the strongly reducing conditions and results in disperse mixtures of oligomeric and polymeric species.[22,23] Our

group, inspired by crystalline silicon's diamond lattice structure, sought to synthesize polymeric silanes with cyclic repeat units.[24] The metal-catalyzed dehydrogenative coupling of hydrosilanes promised greater functional group tolerance than Wurtz polymerization,[25,26] leading to the design and synthesis of the bifunctional cyclosilane monomers **1,4Si$_6$** and **1,3Si$_6$** (Scheme 3.1.1). In earlier reports, we described the structural characterization of the linear and cyclic poly(cyclosilane)s arising from **1,4Si$_6$** and **1,3Si$_6$** dehydropolymerization,[27–30] as well as the effect of poly(cyclosilane) microstructure on thermal properties.[31]

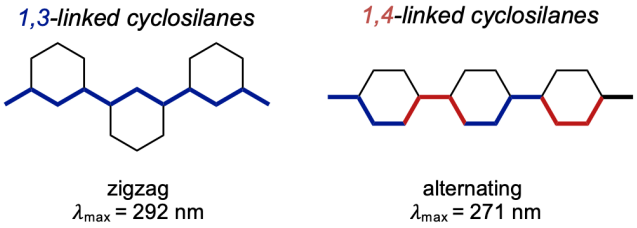

Figure 3.1.1. Connectivity, conformation, and optical properties in poly(cyclosilane)s.

Herein, we report solution-phase UV-vis absorbance spectra of three cyclosilane homopolymers differing in connectivity (1,3- or 1,4-) and architecture (linear or cyclic). We found that *lin*-poly(**1,3Si$_6$**) was bathochromically shifted by 20-nm relative to *lin*-poly(**1,4Si$_6$**). Time-dependent density functional theory (TD-DFT) calculations provided a structure-based hypothesis for this observation. In hexameric model systems, 1,3-linkages led to extended *transoid*-conformation ($|\omega|$=165°)[32] σ-conjugated pathways and low-energy HOMO–LUMO vertical transitions, while 1,4-linkages could not access all *transoid*-conformations. TD-DFT calculations suggested that the HOMO–LUMO transition in 1,4-linked cyclosilanes is symmetry-forbidden, resulting in a shift to higher-energy UV-vis absorption spectra. Based on these design principles, we hypothesized that

statistical copolymers should show vertical transitions intermediate between the homopolymers. Indeed, as the composition of **1,3Si$_6$** increased in statistical copolymers, λ_{max} increased systematically. TD-DFT provides additional insight into the influence of sequence and composition on predicted absorbance spectra.

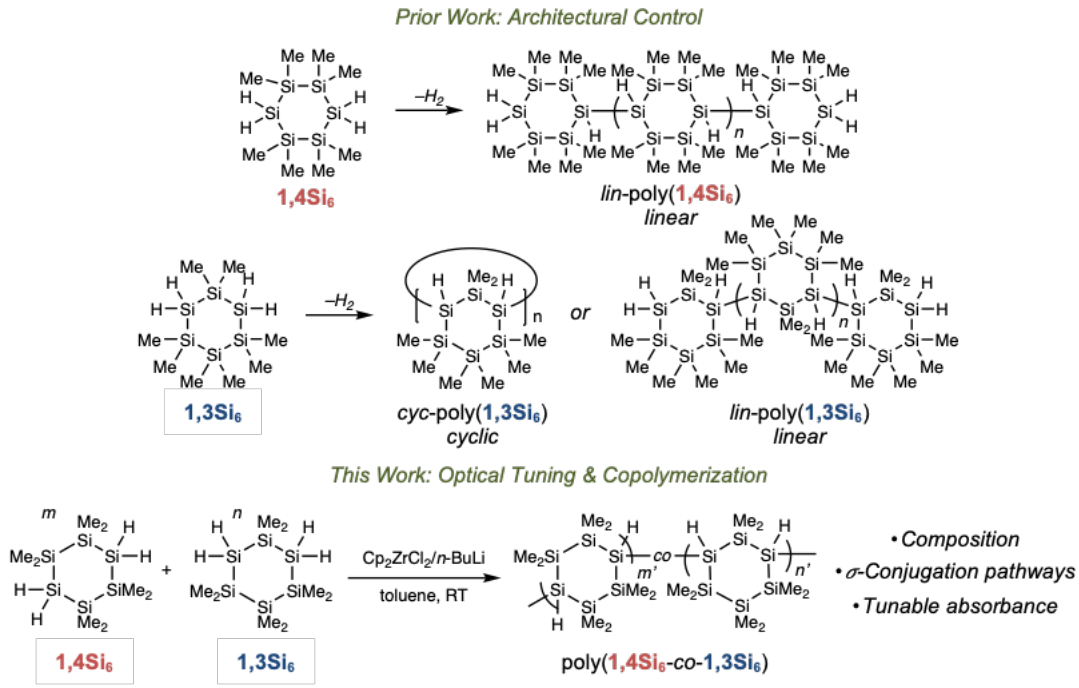

Scheme 3.1.1. Prior work: The structural isomers **1,3Si$_6$** and **1,4Si$_6$** template linear and cyclic poly(cyclosilane) architectures. This work: Cyclosilane copolymerization raises questions of reactivity, sequence, architecture, and physical properties.

Our results establish a conceptual framework for skeletal-based control of polysilane optical properties. An advantage of skeletal control is that in principle every Si atom could contribute to optical activity. An additional key advance in the current work is the coupling of experiment to theory, which provides deeper insights to the relationship between structure and photophysical properties. While the conventional wisdom that σ-conjugation is conformation-dependent implies that non-ideal conformations result in more localized bonds and changes in molecular orbital energies, our finding is that conformation

affects orbital symmetry and the identity of allowed transitions. We hope that the combined impact of these two advances is facilitate the rational design of polymeric silanes with defined optical properties.

3.2 UV-vis spectroscopy: homopolymers

A systematic comparison of poly(cyclosilane) UV-vis absorbance spectra has not previously been reported. Prior work has shown that *lin*-poly(**1,4Si$_6$**) and *cyc*-poly(**1,3Si$_6$**) were bathochromically shifted relative to their respective monomers (Table 3.2.1), but experimental and computational comparison of the homopolymers was not reported. The optical properties of *lin*-poly(**1,3Si$_6$**) have not previously been described in any form.[31]

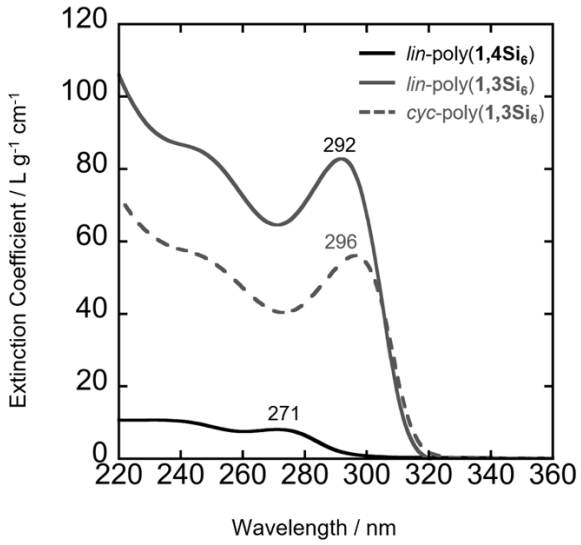

Figure 3.2.1. UV-vis absorbance spectra of homopolymers. [polymer] = 0.012 mg mL^{-1}, THF, room temperature.

A more complete understanding of poly(cyclosilane) UV-vis absorbance spectroscopy was therefore necessary. Solution phase spectra (solvent = THF) of the three distinct homopolymers were collected at room temperature (Figure 3.2.1) and data are summarized in Table 3.2.1. The spectra of the two **1,3Si$_6$** homopolymers, linear and cyclic,

were nearly identical and both were bathochromically shifted relative to poly(**1,4Si$_6$**) by over 20 nm. All three homopolymers absorbed at significantly longer wavelengths (ca. 100 nm) than their respective monomers, which have characteristic sharp absorptions around 190 nm in pentane. These results pointed to skeletal connectivity having a marked effect on the extent of σ-conjugation relative to monomer.

Table 3.2.1. UV-vis spectroscopic properties of cyclosilane monomers and homopolymers.

Polysilanes	λ_{max} (nm)	λ_{onset} (nm)
1,3Si$_6$ [a]	<190	230
cyc-poly(**1,3Si$_6$**)	296	311
lin-poly(**1,3Si$_6$**)	292	308
lin-poly(**1,4Si$_6$**)	271	291
1,4Si$_6$ [a]	194	232

Conditions: [*lin*-poly(**1,3Si$_6$**)] = 0.005 mg mL^{-1}, [*lin*-poly(**1,4Si$_6$**)] = 0.012 mg mL^{-1}, [*cyc*-poly(**1,3Si$_6$**)] = 0.010 mg mL^{-1}, [monomer] = 3.0×10^{-5} M, THF, rt. [a] solvent = pentane.

3.3 Calculated electronic transitions: homopolymers.

The bathochromic shift of *lin*-poly(**1,3Si$_6$**) relative to *lin*-poly(**1,4Si$_6$**) suggested distinct σ-conjugation pathways. That *lin*-poly(**1,3Si$_6$**) appeared to have a longer effective conjugation length despite a lower degree of polymerization was particularly striking (M_n = 1770 g mol^{-1} vs. 2770 g mol^{-1}).

We hypothesized that computational characterization including time-dependent density functional theory (TD-DFT) could shed light on the unique σ-conjugation pathways in each macromolecule. We therefore sought to identify reasonable molecular analogs of each structure. The poly(cyclosilane) absorption bands were similar in position to those of molecular silanes with 8-10 Si atoms. In linear silanes with the general formula

$Me(SiMe_2)_nMe$ (n = 2-8), each additional $SiMe_2$ unit results in a bathochromic shift of ca. 15 nm; the *lin*-poly(**1,4Si$_6$**) transition (λ_{max} = 279 nm) is comparable to the molecular octasilane $Me(SiMe_2)_8Me$ (λ_{max} = 272.5 nm). With degrees of polymerization of ca. 10-20 monomers indicated by size exclusion chromatography (SEC) and solid-state nuclear magnetic resonance (ssNMR) spectroscopy,[27,30] the experimentally observed optical transitions point to an effective conjugation length much shorter than the length of the macromolecule.

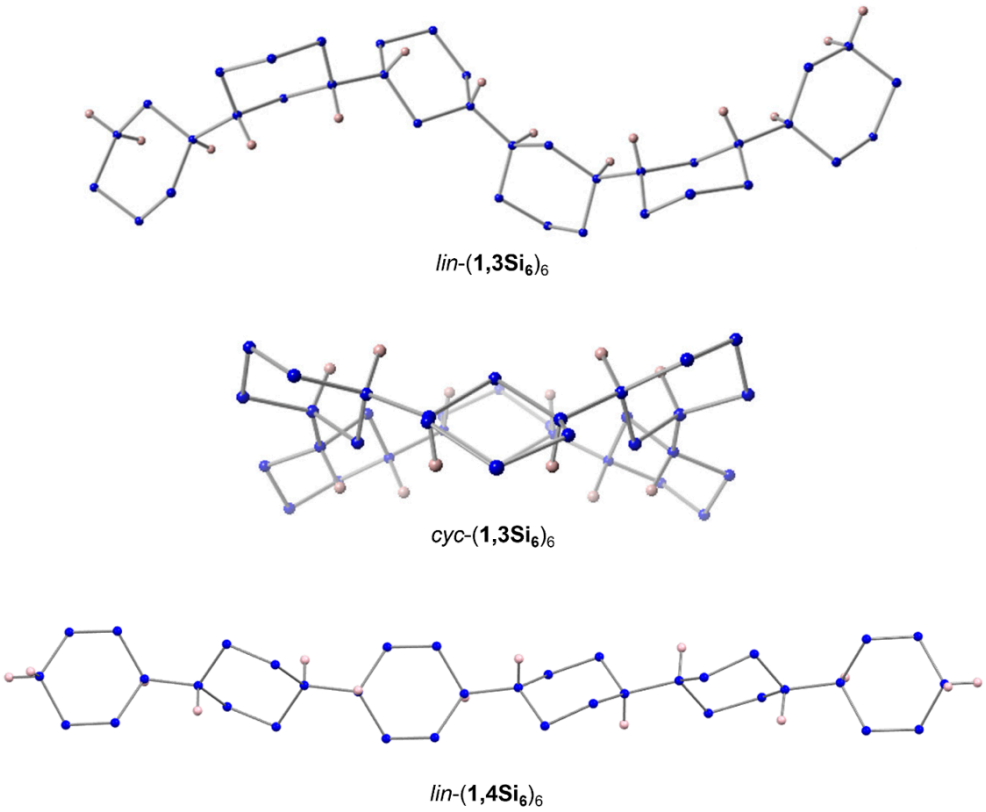

Figure 3.3.1 Geometry-optimized conformations of linear and cyclic hexamers of the cyclosilanes **1,3Si$_6$** and **1,4Si$_6$**. Adapted with permission from *J. Am. Chem. Soc*. **2018**, *140*, 5976, copyright 2018 American Chemical Society. Methyl groups omitted for clarity. B3LYP/6-31G(d).

We therefore chose cyclic and linear hexamers of **1,3Si$_6$** and **1,4Si$_6$** to model σ-conjugation and predict vertical transitions. Diastereomers with *trans* linkages were chosen for *lin*-(**1,4Si$_6$**)$_6$ as ssNMR spectroscopy has indicated this is the major diastereomer.[30] Lower-energy *cis*-linkages were chosen for **1,3Si$_6$** oligomers by analogy. We previously used hexamers to predict distinct infrared (IR) spectra for *lin*- and *cyc*-poly(**1,3Si$_6$**),[29] indicating that hexamers could be computationally tractable. The same functional and basis set were chosen for geometry optimization of a linear hexamer of **1,4Si$_6$** (*lin*-(**1,4Si$_6$**)$_6$) and low energy conformations of all three cyclosilane hexamers are shown in Figure 3.3.1.

While *lin*-(**1,4Si$_6$**)$_6$ was predicted to be linear, **1,3Si$_6$** introduces curvature and bending, as reflected in an almost helical structure for *lin*-(**1,3Si$_6$**)$_6$ and the macrocyclic structure of *cyc*-(**1,3Si$_6$**)$_6$. In all oligomers, individual cyclosilane rings adopted a chair conformation, with some twisting between rings. Prior work has demonstrated that the lowest energy conformation of a cyclohexasilane is chair-like, albeit with lower barriers to inversion than in cyclohexanes.[33–36]

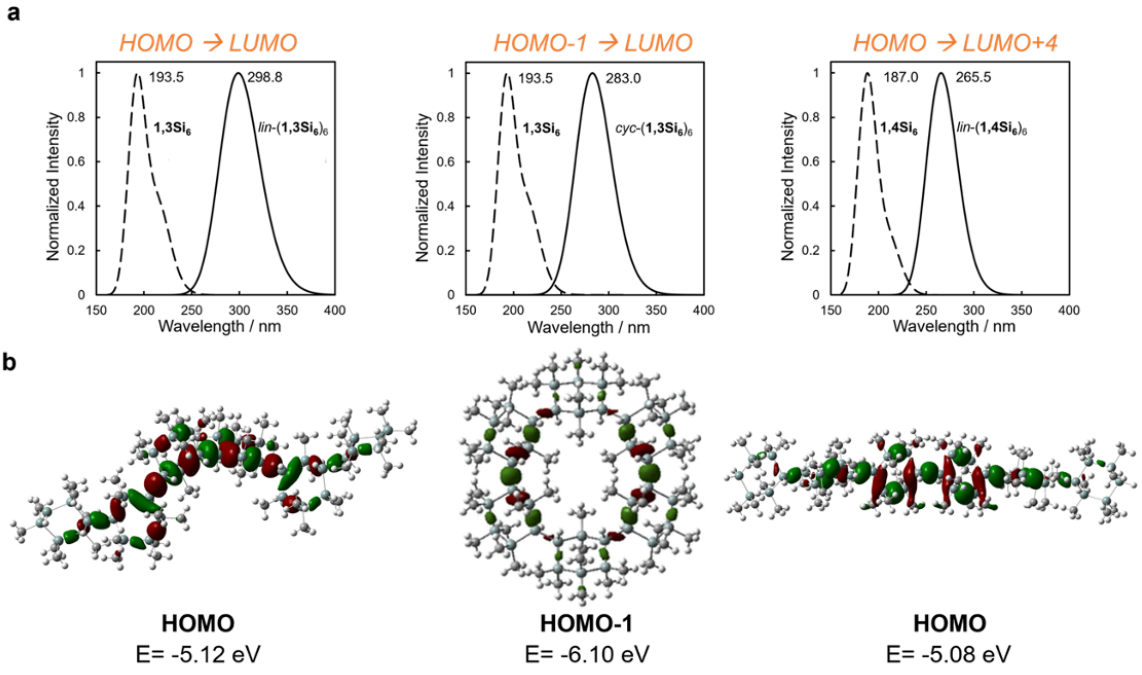

Figure 3.3.2 a) TD-DFT calculated absorbance spectra of *lin*-(**1,3Si$_6$**)$_6$, *cyc*-(**1,3Si$_6$**)$_6$, and *lin*-(**1,4Si$_6$**)$_6$ relative to TD-DFT calculated absorbance spectra of the monomers showed bathochromic shifts and absolute values consistent with experiment. b) Calculated molecular orbital distributions of HOMOs. TD−PBE0/6-311G(d)//B3YLP/6-31G(d). Adapted with permission from *J. Am. Chem. Soc*. **2018**, *140*, 5976. Copyright 2018 American Chemical Society.

From geometry optimized ground state structures, vertical transitions were calculated (TD−PBE0/6-311G(d)//B3YLP/6-31G(d)). This combination was previously reported for simulation of linear hexasilane electronic transitions.[19] The calculated spectral shapes for all three model oligomers (Figure 3.3.1) accurately depicted a sharp transition ca. 190 nm for the monomers, as well as an approximately 100-nm bathochromic shift upon oligomerization. The experimental observation that *lin*-poly(**1,4Si$_6$**) has a higher energy λ_{max} than **1,3Si$_6$** oligomers (265 vs. 299 nm) was also reproduced by the calculations.

The calculated transition wavelengths and oscillator strengths (Table 3.3.1 and Table 3.3.2) showed that *lin*-(**1,4Si$_6$**)$_6$ is distinct from the linear and cyclic hexamers of **1,3Si$_6$**. The most intense vertical transition, with respect to oscillator strength, for *lin*-poly(**1,4Si$_6$**) corresponds to the HOMO→LUMO+4 and was found at 265.5 nm, 35-nm lower than the strong HOMO→LUMO transition of *lin*-(**1,3Si$_6$**)$_6$. In all three oligomers, not all Si atoms contributed to conjugation (Figure 3.3.1), but the extent of HOMO delocalization in *lin*-(**1,4Si$_6$**)$_6$ was clearly less extensive than in *lin*-(**1,3Si$_6$**)$_6$ (e.g., no orbital density on the terminal cyclosilanes).

Table 3.3.1. Calculated vertical electronic transitions in cyclosilane hexamers. TD−PBE0/6-311G(d)//B3YLP/6-31G(d). Relative contributions given in percentages, where H=HOMO and L=LUMO.

Structure	λ (nm)	f	Assignment
lin-(**1,4Si$_6$**)$_6$	265.5	2.738	H→L+4 (39.3%) H→L (24.3%) H-1→L+3 (16.9%) H-1→L+1 (6.3%)
	265.4	1.269	H→L (49.8%) H→L+4 (20.3%) H→L+2 (8.1%) H-1→L+2 (6.3%)
cyc-(**1,3Si$_6$**)$_6$	285.4	1.696	H-1→L (77.1%) H→L+2 (15.8%)
	282.9	1.665	H-2→L (69.6%) H→L+1 (22.6%)
lin-(**1,3Si$_6$**)$_6$	299.4	2.809	H→L (88.7%)

Table 3.3.2. Energy of selected molecular orbitals of *lin*-(**1,4Si$_6$**)$_6$, *lin*-(**1,3Si$_6$**)$_6$ and *cyc*-(**1,3Si$_6$**)$_6$. Calculated at the TD-PBE0/6-311G(d)//B3LYP/6-31G(d) level.

Molecular Orbital	Energy/ eV		
	lin-(**1,4Si$_6$**)$_6$	*lin*-(**1,3Si$_6$**)$_6$	*cyc*-(**1,3Si$_6$**)$_6$
LUMO+5	-0.57	-0.34	-0.32
LUMO+4	-0.57	-0.47	-0.34
LUMO+3	-0.62	-0.48	-0.38
LUMO+2	-0.67	-0.53	-0.73
LUMO+1	-0.72	-0.82	-0.75
LUMO	-0.77	-1.16	-1.16
HOMO	-6.05	-6.00	-5.86
HOMO-1	-6.18	-6.24	-6.10
HOMO-2	-6.37	-6.38	-6.15

HOMO-3	-6.41	-6.42	-6.35
HOMO-4	-6.48	-6.45	-6.38
HOMO-5	-6.56	-6.52	-6.44

Our calculations point to two explanations for the experimental observation of poly(**1,4Si$_6$**)'s higher energy absorption band: reduced σ-conjugation in the ground state HOMO and symmetry-forbidden electronic transitions. Both phenomena are fundamentally conformation dependent. In describing silane conformations, especially torsion angles, we used the nomenclature proposed by Michl and West:[32] *anti*, ω = 180°; *transoid*, |ω|= 165°; *deviant*, |ω| = 150°; *ortho*, |ω| = 90°; gauche, |ω| = 60°, and *cisoid*, |ω| = 40°. σ-Conjugation is suppressed by small torsion angles (e.g., *cisoid*)[20] while torsion angles close to 180° (e.g., *transoid/anti)* extend σ-conjugation by maximizing the interaction of vicinal sp^3 orbitals.[8] We found a *transoid*-pathway across multiple cyclosilanes in *lin*-(**1,3Si$_6$**)$_6$ (Figure 3.3.3a). At the central bond (indicated with green arrow), a 130.6° torsion angle is the smallest angle along the conjugation pathway highlighted in pink. In contrast, because the Si–Si chain in *lin*-(**1,4Si$_6$**)$_6$ must pass through a chair cyclohexasilane, small torsion angles (ca. 60°, *gauche*) cannot be avoided (Figure 3.3.3b). These conformational differences interrupt σ-conjugation in the *lin*-(**1,4Si$_6$**)$_6$ HOMO and also result in changes in symmetry that affect the probability of vertical transitions.

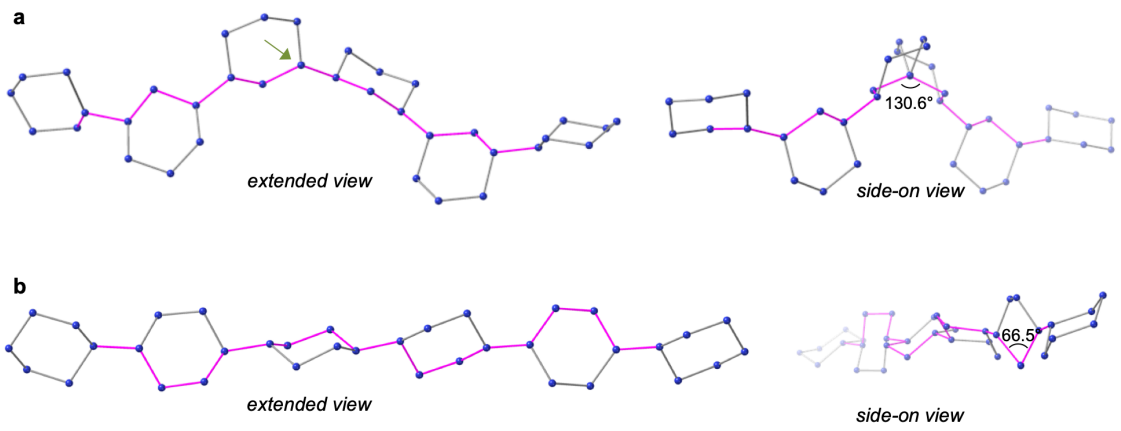

Figure 3.3.3 σ-Conjugation pathways and selected torsion angles in a) *lin*-(**1,3Si$_6$**)$_6$ and b) *lin*-(**1,4Si$_6$**)$_6$. Methyl groups and hydrogens omitted for clarity. Extended Si–Si pathways highlighted in magenta. B3YLP/6-31G(d).

We note that a shortcoming of the calculations reported herein is that they only consider electronic transitions from a single conformation of the ground state oligomer, while the experimental sample at room temperature is an ensemble of different oligomer lengths, conformations, and tacticities. Additionally, these calculations were performed in the gas phase and do not account for the influence of solvent on conformation or vertical transition energies. Nonetheless, the reasonable agreement with experimental UV-vis absorption data bolsters confidence in the general conclusions.

The insight that 1,3-linkages maximize extended conformations inspired interest in statistical copolymers of **1,3Si$_6$** and **1,4Si$_6$**. We hypothesized that a chain with both 1,3- and 1,4-linked cyclosilanes might exhibit properties intermediate between the homopolymers. To test this hypothesis, we sought to prepare the desired statistical copolymers, verify a linear structure with tunable composition, and obtain solution-phase UV-vis spectroscopy. We also pursued TD-DFT calculations to support the experimental observations.

3.4 Copolymer synthesis and microstructure characterization

While statistical copolymerization is broadly used in organic polymers to tune properties such as solubility,[37] self-assembly,[38] glass transition temperature (T_g),[39] and mechanical strength,[40] silane copolymerization has been largely limited to Wurtz polymerization of dichloroorganosilanes.[41] West demonstrated reductive copolymerization of Cl_2SiMe_2/$Cl_2SiMePh$,[42,43] while Fujiki demonstrated Wurtz copolymerization of alkyl and fluoroalkyl comonomers.[44] These studies have typically yielded blocky copolymers. Dehydrocopolymerization of hydrosilanes is limited to phenylsilane with substituted arylsilanes (Waymouth)[26] or methylsilanes (Hengge, Marschner).[45,46] Rieger investigated the copolymerization of *n*-hexylsilane and phenylsilane by Lewis acid catalysis.[47] Given the dearth of prior investigation of zirconocene-catalyzed hydrosilane copolymerization, we identified several critical questions to address through our studies including the relative comonomer reactivity (is a copolymer obtained or a blend of homopolymers?) as well as microstructural characterization (statistical or blocky sequence; linear or cyclic?).

The synthesis of cyclosilane copolymers were investigated by Fan Fang in the Klausen group. The full structural characterization has been performed and published in the following reference: Fang, F.; Jiang, Q.; Klausen, R. S. *J. Am. Chem. Soc.* **2022**, 144, 17, 7834–7843.

Several different comonomer ratios were evaluated for copolymerization upon exposure to Cp_2ZrCl_2/*n*-BuLi in toluene. This system was first identified by Corey as an effective dehydrocoupling catalyst for primary and secondary silanes[48–50] and we have previously demonstrated its effectiveness for homopolymerization of **1,3Si$_6$** and **1,4Si$_6$**.[27–29]

A *linear* architecture of copolymers was assigned by NMR analysis and further supported by differential scanning calorimetry (DSC). This assessment of copolymer microstructure in solution points to a linear copolymer with composition proportional to the comonomer feed ratio. We suggest a statistical sequence is most likely based on the similar structure and reactivity of **1,3Si$_6$** and **1,4Si$_6$**. An alternating A-B copolymer would have resulted in identical compositions of each comonomer in all three copolymerizations. A blocky structure is unlikely as consecutive runs of **1,3Si$_6$** monomers would favor macrocyclization.

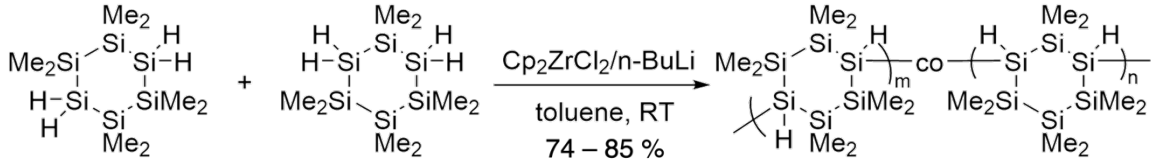

1,4Si$_6$ **1,3Si$_6$** poly(**1,4Si$_6$**-co-**1,3Si$_6$**)

25 % **1,4Si$_6$**, 75% **1,3Si$_6$** : M_n = 4200 g mol^{-1}, M_w/ M_n = 1.72, 84 % yield
50 % **1,4Si$_6$**, 50% **1,3Si$_6$** : M_n = 4110 g mol^{-1}, M_w/ M_n = 1.44, 85 % yield
75 % **1,4Si$_6$**, 25% **1,3Si$_6$** : M_n = 3940 g mol^{-1}, M_w/ M_n = 1.54, 74 % yield

Scheme 3.4.1. Synthesis of cyclosilane copolymers.

3.5 UV-vis spectroscopy: copolymers

UV-vis spectroscopy of the three copolymers under similar conditions (THF, room temperature, Figure 3.5.1) showed a single transition intermediate between the homopolymers, consistent with the overall incorporation of each monomer. The onset of absorption also varied with composition (Table 3.5.1). These results lend support to the conclusion based on DOSY and SEC that binary copolymerization yielded a single copolymer, rather than a blend of homopolymers: a blend of homopolymers would show two optical transitions at 279 and 296 nm at intensities consistent with the concentration of each homopolymer. The observations were also more consistent with a statistical

copolymer, rather than an alternating A-B copolymer as A-B alternating copolymers would have identical connectivities and identical absorption spectra.

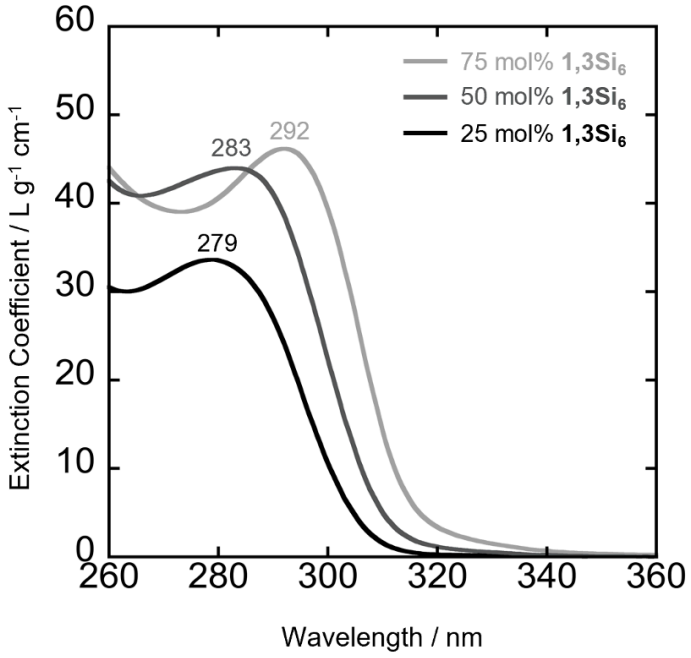

Figure 3.5.1. UV-vis absorbance spectra of copolymers. [copolymer] = 0.012 mg mL^{-1}, THF, room temperature.

The variation of the copolymer optical transition with comonomer composition validated our hypothesis that increasing the probability of consecutive 1,3-linkages increased the wavelength of maximum absorption. We next described TD-DFT calculations that provide additional support for our experimental observations.

Table 3.5.1. UV-vis spectroscopic properties of cyclosilane homopolymers and copolymers.

Polysilanes	λ_{max} (nm)	λ_{onset} (nm)
lin-poly(**1,3Si$_6$**)	<190	230
poly(**1,3Si$_6$**)$_{0.75}$-stat-poly(**1,4Si$_6$**)$_{0.25}$	296	311
poly(**1,3Si$_6$**)$_{0.50}$-stat-poly(**1,4Si$_6$**)$_{0.50}$	292	308

poly(**1,3Si$_6$**)$_{0.25}$-stat-poly(**1,4Si$_6$**)$_{0.75}$	271	291
lin-poly(**1,4Si$_6$**)	194	232

Conditions: Conditions: [copolymer] = 0.012 mg mL^{-1}, [*lin*-poly(**1,3Si$_6$**)] = 0.005 mg mL^{-1}, [*lin*-poly(**1,4Si$_6$**)] = 0.012 mg mL^{-1}, in THF, rt.

3.6 Calculated electronic transitions: copolymers

We considered tetramers with different compositions and sequences as models for the copolymers. The 4-digit numbers used herein abbreviate **1,3Si$_6$** and **1,4Si$_6$** to 3 and 4, respectively. Geometry-optimized ground state conformations are shown in Figure 3.6.1. Vertical transitions were calculated in the same manner as for homopolymer models (TD−PBE0/6-311G(d)//B3YLP/6-31G(d)) and transition wavelengths, oscillator strengths, and assignments are summarized in Table 3.6.1 and Table 3.6.2. The range of predicted wavelengths (262–285 nm) compared favorably to the experimentally observed range (Table 3.6.1, 279–292 nm), suggesting that tetramers were valid models for poly(cyclosilane)s.

We found that both composition and sequence affected vertical transitions. In general, the energy of a vertical transition decreased with increasing **1,3Si$_6$**, but also depended on the position of **1,3Si$_6$** within the tetramer (chain end or interior). Evidence for these trends is summarized below:

1. An interior **1,3Si$_6$** residue increased λ_{max} relative to a chain end **1,3Si$_6$**. For example, 4443 and 4434 have the same composition (25% **1,3Si$_6$**) but the predicted 4434 λ_{max} was bathochromically shifted 14-nm relative to 4443 (Table 3.5.1).
2. When controlled for position, λ_{max} increased with increasing *consecutive* **1,3Si$_6$** residues. Each additional **1,3Si$_6$** residue in the series 4443 to 4433 to 4333 resulted in a bathochromic shift from 262.3 to 278.8 to 283.9 nm. Figure 3.6.2 plots the energy

of a vertical transition versus the number of consecutive **1,3Si$_6$** residues, showing a general trend of increasing λ_{max}.

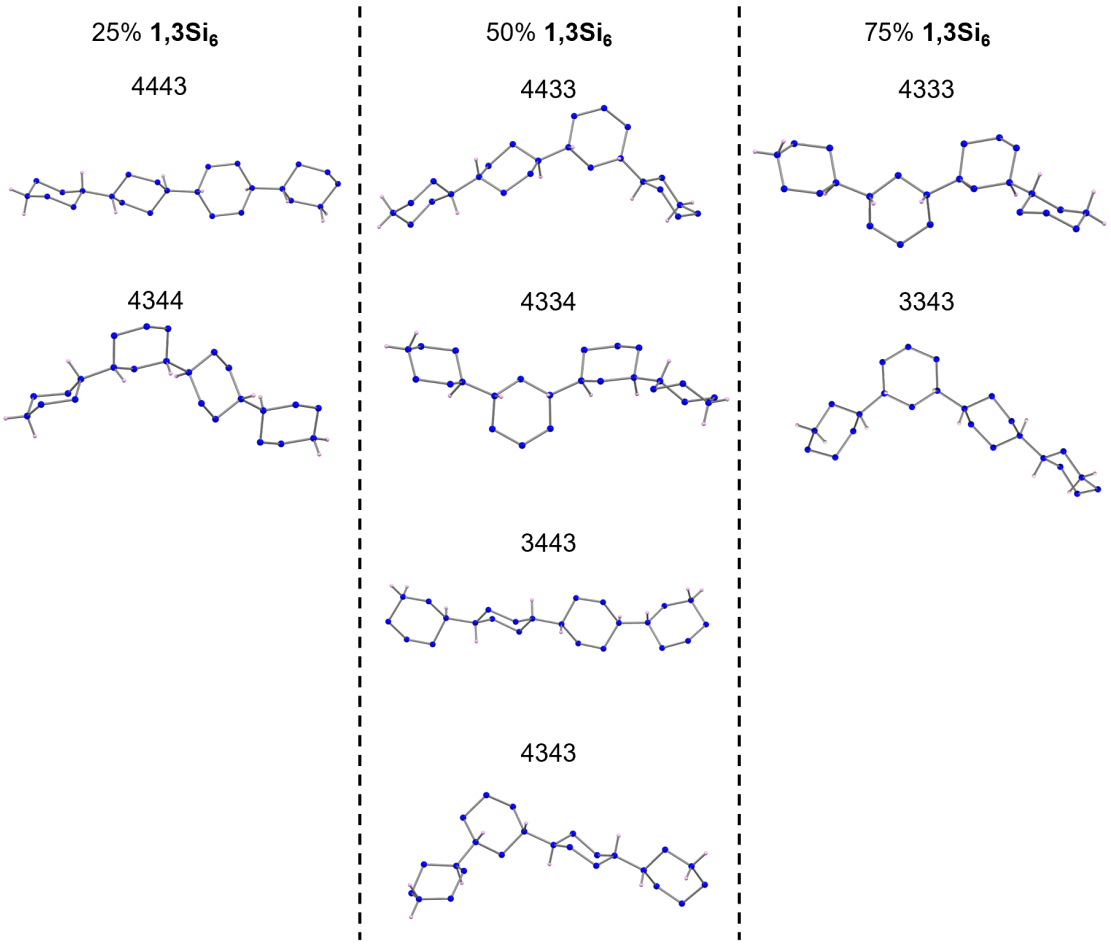

Figure 3.6.1. Ground state conformations of cyclosilane tetramers of different compositions and sequences. Methyl groups omitted for clarity. B3YLP/6-31G(d).

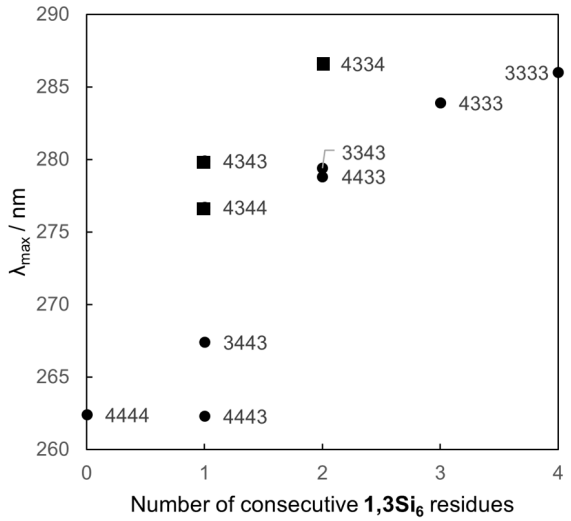

Figure 3.6.2. The predicted λ_{max} versus the number of consecutive **1,3Si$_6$** residues. Squares indicate interior **1,3Si$_6$** residues and circles indicate chain ends **1,3Si$_6$** residues.

Table 3.6.1. Calculated vertical electronic transitions in cyclosilane tetramers. TD−PBE0/6-311G(d)//B3YLP/6-31G(d). Relative contributions given in percentages, where H=HOMO and L=LUMO.

Composition	Sequence	λ_{max} (nm)	f	H-L Gap (eV)	Assignment
0% **1,3Si$_6$**	4444	262.4	1.442	5.35	H→L (38.4%) H→L+2 (36.4%) H-1→L+1 (19.4%)
25% **1,3Si$_6$**	4443	262.3	1.796	5.35	H→L+2 (50.7%) H→L (22.2%) H-1→L+1 (16.6%)
	4344	276.7	1.396	5.18	H→L (86.3%)
50% **1,3Si$_6$**	4433	278.8	1.523	5.16	H→L (86.2%)
	4343	279.9	1.421	5.14	H→L (86.6%)
	4334	284.8	1.730	5.06	H→L (92.2%)
	3443	262.4	1.803	5.35	H→L+2 (51.5%) H→L (20.9%) H-1→L+1 (19.0%)
75% **1,3Si$_6$**	3343	279.4	1.402	5.15	H→L (86.9%)
	4333	283.9	1.700	5.08	H→L (92.0%)
100% **1,3Si$_6$**	3333	286.0	1.769	5.05	H→L (92.8%)

Table 3.6.2. Energy of selected molecular orbitals of tetramers. Calculated at the TD-PBE0/6-311G(d)//B3LYP/6-31G(d) level.

Molecular Orbital	Energy/ eV									
	4444	4443	4344	4433	4343	4334	3443	3343	4333	3333
LUMO+5	-0.23	-0.24	-0.24	-0.21	-0.24	-0.17	-0.23	-0.23	-0.18	-0.18
LUMO+4	-0.27	-0.28	-0.28	-0.26	-0.27	-0.26	-0.29	-0.27	-0.27	-0.24
LUMO+3	-0.30	-0.29	-0.32	-0.29	-0.29	-0.37	-0.32	-0.30	-0.39	-0.31
LUMO+2	-0.60	-0.60	-0.43	-0.34	-0.36	-0.50	-0.60	-0.38	-0.50	-0.48
LUMO+1	-0.68	-0.68	-0.68	-0.66	-0.68	-0.57	-0.68	-0.68	-0.58	-0.55
LUMO	-0.76	-0.76	-0.93	-0.91	-0.95	-1.07	-0.76	-0.94	-1.07	-1.05
HOMO	-6.11	-6.11	-6.12	-6.07	-6.09	-6.13	-6.11	-6.09	-6.15	-6.10
HOMO-1	-6.36	-6.36	-6.35	-6.36	-6.37	-6.35	-6.37	-6.37	-6.36	-6.39
HOMO-2	-6.46	-6.45	-6.45	-6.46	-6.44	-6.46	-6.44	-6.45	-6.47	-6.44
HOMO-3	-6.56	-6.54	-6.53	-6.60	-6.58	-6.49	-6.56	-6.58	-6.48	-6.61
HOMO-4	-6.70	-6.68	-6.64	-6.66	-6.60	-6.63	-6.70	-6.60	-6.66	-6.67
HOMO-5	-6.72	-6.76	-6.80	-6.77	-6.80	-6.81	-6.71	-6.77	-6.76	-6.72

The tetramers 3443 and 4334 illustrate the combined effect of consecutive **1,3Si$_6$** monomers and interior positioning. The tetramers have the same overall composition but in 3443 both **1,3Si$_6$** residues were located at chain ends and were not consecutive, while in 4334 two consecutive **1,3Si$_6$** residues were found only in the interior. 4334 was predicted to have a longer λ_{max} by almost 22 nm (262.4 vs. 284.8 nm).

We noted that the tetramers predicted to have the *shortest* wavelength λ_{max} (3443 and 4443, ca. 262 nm) both had **1,3Si$_6$** residues only at chain ends and were anomalous in the assignment of the most intense vertical transition, which corresponded to the HOMO→LUMO+2 instead of the HOMO→LUMO transition for other tetramers (Table

3.6.1). A shift in the terminating orbital to a LUMO+n was also observed in *lin*-poly(**1,4Si$_6$**) (Table 3.2.2). We expect that this is likely general for segments of consecutive **1,4Si$_6$** residues.

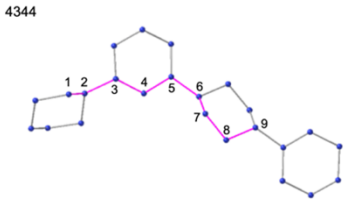

Torsion	deg
∠1-2-3-4	132.2
∠2-3-4-5	170.0
∠3-4-5-6	161.6
∠4-5-6-7	97.09
∠5-6-7-8	162.6
∠6-7-8-9	59.88

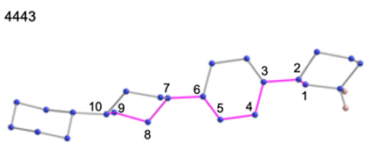

Torsion	deg
∠1-2-3-4	94.31
∠2-3-4-5	161.9
∠3-4-5-6	60.97
∠4-5-6-7	170.9
∠5-6-7-8	2.332
∠6-7-8-9	167.6
∠7-8-9-10	64.50

Figure 3.6.3. Impact of **1,3Si$_6$** position on backbone conformation: interior sites increase consecutive *trans* torsion angles. Methyl groups and hydrogens omitted for clarity. B3YLP/6-31G(d).

We attribute the observed trends in vertical transition energies to changes in conformation with increasing consecutive **1,3Si$_6$** residues. Figure 3.6.3 highlights 4344 and 4443, which had the same overall composition but different sequences. We found that the interior **1,3Si$_6$** reside in 4344 allowed for consecutive torsion angles close to 180° in the vicinity of the **1,3Si$_6$** residue (Figure 3.6.3, blue highlight in Table). This was not possible for 4443. The σ-conjugated pathway (pink) for 4443 resembled *lin*-(**1,4Si$_6$**)$_6$ in having small torsion angles (0–60°, eclipsing and *gauche*) alternate with larger torsion angles. Increasing the number of consecutive **1,3Si$_6$** residues extends this trend.

These computational models validate the experimental observation that increasing the **1,3Si$_6$** concentration in the feed ratio results in bathochromically shifted experimental λ_{max} in the copolymers. Increasing the [**1,3Si$_6$**] in the feed from 25 to 75% during a statistical copolymerization would necessarily result in more consecutive **1,3Si$_6$** residues in the interior of a chain. The longer length of experimental chains relative to tetramers

likely dilutes the strong effect of chain end versus interior position observed computationally. We expect that the experimental observation of increasing λ_{max} with increasing [**1,3Si$_6$**] is tied to **1,3Si$_6$**-enriched interior segments that have symmetry-allowed HOMO-LUMO transitions. In contrast, consecutive runs of **1,4Si$_6$** comonomers effect a change in LUMO symmetry, resulting in a symmetry-forbidden HOMO-LUMO transition and a shift to lower wavelength λ_{max}.[19]

3.7 Conclusion

Herein, we investigated the effect of connectivity on the optical properties of poly(cyclosilane)s. Using the isomeric monomers **1,3Si$_6$** and **1,4Si$_6$**, we prepared a homologous set of linear (co)polymers that were structurally characterized by a suite of NMR spectroscopies. We observed experimentally that across the set of linear polymers possessing from 0 to 100% **1,3Si$_6$** comonomers, λ_{max} and λ_{onset} increased systematically from 271 to 292 nm.

Computational studies provided structural insight into the role of skeletal connectivity in influencing optical properties. We found that oligomeric model systems of 4 or 6 cyclosilanes accurately reproduced polymeric properties. These model systems demonstrated that 1,3-linked cyclosilanes can access extended *transoid* conformations with predicted lower-energy HOMO→LUMO transitions. In contrast, 1,4-connectivity requires endocyclic *gauche* conformations that are associated with a change in LUMO symmetry. As a result of the change in terminating orbital symmetry, the most intense electronic transitions in 1,4-linked cyclosilanes correspond to higher energy HOMO→LUMO+n transitions. Copolymers achieve optical properties intermediate between homopolymers by

increasing the probability of consecutive **1,3Si$_6$** monomers and *transoid*-conformation pathways.

This is the first demonstration of *main chain* control of polysilane optical properties. Prior work focused on the role of alkyl side chains in constraining polysilane conformation and conformation-dependent absorbance spectra. Skeletal control could result in materials in which every Si atom contributes to optical activity. We also report computational insights into the role of conformation in affecting orbital symmetry and photophysical properties. The studies herein point to the potential for structurally complex silane building blocks to define structure-optical property relationships.

3.8 Reference

(1) Klausen, R. S.; Ballestero-Martínez, E. In *Comprehensive Organometallic Chemistry IV*; Elsevier, 2021.
(2) Miller, R. D.; Michl, J. *Chem. Rev.* **1989**, *89*, 1359–1410.
(3) Kumar, V. B.; Leitao, E. M. *Appl. Organomet. Chem.* **2020**, *34*, 1–16.
(4) Priegert, A. M.; Rawe, B. W.; Serin, S. C.; Gates, D. P. *Chem. Soc. Rev.* **2016**, *45*, 922–953.
(5) Vidal, F.; Jäkle, F. *Angew. Chemie - Int. Ed.* **2019**, *58*, 5846–5870.
(6) Gilman, H.; Atwell, W. H.; Schwebke, G. L. *J. Organomet. Chem.* **1964**, *2*, 369–371.
(7) Jovanovic, M.; Michl, J. *J. Am. Chem. Soc.* **2019**, *141*, 13101–13113.
(8) Jovanovic, M.; Michl, J. *J. Am. Chem. Soc.* **2018**, *140*, 11158–11160.
(9) Miller, R. D.; Hofer, D.; Rabolt, J.; Fickes, G. N. *J. Am. Chem. Soc.* **1985**, *107*, 2172–2174.
(10) Rabolt, J. F.; Hofer, D.; Miller, R. D.; Fickes, G. N. *Macromolecules* **1986**, *19*, 611–616.
(11) Trefonas, P.; Damewood, J. R.; West, R.; Miller, R. D. *Organometallics* **1985**, *4*, 1318–1319.
(12) Klausen, R. S.; Widawsky, J. R.; Steigerwald, M. L.; Venkataraman, L.; Nuckolls, C. *J. Am. Chem. Soc.* **2012**, *134*, 4541–4544.
(13) Su, T. A.; Li, H.; Klausen, R. S.; Kim, N. T.; Neupane, M.; Leighton, J. L.; Steigerwald, M. L.; Venkataraman, L.; Nuckolls, C. *Acc. Chem. Res.* **2017**, *50*, 1088–1095.
(14) Su, T. A.; Li, H.; Steigerwald, M. L.; Venkataraman, L.; Nuckolls, C. *Nat. Chem.* **2015**, *7*, 215–220.
(15) Li, H.; Garner, M. H.; Shangguan, Z.; Zheng, Q.; Su, T. A.; Neupane, M.; Li, P.; Velian, A.; Steigerwald, M. L.; Xiao, S.; Nuckolls, C.; Solomon, G. C.;

Venkataraman, L. *Chem. Sci.* **2016**, *7*, 5657–5662.
(16) Garner, M. H.; Li, H.; Chen, Y.; Su, T. A.; Shangguan, Z.; Paley, D. W.; Liu, T.; Ng, F.; Li, H.; Xiao, S.; Nuckolls, C.; Venkataraman, L.; Solomon, G. C. *Nature* **2018**, *558*, 415–419.
(17) Tamao, K.; Tsuji, H.; Terada, M.; Asahara, M.; Yamaguchi, S.; Toshimitsu, A. *Angew. Chemie - Int. Ed.* **2000**, *39*, 3287–3290.
(18) Fukazawa, A.; Tsuji, H.; Tamao, K. *J. Am. Chem. Soc.* **2006**, *128*, 6800–6801.
(19) Kanazawa, Y.; Tsuji, H.; Ehara, M.; Fukuda, R.; Casher, D. L.; Tamao, K.; Nakatsuji, H.; Michl, J. **2016**, 3010–3022.
(20) Tsuji, H.; Terada, M.; Toshimitsu, A.; Tamao, K. *J. Am. Chem. Soc.* **2003**, *125*, 7486–7487.
(21) Burkhard, C. A. *J. Am. Chem. Soc.* **1949**, *71*, 963–964.
(22) Jones, R. G.; Budnik, U.; Holder, S. J.; Wong, W. K. C. *Macromolecules* **1996**, *29*, 8036–8046.
(23) Holder, S. J.; Achilleos, M.; Jones, R. G. *J. Am. Chem. Soc.* **2006**, *128*, 12418–12419.
(24) Marro, E. A.; Klausen, R. S. *Chem. Mater.* **2019**, *31*, 2202–2211.
(25) Tilley, T. D.; Woo, H. *Polym. Prepr.* **1990**, *31*, 228–229.
(26) Banovetz, J. P.; Suzuki, H.; Waymouth, R. M. *Organometallics* **1993**, *12*, 4700–4703.
(27) Press, E. M.; Marro, E. A.; Surampudi, S. K.; Siegler, M. A.; Tang, J. A.; Klausen, R. S. *Angew. Chemie Int. Ed.* **2017**, *56*, 568–572.
(28) Folster, C. P.; Klausen, R. S. *Polym. Chem.* **2018**, *9*, 1938–1941.
(29) Marro, E. A.; Press, E. M.; Siegler, M. A.; Klausen, R. S. *J. Am. Chem. Soc.* **2018**, *140*, 5976–5986.
(30) Dorn, R. W.; Marro, E. A.; Hanrahan, M. P.; Klausen, R. S.; Rossini, A. J. *Chem. Mater.* **2019**, *31*, 9168–9178.
(31) Jiang, Q.; Wong, S.; Klausen, R. S. *Polym. Chem.* **2021**, *12*, 4785–4794.
(32) Michl, J.; West, R. *Acc. Chem. Res.* **2000**, *33*, 821–823.
(33) Tekautz, G.; Binter, A.; Hassler, K.; Flock, M. **2006**, *7*, 421–429.
(34) Casarini, D.; Lunazzi, L.; Mazzanti, A. *Tetrahedron* **1998**, *54*, 13181–13184.
(35) Casarini, D.; Lunazzi, L.; Mazzanti, A. *J. Org. Chem.* **1998**, *63*, 9125–9127.
(36) Ferguson, J. T.; Jiang, Q.; Marro, E. A.; Siegler, M. A.; Klausen, R. S. *Dalt. Trans.* **2020**, *49*, 14951–14961.
(37) van de Wouw, H. L.; Lee, J. Y.; Awuyah, E. C.; Klausen, R. S. *Angew. Chemie - Int. Ed.* **2018**, *57*, 1673–1677.
(38) Panganiban, B.; Qiao, B.; Jiang, T.; DelRe, C.; Obadia, M. M.; Nguyen, T. D.; Smith, A. A. A.; Hall, A.; Sit, I.; Crosby, M. G.; Dennis, P. B.; Drockenmuller, E.; De La Cruz, M. O.; Xu, T. *Science (80-.).* **2018**, *359*, 1239–1243.
(39) Wang, H.; Kolodka, E.; Tande, B. M. *Ind. Eng. Chem. Res.* **2013**, *52*, 5111–5119.
(40) Holmberg, A. L.; Nguyen, N. A.; Karavolias, M. G.; Reno, K. H.; Wool, R. P.; Epps, T. H. *Macromolecules* **2016**, *49*, 1286–1295.
(41) Reuss, V. S.; Frey, H. *Macromolecules* **2010**, *43*, 8462–8467.
(42) West, R.; David, L. D.; Djurovich, P. I.; Stearley, K. L.; Srinivasan, K. S. V.; Yu, H. *J. Am. Chem. Soc.* **1981**, *103*, 7352–7354.
(43) Wolff, A. R.; Nozue, I.; Maxka, J.; West, R. *J. Polym. Sci. Part A Polym. Chem.*

1988, *26*, 701–712.
(44) Kawabe, T.; Naito, M.; Fujiki, M. *Macromolecules* **2008**, *41*, 1952–1960.
(45) Lunzer, F.; Marschner, C. *Materials (Basel).* **2010**, *3*, 1125–1137.
(46) Hengge, E.; Weinberger, M. *J. Organomet. Chem.* **1992**, *441*, 397–410.
(47) Feigl, A.; Chiorescu, I.; Deller, K.; Heidsieck, S. U. H.; Buchner, M. R.; Karttunen, V.; Bockholt, A.; Genest, A.; Rösch, N.; Rieger, B. *Chem. - A Eur. J.* **2013**, *19*, 12526–12536.
(48) Chang, L. S.; Corey, J. Y. *Organometallics* **1989**, *8*, 1885–1893.
(49) Corey, J. Y.; Zhu, X. H.; Bedard, T. C.; Lange, L. D. *Organometallics* **1991**, *10*, 924–930.
(50) Corey, J. Y.; Xiao-Hong, Z. *J. Organomet. Chem.* **1992**, *439*, 1–17.

Chapter 4: Highly selective addition of cyclosilanes to alkynes enabling new conjugated materials

The work presented in this chapter has been published as: Jiang, Q.; Gittens, A. F.; Wong, S.; Siegler, M. A.; Klausen, R. S. *Chem. Sci.* **2022**, *13*, 7587–7593.

4.1 Introduction

We report the synthesis of visible-light absorbing organocyclosilanes via Ru-catalyzed chemoselective, regioselective, and diastereoselective hydrosilylation. While extraordinary progress in predicting and controlling selectivity in organic reactions has been made, the development of similar insights for main group molecules is in its infancy. This lack of synthetic control limits the discovery of structure-property relationships in main group materials. For example, while linear oligosilanes (e.g., $Ar(SiMe)_nAr$) capped with aromatic end groups have been extensively studied for molecular electronics[1,2], metal-organic framework (MOF) secondary building units,[3] charge transport,[4] photoinduced charge transfer,[5–7] and nonlinear optical properties,[8–10] there has been very limited investigation of cyclic σ,π-conjugation,[11] as cyclosilanes are typically synthesized by methods[12–14] that restrict functional group diversity on an organic fragment. Nonetheless, the well-established conformation-dependence of σ-conjugation[15] strongly suggests that the restricted degrees of freedom in cyclosilanes should give rise to properties distinct from linear oligosilanes.

Our group is interested in the synthesis and properties of (macro)molecular mimics of crystalline silicon and we have described new approaches to the selective synthesis of materials based on cyclohexasilanes. We reported the five-step synthesis and

chemoselective polymerization of the cyclohexasilane building blocks **1,4Si$_6$** and **1,3Si$_6$**,[16–21] as well as the seven-step stereocontrolled synthesis of *cis*- and *trans*-**Si$_{10}$H$_4$** (Figure 4.2.1).[22] These works have led to new insights, such as the discovery that the diastereomeric siladecalins have vastly different absorption spectra arising from configuration- and conformation-dependent σ-conjugation.

We envisioned an alternative approach to functionalized cyclosilanes via derivatization of the Si–H bond of our building blocks,[23] but confronted several challenges. First, the $Me_3Si–SiMe_3$ bond is weaker than a $H_3C–CH_3$ bond (BDE: 79 vs 90 kcal mol^{-1})[24] and cross-reactive with reagents for Si–H functionalization; Pd- and Pt-complexes like Karstedt's catalyst fragment Si–Si bonds.[25–27] Second, while the targeted cyclosilanes exhibit *cis/trans* diastereoisomerism, Si-C bonds are longer than C-C bonds,[28] potentially diminishing the steric factors often implicated in asymmetric stereoinduction. Third, the tetrafunctional cyclosilanes pose a significant selectivity challenge: the reaction of **1,4Si$_6$** and phenylacetylene could provide more than 40 distinct products arising from mono-, di-, tri-, or tetra-functionalization, *(E)*/*(Z)*-geometric isomers, α/β-addition, or *cis/trans* diastereoisomerism.

We report herein the extraordinarily selective outcome of the $RuHCl(CO)(PPh_3)_3$-catalyzed[29] reaction between cyclosilanes and aryl acetylenes. We observed perfect regioselectivity for 1,4-difunctionalization and β-addition and perfect (*E*)-selectivity. Products were isolated as a single diastereomer or as a mixture (ca. 2:1) favoring the thermodynamic isomer. The hydrosilylation is highly functional group tolerant: no Si–Si bond cleavage occurred, and functional group tolerance was high. These syntheses enabled a broad probe of the influence of substituent effects, structural isomerism, and

configuration on conjugation in organocyclosilanes, which revealed bathochromic shifts relative to starting materials. We also expect the work herein to expand additional frontiers for the study of conjugated materials. As an initial example, we report the synthesis of a novel thienyl-silane conjugated polymer derived from a *trans*-1,4-bis(thienylvinyl)cyclosilane, which not only absorbs visible light, but is also an entry to stereoregular polysilanes, a class of materials where control of tacticity has been a long-standing challenge.

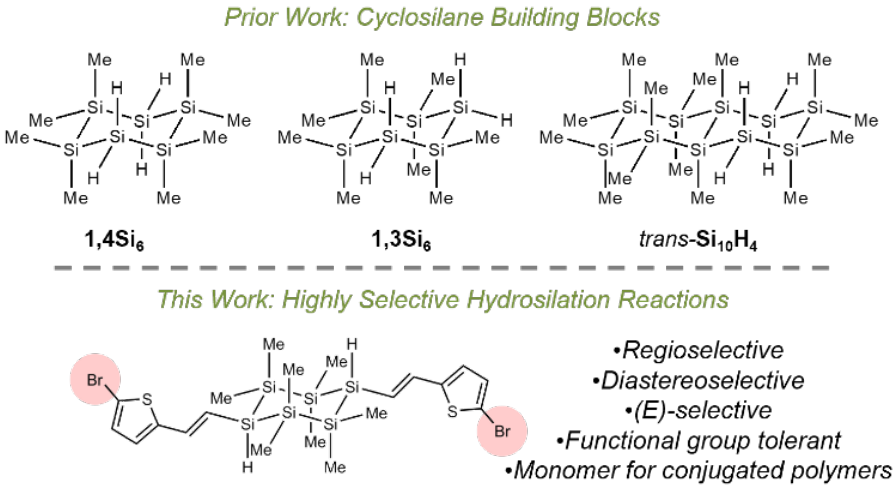

Figure 4.1.1 Highly selective reactions between cyclosilane building blocks and functionalized acetylenes.

4.2 Investigation of regio- and diastereoselectivity

Hydrosilylation is widely used in the industrial preparation of silicones (*e.g.*, Si–O polymers).[30–33] The application of hydrosilylation to oligo- and polysilanes (*e.g.*, Si–Si polymers) has been of interest since at least the 1960's,[34] but as documented by Rosenberg,[35] free-radical[36–38] and many transition-metal catalyzed[34,39] hydrosilylations are accompanied by partial to extensive Si–Si cleavage. Borane Lewis acids are useful for Si–H/X–H dehydrocoupling and Si–H/X=C hydrosilylation without skeletal

fragmentation.[23,40,41] Recently, Kyushin reported Ru-catalyzed *(E)*- or *(Z)*-selective hydrosilylation of alkynes and hydrooligosilanes without Si–Si bond cleavage.[29,42]

Table 4.2.1 Optimization of the $RuHCl(CO)(PPh_3)_3$-catalyzed reaction between phenylacetylene and **1,4Si$_6$**.[a]

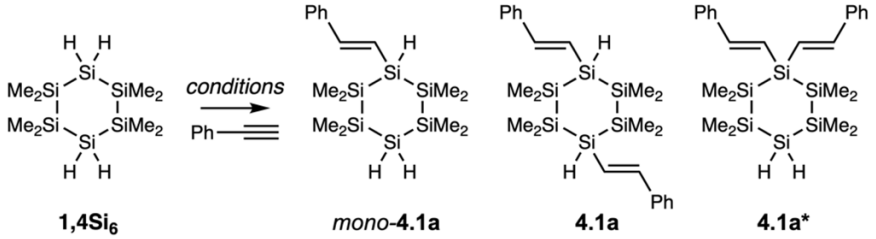

entry	[catalyst][b]	solvent	time	conversion[c]		
				mono-**4.1a**	**4.1a**	**4.1a***
1	5 mol%	toluene	7 d	22%	9%	0%
2[d]	10 mol%	toluene	24 h	42%	50%	0%
3	5 mol%	DCM	24 h	61%	39%	0%
4	10 mol%	DCM	24 h	17%	83%	0%
5[e]	10 mol%	DCM	24 h	45%	25%	0%
6	20 mol%	DCM	2 h	0%	100%	0%
7[f]	20 mol%	DCM	2 h	0%	100%	0%

[a] The reactions were carried out with 0.171 mmol of **1,4Si$_6$** and 0.428 mmol of phenylacetylene in 1 mL of solvent at room temperature under nitrogen protection unless noted. [b] $RuHCl(CO)(PPh_3)_3$ loading was relative to **1,4Si$_6$**. [c] The conversion was determined by ^{1}H NMR spectra of reaction aliquots. [d] The reaction was carried out at 60 °C. [e] The reactions were carried out with 0.171 mmol of **1,4Si$_6$** and 0.171 mmol of phenylacetylene. [f] The reactions were carried out with 0.171 mmol of **1,4Si$_6$** and 1.026 mmol of phenylacetylene.

We envisioned that *(E)*-selective addition of cyclosilanes to alkynes could yield σ,π-conjugated cyclosilanes. As Kyushin's study focused on linear monohydrosilanes like $H–SiMe_2SiMe_2Ph$, our initial focus was regioselectivity with tetrafunctional **1,4Si$_6$** (Table 4.2.1 and Scheme 4.2.1). It was unclear if replacement of one Si–H bond with a vinyl group

would be *activating* (1,1'-functionalization), *deactivating* (1,4-difunctionalization), or *neutral* (mixture). The success of monohydrosilanes suggested the feasibility of fully alkylated Si centers, such as **4.1a***. A first attempt with 2.50 equivalents of phenylacetylene and 5 mol% $RuHCl(CO)(PPh_3)_3$ resulted in mono-**4.1a** (22%) and 1,4-difunctionalized **4.1a** (9%), as determined by ^1H NMR spectroscopy. No 1,1'-difunctionalized **4.1a*** was observed. Further optimization of solvent and catalyst loading led to increased conversion to **4.1a** without residual mono-**4.1a** (entry 6). 1,1'-Difunctionalization was not observed even with excess phenylacetylene (entry 7). The mechanistic origin of the selectivity for monofunctionalization, be it steric, electronic, or a combination of factors, is not yet clear. In all cases, the ^1H NMR spectra were consistent with Si-addition to the phenylacetylene β-position, as α-addition would result in a 1,1-disubsituted alkene.

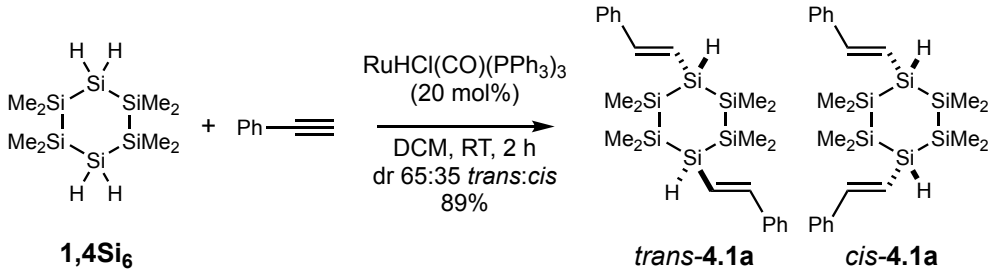

Scheme 4.2.1 Synthesis of *trans* and *cis*-**4.1a** via hydrosilylation of phenylacetylene with **1,4Si$_6$** catalyzed by $RuHCl(CO)(PPh_3)_3$.

Having established regioselectivity, we investigated *(E)*-selectivity and diastereoselectivity under the optimized conditions. **4.1a** was isolated in 89% yield as a 65:35 mixture of two isomeric products, assigned to the *trans* and *cis* diastereomers (Scheme 4.2.1). The isomers were not separable by silica gel chromatography, but recrystallization afforded pure *trans*-**1a** (X-ray crystal structure, Figure 4.2.1), which was confirmed as the major diastereomer. The X-ray crystal structure also confirmed that

hydrosilylation proceeded *without skeletal rearrangement* and with *(E)*- and β-selectivity. In the solid state, *trans*-**1a** adopted a chair conformation with both styryl groups at equatorial positions. This was the expected thermodynamic isomer, in which 1,3-diaxial interactions were minimized. The recrystallization filtrate was enriched in the minor product, which was assigned to *cis*-**1a** based on symmetry consistent with 1,4-difunctionalization. The ca. 1:3 *trans*:*cis* ratio was stable over time but could not be further increased by silica gel column chromatography. The ^{1}H and ^{29}Si NMR spectra of *trans*, *cis* and mixture of diastereomers are shown in Figure 4.2.2.

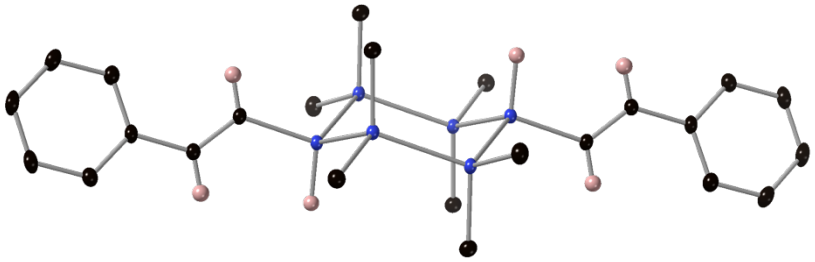

Figure 4.2.1 Displacement ellipsoid plot (30% probability level) of *trans*-**4.1a** at 110(2) K. Blue = Si, Black = C, Pink = H. Hydrogens on methyl and phenyl groups were omitted for clarity.

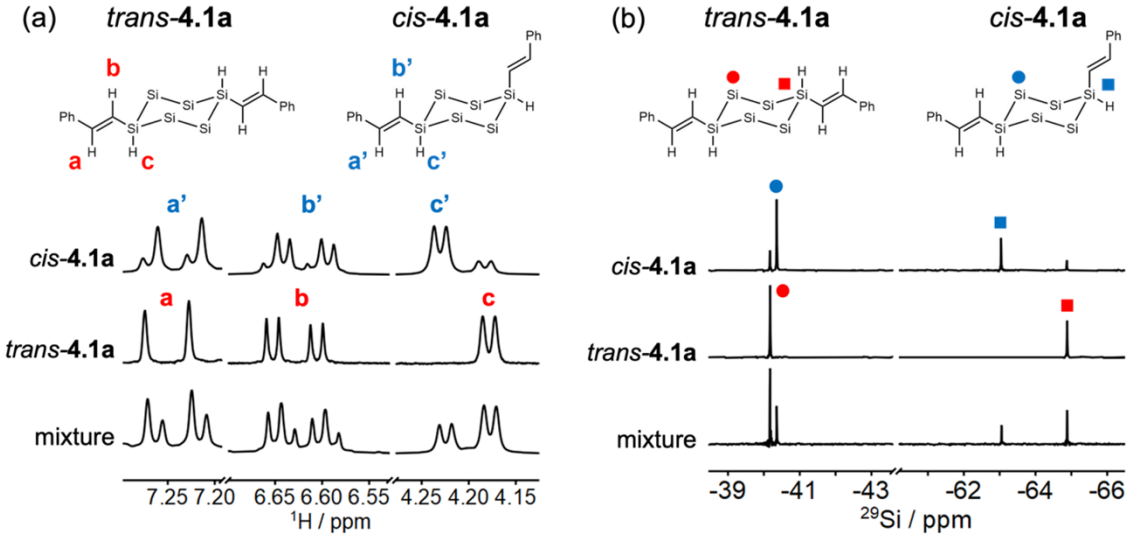

Figure 4.2.2 (a) Cropped ^{1}H NMR spectra (400 MHz, C_6D_6) comparing (top to bottom) *cis*-**4.1a** (dr 25:75 *trans:cis*), *trans*-**4.1a**, and the as-isolated mixture of isomers. (b) Cropped ^{29}Si {^{1}H} DEPT spectra (79 MHz, C_6D_6) comparing (top to bottom) *cis*-**4.1a** (dr 25:75 *trans:cis*), *trans*-**4.1a**, and the as-isolated mixture of isomers. DEPT = distortionless enhancement by polarization transfer. The methyl groups are omitted for clarity.

^{1}H–^{29}Si HSQC and ^{29}Si INEPT+ spectroscopy (Figure 4.2.3 and Figure 4.2.4) allowed assignment of the *Si*Me$_2$ and *Si*H resonances (Figure 4.2.2b). In the ^{1}H–^{29}Si HSQC spectrum of the diastereomer mixture, the Si*H* resonances only correlated with Si peaks at ca. -63.0 ppm and -64.9 ppm, which indicated these Si resonances resulted from *Si*H groups, rather than *Si*Me$_2$. The ^{29}Si INEPT+ spectrum supported assigning the doublet (δ -64.8, $^{1}J_{SiH}$ = 169.8 Hz) to the *Si*H resonance. The experimentally measured coupling constant was consistent with typical one-bond coupling constants between silicon and proton.[43]

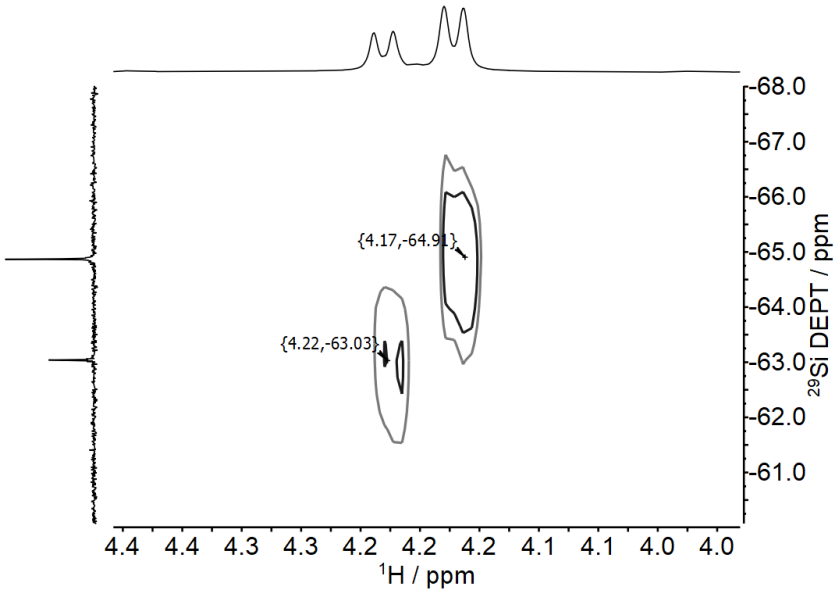

Figure 4.2.3 ^{1}H-^{29}Si HSQC NMR spectrum (400 MHz, C_6D_6) of **4.1a**. $^{1}J_{Si-H}$ = 120 Hz.

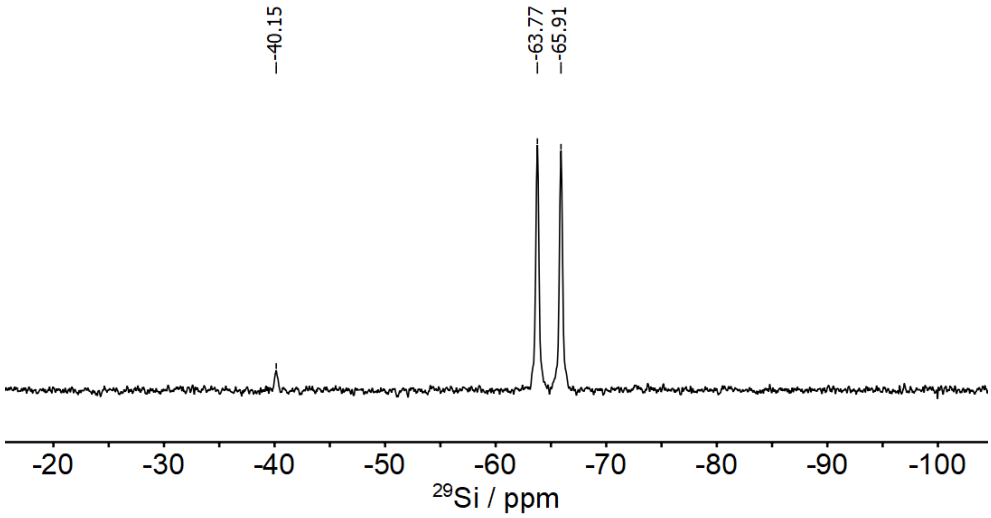

Figure 4.2.4 ^{29}Si INEPT+ NMR spectrum (79 MHz, C_6D_6) of *trans*-**4.1a**.

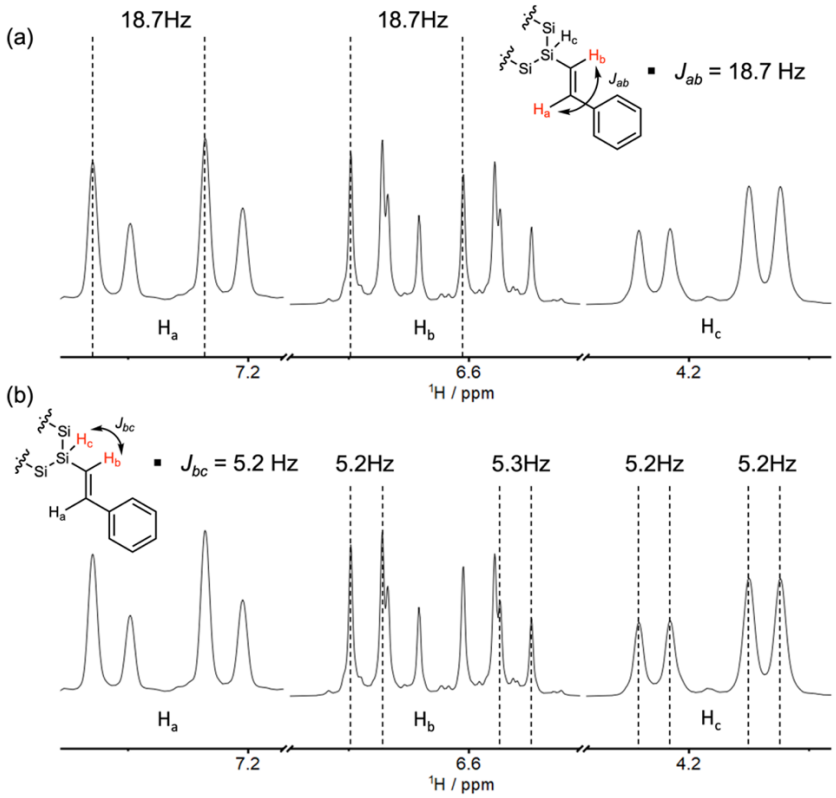

Figure 4.2.5 The coupling constant analysis of ^{1}H NMR spectra of **4.1a**.

The coupling constant analysis of ^{1}H NMR spectra further supported the structure assignment: (*E*)-alkene attached to a tertiary silane (Figure 4.2.5). The coupling constants

of the vinylic peak a (d, J = **18.7** Hz) and b (dd, J = 5.2, **18.7** Hz) were consistent with an (*E*)-alkene (Figure 4.2.5a). Peak c, the doublet assigned as Si*H* resonance (d, J = **5.2** Hz), exhibited the same coupling constant as peak b, the vinylic proton on the neighboring carbon (dd, J = **5.2**, 18.7 Hz) (Figure 4.2.5b).

4.3 Substrate scope

Having established selectivity with **1,4Si$_6$**, we investigated substrate scope (Figure 4.3.1). With a variety of 4-substituted phenylacetylenes, 1,4-bis(styryl)cyclohexasilanes were obtained in >80% yield and without erosion in regio- or diastereoselectivity, as shown by X-ray crystallography (Figure 4.3.2). This provided σ,π-hybrids functionalized with halogens (**4.1b-c**), electron donating groups (**4.1d-f**) and moderately electron withdrawing groups (**4.1g-h**).

The functional groups selected for investigation in Figure 4.3.1 were chosen on the basis of potential applications. Sulfur was tolerated in thiomethyl **4.1d** and thienyl **4.1i-j**, of relevance to molecular electronics.[44] Functional groups that would not be tolerated by the reductive coupling methods traditionally used to prepare cyclosilanes from dihalosilanes were also successfully incorporated, such as methyl ester **4.1h**. Benzoate esters are useful intermediates to a variety of other oxygenated functionality, such as carboxylic acids that have been employed as MOF ligands.[3] In addition, halogenated products (e.g., **4.1b** and **4.1j**) are suitable for catalytic cross-coupling (*vide infra*). Low conversion was observed with strongly electron-withdrawing substituents (*e.g.*, 4-nitro and 4-cyanophenylacetylene) and an electron-poor heterocycle (4-ethynylpyridine).

We also explored the cyclosilane scope. Regioselectivity was maintained (Figure 4.3.1), yielding 1,3- or 1,4-difunctionalized products instead of 1,1'-difunctionalized

cyclosilanes. No skeletal decomposition was observed and perfect *(E)*- and β-selectivities were retained. Interestingly, *cis*-$\mathbf{Si_{10}H_4}$ underwent a slow reaction with phenylacetylene. Low conversion (<5%) was observed in 24 hours.

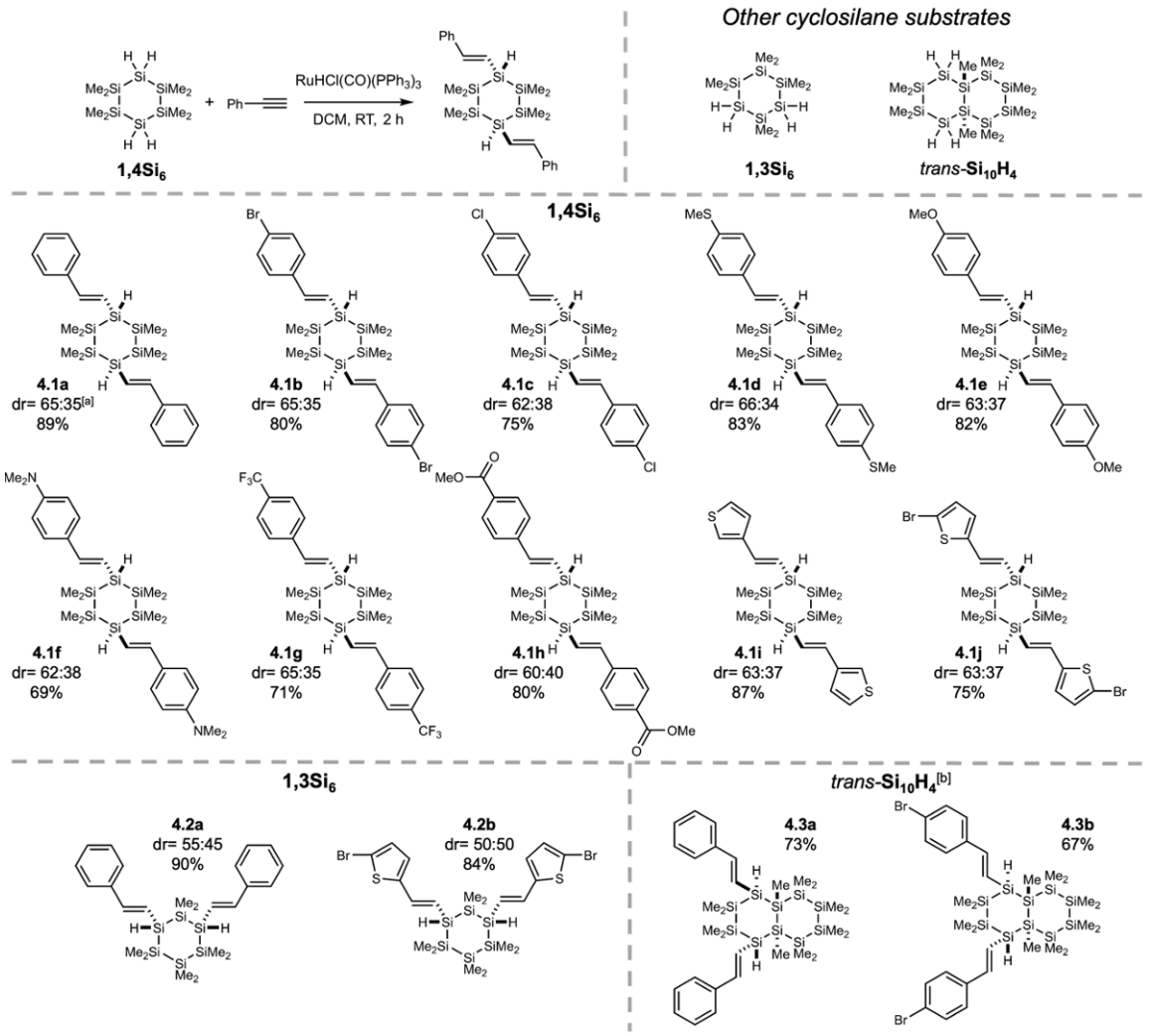

Figure 4.3.1 Substrate scope of hydrosilylation of alkynes with cyclosilanes. For **1,4Si$_6$**, major diastereomers are shown. [a] dr determined by ^{1}H NMR spectroscopy. Isolated yields are reported. [b] Only the *trans* diastereomer was detected.

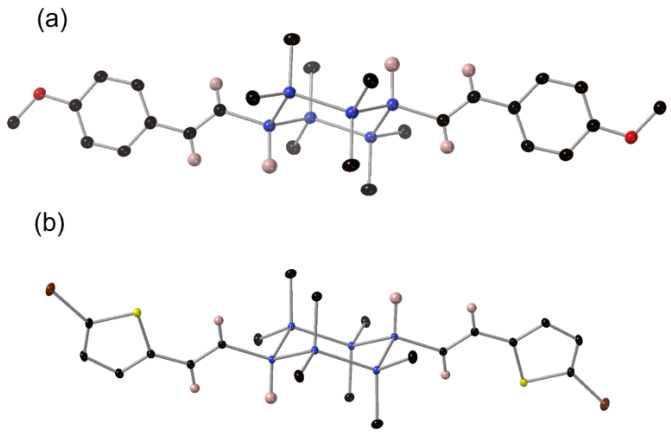

Figure 4.3.2 X-ray crystal structure of (a) *trans*-**4.1e** and (b) *trans*-**4.1j**. Blue = Si, black = C, pink = H, red = O, yellow = S, brown = Br. Hydrogens on methyl and aromatic groups are omitted for clarity.

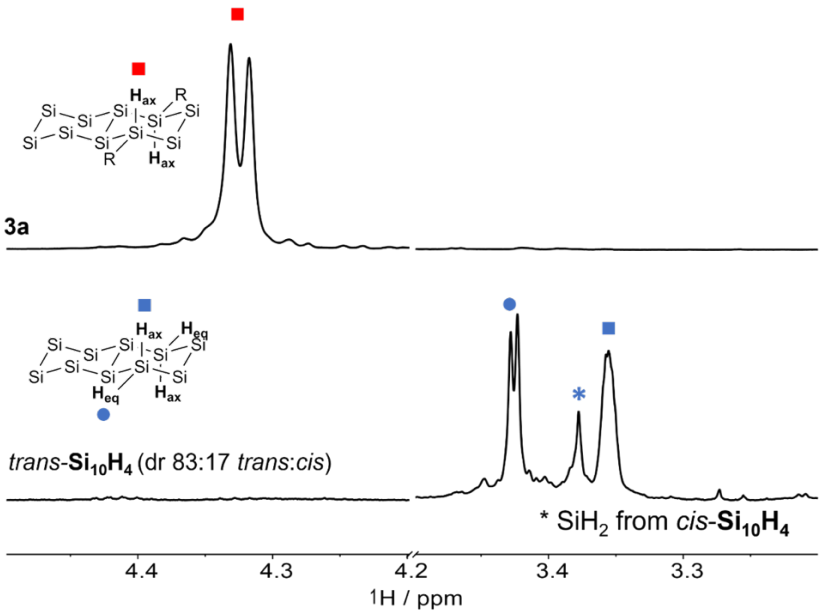

Figure 4.3.3 Cropped ^{1}H NMR spectra (400 MHz, C_6D_6) comparing Si*H* resonances of (top) **4.3a** and *trans*-$\mathbf{Si_{10}H_4}$ (bottom).

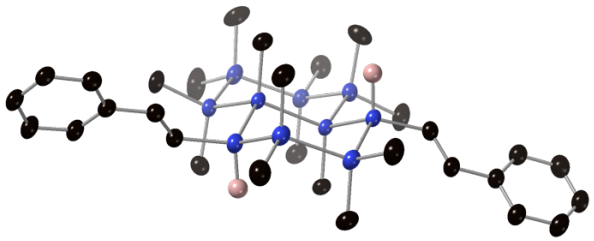

Figure 4.3.4 Displacement ellipsoid plot (30% probability level) of **4.3a** at 173(2) K. Blue = Si, Black = C, Pink = H. Hydrogens on methyl and phenyl groups were omitted for clarity.

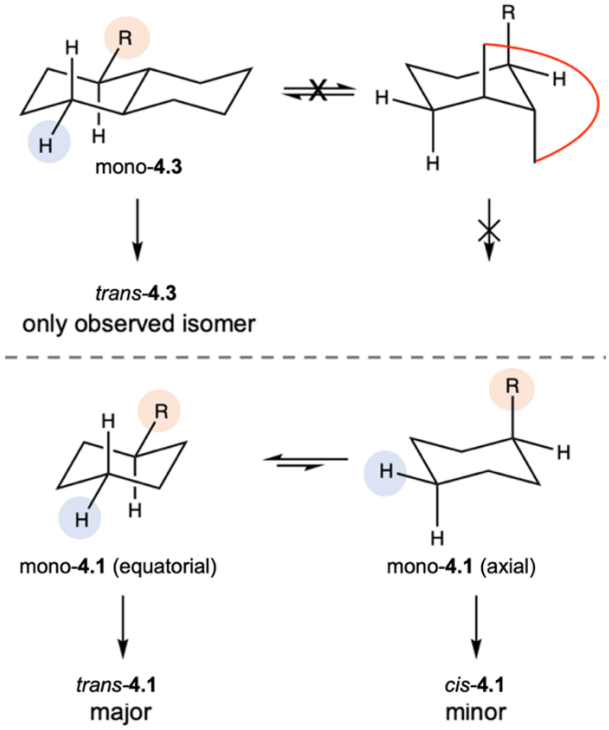

Figure 4.3.5 Model for stereoinduction.

The cyclosilane exerted a striking effect on diastereoselectivity. While diastereomeric ratios (dr) ca. 2:1 were observed for all **1,4Si$_6$**-derived products, the dr decreased to ca. 1:1 for **1,3Si$_6$** and increased dramatically for *trans*-**Si$_{10}$H$_4$**, where only one diastereomer could be detected by ^{1}H NMR spectroscopy (Figure 4.3.3). A relatively complicated SiH resonance was found in the ^{1}H NMR spectrum of *trans*-**Si$_{10}$H$_4$**, as the equatorial (H_{eq}) and axial (H_{ax}) protons showed difference splitting patterns.[22] Only the

axial proton undergoes W-coupling with the neighboring methyl group (H-Si-Si-C-H), leading to a multiplet. The equatorial proton meanwhile exhibits a doublet (J = 2.1 Hz) resulting from geminal coupling to the axial Si-H proton. After the reaction, however, only a single Si*H* resonance (doublet) was observed for **4.3a**, indicating exclusive formation of a single diastereomer. The coupling constant was found to be 5.2 Hz, the same as SiH resonance of **4.1a**. The NMR evidence supports full conversion of the starting *trans*-$\mathbf{Si_{10}H_4}$ in the hydrosilylation reaction.

An X-ray crystal structure of **4.3a** confirmed assignment to the *trans* diastereomer (Figure 4.3.4) with diequatorial styryl groups. Like *trans*-decalin, *trans*-$\mathbf{Si_{10}H_4}$ is conformationally locked,[22] suggesting that hydrosilylation is selective for the equatorial Si–H bond. The reduced diastereoselectivity with **1,3Si$_6$** and **1,4Si$_6$** was attributed to rapid ring inversion[45–47] in a mono-functionalized intermediate (Figure 4.3.5). Hydrosilylation is highly selective for the equatorial proton (blue circle). Interconversion of axial and equatorial conformers (substituent labelled with orange circle) of a mono-functionalized intermediate determines the *trans:cis* ratio of difunctionalized products. Therefore, we expect that the equilibrium between equatorial and axial conformers in mono-functionalized intermediates should determine the dr in difunctionalized products.

4.4 UV-vis absorbance spectra

Finally, we investigated the UV-vis spectroscopic properties of the (bis)styrylcyclosilanes in pentane solution at room temperature. Comparison of *trans*-**4.1a** to **1,4Si$_6$** and phenylacetylene showed that the hybrid material was red-shifted 100-nm compared to purely σ-conjugated and 50-nm relative to purely π-conjugated starting materials (Figure 4.4.1a). DFT calculations showed that the HOMO and LUMO of *trans*-

4.1a is fully delocalized across the entire molecule including both σ (cyclosilane) and π-conjugated (aromatic) moieties (Figure 4.4.2). We also compared the UV-vis spectrum of *trans*-**4.1a** to *cis*-**4.1a** (dr 25:75 *trans:cis*) and found that relative configuration did not strongly influence optical absorbance in solution (Figure 4.4.1b). This observation facilitated comparison of all three cyclosilanes to each other (Figure 4.4.1c), given the different outcomes with respect to dr in the hydrosilylation. While 1,4-difunctionalized **4.1a** and 1,3-difunctionalized **4.2a** were quite similar in the onset of absorption, the onset of absorbance for *trans*-siladecalin **4.3a** was red-shifted by ca. 30 nm relative to monocyclic silanes. Finally, we note the bathochromic influence of thienyl substitution relative to aryl substitution comparing *trans*-**4.1j** to *trans*-**4.1a** (Figure 4.4.1d).

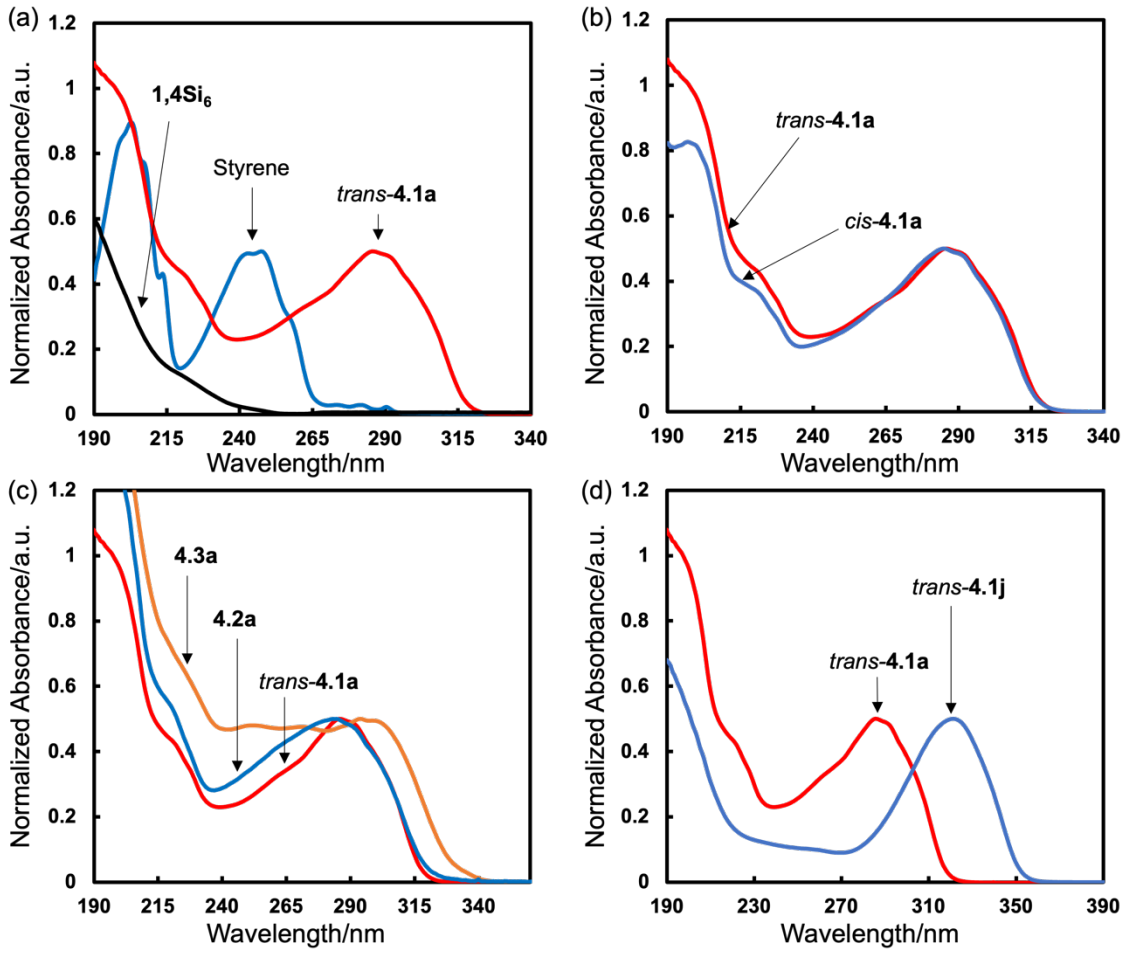

Figure 4.4.1 UV-vis spectra with normalized absorbance ([compound] = 10^{-5} M, in *n*-pentane). (a) Comparison to starting material. Red: *trans*-**4.1a**; black: **1,4Si$_6$**; blue: styrene. (b) Influence of configuration. Red: *trans*-**4.1a**; blue: *cis*-**4.1a** (dr 25:75 *trans:cis*). (c) Cyclosilane comparison. Red: *trans*-**4.1a**; blue: **4.2a** (dr 55:45 *trans:cis*); orange: **4.3a**. (d) Heterocycle effect. Red: *trans*-**4.1a**; blue: *trans*-**4.1j** (dr 90:10 *trans:cis*).

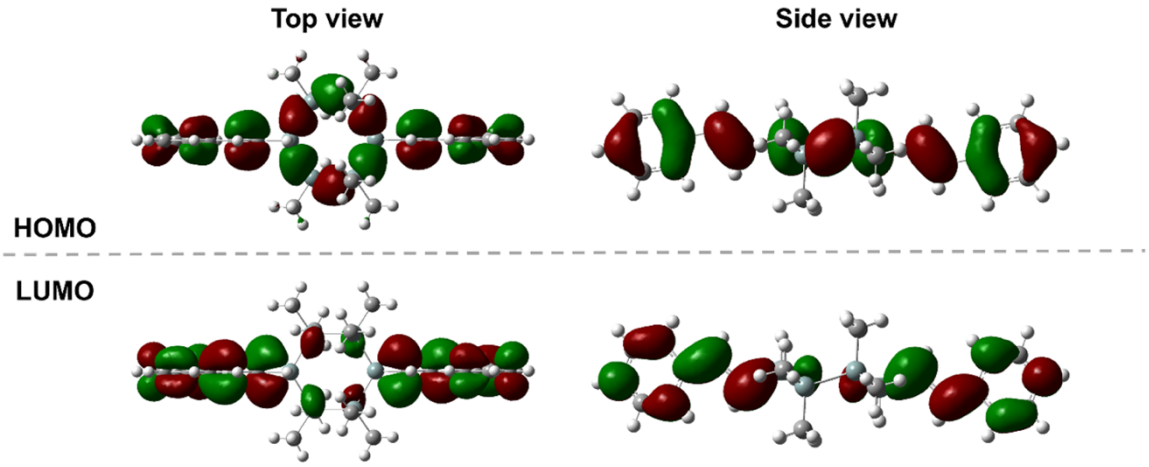

Figure 4.4.2 Calculated HOMO and LUMO of *trans*-**4.1a**. B3YLP/6-31G(d).

4.5 Stereoregular conjugated polymer synthesis

The extended conjugation observed in hybrid molecules suggested a new conjugated polymer design: *stereoregular* copolymers alternating in σ- and π-conjugated motifs could be prepared via copolymerization of a dibrominated building block (e.g., *trans*-**4.1b** or *trans*-**4.1j**) with an appropriate comonomer. Polymers containing Si–Si bonds can be largely divided into two types: polysilanes (e.g., poly(SiR_2))[48,49] and σ,π-copolymers (e.g., poly(Ar($SiMe_2$)$_n$Ar)).[50,51] Polysilanes in which the alkyl substituents are not the same (e.g., poly(SiR'R"), R' ≠ R") are stereogenic at each Si atom, but assignment and control of polysilane tacticity is a long-standing problem with no general solution.[52–57] Use of a stereochemically pre-defined monomer appeals to avoid issues of control of relative configuration during polymerization.

We found that treatment of dibromo *trans*-**4.1j** (dr 90:10 *trans:cis*) with stoichiometric *i*-PrMgCl resulted in quantitative Mg-halogen exchange.[58] The intermediate α,ω-dimagnesiocyclosilane underwent Kumada cross-coupling with 2-bromothiophene, yielding *trans*-**4.1k** in 100% conversion (86% isolated yield) and without cyclosilane skeletal rearrangement or erosion of relative configuration (Scheme 4.5.1a).

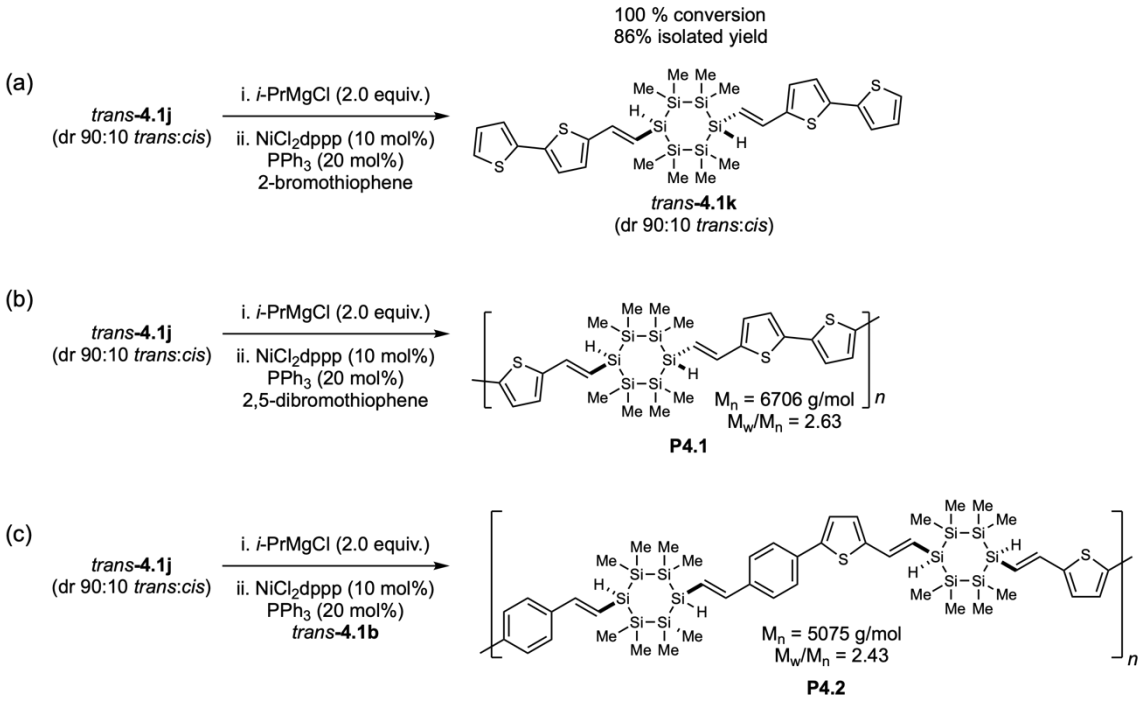

Scheme 4.5.1 a) Model reaction: Kumada cross-coupling of *trans*-**4.1j** and 2-bromothiophene. (b) Kumada polycondensation synthesis of **P4.1**. c) Kumada polycondensation synthesis of **P4.2**.

The novel polymer **P4.1** (M_n = 6706 g/mol, M_w/M_n = 2.63, Figure 4.5.1) was prepared by Kumada polycondensation of 2,5-dibromothiophene with the α,ω-dimagnesiocyclosilane derived from *trans*-**4.1j** (Scheme 4.5.1b and Figure 4.5.1). The dibromo building blocks could in principle serve as either a precursor to a nucleophile for Kumada polymerization, as showed above in the synthesis of **P4.1**, but also as the electrophile. We therefore also synthesized copolymer **P4.2** in which Mg-halogen

exchange of *trans*-**4.1j** was followed by Kumada polycondensation with dibromo *trans*-**4.1b** (M_n = 5075 g mol^{-1}, M_w/M_n = 2.43, Scheme 4.5.1c and Figure 4.5.1).

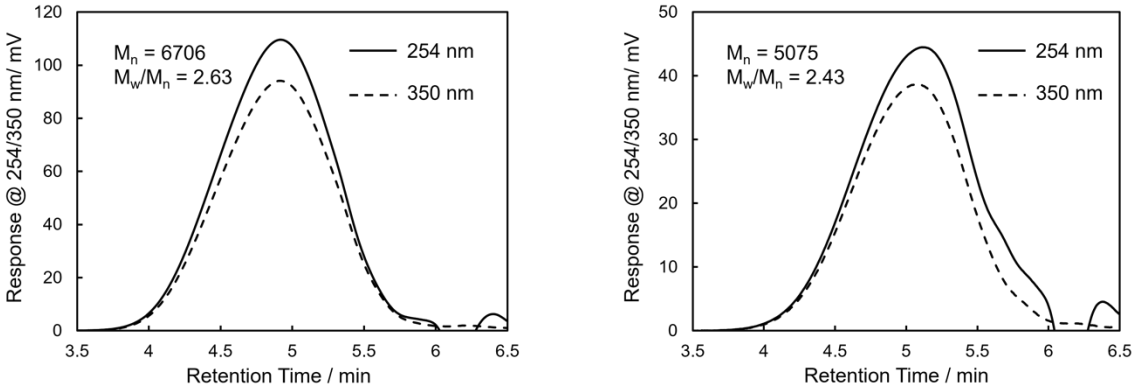

Figure 4.5.1 Size exclusion chromatograms of **P4.1 and P4.2** at 254 nm (solid line) and 350 nm (dotted line). Molecular weight determined relative to polystyrene standards at 254 nm (THF, [**P4.1**] or [**P4.2**] = 0.5 mg mL^{-1}, 40 °C, 0.35 mL min^{-1}, 10 µL injection)

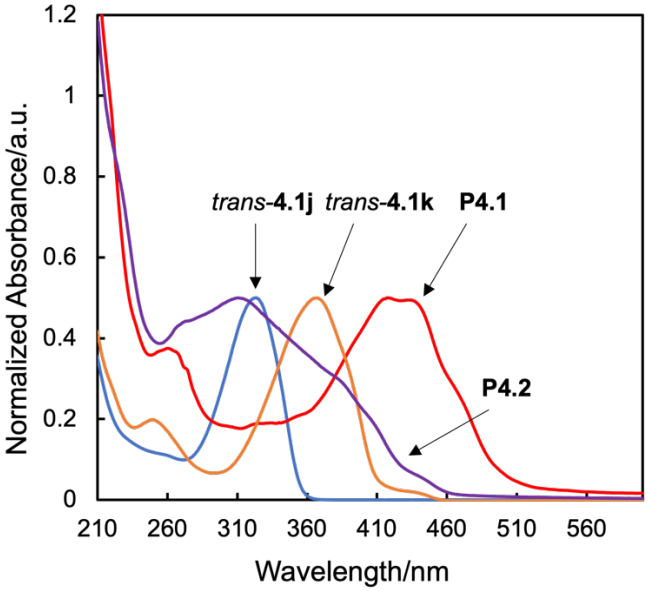

Figure 4.5.2 Comparison of UV-vis spectra of *trans*-**4.1j** (blue), *trans*-**4.1k** (orange), **P4.1** (red) and **P4.2** (purple) in THF. [*trans*-**4.1j**] = 10^{-5} M, [*trans*-**4.1k**] = 10^{-5} M, [**P4.1**] = 0.03 g/L, [**P4.2**] = 0.03 g/L.

The **P4.1** onset of absorption (510 nm) was 140 nm red-shifted from *trans*-**4.1j** itself and 50 nm from *trans*-**4.1k** (Figure 4.5.2), validating the hypothesis that σ,π-mixing

could be extended across a conjugated polymer chain. Comparison of the UV-vis spectra showed that **P4.1** was red-shifted relative to **P4.2**. This was attributed to the difference between dithienyl and phenyl-thienyl units, as we showed (Figure 4.5.2) that molecular thienyl cyclosilanes were red-shifted relative to phenylsilanes. The all-organic conjugated polymer PTVT (poly(thienylenevinylenethienyl)) exhibited a similar absorbance spectrum relative to **P4.1** despite a much longer degree of polymerization (PTVT: λ_{max} = 430 nm, λ_{onset} = 550 nm, M_n = 21,000 g mol^{-1}).[59]

These initial studies on conjugated polymer synthesis highlight the utility of stereodefined σ,π-hybrid materials, as well as the stability of relative configuration to subsequent chemical functionalization. Future work will examine the impact of stereoregularity on physical properties, as tactic polymers can demonstrate enhanced mechanical, thermal, and other properties relative to atactic.[60]

4.6 Conclusion

We demonstrated that Ru-catalyzed addition of tetrafunctional cyclosilanes to functionalized alkynes proceeded with high selectivity across several parameters: chemoselectivity for Si–H over Si–Si bonds, regioselectivity with respect to both cyclosilane and alkyne, and high *(E)/(Z)* and *cis/trans* diastereoselectivity. Broad functional group tolerance was exhibited, providing a complex organocyclosilanes bearing reactive functional groups challenging to incorporate by other means. The diverse functional groups incorporated open up several new possible directions, from MOF synthesis to molecular electronics. We also demonstrated that these synthetic achievements enabled the first broad investigation of structure-property relationships in σ,π-hybrid cyclosilanes, which revealed visible light absorption dependent on both the cyclosilane and

arene identity. As exemplified by the Kumada polycondensation herein, we expect the results of this study to inspire new approaches to stereoregular conjugated materials combining σ- and π-conjugated motifs. We believe this contribution will continue to expand possibilities for the selective synthesis of complex materials from the main group.

4.7 Reference

(1) Klausen, R. S.; Widawsky, J. R.; Steigerwald, M. L.; Venkataraman, L.; Nuckolls, C. *J. Am. Chem. Soc.* **2012**, *134*, 4541–4544.
(2) Su, T. A.; Li, H.; Klausen, R. S.; Widawsky, J. R.; Batra, A.; Steigerwald, M. L.; Venkataraman, L.; Nuckolls, C. *J. Am. Chem. Soc.* **2016**, *138*, 7791–7795.
(3) Burns, D. A.; Press, E. M.; Siegler, M. A.; Klausen, R. S.; Thoi, V. S. *Angew. Chemie Int. Ed.* **2020**, *59*, 763–768.
(4) Surampudi, S.; Yeh, M.-L. L.; Siegler, M. A.; Hardigree, J. F. M. M.; Kasl, T. A.; Katz, H. E.; Klausen, R. S. *Chem. Sci.* **2015**, *6*, 1905–1909.
(5) Zhou, J.; Surampudi, S. K.; Bragg, A. E.; Klausen, R. S. *Chem. - A Eur. J.* **2016**, *22*, 6204–6207.
(6) Zhou, J.; Folster, C. P.; Surampudi, S. K.; Jimenez, D.; Klausen, R. S.; Bragg, A. E. *Dalt. Trans.* **2017**, *46*, 8716–8726.
(7) Barrett, B. J.; Jimenez, D.; Klausen, R. S.; Bragg, A. E. *J. Phys. Chem. B* **2021**, *125*, 8460–8471.
(8) Sharma, H. K.; Pannell, K. H.; Ledoux, I.; Zyss, J.; Ceccanti, A.; Zanello, P. *Organometallics* **2000**, *19*, 770–774.
(9) Shimada, M.; Yamanoi, Y.; Matsushita, T.; Kondo, T.; Nishibori, E.; Hatakeyama, A.; Sugimoto, K.; Nishihara, H. *J. Am. Chem. Soc.* **2015**, *137*, 1024–1027.
(10) Shimada, M.; Tsuchiya, M.; Sakamoto, R.; Yamanoi, Y.; Nishibori, E.; Sugimoto, K.; Nishihara, H. *Angew. Chemie - Int. Ed.* **2016**, *55*, 3022–3026.
(11) Emanuelsson, R.; Löfås, H.; Wallner, A.; Nauroozi, D.; Baumgartner, J.; Marschner, C.; Ahuja, R.; Ott, S.; Grigoriev, A.; Ottosson, H. *Chem. - A Eur. J.* **2014**, *20*, 9304–9311.
(12) Carberry, E. A.; West, R. *J. Am. Chem. Soc.* **1969**, *91*, 5440–5446.
(13) Fischer, R.; Konopa, T.; Ully, S.; Baumgartner, J.; Marschner, C. *J. Organomet. Chem.* **2003**, *685*, 79–92.
(14) Larkin, D. Y.; Korlyukov, A. A.; Matukhina, E. V.; Buzin, M. I.; Chernyavskaya, N. A.; Antipin, M. Y.; Chernyavskii, A. I. *Russ. Chem. Bull.* **2005**, *54*, 1612–1622.
(15) Bande, A.; Michl, J. *Chem. - A Eur. J.* **2009**, *15*, 8504–8517.
(16) Press, E. M.; Marro, E. A.; Surampudi, S. K.; Siegler, M. A.; Tang, J. A.; Klausen, R. S. *Angew. Chemie Int. Ed.* **2017**, *56*, 568–572.
(17) Marro, E. A.; Klausen, R. S. *Chem. Mater.* **2019**, *31*, 2202–2211.
(18) Marro, E. A.; Press, E. M.; Siegler, M. A.; Klausen, R. S. *J. Am. Chem. Soc.* **2018**, *140*, 5976–5986.
(19) Folster, C. P.; Klausen, R. S. *Polym. Chem.* **2018**, *9*, 1938–1941.
(20) Jiang, Q.; Wong, S.; Klausen, R. S. *Polym. Chem.* **2021**, *12*, 4785–4794.

(21) Dorn, R. W.; Marro, E. A.; Hanrahan, M. P.; Klausen, R. S.; Rossini, A. J. *Chem. Mater.* **2019**, *31*, 9168–9178.
(22) Marro, E. A.; Folster, C. P.; Press, E. M.; Im, H.; Ferguson, J. T.; Siegler, M. A.; Klausen, R. S. *J. Am. Chem. Soc.* **2019**, *141*, 17926–17936.
(23) Harrison, D. J.; Edwards, D. R.; McDonald, R.; Rosenberg, L. *Dalt. Trans.* **2008**, No. 26, 3401.
(24) Walsh, R. *Acc. Chem. Res.* **1981**, *14*, 246–252.
(25) Suginome, M.; Ito, Y. *Chem. Rev.* **2000**, *100*, 3221–3256.
(26) Sharma, H. K.; Pannell, K. H. *Chem. Rev.* **1995**, *95*, 1351–1374.
(27) Chen, S.; Zhu, J.; Ke, J.; Li, Y.; He, C. *Angew. Chemie Int. Ed.* **2022**, *61*.
(28) Min, G. K.; Hernández, D.; Skrydstrup, T. *Acc. Chem. Res.* **2013**, *46*, 457–470.
(29) Kanno, K. ichiro; Aikawa, Y.; Kyushin, S. *Tetrahedron Lett.* **2020**, *61*, 152274.
(30) Troegel, D.; Stohrer, J. *Coord. Chem. Rev.* **2011**, *255*, 1440–1459.
(31) Tondreau, A. M.; Atienza, C. C. H.; Weller, K. J.; Nye, S. A.; Lewis, K. M.; Delis, J. G. P. P.; Chirik, P. J. *Science (80-.).* **2012**, *335*, 567–570.
(32) Nakajima, Y.; Shimada, S. *RSC Adv.* **2015**, *5*, 20603–20616.
(33) Moretto, H.-H.; Schulze, M.; Wagner, G. *Ullmann's Encyclopedia of Industrial Chemistry*; 2012; pp 675–712.
(34) Yamamoto, K.; Kumada, M.; Nakajima, I.; Maeda, K.; Imaki, N. *J. Organomet. Chem.* **1968**, *13*, 329–341.
(35) Song, K. C.; Lee, K. M.; Nghia, N. Van; Sung, W. Y.; Do, Y.; Lee, M. H. *Organometallics* **2013**, *32*, 817–823.
(36) Banovetz, J. P.; Hsiao, Y. L.; Waymouth, R. M. *J. Am. Chem. Soc.* **1993**, *115*, 2540–2541.
(37) Hsiao, Y.-L. L.; Waymouth, R. M. *J. Am. Chem. Soc.* **1994**, *116*, 9779–9780.
(38) Shankar, R.; Shahi, V. *J. Organomet. Chem.* **2008**, *693*, 307–315.
(39) Sacarescu, L.; Siokou, A.; Sacarescu, G.; Simionescu, M.; Mangalagiu, I. *Macromolecules* **2008**, *41*, 1019–1024.
(40) Lee, P. T. K. K.; Skjel, M. K.; Rosenberg, L. *Organometallics* **2013**, *32*, 1575–1578.
(41) Lee, P. T. K.; Rosenberg, L. *Dalt. Trans.* **2017**, *46*, 8818–8826.
(42) Kanno, K. ichiro; Noguchi, S.; Ono, Y.; Egawa, S.; Otsuka, N.; Mita, M.; Kyushin, S. *J. Organomet. Chem.* **2022**, *961*, 122234.
(43) Sørensen, O. .; Ernst, R. . *J. Magn. Reson.* **1983**, *51*, 477–489.
(44) Su, T. A.; Li, H.; Klausen, R. S.; Kim, N. T.; Neupane, M.; Leighton, J. L.; Steigerwald, M. L.; Venkataraman, L.; Nuckolls, C. *Acc. Chem. Res.* **2017**, *50*, 1088–1095.
(45) Tekautz, G.; Binter, A.; Hassler, K.; Flock, M. **2006**, *7*, 421–429.
(46) Casarini, D.; Lunazzi, L.; Mazzanti, A. *Tetrahedron* **1998**, *54*, 13181–13184.
(47) Casarini, D.; Lunazzi, L.; Mazzanti, A. *J. Org. Chem.* **1998**, *63*, 9125–9127.
(48) Miller, R. D.; Michl, J. *Chem. Rev.* **1989**, *89*, 1359–1410.
(49) Klausen, R. S.; Ballestero-Martínez, E. *Comprehensive Organometallic Chemistry IV*; Elsevier, 2021.
(50) Fang, F.; Jiang, Q.; Klausen, R. S. *J. Am. Chem. Soc.* **2022**, *144*, 7834–7843.
(51) Morisaki, Y.; Fujimura, F.; Chujo, Y. *Organometallics* **2003**, *22*, 3553–3557.
(52) Banovetz, J. P.; Stein, K. M.; Waymouth, R. M. *Organometallics* **1991**, *10*, 3430–3432.

(53) Choi, N.; Onozawa, S.; Sakakura, T.; Tanaka, M. *Organometallics* **1997**, *16*, 2765–2767.
(54) Grimmond, B. J.; Corey, J. Y. *Organometallics* **2000**, *19*, 3776–3783.
(55) Dioumaev, V. K.; Rahimian, K.; Gauvin, F.; Harrod, J. F. *Organometallics* **1999**, *18*, 2249–2255.
(56) Fossum, E.; Matyjaszewski, K. *Macromolecules* **1995**, *28*, 1618–1625.
(57) Maxka, J.; Mitter, F. K.; Powell, D. R.; West, R. *Organometallics* **1991**, *10*, 660–664.
(58) Knochel, P.; Dohle, W.; Gommermann, N.; Kneisel, F. F.; Kopp, F.; Korn, T.; Sapountzis, I.; Vu, V. A. *Angew. Chemie Int. Ed.* **2003**, *42*, 4302–4320.
(59) Toyoshima, R.; Akagi, K.; Shirakawa, H. *Synth. Met.* **1997**, *84*, 431–432.
(60) Worch, J. C.; Prydderch, H.; Jimaja, S.; Bexis, P.; Becker, M. L.; Dove, A. P. *Nat. Rev. Chem.* **2019**, *3*, 514–535.

Chapter 5: Conjugation in isomeric cyclosilane thioethers

The work presented in this chapter has been published as: Gittens, A. F.; Jiang, Q.; Siegler, M. A.; Klausen, R. S. *Organometallics* **2022**, 41, 23, 3762–3769.

5.1 Introduction

Since the discovery in the 1960's that permethylcyclosilanes exhibit longer-wavelength absorption spectra[1] than cycloalkanes and form stable radical anions,[2] interest in the synthesis of increasingly complex cyclosilanes has only grown.[3] Prismatic solids[4,5] and polycyclic silanes[6] have shed light on the impact of strain and curvature on σ-conjugation, while we have investigated the synthesis of stereochemically defined cyclosilanes.[7–9] An interest in the influence of heteroatomic substitution on optoelectronic properties has inspired work on boron-[10–12] and nitrogen-containing cyclosilanes (Scheme 5.1.1).[13,14] Herein, we report the synthesis of cyclosilane thioethers via chemoselective dehydrocoupling of partially hydrogenated cyclosilanes and arylthiols and examine the effect of structural isomerism on conjugation. Density functional theory (DFT) calculations were used to elucidate potential mechanisms underlying experimental observations.

In recent work, we found that isomeric silanes, both molecular and polymeric, can exhibit strongly different absorbance spectra due to differences in conformation. We have previously reported the synthesis of the partially hydrogenated cyclosilanes **1,3Si$_6$** and **1,4Si$_6$** as monomers for dehydrocoupling polymerization[15–20] and found that linear polymers of **1,3Si$_6$** were red-shifted by 22-nm relative to linear polymers of **1,4Si$_6$** (Scheme 5.1.2),[20] while *cis*-siladecalin is optically inactive compared to *trans*-siladecalin.[7]

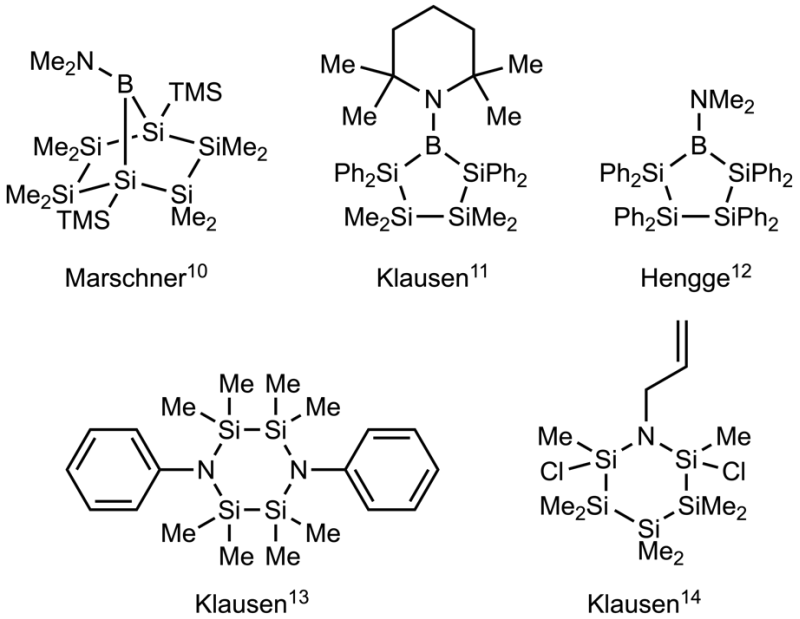

Scheme 5.1.1 Heteroatomic substitution of cyclosilanes.

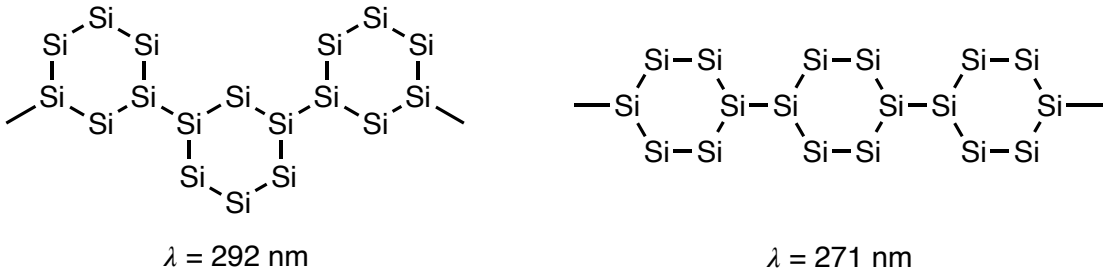

Scheme 5.1.2 Isomeric oligo- and polysilanes with distinct absorption spectra.

Curious about the effect of isomerism on π,n,σ-conjugation, we sought to synthesize two sets of isomeric cyclosilanes bearing exocyclic heteroatoms (Scheme 5.1.2). Based on the high degrees of conversion and chemoselectivity identified by Rosenberg et al. in dehydrocoupling of thiols and linear oligosilanes,[21] we report a combined experimental and computational study probing the effects of sulfur incorporation on the optical properties of isomeric cyclosilanes. Our study demonstrates that the reduced conformational degrees of freedom in cyclosilanes results in a compelling platform to study the effects of isomerism on optical and electronic properties, resulting in the discovery that

changes in skeletal connectivity can have competing effects on conformation and delocalization.

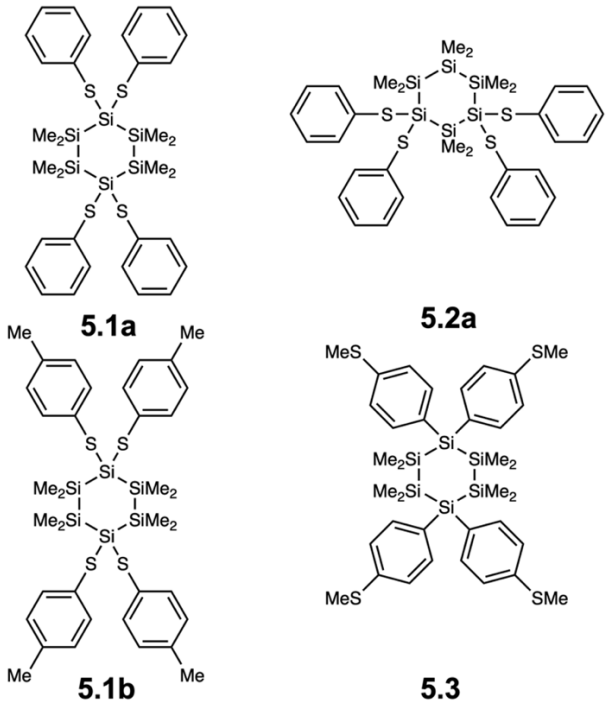

Scheme 5.1.3 Structural isomers of cyclosilane-sulfur hybrids investigated herein. Isomer **5.3** was not synthesized, but computationally evaluated.

5.2 Synthesis of isomeric cyclosilane thiolethers

Identification of methods for the functionalization of Si–H bonds in the presence of Si–Si bonds has been a problem of long-standing interest.[22,23] A consistent challenge has been chemoselectivity, given the susceptibility of Si–Si bonds to cleavage by strong nucleophiles,[24,25] Lewis acids,[26,27] and late transition metals including Rh and Pt.[28,29] In recent years, tris(pentafluorophenyl)borane ($B(C_6F_5)_3$) has been reported as a versatile catalyst for the chemoselective activation of Si–H bonds in linear oligosilanes and polysilanes,[21,30,31] with particularly high yields observed for the dehydrocoupling of thiols

with H-functionalized oligosilanes (Scheme 5.2.1). Therefore, we selected $B(C_6F_5)_3$ as the catalyst for cyclosilane thiolation.

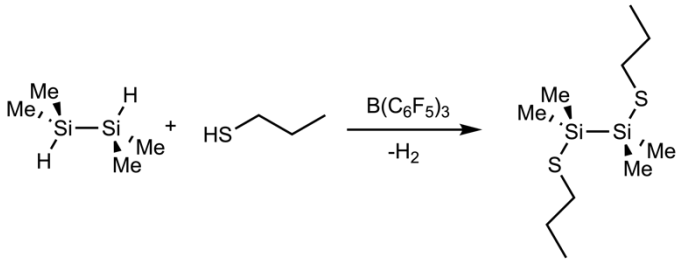

Scheme 5.2.1 Catalytic dehydrocoupling of disilane and propylthiol.

The synthesis of cyclosilane thiolethers were investigated by Alex Gittens in the Klausen group. The full structural characterization has been performed and published in the following reference: Gittens, A. F.; Jiang, Q.; Siegler, M. A.; Klausen, R. S. *Organometallics* **2022**, 41, 23, 3762–3769.

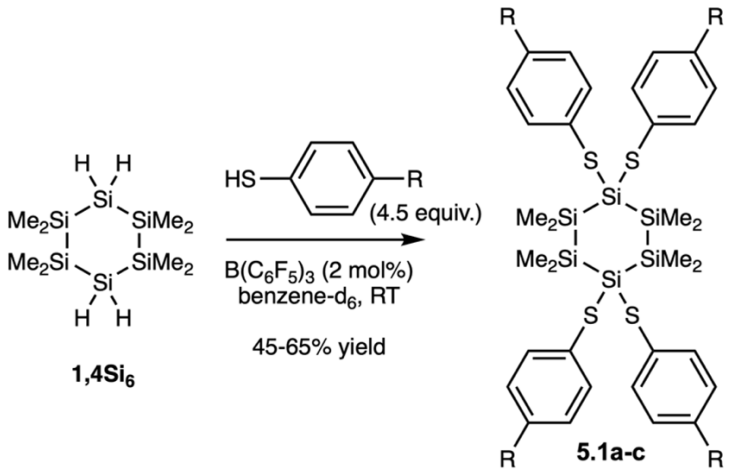

Scheme 5.2.2 Catalytic dehydrocoupling of **1,4Si$_6$** and arylthiols.

In an initial survey of reaction scope, we found that exposing **1,4Si$_6$** to $B(C_6F_5)_3$ and a slight excess of thiophenol resulted in the immediate evolution of hydrogen. A white solid precipitate formed, which was isolated by filtration and proved to be clean tetrafunctionalized cyclosilane thioether **5.1a** (57% yield, Scheme 5.2.2). Full substitution

of all Si–H bonds was notable in comparison to the Ru-catalyzed hydrosilation reaction between **1,4Si$_6$** and alkynes, which yielded the difunctionalized product exclusively.[9] Several other arylthiols were also examined (Scheme 5.2.2). X-ray crystal structures confirmed the structural assignments (Figure 5.2.1).

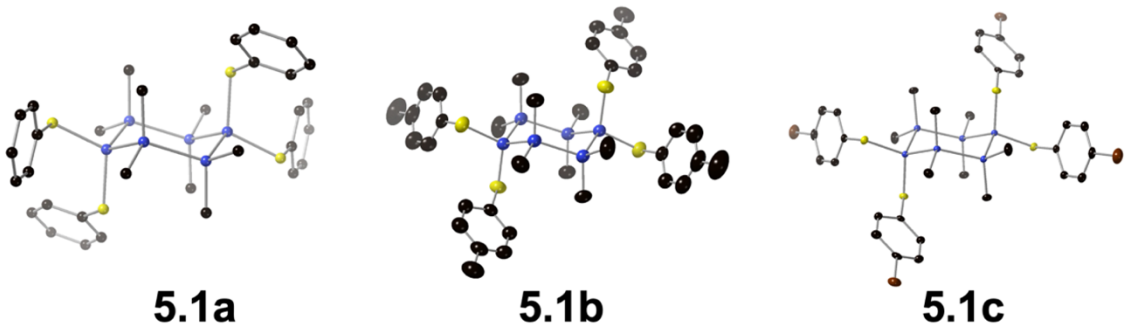

Figure 5.2.1 Displacement ellipsoid plots (50% probability level) of cyclosilane thioethers **5.1a-c** at 110(2) K (**5.1a** and **5.1c**) or at 294(2) K (**5.1b**). Hydrogens omitted for clarity. Blue = silicon, black = carbon, yellow = sulfur, burgundy = bromine.

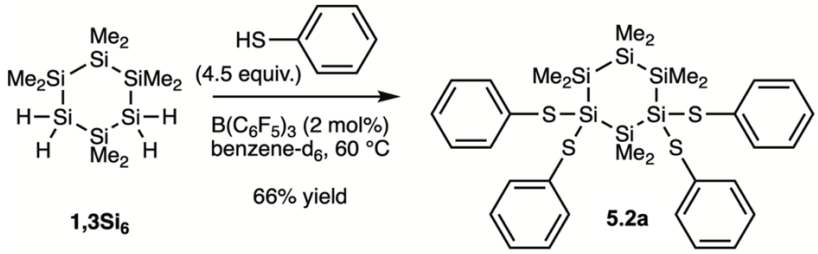

Scheme 5.2.3 Catalytic dehydrocoupling of **1,3Si$_6$** and phenylthiols.

We also examined the reaction of **1,3Si$_6$** with thiophenol. In general, 1,3-functionalized cyclosilanes are more soluble than 1,4-functionalized.[16] No product precipitation was observed from benzene. Instead, reaction progress was monitored by ^{1}H NMR spectroscopy. We found that an increased reaction temperature and longer reaction time were necessary for complete consumption of **1,3Si$_6$**, but ultimately compound **5.2a** could be isolated in 66% yield (Scheme 5.2.3). The observation of complete substitution

of Si–H bonds with minimal byproducts across two sets of cyclosilanes and three distinct thiophenols suggests a promising level of generality and may be appropriate for the synthesis of extended solids.

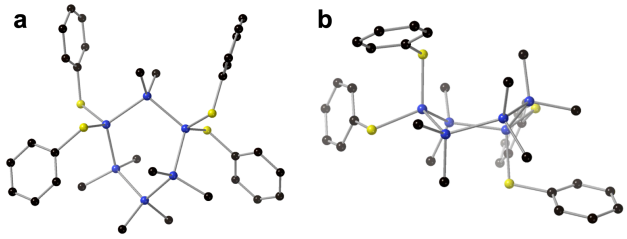

Figure 5.2.2 Displacement ellipsoid plots (50% probability level) of **5.2a** at 110(2) K a) Top down and b) side-on views. Hydrogens omitted for clarity. Black = carbon, blue = silicon, yellow = sulfur.

The crystal structure of **5.2a** was determined (Figure 5.2.2). The central cyclosilane ring adopted a twist-boat conformation in the solid state (Figure 5.2.2). This is distinct both from the 1,4-functionalized cyclosilane thioethers **5.1a-c** and from the crystal structure of a 1,3-tetraarylcyclosilane we previously reported.[16] As it has long been appreciated that oligosilanes have both lower barriers to conformational change than alkanes, we considered two hypotheses for the change in conformation: (1) the twist-boat conformation is lower energy than a chair conformation for **5.2a** or (2) the twist-boat conformation is not the lowest energy conformation, but attractive intermolecular aromatic interactions in the solid-state are maximized in the twist-boat conformation. To investigate these possibilities, we obtained gas-phase conformational data for isomeric **5.1a** and **5.2a**.

5.3 Conformational study via DFT calculations

To understand the conformational differences between **5.1a** and **5.2a** in their crystal structures, we used density functional theory (DFT) calculations to compare the energies of the chair and twist-boat conformers for both **5.1a** and **5.2a**. Geometries were fully

optimized starting from chair or twist-boat conformations respectively without symmetry restrictions using B3LYP hybrid exchange–correlation functional with the 6-311G(d) basis set. Crystal structures were used as starting geometries if applicable. Frequency calculations were performed with the same level of theory, to ensure optimized geometries were local minima on their potential energy surfaces. The calculation indicates that the chair conformation of **5.1a** is of lower energy than the twist-boat conformation by 2.43 kcal mol^{-1} (Table 5.3.1). However, for **5.2a**, the twist-boat conformer is lower energy by 3.06 kcal mol^{-1} compared to the chair conformer. These calculations suggest that the difference in cyclosilane conformation in the crystal structures of **5.1a** and **5.2a** should also be reflected in the gas-phase or solution where intermolecular attractions might be minimized. We hypothesize that 1,3-diaxial interactions between pseudoaxial thiophenol substituents are minimized in the twist-boat conformation.

Table 5.3.1 Calculated energies of conformers **5.1a** and **5.2a**.

Structures	Energies (E_h)		$\Delta E_{chair\text{-}twist}$ (E_h)	$\Delta E_{chair\text{-}twist}$ (kcal mol^{-1})
	chair	twist		
5.1a	-4576.377926	-4576.374056	-0.00387	-2.43
5.2a	-4576.370076	-4576.374962	0.00489	3.07

5.4 Time dependent DFT (TD-DFT) calculations

As oligosilane optical properties are conformation-dependent, these observations suggested that the structural isomers **5.1a** and **5.2a** could have distinct optical properties. Quantum chemical calculations would allow us to directly compare the twist-boat and chair conformers in **5.1a** and **5.2a**, while experimental spectra would reflect different populations of conformers.

Different combinations of functionals and levels of theory were examined by comparing the simulated UV-vis spectra of **5.1a** to the experimental results (Figure 5.4.1). The PBE0 functionals with the 6-311G(d) basis set was selected for its best match of onset and λ_{max} absorption compared to the experimental spectrum (Figure 5.4.1). This combination was previously reported for studying electronic transitions in linear hexasilanes and poly(cyclosilane)s.[20,32] The number of states of TD-DFT calculations was set as 50, as the simulated spectra with higher number of states better matched the broad absorption band from 220 nm to 320 nm in the experimental results (Figure 5.4.2).

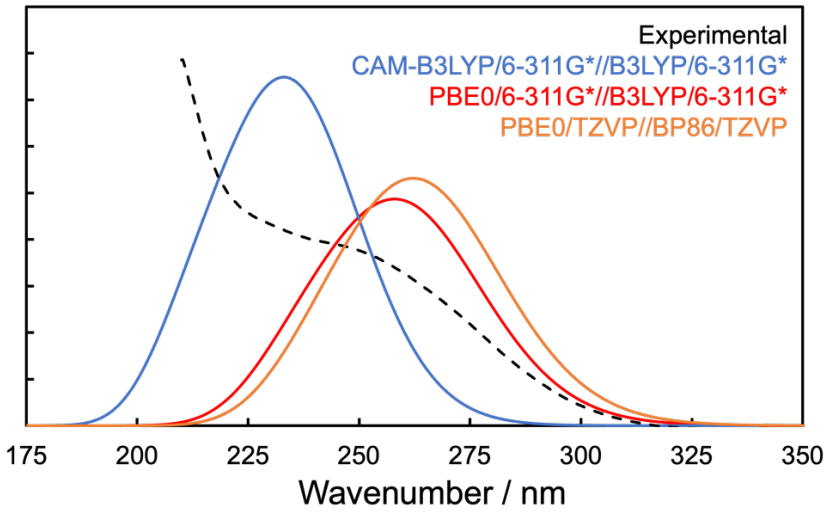

Figure 5.4.1 Comparison of experimental UV-vis spectra and simulated spectra with different functionals and levels of theory.

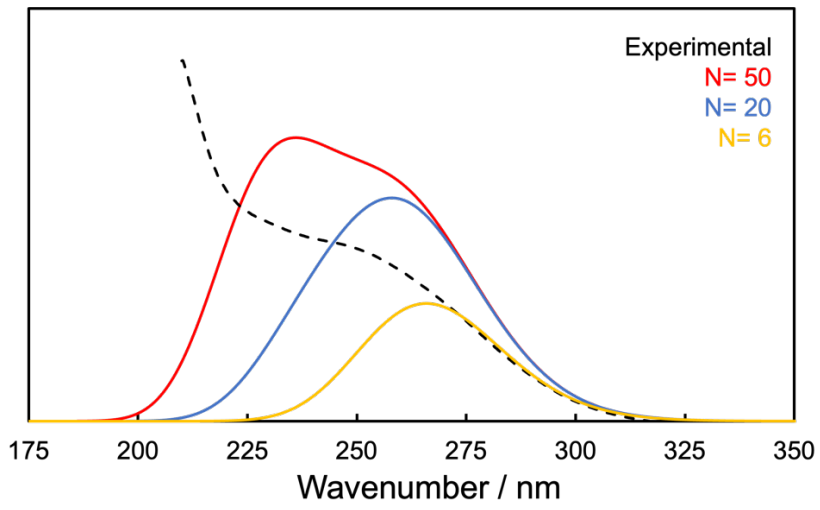

Figure 5.4.2 Comparison of experimental UV-vis spectra and simulated spectra with different numbers of states (N). TD-PBE0/6-311G(d)//B3YLP/6-311G(d).

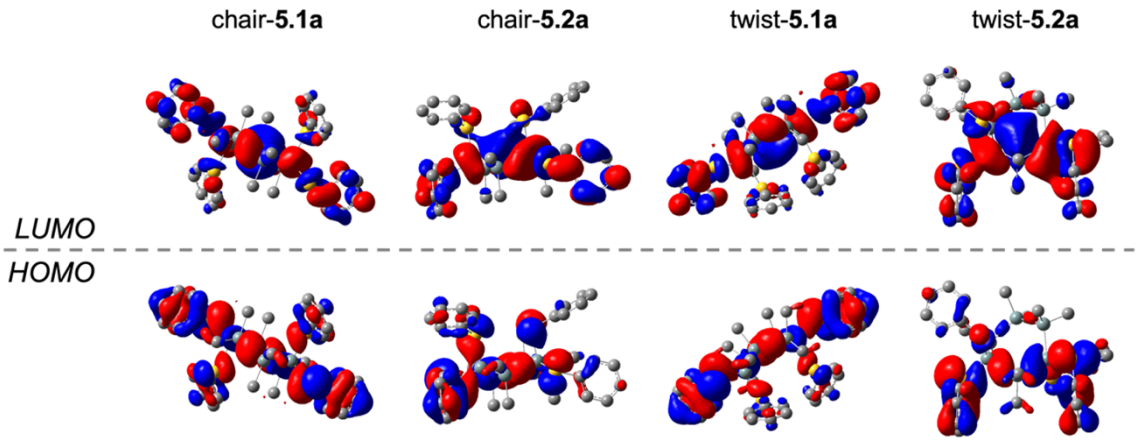

Figure 5.4.3 Calculated frontier orbitals of chair and twist-boat conformers of **5.1a** and **5.2a**. H atoms omitted for clarity. TD-PBE0/6-311G(d)//B3YLP/6-311G(d). Isovalue=0.02.

Conformation-dependent π,n,σ-conjugation in the cyclosilane thioethers was investigated by TD-DFT calculations for both **1,4Si$_6$** and **1,3Si$_6$**-derived compounds. The calculated frontier orbitals of chair cyclosilane thioethers are shown in Figure 5.4.3. The HOMO of chair-**5.1a** delocalizes across the silane ring and all four thioethers. In chair-

5.2a, the electron density on the phenyl groups decreased and the HOMO was predominantly observed on one of the equatorial phenyl groups. LUMOs of chair-**5.1a** and chair-**5.2a** are mostly situated on the silicon frameworks and the equatorial thioethers.

The frontier orbitals of the twist-boat conformers were also studied (Figure 5.4.3). Both HOMOs and LUMOs delocalize across silicon frameworks, sulfur atoms and the equatorial phenyl groups. Interestingly, pseudo π^* orbitals were observed for the LUMO+1 of all four conformers (Figure 5.4.4). These orbitals are assembled by in-phase interaction of σ^*(Si-C/S), similar to the LUMOs of decasilahexahydrotriquinacene and decasilaisotwistane reported by Kyushin.[6] We note that such pseudo π^* orbitals were found partially broken in twist-**5.1a** and chair-**5.2a** (Figure 5.4.4).

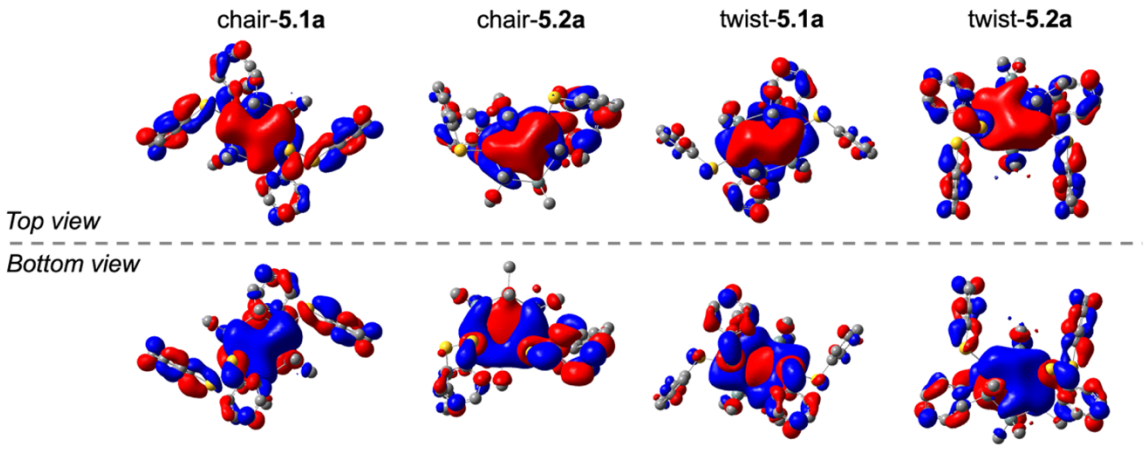

Figure 5.4.4 The LUMO+1 orbital of **5.1a** and **5.2a**. H atoms omitted for clarity. Discontinued pseudo π* orbitals were found on twist-**5.1a** and chair-**5.2a**. TD-PBE0/6-311G(d)//B3YLP/6-311G(d). Isovalue=0.02.

Table 5.4.1. Calculated vertical electronic transitions in cyclosilane thioethers. Only transitions of wavelength above 230 nm and oscillator strength above 0.05 are shown. Relative contributions given in percentages, where H = HOMO and L = LUMO. Assignments are shown if the relative contribution is higher than 10%.

Structure	λ (nm)	f	Assignment	Structure	λ (nm)	f	Assignment
chair-**5.1a**	267.3	0.181	H → L+1 (51.3%)	chair-**5.2a**	288.4	0.102	H → L (84.3.1%)
			H-2 → L (32.8%)		276.7	0.111	H-2 → L (86.4%)
	262.8	0.143	H-1 → L (73.0%)		242.6	0.060	H-2 → L+2 (26.5%)
			H → L+2 (12.0%)		234.4	0.107	H-4 → L+1 (31.1%)
	259.0	0.131	H-3 → L+1 (61.1%)				H-5 → L+1 (17.9%)
			H → L+1 (11.1%)	twist-**5.2a**	282.6	0.155	H → L (92.1%)
	257.5	0.066	H-2 → L (39.2%)		273.9	0.056	H → L+1 (74.5%)
			H → L+1 (24.0%)				H-1 → L (11.5%)
			H-3 → L+1 (11.1%)		269.1	0.09	H-1 → L (73.6%)
	241.8	0.069	H-1 → L+4 (27.2%)		264.1	0.057	H-2 → L (41.8%)
			H → L+6 (11.9%)				H-1 → L+1 (38.1%)
			H-3 → L+2 (10.8%)		244.5	0.059	H-4 → L (39.2%)
	237.2	0.072	H-2 → L+3 (32.0%)				H → L+2 (16.7%)
			H → L+6 (15.6%)		243.7	0.083	H-4 → L (36.8%)
	233.4	0.0624	H-2 → L+7 (16.6%)				H → L+2 (28.9%)
			H-1 → L+3 (10.8%)		234.4	0.053	H-5 → L+1 (77.1%)
	232.8	0.0646	H-1 → L+3 (35.6%)				
			H-5 → L+1 (14.2%)				
	230.9	0.0679	H-3 to L+2 (31.0%)				
			H-4 to L (15.9%)				
			H-2 to L+8 (12.7%)				
twist-**5.1a**	268.7	0.137	H-2 → L (49.0%)				
			H-1 → L (16.7%)				
			H → L+3 (11.6%)				
	266.3	0.097	H-1 → L+1 (49.9%)				
			H-2 → L+1 (26.2%)				
	259.6	0.098	H-1 → L (31.1%)				
			H-2 → L+1 (26.7%)				
			H-1 → L+1 (19.5%)				
	244.0	0.051	H → L+2 (25.6%)				
			H-1 → L+6 (21.5%)				
	243.2	0.091	H-1 → L+4 (27.4%)				
			H-2 → L+4 (10.2%)				
	242.3	0.112	H → L+3 (31.0%)				
			H-2 → L+4 (17.1%)				
	237.1	0.052	H-2 → L+2 (48.8%)				
			H-1 → L+3 (13.9%)				

Electronic transitions in the cyclosilane thioethers are affected by both conformation and connectivity. In the twist and chair **1,4Si$_6$**-derived thioethers, the HOMO → LUMO transition is symmetry forbidden (Table 5.4.1). For chair-**5.1a**, the HOMO → LUMO+1 transition is dominant. However, for twist-1a, the HOMO-2 and HOMO-1 →

LUMO both contribute to the predicted lowest-energy vertical transition. Chair-**5.1a** also shows a more pronounced absorption feature at 260 nm compared to twist-**5.1a** in the simulated UV-vis spectra (Figure 5.4.5a).

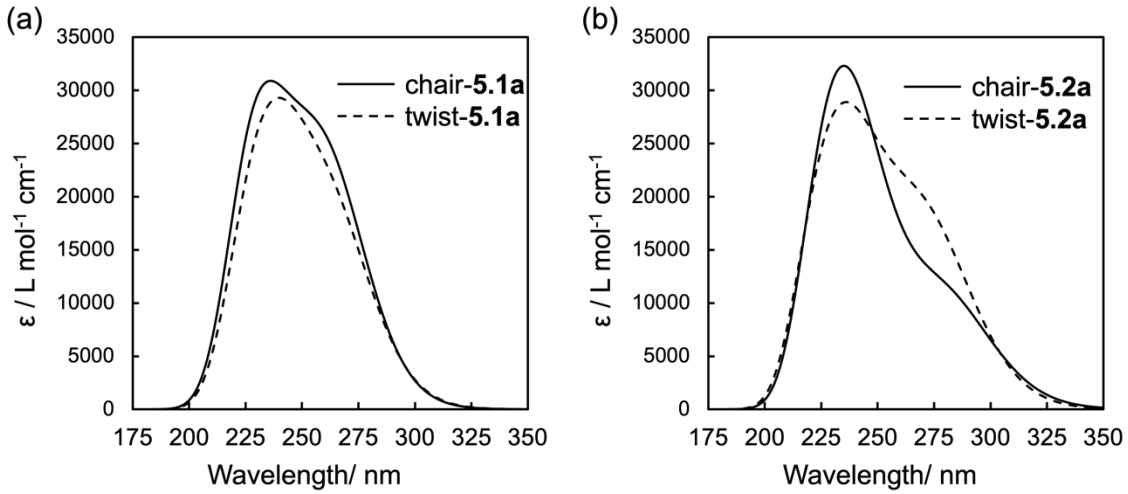

Figure 5.4.5 Simulated UV-vis spectra of (a) **5.1a** and (b) **5.2a**. Solid lines: chair conformations. Dotted lines: twist-boat conformations. TD-PBE0/6-311G(d)//B3YLP/6-311G(d).

Table 5.4.2. Calculated vertical electronic transitions in cyclosilane thioethers. H = HOMO and L = LUMO.

Transition	chair-**5.1a**	twist-**5.1a**	chair-**5.2a**	twist-**5.2a**
H → L	5.48 eV	5.41 eV	5.20 eV	5.28 eV
H → L+1	5.52 eV	5.47 eV	5.51 eV	5.37 eV

In contrast, in chair and twist **1,3Si$_6$**-derived thioethers the HOMO → LUMO transition is allowed (Table 5.4.2), as well as other higher-energy transitions. Twist-**5.2a** has a stronger absorption at 275 nm than chair-**5.2a** (Figure 5.4.5b), resulting from a wider HOMO → LUMO+1 gap in chair-**5.2a** (Table 5.4.3). The LUMO+1 of chair-**5.2a** is found to be a partially broken pseudo π^* orbital (Figure 5.4.4). The discontinued conjugation

raises its energy level, requiring higher energy for HOMO → LUMO+1 transition in chair-**5.2a**.

TD-DFT calculations also facilitated the study of isomeric compounds that have not yet been synthesized. We probed the influence of sulfur connectivity by comparing Ar–S–Si in **5.1b** and MeS–Ar–Si in **5.3** (Figure 5.4.6). In structure **5.3**, sulfur atoms are substituents on the phenyl rings**,** rather than inserted between the cyclosilane and aromatic groups. Cyclosilane thioether **5.1b** has frontier orbitals similar to **5.1a** (Figure 5.4.6).

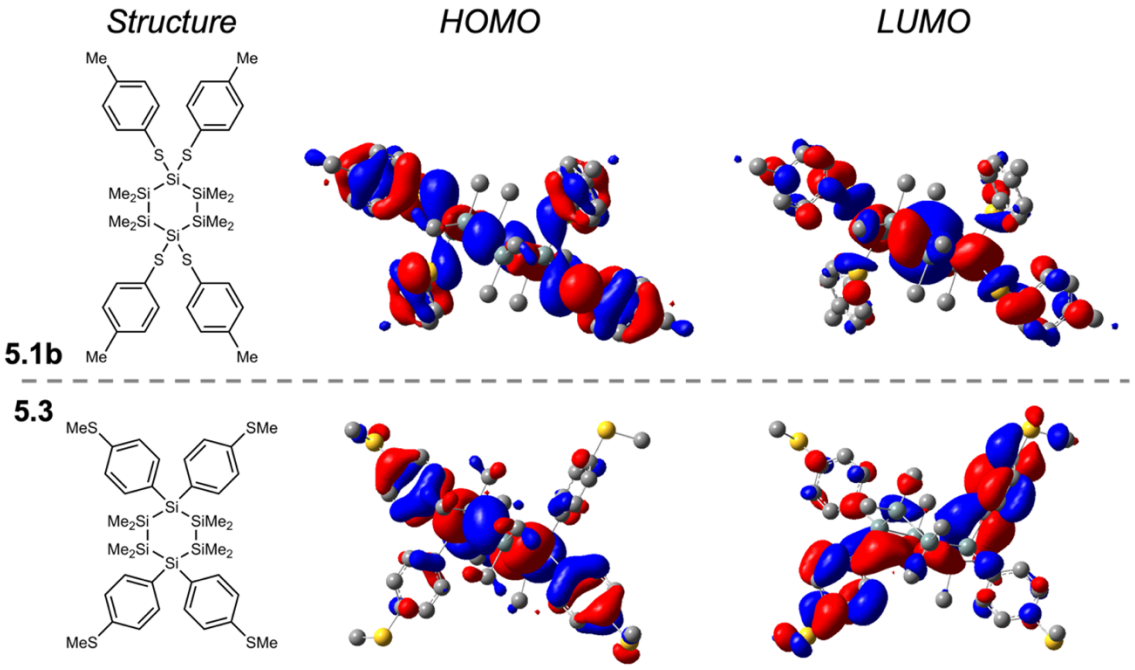

Figure 5.4.6 Comparison of calculated HOMO and LUMO of **5.1b** to its isomeric structure **5.3**. Hydrogen atoms omitted for clarity. TD-PBE0/6-311G(d)//B3YLP/6-311G(d). Isovalue=0.02.

Tetraaryl cyclosilane **5.3** however has a HOMO mainly localized on the equatorial aromatics and the LUMO at the axial aromatics. No pseudo π^* orbital delocalizing through the silicon framework was found in **5.3**. Its LUMO+1 is majorly formed by the π* orbitals of axial phenyl groups (Figure 5.4.7). These results suggest sulfur incorporation (n-electron

donors) facilitates the delocalization between silicon frameworks (σ-conjugation) and aromatic rings (π-conjugation).

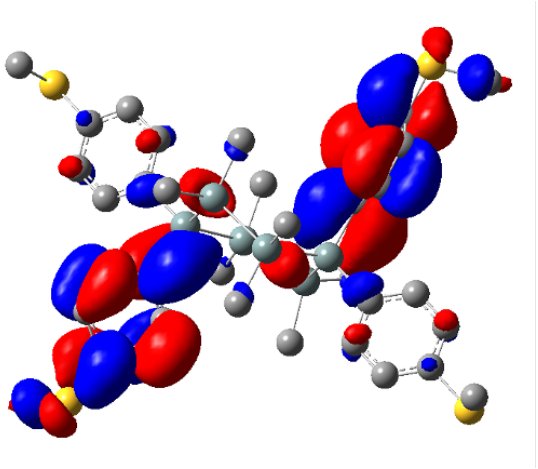

Figure 5.4.7 The LUMO+1 orbital of **5.3**. No pseudo π* orbital delocalizing through the silicon framework was found. Hydrogen atoms omitted for clarity. TD-PBE0/6-311G(d)//B3YLP/6-311G(d). Isovalue=0.02.

5.5 UV-vis spectroscopy

Experimental UV-vis spectra were obtained to evaluate the computational predictions. We first compared the solution-phase UV-vis spectrum of **5.1a** to thiophenol and **1,4Si$_6$**. The cyclosilane thioether exhibited a broad absorption band at 258 nm, which was red-shifted relative to both thiophenol and **1,4Si$_6$** (Figure 5.5.1a). The experimentally observed transition is consistent with the TD-DFT calculated spectrum, which predicted λ_{max} of 260 nm (Figure 5.5.1a). Compared to non-sulfur-incorporated cyclosilane **1,4Si$_6$Ph$_4$**, **5.1a** also exhibited a red-shifted absorption band (Figure 5.5.1b). This observation agrees with the predication made by TD-DFT calculations that sulfur incorporation facilitates delocalization between the π- and σ-fragments. The cyclosilane thioethers **5.1b** and **5.1c** had very similar UV-vis spectra to **5.1a** with respect to the onset of absorption and overall peak shape (Figure 5.5.1c), consistent with the frontier orbital

calculations (Figure 5.5.2 and Table 5.5.1). These observations suggest delocalization of the π- and σ-conjugated systems through the sulfur lone pair and that moderately electron-donating or withdrawing aromatic substituents do not strongly impact that delocalization.

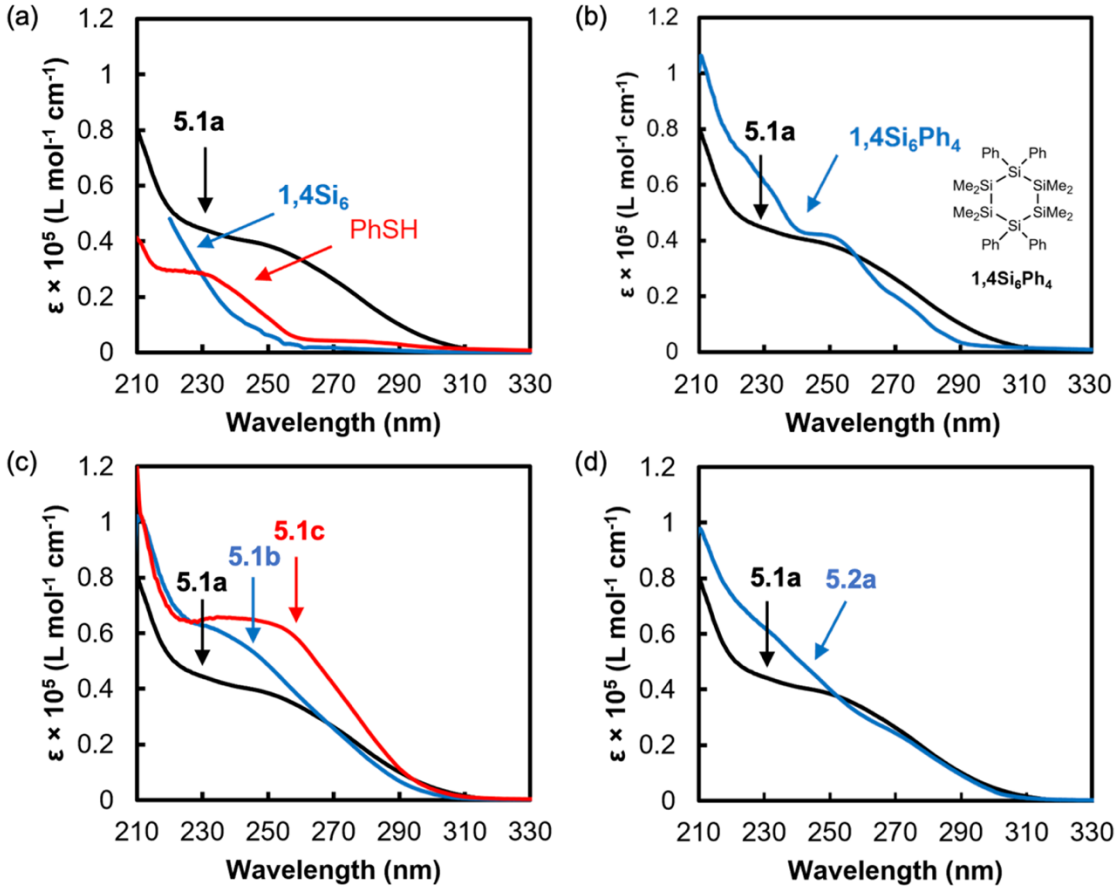

Figure 5.5.1 Solution-phase UV-vis spectra ([compound] = 0.01 mM, THF). a) Comparison of thioether **5.1a** to thiophenol and **1,4Si$_6$** demonstrates red-shift in absorbance. b) Comparison of thioether **5.1a** to **1,4Si$_6$Ph$_4$** demonstrates delocalization between the π- and σ-fragments. c) Comparison of cyclosilane thioethers **5.1a-c**. c) Comparison of isomer cyclosilane thioethers **5.1a** and **5.2a**.

Comparison of the UV-vis spectra of **5.1a** and **5.2a** validated the predictions made by TD-DFT calculations. We predicted similar absorption features for chair-**5.1a** and twist-**5.2a**, the lowest-energy conformers of each cyclosilane thioether (Figure 5.4.5). Despite

stronger absorbance at 230 nm, **5.2a** exhibits similar absorption bands compared to **5.1a** in the experimental UV-vis spectra (Figure 5.5.1d), which agrees with computational studies as we discussed above.

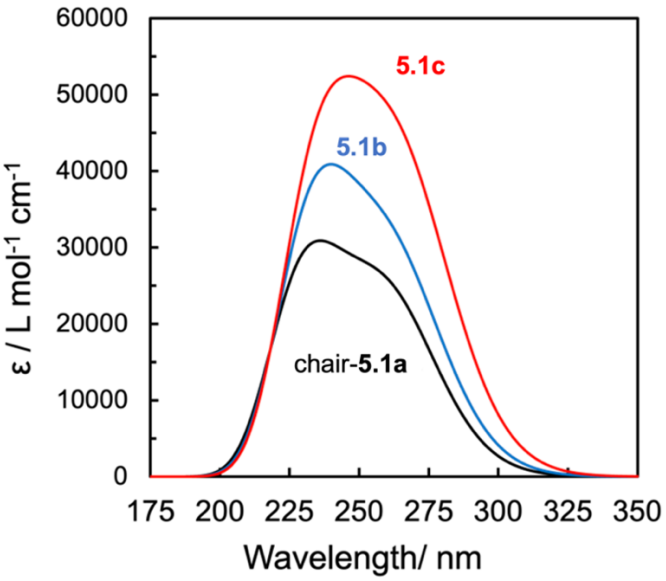

Figure 5.5.2 Simulated UV-vis spectra of chair-**5.1a** (black), **5.1b** (blue) and **5.1c** (red). TD-PBE0/6-311G(d)//B3YLP/6-311G(d).

Table 5.5.1. Calculated band gaps in chair-**5.1a**, **5.1b** and **5.1c.** H = HOMO and L = LUMO. TD-PBE0/6-311G(d)//B3YLP/6-311G(d).

Transition	chair-**5.1a**	**5.1b**	**5.1c**
H → L	5.48 eV	5.42 eV	5.36 eV
H → L+1	5.52 eV	5.46 eV	5.38 eV

5.6 Conclusion

We investigated the effect of conformation and connectivity on conjugation of isomeric cyclosilane thioethers. We prepared thioethers **5.1a-c** and **5.2a** through the $B(C_6F_5)_3$-catalyzed dehydrocoupling of various thioethers and partially hydrogenated

cyclohexasilanes **1,4Si$_6$** and **1,3Si$_6$**. These reactions run with high chemoselectivity for Si-H bonds in the presence of Si-Si bonds, preserving the σ-framework. Their structures were confirmed using ^{1}H and ^{29}Si NMR spectroscopy and single crystal X-ray crystallography. X-ray crystal structures, as well as gas phase calculations, showed that cyclosilanes adopt different conformations depending on skeletal connectivity.

Computational studies were used to probe the factors that influence the photophysical properties of our π,n,σ-conjugated molecules. By comparing isomers **5.1b** and **5.3** using TD-DFT calculations, we see a lack of pseudo π* orbital delocalizing through the silicon framework when sulfur is not connected to both the cyclosilane and phenyl rings. Thus, the insertion of sulfur between the σ-conjugated and π-conjugated systems extends electron delocalization across the whole system.

We demonstrated the important influence of heteroatom substitution in facilitating π- and σ-conjugation in cyclosilane thioethers and observed that constitutional isomers can exhibit distinct conformations and patterns of delocalization. We expanded upon our prior work in building complex silicon building blocks and their precise functionalization. We described their photophysical activity through the use of computational and experimental data. The studies herein provide insight into the potential use of sulfur-influenced conjugated materials.

5.7 Reference

(1) West, R.; Carberry, E. *Science (80-.).* **1975**, *189*, 179–186.
(2) Carberry, E. A.; West, R.; Glass, G. E. *J. Am. Chem. Soc.* **1969**, *91*, 5446–5451.
(3) Heider, Y.; Scheschkewitz, D. *Chem. Rev.* **2021**, *121*, 9674–9718.
(4) Kanemitsu, Y.; Suzuki, K.; Kondo, M.; Kyushin, S.; Matsumoto, H. *Phys. Rev. B* **1995**, *51*, 10666–10670.
(5) Sekiguchi, A.; Yatabe, T.; Kabuto, C.; Sakurai, H. *J. Am. Chem. Soc.* **1993**, *115*, 5853–5854.
(6) Tsurusaki, A.; Koyama, Y.; Kyushin, S. *J. Am. Chem. Soc.* **2017**, *139*, 3982–3985.

(7) Marro, E. A.; Folster, C. P.; Press, E. M.; Im, H.; Ferguson, J. T.; Siegler, M. A.; Klausen, R. S. *J. Am. Chem. Soc.* **2019**, *141*, 17926–17936.
(8) Ferguson, J. T.; Jiang, Q.; Marro, E. A.; Siegler, M. A.; Klausen, R. S. *Dalt. Trans.* **2020**, *49*, 14951–14961.
(9) Jiang, Q.; Gittens, A. F.; Wong, S.; Siegler, M. A.; Klausen, R. S. *Chem. Sci.* **2022**, *13*, 7587–7593.
(10) Markov, J.; Fischer, R.; Wagner, H.; Noormofidi, N.; Baumgartner, J.; Marschner, C. *Dalt. Trans.* **2004**, *51*, 2166.
(11) Purkait, T. K.; Press, E. M.; Marro, E. A.; Siegler, M. A.; Klausen, R. S. *Organometallics* **2019**, *38*, 1688–1698.
(12) Hengge, E.; Wolfer, D. *Angew. Chemie Int. Ed. English* **1973**, *12*, 315–316.
(13) Folster, C. P.; Nguyen, P. N.; Siegler, M. A.; Klausen, R. S. *Organometallics* **2019**, *38*, 2902–2909.
(14) Folster, C. P.; Nguyen, P. N.; Klausen, R. S. *Dalt. Trans.* **2020**, *49*, 16125–16132.
(15) Press, E. M.; Marro, E. A.; Surampudi, S. K.; Siegler, M. A.; Tang, J. A.; Klausen, R. S. *Angew. Chemie Int. Ed.* **2017**, *56*, 568–572.
(16) Marro, E. A.; Press, E. M.; Siegler, M. A.; Klausen, R. S. *J. Am. Chem. Soc.* **2018**, *140*, 5976–5986.
(17) Folster, C. P.; Klausen, R. S. *Polym. Chem.* **2018**, *9*, 1938–1941.
(18) Marro, E. A.; Klausen, R. S. *Chem. Mater.* **2019**, *31*, 2202–2211.
(19) Jiang, Q.; Wong, S.; Klausen, R. S. *Polym. Chem.* **2021**, *12*, 4785–4794.
(20) Fang, F.; Jiang, Q.; Klausen, R. S. *J. Am. Chem. Soc.* **2022**, *144*, 7834–7843.
(21) Harrison, D. J.; Edwards, D. R.; McDonald, R.; Rosenberg, L. *Dalt. Trans.* **2008**, No. 26, 3401.
(22) Banovetz, J. P.; Hsiao, Y. L.; Waymouth, R. M. *J. Am. Chem. Soc.* **1993**, *115*, 2540–2541.
(23) Hsiao, Y.-L. L.; Waymouth, R. M. *J. Am. Chem. Soc.* **1994**, *116*, 9779–9780.
(24) Kayser, C.; Kickelbick, G.; Marschner, C. *Angew. Chemie Int. Ed.* **2002**, *41*, 989–992.
(25) Gilman, H.; Lichtenwalter, G. D. *J. Am. Chem. Soc.* **1958**, *80*, 608–611.
(26) Fischer, J.; Baumgartner, J.; Marschner, C. *Science (80-.).* **2005**, *310*, 825.
(27) Ishikawa, M.; Kumada, M. *J. Chem. Soc. D Chem. Commun.* **1969**, No. 10, 567b – 568.
(28) Rosenberg, L. *Macromol. Symp.* **2003**, *196*, 347–353.
(29) Yamamoto, K.; Kumada, M.; Nakajima, I.; Maeda, K.; Imaki, N. *J. Organomet. Chem.* **1968**, *13*, 329–341.
(30) Lee, P. T. K. K.; Skjel, M. K.; Rosenberg, L. *Organometallics* **2013**, *32*, 1575–1578.
(31) Lee, P. T. K.; Rosenberg, L. *Dalt. Trans.* **2017**, *46*, 8818–8826.
(32) Kanazawa, Y.; Tsuji, H.; Ehara, M.; Fukuda, R.; Casher, D. L.; Tamao, K.; Nakatsuji, H.; Michl, J. **2016**, 3010–3022.

Chapter 6: Impact of stereoregularity on hybrid conjugated polymers

6.1 Introduction

Stereoregularity in the polymer results in pronounced differences in thermal, mechanical and optical properties, and thus well-defined stereoregular polymers are of great interest in both synthesis and applications for decades.[1] In 1927, Staudinger predicted that the main-chain stereochemistry of a polymer would lead to the change of its physical properties[2], and Schildknecht reported the synthesis of the first stereoregular polymer, polyvinyl alkyl ether.[3] The stereoregular polyolefin synthesis catalyzed by transition-metal catalysts has been extensively studied.[4,5]

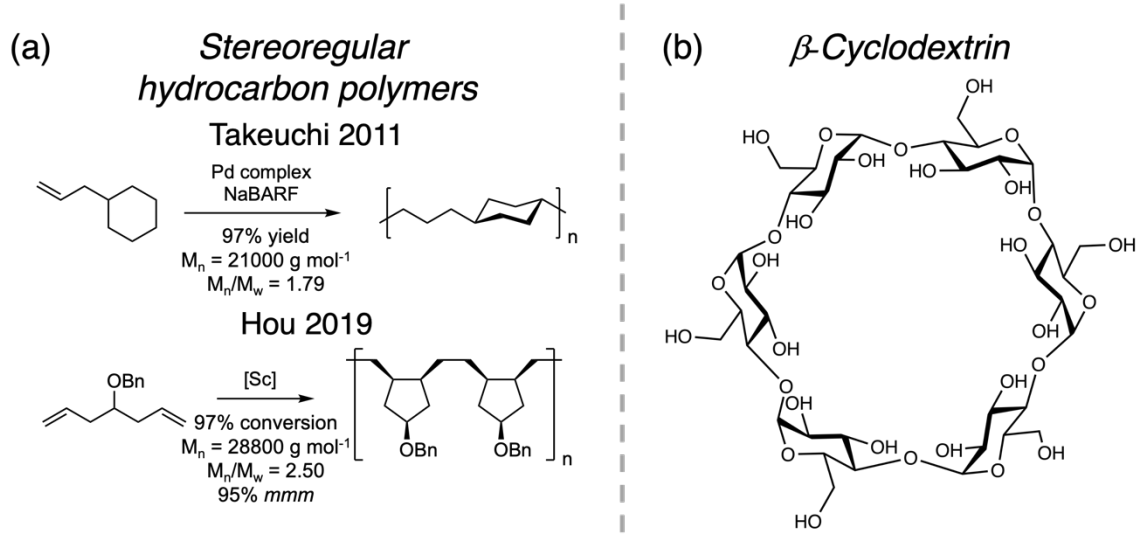

Scheme 6.1.1 Stereoregular polymeric structures containing cyclic units. (a) Stereoregular hydrocarbon polymers. (b) β-Cyclodextrin.

The synthesis of organic polymers with cyclic repeating units in the main chain is an emerging field for their unique physical properties compared to linear polyolefins, including higher melting (T_m) or glass-transition temperatures (T_g), control of polymer rigidity and optical transparency.[6–8] Promotion of stereoregularity of these polymers further improves the beneficial properties. Takeuchi reported a precise isomerization

polymerization of alkenylcyclohexanes yielding stereoregular polymers containing six-membered rings in the polymer backbone (Scheme 6.1.1a).[7] Higher T_g were observed when the ratio of cyclohexyl units increased. More recently, Hou demonstrated the synthesis of functionalized cyclic polyolefins with high isotacticity through the scandium-catalyzed cyclopolymerization of functionalized α,ω-dienes (Scheme 6.1.1a).[8]

The macromolecular structures with stereoregularity can also be constructed with pre-defined stereoregular building blocks. β-Cyclodextrin is an example of highly regulated structures in nature and has found its way in industrial utilization (Scheme 6.1.1b).[9] It is assembled by glucopyranosides, six-membered carbohydrate rings with multiple stereogenic centers.

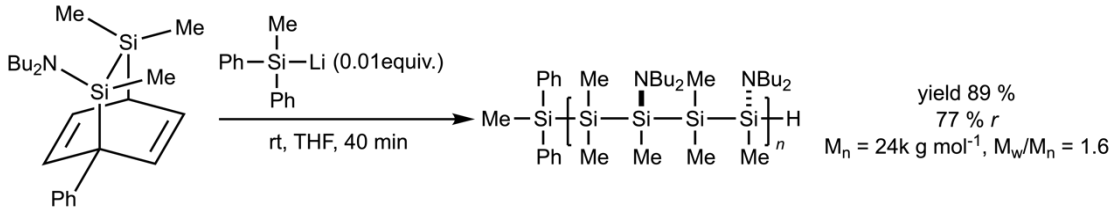

Scheme 6.1.2 Anionic ROP of amino-functionalized masked disilene.

Control of polysilane main-chain stereoregularity, however, has been a long-term challenge to synthetic chemists. The difficulties are from both synthetic methods and characterization of the structures.[10] Though Wurtz polymerization and dehyrocoupling polymerization generated the atactic polysilanes, anionic ring-opening polymerization (ROP) gave some success in the field.[10] Matyjaszewski reported the ROP of all-*trans* cyclotetrasilane resulting in an isotactic polysilane.[11] More recently, polymerization of the amino-functionalized masked disilene was reported by Sakurai and the resulting polysilane was found to be predominately syndiotactic (Scheme 6.1.2).[12] On the other hand, a lack of stereoisomerically pure small molecule model compounds makes the tacticity assignment

of polysilanes complicated through NMR.[10] Conflicting identifications of tacticity were reported in the case of poly(SiMePh) from references.[11,13–15]

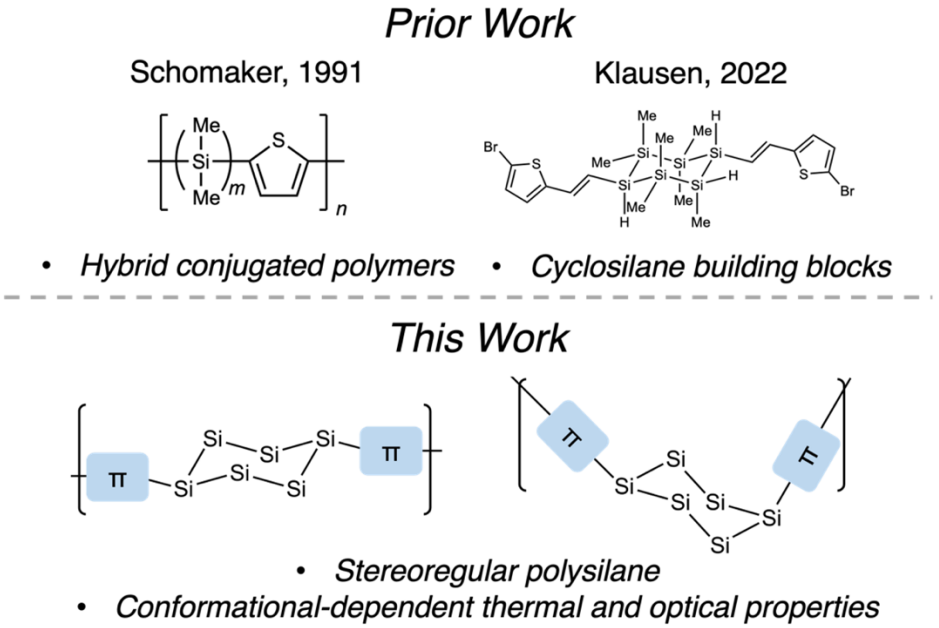

Scheme 6.1.3 (a) Prior work: hybrid conjugated polymer containing linear silane units. (b) Stereoregular polysilane synthesized with cyclosilane building blocks.

The organosilicon materials containing hybrid σ,π-conjugated structures have raised broad interest for their unique optoelectronic properties and potential applications in photoresists, emitting polymers and semiconductive materials.[16] Plenty of study in this field has pursued to increase the structural diversity of π-conjugated units.[17–20] However, the σ fragments in these materials were largely limited to linear oligosilanes[21] (Scheme 6.1.2) due to the limited suitable silane building blocks and synthetic methods.[22] The Klausen lab has extensively explored the design, synthesis, and polymerization of cyclosilanes.[23–26] We recently described a highly selective synthesis of σ,π-conjugated cyclosilanes through $RuHCl(CO)(PPh_3)_3$-catalyzed hydrosilylation.[27] As initial examples,

the copolymerization of the *trans*-bis(thienylvinyl)cyclosilane with dibromo building blocks was also demonstrated.

Herein, we report the synthesis of hybrid conjugated stereoregular polysilanes using *trans* and *cis* cyclosilane building blocks as stereochemically pre-defined monomers. The stereochemistry on cyclosilanes was preserved in the polymerization, enabling well-defined stereoregularity. We observed that stereoregular polysilanes exhibited more pronounced phase transition behaviors in DSC measurements and had more distinct absorption bands in the UV-vis spectra compared to atactic polysilanes. Influence of silane structures (cyclic *versus* linear) and vinyl group incorporation on the polysilane properties was also examined.

6.2 Stereoregular hybrid σ,π-conjugated polymers

We have reported the copolymerization of the building block *trans*-**6.1** and 2,5-dibromothiophene (Table 6.2.1, Entry 1).[27] The building block *trans*-**6.1**, isolated in high diastereomeric purity after recrystallization, can be elaborated to conjugated polymer **P6.1** by Mg/Br exchange[28,29] followed by $NiCl_2$dppp-catalyzed Kumada polycondensation in the presence of PPh_3 ligands (Table 6.2.1, Entry 1). Herein, the reaction conditions were further investigated by varying catalyst and ligand species (Table 6.2.1). At this time, the focus continued to be on Ni-catalyzed Kumada polycondensation as Ni does not cleave Si–Si bonds, whereas the Pd catalysts employed in Stille or Suzuki polycondensation are known to cleave Si–Si bonds.[30–32]

Under the $NiCl_2$dppp-catalyzed conditions, low conversions of starting materials were observed with no additional ligands (Table 6.2.1, Entry 2). Although excess ligands are not usually required in the Kumada catalyst-transfer polycondensation (KCTP) making

poly(3-hexylthiophene)[33], the similar low yield was reported in Kumada couplings of heteroaryl chlorides and lithium tri(quinolyl)magnesates catalyzed by $Ni(acac)_2$ and dppp.[34] The low conversions might arise from a different copolymerization mechanism rather than KCTP. The cyclosilane silane building blocks lacked a continuous π-conjugated backbone, and prevented the Ni catalyst from "walking" along the polymer chain.[33] Therefore, the catalyst required regeneration after a growth of each unit. PPh_3 ligand might improve catalyst recovery and therefore result in a higher conversion of monomers.

Table 6.2.1. Variation of **P6.1** molecular weight characteristics with Ni catalysts and ligands. The relative configuration was maintained in the polymerization (highlighted in red).

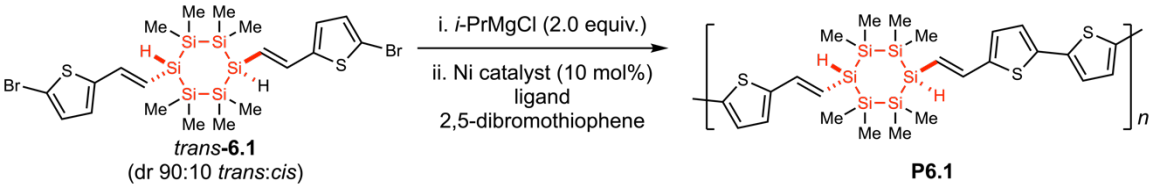

Entry	Catalyst	Ligand	M_n (g mol^{-1}) [a]	M_w/M_n [a]	Yield
1[b]	$NiCl_2$dppp	PPh_3	6.70k	2.63	78%
2	$NiCl_2$dppp	n/a	-	-	Low conversion
3	$NiCl_2$dppp	dppp	-	-	Low conversion
4	$NiCl_2(PPh_3)_2$	PPh_3	4.77k	2.05	63%
5	$NiCl_2(PPh_3)_2$	n/a	4.94k	2.08	65%
6	$NiCl_2(PPh_3)_2$	dppp	4.32k	2.02	55%

[a] Determined by size exclusion chromatography relative to polystyrene standards at 254 nm (THF, [copolymer] = 1 mg mL^{-1}, 40 °C, 0.35 mL min^{-1}, 10 µL injection). [b] Previously reported in reference.[27]

Further experimental exploration supported the above hypothesis. Additional dppp ligands did not improve the polymerization (Table 6.2.1, Entry 3). However, reasonable starting material conversion and molecular weight characteristics of products were

observed in $NiCl_2(PPh_3)_2$-catalyzed polymerizations regardless of the ligand species and amount (Table 6.2.1, Entry 4-6). The reaction condition described in Table 6.2.1, Entry 1 was chosen as the general polymerization condition because of the relatively high molecular weight of products.

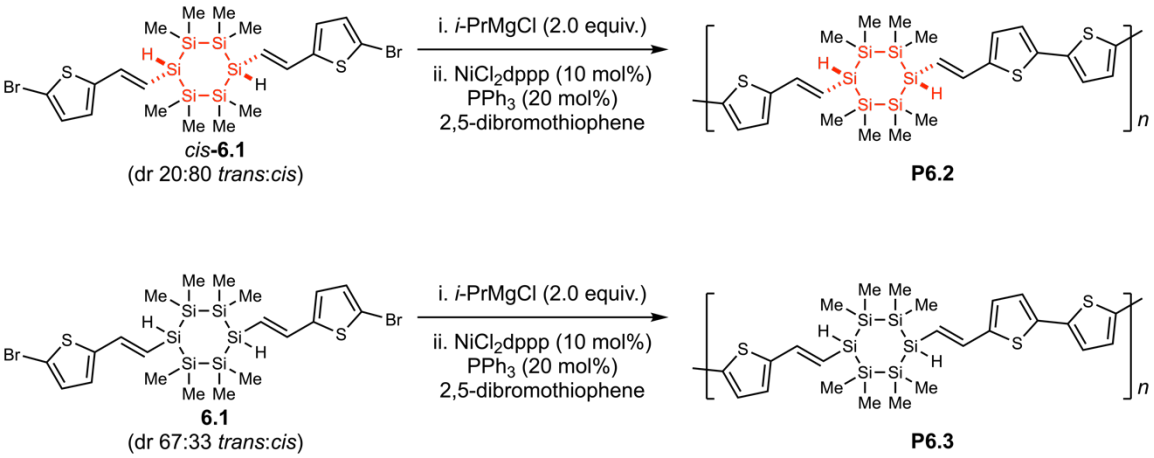

Scheme 6.2.1. Synthesis of hybrid conjugated polymers **P6.2** (predominately *cis*) and **P6.3** (atactic). The relative configuration was maintained in the polymerization (highlighted in red).

Under the optimized polymerization condition, we have now synthesized the stereoisomers of **P6.1** (Table 6.2.1) by variation of the diastereomeric ratio in the starting monomer **6.1**, yielding **P6.2** (predominantly *cis*) and **P6.3** (atactic). We note that *cis*-**6.1** (dr 20:80 *trans*:*cis*) was enriched in the filtrate of **6.1** recrystallization. Similar molecular weight characteristics were determined for all three macromolecules by size exclusion chromatography (Table 6.2.2). However, solubilities of these polymers in $CDCl_3$ were found to be dependent on the degree of stereoregularity (Figure 6.2.1). The atactic **P6.3** formed a clear solution in $CDCl_3$ at room temperature, whereas the stereoregular **P6.1** and **P6.2** both made orange suspension in $CDCl_3$ at the same concentration. The observation

was consistent with polymers of higher crystallinity exhibiting lower solubility in the solution.

Table 6.2.2. Molecular weight characteristics of hybrid conjugated polysilanes.

Cyclosilane	dr (*trans:cis*)	Polymer	M_n (g mol^{-1}) [a]	M_w/M_n [a]	Yield (%)
trans-**6.1**[b]	90:10	**P6.1**	6706	2.63	78
cis-**6.1**	20:80	**P6.2**	6382	2.66	73
6.1	63:37	**P6.3**	6883	2.59	63

[a] Determined by size exclusion chromatography relative to polystyrene standards at 254 nm (THF, [copolymer] = 1 mg mL^{-1}, 40 °C, 0.35 mL min^{-1}, 10 µL injection). [b] Previously reported in reference.[27]

Figure 6.2.1 Solubility characteristics of (left to right) **P6.1**, **P6.3**, and **P6.2** (25 mg polymer in 0.7 mL $CDCl_3$).

The Si-H bonds are known to be diagnostic for NMR spectroscopy[23–25], and the comparison of ^{29}Si NMR spectra of cyclosilane monomers to polysilanes identified the preserved stereochemistry of cyclosilane units in the copolymerization. The *Si*H resonances of cyclosilane conformers had distinct chemical shifts in ^{29}Si NMR spectra:

64.5 ppm for *trans*-**6.1** and 63.0 ppm for *cis*-**6.1** (Figure 6.2.2). Polysilane **P6.1-3** had similar *Si*H resonances to the monomers. Distinct peaks were found at 63.0 and/or 64.8 ppm depending on the diastereomer ratio of their starting cyclosilanes. These features confirmed the remained stereochemistry of the cyclosilane rings and no Si-Si bond cleavage in presence of the Ni catalyst in the polycondensation.

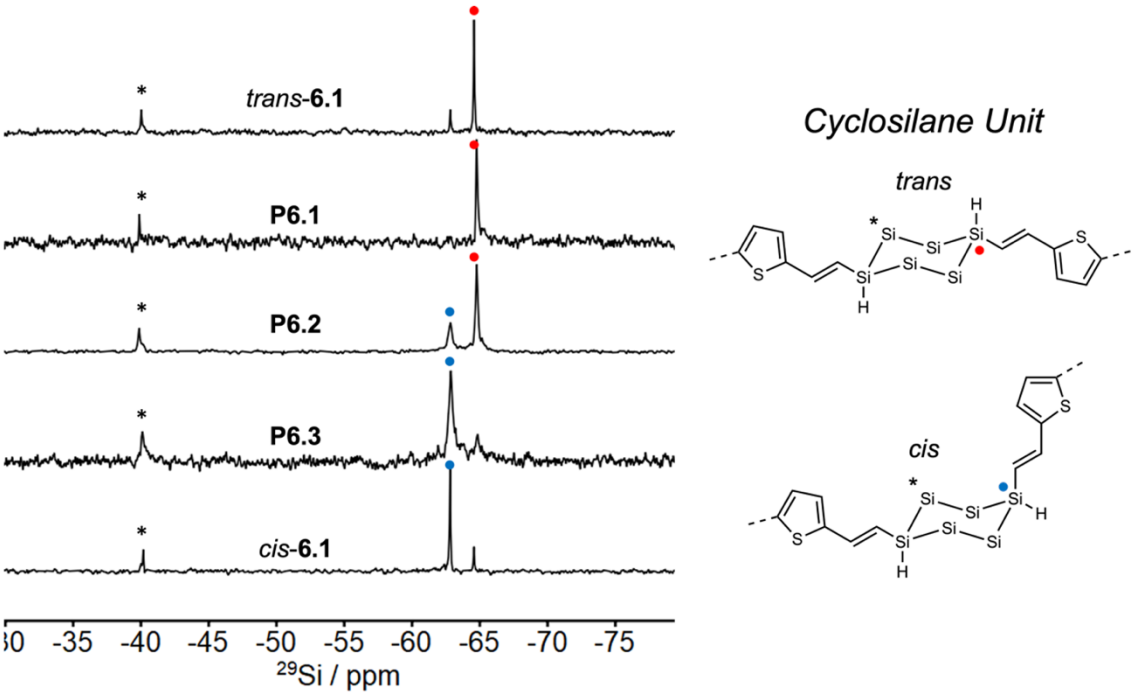

Figure 6.2.2 Cropped ^{29}Si {^{1}H} DEPT spectra (79 MHz, $CDCl_3$) comparing (top to bottom) *trans*-**6.1** (dr 90:10 *trans:cis*), **P6.1**, **P6.2**, **P6.3** and *cis*-**6.1** (dr 20:80 *trans:cis*). $^{1}J_{Si-H}$ = 120 Hz. DEPT = distortionless enhancement by polarization transfer. The methyl groups are omitted for clarity.

6.3 Synthesis of hybrid conjugated polymers containing linear silane units

To address the effect of cyclosilane units on the conjugated polymer properties, a linear silane building block **6.2** was synthesized through $RuHCl(CO)(PPh_3)_3$-catalyzed hydrosilylation using dihydrodisilane and bromoethynylthiophene (Figure 6.3.1a).

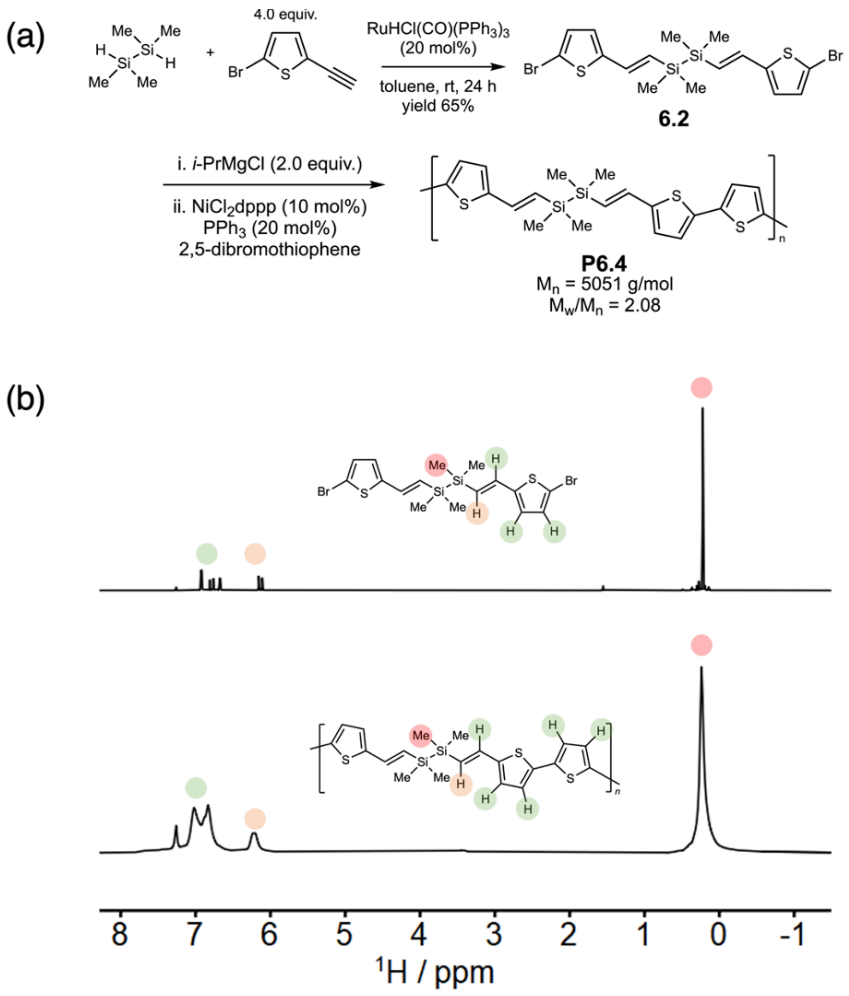

Figure 6.3.1. (a) Synthesis of linear silane building block **6.2** and its polycondensation with dibromothiophene yielding **P6.4**. (b) ^{1}H NMR spectra (400 MHz, $CDCl_3$) of **6.2** (top) and **P6.4** (bottom).

The ^{1}H NMR spectrum confirmed a depletion of Si-H groups for the absence of resonances in 3.0-4.0 ppm, where Si*H* resonances were usually identified (Figure 6.3.1). The coupling constant analysis of alkenyl resonances indicated the selective formation of *(E)*-alkene, which was consistent with literatures.[27,35] The building block **6.2** was then copolymerized with 2,5-dibromothiophene producing the linear silane analog of σ,π-conjugated polysilane (Scheme 6.3.1). The resulting polysilane **P6.4** (M_n = 5051 g mol^{-1}, M_w/M_n = 2.08) was a red powder which was fully soluble in $CDCl_3$. The Si-Me, alkenyl

and thienyl resonances in the ^{1}H NMR spectrum broadened after the copolymerization also indicating the formation of polymeric structures (Figure 6.3.1).

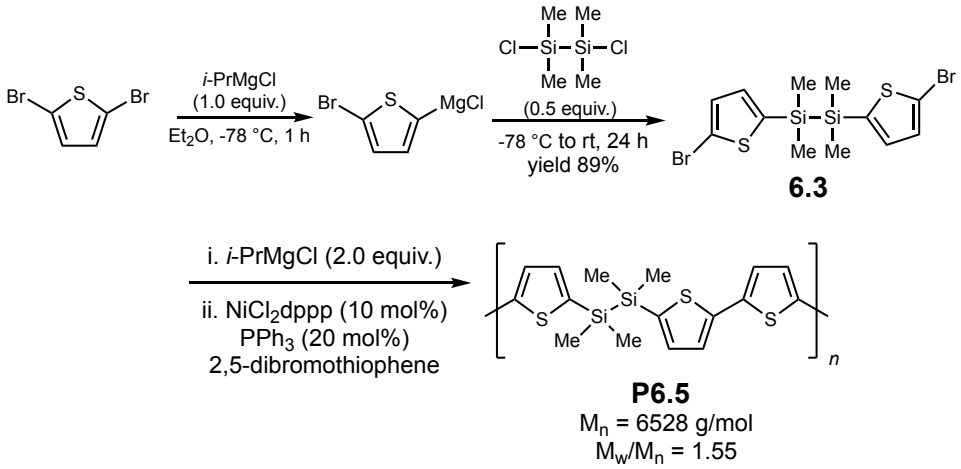

Scheme 6.3.1. Synthesis of linear silane building block **6.3** and its polycondensation with dibromothiophene yielding **P6.5**. Adapted from known procedure.[20]

Known polysilane **P6.5** was synthesized as a comparison to **P6.4** to investigate the influence of vinyl fragments on the thermal and optical properties. The stoichiometrical Mg/Br exchange on one side of 2,5-dibromothiophene was conducted at -78 °C in diethyl ether. Then the bromothienyl magnesium chloride was coupled to dichlorodisilane, affording **6.3**. The linear silane **6.3** was copolymerized with 2,5-dibromothiophene following the standard procedure (Table 6.2.1, Entry 1), resulting in **P6.5**.

6.4 Thermal property study with differential scanning calorimetry

The glass transition temperature of polymers is known to be strongly tacticity-dependent.[36] By achieving control of both relative configuration and molecular weight, it is possible to study the impact of tacticity on polymer properties in isolation. As an example of stereoregularity impact on bulk properties, we found that the three macromolecules exhibited distinct glass transition (T_g) temperatures. The atactic **P6.3** showed a minimal transition, but both *trans* **P6.1** and *cis* **P6.2** showed more pronounced T_g at distinct

temperatures (Figure 6.4.1). The thermal property of atactic **P6.3** is consistent with the absence of phase transition between 40 °C to 200 °C for atactic linear poly(cyclosilane)s.[26]

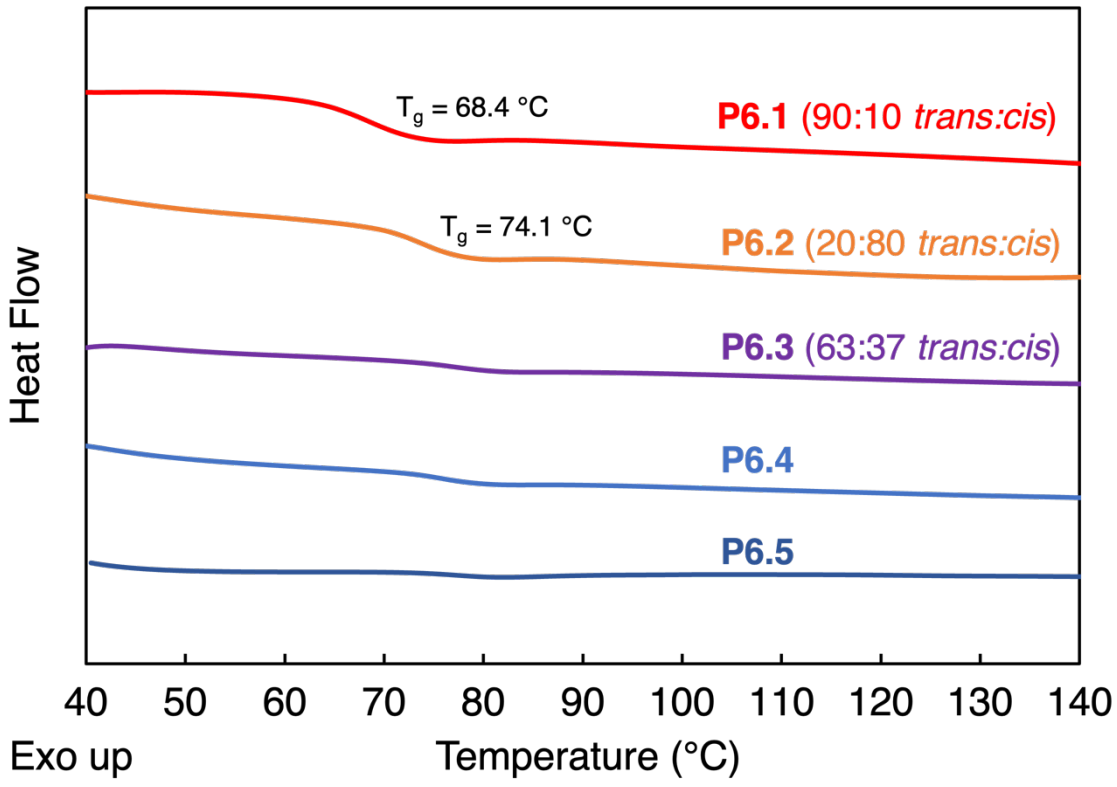

Figure 6.4.1 Cropped DSC curves of **P6.1-5**. The second cycle is shown. Heating rate: 20 °C min^{-1}, cooling rate: 20 °C min^{-1}.

Linear silane-embedded **P6.4** and **P6.5** did not undergo remarkable phase transition between 40 to 180 °C. Based on these comparisons, we attributed the glass transition that **P6.1** and **P6.2** exhibited at 68-74 °C to the ring inversion of cyclohexasilane units. The free-energy profile of cyclohexasilane ring inversion is known to be much lower than cyclohexane.[37] While the temperature increased, the ring inversion would promote mobility of polymer backbones, enhancing glass transition behaviors. We note that **P6.5** was the only polymer that showed melting temperature (T_m) at 203 °C. No T_m was detected

for the other polysilanes before they degraded above 250 °C. This indicated that the incorporation of vinyl groups in the backbone built up polymer rigidity and raised their T_m.

6.5 UV-vis absorbance spectra

We obtained UV-vis spectra of the stereoregular polysilane thin films. The polysilanes were dissolved in THF (2.0 mg/mL), drop-casted on quartz substrates and fully dried under vacuum at room temperature overnight (Figure 6.5.1, blue curves). All three polymers were similar in UV-vis absorption: λ_{max} = *ca.* 420 nm and λ_{onset} = *ca.* 570 nm. No notable difference was identified, which agreed with the similar UV-vis absorption of *trans*- and *cis*-**6.1**.[27]

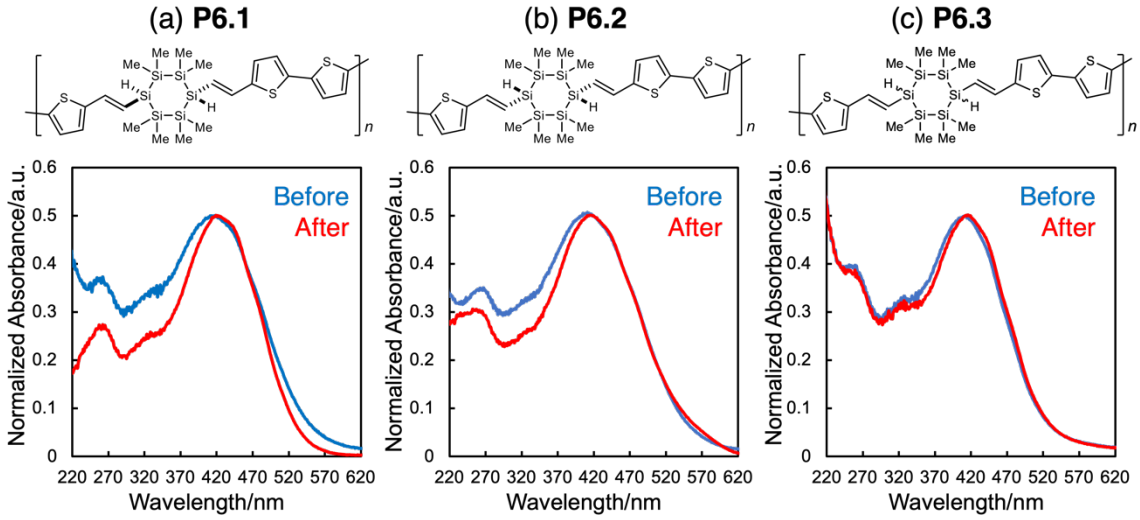

Figure 6.5.1 Comparison of film UV-vis spectra of (a) **P6.1**, (b) **P6.4** and (c) **P6.5**. Before annealing: Blue. After annealing: Red.

The films were then annealed by being heated at 80 °C for 8 hours under vacuum and slowly cooled to room temperature overnight. Compared to UV-vis spectra obtained before annealing, all three annealed polymers showed similar onset (λ_{onset}) and maximum (λ_{max}) absorption, whereas the absorption bands became narrower only in spectra of

annealed **P6.1** and **P6.2**. This is consistent with the DSC results that glass transition were observed in stereoregular **P6.1** and **P6.2** but not atactic **P6.3**. Annealing the stereoregular polymers at temperature above T_g helped form more ordered arrangement of neighboring polymer chains, resulting in more distinct absorption bands.

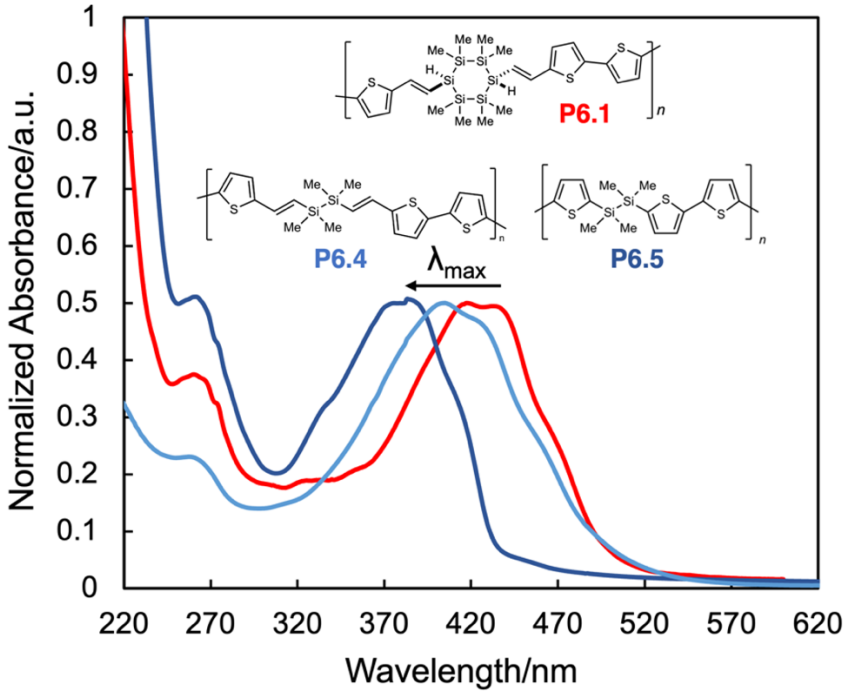

Figure 6.5.2 Comparison of solution UV-vis spectra of **P6.1** (Red), **P6.4** (Blue), and **P6.5** (Prussian) in THF. [polymer] = 0.03 g/L.

The influence of silane and vinyl units embedded in conjugated polymer chains was also investigated through UV-vis spectroscopy (Figure 6.6.2). Despite higher degree of polymerization, λ_{max} of both linear silane-derived polymers were blue-shifted compared to **P6.1**, by *ca*. 10 nm for **P6.4**, and *ca*. 55 nm for **P6.5**. This indicated that cyclosilane units better extended conjugation than their linear analogs. We also note the bathochromic influence of vinyl incorporation as the result of enlarging π-conjugated fragments (**P6.4** *versus* **P6.5**).

6.6 Expanded scope of hybrid conjugated polymers

To further address the impact of stereoregularity on the polysilane optical properties in addition to bulk characteristics, we replaced the comonomer 2,5-dibromothiophene with more sterically hindered **6.4** (Table 6.6.1). The long alkyl side substituents on **6.4** were expected to amplify the influence of cyclosilane stereoregularity on the polymer chain geometry by increasing stereo effects. The standard copolymerization condition (Table 6.2.1, Entry 1) was used. Conjugated polymers **P6.6-8** were synthesized by variation of diastereomer ratio of **6.1** (Table 6.6.1).

Table 6.6.1. Molecular weight characteristics of hybrid conjugated polysilanes. [a]

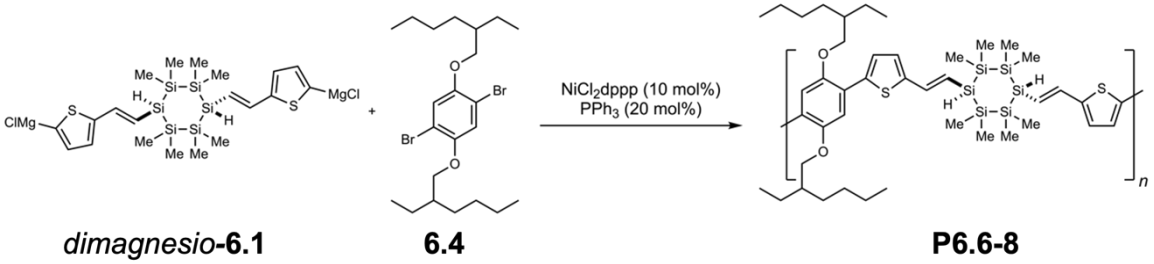

Cyclosilane	dr (*trans:cis*)	Polymer	M_n (g mol^{-1}) [a]	M_w/M_n [a]	Yield (%)
trans-**6.1**	90:10	**P6.6**	4163	2.52	72
cis-**6.1**	20:80	**P6.7**	4051	2.24	68
6.1	63:37	**P6.8**	4468	2.02	56

[a] Determined by size exclusion chromatography relative to polystyrene standards at 254 nm (THF, [copolymer] = 1 mg mL^{-1}, 40 °C, 0.35 mL min^{-1}, 10 μL injection).

As the *trans:cis* ratio in **6.1** tuned from 90:10 to 63:37 to 20:80, the molecular weight characteristics of the copolymer stayed constant (Table 6.6.1), but significantly different absorbance spectra were recorded (Figure 6.6.1). Increasing the ratio of certain diastereomer of cyclosilanes led to a more pronounced transition at ca. 320 nm and a more notable shoulder at 370 nm (Figure 6.6.1).

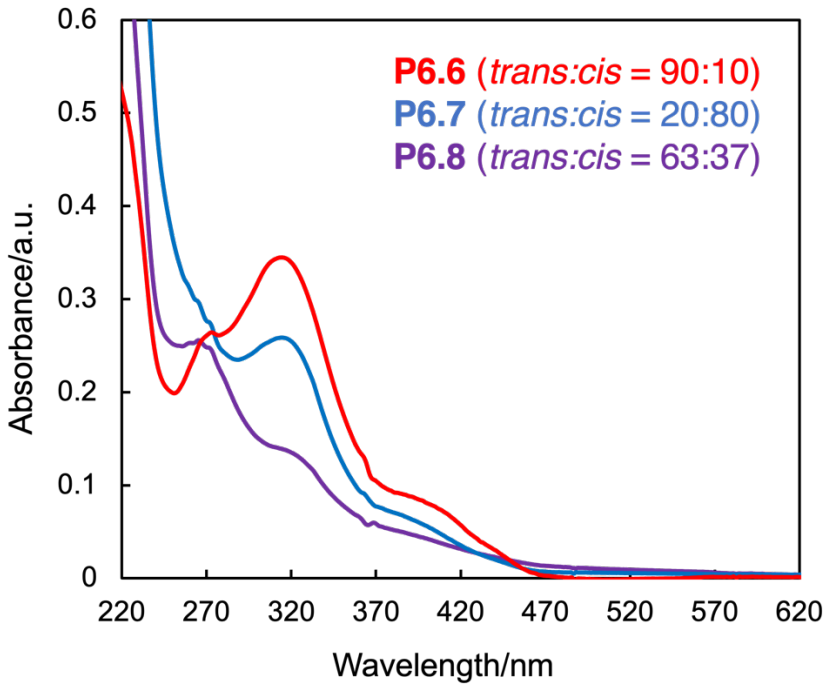

Figure 6.6.1 Comparison of UV-vis spectra of **P6.6** (red), **P6.7** (blue), and **P6.8** (purple) in THF solution. [polymer] = 0.03 g/L.

6.7 Conclusion and future

We demonstrated that stereoregularity showed substantial influence on the thermal and optical properties of hybrid conjugated polymers. A series of stereoregular and atactic σ,π-conjugated polymers derived from sterically pre-defined cyclosilane building blocks were synthesized. Compared to the atactic polymer, the stereoregular polysilanes exhibited notable phase transitions and their optical characteristics better benefitted from annealing. Using blocky aromatic comonomers, the impact of stereoregularity on the optical properties was amplified and the absorption features were more distance in the solution phase. We also demonstrated that the incorporation of cyclosilane and vinyl units into the polymer chain extended conjugation.

Future study of the demonstrated hybrid conjugated polymers will include examining the semicrystallinity by film X-ray diffraction (XRD) and fluorescence

emission properties by fluorescence spectroscopy. More synthetic exploration will be done, including achieving higher stereochemical purity in the building blocks by further purifying cyclosilane monomers with recycling gel permeation chromatography, and altering the electron donor/acceptor profile of aromatic comonomers.

6.8 Reference

(1) Worch, J. C.; Prydderch, H.; Jimaja, S.; Bexis, P.; Becker, M. L.; Dove, A. P. *Nat. Rev. Chem.* **2019**, *3*, 514–535.
(2) Staudinger, H. *Kolloid-Zeitschrift.* **1930**, *51*, 71–89.
(3) Schildknecht, C. E.; Zoss, A. O.; McKinley, C. *Ind. Eng. Chem.* **1947**, *39*, 180–186.
(4) Schrock, R. R. *Acc. Chem. Res.* **2014**, *47*, 2457–2466.
(5) Coates, G. W. *Chem. Rev.* **2000**, *100*, 1223–1252.
(6) Pasini, D.; Takeuchi, D. *Chem. Rev.* **2018**, *118*, 8983–9057.
(7) Takeuchi, D. *J. Am. Chem. Soc.* **2011**, *133*, 11106–11109.
(8) Wang, H.; Zhao, Y.; Nishiura, M.; Yang, Y.; Luo, G.; Luo, Y.; Hou, Z. *J. Am. Chem. Soc.* **2019**, *141*, 12624–12633.
(9) Szejtli, J. *Chem. Rev.* **1998**, *98*, 1743–1754.
(10) Klausen, R. S.; Ballestero-Martínez, E. *Comprehensive Organometallic Chemistry IV*; Elsevier, 2021.
(11) Fossum, E.; Matyjaszewski, K. *Macromolecules* **1995**, *28*, 1618–1625.
(12) Kameta, N.; Hiramatsu, H.; Sanji, T.; Sakurai, H. *J. Inorg. Organomet. Polym. Mater.* **2007**, *17*, 589–594.
(13) Wolff, A. R.; Nozue, I.; Maxka, J.; West, R. *J. Polym. Sci. Part A Polym. Chem.* **1988**, *26*, 701–712.
(14) Maxka, J.; Mitter, F. K.; Powell, D. R.; West, R. *Organometallics* **1991**, *10*, 660–664.
(15) Jones, R. G.; Benfield, R. E.; Evans, P. J.; Holder, S. J.; Locke, J. A. M. *J. Organomet. Chem.* **1996**, *521*, 171–176.
(16) Clegg, P. L. In *Nature*; Jones, R. G., Ando, W., Chojnowski, J., Eds.; Springer Science & Business Media, 1978; Vol. 271, pp 486–486.
(17) Yamaguchi, Y. *Synth. Met.* **1996**, *82*, 149–153.
(18) Morisaki, Y.; Fujimura, F.; Chujo, Y. *Organometallics* **2003**, *22*, 3553–3557.
(19) Wang, Y.; Wang, D.; Xu, C.; Wang, R.; Han, J.; Feng, S. *J. Organomet. Chem.* **2011**, *696*, 3000–3005.
(20) Herrema, J. K.; van Hutten, P. F.; Gill, R. E.; Wildeman, J.; Wieringa, R. H.; Hadziioannou, G. *Macromolecules* **1995**, *28*, 8102–8116.
(21) Wildeman, J.; Herrema, J. K.; Hadziioannou, G.; Schomaker, E. *J. Inorg. Organomet. Polym.* **1991**, *1*, 567–580.
(22) Marro, E. A.; Klausen, R. S. *Chem. Mater.* **2019**, *31*, 2202–2211.
(23) Press, E. M.; Marro, E. A.; Surampudi, S. K.; Siegler, M. A.; Tang, J. A.; Klausen, R. S. *Angew. Chemie Int. Ed.* **2017**, *56*, 568–572.
(24) Marro, E. A.; Press, E. M.; Siegler, M. A.; Klausen, R. S. *J. Am. Chem. Soc.* **2018**,

140, 5976–5986.
(25) Marro, E. A.; Folster, C. P.; Press, E. M.; Im, H.; Ferguson, J. T.; Siegler, M. A.; Klausen, R. S. *J. Am. Chem. Soc.* **2019**, *141*, 17926–17936.
(26) Jiang, Q.; Wong, S.; Klausen, R. S. *Polym. Chem.* **2021**, *12*, 4785–4794.
(27) Jiang, Q.; Gittens, A. F.; Wong, S.; Siegler, M. A.; Klausen, R. S. *Chem. Sci.* **2022**, *13*, 7587–7593.
(28) Knochel, P.; Dohle, W.; Gommermann, N.; Kneisel, F. F.; Kopp, F.; Korn, T.; Sapountzis, I.; Vu, V. A. *Angew. Chemie Int. Ed.* **2003**, *42*, 4302–4320.
(29) Krasovskiy, A.; Knochel, P. *Angew. Chemie Int. Ed.* **2004**, *43*, 3333–3336.
(30) Yamamoto, K.; Kumada, M.; Nakajima, I.; Maeda, K.; Imaki, N. *J. Organomet. Chem.* **1968**, *13*, 329–341.
(31) Yamashita, H.; Reddy, N. P.; Tanaka, M. *Macromolecules* **1993**, *26*, 2143–2144.
(32) Sharma, H. K.; Pannell, K. H. *Chem. Rev.* **1995**, *95*, 1351–1374.
(33) Beryozkina, T.; Senkovskyy, V.; Kaul, E.; Kiriy, A. *Macromolecules* **2008**, *41*, 7817–7823.
(34) Dumouchel, S.; Mongin, F.; Trécourt, F.; Quéguiner, G. *Tetrahedron* **2003**, *59*, 8629–8640.
(35) Kanno, K. ichiro; Aikawa, Y.; Kyushin, S. *Tetrahedron Lett.* **2020**, *61*, 152274.
(36) Thompson, E. V. *J. Polym. Sci. Part A-2 Polym. Phys.* **1966**, *4*, 199–208.
(37) Dorn, R. W.; Marro, E. A.; Hanrahan, M. P.; Klausen, R. S.; Rossini, A. J. *Chem. Mater.* **2019**, *31*, 9168–9178.

Chapter 7: Experimental details

7.1 General information

General Experimental Procedures

All experiments were performed under protection of dry nitrogen or argon with the rigid exclusion of air and moisture using standard Schlenk techniques or in a nitrogen glovebox. All glassware was oven-dried overnight in a 175 °C oven.

Materials

Unless otherwise specified, all chemicals were used as purchased without further purification. Solvents DCM (Fisher, HPLC grade), THF (Fisher, HPLC grade), pentane (Fisher, certified ACS), and toluene (Fisher, certified ACS) were dried on a J. C. Meyer Solvent Dispensing System (SDS) using stainless steel columns packed with neutral alumina (except for toluene which is dried with neutral alumina and Q5 reactant, a copper(II) oxide oxygen scavenger), following the manufacturer's recommendations for solvent preparation and dispensation unless otherwise noted. Acetylenes (4-ethynylthioanisole[1], 4-ethynylbromobenzene[2] and 2-bromo-5-ethynylthiophene[3]) and 1,4-dibromo-2,5-((2-ethylhexyl)oxy)benzene[4] were prepared by adaptation of literature procedures.

Instrumentation

^{1}H NMR, ^{13}C {^{1}H} NMR, ^{19}F {^{1}H} NMR and ^{29}Si {^{1}H} NMR spectra were recorded on either a Bruker Avance 300, 400 or III HD 400 MHz Spectrometer and chemical shifts are reported in parts per million (ppm). Spectra were recorded in benzene-d_6 or chloroform-d_1 with the residual solvent peak as the internal standard (^{1}H NMR: C_6H_6

δ = 7.16; $CHCl_3$ δ = 7.26, ^{13}C NMR: C_6H_6 δ 128.06; $CHCl_3$ δ = 77.16). Chemical shifts of ^{19}F $\{^1H\}$ NMR spectra were calibrated by 0.05% trifluorotoluene in C_6D_6. Chemical shifts of ^{29}Si $\{^1H\}$ NMR spectra were calibrated by tris(Me_3Si)methane in $CDCl_3$. The temperature was room temperature unless otherwise specified. Multiplicities are as indicated: s (singlet), d (doublet), dd (doublet of doublets), m (multiplet) and br (broad). Coupling constants, J, are reported in Hertz, and integration is provided.

Solid-state $^1H \rightarrow ^{29}Si$ and ^{13}C CPMAS spectra were recorded on a Bruker Ascend spectrometer (500 MHz) and chemical shifts were reported in parts per million (ppm). Chemical shifts of $^1H \rightarrow ^{29}Si$ CPMAS spectra were calibrated by silicone rubber. Chemical shifts of $^1H \rightarrow ^{13}C$ CPMAS spectra were calibrated by adamantane. In a glove box, 14 mg of polymer samples were packed into a sample rotor compatible with a 3.2 mm Phoenix HX probe. Spectral data was acquired at a spinning speed of 20 kHz.

All column chromatography was performed on a Teledyne ISCO Combiflash Rf+ using Redisep Rf silica columns. Fourier transformed infrared (FTIR) spectroscopy was performed on a Thermo NicoletNexus 670 FTIR spectrometer. Mass spectrometry and high-resolution mass spectrometry were performed in the Department of Chemistry at Johns Hopkins University using a VG Instruments VG70S/E magnetic sector mass spectrometer with electron ionization (EI) (70 eV). The samples for UV–vis spectroscopy were all prepared in the glove box and packed in sealed quartz cuvettes. UV–vis spectroscopy was performed on a Shimadzu UV-1800 UV–vis spectrophotometer. Molecular weights of polymers were measured by gel permeation chromatography (GPC) on a Tosoh Bioscience EcoSEC GPC workstation with UV detection at 254 nm using butylated hydroxytoluene stabilized tetrahydrofuran (THF) as the eluent (0.35 mL min^{-1},

40 °C) through TSKgel SuperMultipore HZ-M guard column (4.6 mm ID x 2.0 cm, 4 μm, Tosoh Bioscience) and a TSKgel SuperMultipore HZ-M column (4.6 mm ID x 15 cm, 4 μm, Tosoh Bioscience). Polystyrene standards (EasiVial PS-M, Agilent) were used to build a calibration curve. Processing was performed using EcoSEC Data Analysis software (Version 1.14, Tosoh Bioscience). The samples were dissolved in THF (0.5 mg mL^{-1}), filtered through syringe filters (Millex-FG Syringe Filter Unit, 0.20 μm, PTFE, EMD Millipore), and injected by an auto-sampler (10 μL). Differential scanning calorimetry (DSC) was conducted using a TA Instruments DSC Q20 V24.11 Build 124 and processing was performed using Universal V4.5A (TA Instruments). Thermogravimetric analysis (TGA) was conducted using a TA Instruments SDT Q600 under flowing Ar at a heating rate of 5.0 °C min^{-1} from 40 to 600 ˚C.

7.2 Effect of poly(cyclosilane) microstructure on thermal properties

Cp_2ZrMe_2 Synthesis of *lin*-poly(1,3Si_6)

In a nitrogen atmosphere glove box, Cp_2ZrMe_2 (0.056 equiv., 0.019 mmol, 4.8 mg) was added to an oven-dried 2-dram vial equipped with a stir bar. **1,3Si_6** (1.0 equiv., 0.34 mmol, 0.100 g) was added by syringe. The vial was sealed with a septum cap equipped with a vent needle. The mixture was stirred at room temperature in the glove box. After 24 hours, the stir bar was trapped in a dark red glass in the vial. The solid was dissolved in 10 mL of pentane and 0.5 grams of Celite was added. The solution was stirred for 2 hours. The Celite was filtered through a fritted funnel and washed with 5 mL of pentane. The filtrate was then concentrated to a yellow solid under vacuum. The procedure was repeated until a white solid was yielded, which indicated that the catalyst had been fully removed. The solid was further dried under vacuum at 60˚C for 3 hours (85.8 mg, 87%).

Cp_2ZrMe_2 Synthesis of *cyc*-poly(1,3Si_6)

In a nitrogen atmosphere glove box, Cp_2ZrMe_2 (0.056 equiv., 0.019 mmol, 4.8 mg) was added to an oven-dried 2-dram vial equipped with a stir bar and dissolved by 0.5 mL of toluene. **1,3Si_6** (1.0 equiv., 0.34 mmol, 0.100 g) was weighed in a 1-dram vial and diluted by 0.5 mL of toluene. The solution of **1,3Si_6** was added dropwise to the 2-dram vial by syringe. 0.25 mL of toluene was used to rinse the vial and syringe, then added to the 2-dram vial as well. The 2-dram vial was sealed with a septum cap equipped with a vent needle. The mixture was stirred at room temperature in the glove box. After 24 hours, the reaction mixture turned yellow, and deep orange after 4 days. 7 days later, volatile materials were removed under vacuum and the residual solid was dissolved in 10 mL of pentane. 0.5 grams of Celite was added and the solution was stirred for 2 hours. The Celite was filtered

through a fritted funnel and washed with 5 mL of pentane. The filtrate was then concentrated to a yellow solid under vacuum. The procedure was repeated until a white solid was yielded, which indicated that the catalyst had been fully removed. The solid was further dried under vacuum at 60˚C for 3 hours (83.4 mg, 85%).

NMR Spectra

^{1}H NMR Spectrum (400 MHz, Benzene-d_6) of *lin*-poly(**1,3Si$_6$**).

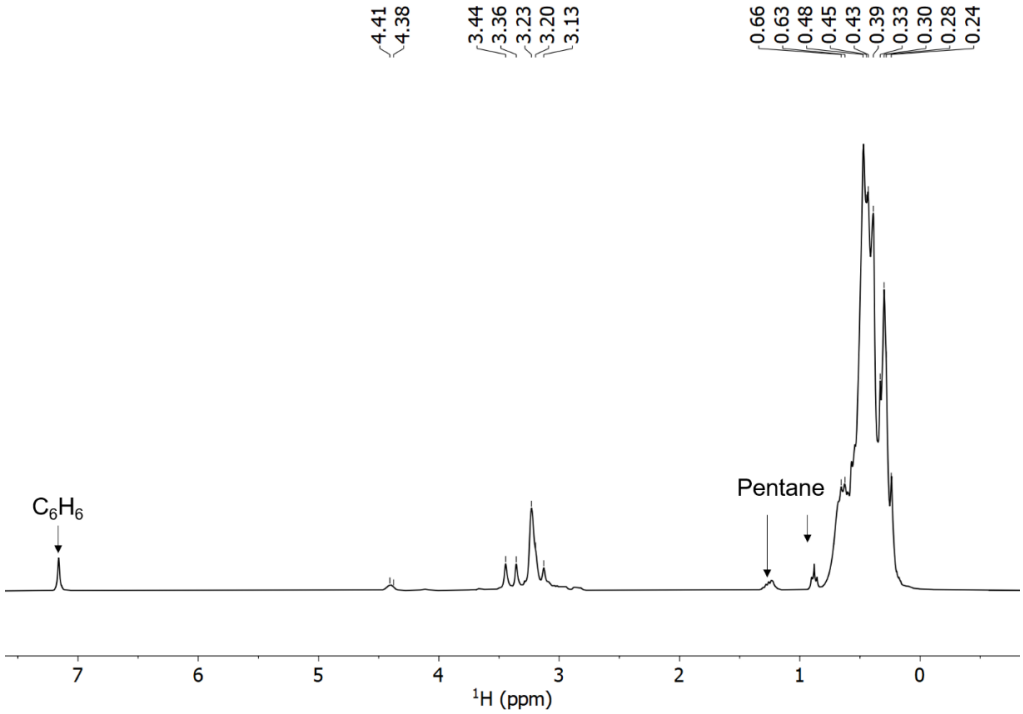

^{29}Si {^{1}H} NMR Spectrum (79 MHz, Benzene-d_6) of *lin*-poly(**1,3Si$_6$**). $^{1}J_{\text{Si-H}}$ = 120 Hz.

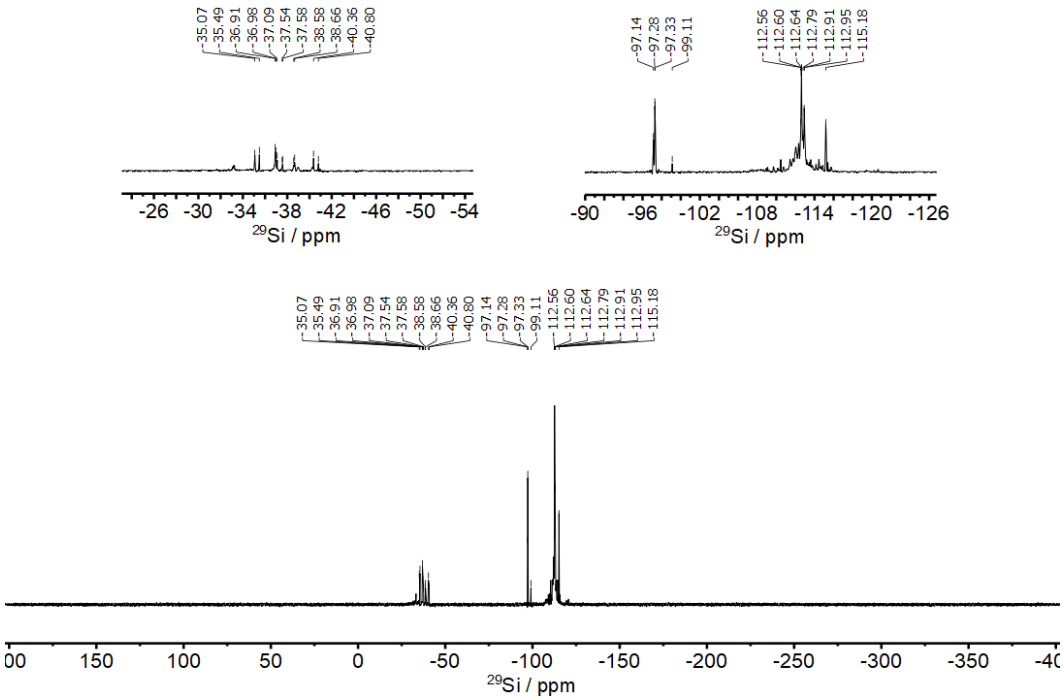

^{13}C {^{1}H} NMR Spectrum (101 MHz, Benzene-d_6) of *lin*-poly(**1,3Si$_6$**).

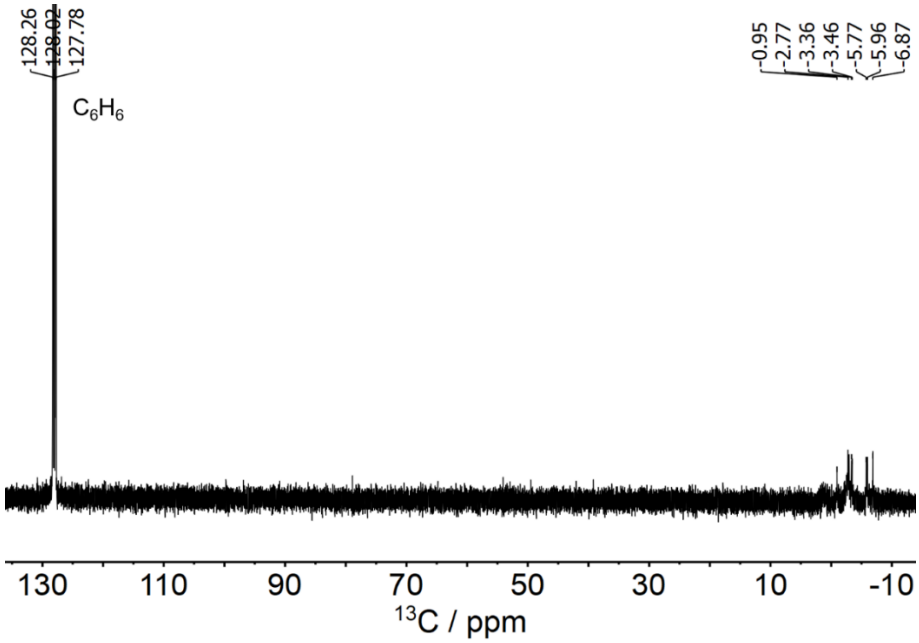

^{1}H- ^{29}Si HSQC NMR spectrum (400 MHz, Benzene-d_6) of *lin*-poly(**1,3Si$_6$**). $^{1}J_{Si\text{-}H}$ = 120 Hz.

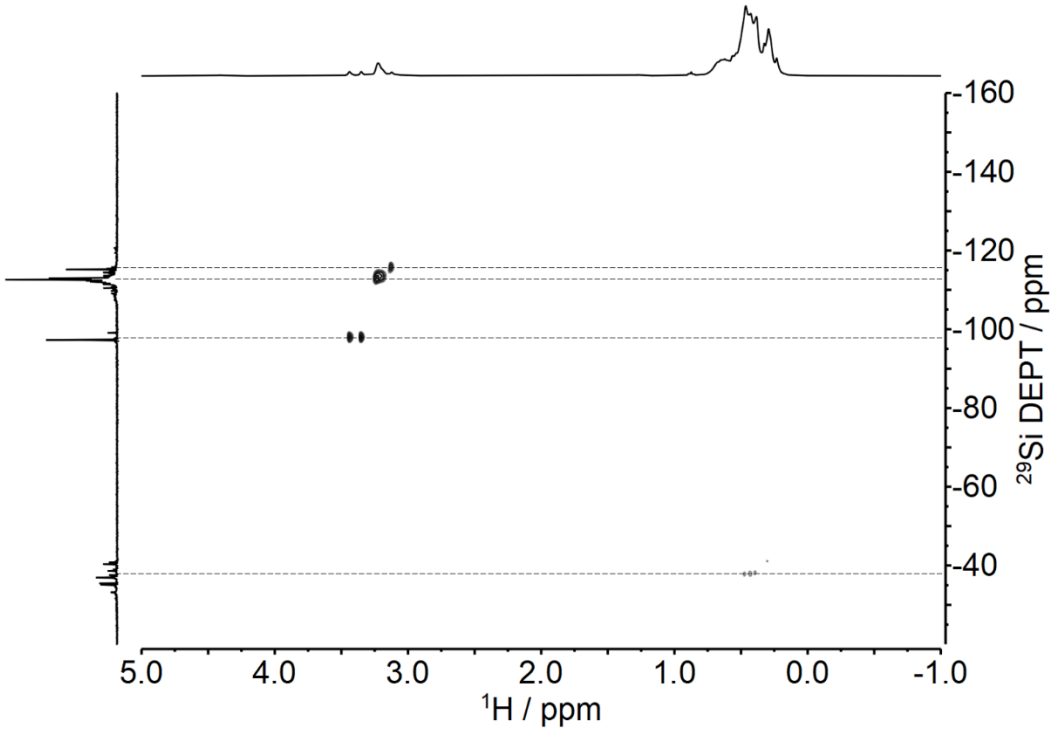

^{1}H NMR Spectrum (400 MHz, Benzene-d_6) of *cyc*-poly(**1,3Si$_6$**) (Cp_2ZrMe_2 synthesis).

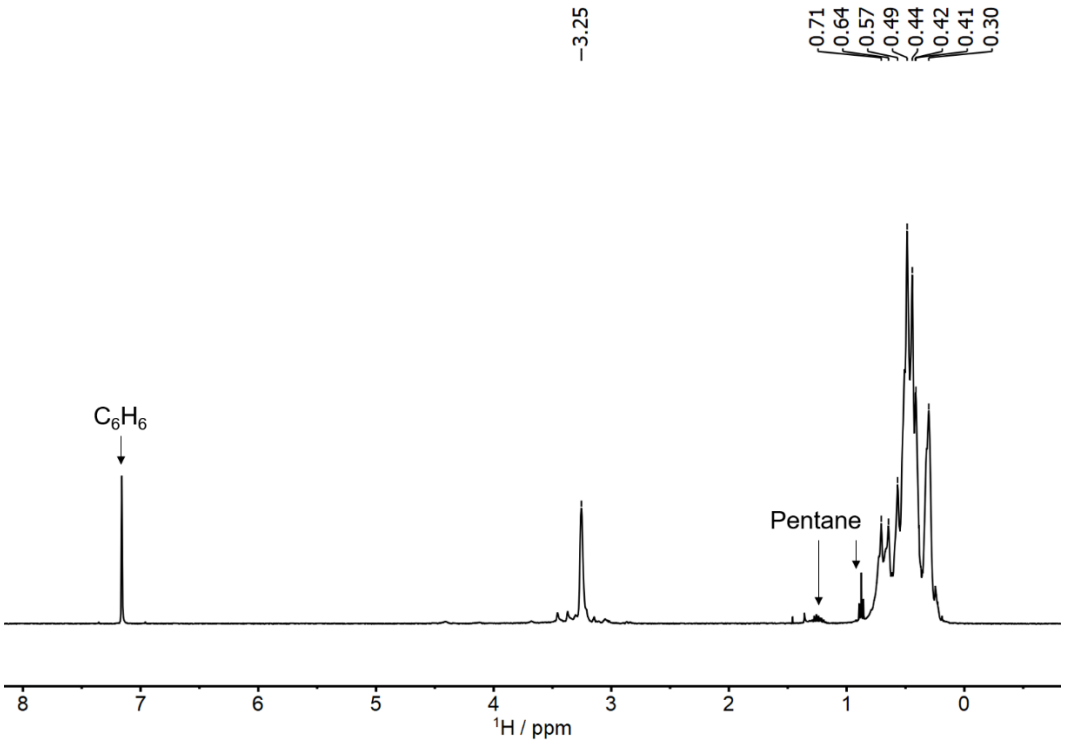

^{29}Si {^{1}H} NMR Spectrum (79 MHz, Benzene-d_6) of *cyc*-poly(**1,3Si$_6$**) (Cp_2ZrMe_2 synthesis).

$^{1}J_{Si\text{-}H}$ = 120 Hz.

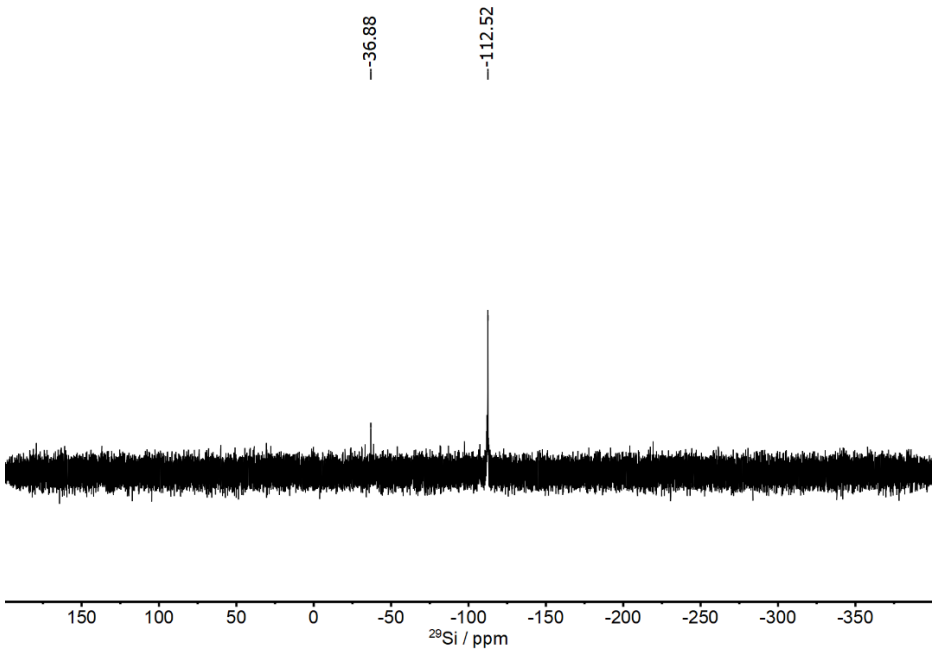

^{1}H NMR Spectrum (400 MHz, Benzene-d_6) of *lin*-poly(**1,4Si$_6$**).

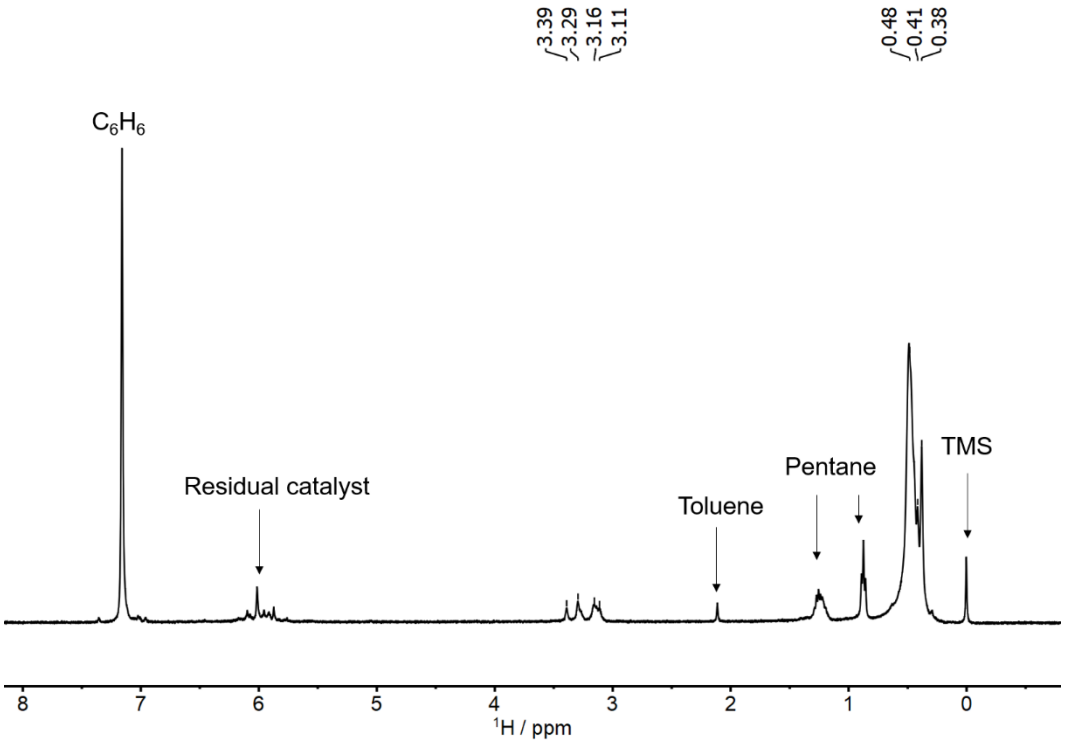

^{29}Si {^{1}H} NMR Spectrum (79 MHz, Benzene-d_6) of *lin*-poly(**1,4Si$_6$**). $^{1}J_{\text{Si-H}}$ = 120 Hz.

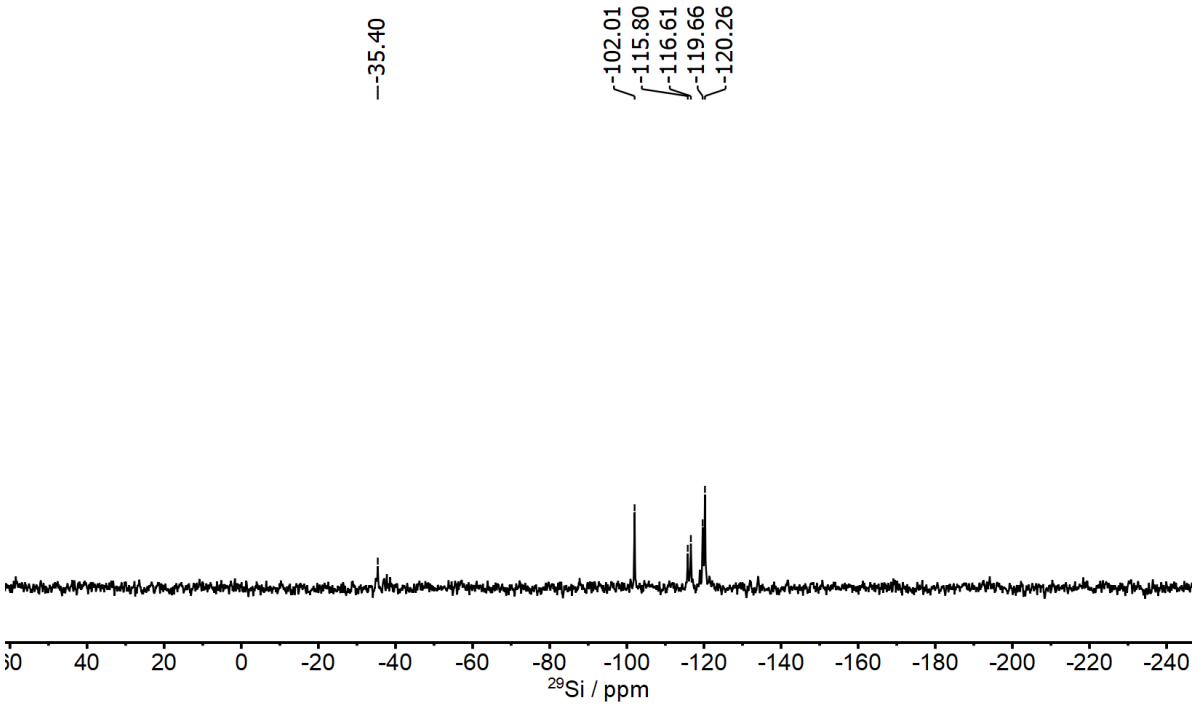

^{1}H NMR Spectrum (400 MHz, Benzene-d_6) of *cyc*-poly(**1,3Si$_6$**) (Cp_2ZrCl_2 synthesis).

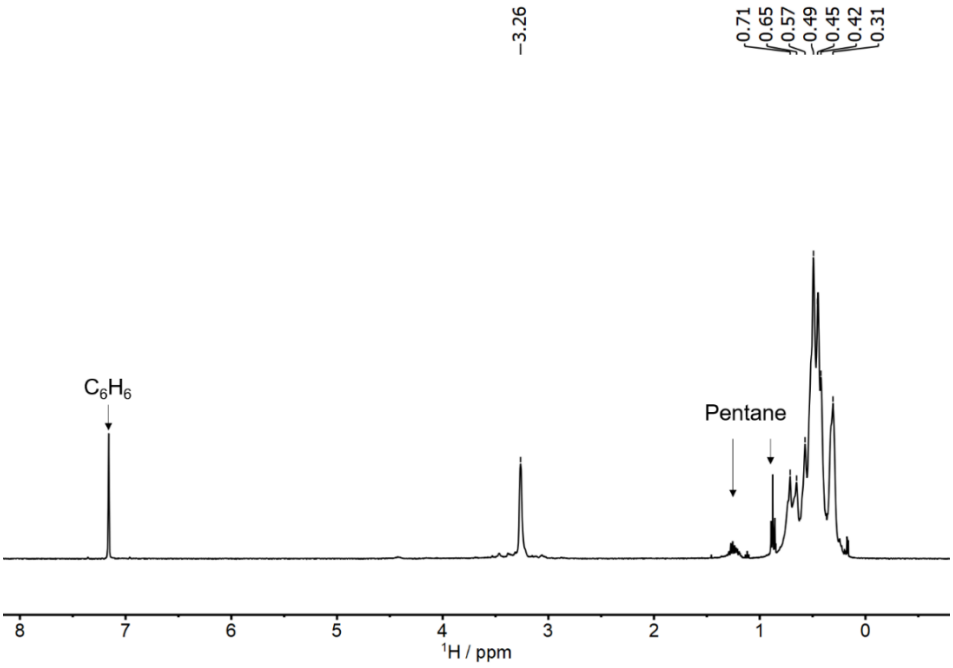

^{29}Si {^{1}H} NMR Spectrum (79 MHz, Benzene-d_6) of *cyc*-poly(**1,3Si$_6$**) (Cp_2ZrCl_2 synthesis).

$^{1}J_{Si\text{-}H}$ = 120 Hz.

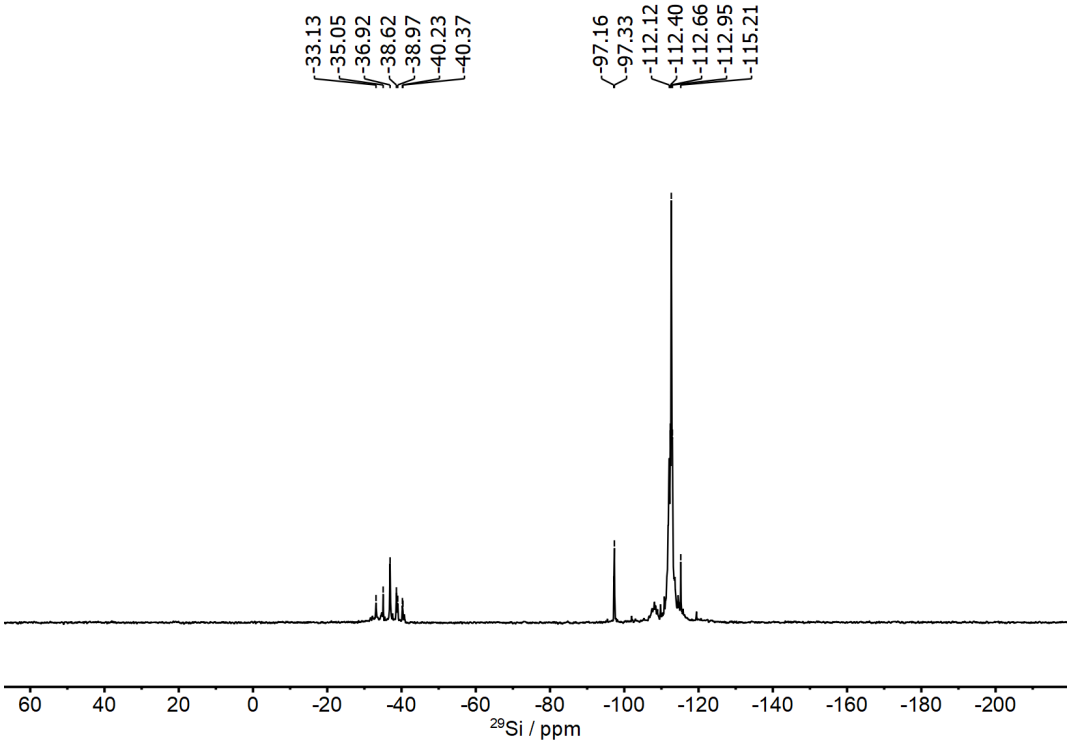

Gel Permeation Chromatography

lin-poly(**1,3Si$_6$**)

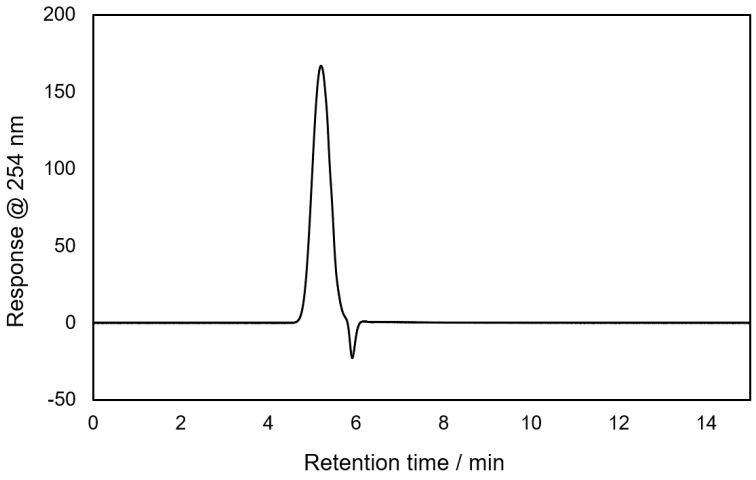

Peak No.	M_n	M_w	M_w / M_n
1	1770	2390	1.35

cyc-poly(**1,3Si$_6$**) (Cp_2ZrMe_2 synthesis)

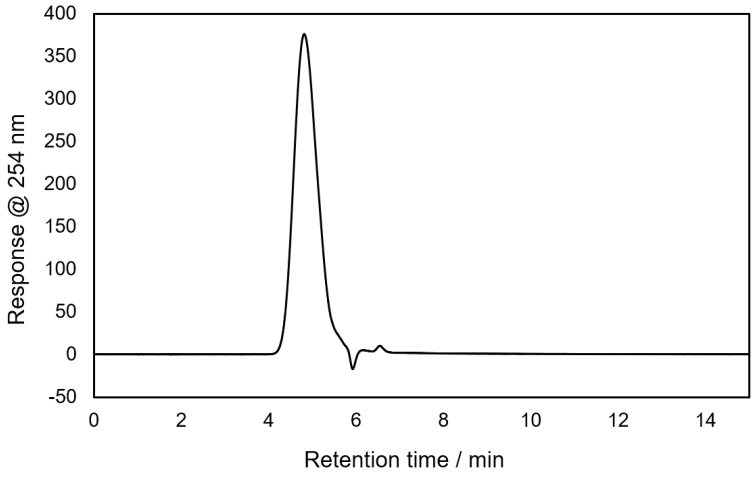

Peak No.	M_n	M_w	M_w / M_n
1	3840	7270	1.90

ATR-FTIR Spectroscopy

ATR-FTIR spectrum of *lin*-poly(**1,3Si$_6$**)

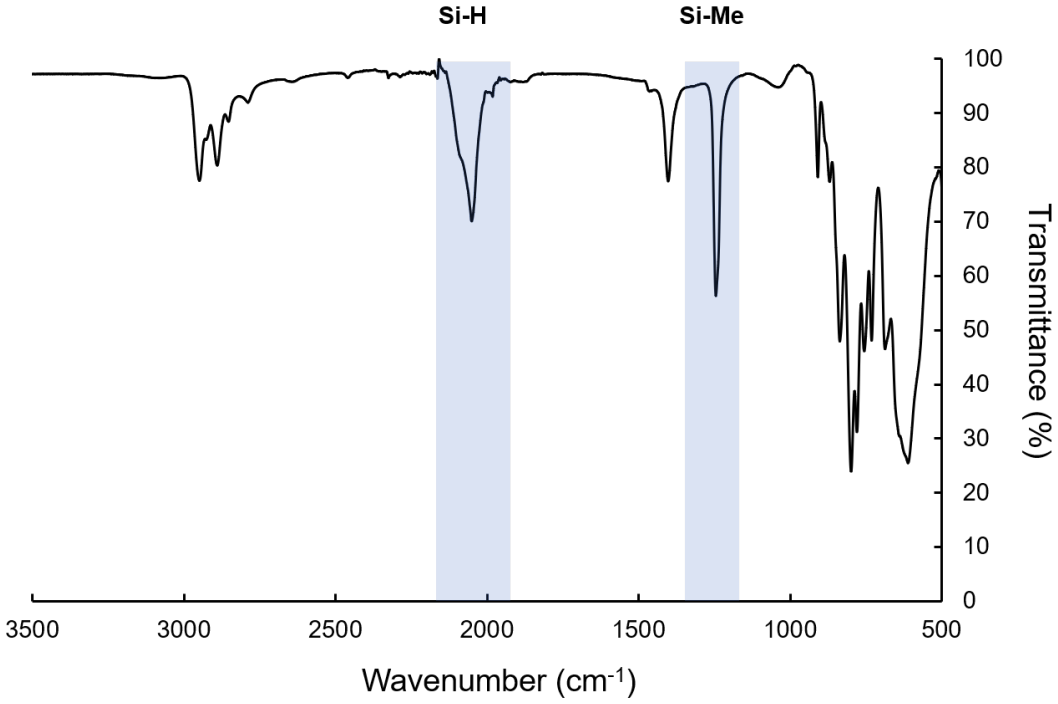

Differential scanning calorimetry

Differential scanning calorimetry (DSC) was conducted using a TA Instruments DSC Q20 V24.11 Build 124 and processing was performed using Universal V4.5A (TA Instruments). Samples were sealed in hermetic aluminum pans, heated from 35 to 200 °C (3 °C min^{-1} for *lin*-poly(**1,4Si$_6$**) and 20 °C min^{-1} for *cyc*-poly(**1,3Si$_6$**) and *lin*-poly(**1,3Si$_6$**)), and cooled from 200 to 35 °C (3 °C min^{-1}), for three cycles under a purge gas of nitrogen (25 mL min^{-1}). Phase transition temperature were calculated from the second heating cycle. The second heating and cooling cycles are shown.

lin-poly(**1,4Si$_6$**)

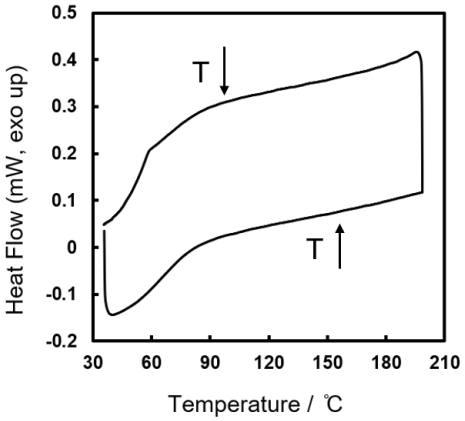

cyc-poly(**1,3Si$_6$**)

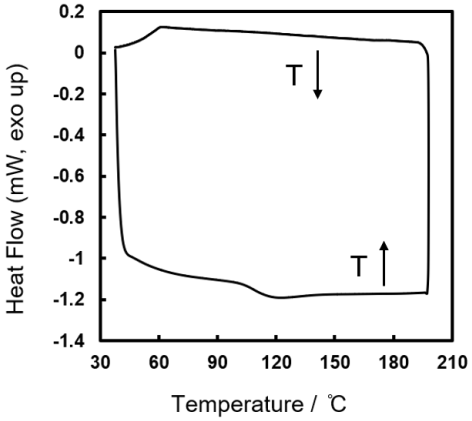

lin-poly(**1,3Si$_6$**)

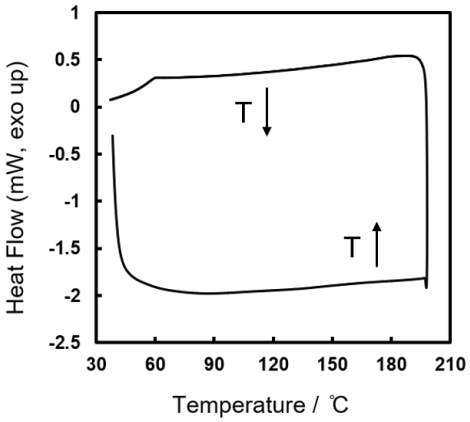

Computational Methods

All the DFT calculations are performed with the Gaussian 09 package.[5] Geometries were optimized using the B3LYP functional with the 6-31G(d) basis. No symmetry restrictions were applied to geometry optimization. Homolytic bond dissociation energies (BDEs) are calculated as follows: BDE = $\sum E_{rs} - E_{cs}$, where $\sum E_{rs}$ is the sum of energy of all radical species, and E_{cs} is the energy of the closed shell species. Hydrogens in optimized structures are omitted for clarity.

Calculated energy of closed shell and radical species of ***1,4Si$_6$****. Radical species are generated by homolytic bond dissociation as labeled on the left column.*

Closed Shell Energies (E_h)	-2058.79738594
Radical Species Energies (E_h)	
Si(1)-H^a	-2058.15686167
Si(1)-H^e	-2058.15931009
Si(2)-Me^a	-2018.83157300
Si(2)-Me^e	-2018.83335389
Si(1)-Si(2)	-2058.68840089
Si(2)-Si(2)	-2058.68886887

*Calculated energy of closed shell and radical species of lin-(****1,4Si$_6$****)$_3$. Radical species are generated by homolytic bond dissociation as labeled on the left column.*

Closed Shell Energies (E_h)	-6174.01411855
Radical Species Energies (E_h)	
Si(1)-H^a	-6173.37304659
Si(1)-H^e	-6173.37569970
Si(4)-H^e	-6173.37738920
Si(6)-Me^a	-6134.05889350
Si(6)-Me^e	-6134.05908879

Si(2)-Si(3)	-6173.91376417
Si(3)-Si(4)	-6173.91906634
Si(4)-Si(5)	-4115.76713951 (dimer)
	-2058.15941768 (monomer)

1,4Si$_6$ and its radical species

1,4Si$_6$ (charge = 0, multiplicity = 1)

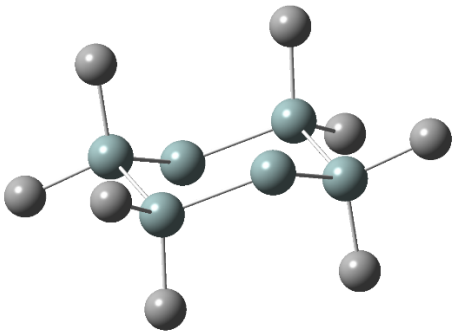

E(RB3LYP) = -2058.79738594 E_h

Center Number	Atomic Number	Atomic Type	Coordinates (Angstroms) X	Y	Z
1	14	0	-2.569659	-0.637739	-0.356331
2	14	0	-3.444674	0.444823	1.565310
3	14	0	-5.801826	0.218408	1.586254
4	1	0	-6.359925	0.921230	2.789080
5	1	0	-6.354401	0.956059	0.403474
6	14	0	-6.615051	-2.004916	1.516256
7	14	0	-5.740036	-3.087478	-0.405385
8	14	0	-3.382885	-2.861063	-0.426328
9	1	0	-2.824786	-3.563885	-1.629155
10	1	0	-2.830309	-3.598714	0.756452
11	6	0	-3.107866	0.296597	-1.932811
12	1	0	-2.709979	1.318702	-1.931222
13	1	0	-2.733556	-0.203925	-2.833797
14	1	0	-4.198159	0.365518	-2.017209
15	6	0	-0.660109	-0.667459	-0.298452
16	1	0	-0.251011	-1.165590	-1.185521
17	1	0	-0.251895	0.350374	-0.269797
18	1	0	-0.291955	-1.202598	0.583814
19	6	0	-6.188827	-4.945224	-0.393908
20	1	0	-7.276495	-5.087715	-0.404310
21	1	0	-5.778485	-5.450660	-1.276307
22	1	0	-5.791974	-5.450396	0.493717

23	6	0	-6.471320	-2.303662	-1.985783
24	1	0	-6.054680	-2.772750	-2.885036
25	1	0	-7.559841	-2.435198	-2.016176
26	1	0	-6.265214	-1.229134	-2.043101
27	6	0	-8.524601	-1.975196	1.458377
28	1	0	-8.932816	-2.993030	1.429722
29	1	0	-8.933700	-1.477065	2.345446
30	1	0	-8.892756	-1.440057	0.576111
31	6	0	-6.076844	-2.939252	3.092736
32	1	0	-6.451155	-2.438731	3.993723
33	1	0	-6.474731	-3.961357	3.091147
34	1	0	-4.986551	-3.008174	3.177135
35	6	0	-2.713390	-0.338994	3.145708
36	1	0	-1.624869	-0.207457	3.176101
37	1	0	-3.130030	0.130095	4.044961
38	1	0	-2.919497	-1.413521	3.203027
39	6	0	-2.995884	2.302569	1.553833
40	1	0	-3.406225	2.808004	2.436232
41	1	0	-1.908215	2.445060	1.564235
42	1	0	-3.392737	2.807741	0.666208

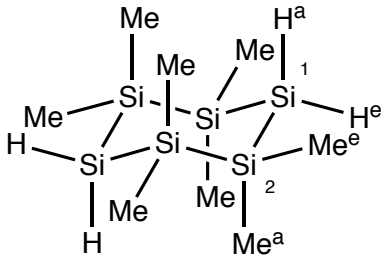

Si(1)-H^a dissociated radical (charge = 0, multiplicity = 2)

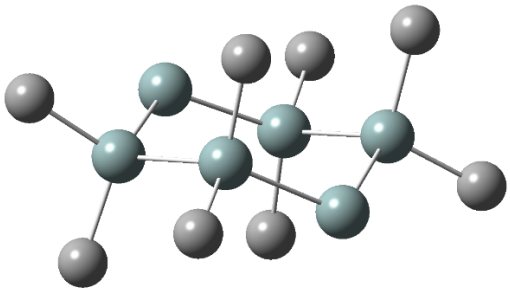

E(UB3LYP) = -2058.15686167 E_h

Center Number	Atomic Number	Atomic Type	Coordinates (Angstroms) X	Y	Z
1	14	0	-2.562477	-0.647836	-0.335273
2	14	0	-3.402079	0.457964	1.588572
3	14	0	-5.731075	0.111982	1.686254

4	1	0	-6.406101	0.965249	2.723273
5	14	0	-6.633225	-2.060017	1.548211
6	14	0	-5.743970	-3.092292	-0.393546
7	14	0	-3.386644	-2.868134	-0.388715
8	1	0	-2.817950	-3.580955	-1.580858
9	1	0	-2.847279	-3.598878	0.804354
10	6	0	-3.104805	0.279928	-1.913514
11	1	0	-2.693149	1.296487	-1.925460
12	1	0	-2.747613	-0.233602	-2.814158
13	1	0	-4.195055	0.362070	-1.984707
14	6	0	-0.652720	-0.692392	-0.290035
15	1	0	-0.253782	-1.198694	-1.177088
16	1	0	-0.235684	0.322136	-0.269760
17	1	0	-0.283039	-1.225712	0.592692
18	6	0	-6.195165	-4.949062	-0.430599
19	1	0	-7.283114	-5.088959	-0.447821
20	1	0	-5.783305	-5.431697	-1.324929
21	1	0	-5.802012	-5.478343	0.444523
22	6	0	-6.463364	-2.267728	-1.957657
23	1	0	-6.037078	-2.708971	-2.866464
24	1	0	-7.551167	-2.401101	-2.001574
25	1	0	-6.259290	-1.191560	-1.979404
26	6	0	-8.536598	-1.939649	1.449016
27	1	0	-8.987008	-2.938743	1.398391
28	1	0	-8.941629	-1.436289	2.334920
29	1	0	-8.861684	-1.377321	0.567120
30	6	0	-6.184438	-3.090562	3.095450
31	1	0	-6.566202	-2.616906	4.007329
32	1	0	-6.624220	-4.093847	3.028454
33	1	0	-5.100658	-3.206256	3.205188
34	6	0	-2.544828	-0.230274	3.153744
35	1	0	-1.463217	-0.048937	3.110638
36	1	0	-2.930548	0.254942	4.057845
37	1	0	-2.700174	-1.309446	3.259740
38	6	0	-3.058014	2.334832	1.504377
39	1	0	-3.476003	2.846639	2.379367
40	1	0	-1.978992	2.532300	1.486986
41	1	0	-3.499162	2.787815	0.610077

Si(1)-H^{e} dissociated radical (charge = 0, multiplicity = 2)

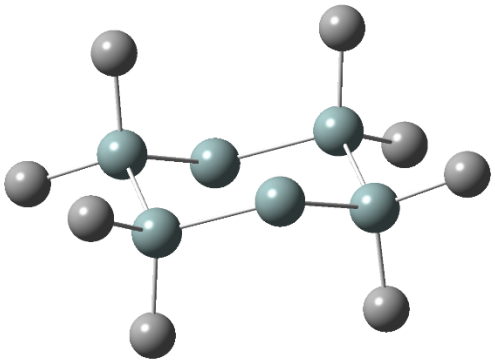

E(UB3LYP) = -2058.15931009 E_h

Center Number	Atomic Number	Atomic Type	Coordinates (Angstroms) X	Y	Z
1	14	0	-2.559998	-0.647007	-0.347115
2	14	0	-3.435971	0.458887	1.569234
3	14	0	-5.775149	0.171354	1.588668
4	1	0	-6.398297	0.989970	0.491356
5	14	0	-6.627592	-2.024390	1.527075
6	14	0	-5.745744	-3.093625	-0.406798
7	14	0	-3.388322	-2.865825	-0.404892
8	1	0	-2.823427	-3.574420	-1.601243
9	1	0	-2.845375	-3.601760	0.783424
10	6	0	-3.092718	0.283486	-1.926951
11	1	0	-2.683101	1.300919	-1.933491
12	1	0	-2.726846	-0.227328	-2.825648
13	1	0	-4.182443	0.363277	-2.006647
14	6	0	-0.649428	-0.689760	-0.292255
15	1	0	-0.246614	-1.196781	-1.177374
16	1	0	-0.234625	0.325563	-0.271516
17	1	0	-0.283185	-1.221686	0.592667
18	6	0	-6.197097	-4.951806	-0.428628
19	1	0	-7.284934	-5.091502	-0.448876
20	1	0	-5.781317	-5.441837	-1.317350
21	1	0	-5.806951	-5.472879	0.452679
22	6	0	-6.467590	-2.283702	-1.977281
23	1	0	-6.045110	-2.737520	-2.881653
24	1	0	-7.555880	-2.414377	-2.017035
25	1	0	-6.260005	-1.208702	-2.012538
26	6	0	-8.534737	-1.975438	1.465830
27	1	0	-8.950903	-2.989354	1.419717
28	1	0	-8.939223	-1.488144	2.360698
29	1	0	-8.895808	-1.422699	0.591715
30	6	0	-6.088581	-2.974055	3.091570
31	1	0	-6.475710	-2.490694	3.996135
32	1	0	-6.471355	-4.001688	3.071170

33	1	0	-4.997831	-3.027985	3.181223
34	6	0	-2.681435	-0.295153	3.151032
35	1	0	-1.591855	-0.169007	3.158795
36	1	0	-3.081649	0.195297	4.046009
37	1	0	-2.892309	-1.367125	3.234078
38	6	0	-3.020245	2.321721	1.522462
39	1	0	-3.420959	2.831124	2.406696
40	1	0	-1.934953	2.480902	1.508267
41	1	0	-3.443723	2.806757	0.636142

Si(2)-Me[a] dissociated radical (charge = 0, multiplicity = 2)

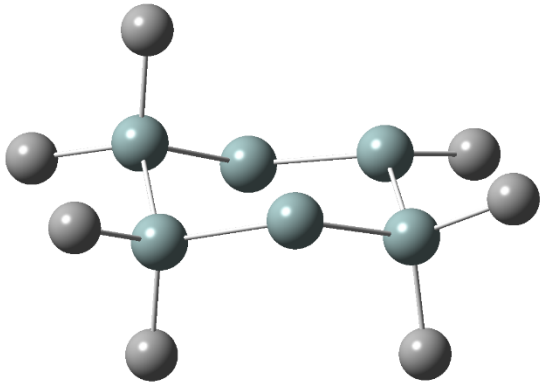

E(UB3LYP) = -2018.83157300 E_h

Center Number	Atomic Number	Atomic Type	Coordinates (Angstroms) X	Y	Z
1	14	0	-2.583903	-0.649939	-0.426802
2	14	0	-3.628982	0.512195	1.341123
3	14	0	-5.960535	0.259839	1.519456
4	1	0	-6.412706	0.940495	2.775678
5	1	0	-6.670030	0.976298	0.407070
6	14	0	-6.622662	-2.011982	1.531712
7	14	0	-5.785946	-3.050832	-0.429023
8	14	0	-3.426469	-2.861994	-0.452566
9	1	0	-2.878399	-3.573256	-1.654903
10	1	0	-2.876804	-3.593623	0.733319
11	6	0	-2.916968	0.181983	-2.116288
12	1	0	-2.529138	1.207484	-2.129343
13	1	0	-2.421562	-0.373976	-2.922080
14	1	0	-3.987025	0.225401	-2.346125
15	6	0	-0.697000	-0.677751	-0.144790
16	1	0	-0.194157	-1.222627	-0.952885
17	1	0	-0.287259	0.339532	-0.123785
18	1	0	-0.440173	-1.165330	0.801468
19	6	0	-6.265794	-4.899727	-0.477595

20	1	0	-7.355779	-5.022945	-0.482191
21	1	0	-5.872262	-5.380301	-1.381248
22	1	0	-5.869711	-5.442715	0.387744
23	6	0	-6.511566	-2.199493	-1.976739
24	1	0	-6.111772	-2.646400	-2.894761
25	1	0	-7.602865	-2.306419	-2.003449
26	1	0	-6.283801	-1.127809	-1.998668
27	6	0	-8.529281	-2.116294	1.590910
28	1	0	-8.864921	-3.160476	1.608489
29	1	0	-8.919611	-1.626598	2.491058
30	1	0	-8.987254	-1.630798	0.721959
31	6	0	-5.910783	-2.856115	3.087380
32	1	0	-6.288256	-2.377090	3.998618
33	1	0	-6.195765	-3.914604	3.124759
34	1	0	-4.816694	-2.803138	3.110801
35	6	0	-3.036219	2.318350	1.580002
36	1	0	-3.431158	2.735224	2.512719
37	1	0	-1.942668	2.370755	1.621565
38	1	0	-3.375254	2.958795	0.756045

Si(2)-Me[e] dissociated radical (charge = 0, multiplicity = 2)

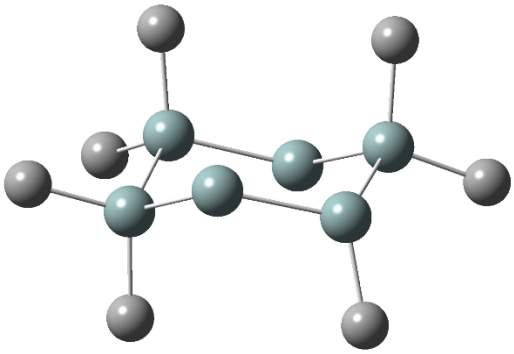

E(UB3LYP) = -2018.83335389 E_h

Center Number	Atomic Number	Atomic Type	Coordinates (Angstroms) X	Y	Z
1	14	0	-2.560124	-0.689025	-0.372079
2	14	0	-3.502819	0.378703	1.509856
3	14	0	-5.846935	0.196682	1.590758
4	1	0	-6.365423	0.888841	2.814146
5	1	0	-6.416786	0.935322	0.419999
6	14	0	-6.631745	-2.043904	1.521334
7	14	0	-5.772836	-3.078695	-0.434483
8	14	0	-3.410560	-2.903702	-0.449284
9	1	0	-2.861838	-3.631977	-1.642536

10	1	0	-2.877732	-3.635862	0.745376
11	6	0	-3.041970	0.250740	-1.959092
12	1	0	-2.617981	1.261721	-1.948095
13	1	0	-2.661861	-0.264403	-2.849411
14	1	0	-4.128093	0.346942	-2.065660
15	6	0	-0.659086	-0.729268	-0.228960
16	1	0	-0.216305	-1.233434	-1.096220
17	1	0	-0.250294	0.287492	-0.186521
18	1	0	-0.333354	-1.263421	0.670143
19	6	0	-6.255027	-4.927465	-0.481671
20	1	0	-7.345092	-5.049586	-0.494253
21	1	0	-5.855381	-5.410461	-1.381341
22	1	0	-5.865928	-5.469069	0.387696
23	6	0	-6.488512	-2.231395	-1.988626
24	1	0	-6.084455	-2.682692	-2.902623
25	1	0	-7.579850	-2.336107	-2.020775
26	1	0	-6.257472	-1.160692	-2.013788
27	6	0	-8.542699	-2.063940	1.515371
28	1	0	-8.924390	-3.092147	1.488071
29	1	0	-8.940547	-1.584910	2.417895
30	1	0	-8.948791	-1.531557	0.648197
31	6	0	-6.018015	-2.966313	3.075979
32	1	0	-6.393391	-2.490023	3.989556
33	1	0	-6.367495	-4.005932	3.075726
34	1	0	-4.923856	-2.984290	3.132949
35	6	0	-2.684603	-0.155402	3.158597
36	1	0	-1.607809	0.045788	3.140290
37	1	0	-3.115570	0.392125	4.003718
38	1	0	-2.821234	-1.227817	3.347683

Si(2)-Si(2) dissociated radical (charge = 0, multiplicity = 3)

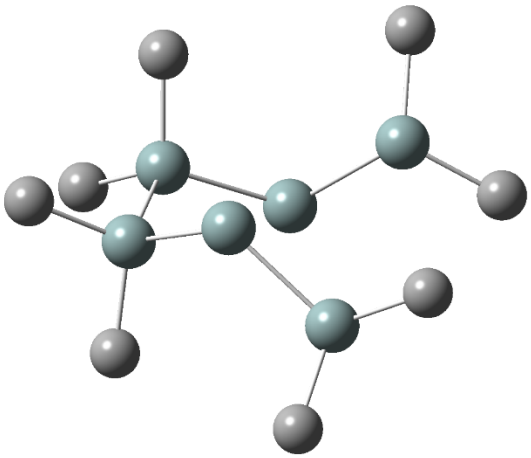

E(UB3LYP) = -2058.68886887 E_h

Center Number	Atomic Number	Atomic Type	Coordinates (Angstroms) X	Y	Z
1	14	0	-2.486994	-0.799159	-1.543249
2	14	0	-3.630160	0.520909	2.848114
3	14	0	-5.722437	0.249924	1.794674
4	1	0	-6.783239	1.002802	2.548484
5	1	0	-5.650697	0.902830	0.450614
6	14	0	-6.425039	-2.002627	1.565812
7	14	0	-5.673539	-2.952117	-0.473798
8	14	0	-3.317829	-2.839407	-0.703030
9	1	0	-2.881315	-3.975327	-1.586664
10	1	0	-2.663389	-3.093488	0.618161
11	6	0	-2.904126	-0.532145	-3.385051
12	1	0	-2.574720	0.459698	-3.716247
13	1	0	-2.401632	-1.278200	-4.015401
14	1	0	-3.981081	-0.607172	-3.568076
15	6	0	-0.611811	-0.593399	-1.264683
16	1	0	-0.043111	-1.337362	-1.838598
17	1	0	-0.278128	0.401073	-1.583940
18	1	0	-0.354122	-0.714529	-0.207571
19	6	0	-6.180966	-4.794808	-0.530569
20	1	0	-7.269569	-4.908200	-0.456337
21	1	0	-5.860634	-5.255948	-1.472376
22	1	0	-5.727896	-5.364461	0.288614
23	6	0	-6.501815	-2.059931	-1.944935
24	1	0	-6.184680	-2.494793	-2.900532
25	1	0	-7.593572	-2.148285	-1.887952
26	1	0	-6.254731	-0.992521	-1.960756
27	6	0	-8.336204	-2.039681	1.598524
28	1	0	-8.714516	-3.065293	1.507528
29	1	0	-8.715951	-1.625774	2.540253
30	1	0	-8.765035	-1.449896	0.780504
31	6	0	-5.778311	-3.026009	3.042204
32	1	0	-6.139995	-2.618260	3.994038
33	1	0	-6.120712	-4.065878	2.976969
34	1	0	-4.683061	-3.036855	3.074902
35	6	0	-3.713306	0.236616	4.732433
36	1	0	-2.711967	0.286876	5.175981
37	1	0	-4.333398	1.000565	5.220446
38	1	0	-4.137352	-0.744384	4.971410
39	6	0	-2.818837	2.204733	2.473575
40	1	0	-3.411456	3.031526	2.887559
41	1	0	-1.815829	2.258972	2.913142
42	1	0	-2.725754	2.363624	1.394257

Si(1)-Si(2) dissociated radical (charge = 0, multiplicity = 3)

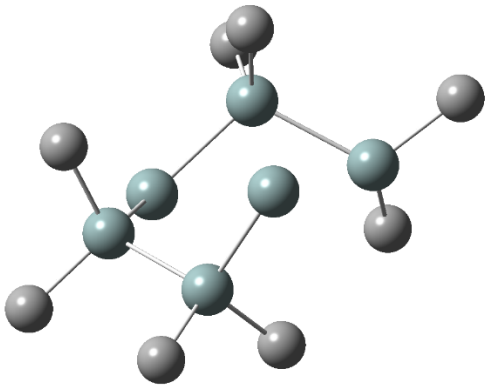

E(UB3LYP) = -2058.68840089 E_h

Center Number	Atomic Number	Atomic Type	Coordinates (Angstroms) X	Y	Z
1	14	0	-2.524417	-0.583065	-0.134458
2	14	0	-2.548274	0.295425	2.057123
3	14	0	-7.539103	0.330929	0.520647
4	1	0	-8.170028	1.219458	1.547101
5	1	0	-8.325293	0.473807	-0.744181
6	14	0	-7.150796	-1.890146	1.208987
7	14	0	-5.831808	-3.009590	-0.419803
8	14	0	-3.498717	-2.745171	-0.099703
9	1	0	-2.837424	-3.564346	-1.170946
10	1	0	-3.122538	-3.417768	1.185581
11	6	0	-3.483497	0.584351	-1.297851
12	1	0	-2.998505	1.566905	-1.347408
13	1	0	-3.519870	0.182050	-2.317461
14	1	0	-4.513755	0.737545	-0.956748
15	6	0	-0.740320	-0.762354	-0.806478
16	1	0	-0.750135	-1.188997	-1.817036
17	1	0	-0.239502	0.212159	-0.856945
18	1	0	-0.135027	-1.419821	-0.172759
19	6	0	-6.198405	-4.883221	-0.313740
20	1	0	-7.259734	-5.087240	-0.500839
21	1	0	-5.614837	-5.434625	-1.060534
22	1	0	-5.946601	-5.291457	0.671580
23	6	0	-6.301922	-2.412239	-2.171149
24	1	0	-5.725781	-2.951580	-2.932612
25	1	0	-7.365357	-2.589033	-2.372922

26	1	0	-6.111469	-1.341475	-2.303059
27	6	0	-8.825193	-2.798826	1.391911
28	1	0	-8.663801	-3.835243	1.714241
29	1	0	-9.456686	-2.307433	2.141039
30	1	0	-9.380682	-2.821858	0.448004
31	6	0	-6.298827	-1.842344	2.911661
32	1	0	-6.941928	-1.358851	3.656599
33	1	0	-6.080965	-2.856901	3.266999
34	1	0	-5.354005	-1.288005	2.871826
35	6	0	-1.429918	-0.660293	3.271904
36	1	0	-0.367823	-0.514409	3.032559
37	1	0	-1.587367	-0.315249	4.300573
38	1	0	-1.636758	-1.735333	3.242775
39	6	0	-2.161129	2.162342	2.158942
40	1	0	-2.325740	2.536529	3.176357
41	1	0	-1.114941	2.369084	1.895567
42	1	0	-2.800043	2.740531	1.483086

---

lin-(**1,4Si$_6$**)$_3$ and its radical species

lin-(**1,4Si$_6$**)$_3$ (charge = 0, multiplicity = 1)

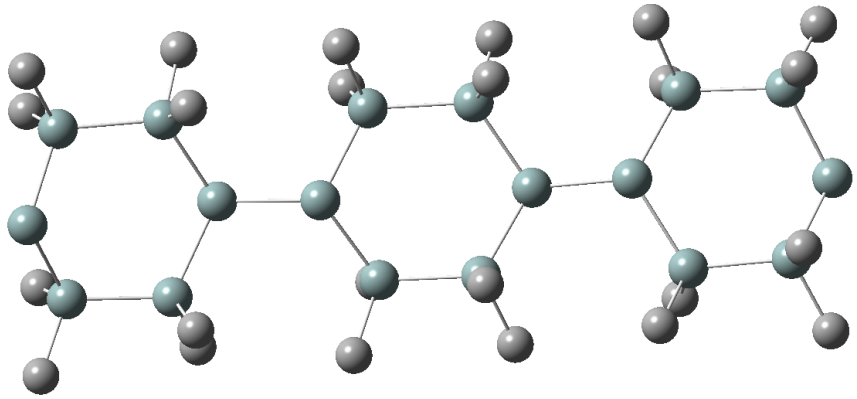

E(RB3LYP) = -6174.01411855 E_h

Center Number	Atomic Number	Atomic Type	Coordinates (Angstroms) X	Y	Z
1	14	0	-0.848100	3.133600	9.954000
2	14	0	0.948700	2.553400	8.540300
3	1	0	2.205000	2.493300	9.355700
4	1	0	1.185600	3.617500	7.509500
5	14	0	0.606800	0.463000	7.502900
6	6	0	-0.516500	4.832100	10.767200
7	1	0	-0.422100	5.614200	10.004300
8	1	0	0.408700	4.824800	11.353700
9	1	0	-1.337600	5.117400	11.436500
10	6	0	-2.459900	3.279400	8.939400
11	1	0	-3.290600	3.597200	9.581300
12	1	0	-2.745400	2.330000	8.473500
13	1	0	-2.354800	4.024000	8.141200
14	6	0	-0.921100	0.560000	6.360500
15	1	0	-0.811900	1.368100	5.627400
16	1	0	-1.845400	0.740500	6.920000
17	1	0	-1.046100	-0.377300	5.805000
18	6	0	2.119100	0.024700	6.418300
19	1	0	1.990200	-0.951900	5.935400
20	1	0	3.041400	-0.011200	7.008200
21	1	0	2.257600	0.771600	5.627300
22	14	0	0.317600	-1.274700	9.103200
23	14	0	-1.083600	1.515800	11.676600
24	6	0	-0.465700	-2.715600	8.114400
25	1	0	-0.664000	-3.600300	8.726200
26	1	0	-1.419600	-2.400800	7.675600

27	1	0	0.193400	-3.021300	7.291800
28	6	0	2.052100	-1.765200	9.735100
29	1	0	2.687800	-2.100400	8.906700
30	1	0	2.550100	-0.912300	10.210900
31	1	0	2.005700	-2.574100	10.471900
32	6	0	0.354300	1.798100	12.902600
33	1	0	0.331100	1.088600	13.735800
34	1	0	1.321500	1.686600	12.398400
35	1	0	0.314800	2.810800	13.322100
36	6	0	-2.767900	1.897900	12.504700
37	1	0	-2.763600	2.902100	12.947100
38	1	0	-3.570700	1.866600	11.759100
39	1	0	-3.028600	1.187600	13.295000
40	14	0	-1.093700	-0.763200	10.965900
41	1	0	-2.494700	-1.012400	10.480000
42	14	0	-1.039400	-4.566800	12.119500
43	14	0	-1.125700	-6.246000	13.820300
44	14	0	-2.138400	-5.722400	15.908600
45	1	0	-3.624200	-5.823400	15.705200
46	14	0	-1.707000	-3.458700	16.491000
47	14	0	-2.054300	-1.889100	14.734900
48	14	0	-0.746400	-2.299200	12.790500
49	1	0	0.689400	-2.148000	13.207700
50	6	0	-2.644900	-4.676200	11.087000
51	1	0	-2.619400	-3.980400	10.240900
52	1	0	-2.789200	-5.686600	10.686700
53	1	0	-3.526400	-4.428000	11.689900
54	6	0	-3.904600	-1.863300	14.259200
55	1	0	-4.232900	-2.832700	13.866400
56	1	0	-4.528400	-1.631100	15.130900
57	1	0	-4.110900	-1.107900	13.491800
58	6	0	-2.906600	-2.866300	17.862000
59	1	0	-2.840900	-3.469000	18.771700
60	1	0	-2.691400	-1.826900	18.139000
61	1	0	-3.944900	-2.908900	17.512800
62	6	0	-2.103100	-7.663100	12.980600
63	1	0	-1.593600	-8.008300	12.072000
64	1	0	-2.236300	-8.529600	13.634600
65	1	0	-3.099900	-7.313800	12.689600
66	6	0	0.672300	-6.803500	14.155800
67	1	0	0.714700	-7.608500	14.897400
68	1	0	1.152100	-7.165300	13.238800
69	1	0	1.275900	-5.972600	14.540300
70	6	0	0.436100	-5.143500	11.042900
71	1	0	0.283600	-6.175000	10.700400
72	1	0	0.580900	-4.520800	10.155800

73	1	0	1.367800	-5.121100	11.619000
74	6	0	-1.601900	-0.220800	15.559300
75	1	0	-1.747500	0.634400	14.894500
76	1	0	-2.223800	-0.056100	16.448000
77	1	0	-0.554400	-0.215500	15.881800
78	6	0	0.097100	-3.286400	17.097300
79	1	0	0.306000	-2.258600	17.418400
80	1	0	0.307200	-3.948800	17.944500
81	1	0	0.807400	-3.533900	16.299800
82	14	0	-1.568300	-7.336700	17.606200
83	1	0	-0.067200	-7.326100	17.692700
84	14	0	-2.317000	-6.692100	19.783300
85	14	0	-2.129400	-8.380400	21.444700
86	14	0	-3.092900	-10.393100	20.684200
87	1	0	-3.055600	-11.443600	21.754400
88	1	0	-4.545300	-10.153200	20.401700
89	14	0	-2.053800	-11.175300	18.718100
90	14	0	-2.149100	-9.567800	16.965800
91	6	0	-2.921700	-12.772300	18.125400
92	1	0	-2.463500	-13.154600	17.204900
93	1	0	-2.844200	-13.557600	18.887000
94	1	0	-3.985800	-12.603400	17.927700
95	6	0	-3.910200	-9.575100	16.227600
96	1	0	-3.999400	-8.877800	15.387000
97	1	0	-4.177800	-10.575100	15.865600
98	1	0	-4.654200	-9.283300	16.978000
99	6	0	-0.896000	-10.223400	15.675800
100	1	0	-1.177600	-11.233800	15.352500
101	1	0	-0.827900	-9.598300	14.781400
102	1	0	0.106500	-10.283600	16.114500
103	6	0	-0.227300	-11.606600	19.078700
104	1	0	-0.148000	-12.346100	19.884400
105	1	0	0.248500	-12.034600	18.187700
106	1	0	0.355200	-10.727100	19.374300
107	6	0	-3.033300	-7.789700	23.022400
108	1	0	-2.930100	-8.529800	23.825000
109	1	0	-2.617500	-6.842300	23.386800
110	1	0	-4.103500	-7.641100	22.841700
111	6	0	-0.292600	-8.653800	21.891500
112	1	0	0.142300	-7.733500	22.300100
113	1	0	-0.183300	-9.437600	22.650500
114	1	0	0.305700	-8.945100	21.021400
115	6	0	-1.220900	-5.257600	20.420200
116	1	0	-1.188200	-4.406300	19.735000
117	1	0	-1.587800	-4.892700	21.388000
118	1	0	-0.190500	-5.602600	20.564800

119	6	0	-4.146300	-6.149000	19.698800
120	1	0	-4.792900	-6.994000	19.434600
121	1	0	-4.484600	-5.764500	20.668700
122	1	0	-4.306400	-5.363400	18.952600

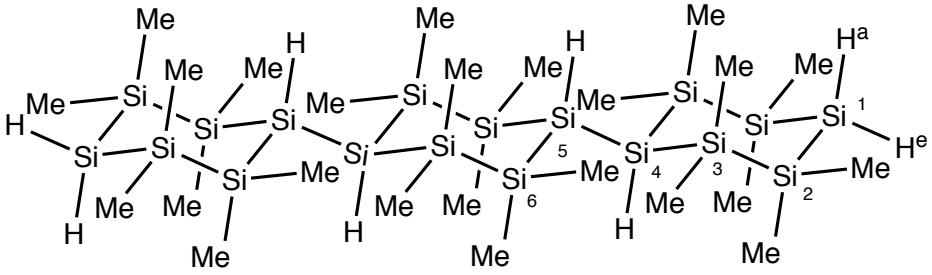

Si(1)-H[a] dissociated radical (charge = 0, multiplicity = 2)

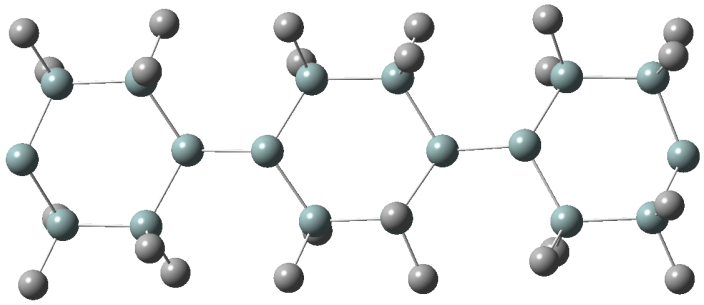

E(UB3LYP) = -6173.37304659 E_h

Center Number	Atomic Number	Atomic Type	Coordinates (Angstroms) X	Y	Z
1	14	0	-0.897227	3.143234	9.958021
2	14	0	0.870825	2.531058	8.540819
3	1	0	1.331312	3.626779	7.620464
4	14	0	0.624216	0.446989	7.488996
5	6	0	-0.541088	4.841213	10.758649
6	1	0	-0.437476	5.617079	9.990715
7	1	0	0.383402	4.826080	11.345712
8	1	0	-1.359800	5.139902	11.425170
9	6	0	-2.530697	3.295029	8.972920
10	1	0	-3.354218	3.590121	9.635506
11	1	0	-2.808453	2.350031	8.493376
12	1	0	-2.443631	4.055250	8.187874
13	6	0	-0.860357	0.482775	6.282076
14	1	0	-0.725699	1.261400	5.522251
15	1	0	-1.805316	0.680831	6.799604
16	1	0	-0.956443	-0.479174	5.762988
17	6	0	2.187260	0.043416	6.466805
18	1	0	2.095351	-0.935153	5.979253
19	1	0	3.086156	0.025499	7.092067

20	1	0	2.340493	0.793125	5.681298
21	14	0	0.315438	-1.275001	9.102967
22	14	0	-1.108195	1.518638	11.676584
23	6	0	-0.469508	-2.717670	8.117631
24	1	0	-0.676101	-3.597653	8.733345
25	1	0	-1.419071	-2.401006	7.671039
26	1	0	0.193004	-3.032099	7.300971
27	6	0	2.044691	-1.769845	9.745017
28	1	0	2.684616	-2.108231	8.921183
29	1	0	2.541262	-0.917085	10.222509
30	1	0	1.991192	-2.577239	10.482931
31	6	0	0.330401	1.812918	12.898131
32	1	0	0.320883	1.097237	13.726368
33	1	0	1.296222	1.718588	12.387891
34	1	0	0.278413	2.821979	13.324912
35	6	0	-2.793000	1.884418	12.510842
36	1	0	-2.799017	2.891852	12.946127
37	1	0	-3.599434	1.837724	11.769958
38	1	0	-3.040325	1.177022	13.307907
39	14	0	-1.102010	-0.758843	10.960669
40	1	0	-2.500952	-1.015031	10.472559
41	14	0	-1.049333	-4.562864	12.116405
42	14	0	-1.137013	-6.242936	13.816462
43	14	0	-2.138956	-5.717501	15.909489
44	1	0	-3.625976	-5.813521	15.712822
45	14	0	-1.697159	-3.455568	16.490071
46	14	0	-2.050921	-1.885203	14.735896
47	14	0	-0.751025	-2.295041	12.785763
48	1	0	0.686360	-2.145850	13.198193
49	6	0	-2.656651	-4.668888	11.086383
50	1	0	-2.631531	-3.972707	10.240527
51	1	0	-2.803631	-5.678839	10.685881
52	1	0	-3.536547	-4.419298	11.691015
53	6	0	-3.903332	-1.860447	14.268068
54	1	0	-4.232447	-2.830324	13.877034
55	1	0	-4.523649	-1.628636	15.142347
56	1	0	-4.113782	-1.105626	13.501425
57	6	0	-2.887227	-2.859967	17.867936
58	1	0	-2.820126	-3.465046	18.776012
59	1	0	-2.665575	-1.822254	18.146122
60	1	0	-3.927389	-2.896828	17.523734
61	6	0	-2.123726	-7.655148	12.979479
62	1	0	-1.619007	-8.002267	12.068880
63	1	0	-2.258727	-8.521284	13.633496
64	1	0	-3.119873	-7.300932	12.692126
65	6	0	0.660090	-6.807478	14.145012

66	1	0	0.702619	-7.610975	14.888201
67	1	0	1.134355	-7.173136	13.226698
68	1	0	1.268813	-5.978226	14.524957
69	6	0	0.423943	-5.143741	11.038879
70	1	0	0.267206	-6.174116	10.694757
71	1	0	0.572014	-4.520412	10.152965
72	1	0	1.355469	-5.126252	11.615463
73	6	0	-1.595008	-0.217849	15.560385
74	1	0	-1.742585	0.638630	14.897642
75	1	0	-2.213235	-0.054279	16.451759
76	1	0	-0.546212	-0.213619	15.878724
77	6	0	0.110676	-3.289464	17.086715
78	1	0	0.325160	-2.262368	17.406234
79	1	0	0.322586	-3.952322	17.933105
80	1	0	0.815902	-3.540131	16.285649
81	14	0	-1.566488	-7.334750	17.603294
82	1	0	-0.065023	-7.328806	17.683788
83	14	0	-2.304584	-6.689886	19.783842
84	14	0	-2.117350	-8.380776	21.442811
85	14	0	-3.088132	-10.390322	20.683158
86	1	0	-3.049763	-11.441954	21.752245
87	1	0	-4.540904	-10.146729	20.405891
88	14	0	-2.057711	-11.172972	18.712720
89	14	0	-2.156749	-9.563409	16.962777
90	6	0	-2.931140	-12.767726	18.121820
91	1	0	-2.476363	-13.150668	17.199903
92	1	0	-2.853427	-13.553512	18.882878
93	1	0	-3.995348	-12.596175	17.927110
94	6	0	-3.921422	-9.564591	16.233125
95	1	0	-4.013548	-8.863887	15.395737
96	1	0	-4.192577	-10.562763	15.868623
97	1	0	-4.661167	-9.274431	16.988364
98	6	0	-0.911923	-10.220620	15.665604
99	1	0	-1.198782	-11.229163	15.341157
100	1	0	-0.845601	-9.593627	14.772452
101	1	0	0.092400	-10.285679	16.099519
102	6	0	-0.230895	-11.608416	19.066198
103	1	0	-0.150331	-12.349536	19.870356
104	1	0	0.240939	-12.035780	18.172872
105	1	0	0.354338	-10.730613	19.361406
106	6	0	-3.015584	-7.789261	23.023452
107	1	0	-2.912217	-8.530415	23.825127
108	1	0	-2.596348	-6.843287	23.387710
109	1	0	-4.085825	-7.637700	22.845762
110	6	0	-0.280155	-8.659263	21.884895
111	1	0	0.158061	-7.740383	22.293195

112	1	0	-0.171015	-9.443844	22.643084
113	1	0	0.315505	-8.951418	21.013238
114	6	0	-1.200984	-5.260113	20.418590
115	1	0	-1.168440	-4.407442	19.734964
116	1	0	-1.562619	-4.895861	21.388604
117	1	0	-0.171147	-5.608716	20.558134
118	6	0	-4.132071	-6.139829	19.706605
119	1	0	-4.783070	-6.982395	19.445345
120	1	0	-4.464934	-5.753589	20.677669
121	1	0	-4.292175	-5.353935	18.960661

Si(1)-H^{e} dissociated radical (charge = 0, multiplicity = 2)

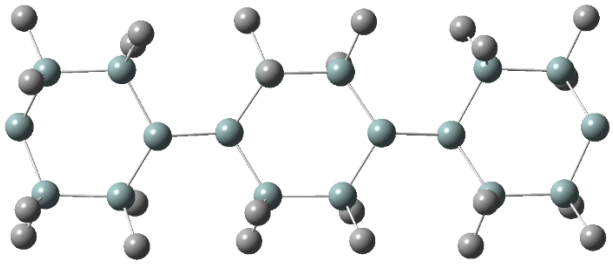

E(UB3LYP) = -6173.37569970 E_h

Center Number	Atomic Number	Atomic Type	Coordinates (Angstroms) X	Y	Z
1	14	0	-0.856206	3.144317	9.960147
2	14	0	0.914921	2.536780	8.544028
3	1	0	2.217217	2.560774	9.296391
4	14	0	0.612720	0.459763	7.492902
5	6	0	-0.511555	4.832638	10.785027
6	1	0	-0.429138	5.621867	10.028457
7	1	0	0.422151	4.818854	11.357607
8	1	0	-1.322952	5.109687	11.469492
9	6	0	-2.472348	3.293439	8.955769
10	1	0	-3.305286	3.585745	9.606738
11	1	0	-2.746075	2.350420	8.469932
12	1	0	-2.377023	4.056188	8.174069
13	6	0	-0.906289	0.541062	6.340256
14	1	0	-0.782949	1.329503	5.588662
15	1	0	-1.831468	0.746001	6.890058
16	1	0	-1.038224	-0.409194	5.809006
17	6	0	2.139414	0.021250	6.431518
18	1	0	2.023995	-0.964320	5.963571
19	1	0	3.055758	0.003536	7.031267
20	1	0	2.277384	0.756960	5.630385

21	14	0	0.311886	-1.279759	9.100992
22	14	0	-1.094466	1.511867	11.679027
23	6	0	-0.465746	-2.725073	8.112374
24	1	0	-0.664381	-3.608287	8.726467
25	1	0	-1.418549	-2.413379	7.669362
26	1	0	0.197550	-3.031384	7.293400
27	6	0	2.046613	-1.762490	9.736465
28	1	0	2.683606	-2.102498	8.911083
29	1	0	2.541238	-0.904391	10.206200
30	1	0	2.000885	-2.566069	10.479083
31	6	0	0.344766	1.792775	12.902653
32	1	0	0.327340	1.075841	13.729685
33	1	0	1.310274	1.690307	12.393697
34	1	0	0.300933	2.801537	13.330952
35	6	0	-2.778205	1.891678	12.511545
36	1	0	-2.772129	2.894392	12.957316
37	1	0	-3.582566	1.863000	11.767597
38	1	0	-3.036881	1.178501	13.300075
39	14	0	-1.102782	-0.763876	10.959535
40	1	0	-2.503891	-1.017352	10.476519
41	14	0	-1.040109	-4.566367	12.117645
42	14	0	-1.127095	-6.245545	13.818560
43	14	0	-2.138540	-5.721576	15.907368
44	1	0	-3.624466	-5.821948	15.704741
45	14	0	-1.705382	-3.458045	16.488515
46	14	0	-2.055215	-1.888135	14.733140
47	14	0	-0.750049	-2.297473	12.786407
48	1	0	0.686298	-2.143198	13.200441
49	6	0	-2.644492	-4.677946	11.083674
50	1	0	-2.619831	-3.981649	10.237890
51	1	0	-2.786812	-5.688392	10.682739
52	1	0	-3.526784	-4.431680	11.686157
53	6	0	-3.906224	-1.863706	14.259869
54	1	0	-4.233947	-2.833467	13.867396
55	1	0	-4.529116	-1.632487	15.132478
56	1	0	-4.114675	-1.108574	13.492961
57	6	0	-2.902655	-2.864883	17.861188
58	1	0	-2.835883	-3.467730	18.770763
59	1	0	-2.686487	-1.825650	18.137977
60	1	0	-3.941491	-2.907010	17.513613
61	6	0	-2.105853	-7.661753	12.979013
62	1	0	-1.596751	-8.007483	12.070319
63	1	0	-2.239647	-8.528029	13.633101
64	1	0	-3.102390	-7.311556	12.688133
65	6	0	0.670588	-6.804379	14.153377
66	1	0	0.712565	-7.609285	14.895102

67	1	0	1.149777	-7.166775	13.236312
68	1	0	1.275131	-5.973994	14.537474
69	6	0	0.437615	-5.142230	11.043545
70	1	0	0.285896	-6.173671	10.700376
71	1	0	0.584609	-4.519402	10.157040
72	1	0	1.368056	-5.120082	11.621721
73	6	0	-1.602412	-0.220728	15.559372
74	1	0	-1.748121	0.636144	14.896718
75	1	0	-2.223607	-0.057800	16.448805
76	1	0	-0.554708	-0.216231	15.881249
77	6	0	0.099661	-3.286641	17.092248
78	1	0	0.309847	-2.258904	17.412534
79	1	0	0.310331	-3.948768	17.939503
80	1	0	0.808786	-3.535231	16.293975
81	14	0	-1.567875	-7.335729	17.604772
82	1	0	-0.066673	-7.326205	17.689606
83	14	0	-2.313886	-6.690187	19.782450
84	14	0	-2.126495	-8.378583	21.443847
85	14	0	-3.092371	-10.390451	20.684227
86	1	0	-3.055096	-11.440862	21.754540
87	1	0	-4.544775	-10.149315	20.402966
88	14	0	-2.055434	-11.173705	18.717429
89	14	0	-2.151200	-9.566410	16.965073
90	6	0	-2.924927	-12.770262	18.125596
91	1	0	-2.467085	-13.153340	17.205255
92	1	0	-2.848074	-13.555254	18.887560
93	1	0	-3.988861	-12.600493	17.927861
94	6	0	-3.912970	-9.572073	16.228531
95	1	0	-4.002623	-8.873902	15.388765
96	1	0	-4.181383	-10.571630	15.865819
97	1	0	-4.656105	-9.280686	16.979967
98	6	0	-0.899808	-10.222863	15.673836
99	1	0	-1.182835	-11.232729	15.350145
100	1	0	-0.831493	-9.597399	14.779734
101	1	0	0.102926	-10.284599	16.111887
102	6	0	-0.229080	-11.606409	19.076732
103	1	0	-0.149961	-12.346247	19.882215
104	1	0	0.245876	-12.034544	18.185425
105	1	0	0.354294	-10.727508	19.372354
106	6	0	-3.028841	-7.786710	23.021998
107	1	0	-2.925856	-8.526741	23.824758
108	1	0	-2.611921	-6.839608	23.385984
109	1	0	-4.098987	-7.637133	22.842029
110	6	0	-0.289674	-8.653441	21.889597
111	1	0	0.146241	-7.733450	22.297840
112	1	0	-0.180583	-9.437139	22.648702

113	1	0	0.308013	-8.945402	21.019264
114	6	0	-1.215851	-5.256672	20.418299
115	1	0	-1.183233	-4.405181	19.733241
116	1	0	-1.581356	-4.891627	21.386557
117	1	0	-0.185605	-5.602548	20.561601
118	6	0	-4.142750	-6.145585	19.699525
119	1	0	-4.790368	-6.990238	19.436596
120	1	0	-4.479724	-5.760107	20.669470
121	1	0	-4.303054	-5.360384	18.952903

Si(4)-H dissociated radical (charge = 0, multiplicity = 2)

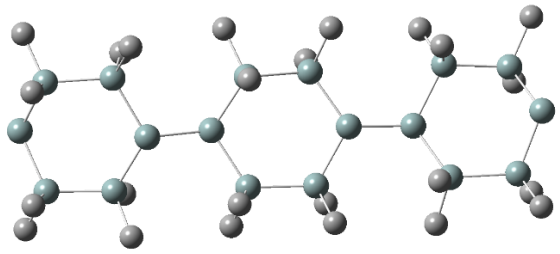

E(UB3LYP) = 12 E_h

Center Number	Atomic Number	Atomic Type	Coordinates (Angstroms) X	Y	Z
1	14	0	-1.389025	3.019528	9.805204
2	14	0	0.486642	2.703877	8.410357
3	1	0	1.727227	2.933247	9.219416
4	1	0	0.522376	3.726572	7.313444
5	14	0	0.542512	0.530373	7.498111
6	6	0	-1.414266	4.814582	10.463190
7	1	0	-1.480036	5.528783	9.633564
8	1	0	-0.507886	5.048674	11.032537
9	1	0	-2.277590	4.985154	11.118110
10	6	0	-3.004109	2.726120	8.829411
11	1	0	-3.877118	2.917002	9.465529
12	1	0	-3.081898	1.696928	8.462162
13	1	0	-3.071855	3.397040	7.964724
14	6	0	-0.890318	0.349441	6.246393
15	1	0	-0.824064	1.115589	5.464576
16	1	0	-1.871799	0.445488	6.723547
17	1	0	-0.853441	-0.630249	5.755106
18	6	0	2.181369	0.264402	6.550148
19	1	0	2.228220	-0.742644	6.117201
20	1	0	3.050297	0.389046	7.205372
21	1	0	2.275909	0.984538	5.728468

22	14	0	0.373563	-1.173006	9.155083
23	14	0	-1.238022	1.523481	11.642980
24	6	0	-0.217850	-2.712526	8.182283
25	1	0	-0.325821	-3.599195	8.813178
26	1	0	-1.190146	-2.519357	7.715151
27	1	0	0.491926	-2.958617	7.382050
28	6	0	2.119673	-1.482469	9.864156
29	1	0	2.829739	-1.728537	9.065471
30	1	0	2.498528	-0.594739	10.384005
31	1	0	2.120325	-2.309800	10.582434
32	6	0	0.331804	1.977926	12.631457
33	1	0	0.492433	1.306364	13.481446
34	1	0	1.222097	1.925999	11.993907
35	1	0	0.265037	3.001231	13.021034
36	6	0	-2.805208	1.835915	12.695125
37	1	0	-2.848806	2.886553	13.008792
38	1	0	-3.707401	1.627489	12.108279
39	1	0	-2.848800	1.219462	13.597790
40	14	0	-1.139555	-0.760302	10.961119
41	1	0	-2.504679	-1.058234	10.398440
42	14	0	-0.847080	-4.590748	12.130254
43	14	0	-0.967593	-6.246270	13.853797
44	14	0	-1.939031	-5.679744	15.952547
45	1	0	-3.428812	-5.654127	15.759378
46	14	0	-1.297243	-3.466904	16.546508
47	14	0	-1.750042	-1.844274	14.865637
48	14	0	-0.774167	-2.306319	12.761500
49	6	0	-2.352245	-4.837509	10.971987
50	1	0	-2.324979	-4.134020	10.132643
51	1	0	-2.372867	-5.854106	10.560811
52	1	0	-3.293431	-4.672379	11.508561
53	6	0	-3.647583	-1.674884	14.683870
54	1	0	-4.099117	-2.616525	14.352084
55	1	0	-4.108298	-1.400487	15.641500
56	1	0	-3.910679	-0.903802	13.951307
57	6	0	-2.288700	-2.797134	18.041591
58	1	0	-2.165152	-3.402106	18.943357
59	1	0	-1.965094	-1.776903	18.282936
60	1	0	-3.359663	-2.758347	17.811723
61	6	0	-1.972677	-7.649470	13.026207
62	1	0	-1.479603	-7.991713	12.107466
63	1	0	-2.095768	-8.518069	13.678434
64	1	0	-2.972535	-7.295097	12.752589
65	6	0	0.814266	-6.854302	14.189981
66	1	0	0.826910	-7.670472	14.920851
67	1	0	1.290064	-7.217681	13.271533

68	1	0	1.440035	-6.048046	14.590739
69	6	0	0.742476	-5.071724	11.175739
70	1	0	0.679331	-6.108182	10.819889
71	1	0	0.918454	-4.434832	10.304267
72	1	0	1.622078	-4.996704	11.824366
73	6	0	-1.057738	-0.217647	15.599242
74	1	0	-1.217338	0.639683	14.939356
75	1	0	-1.543277	0.008295	16.556802
76	1	0	0.019629	-0.299498	15.782407
77	6	0	0.566197	-3.445053	16.965421
78	1	0	0.892550	-2.438706	17.254724
79	1	0	0.799769	-4.122731	17.795007
80	1	0	1.170978	-3.754618	16.104995
81	14	0	-1.492747	-7.368602	17.615217
82	1	0	0.005013	-7.464079	17.708057
83	14	0	-2.197051	-6.692733	19.793554
84	14	0	-2.371979	-8.411622	21.424908
85	14	0	-3.526869	-10.263698	20.530919
86	1	0	-3.737706	-11.319263	21.576049
87	1	0	-4.898575	-9.821142	20.119188
88	14	0	-2.420975	-11.160491	18.651150
89	14	0	-2.218203	-9.540347	16.922905
90	6	0	-3.414457	-12.641397	17.961379
91	1	0	-2.925976	-13.067139	17.076107
92	1	0	-3.493678	-13.436183	18.712784
93	1	0	-4.430771	-12.348265	17.676848
94	6	0	-3.925999	-9.402568	16.077056
95	1	0	-3.916796	-8.694591	15.241493
96	1	0	-4.247531	-10.376426	15.688076
97	1	0	-4.687655	-9.062836	16.788815
98	6	0	-0.933063	-10.282139	15.711864
99	1	0	-1.279124	-11.252465	15.333118
100	1	0	-0.734098	-9.642100	14.847698
101	1	0	0.021449	-10.448217	16.224536
102	6	0	-0.697240	-11.805587	19.162499
103	1	0	-0.778613	-12.541355	19.971501
104	1	0	-0.204621	-12.297648	18.315339
105	1	0	-0.039250	-11.001085	19.508298
106	6	0	-3.327484	-7.713320	22.926754
107	1	0	-3.408189	-8.468276	23.718031
108	1	0	-2.814874	-6.840493	23.349831
109	1	0	-4.342839	-7.407386	22.652410
110	6	0	-0.643053	-8.946675	22.035101
111	1	0	-0.131320	-8.106338	22.519550
112	1	0	-0.720111	-9.755987	22.770966
113	1	0	-0.004272	-9.298414	21.217845

114	6	0	-0.897428	-5.464834	20.480234
115	1	0	-0.660362	-4.657496	19.780746
116	1	0	-1.247442	-5.006397	21.413822
117	1	0	0.038849	-5.991210	20.699107
118	6	0	-3.920012	-5.874562	19.679931
119	1	0	-4.680251	-6.614304	19.402150
120	1	0	-4.213571	-5.446349	20.646167
121	1	0	-3.950434	-5.073443	18.934739

Si(6)-Me[a] dissociated radical (charge = 0, multiplicity = 2)

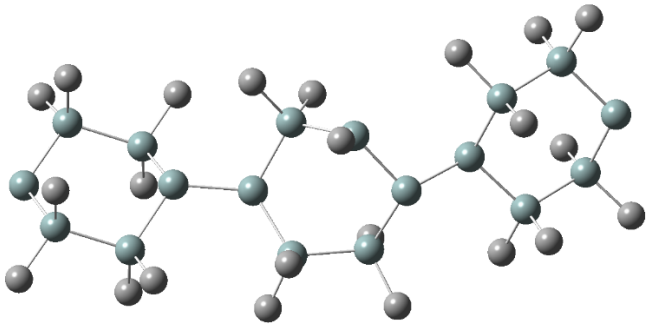

E(UB3LYP) = -6134.05889350 E_h

Center Number	Atomic Number	Atomic Type	Coordinates (Angstroms) X	Y	Z
1	14	0	0.710202	2.702833	10.968946
2	14	0	0.594593	2.492830	8.617206
3	1	0	1.933257	2.043229	8.114360
4	1	0	0.365499	3.837532	7.991715
5	14	0	-1.042737	0.969674	7.849378
6	6	0	2.193633	3.813582	11.436762
7	1	0	2.081278	4.815800	11.006064
8	1	0	3.138287	3.397017	11.070108
9	1	0	2.274334	3.925480	12.525175
10	6	0	-0.884992	3.524579	11.622569
11	1	0	-0.824013	3.678113	12.706935
12	1	0	-1.770793	2.911157	11.423638
13	1	0	-1.043081	4.504729	11.157218
14	6	0	-2.783667	1.634918	8.264713
15	1	0	-2.946054	2.619640	7.810423
16	1	0	-2.934596	1.734333	9.345141
17	1	0	-3.558945	0.960194	7.881467
18	6	0	-0.903289	0.803231	5.949870
19	1	0	-1.653911	0.105817	5.557813
20	1	0	0.085031	0.438442	5.649014

21	1	0	-1.063255	1.772518	5.462487
22	14	0	-0.732429	-1.161560	8.856617
23	14	0	0.954841	0.554646	11.948709
24	6	0	-2.146362	-2.296820	8.250279
25	1	0	-2.008035	-3.328264	8.592219
26	1	0	-3.122559	-1.951562	8.608983
27	1	0	-2.180974	-2.315109	7.153718
28	6	0	0.920153	-1.907110	8.257144
29	1	0	0.894315	-2.059016	7.170988
30	1	0	1.770008	-1.252505	8.478223
31	1	0	1.119281	-2.879289	8.722390
32	6	0	2.647559	-0.199549	11.488023
33	1	0	2.757120	-1.200512	11.922341
34	1	0	2.785682	-0.287270	10.405213
35	1	0	3.462323	0.423065	11.877674
36	6	0	0.929558	0.748542	13.849708
37	1	0	1.728681	1.425121	14.177640
38	1	0	-0.021190	1.156267	14.210472
39	1	0	1.092392	-0.217497	14.341060
40	14	0	-0.788742	-0.900267	11.224070
41	1	0	-2.084465	-0.182487	11.478896
42	14	0	-1.326194	-4.966670	11.759495
43	14	0	-1.051426	-6.583271	13.483184
44	14	0	-2.715958	-6.338187	15.180031
45	1	0	-3.896067	-7.163628	14.748254
46	14	0	-3.511234	-4.112962	15.241697
47	14	0	-1.980044	-2.405915	14.697102
48	14	0	-0.804032	-2.824676	12.646156
49	1	0	0.632403	-2.984016	13.067863
50	6	0	-3.095179	-5.068494	11.051383
51	1	0	-3.257410	-4.331840	10.257017
52	1	0	-3.278339	-6.062660	10.625304
53	1	0	-3.850213	-4.897472	11.825200
54	6	0	-2.936361	-0.756485	14.642044
55	1	0	-3.701873	-0.753974	13.858647
56	1	0	-3.433227	-0.571343	15.602002
57	1	0	-2.260321	0.083247	14.444894
58	6	0	-5.240813	-3.922583	14.432903
59	1	0	-5.940836	-4.654792	14.849954
60	1	0	-5.644841	-2.921877	14.622986
61	1	0	-5.214293	-4.071188	13.346442
62	6	0	-1.209750	-8.313777	12.681306
63	1	0	-0.432579	-8.460449	11.920917
64	1	0	-1.111996	-9.120674	13.416102
65	1	0	-2.183719	-8.430795	12.192654
66	6	0	0.696950	-6.382520	14.221929

67	1	0	0.896221	-7.130944	14.995710
68	1	0	1.459594	-6.497296	13.441670
69	1	0	0.831632	-5.391715	14.670021
70	6	0	-0.097562	-5.403001	10.359516
71	1	0	-0.284642	-6.414379	9.977902
72	1	0	-0.189800	-4.709083	9.516373
73	1	0	0.939810	-5.363739	10.710630
74	6	0	-0.690128	-2.330143	16.102177
75	1	0	0.058748	-1.552842	15.912834
76	1	0	-1.177301	-2.105689	17.058341
77	1	0	-0.162027	-3.284109	16.212815
78	14	0	-2.118186	-7.118962	17.360954
79	1	0	-0.964679	-6.264995	17.806443
80	14	0	-3.886270	-6.756223	18.923853
81	14	0	-3.246026	-7.400433	21.119669
82	14	0	-2.499362	-9.640769	21.136557
83	1	0	-2.099704	-10.047671	22.524410
84	1	0	-3.646451	-10.533589	20.770865
85	14	0	-0.728251	-10.031987	19.625052
86	14	0	-1.360562	-9.381370	17.428379
87	6	0	-0.280963	-11.890969	19.623308
88	1	0	0.542336	-12.099591	18.928882
89	1	0	0.036332	-12.214728	20.621905
90	1	0	-1.135165	-12.510474	19.328311
91	6	0	-2.739412	-10.537290	16.787905
92	1	0	-3.043583	-10.266811	15.769712
93	1	0	-2.391491	-11.577326	16.766365
94	1	0	-3.631850	-10.499427	17.422401
95	6	0	0.184767	-9.640616	16.332764
96	1	0	0.519677	-10.683908	16.391951
97	1	0	-0.015535	-9.418420	15.279954
98	1	0	1.017364	-9.005984	16.656523
99	6	0	0.817364	-9.050991	20.168611
100	1	0	1.135719	-9.346832	21.175390
101	1	0	1.655013	-9.240212	19.486295
102	1	0	0.634951	-7.970875	20.179775
103	6	0	-4.739271	-7.217990	22.299376
104	1	0	-4.460456	-7.492331	23.323909
105	1	0	-5.102392	-6.183130	22.318741
106	1	0	-5.572965	-7.861585	21.997270
107	6	0	-1.852663	-6.251660	21.741581
108	1	0	-2.204764	-5.214298	21.796456
109	1	0	-1.518529	-6.542322	22.744670
110	1	0	-0.980626	-6.270710	21.078566
111	6	0	-4.372547	-4.910996	19.010874
112	1	0	-4.730756	-4.541346	18.043362

113	1	0	-5.172785	-4.761635	19.747139
114	1	0	-3.522629	-4.285523	19.305979
115	6	0	-5.423337	-7.751178	18.381672
116	1	0	-5.230416	-8.829542	18.365096
117	1	0	-6.258562	-7.573525	19.070077
118	1	0	-5.750065	-7.456107	17.377379

Si(6)-Me^{e} dissociated radical (charge = 0, multiplicity = 2)

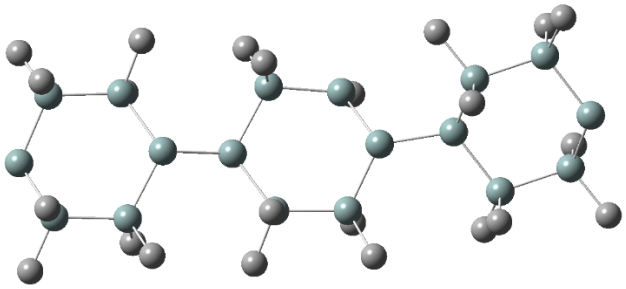

E(UB3LYP) = -6134.05908879 E_h

Center Number	Atomic Number	Atomic Type	Coordinates (Angstroms) X	Y	Z
1	14	0	-0.496714	3.142268	10.307288
2	14	0	0.414996	2.477347	8.237192
3	1	0	1.879938	2.214326	8.414804
4	1	0	0.320987	3.588549	7.233665
5	14	0	-0.611985	0.520632	7.417316
6	6	0	0.393890	4.714113	10.932950
7	1	0	0.254044	5.542237	10.227751
8	1	0	1.471100	4.550135	11.045205
9	1	0	-0.002087	5.033526	11.904871
10	6	0	-2.346671	3.567456	10.093879
11	1	0	-2.762944	3.950941	11.033157
12	1	0	-2.940597	2.695614	9.798743
13	1	0	-2.486067	4.341124	9.329414
14	6	0	-2.462451	0.845086	7.071365
15	1	0	-2.591839	1.666299	6.356330
16	1	0	-3.014354	1.104352	7.981414
17	1	0	-2.933523	-0.046964	6.640674
18	6	0	0.210223	0.008488	5.768527
19	1	0	-0.237054	-0.909991	5.368857
20	1	0	1.284708	-0.165311	5.891565
21	1	0	0.083758	0.795284	5.015068
22	14	0	-0.377757	-1.270647	8.961992
23	14	0	-0.238845	1.429041	11.935393

24	6	0	-1.556915	-2.626530	8.300537
25	1	0	-1.550750	-3.539016	8.902782
26	1	0	-2.587694	-2.254465	8.275732
27	1	0	-1.280493	-2.904808	7.275445
28	6	0	1.435688	-1.867103	8.881841
29	1	0	1.690620	-2.204485	7.869815
30	1	0	2.124766	-1.055294	9.143342
31	1	0	1.628124	-2.696822	9.570478
32	6	0	1.598384	1.367552	12.453736
33	1	0	1.776365	0.612856	13.227782
34	1	0	2.240678	1.122855	11.599642
35	1	0	1.926337	2.336876	12.848285
36	6	0	-1.318850	1.997387	13.410377
37	1	0	-0.982694	2.975860	13.776631
38	1	0	-2.365372	2.101050	13.101050
39	1	0	-1.292863	1.301517	14.253341
40	14	0	-0.933952	-0.747314	11.229720
41	1	0	-2.436440	-0.725414	11.281401
42	14	0	-0.917641	-4.658604	12.101564
43	14	0	-0.615304	-6.403013	13.697608
44	14	0	-1.605196	-5.822739	15.774589
45	1	0	-3.027814	-5.460851	15.454661
46	14	0	-0.570156	-3.835437	16.477822
47	14	0	-0.810486	-1.976079	15.046852
48	14	0	-0.239034	-2.467439	12.773530
49	1	0	1.263735	-2.482544	12.737015
50	6	0	-2.761740	-4.621599	11.605434
51	1	0	-2.959483	-3.869173	10.834024
52	1	0	-3.083274	-5.594731	11.215011
53	1	0	-3.394730	-4.384753	12.468589
54	6	0	-2.628401	-1.404617	15.131563
55	1	0	-3.305693	-2.218922	14.848792
56	1	0	-2.889704	-1.094842	16.150278
57	1	0	-2.824369	-0.562384	14.458872
58	6	0	-1.419132	-7.965332	12.936343
59	1	0	-0.996059	-8.181295	11.947193
60	1	0	-1.252247	-8.847221	13.564890
61	1	0	-2.501199	-7.839991	12.816923
62	6	0	1.249949	-6.744836	13.921841
63	1	0	1.428642	-7.539143	14.655722
64	1	0	1.696195	-7.065313	12.972680
65	1	0	1.790253	-5.853009	14.257610
66	6	0	0.152168	-5.227192	10.617565
67	1	0	-0.184976	-6.205120	10.251148
68	1	0	0.119971	-4.529857	9.776437
69	1	0	1.200965	-5.329467	10.919779

70	6	0	0.355901	-0.642219	15.763880
71	1	0	0.358014	0.283108	15.180767
72	1	0	0.057526	-0.391047	16.789226
73	1	0	1.386184	-1.014153	15.798370
74	6	0	1.234656	-4.118105	17.057027
75	1	0	1.641717	-3.207908	17.511361
76	1	0	1.280530	-4.918074	17.804088
77	1	0	1.892421	-4.398729	16.224723
78	14	0	-1.688280	-7.357183	17.599825
79	1	0	-0.482825	-7.036365	18.438966
80	14	0	-3.604231	-6.814044	18.904267
81	14	0	-3.600041	-8.019930	20.947981
82	14	0	-3.394844	-10.330481	20.487337
83	1	0	-3.386721	-11.112336	21.768238
84	1	0	-4.621479	-10.781944	19.753227
85	14	0	-1.499735	-10.896973	19.191478
86	14	0	-1.507729	-9.684289	17.148134
87	6	0	-1.520708	-12.771808	18.818455
88	1	0	-0.650720	-13.063404	18.217103
89	1	0	-1.493688	-13.353924	19.747445
90	1	0	-2.422714	-13.063098	18.269070
91	6	0	-2.952474	-10.289960	16.056281
92	1	0	-2.976776	-9.765314	15.094226
93	1	0	-2.851916	-11.362104	15.847110
94	1	0	-3.921842	-10.137495	16.543748
95	6	0	0.136970	-10.054921	16.245065
96	1	0	0.244505	-11.131247	16.060549
97	1	0	0.190266	-9.546040	15.276324
98	1	0	0.998461	-9.730688	16.839803
99	6	0	0.092740	-10.502949	20.169770
100	1	0	0.115769	-11.049758	21.120009
101	1	0	0.981192	-10.795739	19.596926
102	1	0	0.181293	-9.434624	20.396206
103	6	0	-5.226900	-7.703230	21.900130
104	1	0	-5.238733	-8.255401	22.847536
105	1	0	-5.344233	-6.637796	22.133939
106	1	0	-6.101005	-8.018281	21.319662
107	6	0	-2.144831	-7.451225	22.046071
108	1	0	-2.249804	-6.391141	22.307470
109	1	0	-2.110991	-8.022436	22.981449
110	1	0	-1.179580	-7.574559	21.542596
111	6	0	-3.633143	-4.940130	19.272068
112	1	0	-3.668269	-4.356421	18.344885
113	1	0	-4.516404	-4.677345	19.867900
114	1	0	-2.744637	-4.622810	19.828841
115	6	0	-5.179235	-7.246125	17.914218

116	1	0	-5.259232	-8.320743	17.715483
117	1	0	-6.076365	-6.944164	18.468575
118	1	0	-5.193093	-6.723957	16.950197

Si(2)-Si(3) dissociated radical (charge = 0, multiplicity = 3)

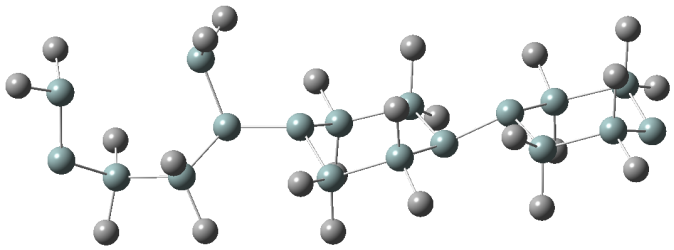

E(UB3LYP) = -6173.91376417 E_h

Center Number	Atomic Number	Atomic Type	Coordinates (Angstroms) X	Y	Z
1	14	0	-1.639123	2.031408	8.866302
2	14	0	0.005651	3.690091	8.463108
3	1	0	-0.031470	4.690710	9.577170
4	1	0	-0.395277	4.459703	7.234345
5	14	0	2.243055	2.971417	8.284040
6	6	0	-3.338845	2.905692	8.821013
7	1	0	-3.510152	3.363747	7.839586
8	1	0	-3.412803	3.696522	9.575559
9	1	0	-4.151927	2.192400	9.003655
10	6	0	-1.614088	0.748786	7.455333
11	1	0	-2.429678	0.025993	7.576842
12	1	0	-0.675127	0.184893	7.431599
13	1	0	-1.742898	1.238811	6.482630
14	6	0	2.557713	1.755233	6.851364
15	1	0	2.364284	2.228145	5.879080
16	1	0	1.917959	0.869985	6.931071
17	1	0	3.600760	1.417356	6.855644
18	6	0	3.465482	4.431847	8.180030
19	1	0	4.501655	4.075582	8.221155
20	1	0	3.315958	5.133366	9.007273
21	1	0	3.339257	4.986348	7.240438
22	14	0	1.054511	-1.707808	9.674679
23	14	0	-1.326682	1.048504	11.023078
24	6	0	1.217787	-3.476059	8.978727
25	1	0	1.286306	-4.212406	9.790644
26	1	0	0.361762	-3.743437	8.351126
27	1	0	2.125832	-3.566439	8.370455

28	6	0	2.585848	-1.320880	10.742437
29	1	0	3.505103	-1.470298	10.163685
30	1	0	2.580572	-0.287253	11.103251
31	1	0	2.630623	-1.984374	11.616740
32	6	0	0.157609	1.853737	11.910290
33	1	0	0.343056	1.393556	12.887707
34	1	0	1.074128	1.766907	11.315626
35	1	0	-0.026231	2.922527	12.074572
36	6	0	-2.896366	1.390439	12.057213
37	1	0	-3.094294	2.467553	12.117673
38	1	0	-3.781178	0.914430	11.619700
39	1	0	-2.785205	1.015584	13.080545
40	14	0	-0.983619	-1.292707	10.789698
41	1	0	-2.058864	-1.760606	9.850791
42	14	0	-2.487243	-4.618867	12.163704
43	14	0	-2.274452	-6.373707	13.760189
44	14	0	-2.373184	-5.714658	16.055699
45	1	0	-3.830466	-5.502458	16.358082
46	14	0	-1.324959	-3.608586	16.470012
47	14	0	-1.761290	-1.942600	14.828503
48	14	0	-1.135144	-2.747433	12.691840
49	1	0	0.259260	-3.274832	12.893401
50	6	0	-4.314124	-4.078732	12.026121
51	1	0	-4.428586	-3.275084	11.288777
52	1	0	-4.936277	-4.920364	11.697678
53	1	0	-4.717166	-3.719171	12.978604
54	6	0	-3.610981	-1.471459	14.911027
55	1	0	-4.258267	-2.348443	14.802955
56	1	0	-3.838454	-1.011940	15.880983
57	1	0	-3.889207	-0.753178	14.131750
58	6	0	-2.008502	-2.839836	18.085697
59	1	0	-1.861175	-3.475744	18.962562
60	1	0	-1.518888	-1.878825	18.288504
61	1	0	-3.084020	-2.650072	17.991904
62	6	0	-3.727924	-7.554803	13.361574
63	1	0	-3.665315	-7.899503	12.321465
64	1	0	-3.750352	-8.440463	14.002526
65	1	0	-4.685519	-7.035240	13.481246
66	6	0	-0.608301	-7.249513	13.431167
67	1	0	-0.447817	-8.093662	14.110622
68	1	0	-0.565056	-7.632534	12.404356
69	1	0	0.230596	-6.555856	13.562296
70	6	0	-1.987759	-5.334695	10.462478
71	1	0	-2.598782	-6.210528	10.210453
72	1	0	-2.136370	-4.587553	9.673696
73	1	0	-0.936306	-5.640196	10.439603

74	6	0	-0.737387	-0.401253	15.314802
75	1	0	-0.966641	0.448958	14.662143
76	1	0	-0.956804	-0.093636	16.344768
77	1	0	0.338909	-0.595078	15.245550
78	6	0	0.565407	-3.844354	16.602151
79	1	0	1.059941	-2.899276	16.857412
80	1	0	0.832179	-4.579695	17.368987
81	1	0	0.984083	-4.190715	15.650273
82	14	0	-1.634359	-7.458130	17.549729
83	1	0	-0.190044	-7.710097	17.216573
84	14	0	-1.653457	-6.772771	19.841043
85	14	0	-1.362111	-8.514803	21.431387
86	14	0	-2.822948	-10.305856	20.970944
87	1	0	-2.704947	-11.377025	22.014507
88	1	0	-4.234645	-9.809172	21.056594
89	14	0	-2.455810	-11.193860	18.818224
90	14	0	-2.758460	-9.531394	17.145939
91	6	0	-3.694372	-12.612328	18.486719
92	1	0	-3.551171	-13.040582	17.486828
93	1	0	-3.560309	-13.419917	19.216475
94	1	0	-4.731221	-12.266337	18.559351
95	6	0	-4.633866	-9.211599	16.971233
96	1	0	-4.851313	-8.465373	16.199274
97	1	0	-5.163346	-10.134342	16.704751
98	1	0	-5.059380	-8.845908	17.913173
99	6	0	-2.075640	-10.337192	15.549099
100	1	0	-2.602099	-11.277623	15.341479
101	1	0	-2.177934	-9.699868	14.666659
102	1	0	-1.011275	-10.572160	15.664944
103	6	0	-0.692593	-11.920398	18.708155
104	1	0	-0.528025	-12.673878	19.487598
105	1	0	-0.538340	-12.408033	17.738015
106	1	0	0.079206	-11.150984	18.819129
107	6	0	-1.730267	-7.805905	23.168929
108	1	0	-1.569344	-8.570004	23.938995
109	1	0	-1.072946	-6.958154	23.399007
110	1	0	-2.766608	-7.460893	23.253570
111	6	0	0.447795	-9.124869	21.423452
112	1	0	1.129054	-8.308061	21.691371
113	1	0	0.594000	-9.931041	22.152246
114	1	0	0.752994	-9.502715	20.441700
115	6	0	-0.199469	-5.571559	20.171031
116	1	0	-0.208392	-4.694974	19.518036
117	1	0	-0.228786	-5.213342	21.208025
118	1	0	0.758564	-6.083625	20.024267
119	6	0	-3.320253	-5.920770	20.226092

120	1	0	-4.149924	-6.633130	20.145921
121	1	0	-3.327023	-5.518624	21.246515
122	1	0	-3.527576	-5.093623	19.538791

Si(3)-Si(4) dissociated radical (charge = 0, multiplicity = 3)

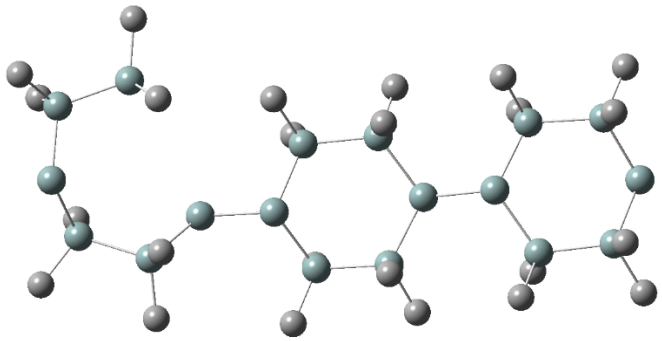

E(UB3LYP) = -6173.91906634 E_h

Center Number	Atomic Number	Atomic Type	Coordinates (Angstroms) X	Y	Z
1	14	0	-1.125970	3.172216	9.521424
2	14	0	0.397611	2.457348	7.870532
3	1	0	1.787300	2.526801	8.428120
4	1	0	0.383975	3.390782	6.696089
5	14	0	-0.046717	0.246733	7.185005
6	6	0	-0.699051	4.955345	10.064312
7	1	0	-0.769524	5.644077	9.213789
8	1	0	0.318552	5.022957	10.464299
9	1	0	-1.390197	5.311296	10.838316
10	6	0	-2.897637	3.190425	8.807033
11	1	0	-3.604650	3.590273	9.544003
12	1	0	-3.242402	2.189483	8.525653
13	1	0	-2.954509	3.826056	7.915284
14	6	0	-1.786320	0.153043	6.401711
15	1	0	-1.885210	0.866691	5.575109
16	1	0	-2.578070	0.370410	7.126847
17	1	0	-1.971611	-0.849575	5.997890
18	6	0	1.220310	-0.292088	5.857898
19	1	0	1.039195	-1.324407	5.533817
20	1	0	2.248215	-0.232192	6.231966
21	1	0	1.149403	0.351531	4.972772
22	14	0	0.107404	-1.258416	9.018570
23	14	0	-1.019516	1.765092	11.434299
24	6	0	-0.652116	-2.892812	8.373501
25	1	0	-0.647855	-3.688537	9.123244

26	1	0	-1.692497	-2.735432	8.066377
27	1	0	-0.098721	-3.256603	7.498439
28	6	0	1.961172	-1.498167	9.412061
29	1	0	2.502656	-1.865743	8.531842
30	1	0	2.421937	-0.549472	9.711281
31	1	0	2.119100	-2.213420	10.226565
32	6	0	0.576438	2.229687	12.377299
33	1	0	0.717367	1.626801	13.280144
34	1	0	1.458284	2.084225	11.742205
35	1	0	0.556917	3.284279	12.678119
36	6	0	-2.572074	2.215189	12.460730
37	1	0	-2.543780	3.269354	12.764757
38	1	0	-3.476499	2.067622	11.859164
39	1	0	-2.680623	1.611107	13.366213
40	14	0	-1.045803	-0.585972	11.002167
41	1	0	-2.490976	-0.917639	10.751779
42	14	0	-0.562680	-4.240072	12.528828
43	14	0	-0.374746	-5.663210	14.430831
44	14	0	-1.575844	-4.892057	16.317915
45	1	0	-3.037365	-4.911858	15.975252
46	14	0	-0.972062	-2.649716	16.788796
47	14	0	-1.480761	-1.232911	14.947922
48	14	0	-0.390342	-1.885774	12.924614
49	1	0	1.070893	-1.605834	13.138544
50	6	0	-2.245472	-4.603829	11.699119
51	1	0	-2.380610	-4.025826	10.778461
52	1	0	-2.333123	-5.666898	11.444217
53	1	0	-3.076537	-4.354433	12.369377
54	6	0	-3.371749	-1.233529	14.679907
55	1	0	-3.735536	-2.238487	14.436166
56	1	0	-3.894753	-0.902724	15.585441
57	1	0	-3.666685	-0.567091	13.861397
58	6	0	-1.934865	-2.019818	18.315327
59	1	0	-1.703598	-2.633149	19.194420
60	1	0	-1.666834	-0.982939	18.552928
61	1	0	-3.018293	-2.058344	18.155275
62	6	0	-1.036281	-7.382974	13.919150
63	1	0	-0.489265	-7.778420	13.054121
64	1	0	-0.920123	-8.096481	14.744617
65	1	0	-2.099267	-7.343424	13.656711
66	6	0	1.465157	-5.868840	14.899997
67	1	0	1.575185	-6.565897	15.739259
68	1	0	2.035624	-6.273191	14.054900
69	1	0	1.929091	-4.920311	15.191187
70	6	0	0.865429	-4.826969	11.395767
71	1	0	0.761389	-5.897627	11.177558

72	1	0	0.906699	-4.298753	10.439401
73	1	0	1.830186	-4.684134	11.895602
74	6	0	-0.914877	0.501737	15.528227
75	1	0	-1.110699	1.288251	14.794792
76	1	0	-1.438051	0.774874	16.453428
77	1	0	0.160186	0.507781	15.742659
78	6	0	0.891141	-2.546826	17.189704
79	1	0	1.166777	-1.522327	17.468632
80	1	0	1.152444	-3.201873	18.029103
81	1	0	1.511111	-2.834483	16.333643
82	14	0	-1.298837	-6.363851	18.124582
83	1	0	0.091949	-6.272220	18.680100
84	14	0	-2.907977	-6.666291	19.818559
85	14	0	-2.392164	-8.639217	21.047912
86	14	0	-3.399601	-10.592680	20.146724
87	1	0	-3.736448	-11.465214	21.322511
88	1	0	-4.726183	-10.233070	19.551176
89	14	0	-2.242011	-11.990320	18.622557
90	14	0	-2.048667	-11.004812	16.484635
91	6	0	-3.219082	-13.635206	18.526332
92	1	0	-2.725708	-14.342950	17.848986
93	1	0	-3.284051	-14.105478	19.515204
94	1	0	-4.240230	-13.477108	18.162270
95	6	0	-3.641629	-10.159053	15.863239
96	1	0	-3.460899	-9.650277	14.909323
97	1	0	-4.446723	-10.889363	15.705183
98	1	0	-4.002777	-9.411585	16.577522
99	6	0	-1.428345	-12.230956	15.156487
100	1	0	-2.179095	-13.004290	14.944205
101	1	0	-1.217874	-11.707469	14.216331
102	1	0	-0.507222	-12.733422	15.471168
103	6	0	-0.498802	-12.393168	19.287050
104	1	0	-0.556175	-12.870754	20.272729
105	1	0	0.020911	-13.085981	18.613803
106	1	0	0.118419	-11.493775	19.381878
107	6	0	-3.093499	-8.442849	22.816402
108	1	0	-2.856561	-9.322729	23.426174
109	1	0	-2.666786	-7.563372	23.313644
110	1	0	-4.183475	-8.328451	22.809951
111	6	0	-0.501276	-8.856019	21.186555
112	1	0	-0.047575	-7.993888	21.690448
113	1	0	-0.246427	-9.751219	21.766281
114	1	0	-0.032500	-8.946815	20.200586
115	6	0	-2.911291	-5.186697	21.033536
116	1	0	-3.161859	-4.255142	20.512989
117	1	0	-3.655179	-5.339691	21.825688

118	1	0	-1.934795	-5.051653	21.511724
119	6	0	-4.631178	-6.765057	19.010480
120	1	0	-4.698838	-7.591474	18.295053
121	1	0	-5.408824	-6.916869	19.768823
122	1	0	-4.863021	-5.837029	18.474582

Si(4)-Si(5) dissociated dimer radical (charge = 0, multiplicity = 2)

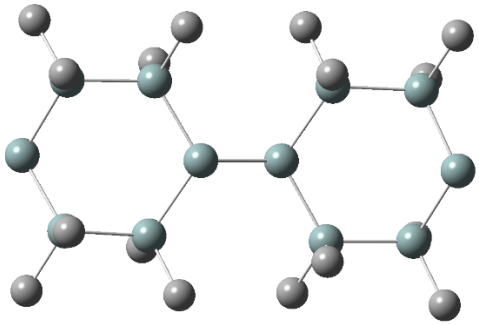

E(UB3LYP) = -4115.76713951 E_h

Center Number	Atomic Number	Atomic Type	Coordinates (Angstroms) X	Y	Z
1	14	0	-0.669829	3.145642	9.998197
2	14	0	0.794816	2.491810	8.270884
3	1	0	2.186075	2.388137	8.818080
4	1	0	0.853277	3.545127	7.204492
5	14	0	0.178817	0.404175	7.365543
6	6	0	-0.047846	4.766781	10.799307
7	1	0	-0.005450	5.573139	10.057209
8	1	0	0.956051	4.648994	11.221786
9	1	0	-0.716725	5.092625	11.605788
10	6	0	-2.400128	3.489806	9.264569
11	1	0	-3.083625	3.852646	10.041615
12	1	0	-2.848676	2.596056	8.817510
13	1	0	-2.345300	4.259717	8.485554
14	6	0	-1.577733	0.497358	6.619929
15	1	0	-1.644301	1.284133	5.859066
16	1	0	-2.338880	0.701884	7.380877
17	1	0	-1.839171	-0.452581	6.137692
18	6	0	1.384395	-0.080034	5.962056
19	1	0	1.122217	-1.055711	5.534578
20	1	0	2.419090	-0.135242	6.318101
21	1	0	1.350035	0.658049	5.151624
22	14	0	0.255217	-1.278710	9.041476
23	14	0	-0.813904	1.501714	11.711031

24	6	0	-0.431942	-2.838952	8.170394
25	1	0	-0.454020	-3.723009	8.812766
26	1	0	-1.454796	-2.660659	7.818714
27	1	0	0.181942	-3.081893	7.293652
28	6	0	2.082265	-1.547701	9.529614
29	1	0	2.678121	-1.845336	8.658103
30	1	0	2.520595	-0.625989	9.929832
31	1	0	2.194323	-2.325383	10.293190
32	6	0	0.752253	1.661081	12.794036
33	1	0	0.742628	0.952303	13.629073
34	1	0	1.657737	1.466650	12.207101
35	1	0	0.838435	2.671776	13.210934
36	6	0	-2.361394	2.020708	12.712569
37	1	0	-2.253153	3.052516	13.070999
38	1	0	-3.255957	1.982925	12.080268
39	1	0	-2.546469	1.387100	13.583924
40	14	0	-1.028927	-0.771170	10.993124
41	1	0	-2.465431	-0.930434	10.578356
42	14	0	-0.803036	-4.599759	12.079309
43	14	0	-0.939514	-6.228072	13.814668
44	14	0	-2.618819	-5.622203	15.337877
45	1	0	-3.968520	-5.666153	14.676038
46	14	0	-2.264708	-3.530098	16.340429
47	14	0	-2.062817	-1.814748	14.692974
48	14	0	-0.683791	-2.327397	12.806528
49	1	0	0.732442	-2.122344	13.266856
50	6	0	-2.350950	-4.825990	10.983821
51	1	0	-2.371569	-4.113961	10.152235
52	1	0	-2.388542	-5.837793	10.562321
53	1	0	-3.264866	-4.676832	11.570703
54	6	0	-3.826740	-1.407892	14.085018
55	1	0	-4.297760	-2.290102	13.635916
56	1	0	-4.461273	-1.079768	14.917054
57	1	0	-3.824883	-0.614147	13.330570
58	6	0	-3.731075	-3.078860	17.478480
59	1	0	-3.820377	-3.802705	18.297116
60	1	0	-3.593423	-2.085908	17.924179
61	1	0	-4.679790	-3.073724	16.931139
62	6	0	-1.334880	-7.915377	13.010193
63	1	0	-0.564026	-8.194755	12.281283
64	1	0	-1.376707	-8.704620	13.770089
65	1	0	-2.299243	-7.899305	12.490947
66	6	0	0.733262	-6.382054	14.720916
67	1	0	0.686968	-7.160254	15.491799
68	1	0	1.529837	-6.656032	14.018594
69	1	0	1.027933	-5.446711	15.209297

70	6	0	0.784430	-5.055610	11.108441
71	1	0	0.712906	-6.078947	10.718506
72	1	0	0.980010	-4.391972	10.261415
73	1	0	1.657879	-5.013158	11.769377
74	6	0	-1.324196	-0.323911	15.643055
75	1	0	-1.197651	0.565162	15.018971
76	1	0	-1.971725	-0.048887	16.485471
77	1	0	-0.340591	-0.582582	16.051267
78	6	0	-0.682403	-3.587283	17.406479
79	1	0	-0.524290	-2.627623	17.913247
80	1	0	-0.758945	-4.363062	18.177226
81	1	0	0.210816	-3.798109	16.808084

Si(4)-Si(5) dissociated monomer radical (charge = 0, multiplicity = 2)

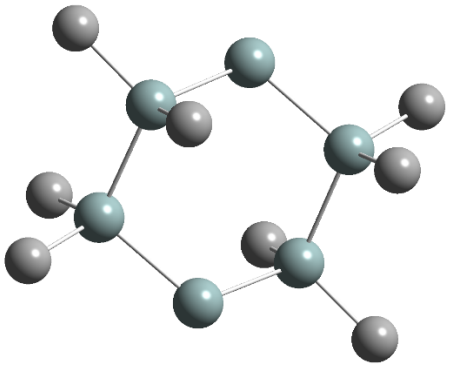

E(UB3LYP) = -2058.15941768 E_h

Center Number	Atomic Number	Atomic Type	Coordinates (Angstroms) X	Y	Z
1	14	0	-0.862114	3.188792	9.950872
2	14	0	0.880150	2.525404	8.489163
3	1	0	2.156684	2.457911	9.272907
4	1	0	1.102860	3.594291	7.459558
5	14	0	0.560952	0.443752	7.405534
6	6	0	-0.410287	4.861924	10.759025
7	1	0	-0.272095	5.636936	9.995465
8	1	0	0.517789	4.793904	11.337268
9	1	0	-1.205448	5.198279	11.435854
10	6	0	-2.476681	3.422338	8.959529
11	1	0	-3.288903	3.760454	9.614482
12	1	0	-2.800755	2.491867	8.480811
13	1	0	-2.347323	4.176515	8.174083
14	6	0	-0.987982	0.525481	6.293169
15	1	0	-0.896909	1.327696	5.551210

16	1	0	-1.898081	0.708126	6.875014
17	1	0	-1.124184	-0.416947	5.748966
18	6	0	2.075410	0.065228	6.301766
19	1	0	1.955457	-0.895926	5.786859
20	1	0	2.999485	0.020065	6.888442
21	1	0	2.202988	0.840520	5.536652
22	14	0	0.281337	-1.252517	9.050982
23	14	0	-1.166930	1.512987	11.613042
24	6	0	-0.204236	-2.907801	8.232724
25	1	0	-0.319503	-3.695381	8.986566
26	1	0	-1.150680	-2.825652	7.687116
27	1	0	0.566475	-3.234165	7.523489
28	6	0	1.916063	-1.497005	10.003849
29	1	0	2.717464	-1.813559	9.325170
30	1	0	2.242985	-0.574080	10.495676
31	1	0	1.806836	-2.267655	10.775733
32	6	0	0.355355	1.470550	12.762186
33	1	0	0.245663	0.694967	13.529064
34	1	0	1.278396	1.265795	12.208216
35	1	0	0.481617	2.432385	13.273917
36	6	0	-2.718242	1.891241	12.659218
37	1	0	-2.629928	2.869102	13.148539
38	1	0	-3.624280	1.903617	12.043567
39	1	0	-2.855671	1.136599	13.442448
40	14	0	-1.412329	-0.572769	10.543532
41	1	0	-2.751506	-0.645069	9.863038

7.3 Poly(cyclosilane) connectivity tunes optical absorbance

The synthesis of cyclosilane copolymers were investigated by Fan Fang in the Klausen group. The full structural characterization has been performed and published in the following reference: Fang, F.; Jiang, Q.; Klausen, R. S. *J. Am. Chem. Soc.* **2022**, 144, 17, 7834–7843.

All DFT calculations were performed using the Gaussian 09 package.[5] Geometries were optimized using the B3LYP functional with the 6-31G(d) basis set employing tight optimization parameters and an ultrafine integration grid. No symmetry restrictions were applied to geometry optimizations. All optimized structures possess zero imaginary frequencies. TD-DFT calculations were performed using the PBE0 functional with the 6-311G(d) basis set on geometries optimized with the B3LYP functional. Coordinates of optimized structures can be found in the following reference: Fang, F.; Jiang, Q.; Klausen, R. S. *J. Am. Chem. Soc.* **2022**, 144, 17, 7834–7843.

TD-PBE0 Excitations
1,3Si_6-1,3Si_6-1,3Si_6-1,3Si_6
Excitation energies and oscillator strengths:
Excited State 1: Singlet-?Sym 4.3346 eV 286.03 nm f=1.7691 <S**2>=0.000
317 -> 318 0.68139
Excited State 2: Singlet-?Sym 4.5953 eV 269.80 nm f=0.0276 <S**2>=0.000
315 -> 318 0.63059
316 -> 318 -0.16255
Excited State 3: Singlet-?Sym 4.6863 eV 264.57 nm f=0.1182 <S**2>=0.000
314 -> 318 0.13027
315 -> 318 0.18426
316 -> 318 0.61809
317 -> 319 0.14426

1,3Si_6-1,4Si_6-1,3Si_6-1,3Si_6
Excitation energies and oscillator strengths:
Excited State 1: Singlet-?Sym 4.4377 eV 279.39 nm f=1.4018 <S**2>=0.000
316 -> 318 -0.13408
317 -> 318 0.65928
317 -> 319 0.10340

Excited State 2: Singlet-?Sym 4.6895 eV 264.39 nm f=0.0067 <S**2>=0.000
313 -> 318 0.23880
315 -> 318 0.60298
317 -> 320 -0.11206
Excited State 3: Singlet-?Sym 4.7443 eV 261.33 nm f=0.5212 <S**2>=0.000
316 -> 319 0.27206
317 -> 318 -0.12014
317 -> 319 0.60602

1,3Si$_6$-1,4Si$_6$-1,4Si$_6$-1,3Si$_6$

Excitation energies and oscillator strengths:

Excited State 1: Singlet-?Sym 4.7037 eV 263.59 nm f=0.3719 <S**2>=0.000
317 -> 318 0.56536
317 -> 320 -0.36887
Excited State 2: Singlet-?Sym 4.7246 eV 262.42 nm f=1.8032 <S**2>=0.000
316 -> 319 0.30821
317 -> 318 0.32362
317 -> 320 0.50746
Excited State 3: Singlet-?Sym 4.7619 eV 260.37 nm f=0.0103 <S**2>=0.000
316 -> 318 0.25770
316 -> 320 0.15420
317 -> 318 -0.10938
317 -> 319 0.59700

1,4Si$_6$-1,3Si$_6$-1,3Si$_6$-1,3Si$_6$

Excitation energies and oscillator strengths:

Excited State 1: Singlet-?Sym 4.3667 eV 283.93 nm f=1.7003 <S**2>=0.000
317 -> 318 0.67818
Excited State 2: Singlet-?Sym 4.5855 eV 270.38 nm f=0.0525 <S**2>=0.000
314 -> 318 0.31666
315 -> 318 0.47311
316 -> 318 -0.31374
Excited State 3: Singlet-?Sym 4.6416 eV 267.12 nm f=0.0742 <S**2>=0.000
314 -> 318 0.21169
315 -> 318 0.24036
315 -> 319 0.11962
316 -> 318 0.56413
317 -> 319 -0.13531

1,4Si$_6$-1,3Si$_6$-1,3Si$_6$-1,4Si$_6$

Excitation energies and oscillator strengths:

Excited State 1: Singlet-?Sym 4.3526 eV 284.85 nm f=1.7297 <S**2>=0.000
317 -> 318 0.67903
Excited State 2: Singlet-?Sym 4.5813 eV 270.63 nm f=0.0464 <S**2>=0.000
315 -> 318 0.63590
Excited State 3: Singlet-?Sym 4.6295 eV 267.81 nm f=0.0710 <S**2>=0.000

313 -> 318 0.10926
316 -> 318 0.63839
317 -> 319 -0.15339

1,4Si$_6$-1,3Si$_6$-1,4Si$_6$-1,3Si$_6$
Excitation energies and oscillator strengths:
Excited State 1: Singlet-?Sym 4.4291 eV 279.93 nm f=1.4209 <S**2>=0.000
316 -> 318 0.14897
317 -> 318 0.65818
317 -> 319 0.10164
Excited State 2: Singlet-?Sym 4.6653 eV 265.76 nm f=0.0052 <S**2>=0.000
313 -> 318 -0.17272
315 -> 318 0.60721
316 -> 318 -0.16669
317 -> 318 0.10160
Excited State 3: Singlet-?Sym 4.7452 eV 261.28 nm f=0.1950 <S**2>=0.000
314 -> 318 -0.32208
315 -> 318 0.17339
316 -> 318 0.49159
316 -> 319 0.16061
317 -> 319 -0.20475

1,4Si$_6$-1,4Si$_6$-1,3Si$_6$-1,3Si$_6$
Excitation energies and oscillator strengths:
Excited State 1: Singlet-?Sym 4.4470 eV 278.80 nm f=1.5229 <S**2>=0.000
316 -> 318 -0.15323
317 -> 318 0.65658
317 -> 319 -0.11994
Excited State 2: Singlet-?Sym 4.7324 eV 261.99 nm f=0.4618 <S**2>=0.000
315 -> 318 -0.12058
316 -> 318 0.21053
316 -> 319 0.21840
317 -> 318 0.17126
317 -> 319 0.56356
Excited State 3: Singlet-?Sym 4.7347 eV 261.86 nm f=0.1131 <S**2>=0.000
314 -> 318 0.25961
315 -> 318 0.45660
316 -> 318 -0.27300
316 -> 319 0.15835
317 -> 319 0.22227
317 -> 320 -0.10428

1,4Si$_6$-1,4Si$_6$-1,3Si$_6$-1,4Si$_6$
Excitation energies and oscillator strengths:
Excited State 1: Singlet-?Sym 4.4814 eV 276.67 nm f=1.3964 <S**2>=0.000
314 -> 318 -0.11938

316 -> 318 0.10949
317 -> 318 0.65682
317 -> 319 -0.12048
Excited State 2: Singlet-?Sym 4.6802 eV 264.91 nm f=0.0206 <S**2>=0.000
313 -> 318 0.10569
314 -> 318 0.30214
315 -> 318 0.44830
316 -> 318 0.32739
317 -> 320 0.10082
Excited State 3: Singlet-?Sym 4.7386 eV 261.65 nm f=0.4758 <S**2>=0.000
314 -> 319 0.10090
315 -> 318 0.13201
316 -> 318 -0.32264
316 -> 319 -0.20409
317 -> 318 0.14972
317 -> 319 0.51808

1,4Si_6-1,4Si_6-1,4Si_6-1,3Si_6
Excitation energies and oscillator strengths:
Excited State 1: Singlet-?Sym 4.7033 eV 263.61 nm f=0.4006 <S**2>=0.000
317 -> 318 0.56394
317 -> 320 0.37783
Excited State 2: Singlet-?Sym 4.7261 eV 262.34 nm f=1.7960 <S**2>=0.000
315 -> 319 0.10851
316 -> 319 -0.28823
317 -> 318 -0.33315
317 -> 320 0.50344
Excited State 3: Singlet-?Sym 4.7633 eV 260.29 nm f=0.0664 <S**2>=0.000
316 -> 318 0.25409
316 -> 320 -0.15433
317 -> 319 0.60162

1,4Si_6-1,4Si_6-1,4Si_6-1,4Si_6
Excitation energies and oscillator strengths:
Excited State 1: Singlet-?Sym 4.7034 eV 263.60 nm f=0.7834 <S**2>=0.000
312 -> 318 -0.10311
317 -> 318 0.49851
317 -> 320 0.45426
Excited State 2: Singlet-?Sym 4.7256 eV 262.37 nm f=1.4417 <S**2>=0.000
316 -> 319 0.31182
317 -> 318 0.43807
Excited State 3: Singlet-?Sym 4.7643 eV 260.24 nm f=0.0008 <S**2>=0.000
316 -> 318 0.25707
316 -> 320 -0.17073
317 -> 319 0.60358

lin-(**1,4Si$_6$**)$_6$
Excitation energies and oscillator strengths:
Excited State 1: Singlet-?Sym 4.6694 eV 265.52 nm f=2.7381 <S**2>=0.000
469 -> 477 -0.10422
474 -> 477 0.17567
474 -> 479 0.29107
475 -> 476 -0.34861
475 -> 480 0.44405
Excited State 2: Singlet-?Sym 4.6708 eV 265.44 nm f=1.2688 <S**2>=0.000
473 -> 478 0.17712
474 -> 477 -0.10062
474 -> 479 0.10824
475 -> 476 0.49892
475 -> 478 0.20151
475 -> 480 0.31892
Excited State 3: Singlet-?Sym 4.7048 eV 263.53 nm f=0.0448 <S**2>=0.000
474 -> 476 -0.29905
474 -> 480 0.16260
475 -> 477 0.46710
475 -> 479 0.31614

lin-(**1,3Si$_6$**)$_6$
Excitation energies and oscillator strengths:
Excited State 1: Singlet-?Sym 4.1418 eV 299.35 nm f=2.8090 <S**2>=0.000
474 -> 477 0.14937
475 -> 476 0.66597
Excited State 2: Singlet-?Sym 4.4803 eV 276.73 nm f=0.1542 <S**2>=0.000
473 -> 477 0.11913
474 -> 476 0.55633
475 -> 477 0.35760
Excited State 3: Singlet-?Sym 4.5681 eV 271.41 nm f=0.0044 <S**2>=0.000
470 -> 476 -0.17234
471 -> 476 -0.23069
471 -> 477 -0.22515
472 -> 476 0.50680
472 -> 477 0.13500

7.4 Highly selective addition of cyclosilanes to alkynes enabling new conjugated materials

Hydrosilation of acetylenes with 1,4Si$_6$

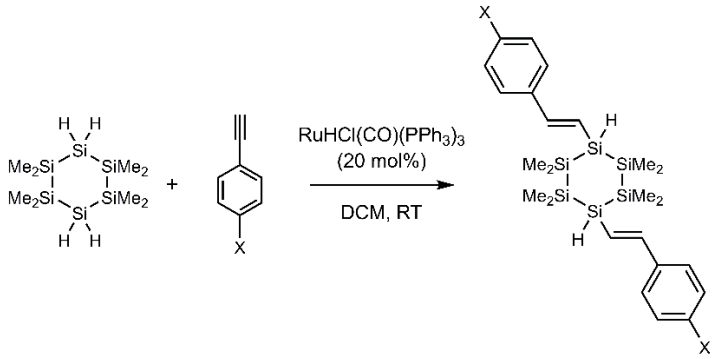

Synthesis of **4.1a**

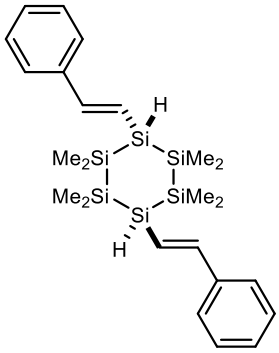

In a glove box, an oven-dried scintillation vial with stir bar was charged with **1,4Si$_6$** (1.0 equiv., 1.71 mmol, 0.500 g) and RuHCl(CO)(PPh$_3$)$_3$ (0.2 equiv., 0.342 mmol, 0.325 g). DCM (10 mL) was added to dissolve the reagents. Phenylacetylene (2.5 equiv., 4.27 mmol, 0.47 mL) was added dropwise by syringe. After the addition was complete, the reaction mixture turned dark red and was stirred for 2 hours at room temperature. The solution was concentrated under vacuum, transferred to a silica gel cartridge, and then dried on it under vacuum. The cartridge was subjected to automated column chromatography with 100% hexanes to yield **4.1a** (dr 65:35 *trans:cis*) as a white solid (0.756 g, 89%).

Isolation of *trans*-**4.1a**: In a scintillation vial, 0.500 g of **4.1a** (dr 65:35 *trans:cis*) was dissolved in 3 mL of DCM and layered with 17 mL of dry methanol. The solution was allowed to sit overnight in a glove box and colorless crystals were found at the bottom. The mixture was filtered through a fritted funnel, washed with 5 mL of dry methanol and dried under vacuum. *trans*-**4.1a** (0.249 g, 77%) was collected as a colorless crystal. X-ray quality crystals were grown by liquid-liquid diffusion using THF as the solvent and methanol as the antisolvent.

Enrichment of *cis*-**1a**: The filtrate was dried under vacuum yielding a white solid. The solid was determined as enriched *cis*-**4.1a** (dr 25:75 *trans:cis*) through ^{1}H NMR spectroscopy.

*Tabulated Characterization Data for **1a***

δ_H (400 MHz, C_6D_6)	*trans*-**4.1a**: 7.36 – 7.32 (m, 4H, Ar*H*), 7.25 (d, *J* = 18.8 Hz, 2H, vinyl), 7.15 – 7.09 (m, 4H, Ar*H*), 7.08 - 7.06 (m, 2H, Ar*H*), 6.63 (dd, *J* = 18.7, 5.2 Hz, 2H, vinyl), 4.18 (d, *J* = 5.2 Hz, 2H, Si*H*), 0.42 (s, 12H, -CH_3), 0.39 (s, 12H, -CH_3). *cis*-**4.1a**: 7.36 – 7.32 (m, 4H, Ar*H*), 7.23 (d, *J* = 18.8 Hz, 2H, vinyl), 7.15 – 7.09 (m, 4H, Ar*H*), 7.08 - 7.06 (m, 2H, Ar*H*), 6.61 (dd, *J* = 18.7, 5.2 Hz, 2H, vinyl), 4.23 (d, *J* = 5.2 Hz, 2H, Si*H*), 0.42 (s, 12H, -CH_3), 0.38 (s, 12H, -CH_3).
δ_C (101 MHz, C_6D_6)	*trans*-**4.1a**: 147.62 (vinyl), 138.90 (*Ar*), 128.93 (*Ar*), 126.70 (*Ar*), 119.98 (vinyl), -4.54 (-*C*H$_3$), -4.56 (-*C*H$_3$). *cis*-**4.1a:** 147.68 (vinyl), 138.87 (*Ar*), 128.95 (*Ar*), 126.65 (*Ar*), 120.37 (vinyl), -4.28 (-*C*H$_3$), -4.43 (-*C*H$_3$).
δ_{Si} (79 MHz, C_6D_6)	*trans*-**4.1a**: -40.17 (*Si*Me$_2$), -64.88 (*Si*H). *cis*-**4.1a**: -40.36 (*Si*Me$_2$), -63.04 (*Si*H).
HRMS	Calcd. for $C_{24}H_{40}Si_6$: 496.1746. Found: 496.1738.
IR (cm^{-1})	2084 (SiH).
λ_{max} (pentane) /nm	*trans*-**4.1a**: 286 (ε/dm^3 mol^{-1} cm^{-1} 51900) *cis*-**4.1a**: 285 (ε/dm^3 mol^{-1} cm^{-1} 42400)

Synthesis of **4.1b**

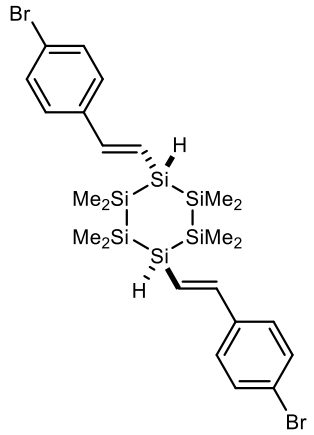

In a glove box, an oven-dried 2-dram vial with stir bar was charged with **1,4Si$_6$** (1.0 equiv., 0.342 mmol, 0.100 g) and RuHCl(CO)(PPh$_3$)$_3$ (0.2 equiv., 0.068 mmol, 0.0651 g). DCM (1 mL) was added to dissolve the reagents. 4-ethynylbromobenzene (2.5 equiv., 0.854 mmol, 0.155 g) was dissolved by 0.5 mL of DCM in a 1-dram vial and added dropwise into the reaction mixture by pipette. The vial was rinsed by 0.5 mL of DCM and the solution was added to the reaction as well. After the addition was complete, the reaction mixture turned dark red and was stirred for 2 hours at room temperature. The solution was transferred to a silica gel cartridge, and then dried on it under vacuum. The cartridge was subjected to automated column chromatography with 100% hexanes to yield **4.1b** (dr 65:35 *trans:cis*) as a white solid (0.179 g, 80%).

Isolation of *trans*-**4.1b**: In a scintillation vial, 0.500 g of **4.1b** (dr 65:35 *trans:cis*) was dissolved in 3 mL of DCM and layered with 17 mL of dry methanol. The solution was allowed to sit overnight in a glove box and colorless crystals were found at the bottom. The

mixture was filtered through a fritted funnel, washed with 5 mL of dry methanol and dried under vacuum. *trans*-**4.1b** (0.233 g, 72%) was collected as a colorless crystal.

*Tabulated Characterization Data for **4.1b***

δ_H (400 MHz, C_6D_6)	*trans*-**4.1b**: 7.22 (t, *J* = 8.5 Hz, 4H, Ar*H*), 7.01 (d, *J* = 18.7 Hz, 2H, vinyl), 6.93 (d, *J* = 8.5 Hz, 4H, Ar*H*), 6.50 (dd, *J* = 18.7, 5.2 Hz, 2H, vinyl), 4.11 (d, *J* = 5.2 Hz, 2H, Si*H*), 0.4 (s, 12H, -CH_3), 0.38 (s, 12H, -CH_3). *cis*-**4.1b**: 7.22 (t, *J* = 8.5 Hz, 4H, Ar*H*), 7.03 (d, *J* = 18.7 Hz, 2H, vinyl), 6.93 (d, *J* = 8.5 Hz, 4H, Ar*H*), 6.48 (dd, *J* = 18.7, 5.2 Hz, 2H, vinyl), 4.11 (d, *J* = 5.2 Hz, 2H, Si*H*), 0.40 (s, 3H, -CH_3), 0.37 (s, 3H, -CH_3).
δ_C (101 MHz, C_6D_6)	*trans*-**4.1b**: 146.11 (vinyl), 137.55 (*Ar*), 132.05 (*Ar*), 122.24 (*Ar*), 121.19 (vinyl), -4.58 (-*C*H_3), -4.59 (-*C*H_3). *cis*-**4.1b:** 146.19 (vinyl), 137.49 (*Ar*), 132.08 (*Ar*), 122.29 (*Ar*), 121.59 (vinyl), -4.28 (-*C*H_3), -4.43 (-*C*H_3).
δ_{Si} (79 MHz, C_6D_6)	*trans*-**4.1b**: -40.10 (*Si*Me_2), -64.84 (*Si*H). *cis*-**4.1b**: -40.41 (*Si*Me_2), -63.00 (*Si*H).
HRMS	Calcd. for $C_{24}H_{38}Br_2Si_6$: 651.9956. Found: 651.9965.
IR (cm^{-1})	2068 (SiH).
λ_{max} (pentane) /nm	*trans*-**4.1b**: 296 (ε/dm^3 mol^{-1} cm^{-1} 49300)

Synthesis of **4.1c**

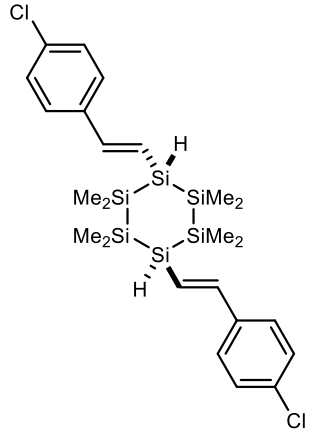

In a glove box, an oven-dried scintillation vial with stir bar was charged with **1,4Si$_6$** (1.0 equiv., 0.342 mmol, 0.100 g) and $RuHCl(CO)(PPh_3)_3$ (0.2 equiv., 0.068 mmol, 0.0651 g). DCM (1 mL) was added to dissolve the reagents. 4-ethynylchlorobenzene (2.5 equiv., 0.854 mmol, 0.117 g) was dissolved by 0.5 mL of DCM in a 1-dram vial and added dropwise into the reaction mixture by pipette. The vial was rinsed by 0.5 mL of DCM and the solution was added to the reaction as well. After the addition was complete, the reaction mixture turned dark red and was stirred for 2 hours at room temperature. The solution was transferred to a silica gel cartridge, and then dried on it under vacuum. The cartridge was subjected to automated column chromatography with 100% hexanes to yield **4.1c** (dr 62:38 *trans:cis*) as a white solid (0.145 g, 75%).

*Tabulated Characterization Data for **4.1c***

δ_H (400 MHz, C_6D_6)	*trans*-**4.1c**: 7.10 – 7.03 (m, 6H, Ar*H* and vinyl), 7.03 – 6.97 (m, 4H, Ar*H*), 6.49 (dd, *J* = 18.7, 5.2 Hz, 2H, vinyl), 4.13 (d, *J* = 5.2 Hz, 2H, Si*H*), 0.41 (s, 12H, -CH_3), 0.39 (s, 12H, -CH_3). *cis*-**4.1c**: 7.10 – 7.03 (m, 6H, Ar*H* and vinyl), 7.03 – 6.97 (m, 4H, Ar*H*), 6.47 (dd, *J* = 18.7, 5.2 Hz, 2H, vinyl), 4.18 (d, *J* = 5.2 Hz, 2H, Si*H*), 0.40 (s, 12H, -CH_3), 0.38 (s, 12H, -CH_3).
δ_C (101 MHz, C_6D_6)	*trans*-**4.1c**: 146.05 (vinyl), 137.17 (*Ar*), 134.00 (*Ar*), 129.12 (*Ar*), 129.09 (vinyl), -4.57 (-*C*H$_3$), -4.59 (-*C*H$_3$). *cis*-**4.1c:** 146.05 (vinyl), 137.17 (*Ar*), 134.00 (*Ar*), 129.09 (*Ar*), 120.99 (vinyl), -4.28 (-*C*H$_3$), -4.43 (-*C*H$_3$).
δ_{Si} (79 MHz, C_6D_6)	*trans*-**4.1c**: -40.09 (*Si*Me$_2$), -64.93 (*Si*H). *cis*-**4.1c**: -40.39 (*Si*Me$_2$), -63.06 (*Si*H).
HRMS	Calcd. for $C_{24}H_{40}Si_6$: 568.0907. Found: 568.0932.
IR (cm^{-1})	2061 (SiH).
λ_{max} (pentane) /nm	290 (ε/dm^3 mol^{-1} cm^{-1} 47400)

Synthesis of **4.1d**

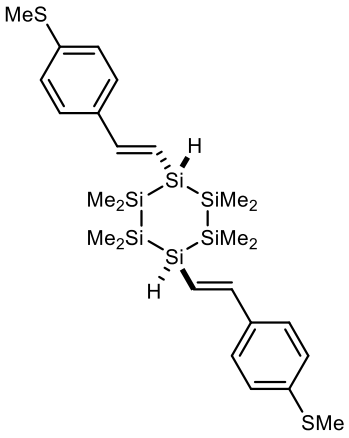

In a glove box, an oven-dried scintillation vial with stir bar was charged with **1,4Si$_6$** (1.0 equiv., 0.342 mmol, 0.100 g) and RuHCl(CO)(PPh$_3$)$_3$ (0.2 equiv., 0.068 mmol, 0.0651 g). DCM (1 mL) was added to dissolve the reagents. 4-ethynylmethylthiobenzene (2.5 equiv., 0.854 mmol, 0.127 g) was dissolved by 0.5 mL of DCM in a 1-dram vial and added dropwise into the reaction mixture by pipette. The vial was rinsed by 0.5 mL of DCM and the solution was added to the reaction as well. After the addition was complete, the reaction mixture turned dark red and was stirred for 2 hours at room temperature. The solution was transferred to a silica gel cartridge, and then dried on it under vacuum. The cartridge was subjected to automated column chromatography with 95% hexanes/5% ethyl acetate to yield **4.1d** (dr 66:34 *trans:cis*) as a white solid (0.167 g, 83%).

*Tabulated Characterization Data for **4.1d***

δ_H (400 MHz, C_6D_6)	*trans*-**4.1d**: 7.24 – 7.17 (m, 6H, Ar*H* and vinyl), 7.07 (d*, J* = 8.5 Hz, 4H, Ar*H*), 6.57 (dd*, J* = 18.7, 5.2 Hz, 2H, vinyl), 4.20 (d, J=5.2 Hz, 2H, Si*H*), 1.98 (s, 6H, -S*Me*), 0.44 (d*, J* = 0.5 Hz, 12H, -CH_3), 0.41 (s, 12H, -CH_3). *cis*-**4.1d**: 7.24 – 7.17 (m, 6H, Ar*H* and vinyl), 7.04 (d*, J* = 8.5 Hz, 4H, Ar*H*), 6.55 (dd*, J* = 18.7, 5.2 Hz, 2H, vinyl), 4.24 (d*, J* = 5.2 Hz, 2H, Si*H*), 1.98 (s, 6H, -S*Me*), 0.45 (s, 12H, -CH_3), 0.40 (s, 12H, -CH_3).

δ_C (101 MHz, C_6D_6)	*trans*-**4.1d**: 146.95 (vinyl), 139.26 (*Ar*), 135.74 (*Ar*), 128.87 (*Ar*), 127.11 (*Ar*), 126.88 (*Ar*), 118.98 (vinyl), 15.31 (-S*Me*), -4.50 (-*C*H_3), -4.52 (-*C*H_3). *cis*-**4.1d:** 147.03 (vinyl), 139.30 (*Ar*), 135.65 (*Ar*), 128.79 (*Ar*), 127.06 (*Ar*), 126.84 (*Ar*), 119.38 (vinyl), 15.26 (-S*Me*), -4.22 (-*C*H_3), -4.36 (-*C*H_3).
δ_{Si} (79 MHz, C_6D_6)	*trans*-**4.1d**: -40.15 (*Si*Me_2), -64.74 (*Si*H). *cis*-**4.1d**: -40.50 (*Si*Me_2), -62.87 (*Si*H).
HRMS	Calcd. for $C_{26}H_{44}S_2Si_6$: 588.1500. Found: 588.1492.
IR (cm^{-1})	2077 (SiH).

Synthesis of **4.1e**

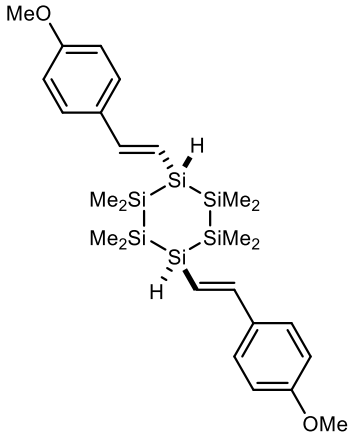

In a glove box, an oven-dried scintillation vial with stir bar was charged with **1,4Si$_6$** (1.0 equiv., 0.342 mmol, 0.100 g) and $RuHCl(CO)(PPh_3)_3$ (0.2 equiv., 0.068 mmol, 0.0651 g). DCM (2 mL) was added to dissolve the reagents. 4-ethynylanisole (2.5 equiv., 0.854 mmol, 0.11 mL) was added dropwise into the reaction mixture by syringe. After the addition was complete, the reaction mixture turned dark red and was stirred for 2 hours at room temperature. The solution was transferred to a silica gel cartridge, and then dried on it under vacuum. The cartridge was subjected to automated column chromatography with 90% hexanes/10% ethyl acetate to yield **4.1e** (dr 63:37 *trans:cis*) as a white solid (0.156 g, 82%). X-ray quality crystals were grown by liquid-liquid diffusion using THF as the solvent and methanol as the antisolvent.

*Tabulated Characterization Data for **4.1e***

δ_H (400 MHz, C_6D_6)	*trans*-**4.1e**: 7.42 –7.29 (m, 2H, Ar*H*), 7.25 (d*, J* = 18.7 Hz, 2H, vinyl), 7.08 – 7.01 (m, 2H, Ar*H*), 6.73 (t*, J* = 8.9 Hz, 4H, Ar*H*), 6.49 (dd*, J* = 18.7, 5.2 Hz, 2H, vinyl), 4.22 (d*, J* = 5.2 Hz, 2H, Si*H*), 3.28 (s, 6H, -O*Me*), 0.46 (s, 12H, -CH_3), 0.43 (s, 12H, -CH_3). *cis*-**4.1e**: 7.42 –7.29 (m, 2H, Ar*H*), 7.24 (d*, J* = 18.7 Hz, 2H, vinyl), 7.08 – 7.01 (m, 2H, Ar*H*), 6.73 (t*, J* = 8.9 Hz, 4H, Ar*H*), 6.47 (dd*, J* = 18.7, 5.2 Hz, 2H, vinyl), 4.27 (d*, J* = 5.2 Hz, 2H, Si*H*), 3.28 (s, 6H, -O*Me*), 0.47 (s, 12H, -CH_3), 0.41 (s, 12H, -CH_3).
δ_C (101 MHz, C_6D_6)	*trans*-**4.1e**: 160.25 (vinyl), 147.18 (*Ar*), 132.03 (*Ar*), 128.86 (*Ar*), 127.98 (*Ar*), 116.61(*Ar*), 114.40 (vinyl), 54.83 (-O*Me*), -4.46 (-*C*H$_3$), -4.49 (-*C*H$_3$). *cis*-**4.1e:** 160.25 (vinyl), 147.18 (*Ar*), 131.97 (*Ar*), 128.79 (*Ar*), 127.94 (*Ar*), 117.02 (*Ar*), 114.42 (vinyl), 54.81 (-O*Me*), -4.19 (-*C*H$_3$), -4.34 (-*C*H$_3$).
δ_{Si} (79 MHz, C_6D_6)	*trans*-**4.1e**: -40.24 (*Si*Me$_2$), -64.84 (*Si*H). *cis*-**4.1e**: -40.46 (*Si*Me$_2$), -63.01(*Si*H).
HRMS	Calcd. for $C_{26}H_{44}O_2Si_6$: 556.1957. Found: 556.1966.
IR (cm^{-1})	2064 (SiH).
λ_{max} (pentane) /nm	*trans*-**4.1e**: 292 (ε/dm^3 mol^{-1} cm^{-1} 53000)

Synthesis of **4.1f**

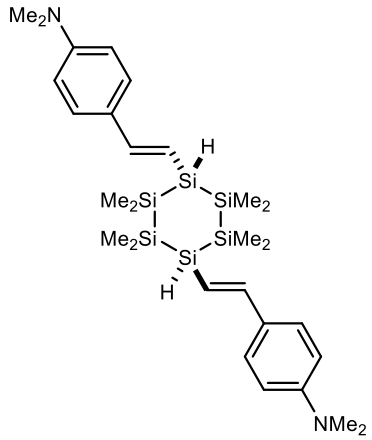

In a glove box, an oven-dried scintillation vial with stir bar was charged with **1,4Si$_6$** (1.0 equiv., 0.342 mmol, 0.100 g) and RuHCl(CO)(PPh$_3$)$_3$ (0.2 equiv., 0.068 mmol, 0.0651 g). DCM (1 mL) was added to dissolve the reagents. 4-ethynyl-N,N-dimethylanilline (2.5

equiv., 0.854 mmol, 0.124 g) was dissolved by 0.5 mL of DCM in a 1-dram vial and added dropwise into the reaction mixture by pipette. The vial was rinsed by 0.5 mL of DCM and the solution was added to the reaction as well. After the addition was complete, the reaction mixture turned dark red and was stirred for 2 hours at room temperature. The solution was transferred to a silica gel cartridge, and then dried on it under vacuum. The cartridge was subjected to automated column chromatography with 85% hexanes/15% ethyl acetate to yield **4.1f** (dr 62:38 *trans:cis*) as a white solid (0.137 g, 69%). The NMRs were collected at 50 ˚C for the poor solubility of the *trans* isomer at room temperature.

*Tabulated Characterization Data for **4.1f***

δ_H (400 MHz, C_6D_6)	*trans*-**4.1f**: 7.44 – 7.37 (m, 4H, Ar*H*), 7.30 (d, *J* = 18.6 Hz, 2H, vinyl), 6.53 (t, *J* = 8.3 Hz, 4H, Ar*H*), 6.44 (dd, *J* = 18.6, 5.2 Hz, 2H, vinyl), 4.25 (d, *J* = 5.2 Hz, 2H, Si*H*), 2.52 (s, 12H, -N*Me*$_2$), 0.47 (s, 12H, -C*H*$_3$), 0.45 (s, 12H, -C*H*$_3$). *cis*-**4.1f**: 7.44 – 7.37 (m, 4H, Ar*H*), 7.28 (d, *J* = 18.6 Hz, 2H, vinyl), 6.53 (t, *J* = 8.3 Hz, 4H, Ar*H*), 6.43 (dd, *J* = 18.6, 5.2 Hz, 2H, vinyl), 4.28 (d, *J* = 5.2 Hz, 2H, Si*H*), 2.52 (s, 12H, -N*Me*$_2$), 0.50 (s, 12H, -C*H*$_3$), 0.43 (s, 12H, -C*H*$_3$).
δ_C (101 MHz, C_6D_6)	*trans*-**4.1f**: 150.34 (vinyl), 147.57 (*Ar*), 113.30 (*Ar*), 112.88 (*Ar*), 112.29 (vinyl), 39.64 (-N*Me*$_2$), -4.77 (-*C*H$_3$), -4.81(-*C*H$_3$). *cis*-**4.1f:** 150.34 (vinyl), 147.62 (*Ar*), 112.88 (*Ar*), 112.27 (*Ar*), 39.64 (-N*Me*$_2$), -4.52 (-*C*H$_3$), -4.66 (-*C*H$_3$).
δ_{Si} (79 MHz, C_6D_6)	*trans*-**4.1f**: -40.30 (*Si*Me$_2$), -64.48 (*Si*H). *cis*-**4.1f**: -40.45 (*Si*Me$_2$), -62.86 (*Si*H).
HRMS	Calcd. for $C_{28}H_{50}N_2Si_6$: 582.2590. Found: 582.2593.
IR (cm^{-1})	2051(SiH).

Synthesis of **4.1g**

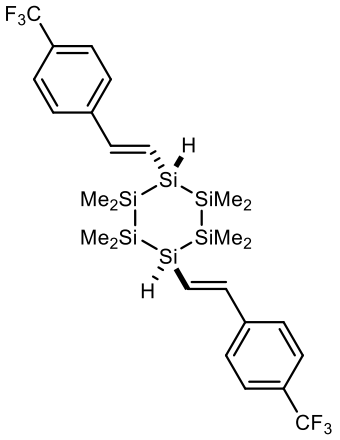

In a glove box, an oven-dried scintillation vial with stir bar was charged with **1,4Si$_6$** (1.0 equiv., 0.342 mmol, 0.100 g) and RuHCl(CO)(PPh$_3$)$_3$ (0.2 equiv., 0.068 mmol, 0.0651 g). DCM (1 mL) was added to dissolve the reagents. 4-ethynyltrifluoromethylbenzene (2.5 equiv., 0.854 mmol, 0.12 mL) was added dropwise into the reaction mixture by syringe. The vial was rinsed by 0.5 mL of DCM and the solution was added to the reaction as well. After the addition was complete, the reaction mixture turned dark red and was stirred for 2 hours at room temperature. The solution was transferred to a silica gel cartridge, and then dried on it under vacuum. The cartridge was subjected to automated column chromatography with 100% hexanes to yield **4.1g** (dr 65:35 *trans:cis*) as a white solid (0.154 g, 71%).

*Tabulated Characterization Data for **4.1g***

δ_H (400 MHz, C_6D_6)	*trans*-**4.1g**: 7.38 – 7.27 (m, 4H, Ar*H*), 7.12 - 7.05 (m, 6H, Ar*H* and vinyl), 6.61 (dd, *J* = 18.5, 5.4 Hz, 2H, vinyl), 4.14 (d, *J* = 5.4 Hz, 2H, Si*H*), 0.42 (s, 12H, -CH_3), 0.40 (s, 12H, -CH_3). *cis*-**4.1g**: 7.38 – 7.27 (m, 4H, Ar*H*), 7.12 - 7.05 (m, 6H, Ar*H* and vinyl), 6.60 (dd, *J* = 18.7, 5.4 Hz, 2H, vinyl), 4.18 (d, *J* = 5.4 Hz, 2H, Si*H*), 0.42 (s, 12H, -CH_3), 0.39 (s, 12H, -CH_3).

δ_C (101 MHz, C_6D_6)	*trans*-**4.1g**: 145.80 (vinyl), 141.71 (*Ar*), 126.72 (*Ar*), 125.89 (*Ar*), 124.00 (vinyl), -4.61 (-*C*H_3). *cis*-**4.1g:** 145.89 (vinyl), 141.71 (*Ar*), 126.65 (*Ar*), 125.86 (*Ar*), 124.36 (vinyl), -4.33 (-*C*H_3), -4.48 (-*C*H_3).
δ_F (376 MHz, C_6D_6)	*trans*-**4.1g**: -62.18 (-C*F*$_3$). *cis*-**4.1g**: -62.24 (-C*F*$_3$).
δ_{Si} (79 MHz, C_6D_6)	*trans*-**4.1g**: -39.98 (*Si*Me_2), -64.54 (*Si*H). *cis*-**4.1g**: -40.31 (*Si*Me_2), -62.73 (*Si*H).
HRMS	Calcd. for $C_{26}H_{38}F_6Si_6$: 632.1493. Found: 632.1499.
IR (cm^{-1})	2082 (SiH).
λ_{max} (pentane) /nm	294 (ε/dm^3 mol^{-1} cm^{-1} 40000)

Synthesis of **4.1h**

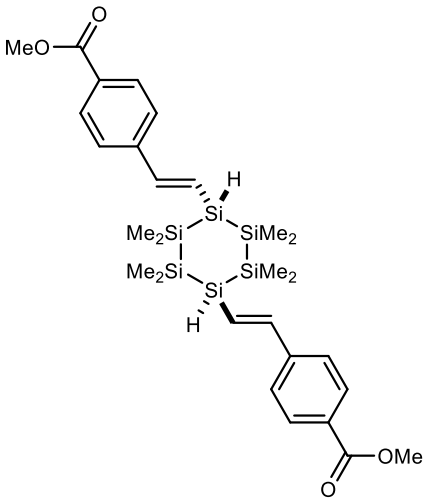

In a glove box, an oven-dried scintillation vial with stir bar was charged with **1,4Si$_6$** (1.0 equiv., 0.342 mmol, 0.100 g) and $RuHCl(CO)(PPh_3)_3$ (0.2 equiv., 0.068 mmol, 0.0651 g). DCM (1 mL) was added to dissolve the reagents. Methyl 4-ethynylbenzoate (2.5 equiv., 0.854 mmol, 0.137 g) was dissolved by 0.5 mL of DCM in a 1-dram vial and added dropwise into the reaction mixture by pipette. The vial was rinsed by 0.5 mL of DCM and the solution was added to the reaction as well. After the addition was complete, the reaction mixture turned dark red and was stirred for 2 hours at room temperature. The solution was transferred to a silica gel cartridge, and then dried on it under vacuum. The cartridge was

subjected to automated column chromatography with 85% hexanes/15% ethyl acetate to yield **4.1h** (dr 60:40 *trans:cis*) as a white solid (0.168 g, 80%).

*Tabulated Characterization Data for **4.1h***

δ_H (400 MHz, C_6D_6)	*trans*-**4.1h**: 8.13 (d, *J* = 8.3 Hz, 4H, Ar*H*), 7.24 (d, *J* = 8.3 Hz, 4H, Ar*H*), 7.15 (d, *J* = 18.8 Hz, 2H, vinyl), 6.68 (dd, *J* = 18.8, 5.3 Hz, 2H, vinyl), 4.13 (d, *J* = 5.3 Hz, 2H, Si*H*), 3.50 (s, 6H, -COO*Me*), 0.41 (s, 12H, -CH_3), 0.37 (s, 12H, -CH_3). *cis*-**4.1h**: 8.10 (d, *J* = 8.3 Hz, 2H, Ar*H*), 7.24 (d, *J* = 8.3 Hz, 4H, Ar*H*), 7.15 (d, *J* = 18.8 Hz, 2H, vinyl), 6.65 (dd, *J* = 18.8, 5.3 Hz, 2H, vinyl), 4.13 (d, *J* = 5.3 Hz, 2H, Si*H*), 3.50 (s, 6H, -COO*Me*), 0.39 (s, 12H, -CH_3), 0.37 (s, 12H, -CH_3).
δ_C (101 MHz, C_6D_6)	*trans*-**4.1h**: 166.45 (*C*=O), 146.46 (vinyl), 142.51 (*Ar*), 130.46 (*Ar*), 130.20 (*Ar*), 126.47 (*Ar*), 124.30 (vinyl), 51.64 (-COO*Me*), -4.59 (-*C*H_3), -4.63 (-*C*H_3). *cis*-**4.1h**: 166.41 (*C*=O), 146.37 (vinyl), 142.57 (*Ar*), 130.44 (*Ar*), 130.18 (*Ar*), 126.55 (*Ar*), 123.91 (vinyl), 51.64 (-COO*Me*), -4.29 (-*C*H_3), -4.45 (-*C*H_3).
δ_{Si} (79 MHz, C_6D_6)	*trans*-**4.1h**: -39.88 (*Si*Me_2), -64.86 (*Si*H). *cis*-**4.1h**: -40.29 (*Si*Me_2), -62.90 (*Si*H).
HRMS	Calcd. for $C_{28}H_{44}O_4Si_6$: 612.1855. Found: 612.1843.
IR (cm^{-1})	1718 (C=O), 2073 (SiH).
λ_{max} (pentane) /nm	308 (ε/dm^3 mol^{-1} cm^{-1} 43100)

Synthesis of **4.1i**

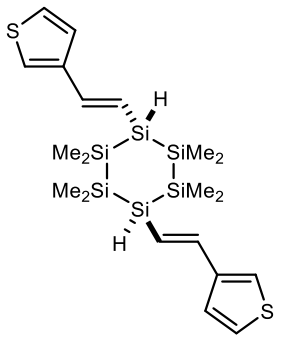

In a glove box, an oven-dried scintillation vial with stir bar was charged with **1,4Si$_6$** (1.0 equiv., 0.342 mmol, 0.100 g) and $RuHCl(CO)(PPh_3)_3$ (0.2 equiv., 0.068 mmol, 0.0651

g). DCM (1 mL) was added to dissolve the reagents. 3-ethynylthiophene (2.5 equiv., 0.854 mmol, 0.092 g) was diluted by 0.5 mL of DCM in a 1-dram vial and added dropwise into the reaction mixture by pipette. The vial was rinsed by 0.5 mL of DCM and the solution was added to the reaction as well. After the addition was complete, the reaction mixture turned dark red and was stirred for 30 minutes at room temperature. The solution was transferred to a silica gel cartridge, and then dried on it under vacuum. The cartridge was subjected to automated column chromatography with 100% hexanes to yield **4.1i** (dr 63:37 *trans:cis*) as a white solid (0.151 g, 87%).

*Tabulated Characterization Data for **4.1i***

δ_H (400 MHz, C_6D_6)	*trans*-**4.1i**: 7.14 (d, *J* = 18.7 Hz, 2H, vinyl), 7.06 (dt, *J* = 4.5, 2.1 Hz, 2H, thienyl), 6.79 – 6.74 (m, 4H, thienyl), 6.33 (dd, *J* = 18.7, 5.3 Hz, 2H, vinyl), 4.11 (d, *J* = 5.3 Hz, 2H, Si*H*), 0.39 (s, 12H, -CH_3), 0.37 (s, 12H, -CH_3). *cis*-**4.1i**: 7.12 (d, *J* = 18.7 Hz, 2H, vinyl), 7.06 (dt, *J* = 4.5, 2.1 Hz, 2H, thienyl), 6.79 – 6.74 (m, 4H, thienyl), 6.31 (dd, *J* = 18.6, 5.3 Hz, 2H, vinyl), 4.16 (d, *J* = 5.3 Hz, 2H, Si*H*), 0.39 (s, 12H, -CH_3), 0.36 (s, 12H, -CH_3).
δ_C (101 MHz, C_6D_6)	*trans*-**4.1i**: 142.48 (vinyl), 141.38 (thienyl), 126.14 (thienyl), 125.05 (thienyl), 122.83 (thienyl), 119.18 (vinyl), -4.53 (-*C*H_3), -4.55 (-*C*H_3). *cis*-**4.1i:** 142.43 (vinyl), 141.45 (thienyl), 126.20 (thienyl), 124.96 (thienyl), 122.83 (thienyl), 119.61 (vinyl), -4.25 (-*C*H_3), -4.42 (-*C*H_3).
δ_{Si} (79 MHz, C_6D_6)	*trans*-**4.1i**: -40.28 (*Si*Me_2), -65.22 (*Si*H). *cis*-**4.1i**: -40.50 (*Si*Me_2), -63.32 (*Si*H).
HRMS	Calcd. for $C_{20}H_{36}S_2Si_6$: 508.0874. Found: 508.0871.
IR (cm^{-1})	2051, 2085 (SiH).

Synthesis of **4.1j**

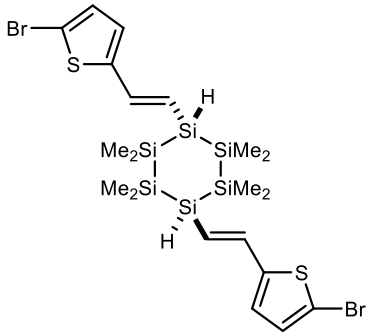

In a glove box, an oven-dried scintillation vial with stir bar was charged with **1,4Si$_6$** (1.0 equiv., 1.708 mmol, 0.500 g) and RuHCl(CO)(PPh$_3$)$_3$ (0.2 equiv., 0.342 mmol, 0.325 g). DCM (8 mL) was added to dissolve the reagents. 2-bromo-5-ethynylthiophene (2.5 equiv., 4.269 mmol, 0.799 g) was diluted by 1 mL of DCM in a 1-dram vial and added dropwise into the reaction mixture by pipette. The vial was rinsed by 1 mL of DCM and the solution was added to the reaction as well. After the addition was complete, the reaction mixture turned dark red and was stirred for 30 minutes at room temperature. The solution was concentrated under vacuum, transferred to a silica gel cartridge, and then dried on it under vacuum. The cartridge was subjected to automated column chromatography with 100% hexanes to yield **4.1j** (dr 63:37 *trans:cis*) as a white solid (0.849 g, 75%).

Isolation of *trans*-**4.1j**: In a scintillation vial, 0.500 g of **4.1j** (dr 63:37 *trans:cis*) was dissolved in 2 mL of DCM and layered with 18 mL of dry methanol. The solution was allowed to sit overnight in a glove box and colorless crystals were found at the bottom. The mixture was filtered through a fritted funnel, washed with 5 mL of dry methanol and dried under vacuum. *trans*-**4.1j** (dr 90:10 *trans:cis*) (0.270 g, 83%) was collected as a colorless crystal. X-ray quality crystals were grown by liquid-liquid diffusion using THF as the solvent and methanol as the antisolvent.

*Tabulated Characterization Data for **4.1j***

δ_H (400 MHz, C_6D_6)	*trans*-**4.1j**: 7.03 (d, *J* = 18.7 Hz, 2H, vinyl), 6.56 (d, *J* = 3.8 Hz, 2H, thienyl), 6.24 (dd, *J* = 18.7, 5.3 Hz, 2H, vinyl), 6.22 (d, *J* = 3.8 Hz, 2H, thienyl), 4.03 (d, *J* = 5.6 Hz, 2H, Si*H*), 0.33 (s, 12H, -CH_3), 0.33 (s, 12H, -CH_3). *cis*-**4.1j**: 7.01 (d, *J* = 18.7 Hz, 2H, vinyl), 6.56 (d, *J* = 3.8 Hz, 2H, thienyl), 6.22 (dd, *J* = 18.7, 5.3 Hz, 2H, vinyl), 6.22 (d, *J* = 3.8 Hz, 2H, thienyl), 4.08 (d, *J* = 5.6 Hz, 2H, Si*H*), 0.35 (s, 12H, -CH_3), 0.32 (s, 12H, -CH_3).
δ_C (101 MHz, C_6D_6)	*trans*-**4.1j**: 147.03 (vinyl), 138.90 (thienyl), 130.81 (thienyl), 125.90 (thienyl), 120.87 (thienyl), 112.31 (vinyl), -4.61 (-*C*H_3), -4.72 (-*C*H_3). *cis*-**4.1j:** 146.99 (vinyl), 138.99 (thienyl), 130.84 (thienyl), 125.92 (thienyl), 121.17 (thienyl), 112.38 (vinyl), -4.61 (-*C*H_3), -4.72 (-*C*H_3).
δ_{Si} (79 MHz, C_6D_6)	*trans*-**4.1j**: -40.23 (*Si*Me_2), -64.37 (*Si*H). *cis*-**4.1j**: -40.38 (*Si*Me_2), -62.85 (*Si*H).
HRMS	Calcd. for $C_{20}H_{34}Br_2S_2Si_6$: 663.9084. Found: 663.9064.
IR (cm^{-1})	2051, 2083 (SiH).
λ_{max} (pentane) /nm	*trans*-**4.1j**: 321 (ε/dm^3 mol^{-1} cm^{-1} 61100)
λ_{max} (THF) /nm	*trans*-**4.1j**: 323 (ε/dm^3 mol^{-1} cm^{-1} 51500)

Hydrosilation of acetylenes with 1,3Si$_6$

Synthesis of **4.2a**

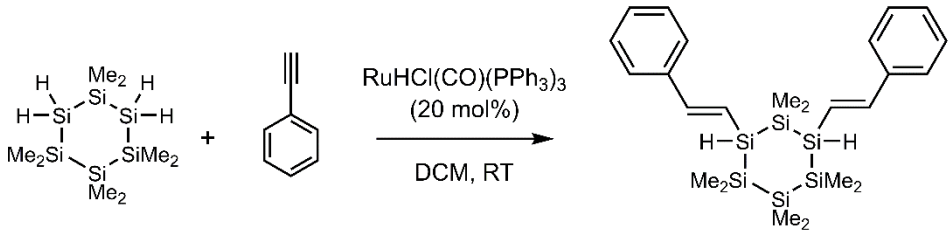

In a glove box, an oven-dried 2-dram vial with stir bar was charged with RuHCl(CO)(PPh_3)$_3$ (0.2 equiv., 0.068 mmol, 0.0651 g) and DCM (1.0 mL). **1,3Si$_6$** (1.0 equiv., 0.342 mmol, 0.100 g) was diluted by 1.0 mL of DCM added to the vial.

Phenylacetylene (2.5 equiv., 0.854 mmol, 94 μL) was added dropwise into the reaction mixture by micro syringe. After the addition was complete, the reaction mixture turned dark red and was stirred for 2 hours at room temperature. The solution was transferred to a silica gel cartridge, and then dried on it under vacuum. The cartridge was subjected to automated column chromatography with 100% hexanes to yield **4.2a** (dr 55:45 *trans:cis*) as a white oily solid (0.152 g, 90%).

*Tabulated Characterization Data for **4.2a***

δ_H (400 MHz, C_6D_6)	*trans*-**4.2a**: 7.37 – 7.32 (m, 2H, Ar*H*), 7.33 – 7.26 (m, 2H, Ar*H*), 7.26 (d, *J* = 18.7 Hz, 2H, vinyl), 7.14 – 7.01 (m, 4H, Ar*H*), 6.62 (dd, *J* = 18.7, 5.1 Hz, 2H, vinyl), 4.22 (d, *J* = 5.1 Hz, 2H, Si*H*), 0.53 (s, 6H, -CH_3), 0.40 (s, 12H, CH_3), 0.29 (s, 6H, -CH_3). *cis*-**4.2a**: 7.37 – 7.32 (m, 2H, Ar*H*), 7.33 – 7.26 (m, 2H, Ar*H*), 7.23 (d, *J* = 18.7 Hz, 2H, vinyl), 7.14 – 7.01 (m, 4H, Ar*H*), 6.61 (dd, *J* = 18.7, 5.1 Hz, 2H, vinyl), 4.27 (d, *J* = 5.3 Hz, 2H, Si*H*), 0.51 (s, 3H, -CH_3), 0.50 (s, 3H, -CH_3), 0.38 (s, 6H, -CH_3), 0.37 (s, 6H, -CH_3), 0.29 (s, 3H, -CH_3), 0.28 (s, 3H, -CH_3).
δ_C (101 MHz, C_6D_6)	*trans*-**4.2a**: 147.38 (vinyl), 138.42 (*Ar*), 128.53 (*Ar*), 126.35 (*Ar*), 119.75 (vinyl), -3.13 (-*C*H_3), -4.57 (-*C*H_3), -4.77 (-*C*H_3). *cis*-**4.2a:** 147.37 (vinyl), 138.51 (*Ar*), 128.55 (*Ar*), 126.32 (*Ar*), 119.71 (vinyl), -2.54 (-*C*H_3), -3.61 (-*C*H_3), -6.43 (-*C*H_3), -6.52 (-*C*H_3).
δ_{Si} (79 MHz, C_6D_6)	*trans*-**4.2a**: -40.20 (*Si*Me_2), -40.67 (*Si*Me_2), -41.28 (*Si*Me_2), -62.68 (*Si*H). *cis*-**4.2a**: -40.42 (*Si*Me_2), -40.87 (*Si*Me_2), -41.09 (*Si*Me_2), -62.53 (*Si*H).
HRMS	Calcd. for $C_{24}H_{40}Si_6$: 496.1746. Found: 496.1763.
IR (cm^{-1})	2051, 2072 (SiH).
λ_{max} (pentane) /nm	284 (ε/dm^3 mol^{-1} cm^{-1} 38900)

Synthesis of **4.2b**

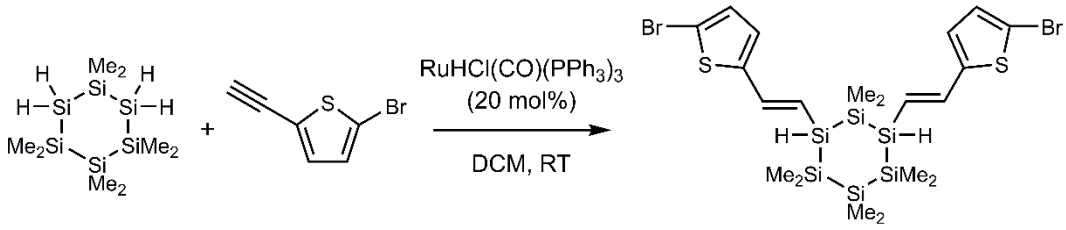

In a glove box, an oven-dried 2-dram vial with stir bar was charged with $RuHCl(CO)(PPh_3)_3$ (0.2 equiv., 0.068 mmol, 0.0651 g) and DCM (1.0 mL). **1,3Si$_6$** (1.0 equiv., 0.342 mmol, 0.100 g) was diluted by 0.5 mL of DCM added to the vial. 2-bromo-5-ethynylthiophene (2.5 equiv., 4.269 mmol, 0.160 g) was weighed in a 1-dram vial, diluted by 0.5 mL of DCM and added dropwise into the reaction mixture by pipette. The vial was rinsed by 0.5 mL of DCM and the solution was added to the reaction as well. After the addition was complete, the reaction mixture turned dark red and was stirred for 30 minutes at room temperature. The solution was transferred to a silica gel cartridge, and then dried on it under vacuum. The cartridge was subjected to automated column chromatography with 100% hexanes to yield **4.2b** (dr 50:50 *trans:cis*) as a pale yellow oil (0.188 g, 84%).

*Tabulated Characterization Data for **4.2b***

δ_H (400 MHz, C_6D_6)	*trans*-**4.2b**: 7.03 (d, J = 18.4 Hz, 2H, vinyl), 6.57 (d, J = 3.8 Hz, 2H, thienyl), 6.29 – 6.15 (m, 4H, vinyl and thienyl), 4.08 (d, J = 5.3 Hz, 2H, Si*H*), 0.42 (s, 6H, -CH_3), 0.33 (s, 12H, -CH_3), 0.26 (s, 6H, -CH_3). *cis*-**4.2b**: 7.00 (d, J = 18.4 Hz, 2H, vinyl), 6.55 (d, J = 3.8 Hz, 2H, thienyl), 6.29 – 6.15 (m, 4H, vinyl and thienyl), 4.11 (d, J = 5.3 Hz, 2H, Si*H*), 0.41 (s, 6H, -CH_3), 0.31 (s, 12H, -CH_3), 0.24 (s, 6H, -CH_3).
δ_C (101 MHz, C_6D_6)	*trans*-**4.2b**: 146.99 (vinyl), 139.01 (thienyl), 130.81 (thienyl), 125.94 (thienyl), 120.87 (thienyl), 112.36 (vinyl), -2.95 (-*C*H$_3$), -4.28 (-*C*H$_3$), -4.33 (-*C*H$_3$), -4.54 (-*C*H$_3$), -4.56 (-*C*H$_3$).

	cis-**4.2b:** 146.94 (vinyl), 139.14 (thienyl), 130.79 (thienyl), 126.04 (thienyl), 120.82 (thienyl), 112.49 (vinyl), -2.37 (-*C*H_3), -3.35 (-*C*H_3), -6.08 (-*C*H_3), -6.15 (-*C*H_3), -6.21 (-*C*H_3).
δ_{Si} (79 MHz, C_6D_6)	*trans*-**4.2b**: 40.30 (*Si*Me_2), -40.78 (*Si*Me_2), -41.32 (*Si*Me_2), -62.54 (*Si*H). *cis*-**4.2b:** -40.37 (*Si*Me_2), -40.82 (*Si*Me_2), -41.14 (*Si*Me_2), -62.33 (*Si*H).
HRMS	Calcd. for $C_{20}H_{34}BrS_2Si_6$ ($[M-^{79}Br]^+$): 584.9901. Found: 584.9899.
IR (cm^{-1})	2051, 2062 (SiH).

Hydrosilation of acetylenes with *trans*-$Si_{10}H_4$

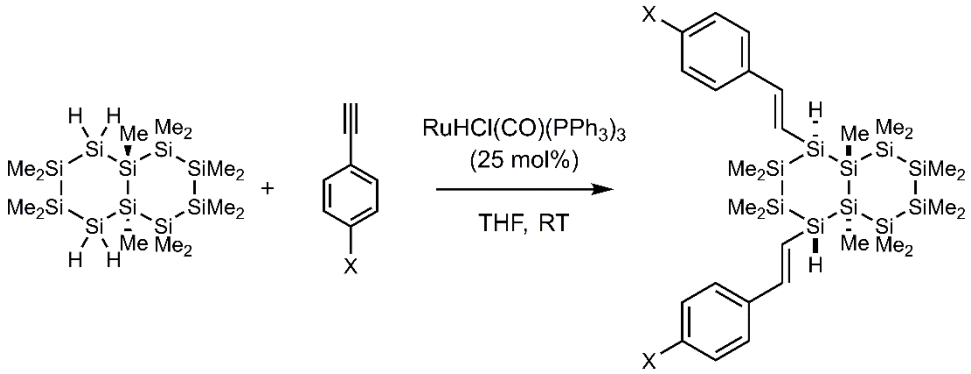

Synthesis of **4.3a**

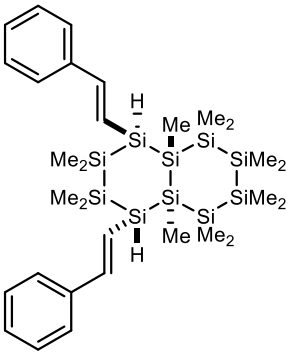

In a glove box, an oven-dried 2-dram vial with stir bar was charged with *trans*-**$Si_{10}H_4$** (dr 83:17 *trans*:*cis*, 1.0 equiv., 0.202 mmol, 0.100 g) and $RuHCl(CO)(PPh_3)_3$ (0.25 equiv., 0.051 mmol, 0.048 g). THF (1.0 mL) was added to dissolve the reagents. Phenylacetylene (4.0 equiv., 0.832 mmol, 0.085 g) was weighed in a 1-dram vial, diluted

by 0.5 mL of THF and added dropwise to the reaction mixture by syringe. The vial was rinsed by 0.5 mL of THF, and the solution was added to the reaction as well. After the addition was complete, the reaction mixture turned dark red and was stirred for 24 hours at room temperature. The solution was transferred to a silica gel cartridge, and then dried on it under vacuum. The cartridge was subjected to automated column chromatography with 100% hexanes to yield **4.3a** as a white solid (0.102 g, 73%).

*Tabulated Characterization Data for **4.3a***

δ_H (400 MHz, C_6D_6)	7.38 – 7.34 (m, 4H, Ar*H*), 7.28 (d, *J* = 18.7, 2H, vinyl), 7.18 – 7.10 (m, 4H, Ar*H*), 7.08 – 7.03 (m, 2H, Ar*H*), 6.69 (dd, *J* = 18.7, 5.5, 2H, vinyl), 4.32 (d, *J* = 5.5, 2H, Si*H*), 0.57 (s, 6H, -CH_3), 0.49 (s, 6H, -CH_3), 0.44 (s, 6H, -CH_3), 0.42 (s, 6H, -CH_3), 0.33 (s, 6H, -CH_3), 0.26 (s, 6H, -CH_3), 0.21 (s, 6H, -CH_3).
δ_C (101 MHz, C_6D_6)	146.90 (vinyl), 138.96 (*Ar*), 128.97 (*Ar*), 126.69 (*Ar*), 121.54 (vinyl), -3.19 (-*C*H_3), -4.04 (-*C*H_3), -4.19 (-*C*H_3), -4.41 (-*C*H_3), -4.50 (-*C*H_3), -6.47 (-*C*H_3), -8.41 (-*C*H_3).
δ_{Si} (79 MHz, C_6D_6)	-36.12 (*Si*Me_2), -36.51 (*Si*Me_2), -39.96(*Si*Me_2), -67.78 (*Si*H), -75.89 (*Si*Si_2Me).
HRMS	Calcd. for $C_{30}H_{58}Si_{10}$: 698.2231. Found: 698.2194.
IR (cm^{-1})	2072 (SiH).
λ_{max} (pentane) /nm	298 (ε/dm^3 mol^{-1} cm^{-1} 29200), 294 (ε/dm^3 mol^{-1} cm^{-1} 29500)

Synthesis of **4.3b**

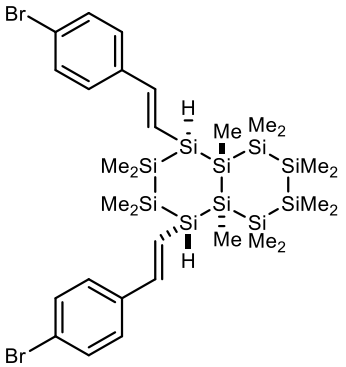

In a glove box, an oven-dried 2-dram vial with stir bar was charged with *trans*-**$Si_{10}H_4$** (dr 83:17 *trans*:*cis,* 1.0 equiv., 0.149 mmol, 0.074 g) and $RuHCl(CO)(PPh_3)_3$ (0.25 equiv., 0.042 mmol, 0.036 g). THF (0.75 mL) was added to dissolve the reagents. 4-Ethynylbromobenzene (4.0 equiv., 0.042 mmol, 0.108 g) was weighed in a 1-dram vial, diluted by 0.5 mL of THF and added dropwise to the reaction mixture by syringe. The vial was rinsed by 0.25 mL of THF, and the solution was added to the reaction as well. After the addition was complete, the reaction mixture turned dark red and was stirred for 24 hours at room temperature. The solution was transferred to a silica gel cartridge, and then dried on it under vacuum. The cartridge was subjected to automated column chromatography with 100% hexanes to yield **4.3b** as a white solid (0.072 g, 67%).

*Tabulated Characterization Data for **4.3b***

δ_H (400 MHz, C_6D_6)	7.25 (d, *J*=8.5, 4H, Ar*H*), 7.08 (d, *J* = 18.7, 2H, vinyl), 6.95 (d, *J* = 8.5, 4H, Ar*H*), 6.58 (dd, *J* = 18.7, 5.6, 2H, vinyl), 4.29 (d, *J* = 5.6, 2H, Si*H*), 0.56 (s, 6H, -CH_3), 0.48 (s, 6H, -CH_3), 0.44 (s, 6H, -CH_3), 0.41 (s, 6H, -CH_3), 0.30 (s, 6H, -CH_3), 0.27 (s, 6H, -CH_3), 0.22 (s, 6H, -CH_3).
δ_C (101 MHz, C_6D_6)	145.37 (vinyl), 137.60 (*Ar*), 132.12 (*Ar*), 122.79 (*Ar*), 122.26 (vinyl), 1.42 (-*C*H_3), -3.21 (-*C*H_3), -4.08 (-*C*H_3), -4.23 (-*C*H_3), -4.44 (-*C*H_3), -4.53 (-*C*H_3), -6.51 (-*C*H_3), -8.43 (-*C*H_3).
δ_{Si} (79 MHz, C_6D_6)	-36.08 (*Si*Me_2), -36.50 (*Si*Me_2), -39.89 (*Si*Me_2), -67.54 (*Si*H), -75.85 (*Si*Si_2Me).
HRMS	Calcd. for $C_{30}H_{56}Br_2Si_{10}$: 854.0441. Found: 854.0457.
IR (cm^{-1})	2065 (SiH).

Model reaction: Kumada cross-coupling of 4.1j and 2-bromothiophene

In a glove box, an oven-dried 2-dram vial with stir bar was charged with *trans*-**4.1j** (dr 90:10 *trans:cis*) (1.0 equiv., 0.075 mmol, 50.0 mg) and THF (1.0 mL). *i*-PrMgCl (2.0 M in THF) (75 μL) was added by micro syringe. The solution was stirred at room

temperature for 30 minutes, yielding a di-Grignard intermediate. $NidpppCl_2$ (0.1 equiv., 0.007 mmol, 4.1 mg), triphenylphosphine (0.2 equiv., 0.014 mmol, 3.9 mg) and 2-bromothiophene (2.5 equiv., 0.187 mmol, 30.6 mg) were weighed in a 2-dram vial with stir bar and dissolved in THF (1.0 mL). The di-Grignard solution was quickly added to the reaction mixture by pipette, yielding a dark red solution. 0.5 mL of THF was used to rinse the vial and combined with the reaction mixture. The reaction was heated to 40 ˚C and allowed to stir for 24 hours in a glove box. The solution turned bright orange after 16 hours.

The reaction was cooled to room temperature and quenched by 0.1 mL of dry methanol. The solution was transferred to a silica gel cartridge, and then dried on it under vacuum. The cartridge was subjected to automated column chromatography with 100% hexanes to yield *trans*-**4.1k** (dr 90:10 *trans:cis*) as a yellow solid (43.5 mg, 86%).

*Tabulated Characterization Data for trans-**4.1k***

δ_H (400 MHz, C_6D_6)	7.21 (d, *J* = 18.3 Hz, 2H, vinyl), 6.98 (d, *J* = 3.6 Hz, 2H, thienyl), 6.84 (d, *J* = 3.7 Hz, 2H, thienyl), 6.69 (d, *J* = 5.2 Hz, 2H, thienyl), 6.65 – 6.58 (m, 2H, thienyl), 6.55 (d, *J* = 3.8 Hz, 2H, thienyl), 6.42 (dd, *J* = 18.4, 5.5 Hz, 2H, vinyl), 4.12 (d, *J* = 5.6 Hz, 2H, Si*H*), 0.39 (s, 12H, -CH_3), 0.38 (s, 12H, (thienyl)H_3).
δ_C (101 MHz, C_6D_6)	144.00 (vinyl), 139.23 (thienyl), 137.46 (thienyl), 136.84 (thienyl), 126.49 (thienyl), 124.39 (thienyl), 124.06 (thienyl), 123.83 (thienyl), 119.74 (vinyl), -4.93 (-CH$_3$), -5.01 (-CH$_3$).
δ_{Si} (79 MHz, C_6D_6)	-40.09 (*Si*Me$_2$), -64.57 (*Si*H).
HRMS	Calcd. for $C_{28}H_{40}S_4Si_6$: 672.0627. Found: 672.0623.
IR (cm^{-1})	2084 (SiH).
λ_{max} (THF) /nm	367 (ε/dm^3 mol^{-1} cm^{-1} 32600)

Synthesis of P4.1 via Kumada Polycondensation

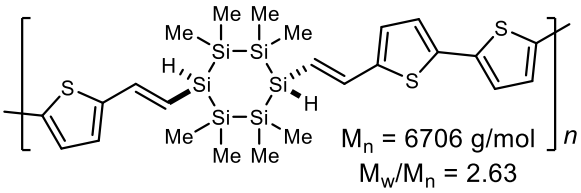

In a glove box, an oven-dried 2-dram vial with stir bar was charged with **4.1j** (dr 90:10 *trans:cis*) (1.0 equiv., 0.075 mmol, 50.0 mg) and THF (1.0 mL). *i*-PrMgCl (2.0 M in THF) (75 μL) was added by micro syringe. The solution was stirred at room temperature for 30 minutes, yielding a di-Grignard intermediate. 0.1 mL of reaction mixture was taken as an aliquot, quenched by methanol and dried under vacuum. The clean ^{1}H NMR spectrum of the quenched intermediate showed a full conversion of the starting cyclosilane. $NidpppCl_2$ (0.1 equiv., 0.007 mmol, 4.1 mg), triphenylphosphine (0.2 equiv., 0.014 mmol, 3.9 mg) and 2,5-dibromothiophene (1.5 equiv., 0.112 mmol, 27.2 mg) were weighed in a 2-dram vial with stir bar and dissolved in THF (1.0 mL). The di-Grignard solution was quickly added to the reaction mixture by pipette, yielding a dark red solution. 0.5 mL of THF was used to rinse the vial and combined with the reaction mixture. The reaction was heated to 40 ˚C and allowed to stir for 24 hours in a glove box. The solution turned bright orange after 16 hours.

After 24 hours, the reaction was quenched by adding the orange solution dropwise to 15 mL of dry methanol in a scintillation vial. Formation of orange precipitates was observed. The suspension was allowed to sit overnight, and the top clear yellow solution was removed. 10 mL of methanol were added, and precipitates were washed sufficiently by shaking the vial. The suspension was allowed to sit until the precipitates settled at the bottom. The above washing procedure was repeated 2 more times. Then the suspension

was filtered through a Buchner funnel and the solid was dried under vacuum, yielding an orange powder (36.8 mg, 80%).

Tabulated Characterization Data for ***P4.1***

δ_H (400 MHz, $CDCl_3$)	7.03 (br, 4H, vinyl and thienyl), 6.82 (br, 2H, thienyl), 6.14 (br, 2H, vinyl), 3.77 (br, 2H, Si*H*), 0.31 (br, 24H, -C*H*$_3$).
δ_C (101 MHz, $CDCl_3$)	144.43 (vinyl), 138.64 (thienyl), 136.55 (thienyl), 136.24 (thienyl), 130.47 (thienyl), 126.36 (thienyl), 125.34 (thienyl), 124.56 (thienyl), 124.12 (thienyl), 120.92 (vinyl), 120.84 (vinyl), -4.35 (-*C*H$_3$), -4.59 (-*C*H$_3$), -4.67 (-*C*H$_3$).
δ_C (125.7 MHz, CPMAS)	141.58 (aromatic and vinyl), 134.03 (aromatic), 121.74 (aromatic and vinyl), -6.89 (-*C*H$_3$).
δ_{Si} (79 MHz, $CDCl_3$)	-39.88 (*Si*Me$_2$), -64.76 (*Si*H).
δ_{Si} (99.3 MHz, CPMAS)	-33.23 (*Si*Me$_2$), -62.68 (br, *Si*H)
IR (cm^{-1})	2051 (SiH).
λ_{max} (THF) /nm	433 (ε/dm^3 g^{-1} cm^{-1} 8.17), 418 (ε/dm^3 g^{-1} cm^{-1} 8.27)

Synthesis of P4.2 via Kumada Polycondensation

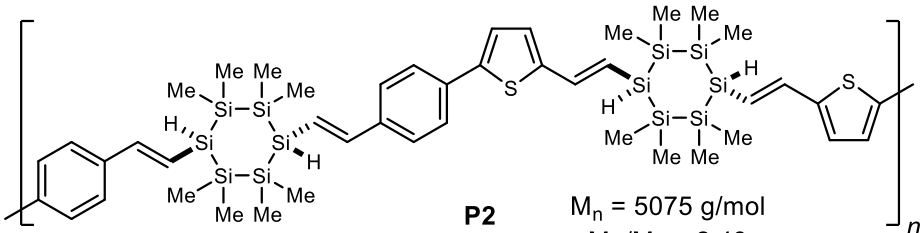

In a glove box, an oven-dried 2-dram vial with stir bar was charged with **4.1j** (dr 90:10 *trans:cis*) (1.0 equiv., 0.075 mmol, 50.0 mg) and THF (1.0 mL). *i*-PrMgCl (2.0 M in THF) (75 μL) was added by micro syringe. The solution was stirred at room temperature for 30 minutes, yielding a di-Grignard intermediate. NidpppCl$_2$ (0.1 equiv., 0.007 mmol, 4.1 mg), triphenylphosphine (0.2 equiv., 0.014 mmol, 3.9 mg) and *trans*-**4.1b** (1.1 equiv., 0.082 mmol, 54.0 mg) were weighed in a 2-dram vial with stir bar and dissolved in THF (1.0 mL). The di-Grignard solution was quickly added to the reaction mixture by pipette,

yielding a dark red solution. 0.5 mL of THF was used to rinse the vial and combined with the reaction mixture. The reaction was heated to 40 ˚C and allowed to stir for 24 hours in a glove box. The solution turned dark red after 16 hours.

After 24 hours, the reaction was quenched by adding the orange solution dropwise to 15 mL of dry methanol in a scintillation vial. Formation of orange precipitates was observed. The suspension was allowed to sit overnight, and the top clear yellow solution was removed. 10 mL of methanol were added, and precipitates were washed sufficiently by shaking the vial. The suspension was allowed to sit until the precipitates settled at the bottom. The above washing procedure was repeated 2 more times. Then the suspension was filtered through a Buchner funnel and the solid was dried under vacuum, yielding a yellow powder (46.7 mg, 60%). Solid-state $^{1}H \rightarrow ^{29}Si$ and ^{13}C CPMAS spectra were recorded for its low solubility in $CDCl_3$. The broadness of peaks arises from the residual Ni catalyst.

Tabulated Characterization Data for ***P4.2***

δ_H (400 MHz, $CDCl_3$)	7.70-7.65 (br, 4H, aromatic), 7.55-6.98 (br, 8H, vinyl and aromatic), 7.03-6.98 (br, 4H, vinyl and aromatic), 6.47 (br, 2H, vinyl), 6.20 (br, 2H, vinyl), 3.77 (br, 2H, Si*H*), 3.53 (br, 2H, Si*H*), 0.30 (br, 48H).
δ_C (125.7 MHz, CPMAS)	142.32 (aromatic and vinyl), 135.80 (aromatic), 128.93 (aromatic and vinyl), 124.61 (aromatic), -1.14 (-*C*H_3), -6.70 (-*C*H_3).
δ_{Si} (99.3 MHz, CPMAS)	-34.10 (*Si*Me_2), -65.98 (br, *Si*H)
IR (cm^{-1})	2064 (SiH).
λ_{max} (THF) /nm	311 (ε/dm^3 g^{-1} cm^{-1} 8.93)

NMR Spectra

NMR Spectra of 4.1a

^{1}H NMR Spectrum (400 MHz, C_6D_6)

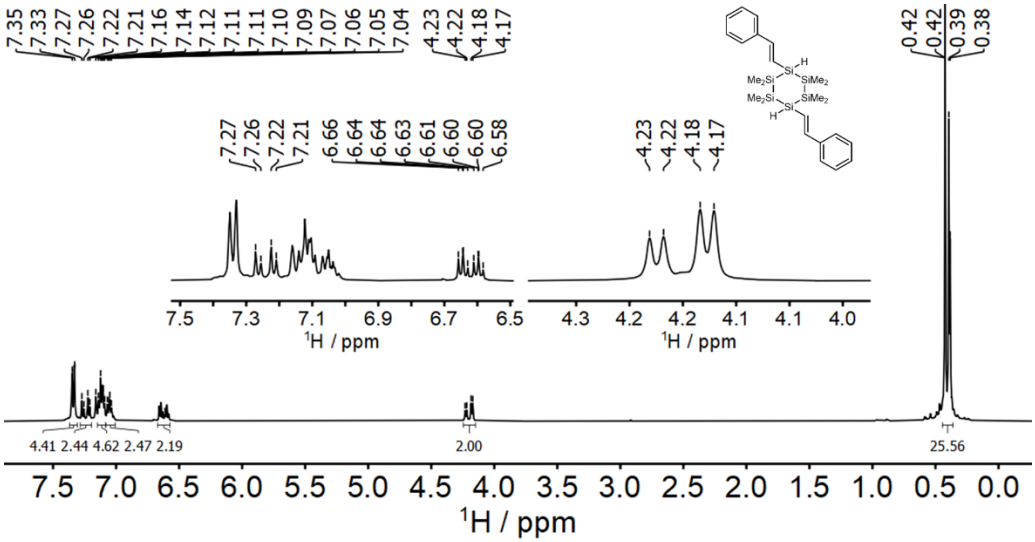

^{13}C{^{1}H} NMR Spectrum (101 MHz, C_6D_6)

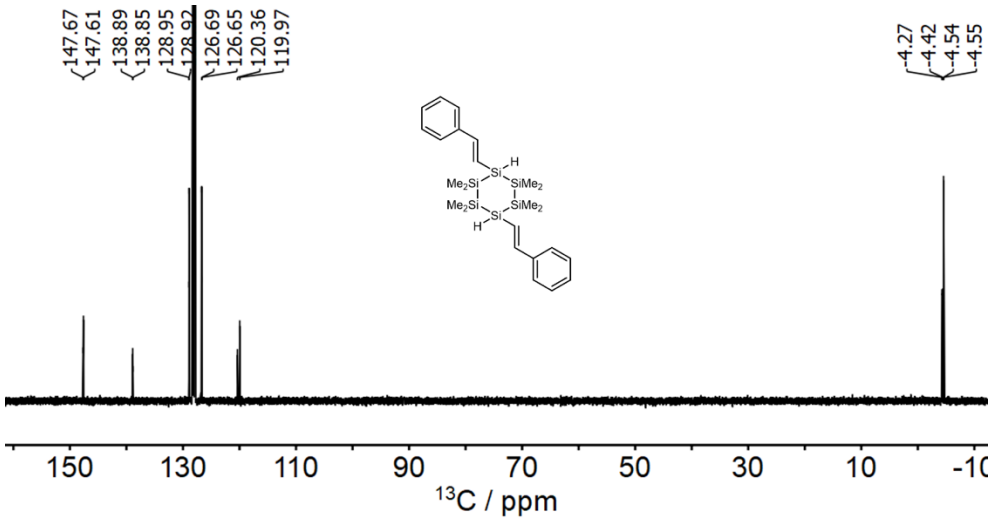

$^{29}Si\{^{1}H\}$ NMR Spectrum (79 MHz, C_6D_6). $^{1}J_{Si\text{-}H}$ = 7 Hz.

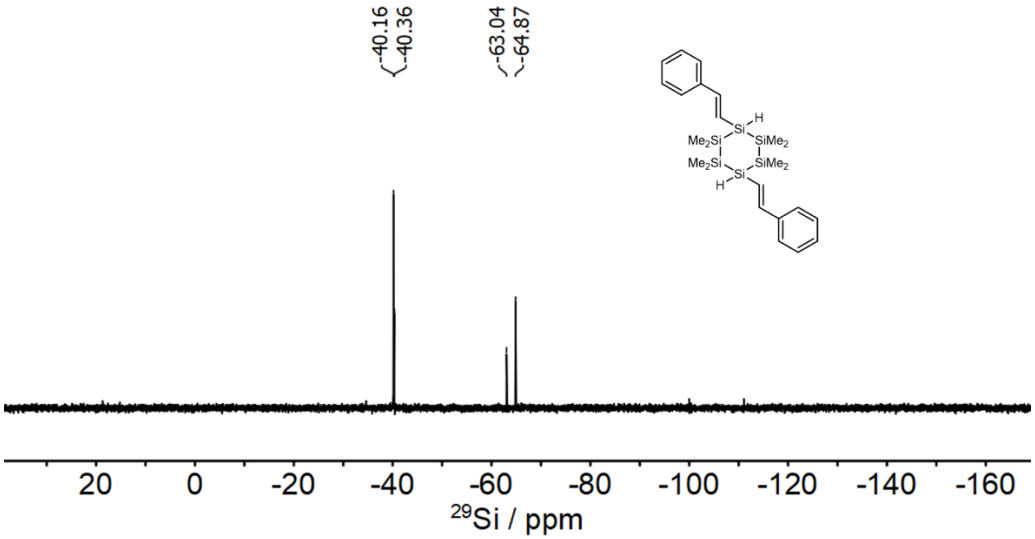

NMR Spectra of 4.1b

^{1}H NMR Spectrum (400 MHz, C_6D_6)

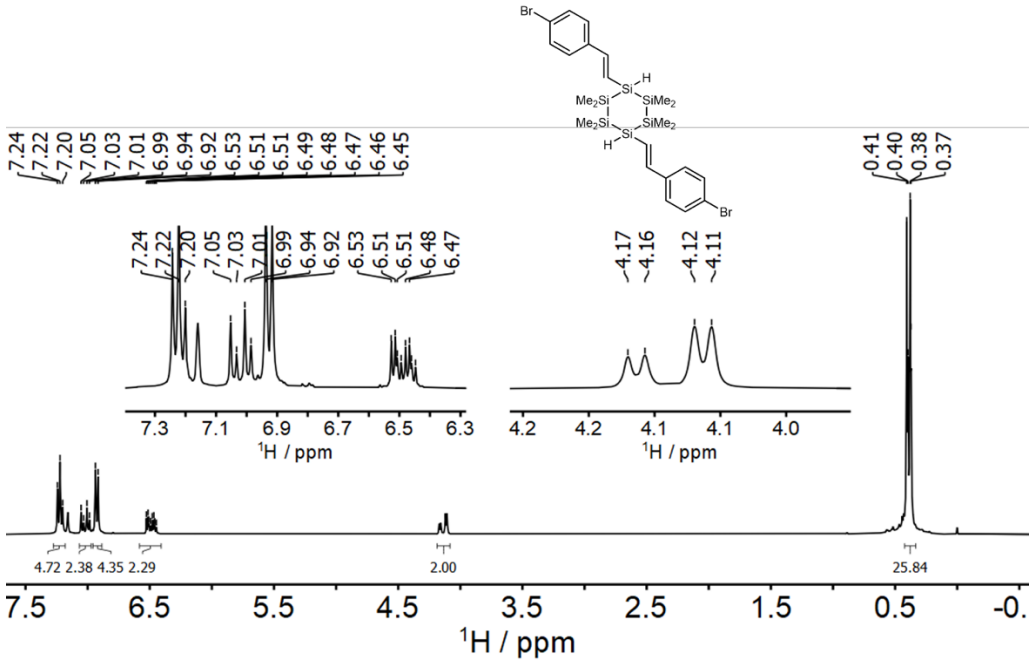

$^{13}C\{^{1}H\}$ NMR Spectrum (101 MHz, C_6D_6)

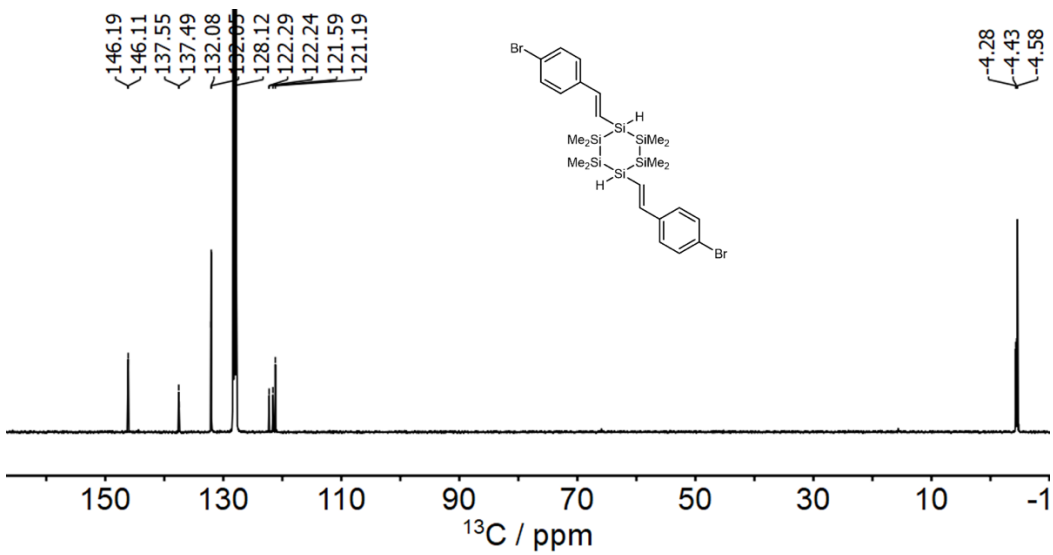

$^{29}Si\{^{1}H\}$ NMR Spectrum (79 MHz, C_6D_6). $^{1}J_{Si\text{-}H}$ = 7 Hz.

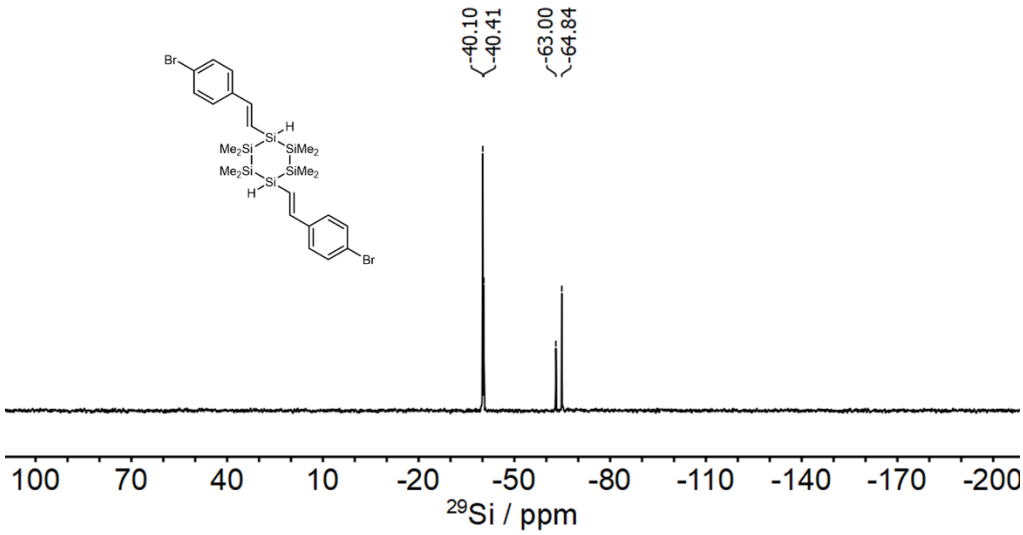

NMR Spectra of 4.1c

^{1}H NMR Spectrum (400 MHz, C_6D_6)

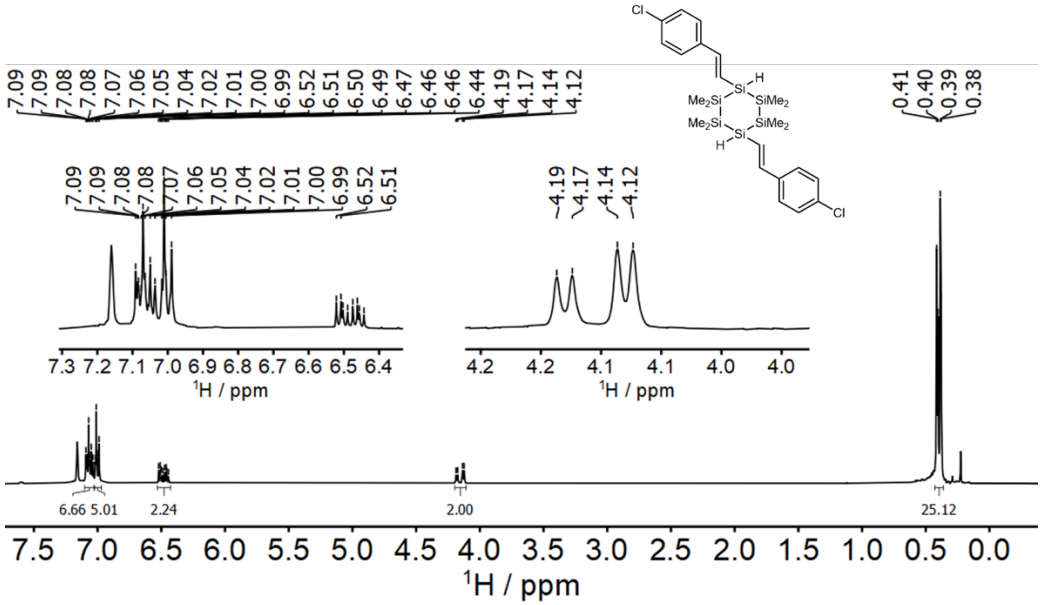

^{13}C{^{1}H} NMR Spectrum (101 MHz, C_6D_6)

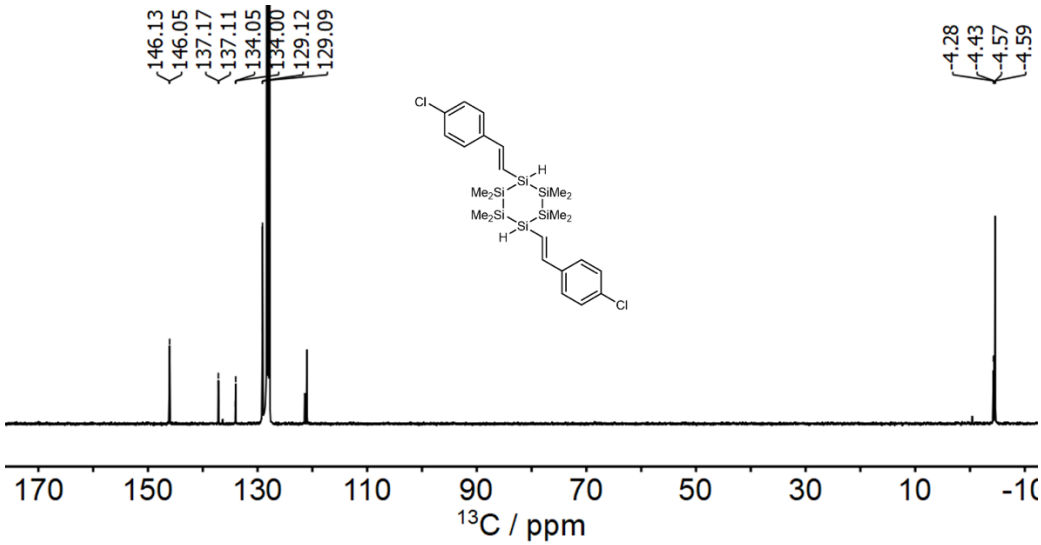

$^{29}Si\{^{1}H\}$ NMR Spectrum (79 MHz, C_6D_6). $^{1}J_{Si\text{-}H}$ = 7 Hz.

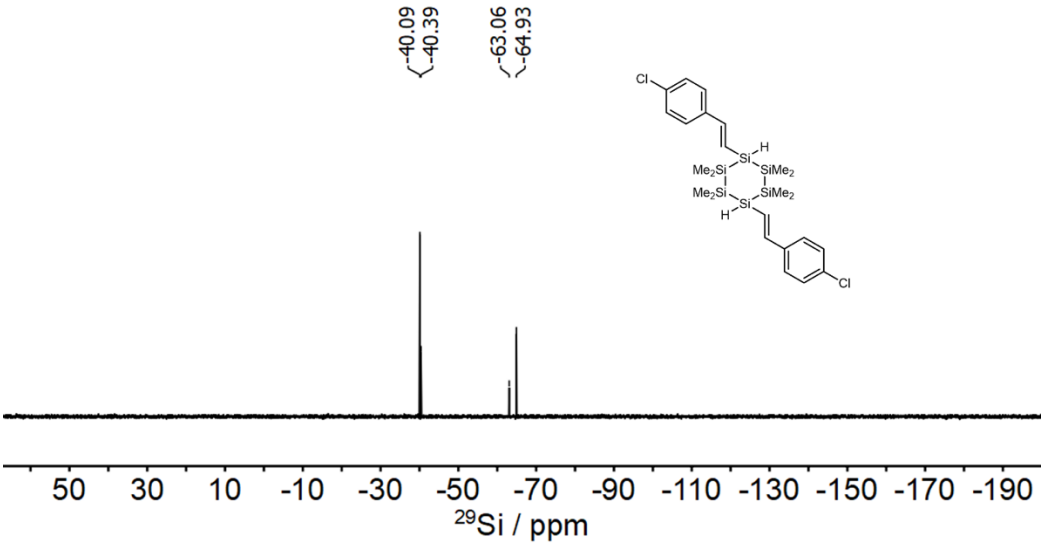

NMR Spectra of 4.1d

^{1}H NMR Spectrum (400 MHz, C_6D_6)

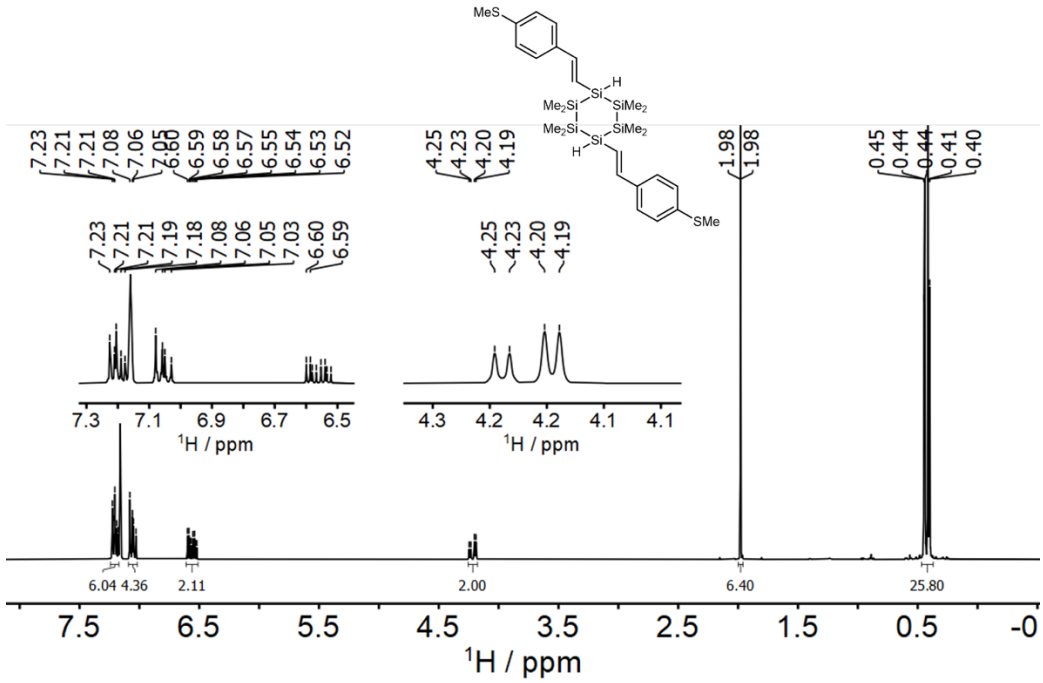

$^{13}C\{^{1}H\}$ NMR Spectrum (101 MHz, C_6D_6)

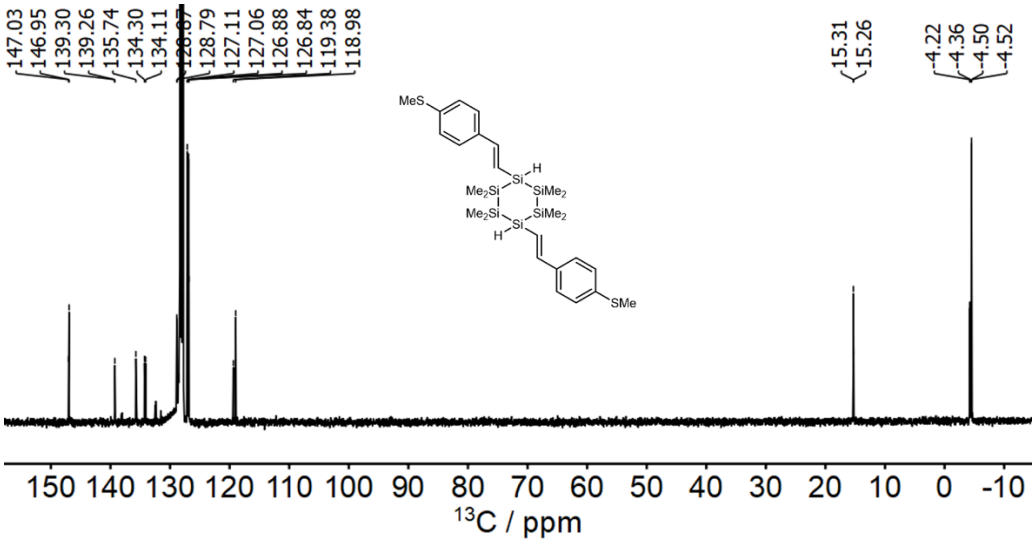

$^{29}Si\{^{1}H\}$ NMR Spectrum (79 MHz, C_6D_6). $^{1}J_{Si\text{-}H}$ = 7 Hz.

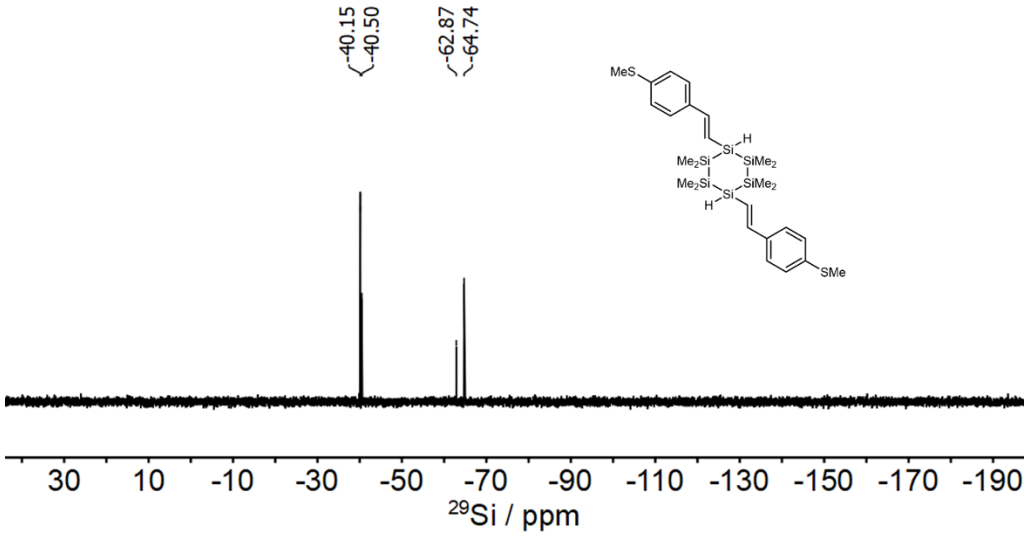

NMR Spectra of 4.1e

^{1}H NMR Spectrum of (400 MHz, C_6D_6)

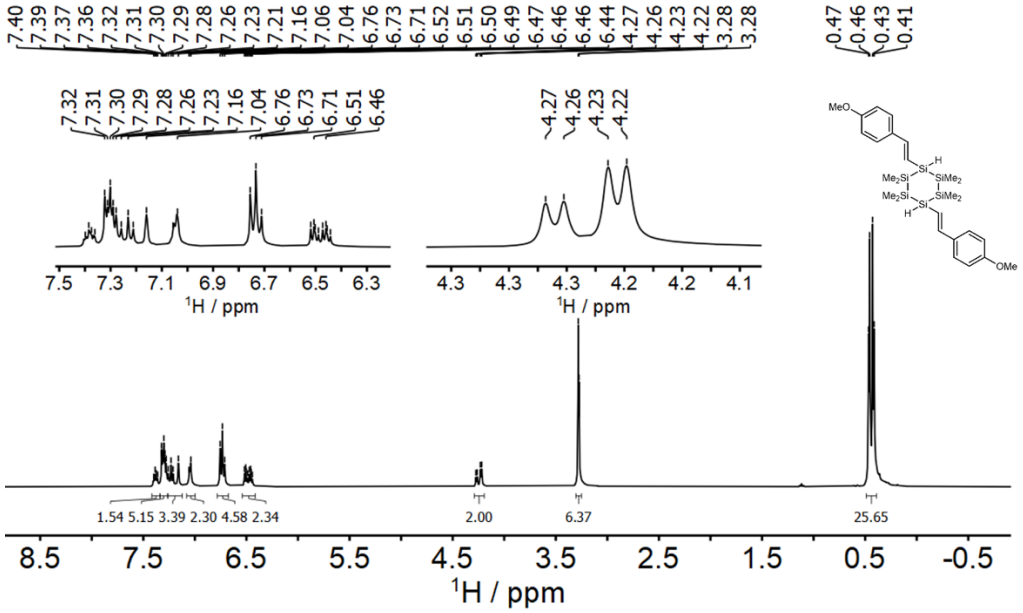

^{13}C{^{1}H} NMR Spectrum (101 MHz, C_6D_6)

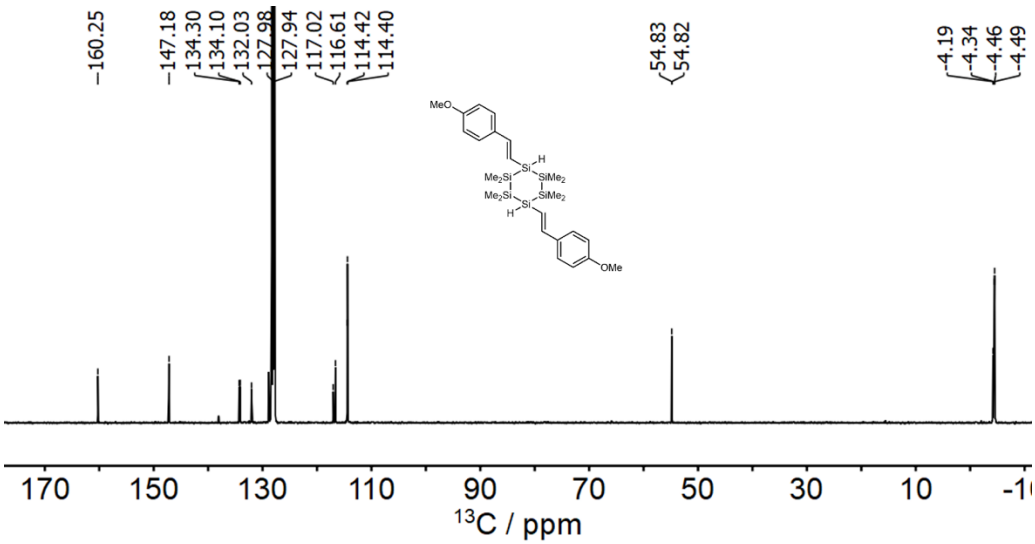

$^{29}Si\{^{1}H\}$ NMR Spectrum (79 MHz, C_6D_6). $^{1}J_{Si\text{-}H}$ = 7 Hz.

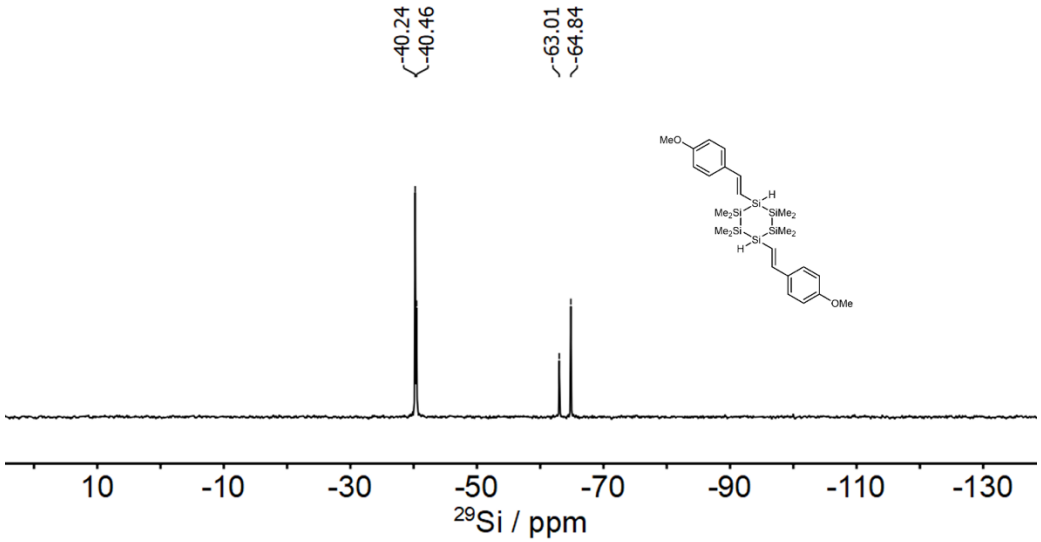

NMR Spectra of 4.1f

^{1}H NMR Spectrum (400 MHz, C_6D_6)

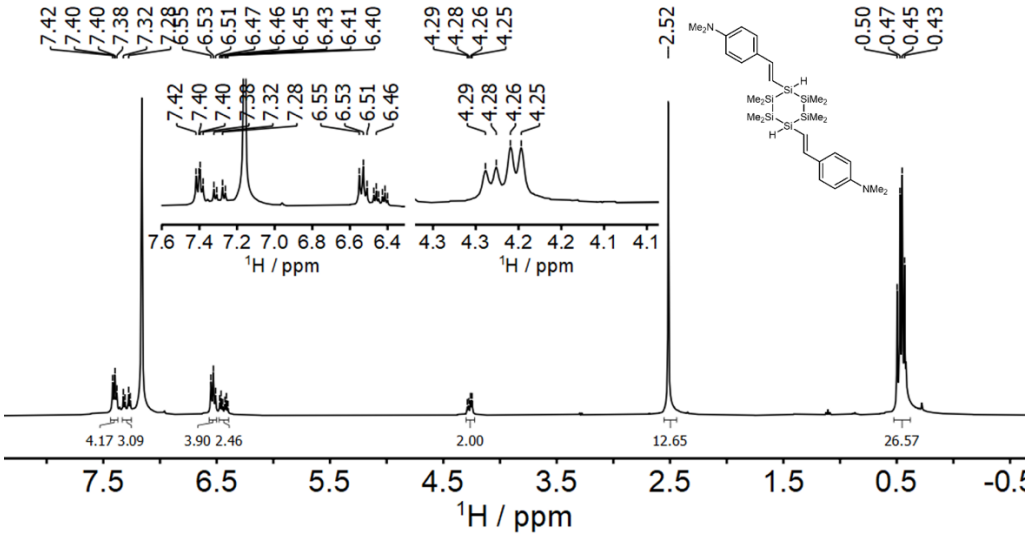

$^{13}C\{^{1}H\}$ NMR Spectrum (101 MHz, C_6D_6)

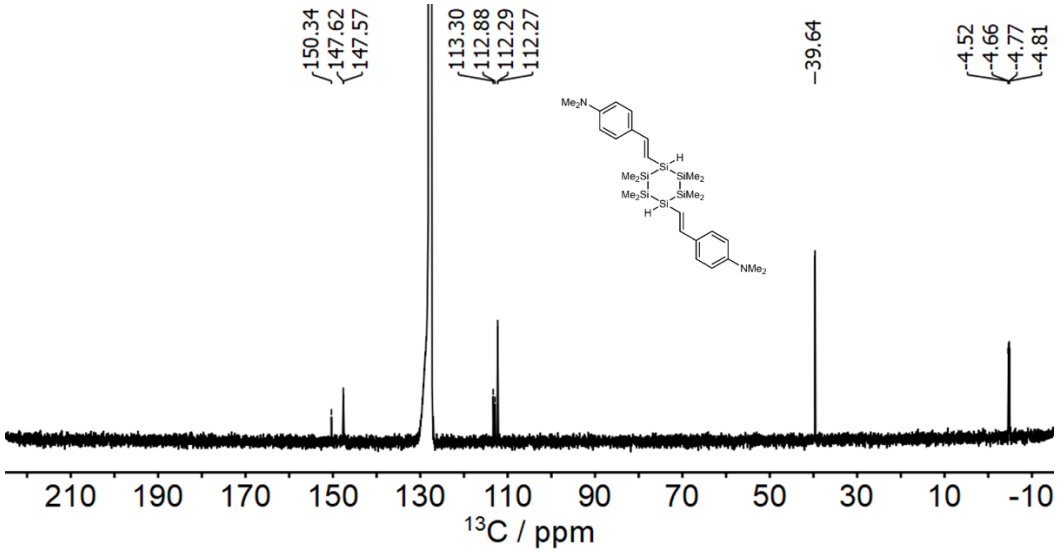

$^{29}Si\{^{1}H\}$ NMR Spectrum (79 MHz, C_6D_6). $^{1}J_{Si\text{-}H}$ = 7 Hz.

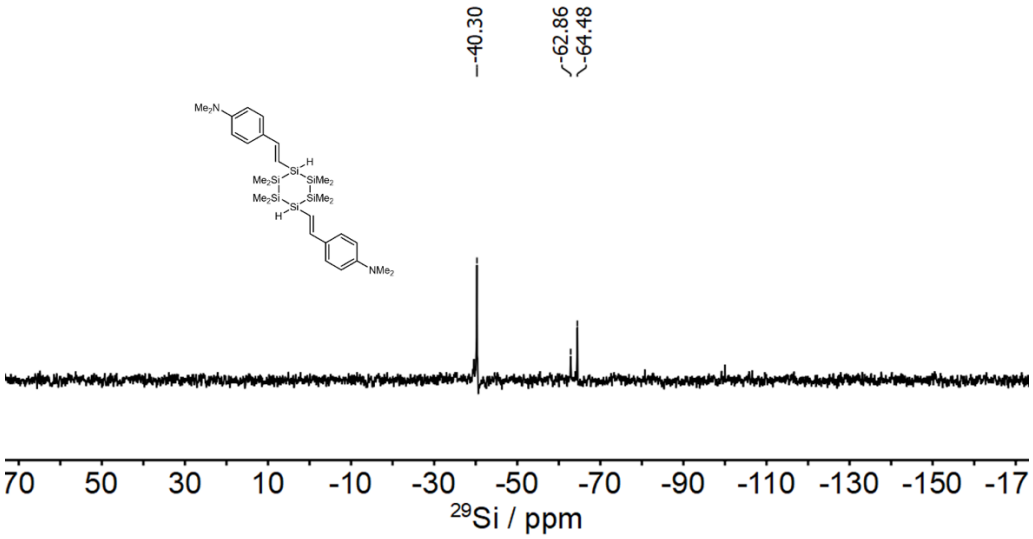

NMR Spectra of 4.1g

^{1}H NMR Spectrum (400 MHz, C_6D_6)

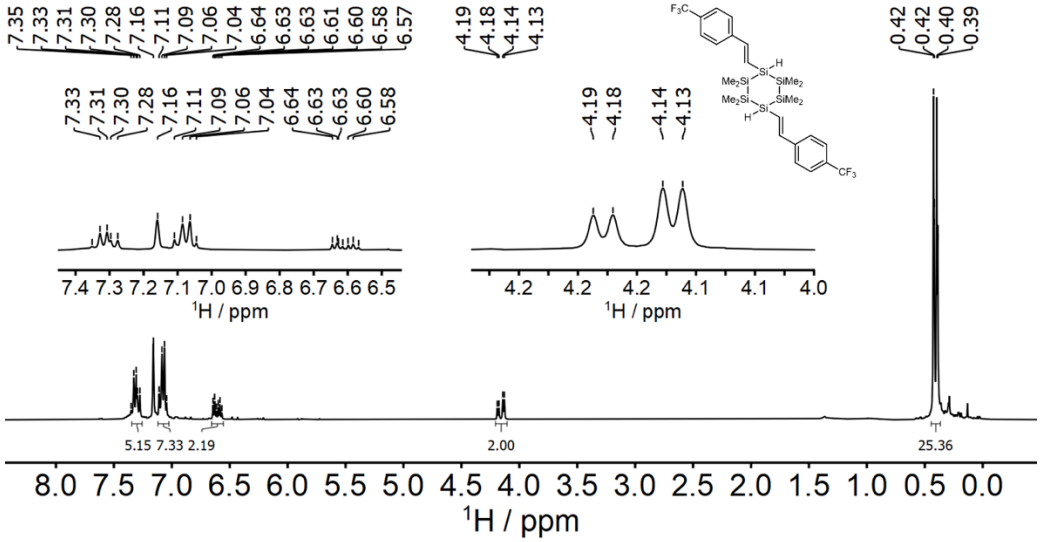

^{13}C{^{1}H} NMR Spectrum (101 MHz, C_6D_6)

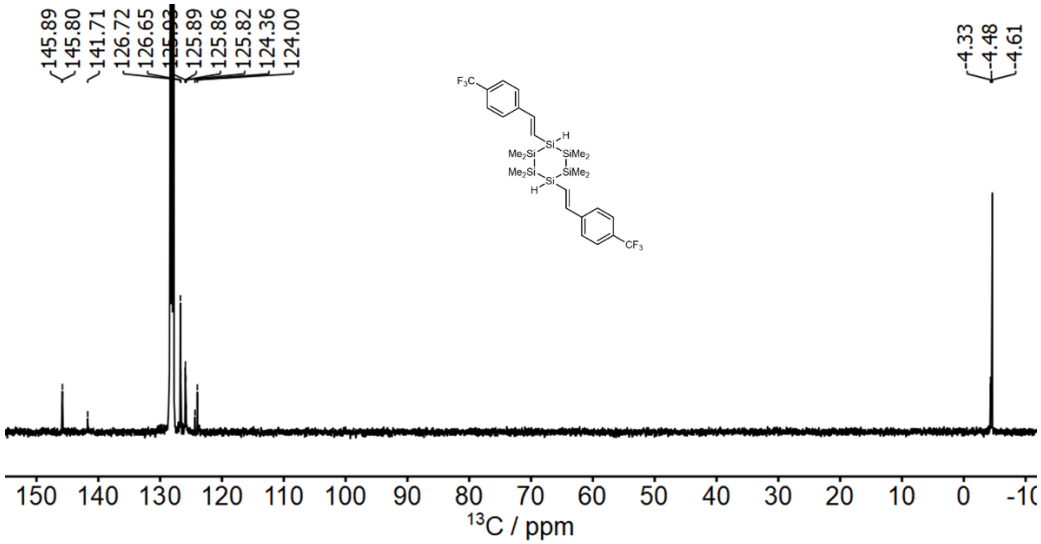

$^{19}F\{^{1}H\}$ NMR Spectrum (376 MHz, C_6D_6).

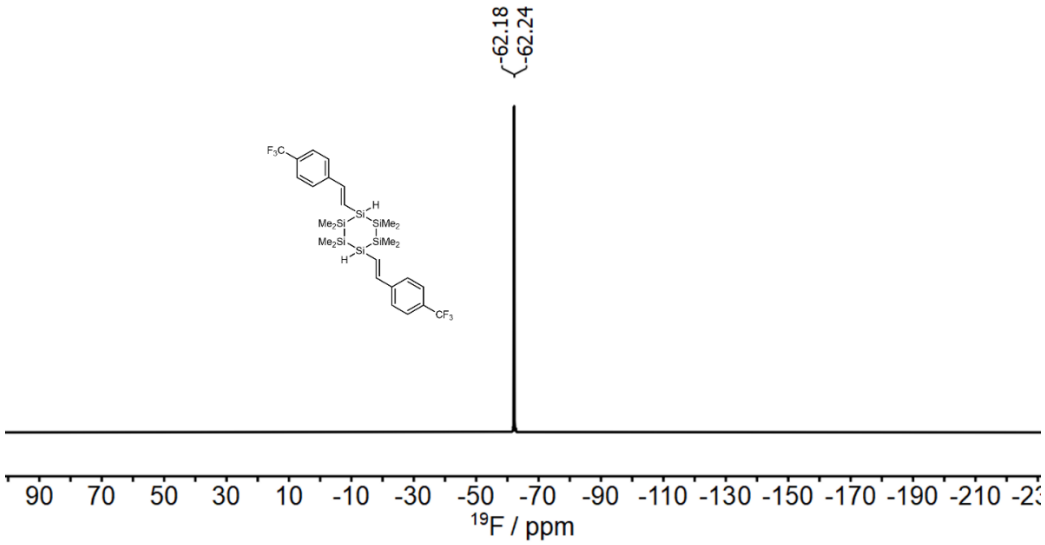

$^{29}Si\{^{1}H\}$ NMR Spectrum (79 MHz, C_6D_6). $^{1}J_{Si\text{-}H}$ = 7 Hz.

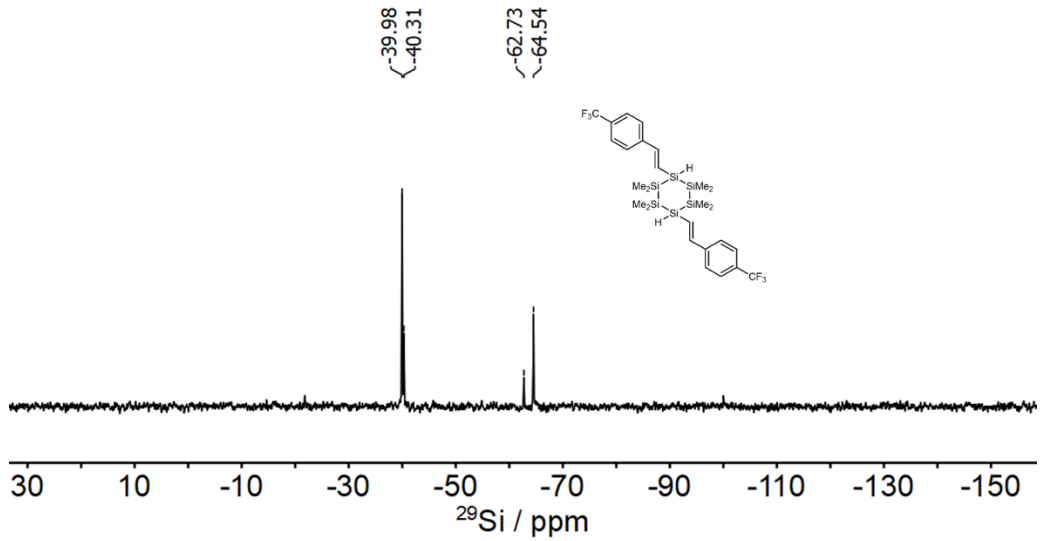

NMR Spectra of 4.1h

^{1}H NMR Spectrum (400 MHz, C_6D_6)

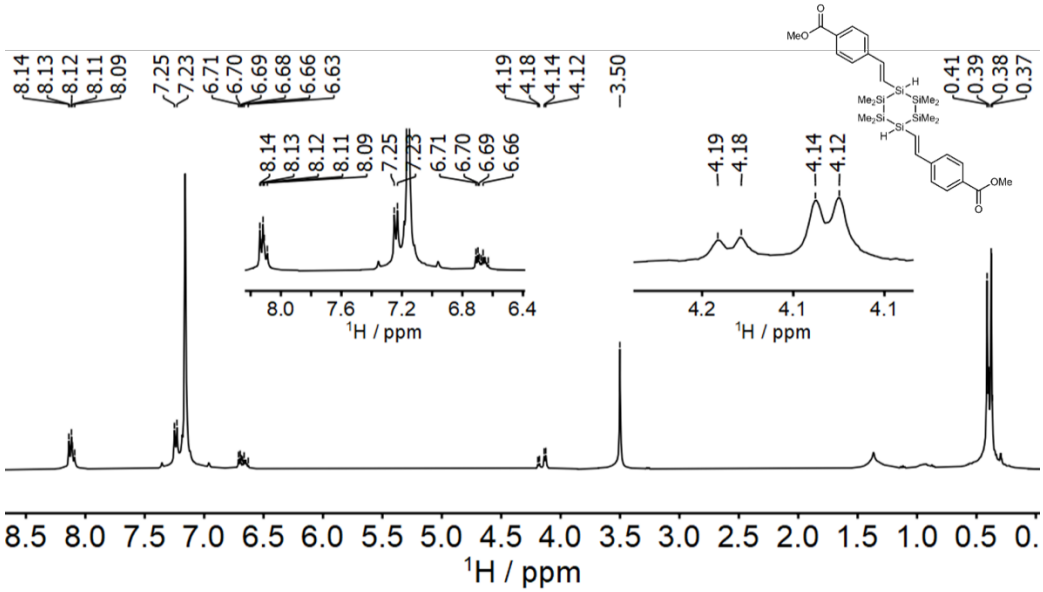

^{13}C{^{1}H} NMR Spectrum (101 MHz, C_6D_6)

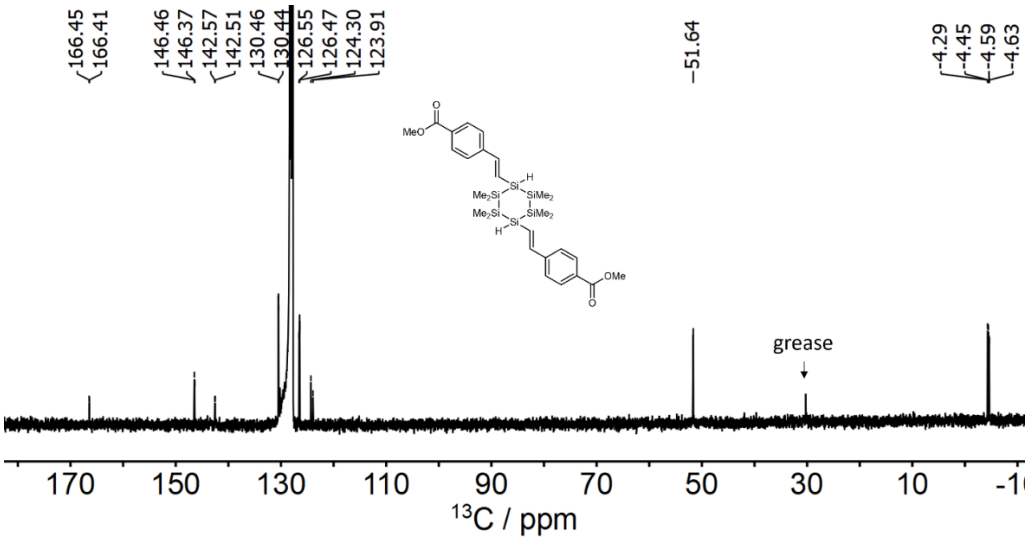

$^{29}Si\{^{1}H\}$ NMR Spectrum (79 MHz, C_6D_6). $^{1}J_{Si\text{-}H}$ = 7 Hz.

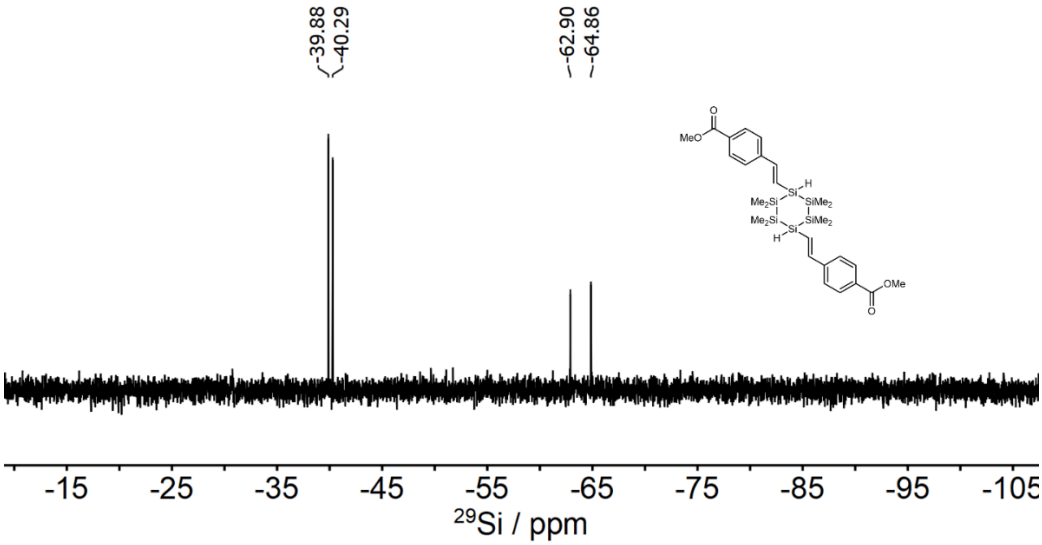

NMR Spectra of 4.1i

^{1}H NMR Spectrum (400 MHz, C_6D_6)

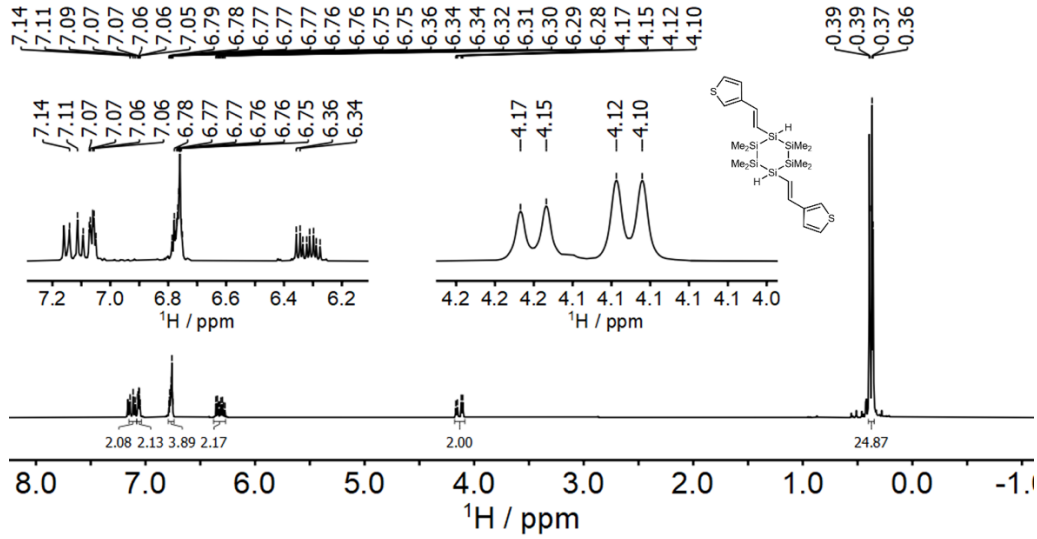

$^{13}C\{^{1}H\}$ NMR Spectrum of (101 MHz, C_6D_6)

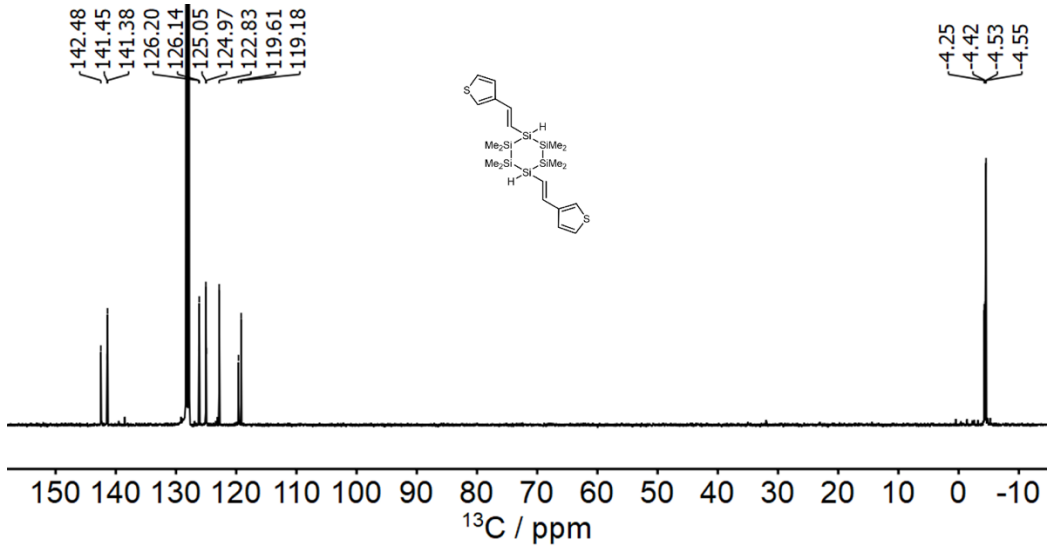

$^{29}Si\{^{1}H\}$ NMR Spectrum (79 MHz, C_6D_6). $^{1}J_{Si\text{-}H}$ = 7 Hz.

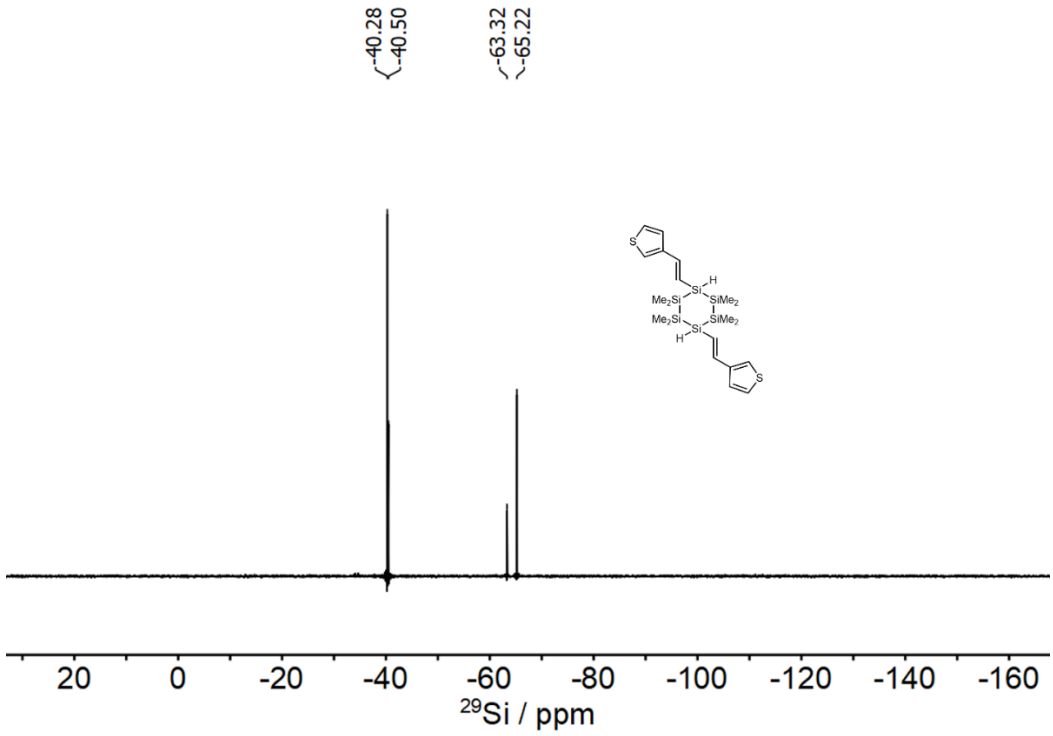

NMR Spectra of 4.1j

^{1}H NMR Spectrum (400 MHz, C_6D_6)

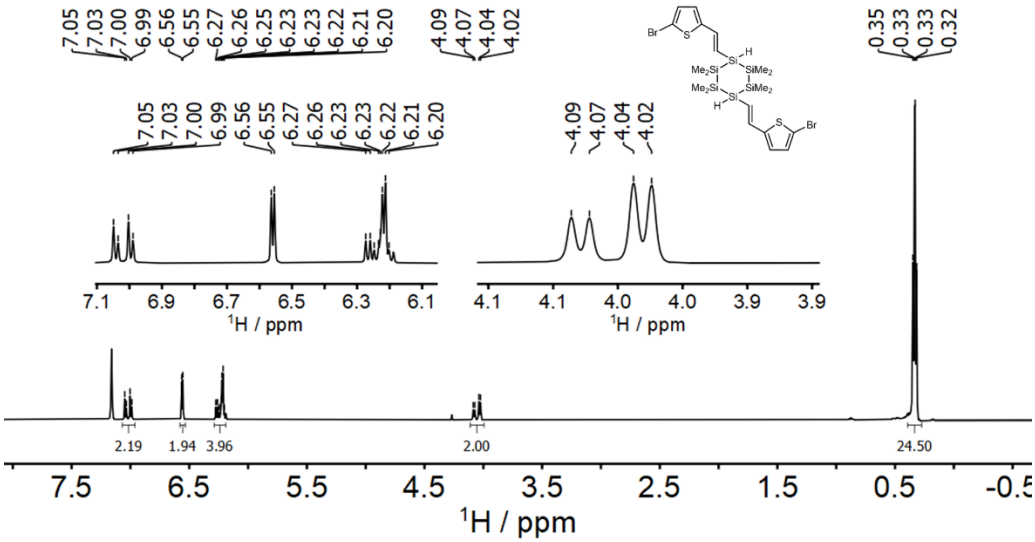

^{13}C{^{1}H} NMR Spectrum (101 MHz, C_6D_6)

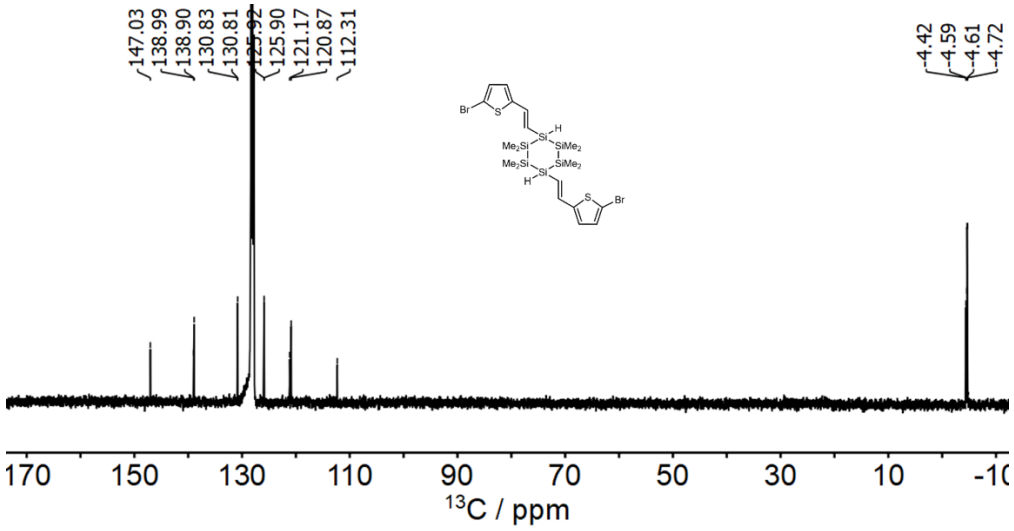

$^{29}Si\{^{1}H\}$ NMR Spectrum (79 MHz, C_6D_6). $^{1}J_{Si\text{-}H}$ = 7 Hz.

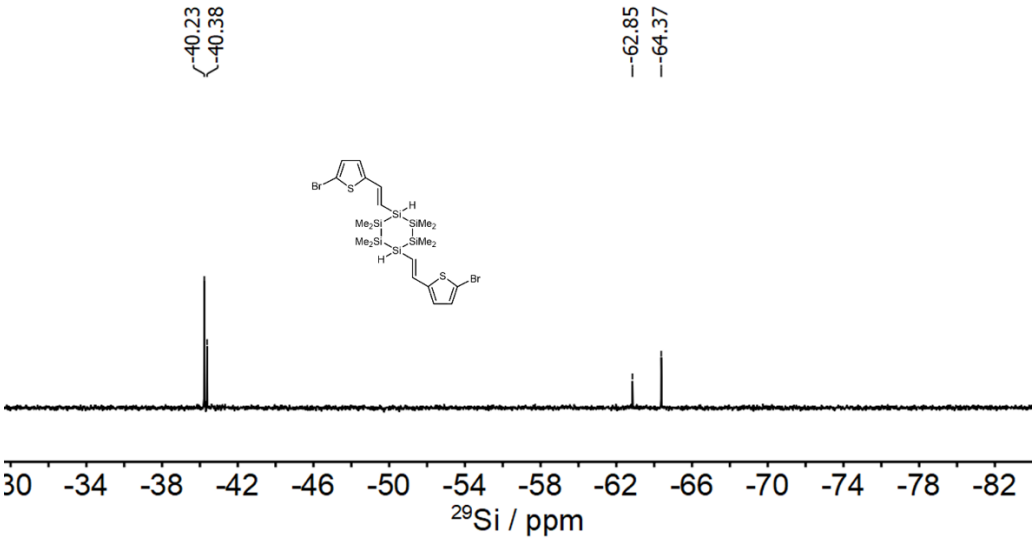

NMR Spectra of 4.2a

^{1}H NMR Spectrum of **2a** (400 MHz, C_6D_6)

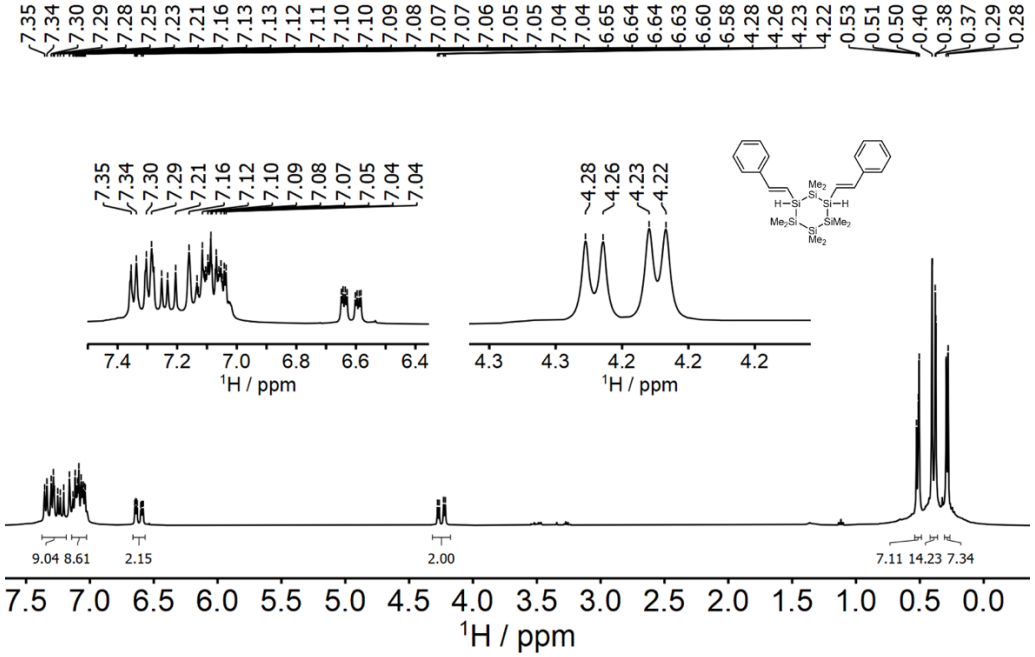

$^{13}C\{^{1}H\}$ NMR Spectrum (101 MHz, C_6D_6)

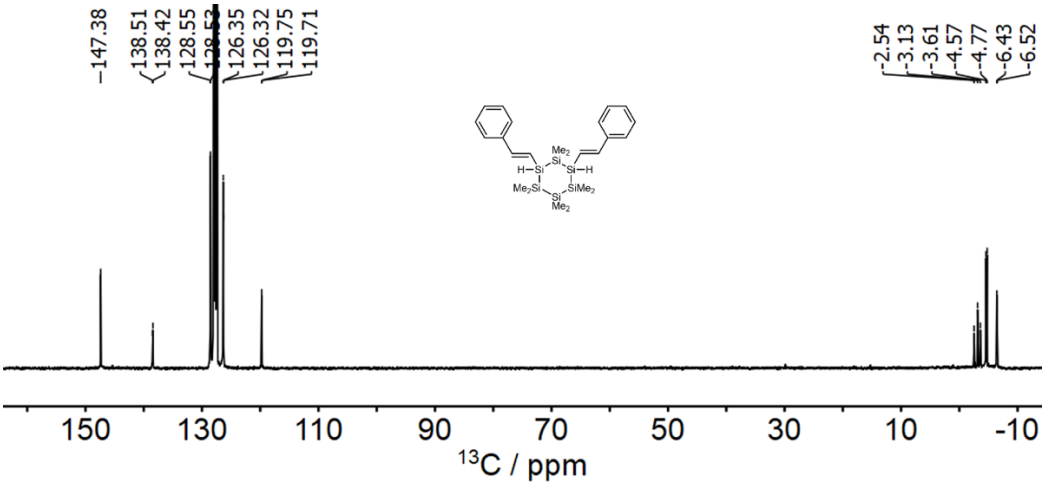

$^{29}Si\{^{1}H\}$ NMR Spectrum (79 MHz, C_6D_6). $^{1}J_{Si\text{-}H}$ = 7 Hz.

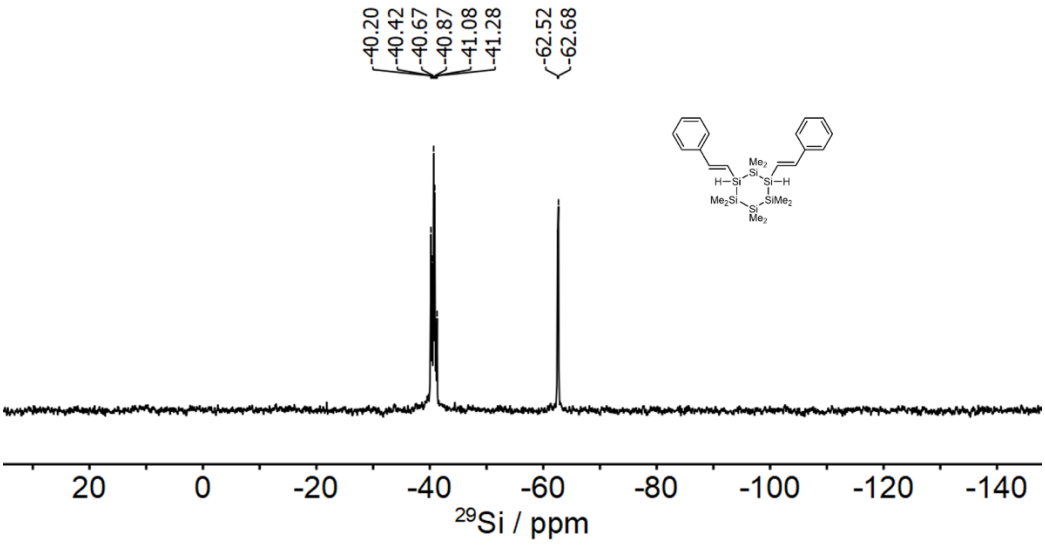

^{1}H-^{29}Si HSQC NMR spectrum (400 MHz, C_6D_6) of **2a.** $^{1}J_{Si-H}$ = 120 Hz.

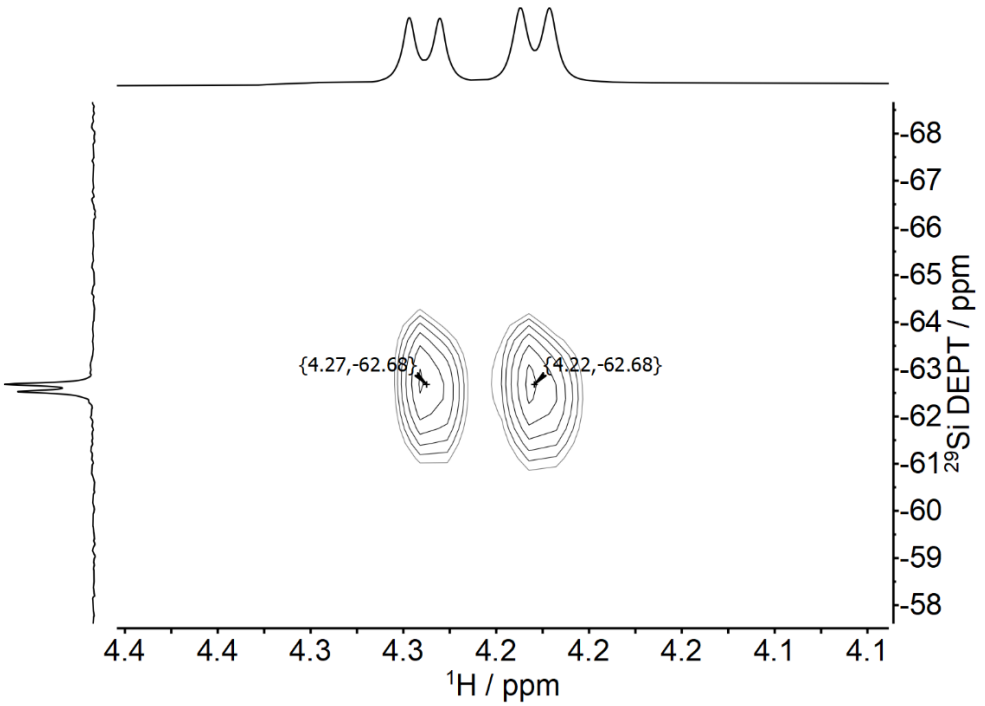

NMR Spectra of 4.2b

^{1}H NMR Spectrum (400 MHz, C_6D_6)

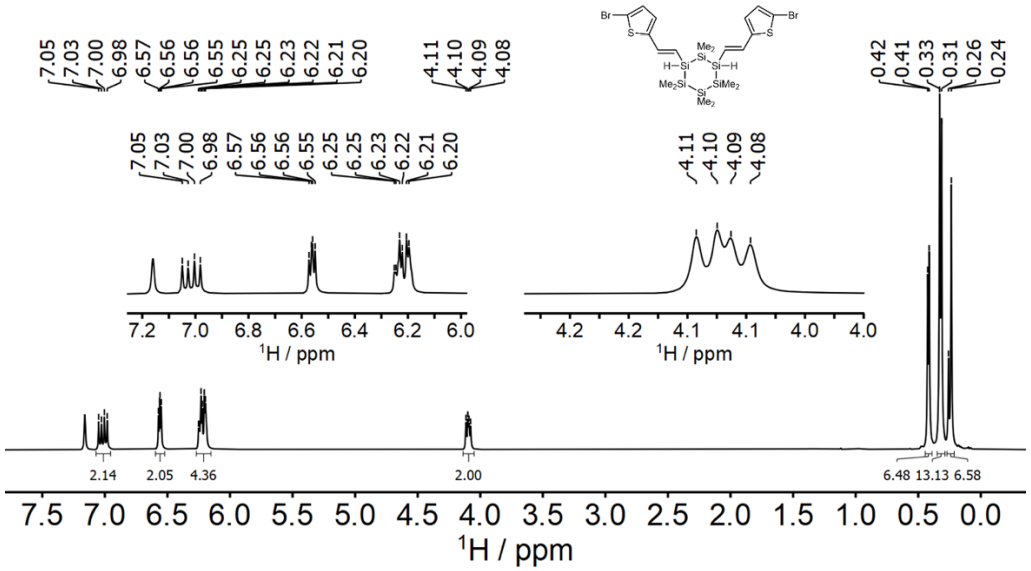

$^{13}C\{^{1}H\}$ NMR Spectrum (101 MHz, C_6D_6)

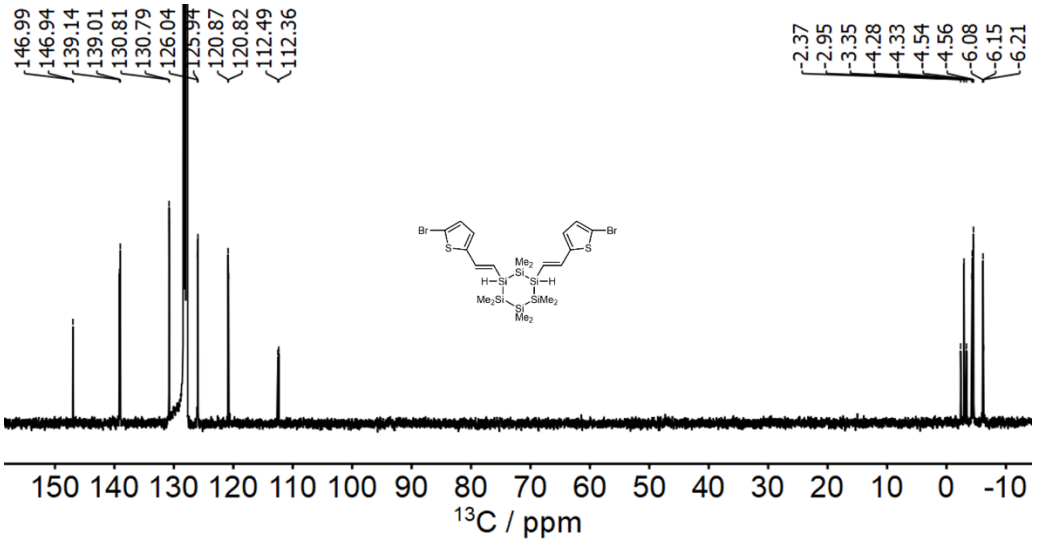

$^{29}Si\{^{1}H\}$ NMR Spectrum (79 MHz, C_6D_6). $^{1}J_{Si\text{-}H}$ = 7 Hz.

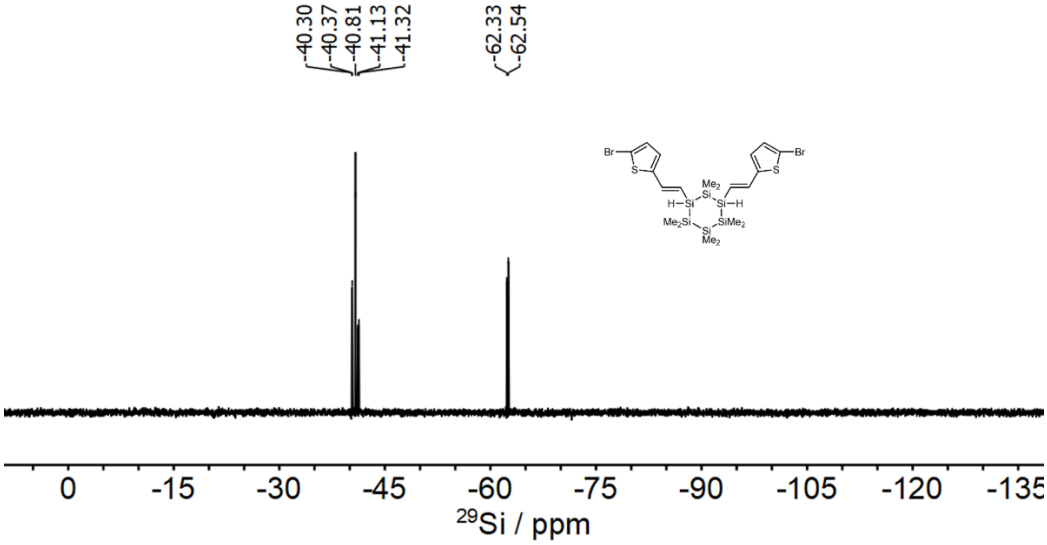

NMR Spectra of 4.3a

^{1}H NMR Spectrum (400 MHz, C_6D_6)

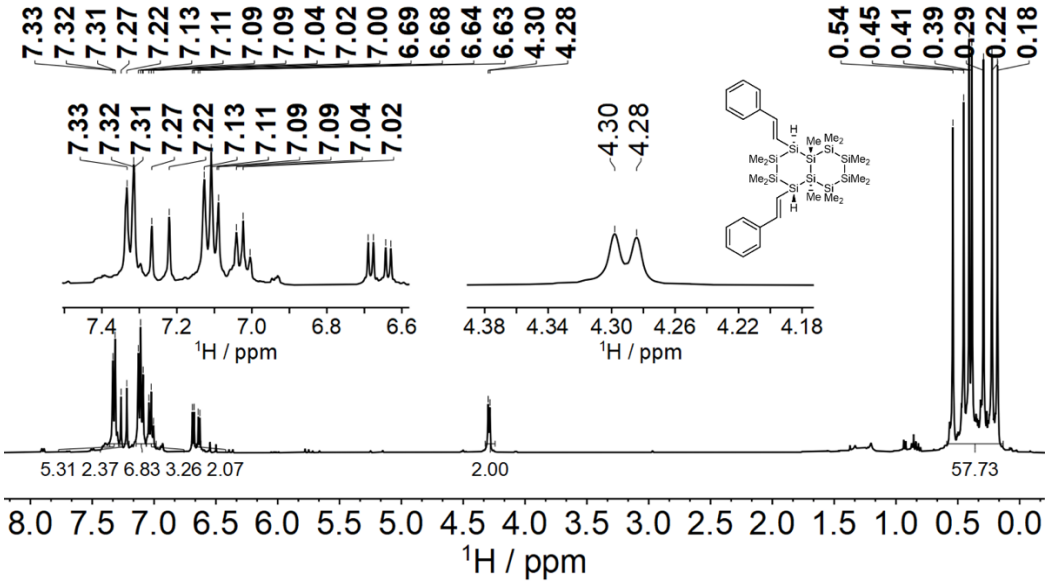

^{13}C{^{1}H} NMR Spectrum (101 MHz, C_6D_6)

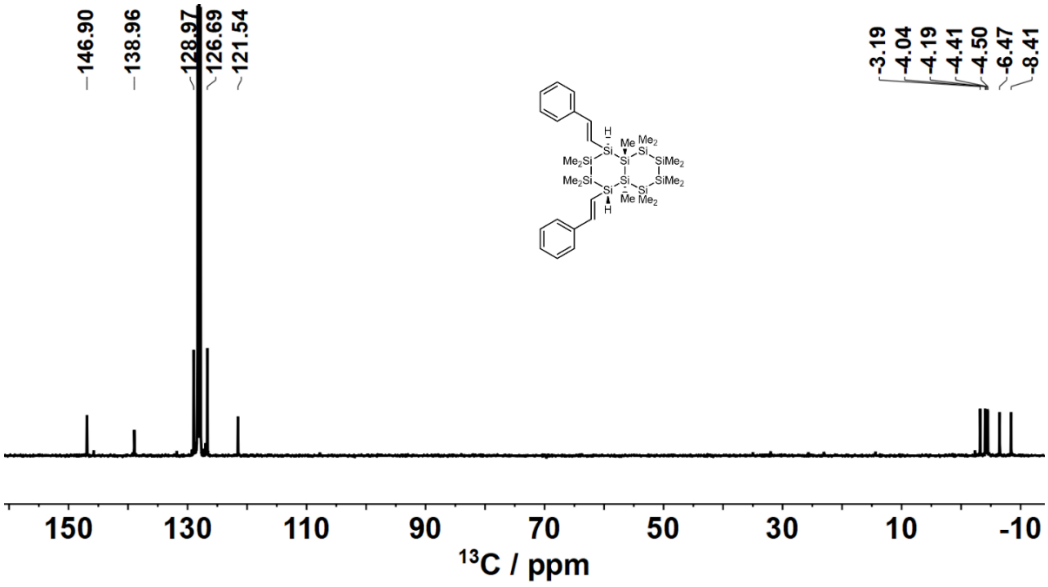

$^{29}Si\{^{1}H\}$ NMR Spectrum (79 MHz, C_6D_6). $^{1}J_{Si\text{-}H}$ = 7 Hz.

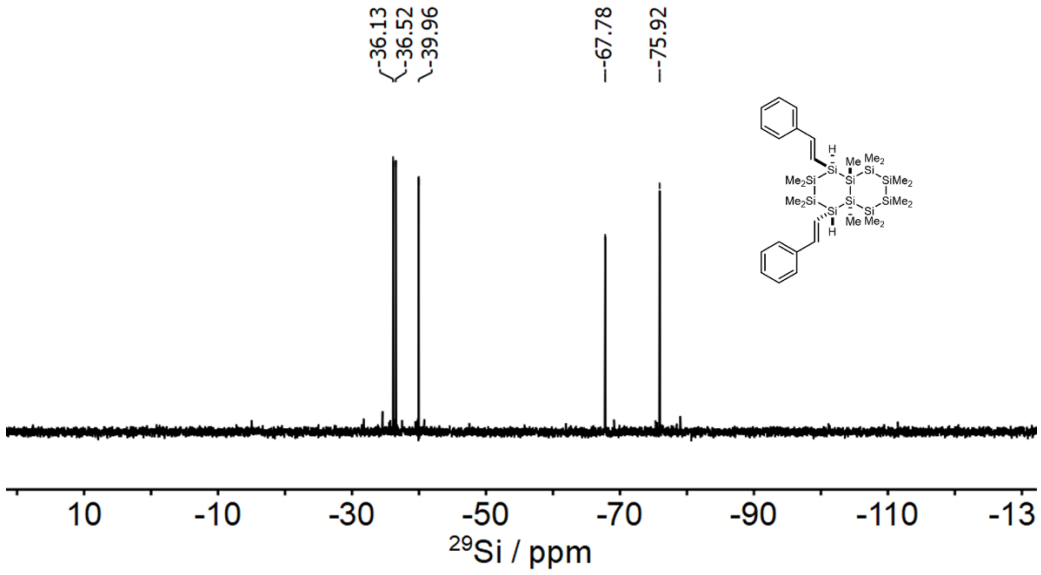

^{1}H-^{29}Si HSQC NMR spectrum (400 MHz, C_6D_6). $^{1}J_{Si\text{-}H}$ = 120 Hz.

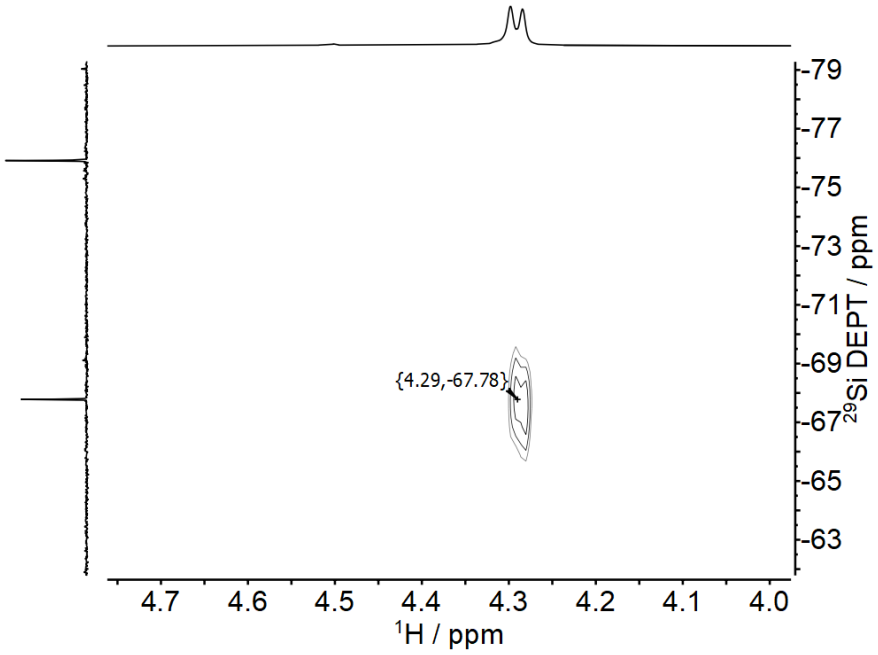

NMR Spectra of 3b

^{1}H NMR Spectrum (400 MHz, C_6D_6)

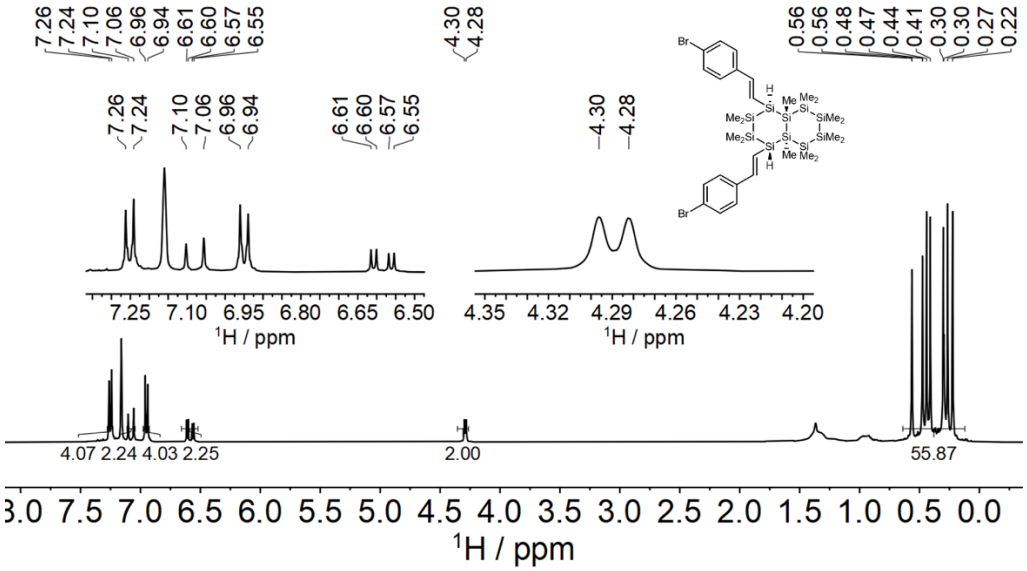

$^{13}C\{^{1}H\}$ NMR Spectrum (101 MHz, C_6D_6)

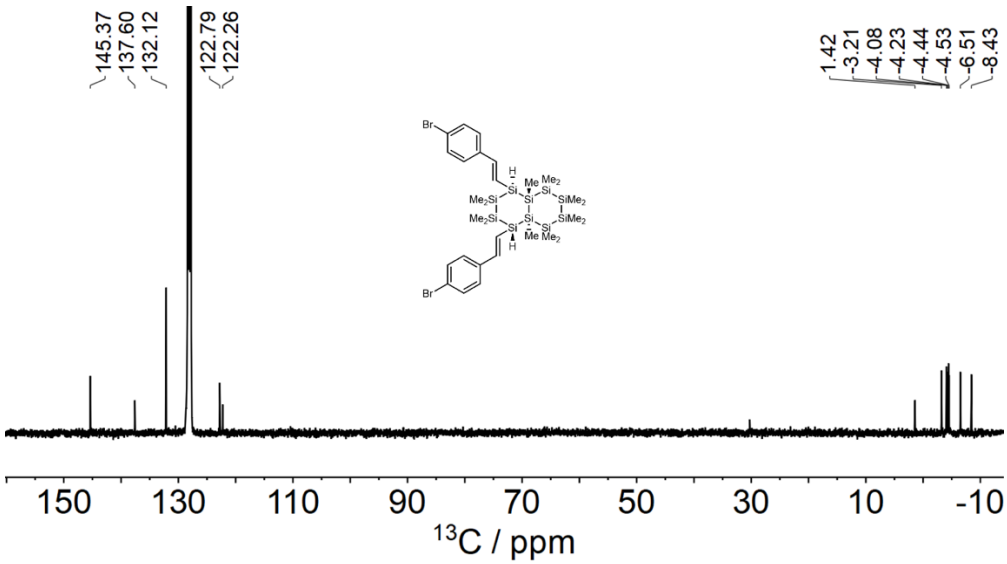

$^{29}Si\{^{1}H\}$ NMR Spectrum (79 MHz, C_6D_6). $^{1}J_{Si\text{-}H}$ = 7 Hz.

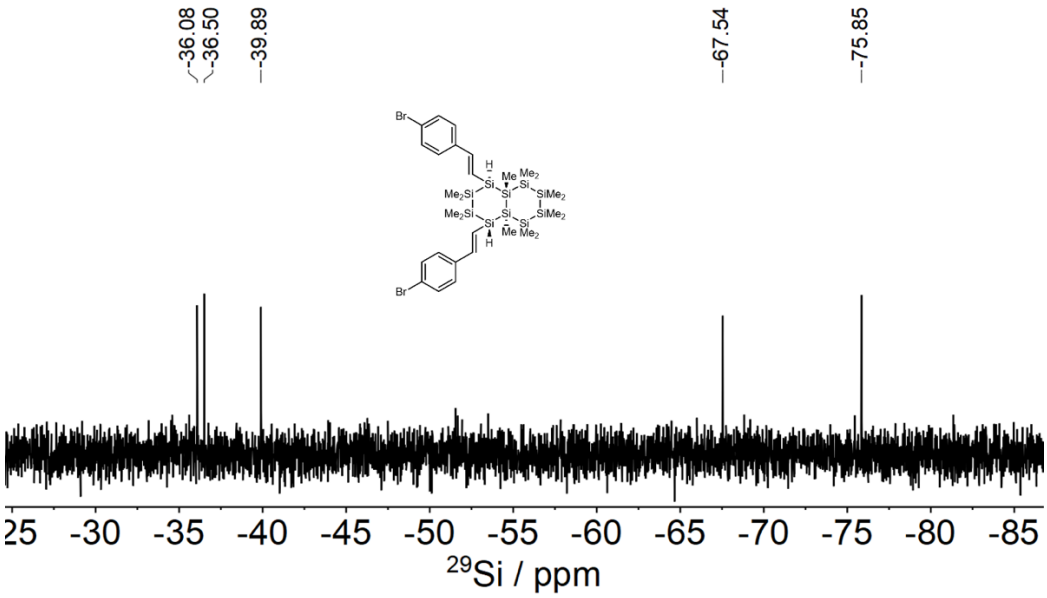

$^{29}Si\{^{1}H\}$ NMR Spectrum (79 MHz, C_6D_6). $^{1}J_{Si\text{-}H}$ = 120 Hz.

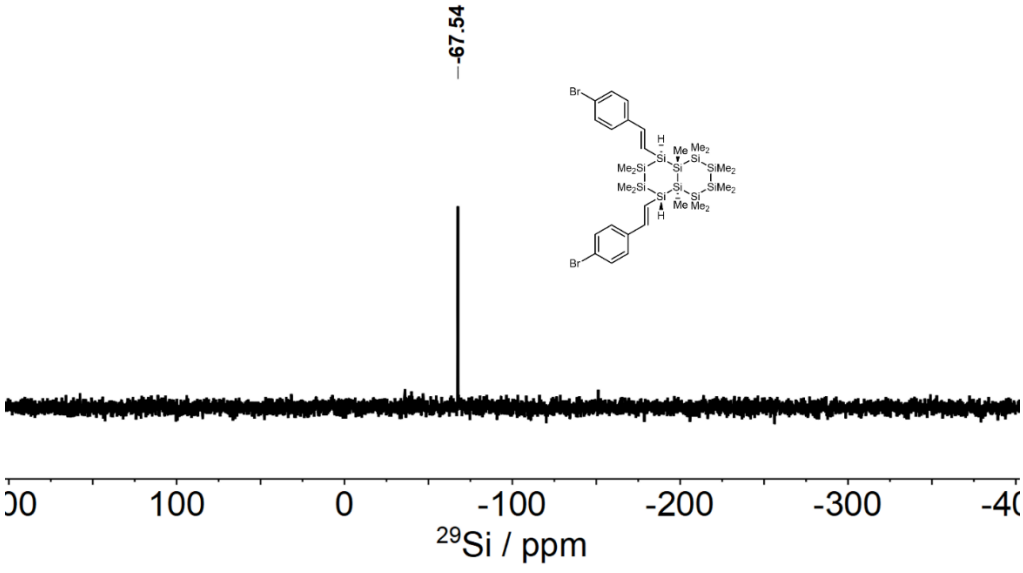

NMR Spectra of 4.1k

^{1}H NMR Spectrum (400 MHz, C_6D_6)

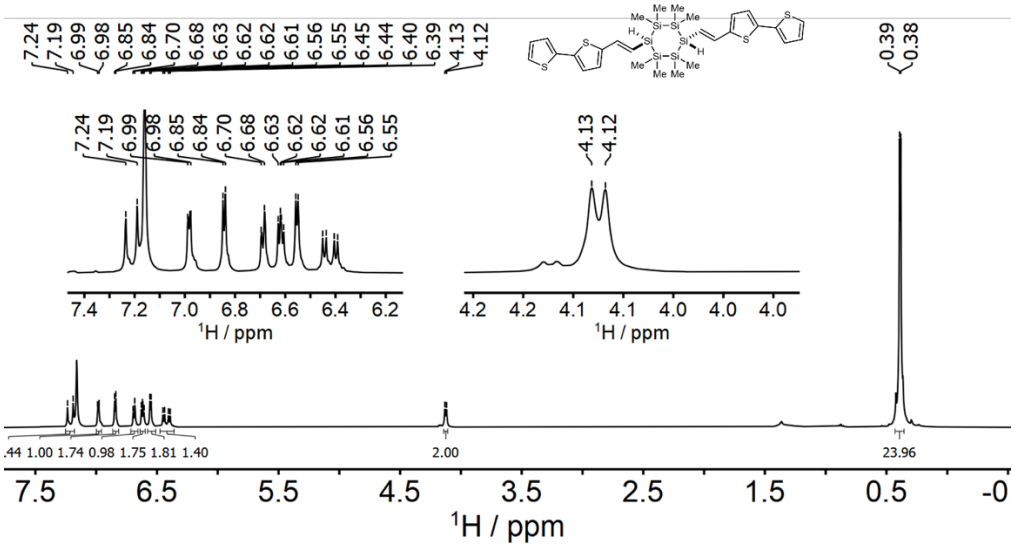

$^{13}C\{^{1}H\}$ NMR Spectrum (101 MHz, C_6D_6)

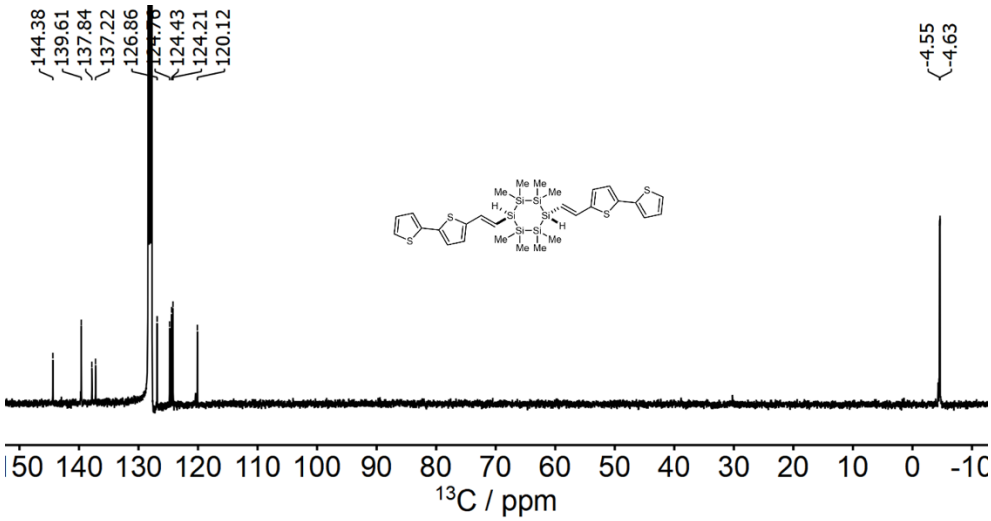

$^{29}Si\{^{1}H\}$ NMR Spectrum (79 MHz, C_6D_6). $^{1}J_{Si\text{-}H}$ = 7 Hz.

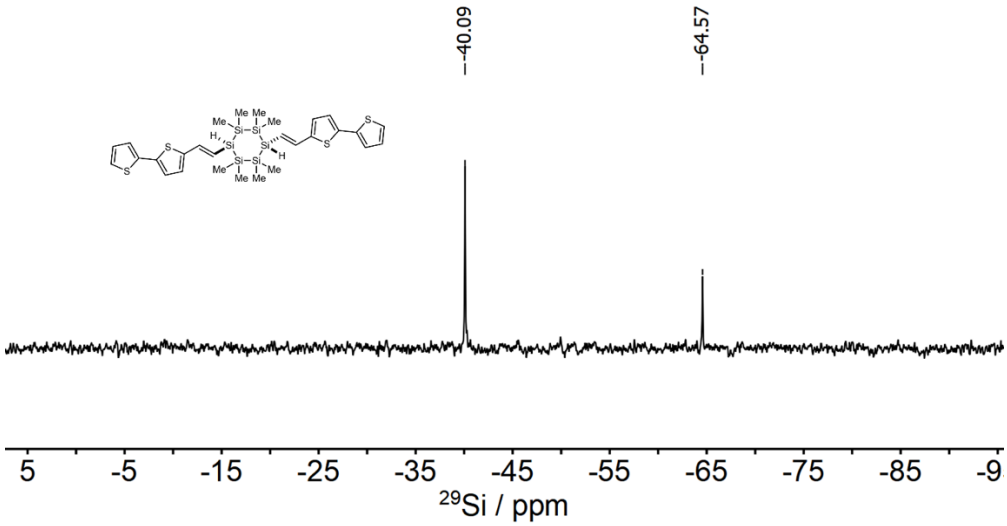

NMR Spectra of P4.1

^{1}H NMR Spectrum (400 MHz, $CDCl_3$)

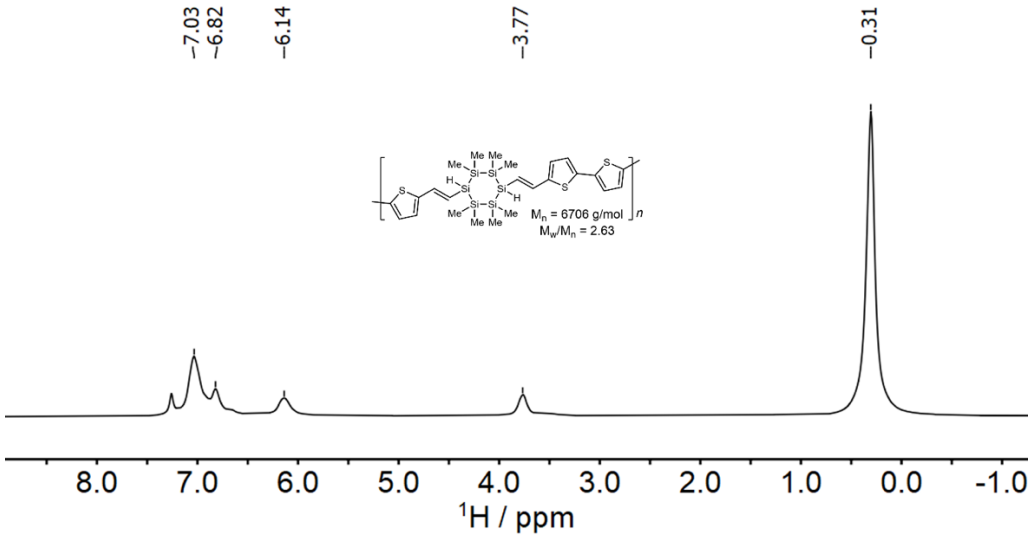

$^{13}C\{^{1}H\}$ NMR Spectrum (101 MHz, $CDCl_3$)

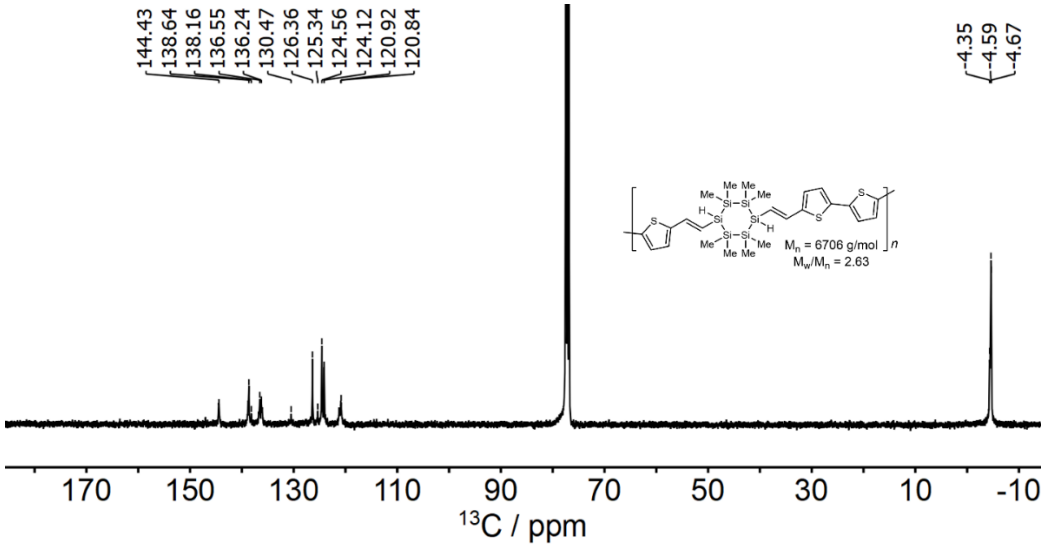

$^{29}Si\{^{1}H\}$ NMR Spectrum (79 MHz, $CDCl_3$). $^{1}J_{Si\text{-}H}$ = 120 Hz.

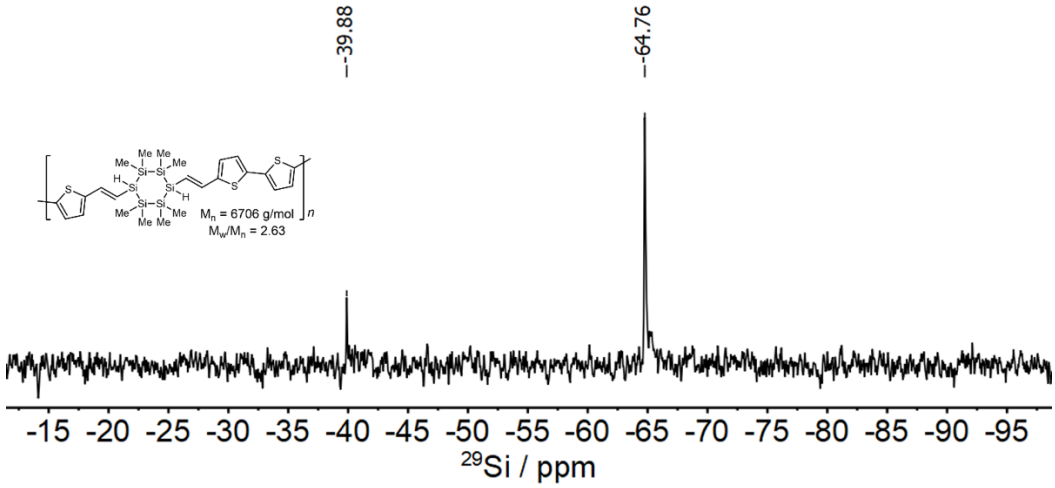

$^{1}H \rightarrow {}^{13}C$ CPMAS spectrum (126 MHz).

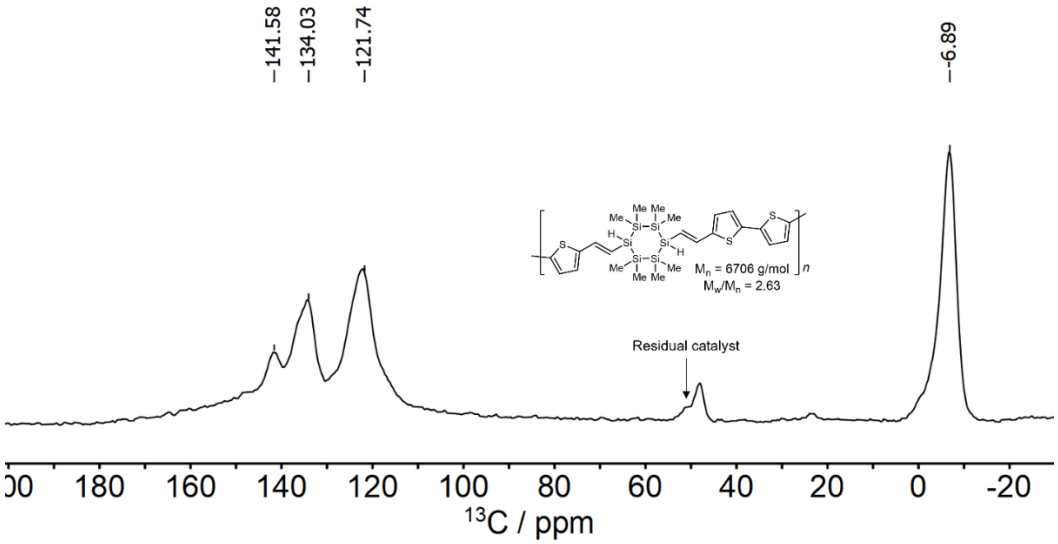

$^{1}H \rightarrow {}^{29}Si$ CPMAS spectrum (99 MHz).

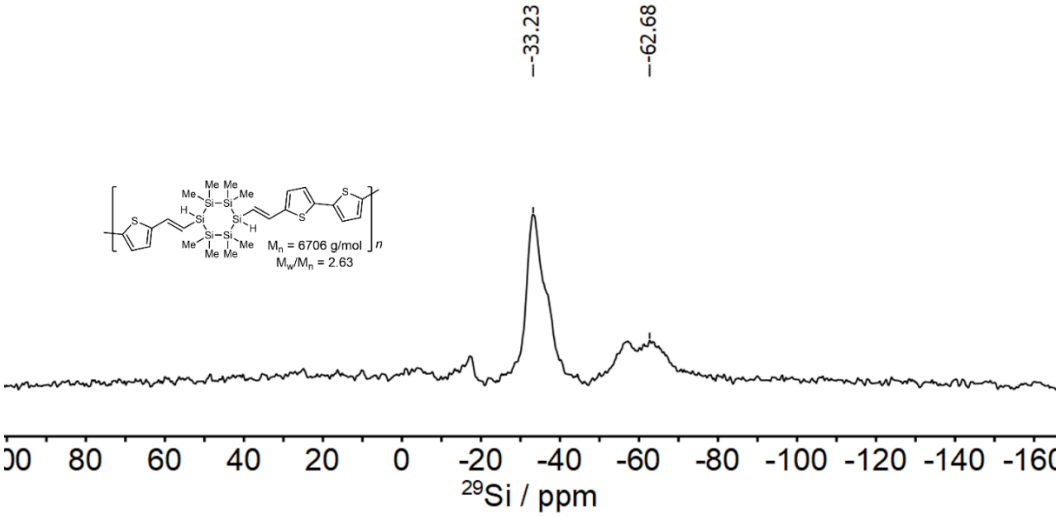

^{1}H NMR Spectrum of the quenched intermediate (400 MHz, C_6D_6).

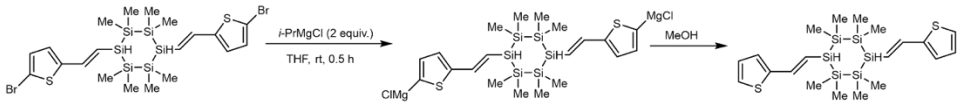

- 100 % conversion, clean NMR without purification

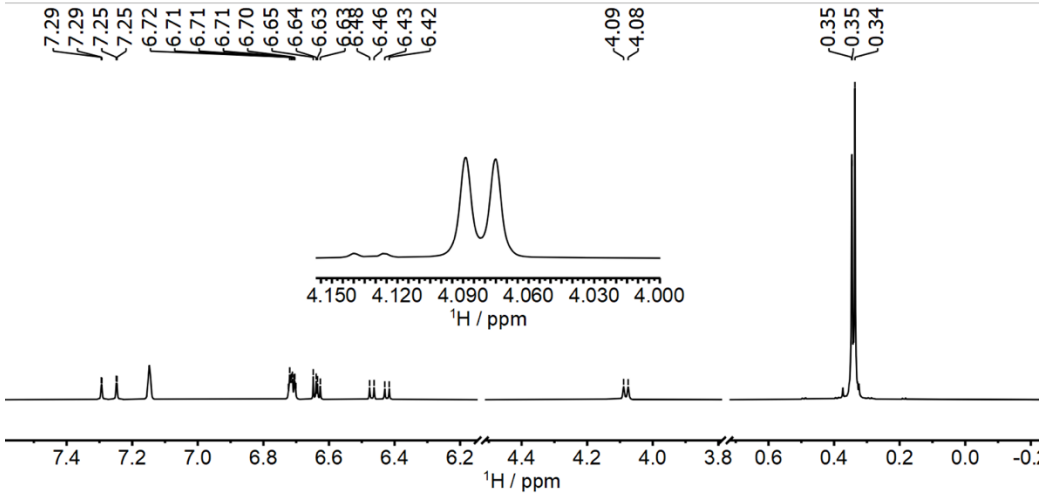

NMR Spectra of P4.2

^{1}H NMR Spectrum (400 MHz, $CDCl_3$)

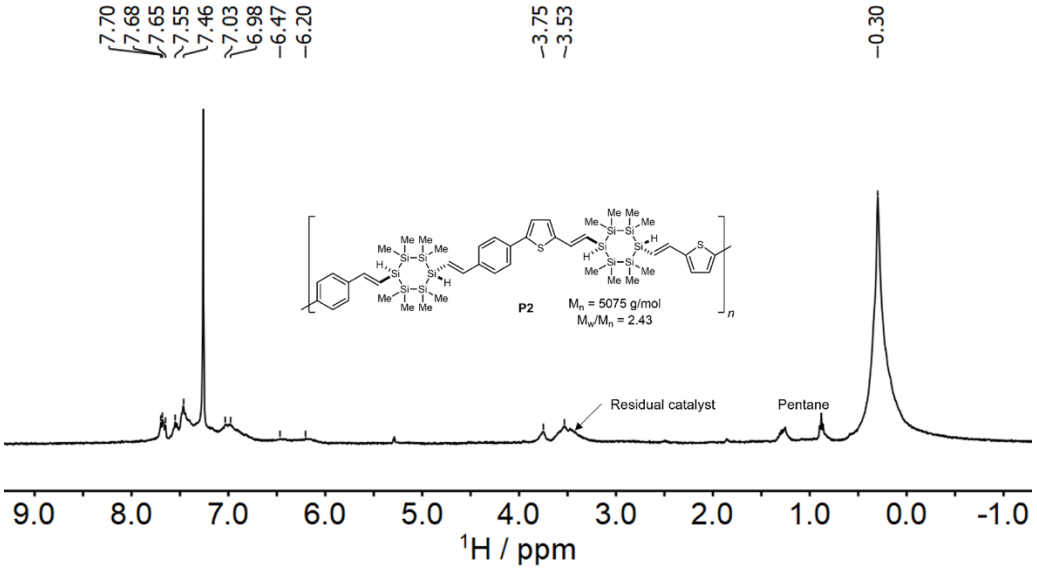

$^{1}H \rightarrow {}^{13}C$ CPMAS spectrum (126 MHz).

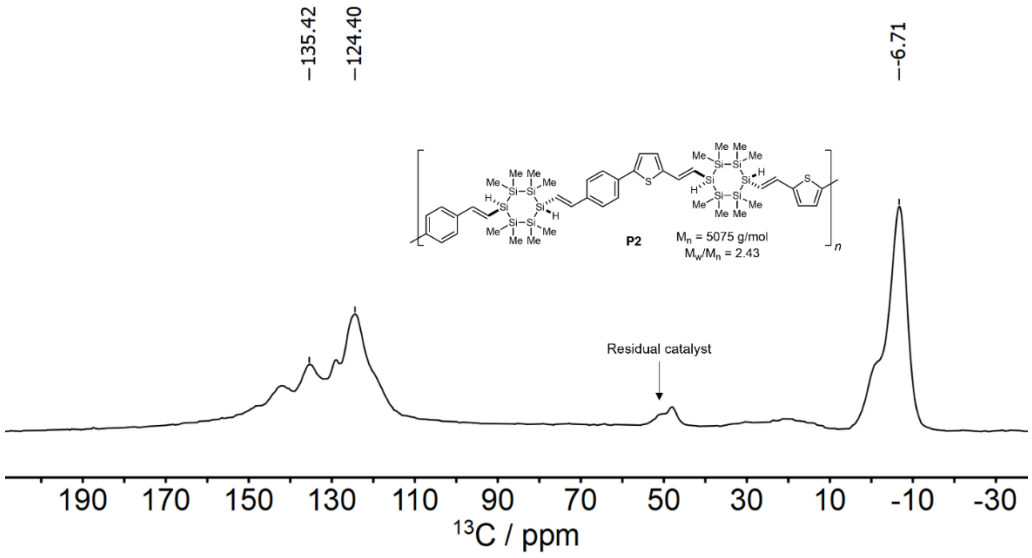

$^{1}H \rightarrow {}^{29}Si$ CPMAS spectrum (99 MHz).

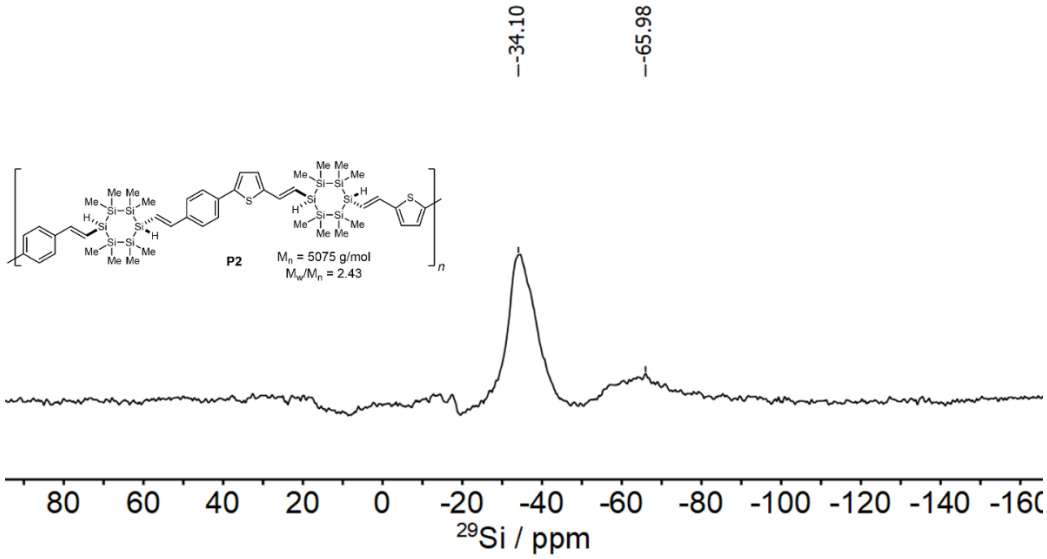

Single Crystal X-Ray Crystallography

All reflection intensities were measured either at 110(2) K for **4.1a**, **4.1e** and **4.1j** or at 173 K for **4.3a** using a SuperNova diffractometer (equipped with Atlas detector) either with Mo *K*α radiation (λ = 0.71073 Å) for **4.1a** and **4.1j** or with Cu *K*α radiation (λ = 1.54178 Å) for **4.1e** and **4.3a** under the program CrysAlisPro (Version CrysAlisPro 1.171.39.29c, Rigaku OD, 2017). The same program was used to refine the cell dimensions and for data reduction. The structure was solved with the program SHELXS-2018/3 (Sheldrick, 2018) and was refined on F^2 with SHELXL-2018/3 (Sheldrick, 2018). Numerical absorption correction based on gaussian integration over a multifaceted crystal model was applied using CrysAlisPro for **4.1a** and **4.1j**. Analytical numeric absorption correction using a multifaceted crystal was applied using CrysAlisPro for **4.1e** and **4.3a**. The temperature of the data collection was controlled using the system Cryojet (manufactured by Oxford Instruments). The H atoms were placed at calculated positions (unless otherwise specified) using the instructions AFIX 43 or AFIX 137 with isotropic displacement parameters having values 1.2 or 1.5 U_{eq} of the attached C atoms.

4.1a: The H atoms attached to Si1, Si4 and Si7 were found from difference Fourier maps, and their coordinates were refined freely. The structure is ordered. The asymmetric unit contains 1 + ½ crystallographically independent molecules. One of the two molecules is found at one site of inversion symmetry, and thus only one half is crystallographically independent.

4.1e/4.1j: The H atom attached to Si1 was found from difference Fourier map, and its coordinates were refined freely. The structure is ordered. The asymmetric unit contains ½ crystallographically independent molecule as it is found at one site of inversion symmetry.

4.3a: Some crystals were initially flashcooled from room temperature to 110 K, but these crystals cracked and the diffraction pattern was not of great quality. Another crystal was flashcooled from room temperature to 173 K, and the diffraction pattern was consistent with that of a single crystal. The H atoms attached to Si1, Si8, Si11 and Si18 were found from difference Fourier maps, and their coordinates were refined pseudofreely using the DFIX instruction in order to keep the Si–H within and acceptable range. The asymmetric unit contains two crystallographically independent molecules of the target compound. The C1A→C8A fragment is disordered over two orientations, and the occupancy factor of the major component of the disorder refines to 0.836(7).

Crystallographic data for 4.1a

	4.1a
Crystal data	
Chemical formula	$C_{24}H_{40}Si_6$
M_r	497.10
Crystal system, space group	Monoclinic, $P2_1/c$
Temperature (K)	110
a, b, c (Å)	36.3350 (8), 6.64881 (13), 18.7594 (4)
(°)	95.565 (2)
V (Å^3)	4510.62 (16)
Z	6
Radiation type	Mo K
(mm^{-1})	0.29

Crystal size (mm)	0.54 × 0.35 × 0.14
Data collection	
Diffractometer	SuperNova, Dual, Cu at zero, Atlas
Absorption correction	Gaussian *CrysAlis PRO* 1.171.39.46 (Rigaku Oxford Diffraction, 2018) Numerical absorption correction based on gaussian integration over a multifaceted crystal model Empirical absorption correction using spherical harmonics, implemented in SCALE3 ABSPACK scaling algorithm.
T_{min}, T_{max}	0.410, 1.000
No. of measured, independent and observed [$I >$ 2 (I)] reflections	44126, 10362, 8191
R_{int}	0.037
(sin /)$_{max}$ (Å^{-1})	0.650
Refinement	
$R[F^2 >$ 2 $(F^2)]$, $wR(F^2)$, S	0.040, 0.095, 1.09
No. of reflections	10362
No. of parameters	427
H-atom treatment	H atoms treated by a mixture of independent and constrained refinement
ρ_{max}, ρ_{min} (e Å^{-3})	0.53, -0.26

Crystallographic data for 4.1e

	4.1e
Crystal data	
Chemical formula	$C_{26}H_{44}O_2Si_6$
M_r	557.15
Crystal system, space group	Monoclinic, $P2_1/c$
Temperature (K)	110
a, b, c (Å)	10.3662 (5), 11.2796 (6), 14.0764 (7)
(°)	91.466 (4)
V (Å^3)	1645.37 (14)
Z	2

Radiation type	Cu *K*
(mm^{-1})	2.53
Crystal size (mm)	0.09 × 0.07 × 0.04
Data collection	
Diffractometer	SuperNova, Dual, Cu at zero, Atlas
Absorption correction	Analytical *CrysAlis PRO* 1.171.39.46 (Rigaku Oxford Diffraction, 2018) Analytical numeric absorption correction using a multifaceted crystal model based on expressions derived by R.C. Clark & J.S. Reid. (Clark, R. C. & Reid, J. S. (1995). Acta Cryst. A51, 887-897) Empirical absorption correction using spherical harmonics, implemented in SCALE3 ABSPACK scaling algorithm.
T_{min}, T_{max}	0.864, 0.917
No. of measured, independent and observed [$I >$ 2 (I)] reflections	9929, 2958, 2235
R_{int}	0.054
(sin /)$_{max}$ (Å^{-1})	0.598
Refinement	
$R[F^2 > 2$ (F^2)], $wR(F^2)$, S	0.051, 0.139, 1.04
No. of reflections	2958
No. of parameters	163
H-atom treatment	H atoms treated by a mixture of independent and constrained refinement
ρ_{max}, ρ_{min} (e Å^{-3})	0.92, -0.32

Crystallographic data for 4.1j

	4.1j
Crystal data	
Chemical formula	$C_{20}H_{34}Br_2S_2Si_6$
M_r	666.95
Crystal system, space group	Monoclinic, *C*2/*c*
Temperature (K)	110
a, *b*, *c* (Å)	22.2430 (8), 8.33206 (19), 18.2305 (6)

(°)	113.890 (4)
V (Å^3)	3089.19 (19)
Z	4
Radiation type	Mo K
(mm^{-1})	3.00
Crystal size (mm)	0.33 × 0.25 × 0.10
Data collection	
Diffractometer	SuperNova, Dual, Cu at zero, Atlas
Absorption correction	Gaussian *CrysAlis PRO* 1.171.41.93a (Rigaku Oxford Diffraction, 2020) Numerical absorption correction based on gaussian integration over a multifaceted crystal model Empirical absorption correction using spherical harmonics, implemented in SCALE3 ABSPACK scaling algorithm.
T_{min}, T_{max}	0.593, 1.000
No. of measured, independent and observed [$I >$ 2 (I)] reflections	22208, 3551, 3249
R_{int}	0.027
(sin /)$_{max}$ (Å^{-1})	0.650
Refinement	
$R[F^2 > 2$ (F^2)], $wR(F^2)$, S	0.020, 0.047, 1.02
No. of reflections	3551
No. of parameters	144
H-atom treatment	H atoms treated by a mixture of independent and constrained refinement
ρ_{max}, ρ_{min} (e Å^{-3})	0.53, -0.36

Crystallographic data for 4.3a

	4.3a
Crystal data	
Chemical formula	$C_{30}H_{58}Si_{10}$
M_r	699.66
Crystal system, space group	Triclinic, P-1

Temperature (K)	173
a, *b*, *c* (Å)	8.8909 (3), 13.8639 (4), 37.0010 (12)
, , (°)	86.116 (2), 83.625 (2), 81.600 (2)
V (Å^3)	4477.9 (2)
Z	4
Radiation type	Cu *K*
(mm^{-1})	2.90
Crystal size (mm)	0.27 × 0.16 × 0.06
Data collection	
Diffractometer	SuperNova, Dual, Cu at zero, Atlas
Absorption correction	Analytical *CrysAlis PRO* 1.171.41.93a (Rigaku Oxford Diffraction, 2020) Analytical numeric absorption correction using a multifaceted crystal model based on expressions derived by R.C. Clark & J.S. Reid. (Clark, R. C. & Reid, J. S. (1995). Acta Cryst. A51, 887-897) Empirical absorption correction using spherical harmonics, implemented in SCALE3 ABSPACK scaling algorithm.
T_{min}, T_{max}	0.555, 0.864
No. of measured, independent and observed [$I >$ 2 (I)] reflections	55290, 16062, 13297
R_{int}	0.046
(sin /)$_{max}$ (Å^{-1})	0.598
Refinement	
$R[F^2 > 2$ (F^2)], $wR(F^2)$, S	0.068, 0.193, 1.10
No. of reflections	16062
No. of parameters	834
No. of restraints	261
H-atom treatment	H atoms treated by a mixture of independent and constrained refinement
ρ_{max}, ρ_{min} (e Å^{-3})	0.86, -0.39

Computer programs: *CrysAlis PRO* 1.171.39.29c (Rigaku OD, 2017), *SHELXS2018*/3 (Sheldrick, 2018), *SHELXL2018*/3 (Sheldrick, 2018), *SHELXTL* v6.10 (Sheldrick, 2008).

References:

Sheldrick, G. M. (2015). Acta Cryst. C71, 3-8.

Computational methods

All DFT calculations were performed using the Gaussian 09 package.[5] Geometries were optimized using the B3LYP functional with the 6-31G(d) basis set starting from the crystal structure employing tight optimization parameters and an ultrafine integration grid. No symmetry restrictions were applied to geometry optimizations. Frequency calculations carried out at the same level of theory on fully optimized geometries showed no imaginary frequencies, confirming optimized geometries as local minima on their potential surfaces. Energy calculations carried out at the same level of theory and visualization of optimized geometries and molecular orbitals were performed using GaussView 5.0.9. Coordinates of the optimized structure can be found in the following reference: Jiang, Q.; Gittens, A. F.; Wong, S.; Siegler, M. A.; Klausen, R. S. *Chem. Sci.* **2022**, *13*, 7587–7593.

7.5 Conjugation in isomeric cyclosilane thioethers

The synthesis of cyclosilane thiolethers were investigated by Alex Gittens in the Klausen group. The full structural characterization has been performed and published in the following reference: Gittens, A. F.; Jiang, Q.; Siegler, M. A.; Klausen, R. S. *Organometallics* **2022**, 41, 23, 3762–3769.

All the DFT calculations are performed with the Gaussian 16 package.[6] Geometry optimizations and energy calculations were carried out using the B3LYP functional with the 6-311G(d) basis. No symmetry restrictions were applied to geometry optimization. Crystal structures were used as starting geometries on chair-**5.1a** and twist-**5.2a**. All optimized structures possess zero imaginary frequencies.TD-DFT calculations were caried out with the PBE0 function with the 6-311G(d) basis. Numbers of states were set as 50. Molecular orbitals were visualized in GaussView 5.0. with isovalue=0.02. Coordinates of optimized structures can be found in the following reference: Gittens, A. F.; Jiang, Q.; Siegler, M. A.; Klausen, R. S. *Organometallics* **2022**, 41, 23, 3762–3769.

TD-DFT Calculations

chair-**5.1a**

Excitation energies and oscillator strengths:

```
 Excited state symmetry could not be determined.
 Excited State   1:      Singlet-?Sym    4.6297 eV  267.80 nm  f=0.0000  <S**2>=0.000
    189 ->193        -0.15002
    190 ->194         0.18336
    190 ->195         0.16593
    192 ->193         0.61007
 This state for optimization and/or second-order correction.
 Total Energy, E(TD-HF/TD-DFT) =  -4573.24328628
 Copying the excited state density for this state as the 1-particle RhoCI density.
```

Excited state symmetry could not be determined.
Excited State 2: Singlet-?Sym 4.6387 eV 267.28 nm f=0.1807 <S**2>=0.000
189 ->194 -0.10119
189 ->195 -0.13403
190 ->193 0.40508
192 ->194 0.50638

Excited state symmetry could not be determined.
Excited State 3: Singlet-?Sym 4.7065 eV 263.43 nm f=0.0000 <S**2>=0.000
189 ->193 -0.33709
189 ->196 -0.11381
190 ->194 0.46188
191 ->194 -0.24323
191 ->195 -0.10752
192 ->193 -0.18380
192 ->196 0.10431

Excited state symmetry could not be determined.
Excited State 4: Singlet-?Sym 4.7172 eV 262.83 nm f=0.1426 <S**2>=0.000
190 ->193 0.10723
191 ->193 0.60404
191 ->196 -0.11541
192 ->195 0.24518

Excited state symmetry could not be determined.
Excited State 5: Singlet-?Sym 4.7384 eV 261.66 nm f=0.0000 <S**2>=0.000
189 ->193 -0.34014
189 ->196 0.17656
191 ->194 0.46723
191 ->195 -0.19589
192 ->193 -0.12929
192 ->196 0.15809

Excited state symmetry could not be determined.
Excited State 6: Singlet-?Sym 4.7864 eV 259.03 nm f=0.1311 <S**2>=0.000
189 ->194 0.55263
190 ->193 -0.15943
190 ->196 -0.14829
191 ->196 0.19314
192 ->194 0.23557

Excited state symmetry could not be determined.
Excited State 7: Singlet-?Sym 4.8158 eV 257.45 nm f=0.0659 <S**2>=0.000
189 ->194 0.23587
189 ->195 -0.13604

190 ->193 0.44244
190 ->196 -0.17037
191 ->193 -0.13385
192 ->194 -0.34635
192 ->195 0.11287

Excited state symmetry could not be determined.
Excited State 8: Singlet-?Sym 4.8626 eV 254.98 nm f=0.0000 <S**2>=0.000
189 ->193 0.37582
189 ->197 -0.10369
190 ->194 0.35854
190 ->198 0.10033
191 ->194 0.32361
192 ->196 0.21050

Excited state symmetry could not be determined.
Excited State 9: Singlet-?Sym 5.0541 eV 245.31 nm f=0.0000 <S**2>=0.000
183 ->194 0.10019
188 ->194 -0.16613
189 ->193 0.14172
189 ->196 0.20744
189 ->201 0.10107
190 ->194 0.11351
190 ->198 -0.17647
190 ->202 0.13812
191 ->195 -0.12265
191 ->199 -0.23950
192 ->197 -0.16593
192 ->200 0.31748

Excited state symmetry could not be determined.
Excited State 10: Singlet-?Sym 5.0542 eV 245.31 nm f=0.0140 <S**2>=0.000
183 ->196 0.13097
184 ->194 0.10544
188 ->193 0.13736
189 ->195 -0.15627
189 ->198 0.16108
189 ->199 -0.18419
190 ->197 -0.12077
191 ->193 0.11739
191 ->196 0.14322
191 ->200 0.31495
192 ->198 -0.11509
192 ->199 -0.28664

Excited state symmetry could not be determined.

Excited State 11: Singlet-?Sym 5.0561 eV 245.22 nm f=0.0000 <S**2>=0.000
187 ->193 0.10358
188 ->194 -0.11402
189 ->193 -0.10775
189 ->200 -0.24320
190 ->198 -0.10885
191 ->195 0.24337
191 ->198 -0.14267
191 ->199 0.21271
192 ->193 -0.16123
192 ->196 -0.22521
192 ->197 -0.13761
192 ->201 -0.18036

Excited state symmetry could not be determined.
Excited State 12: Singlet-?Sym 5.0675 eV 244.66 nm f=0.0329 <S**2>=0.000
189 ->195 0.13630
189 ->198 0.11765
189 ->199 0.14826
190 ->193 -0.13006
190 ->197 -0.15205
190 ->200 0.17633
190 ->201 -0.10989
191 ->193 -0.20543
191 ->196 -0.18487
191 ->201 -0.17974
192 ->194 0.12897
192 ->195 0.29012
192 ->198 -0.22996
192 ->202 0.11388

Excited state symmetry could not be determined.
Excited State 13: Singlet-?Sym 5.1044 eV 242.90 nm f=0.0000 <S**2>=0.000
186 ->194 0.13220
188 ->194 0.18353
189 ->196 -0.24549
189 ->197 0.28364
190 ->198 -0.16015
190 ->199 -0.12216
191 ->194 0.13797
191 ->195 0.24357
191 ->198 0.19275
191 ->199 -0.10686
191 ->202 0.13502
192 ->200 0.14890
192 ->201 -0.10558

Excited state symmetry could not be determined.
Excited State 14: Singlet-?Sym 5.1272 eV 241.82 nm f=0.0692 <S**2>=0.000
189 ->194 0.17758
189 ->195 0.23194
189 ->198 0.19787
189 ->202 0.13754
190 ->201 0.10117
191 ->196 -0.16204
191 ->197 0.36908
191 ->200 0.10031
192 ->198 0.24427

Excited state symmetry could not be determined.
Excited State 15: Singlet-?Sym 5.1565 eV 240.44 nm f=0.0483 <S**2>=0.000
188 ->193 0.20878
189 ->195 -0.21235
190 ->193 -0.13855
190 ->196 0.11157
190 ->197 0.26711
190 ->201 -0.10537
192 ->195 0.41203
192 ->198 0.19771

Excited state symmetry could not be determined.
Excited State 16: Singlet-?Sym 5.1636 eV 240.11 nm f=0.0000 <S**2>=0.000
186 ->194 0.10069
188 ->194 0.21403
189 ->196 -0.10193
189 ->197 -0.18045
189 ->200 -0.10472
189 ->201 0.10669
190 ->194 -0.10914
190 ->195 0.20792
190 ->199 -0.19823
191 ->194 -0.16895
191 ->198 -0.15155
192 ->196 0.34682
192 ->201 -0.18740

Excited state symmetry could not be determined.
Excited State 17: Singlet-?Sym 5.1900 eV 238.89 nm f=0.0000 <S**2>=0.000
187 ->193 0.10182
189 ->197 -0.12790
190 ->195 0.31028
190 ->198 0.14929

192 ->196 -0.18649
192 ->197 0.39697
192 ->200 0.17657
192 ->203 -0.16812

Excited state symmetry could not be determined.
Excited State 18: Singlet-?Sym 5.2279 eV 237.16 nm f=0.0721 <S**2>=0.000
188 ->193 -0.16387
189 ->194 0.15456
189 ->199 0.22107
190 ->196 0.40031
190 ->200 0.17113
192 ->195 -0.19275
192 ->199 -0.27898

Excited state symmetry could not be determined.
Excited State 19: Singlet-?Sym 5.2684 eV 235.34 nm f=0.0000 <S**2>=0.000
186 ->194 -0.17885
188 ->194 -0.34202
189 ->196 0.11359
189 ->200 -0.10612
190 ->194 -0.14924
190 ->195 -0.12574
191 ->195 0.19973
192 ->196 0.36610
192 ->197 0.17897

Excited state symmetry could not be determined.
Excited State 20: Singlet-?Sym 5.2723 eV 235.16 nm f=0.0142 <S**2>=0.000
186 ->193 0.15178
188 ->193 0.48088
189 ->198 0.15766
189 ->199 0.12143
190 ->196 0.13064
190 ->197 -0.13328
191 ->196 -0.14849
191 ->200 -0.13284
192 ->195 -0.20906
192 ->199 0.13600

Excited state symmetry could not be determined.
Excited State 21: Singlet-?Sym 5.3086 eV 233.55 nm f=0.0000 <S**2>=0.000
189 ->196 -0.17555
189 ->200 -0.22818
190 ->195 -0.24992
190 ->199 -0.20074

190 ->204 0.10276
191 ->195 -0.19882
191 ->199 0.12980
192 ->200 0.24452
192 ->201 0.29795
192 ->203 -0.17552

Excited state symmetry could not be determined.
Excited State 22: Singlet-?Sym 5.3121 eV 233.40 nm f=0.0624 <S**2>=0.000
189 ->194 -0.15064
189 ->198 0.13134
189 ->199 0.21285
190 ->196 -0.22182
190 ->200 0.28852
190 ->203 -0.12511
191 ->196 0.23194
191 ->197 0.20509
191 ->200 -0.18946
192 ->198 0.16027

Excited state symmetry could not be determined.
Excited State 23: Singlet-?Sym 5.3173 eV 233.17 nm f=0.0000 <S**2>=0.000
189 ->193 0.15737
189 ->197 0.27772
189 ->200 -0.16253
190 ->195 0.22215
190 ->198 -0.25243
191 ->195 -0.21461
191 ->198 0.27038
191 ->199 0.18001
192 ->200 -0.13479

Excited state symmetry could not be determined.
Excited State 24: Singlet-?Sym 5.3250 eV 232.84 nm f=0.0646 <S**2>=0.000
187 ->194 0.26664
189 ->195 0.12694
189 ->198 0.10942
190 ->196 0.16925
190 ->197 -0.18300
190 ->200 -0.12154
191 ->196 0.42199
191 ->197 0.13637
191 ->200 -0.10693
191 ->201 -0.10194
192 ->195 0.13569
192 ->202 -0.11527

Excited state symmetry could not be determined.
Excited State 25: Singlet-?Sym 5.3274 eV 232.73 nm f=0.0000 <S**2>=0.000
187 ->193 0.50760
188 ->195 -0.14460
189 ->200 0.12029
190 ->199 0.13018
191 ->195 0.12386
191 ->199 -0.10930
192 ->196 0.15131
192 ->197 -0.14624
192 ->201 0.17740

Excited state symmetry could not be determined.
Excited State 26: Singlet-?Sym 5.3666 eV 231.03 nm f=0.0000 <S**2>=0.000
185 ->193 -0.18523
187 ->193 -0.17847
188 ->194 0.28787
189 ->196 0.33116
189 ->201 -0.15016
190 ->205 -0.10543
191 ->195 0.24456
192 ->201 0.10413
192 ->203 -0.14676

Excited state symmetry could not be determined.
Excited State 27: Singlet-?Sym 5.3694 eV 230.91 nm f=0.0679 <S**2>=0.000
188 ->193 0.28225
189 ->195 0.39394
189 ->198 -0.20181
190 ->197 0.13410
190 ->201 0.25198
191 ->196 0.11274
191 ->201 -0.13256
192 ->199 -0.14187

Excited state symmetry could not be determined.
Excited State 28: Singlet-?Sym 5.3938 eV 229.87 nm f=0.1160 <S**2>=0.000
185 ->194 0.24760
187 ->194 0.46664
188 ->196 -0.13011
190 ->201 0.10596
190 ->203 -0.12630
191 ->196 -0.14571
191 ->203 -0.10837
192 ->202 0.11469

Excited state symmetry could not be determined.
Excited State 29: Singlet-?Sym 5.4014 eV 229.54 nm f=0.0000 <S**2>=0.000
185 ->193 -0.15908
187 ->193 -0.25929
188 ->194 -0.14041
189 ->196 -0.22509
189 ->200 0.13861
190 ->195 0.29484
190 ->199 0.13936
191 ->195 0.13561
192 ->193 -0.11358
192 ->196 0.12520
192 ->197 -0.21231
192 ->201 0.20647

Excited state symmetry could not be determined.
Excited State 30: Singlet-?Sym 5.4343 eV 228.15 nm f=0.0004 <S**2>=0.000
185 ->194 0.13070
190 ->193 0.10651
190 ->196 -0.11947
190 ->197 0.13350
190 ->200 -0.12133
190 ->201 -0.18580
190 ->203 0.14230
191 ->201 -0.23440
191 ->203 0.11068
192 ->195 -0.10042
192 ->198 0.25925
192 ->202 0.13624
192 ->205 0.21709

Excited state symmetry could not be determined.
Excited State 31: Singlet-?Sym 5.4563 eV 227.23 nm f=0.0970 <S**2>=0.000
181 ->194 0.12409
185 ->194 -0.32044
186 ->193 0.40081
187 ->194 0.14310
187 ->195 0.14993
188 ->196 0.11482
190 ->196 -0.13961
191 ->200 0.11951
192 ->202 0.12727

Excited state symmetry could not be determined.
Excited State 32: Singlet-?Sym 5.4733 eV 226.52 nm f=0.0053 <S**2>=0.000

188 ->193 0.11145
189 ->195 0.17650
189 ->199 0.18823
189 ->205 -0.18345
189 ->207 0.11748
190 ->196 -0.19488
190 ->201 -0.26285
190 ->203 0.15750
191 ->193 -0.10046
191 ->201 0.29954
191 ->203 -0.19193
191 ->208 0.10933
192 ->202 -0.10393

Excited state symmetry could not be determined.
Excited State 33: Singlet-?Sym 5.4801 eV 226.25 nm f=0.0000 <S**2>=0.000
187 ->200 0.12501
189 ->196 0.19261
189 ->201 0.30201
189 ->203 -0.10013
190 ->199 -0.23677
191 ->195 0.15643
191 ->199 0.13489
191 ->204 -0.14437
191 ->205 -0.16186
192 ->197 -0.13924
192 ->201 0.13265

Excited state symmetry could not be determined.
Excited State 34: Singlet-?Sym 5.4869 eV 225.96 nm f=0.0000 <S**2>=0.000
181 ->193 -0.11939
185 ->193 0.47894
186 ->194 -0.12149
186 ->195 -0.19942
187 ->193 -0.16968
188 ->194 0.13264
188 ->195 -0.10462
189 ->201 -0.16865
189 ->203 0.10788
190 ->195 0.15899

Excited state symmetry could not be determined.
Excited State 35: Singlet-?Sym 5.5234 eV 224.47 nm f=0.0000 <S**2>=0.000
185 ->193 -0.17002
186 ->194 0.11646
187 ->200 0.10936

188 ->194 -0.15438
189 ->200 -0.12614
189 ->201 -0.18347
189 ->203 0.22936
190 ->199 -0.12530
191 ->195 0.10616
191 ->198 0.17728
191 ->199 -0.17563
191 ->207 -0.12977
192 ->197 -0.21915
192 ->203 0.22347

Excited state symmetry could not be determined.
Excited State 36: Singlet-?Sym 5.5258 eV 224.37 nm f=0.0070 <S**2>=0.000
185 ->194 0.20532
186 ->193 0.16746
186 ->196 -0.15046
187 ->194 -0.22368
190 ->196 0.18052
190 ->197 -0.20009
191 ->196 0.10046
191 ->197 -0.13903
191 ->201 0.12113
191 ->203 -0.11690
192 ->198 0.22062
192 ->202 0.27793

Excited state symmetry could not be determined.
Excited State 37: Singlet-?Sym 5.5304 eV 224.19 nm f=0.0126 <S**2>=0.000
185 ->194 -0.24540
186 ->193 -0.12209
187 ->198 0.10609
190 ->200 0.12896
191 ->196 0.10786
192 ->199 0.31149
192 ->202 0.27359
192 ->204 -0.13073

Excited state symmetry could not be determined.
Excited State 38: Singlet-?Sym 5.5448 eV 223.60 nm f=0.0105 <S**2>=0.000
185 ->194 0.12772
187 ->194 -0.17328
190 ->196 0.11277
190 ->197 0.19450
191 ->197 0.31003
191 ->200 0.15698

191 ->201 -0.10152
191 ->203 -0.24622
192 ->198 -0.21053
192 ->199 0.17461

Excited state symmetry could not be determined.
Excited State 39: Singlet-?Sym 5.5632 eV 222.86 nm f=0.0000 <S**2>=0.000
182 ->194 -0.10664
184 ->193 0.12897
186 ->194 0.34656
186 ->195 -0.11409
187 ->196 0.15147
187 ->197 0.11985
188 ->194 -0.12066
188 ->198 -0.14841
189 ->197 0.10665
190 ->198 0.20979
191 ->199 0.11918
191 ->204 -0.11686
192 ->200 -0.10076
192 ->201 0.12827

Excited state symmetry could not be determined.
Excited State 40: Singlet-?Sym 5.5735 eV 222.45 nm f=0.0732 <S**2>=0.000
181 ->194 -0.10158
185 ->194 0.17300
186 ->193 0.30579
187 ->199 -0.10019
188 ->200 -0.11781
189 ->195 0.11082
189 ->198 0.10699
190 ->197 0.22647
190 ->200 0.17182
191 ->203 0.20319
192 ->198 -0.15852
192 ->199 0.12116
192 ->204 -0.14910

Excited state symmetry could not be determined.
Excited State 41: Singlet-?Sym 5.5932 eV 221.67 nm f=0.0000 <S**2>=0.000
186 ->194 -0.16609
188 ->195 -0.12974
189 ->201 -0.11747
189 ->203 -0.20476
190 ->198 0.31358
190 ->204 -0.10961

191 ->198 0.12469
191 ->202 0.22490
192 ->200 0.22456
192 ->203 0.17840

Excited state symmetry could not be determined.
Excited State 42: Singlet-?Sym 5.5982 eV 221.47 nm f=0.0000 <S**2>=0.000
180 ->193 -0.14619
183 ->194 -0.10405
185 ->193 0.11846
186 ->194 0.23818
188 ->195 -0.11927
189 ->196 0.17660
189 ->200 0.13040
190 ->202 -0.20761
191 ->198 0.18818
191 ->204 0.10834
192 ->197 -0.14645
192 ->201 -0.10584
192 ->203 -0.15080
192 ->206 0.14140

Excited state symmetry could not be determined.
Excited State 43: Singlet-?Sym 5.6140 eV 220.85 nm f=0.0000 <S**2>=0.000
186 ->194 -0.18853
188 ->195 0.19322
189 ->197 -0.26004
189 ->203 0.12448
189 ->206 -0.10951
190 ->198 -0.11322
190 ->202 -0.17726
191 ->198 0.16040
191 ->202 0.33884
192 ->200 -0.10191
192 ->203 -0.11597

Excited state symmetry could not be determined.
Excited State 44: Singlet-?Sym 5.6160 eV 220.77 nm f=0.0080 <S**2>=0.000
189 ->195 0.12993
189 ->198 0.39171
190 ->197 0.15926
190 ->201 -0.13849
190 ->203 -0.21022
191 ->197 -0.25212
192 ->198 0.13102
192 ->204 0.14250

Excited state symmetry could not be determined.
Excited State 45: Singlet-?Sym 5.6199 eV 220.62 nm f=0.0000 <S**2>=0.000
188 ->199 -0.10531
189 ->197 -0.19409
189 ->200 -0.10884
189 ->201 0.17201
189 ->206 0.14174
190 ->199 0.18679
190 ->202 0.28715
191 ->198 0.38149
191 ->202 -0.16086

Excited state symmetry could not be determined.
Excited State 46: Singlet-?Sym 5.6258 eV 220.38 nm f=0.0000 <S**2>=0.000
186 ->194 0.14306
188 ->194 -0.10912
189 ->197 -0.17789
190 ->198 -0.28247
190 ->202 -0.17391
190 ->204 -0.12702
192 ->197 0.17683
192 ->200 0.19191
192 ->201 0.20342
192 ->203 0.32785

Excited state symmetry could not be determined.
Excited State 47: Singlet-?Sym 5.6361 eV 219.98 nm f=0.0039 <S**2>=0.000
185 ->194 0.15467
188 ->196 0.12656
189 ->194 -0.10645
189 ->199 0.16970
189 ->202 0.44259
190 ->201 0.18405
190 ->203 0.16151
190 ->206 0.12983
191 ->197 -0.17128
191 ->206 -0.14854

Excited state symmetry could not be determined.
Excited State 48: Singlet-?Sym 5.6655 eV 218.84 nm f=0.0116 <S**2>=0.000
181 ->194 -0.10022
182 ->193 0.14588
186 ->193 -0.18404
187 ->198 -0.10950
188 ->197 0.13265

189 ->202 0.13508
190 ->201 -0.18294
192 ->198 -0.18489
192 ->202 0.39545
192 ->204 0.16341

Excited state symmetry could not be determined.
Excited State 49: Singlet-?Sym 5.6723 eV 218.58 nm f=0.0000 <S**2>=0.000
182 ->194 0.11243
187 ->200 0.14277
188 ->199 0.13905
189 ->200 0.13146
189 ->201 -0.11600
190 ->199 0.16510
190 ->202 0.14262
191 ->199 0.29733
191 ->204 -0.12820
192 ->200 0.22500
192 ->201 -0.29354

Excited state symmetry could not be determined.
Excited State 50: Singlet-?Sym 5.6800 eV 218.28 nm f=0.0105 <S**2>=0.000
187 ->199 -0.11095
190 ->197 -0.17527
190 ->200 0.17346
190 ->201 -0.17987
191 ->200 0.32629
191 ->201 -0.26947
192 ->198 0.11128
192 ->199 0.27244
192 ->202 -0.13970
192 ->205 0.11300

twist-**5.1a**

Excitation energies and oscillator strengths:

Excited state symmetry could not be determined.
Excited State 1: Singlet-?Sym 4.5701 eV 271.29 nm f=0.0025 <S**2>=0.000
190 ->196 -0.16844
191 ->196 0.11458
192 ->193 0.63935
This state for optimization and/or second-order correction.
Total Energy, E(TD-HF/TD-DFT) = -4573.24184517
Copying the excited state density for this state as the 1-particle RhoCI density.

Excited state symmetry could not be determined.
Excited State 2: Singlet-?Sym 4.6141 eV 268.71 nm f=0.1366 <S**2>=0.000
190 ->193 0.49509
190 ->194 -0.21199
191 ->193 -0.28916
191 ->194 -0.14886
192 ->196 -0.24073

Excited state symmetry could not be determined.
Excited State 3: Singlet-?Sym 4.6247 eV 268.09 nm f=0.0299 <S**2>=0.000
191 ->195 -0.16396
192 ->194 0.64745

Excited state symmetry could not be determined.
Excited State 4: Singlet-?Sym 4.6554 eV 266.32 nm f=0.0969 <S**2>=0.000
189 ->195 -0.14154
190 ->193 0.17843
190 ->194 0.36211
191 ->193 -0.15024
191 ->194 0.49940

Excited state symmetry could not be determined.
Excited State 5: Singlet-?Sym 4.6688 eV 265.56 nm f=0.0111 <S**2>=0.000
189 ->196 0.10088
190 ->193 0.33614
190 ->194 0.30326
191 ->193 0.41609
191 ->194 -0.20295
192 ->195 0.18629

Excited state symmetry could not be determined.
Excited State 6: Singlet-?Sym 4.7757 eV 259.61 nm f=0.0979 <S**2>=0.000
190 ->193 0.14748
190 ->194 -0.36551
190 ->197 0.10612
191 ->193 0.39433
191 ->194 0.31190
192 ->195 -0.17589

Excited state symmetry could not be determined.
Excited State 7: Singlet-?Sym 4.8072 eV 257.91 nm f=0.0175 <S**2>=0.000
189 ->193 0.17082
189 ->194 0.50108
190 ->195 -0.28438
190 ->196 0.15888

191 ->195 -0.20918
191 ->196 0.12052

Excited state symmetry could not be determined.
Excited State 8: Singlet-?Sym 4.8526 eV 255.50 nm f=0.0090 <S**2>=0.000
189 ->193 0.56304
189 ->194 -0.13689
190 ->195 0.11969
190 ->196 0.17805
191 ->195 0.12726
191 ->200 0.10831
192 ->193 0.14833
192 ->194 0.10449

Excited state symmetry could not be determined.
Excited State 9: Singlet-?Sym 5.0108 eV 247.44 nm f=0.0056 <S**2>=0.000
182 ->193 0.10658
188 ->194 0.15036
190 ->194 -0.13476
190 ->197 -0.18048
190 ->198 0.12847
190 ->201 0.16559
191 ->194 0.12799
191 ->195 -0.11416
191 ->201 -0.11415
192 ->195 0.15551
192 ->196 0.19457
192 ->197 -0.15041
192 ->198 0.21435
192 ->200 -0.17723
192 ->201 0.14315

Excited state symmetry could not be determined.
Excited State 10: Singlet-?Sym 5.0135 eV 247.30 nm f=0.0026 <S**2>=0.000
182 ->196 0.12460
189 ->197 -0.10111
190 ->196 -0.13113
190 ->197 -0.10663
190 ->198 -0.21684
190 ->200 0.14823
190 ->201 0.10243
191 ->195 0.18932
192 ->194 0.12347
192 ->196 0.11130
192 ->197 0.24074
192 ->198 0.13249

192 ->199 -0.11798
192 ->200 -0.10753
192 ->201 -0.23592

Excited state symmetry could not be determined.
Excited State 11: Singlet-?Sym 5.0693 eV 244.58 nm f=0.0162 <S**2>=0.000
187 ->194 0.12172
189 ->194 0.32136
189 ->199 0.16337
189 ->201 -0.11364
190 ->195 0.13230
191 ->195 0.36030
191 ->196 -0.12367
191 ->200 0.21662
192 ->197 -0.13809
192 ->199 0.14345

Excited state symmetry could not be determined.
Excited State 12: Singlet-?Sym 5.0820 eV 243.97 nm f=0.0508 <S**2>=0.000
183 ->195 0.10031
189 ->195 0.16214
189 ->200 0.16073
191 ->194 0.13171
191 ->199 0.32793
192 ->195 0.35782
192 ->196 -0.16823
192 ->200 0.17880

Excited state symmetry could not be determined.
Excited State 13: Singlet-?Sym 5.0901 eV 243.58 nm f=0.0088 <S**2>=0.000
184 ->195 -0.10448
187 ->193 -0.20218
189 ->193 -0.13472
189 ->194 -0.16012
189 ->197 0.17122
189 ->199 0.12051
190 ->195 -0.14616
190 ->198 0.20157
191 ->196 0.22108
191 ->198 0.27890
191 ->200 0.20885

Excited state symmetry could not be determined.
Excited State 14: Singlet-?Sym 5.0980 eV 243.20 nm f=0.0909 <S**2>=0.000
186 ->194 -0.10916
188 ->194 0.18146

189 ->195 -0.17122
189 ->196 0.15041
189 ->198 0.13729
190 ->193 -0.10737
190 ->197 0.22620
190 ->199 -0.18068
190 ->201 0.12599
191 ->197 0.37028
191 ->201 0.11415
192 ->196 -0.18404
192 ->198 0.16006

Excited state symmetry could not be determined.
Excited State 15: Singlet-?Sym 5.1161 eV 242.34 nm f=0.1121 <S**2>=0.000
188 ->194 -0.11382
189 ->198 0.19576
189 ->200 0.10659
190 ->193 0.10152
190 ->197 0.29263
190 ->199 0.20484
191 ->193 -0.16784
191 ->197 0.15362
191 ->202 -0.11326
192 ->196 0.39340

Excited state symmetry could not be determined.
Excited State 16: Singlet-?Sym 5.1412 eV 241.16 nm f=0.0015 <S**2>=0.000
185 ->193 -0.11189
189 ->193 -0.16794
189 ->199 -0.15050
190 ->196 0.38391
190 ->198 -0.21523
190 ->200 -0.14847
191 ->196 -0.11527
192 ->193 0.10786
192 ->197 0.19481
192 ->199 0.27218
192 ->202 0.10145

Excited state symmetry could not be determined.
Excited State 17: Singlet-?Sym 5.1601 eV 240.27 nm f=0.0289 <S**2>=0.000
188 ->193 -0.16475
189 ->200 -0.14558
190 ->197 0.20311
190 ->199 -0.11697
191 ->199 -0.20544

192 ->195 0.44024
192 ->198 -0.24992

Excited state symmetry could not be determined.
Excited State 18: Singlet-?Sym 5.2060 eV 238.16 nm f=0.0265 <S**2>=0.000
186 ->193 -0.12144
186 ->194 -0.18256
188 ->193 0.21649
188 ->194 0.37820
190 ->194 0.13729
190 ->199 0.19989
190 ->205 0.10190
192 ->198 -0.22435
192 ->200 -0.17233

Excited state symmetry could not be determined.
Excited State 19: Singlet-?Sym 5.2102 eV 237.97 nm f=0.0011 <S**2>=0.000
185 ->193 -0.11066
187 ->193 -0.13011
189 ->199 -0.15770
190 ->196 0.23138
190 ->198 0.10685
191 ->195 0.25931
191 ->196 0.28989
191 ->200 -0.21848
192 ->197 -0.25007
192 ->199 -0.18203

Excited state symmetry could not be determined.
Excited State 20: Singlet-?Sym 5.2288 eV 237.12 nm f=0.0524 <S**2>=0.000
189 ->194 0.14549
190 ->195 0.49383
191 ->196 0.26403
191 ->198 0.11074
192 ->197 0.24956
192 ->199 -0.10010
192 ->201 0.17691

Excited state symmetry could not be determined.
Excited State 21: Singlet-?Sym 5.2539 eV 235.98 nm f=0.0058 <S**2>=0.000
185 ->193 0.14808
187 ->193 0.51912
188 ->196 -0.10202
189 ->193 -0.14753
190 ->198 0.14305
191 ->195 0.18578

191 ->198 0.16328

Excited state symmetry could not be determined.
Excited State 22: Singlet-?Sym 5.2587 eV 235.77 nm f=0.0060 <S**2>=0.000
186 ->194 -0.11637
188 ->194 0.22862
189 ->196 0.14628
190 ->199 -0.24834
190 ->201 -0.12840
191 ->197 -0.14133
192 ->196 0.33874
192 ->200 0.30768

Excited state symmetry could not be determined.
Excited State 23: Singlet-?Sym 5.2769 eV 234.96 nm f=0.0224 <S**2>=0.000
186 ->193 -0.18363
188 ->193 0.53663
188 ->194 -0.26289
191 ->199 -0.11919
192 ->195 0.12499

Excited state symmetry could not be determined.
Excited State 24: Singlet-?Sym 5.2868 eV 234.51 nm f=0.0048 <S**2>=0.000
185 ->194 0.12067
187 ->193 -0.15544
187 ->194 0.46357
188 ->195 0.13979
189 ->197 0.14362
190 ->198 0.10541
191 ->196 -0.18752
191 ->198 0.15189
191 ->200 -0.13530
192 ->197 0.20603

Excited state symmetry could not be determined.
Excited State 25: Singlet-?Sym 5.3017 eV 233.86 nm f=0.0003 <S**2>=0.000
190 ->195 0.11687
190 ->196 0.23650
190 ->198 0.16463
190 ->200 0.34323
191 ->196 -0.32222
192 ->193 0.12411
192 ->199 -0.14473
192 ->201 -0.14564
192 ->202 0.11683
192 ->205 -0.11821

Excited state symmetry could not be determined.
Excited State 26: Singlet-?Sym 5.3348 eV 232.41 nm f=0.0257 <S**2>=0.000
187 ->194 0.39870
189 ->194 -0.18222
189 ->197 -0.20902
190 ->198 -0.18307
190 ->200 0.15997
191 ->195 -0.21986
191 ->196 0.16766
191 ->200 0.13641
192 ->197 -0.13940
192 ->201 -0.10939

Excited state symmetry could not be determined.
Excited State 27: Singlet-?Sym 5.3575 eV 231.42 nm f=0.0041 <S**2>=0.000
189 ->195 0.48464
189 ->196 0.21146
190 ->201 -0.19459
191 ->197 0.14609
191 ->199 -0.14470
191 ->201 -0.10492
192 ->200 -0.17484
192 ->203 -0.13342

Excited state symmetry could not be determined.
Excited State 28: Singlet-?Sym 5.3646 eV 231.12 nm f=0.0070 <S**2>=0.000
182 ->196 -0.10084
187 ->193 0.12135
190 ->195 -0.17130
190 ->200 0.14492
190 ->203 0.21069
191 ->195 0.13953
191 ->198 -0.15653
191 ->203 -0.11870
192 ->197 0.21814
192 ->201 0.24267
192 ->202 0.14846
192 ->205 -0.19043

Excited state symmetry could not be determined.
Excited State 29: Singlet-?Sym 5.3737 eV 230.72 nm f=0.0145 <S**2>=0.000
186 ->193 0.15018
187 ->195 -0.10910
189 ->195 -0.21670
189 ->196 0.30300

189 ->200 0.11083
190 ->199 -0.12314
190 ->201 0.13300
190 ->202 -0.16585
190 ->205 0.13008
191 ->197 -0.15984
192 ->200 -0.16552
192 ->203 -0.20984

Excited state symmetry could not be determined.
Excited State 30: Singlet-?Sym 5.3937 eV 229.87 nm f=0.0198 <S**2>=0.000
182 ->193 0.11157
186 ->193 -0.12217
186 ->194 0.14408
189 ->196 0.23718
190 ->197 0.16944
190 ->205 -0.10746
191 ->197 -0.24497
191 ->201 -0.20882
191 ->202 -0.13387
192 ->195 -0.10128
192 ->198 -0.10115
192 ->203 0.24960

Excited state symmetry could not be determined.
Excited State 31: Singlet-?Sym 5.4088 eV 229.23 nm f=0.0027 <S**2>=0.000
185 ->193 -0.18828
190 ->195 -0.14706
190 ->203 -0.14281
190 ->206 -0.10638
191 ->198 -0.11190
191 ->200 0.18944
191 ->203 0.16841
192 ->199 -0.22717
192 ->201 0.24201
192 ->202 -0.21200
192 ->205 0.24480

Excited state symmetry could not be determined.
Excited State 32: Singlet-?Sym 5.4229 eV 228.63 nm f=0.0950 <S**2>=0.000
186 ->193 0.46751
186 ->194 -0.13870
187 ->196 -0.10545
188 ->193 0.14589
189 ->196 -0.16171
190 ->201 0.10529

190 ->202 0.15554
191 ->199 -0.12527
191 ->201 -0.11278
192 ->203 0.14594

Excited state symmetry could not be determined.
Excited State 33: Singlet-?Sym 5.4642 eV 226.90 nm f=0.0275 <S**2>=0.000
186 ->194 0.46268
188 ->194 0.21647
189 ->195 -0.14229
190 ->199 -0.10157
190 ->201 -0.15489
191 ->201 -0.11162
192 ->203 -0.20421

Excited state symmetry could not be determined.
Excited State 34: Singlet-?Sym 5.4776 eV 226.35 nm f=0.0047 <S**2>=0.000
181 ->193 0.10786
185 ->193 0.34098
186 ->196 0.12365
187 ->193 -0.10102
190 ->196 0.19730
191 ->204 -0.10033
192 ->198 -0.11790
192 ->199 -0.28837

Excited state symmetry could not be determined.
Excited State 35: Singlet-?Sym 5.4805 eV 226.23 nm f=0.0362 <S**2>=0.000
185 ->193 0.11314
186 ->193 -0.15549
186 ->194 -0.15790
188 ->194 -0.10762
189 ->196 -0.11763
190 ->197 0.28033
191 ->197 -0.24681
191 ->201 -0.16998
192 ->198 0.35848
192 ->203 -0.15492

Excited state symmetry could not be determined.
Excited State 36: Singlet-?Sym 5.4972 eV 225.54 nm f=0.0318 <S**2>=0.000
186 ->193 -0.11943
186 ->194 0.12954
189 ->195 0.22749
189 ->196 -0.19317
189 ->198 -0.16373

190 ->199 -0.27707
190 ->201 0.35475
191 ->201 0.16837

Excited state symmetry could not be determined.
Excited State 37: Singlet-?Sym 5.5018 eV 225.35 nm f=0.0010 <S**2>=0.000
180 ->193 0.13626
185 ->193 0.32191
185 ->194 0.18721
186 ->196 0.12104
187 ->193 -0.16076
190 ->200 0.15170
191 ->203 0.14410
192 ->199 0.23887

Excited state symmetry could not be determined.
Excited State 38: Singlet-?Sym 5.5091 eV 225.05 nm f=0.0015 <S**2>=0.000
186 ->193 0.16978
186 ->194 0.16915
188 ->193 0.10601
189 ->196 0.18373
189 ->200 0.11365
190 ->199 0.18118
190 ->201 0.14442
191 ->197 -0.19245
191 ->199 -0.16634
191 ->201 0.27327
192 ->198 0.24079
192 ->200 0.10938
192 ->204 0.10268

Excited state symmetry could not be determined.
Excited State 39: Singlet-?Sym 5.5110 eV 224.98 nm f=0.0001 <S**2>=0.000
185 ->193 0.13595
189 ->197 -0.11274
189 ->199 -0.10446
190 ->198 -0.16496
191 ->198 0.39224
191 ->200 0.15745
192 ->197 -0.19653
192 ->199 -0.19253
192 ->202 0.22909
192 ->205 0.10737

Excited state symmetry could not be determined.
Excited State 40: Singlet-?Sym 5.5534 eV 223.26 nm f=0.0113 <S**2>=0.000

186 ->193 0.16269
189 ->198 -0.13933
189 ->200 -0.17545
190 ->197 0.12194
190 ->199 -0.10324
190 ->202 -0.14933
191 ->199 0.38951
191 ->208 -0.10249
192 ->196 0.12374
192 ->200 -0.19204
192 ->206 -0.13420

Excited state symmetry could not be determined.
Excited State 41: Singlet-?Sym 5.5572 eV 223.11 nm f=0.0204 <S**2>=0.000
181 ->194 0.12661
183 ->194 -0.10181
185 ->194 0.42119
186 ->195 -0.19528
187 ->194 -0.13545
189 ->197 -0.19671
190 ->203 0.15014
191 ->198 0.17809
192 ->201 0.10515
192 ->202 -0.10428
192 ->205 -0.14347

Excited state symmetry could not be determined.
Excited State 42: Singlet-?Sym 5.5734 eV 222.46 nm f=0.0055 <S**2>=0.000
185 ->194 0.15946
189 ->197 0.38524
189 ->199 -0.11854
189 ->201 0.29066
190 ->198 -0.27903
190 ->204 0.11847
191 ->200 0.17375

Excited state symmetry could not be determined.
Excited State 43: Singlet-?Sym 5.5875 eV 221.90 nm f=0.0028 <S**2>=0.000
185 ->194 0.14094
186 ->195 -0.12383
189 ->199 -0.12155
189 ->201 -0.14378
190 ->198 0.19439
190 ->200 -0.10483
190 ->206 0.12939
191 ->198 -0.14664

191 ->200 0.28988
191 ->204 -0.13149
192 ->197 0.12323
192 ->201 -0.19850
192 ->202 0.29762

Excited state symmetry could not be determined.
Excited State 44: Singlet-?Sym 5.5984 eV 221.47 nm f=0.0239 <S**2>=0.000
189 ->203 0.13524
190 ->202 -0.30392
190 ->205 0.16663
191 ->197 0.12343
191 ->199 -0.10988
191 ->201 -0.27641
192 ->200 0.34810
192 ->204 -0.10658

Excited state symmetry could not be determined.
Excited State 45: Singlet-?Sym 5.6132 eV 220.88 nm f=0.0004 <S**2>=0.000
180 ->194 0.17925
185 ->194 0.10831
187 ->201 0.10313
188 ->195 0.20532
188 ->200 -0.12078
189 ->208 0.13810
190 ->200 0.24276
190 ->203 -0.18032
191 ->203 -0.16374
191 ->204 -0.10293
191 ->207 -0.22029
192 ->199 0.13228
192 ->201 -0.10499
192 ->202 -0.10081

Excited state symmetry could not be determined.
Excited State 46: Singlet-?Sym 5.6341 eV 220.06 nm f=0.0007 <S**2>=0.000
189 ->196 0.19598
189 ->206 -0.14746
190 ->197 -0.11452
190 ->201 0.16732
190 ->202 0.37071
190 ->205 0.12574
191 ->199 0.14645
191 ->202 0.24815
192 ->200 0.15218
192 ->207 0.16349

Excited state symmetry could not be determined.
Excited State 47: Singlet-?Sym 5.6418 eV 219.76 nm f=0.0098 <S**2>=0.000
189 ->197 0.17661
189 ->199 0.25053
190 ->198 -0.10038
190 ->200 0.14368
190 ->204 -0.13312
191 ->200 -0.21540
192 ->197 -0.12753
192 ->201 0.20463
192 ->202 0.29950
192 ->205 0.13856

Excited state symmetry could not be determined.
Excited State 48: Singlet-?Sym 5.6595 eV 219.07 nm f=0.0056 <S**2>=0.000
187 ->195 0.12252
187 ->198 0.12795
189 ->196 -0.11669
189 ->198 0.45018
189 ->200 0.13742
190 ->197 -0.15318
190 ->199 -0.21537
191 ->197 -0.11656
191 ->201 0.10416

Excited state symmetry could not be determined.
Excited State 49: Singlet-?Sym 5.6612 eV 219.01 nm f=0.0004 <S**2>=0.000
180 ->194 0.11561
188 ->195 0.22904
189 ->199 0.27649
189 ->201 -0.18643
189 ->202 0.10089
190 ->200 -0.16439
190 ->203 0.11577
190 ->206 -0.16716
191 ->198 0.10870
191 ->203 0.14819
191 ->206 -0.12065
191 ->207 0.10566
192 ->201 -0.18624

Excited state symmetry could not be determined.
Excited State 50: Singlet-?Sym 5.6762 eV 218.43 nm f=0.0015 <S**2>=0.000
182 ->193 0.12087
189 ->197 0.14943

189 ->199 -0.14380
189 ->201 -0.13789
189 ->205 0.11067
190 ->203 0.23684
190 ->204 -0.13217
190 ->207 -0.10202
191 ->201 0.11631
191 ->203 0.12179
191 ->204 -0.14447
191 ->207 -0.12236
192->202 -0.14672

5.1b

Excitation energies and oscillator strengths:

Excited state symmetry could not be determined.
Excited State 1: Singlet-?Sym 4.5987 eV 269.61 nm f=0.0000 <S**2>=0.000
205 -> 211 0.11877
207 -> 210 -0.15702
207 -> 211 0.12911
208 -> 209 0.63262
This state for optimization and/or second-order correction.
Total Energy, E(TD-HF/TD-DFT) = -4730.34793303
Copying the excited state density for this state as the 1-particle RhoCI density.

Excited state symmetry could not be determined.
Excited State 2: Singlet-?Sym 4.6173 eV 268.52 nm f=0.2817 <S**2>=0.000
205 -> 209 -0.33976
206 -> 211 0.10991
207 -> 209 -0.12981
207 -> 212 -0.10948
208 -> 210 0.54472

Excited state symmetry could not be determined.
Excited State 3: Singlet-?Sym 4.6681 eV 265.60 nm f=0.1088 <S**2>=0.000
207 -> 209 0.60888
207 -> 212 -0.11943
208 -> 210 0.10276
208 -> 211 0.23154

Excited state symmetry could not be determined.
Excited State 4: Singlet-?Sym 4.6961 eV 264.02 nm f=0.0000 <S**2>=0.000
205 -> 210 0.36089

205 -> 211 -0.12405
206 -> 209 0.45815
207 -> 210 0.14853
207 -> 211 0.14714
208 -> 209 0.13322
208 -> 212 -0.17530

Excited state symmetry could not be determined.
Excited State 5: Singlet-?Sym 4.7163 eV 262.89 nm f=0.0000 <S**2>=0.000
204 -> 210 0.13179
205 -> 210 -0.36273
206 -> 212 -0.16582
207 -> 210 0.50611
208 -> 212 -0.11838

Excited state symmetry could not be determined.
Excited State 6: Singlet-?Sym 4.7692 eV 259.97 nm f=0.1781 <S**2>=0.000
203 -> 210 0.11812
205 -> 209 0.33782
205 -> 212 0.11657
206 -> 210 0.46117
207 -> 212 -0.12263
208 -> 210 0.28054

Excited state symmetry could not be determined.
Excited State 7: Singlet-?Sym 4.8022 eV 258.18 nm f=0.0553 <S**2>=0.000
205 -> 209 0.40850
205 -> 212 -0.21964
206 -> 210 -0.38048
206 -> 211 -0.15719
208 -> 210 0.21358

Excited state symmetry could not be determined.
Excited State 8: Singlet-?Sym 4.8209 eV 257.18 nm f=0.0000 <S**2>=0.000
205 -> 210 -0.32620
205 -> 211 -0.10600
205 -> 214 -0.11104
206 -> 209 0.40593
206 -> 212 -0.12190
207 -> 210 -0.29690
208 -> 212 0.18322

Excited state symmetry could not be determined.

Excited State 9: Singlet-?Sym 4.9908 eV 248.43 nm f=0.0187 <S**2>=0.000
199 -> 212 0.12092
204 -> 209 0.16459
205 -> 209 -0.12211
205 -> 213 0.15504
205 -> 217 -0.10432
206 -> 211 -0.11361
206 -> 214 -0.22013
206 -> 215 0.10397
207 -> 213 -0.10140
207 -> 216 0.32696
208 -> 215 0.31868

Excited state symmetry could not be determined.
Excited State 10: Singlet-?Sym 4.9910 eV 248.41 nm f=0.0000 <S**2>=0.000
204 -> 210 0.16651
205 -> 215 0.16532
205 -> 218 0.10817
206 -> 216 -0.19817
207 -> 210 -0.10423
207 -> 211 0.18693
207 -> 214 0.22575
208 -> 209 -0.15668
208 -> 212 -0.21648
208 -> 213 0.21079
208 -> 216 0.10671
208 -> 217 -0.18260

Excited state symmetry could not be determined.
Excited State 11: Singlet-?Sym 5.0013 eV 247.90 nm f=0.0000 <S**2>=0.000
199 -> 210 -0.11157
203 -> 209 0.12664
205 -> 214 0.15663
206 -> 209 0.17012
206 -> 212 0.10554
206 -> 213 -0.17081
206 -> 216 0.12254
206 -> 217 0.12343
207 -> 210 -0.10043
207 -> 211 -0.10914
207 -> 215 0.31771
208 -> 216 0.33750

Excited state symmetry could not be determined.
Excited State 12: Singlet-?Sym 5.0098 eV 247.48 nm f=0.0157 <S**2>=0.000
205 -> 216 0.18307
206 -> 215 -0.19008
207 -> 209 -0.21449
207 -> 212 -0.17611
207 -> 213 0.14682
207 -> 217 -0.20167
208 -> 210 -0.10585
208 -> 211 0.25828
208 -> 214 0.27177

Excited state symmetry could not be determined.
Excited State 13: Singlet-?Sym 5.0911 eV 243.53 nm f=0.1767 <S**2>=0.000
206 -> 210 0.17483
206 -> 211 -0.16717
206 -> 214 0.13579
206 -> 218 -0.12924
207 -> 209 0.11232
207 -> 212 0.15915
207 -> 213 0.36172
208 -> 211 -0.30365
208 -> 214 0.25790

Excited state symmetry could not be determined.
Excited State 14: Singlet-?Sym 5.0920 eV 243.49 nm f=0.0000 <S**2>=0.000
202 -> 210 -0.13095
204 -> 210 -0.10334
205 -> 211 -0.10528
205 -> 214 0.10320
205 -> 218 -0.11550
206 -> 212 -0.20751
206 -> 213 -0.23662
207 -> 210 -0.14740
207 -> 211 0.31565
207 -> 214 -0.20895
207 -> 218 0.12627
208 -> 212 -0.12680
208 -> 213 -0.24859

Excited state symmetry could not be determined.
Excited State 15: Singlet-?Sym 5.1409 eV 241.17 nm f=0.0000 <S**2>=0.000
202 -> 210 -0.19264

204 -> 210 -0.29034
205 -> 215 0.13035
206 -> 212 -0.16756
207 -> 210 0.11761
207 -> 214 0.10617
208 -> 212 0.35229
208 -> 213 0.22428
208 -> 217 -0.19460
208 -> 219 0.10256

Excited state symmetry could not be determined.
Excited State 16: Singlet-?Sym 5.1423 eV 241.11 nm f=0.1025 <S**2>=0.000
202 -> 209 0.10318
204 -> 209 0.31419
205 -> 213 -0.25917
205 -> 217 -0.11704
206 -> 211 -0.26082
206 -> 214 0.15633
207 -> 212 0.15535
208 -> 211 0.31579
208 -> 214 -0.11555

Excited state symmetry could not be determined.
Excited State 17: Singlet-?Sym 5.1612 eV 240.22 nm f=0.0000 <S**2>=0.000
203 -> 209 0.16492
205 -> 210 -0.11688
205 -> 211 -0.28810
205 -> 214 0.18973
205 -> 215 -0.12747
206 -> 213 -0.23502
207 -> 210 -0.10584
208 -> 213 0.29070
208 -> 216 -0.18855
208 -> 219 0.16249

Excited state symmetry could not be determined.
Excited State 18: Singlet-?Sym 5.1964 eV 238.60 nm f=0.0375 <S**2>=0.000
203 -> 210 -0.15187
204 -> 209 0.39665
205 -> 212 -0.21368
205 -> 213 0.11952
205 -> 216 -0.14093
206 -> 210 0.10075

206 -> 214 -0.11201
206 -> 215 0.12348
207 -> 212 -0.15231
207 -> 216 -0.11320
208 -> 215 -0.27909

Excited state symmetry could not be determined.
Excited State 19: Singlet-?Sym 5.2278 eV 237.16 nm f=0.0000 <S**2>=0.000
202 -> 210 0.18273
203 -> 209 0.22467
204 -> 210 0.31480
204 -> 211 0.10016
205 -> 210 0.13704
205 -> 211 -0.11594
206 -> 209 -0.10822
206 -> 212 0.10982
207 -> 211 0.15037
208 -> 212 0.34513
208 -> 213 -0.12261
208 -> 217 -0.14154

Excited state symmetry could not be determined.
Excited State 20: Singlet-?Sym 5.2418 eV 236.53 nm f=0.0586 <S**2>=0.000
202 -> 209 0.11403
203 -> 210 0.21174
204 -> 209 0.31713
204 -> 212 -0.12804
205 -> 209 0.10454
205 -> 212 0.28835
205 -> 213 0.12070
205 -> 216 0.12388
206 -> 210 -0.17502
206 -> 215 -0.17530
206 -> 218 0.11004
208 -> 211 -0.25497

Excited state symmetry could not be determined.
Excited State 21: Singlet-?Sym 5.2562 eV 235.88 nm f=0.0000 <S**2>=0.000
203 -> 209 0.50392
204 -> 210 -0.15566
204 -> 211 0.14501
205 -> 214 -0.17167
206 -> 209 -0.11423

206 -> 213 0.20258
208 -> 212 -0.19092

Excited state symmetry could not be determined.
Excited State 22: Singlet-?Sym 5.2739 eV 235.09 nm f=0.1127 <S**2>=0.000
203 -> 210 -0.29336
204 -> 212 0.11715
205 -> 212 -0.15408
205 -> 213 -0.12567
205 -> 216 0.30219
205 -> 219 -0.11388
206 -> 210 0.11349
206 -> 215 -0.26876
208 -> 211 -0.20156
208 -> 214 -0.15523
208 -> 215 0.11136
208 -> 220 0.11397

Excited state symmetry could not be determined.
Excited State 23: Singlet-?Sym 5.2796 eV 234.84 nm f=0.0118 <S**2>=0.000
203 -> 210 0.10704
205 -> 212 -0.17932
205 -> 213 0.20167
206 -> 210 0.10473
206 -> 214 -0.19822
207 -> 212 0.47499
207 -> 213 -0.13162
207 -> 216 -0.16827

Excited state symmetry could not be determined.
Excited State 24: Singlet-?Sym 5.2924 eV 234.27 nm f=0.0000 <S**2>=0.000
203 -> 209 -0.10305
204 -> 210 0.11045
205 -> 214 -0.19357
205 -> 215 -0.24471
206 -> 213 0.13729
206 -> 216 0.32636
207 -> 211 0.27678
207 -> 214 0.12107
207 -> 215 0.22227
208 -> 219 0.10919

Excited state symmetry could not be determined.

Excited State 25: Singlet-?Sym 5.2970 eV 234.06 nm f=0.0000 <S**2>=0.000
203 -> 209 0.10099
205 -> 210 -0.10755
205 -> 211 0.38273
205 -> 214 0.10978
205 -> 215 -0.11914
206 -> 212 0.21551
206 -> 217 0.12528
208 -> 216 -0.27369
208 -> 217 -0.24059
208 -> 219 0.12073

Excited state symmetry could not be determined.
Excited State 26: Singlet-?Sym 5.3271 eV 232.74 nm f=0.2653 <S**2>=0.000
202 -> 209 -0.17075
203 -> 210 -0.32918
203 -> 211 0.12776
204 -> 209 0.15306
205 -> 209 0.12599
205 -> 212 0.12940
206 -> 211 0.32925
207 -> 212 0.22869
207 -> 217 -0.12090
208 -> 215 0.11332
208 -> 218 -0.15864

Excited state symmetry could not be determined.
Excited State 27: Singlet-?Sym 5.3308 eV 232.58 nm f=0.0000 <S**2>=0.000
203 -> 212 0.12699
204 -> 210 -0.27218
205 -> 210 -0.12048
205 -> 215 -0.12648
205 -> 218 0.12074
206 -> 212 0.28750
206 -> 217 -0.14849
207 -> 211 0.31362
208 -> 212 0.14443
208 -> 217 0.16672
208 -> 219 -0.16875

Excited state symmetry could not be determined.
Excited State 28: Singlet-?Sym 5.3486 eV 231.81 nm f=0.0066 <S**2>=0.000
201 -> 210 0.15963

203 -> 210 0.28620
204 -> 209 0.12968
205 -> 212 -0.24092
205 -> 213 -0.16339
205 -> 217 0.23729
206 -> 211 0.27128
206 -> 214 0.13472
206 -> 218 -0.13292
207 -> 216 0.11572
207 -> 219 -0.10897

Excited state symmetry could not be determined.
Excited State 29: Singlet-?Sym 5.3747 eV 230.68 nm f=0.0000 <S**2>=0.000
201 -> 209 0.13168
203 -> 209 0.15709
204 -> 210 0.13774
205 -> 210 0.10549
205 -> 211 0.29958
205 -> 218 -0.10132
206 -> 212 -0.24462
207 -> 211 0.13559
207 -> 221 0.10251
208 -> 209 -0.10788
208 -> 213 0.23162
208 -> 217 0.25219
208 -> 219 -0.12969

Excited state symmetry could not be determined.
Excited State 30: Singlet-?Sym 5.3901 eV 230.02 nm f=0.0027 <S**2>=0.000
202 -> 209 0.17114
205 -> 216 0.11940
205 -> 217 0.11322
205 -> 219 -0.10208
207 -> 216 0.13632
207 -> 217 0.25387
207 -> 219 -0.19008
208 -> 214 0.30711
208 -> 218 -0.13753
208 -> 221 0.19972

Excited state symmetry could not be determined.
Excited State 31: Singlet-?Sym 5.4195 eV 228.78 nm f=0.0582 <S**2>=0.000
196 -> 210 0.11252

201 -> 210 -0.25351
202 -> 209 0.43859
203 -> 211 -0.13284
206 -> 211 0.13187
206 -> 215 0.11352
207 -> 217 -0.18402
208 -> 215 0.11716
208 -> 218 0.15914

Excited state symmetry could not be determined.
Excited State 32: Singlet-?Sym 5.4410 eV 227.87 nm f=0.0000 <S**2>=0.000
201 -> 209 0.32117
202 -> 210 -0.29841
203 -> 216 0.12612
204 -> 210 0.15670
204 -> 215 0.12148
205 -> 215 -0.17959
206 -> 217 -0.15612
207 -> 211 -0.10543
208 -> 213 -0.12868
208 -> 219 -0.11196

Excited state symmetry could not be determined.
Excited State 33: Singlet-?Sym 5.4598 eV 227.08 nm f=0.0000 <S**2>=0.000
201 -> 209 -0.19864
202 -> 210 0.28409
203 -> 216 0.14144
204 -> 210 -0.14257
204 -> 215 0.11494
205 -> 215 -0.15120
206 -> 212 -0.21302
207 -> 211 -0.12405
207 -> 214 0.20392
208 -> 213 -0.20811
208 -> 219 -0.13587

Excited state symmetry could not be determined.
Excited State 34: Singlet-?Sym 5.4653 eV 226.86 nm f=0.0112 <S**2>=0.000
205 -> 212 0.12578
205 -> 213 0.13303
205 -> 216 0.11630
205 -> 217 0.26594
205 -> 219 -0.19307

206 -> 211 -0.10131
206 -> 214 -0.11771
206 -> 215 0.10077
206 -> 221 -0.14098
206 -> 223 -0.11763
207 -> 213 0.29409
207 -> 219 0.19944
208 -> 214 -0.16191
208 -> 220 0.11670

Excited state symmetry could not be determined.
Excited State 35: Singlet-?Sym 5.4769 eV 226.38 nm f=0.0000 <S**2>=0.000
201 -> 209 0.14588
205 -> 221 -0.12473
206 -> 212 0.11353
206 -> 217 0.29224
206 -> 219 -0.22756
207 -> 214 0.24382
207 -> 215 -0.16244
207 -> 220 -0.17211
207 -> 221 0.10090
207 -> 223 0.10969
208 -> 213 -0.16199
208 -> 217 0.10253
208 -> 224 0.10100

Excited state symmetry could not be determined.
Excited State 36: Singlet-?Sym 5.4821 eV 226.16 nm f=0.0119 <S**2>=0.000
201 -> 210 -0.16231
202 -> 209 -0.10461
205 -> 213 -0.19015
205 -> 217 0.15355
205 -> 219 -0.14997
206 -> 211 -0.10637
206 -> 215 0.12625
207 -> 213 -0.28431
207 -> 217 -0.24599
208 -> 214 0.29423
208 -> 215 -0.10017
208 -> 218 -0.10431

Excited state symmetry could not be determined.
Excited State 37: Singlet-?Sym 5.4899 eV 225.84 nm f=0.0021 <S**2>=0.000

201 -> 210 0.25544
202 -> 212 -0.13369
203 -> 210 -0.19612
203 -> 215 0.13891
204 -> 212 -0.10481
204 -> 216 0.12717
205 -> 212 0.26116
205 -> 217 0.12166
206 -> 211 -0.11997
207 -> 212 0.10672
207 -> 216 0.12735
207 -> 219 -0.20483
208 -> 218 0.22416

Excited state symmetry could not be determined.
Excited State 38: Singlet-?Sym 5.4953 eV 225.62 nm f=0.0221 <S**2>=0.000
201 -> 210 -0.15365
203 -> 214 0.13605
204 -> 213 0.15107
204 -> 217 -0.10429
205 -> 216 0.15803
205 -> 217 0.10139
207 -> 212 0.10198
207 -> 213 0.13385
208 -> 215 -0.26356
208 -> 218 0.31446
208 -> 220 -0.16414

Excited state symmetry could not be determined.
Excited State 39: Singlet-?Sym 5.4989 eV 225.47 nm f=0.0000 <S**2>=0.000
200 -> 209 0.13210
201 -> 209 0.37265
202 -> 210 0.25603
202 -> 211 0.18237
203 -> 212 0.15931
203 -> 217 0.10094
204 -> 214 -0.14551
207 -> 215 0.10567
208 -> 216 0.10051
208 -> 217 -0.14277
208 -> 219 0.11146

Excited state symmetry could not be determined.

Excited State 40: Singlet-?Sym 5.5217 eV 224.54 nm f=0.0642 <S**2>=0.000
196 -> 210 -0.15934
201 -> 210 0.36481
202 -> 209 0.24854
202 -> 212 -0.15106
204 -> 216 -0.12514
205 -> 213 -0.13563
205 -> 216 0.10824
207 -> 219 0.20025
208 -> 214 0.12310
208 -> 220 -0.15205

Excited state symmetry could not be determined.
Excited State 41: Singlet-?Sym 5.5348 eV 224.01 nm f=0.0000 <S**2>=0.000
202 -> 210 -0.14309
203 -> 213 -0.11485
203 -> 216 -0.13223
204 -> 214 -0.13187
204 -> 215 -0.13047
205 -> 214 0.24887
206 -> 219 0.10367
207 -> 214 0.31499
207 -> 215 0.11213
207 -> 218 -0.27318
208 -> 213 -0.14429
208 -> 222 0.11505

Excited state symmetry could not be determined.
Excited State 42: Singlet-?Sym 5.5508 eV 223.36 nm f=0.0000 <S**2>=0.000
196 -> 209 -0.10740
201 -> 209 0.11325
202 -> 210 0.13897
203 -> 216 -0.11526
203 -> 217 -0.11776
204 -> 211 0.11129
204 -> 214 0.10080
205 -> 221 0.12662
206 -> 212 -0.11879
206 -> 216 -0.12385
206 -> 217 -0.19321
206 -> 219 0.13870
207 -> 214 0.24076
207 -> 218 0.17525

208 -> 213 -0.13215
208 -> 216 -0.12294
208 -> 217 0.11857
208 -> 219 0.20081
208 -> 222 -0.12503

Excited state symmetry could not be determined.
Excited State 43: Singlet-?Sym 5.5587 eV 223.04 nm f=0.0000 <S**2>=0.000
202 -> 210 -0.10710
204 -> 211 -0.14644
205 -> 220 -0.14565
206 -> 216 -0.10345
206 -> 219 -0.13138
207 -> 215 -0.12466
208 -> 213 -0.13855
208 -> 216 0.30098
208 -> 217 0.18571
208 -> 219 0.38688

Excited state symmetry could not be determined.
Excited State 44: Singlet-?Sym 5.5714 eV 222.54 nm f=0.0239 <S**2>=0.000
202 -> 209 -0.12427
203 -> 215 -0.11235
204 -> 213 -0.13598
204 -> 216 -0.13239
205 -> 213 0.12234
205 -> 219 0.11123
206 -> 214 0.32334
207 -> 213 -0.13600
207 -> 216 -0.13167
208 -> 214 0.17289
208 -> 215 0.21042
208 -> 218 0.31812

Excited state symmetry could not be determined.
Excited State 45: Singlet-?Sym 5.5829 eV 222.08 nm f=0.0000 <S**2>=0.000
200 -> 209 -0.11746
204 -> 211 0.20779
204 -> 215 0.10849
205 -> 214 0.31260
205 -> 218 0.11663
206 -> 212 -0.12057
206 -> 213 0.29348

206 -> 217 0.21483
206 -> 219 0.14144
207 -> 214 -0.20349
207 -> 218 -0.10253
208 -> 217 0.10760

Excited state symmetry could not be determined.
Excited State 46: Singlet-?Sym 5.5990 eV 221.44 nm f=0.0000 <S**2>=0.000
201 -> 209 -0.11716
205 -> 214 0.16629
205 -> 218 -0.31097
206 -> 212 0.12158
206 -> 213 0.24945
206 -> 216 0.13253
206 -> 222 -0.14104
207 -> 215 -0.17701
207 -> 218 0.31425
208 -> 216 0.15961

Excited state symmetry could not be determined.
Excited State 47: Singlet-?Sym 5.6075 eV 221.10 nm f=0.0046 <S**2>=0.000
202 -> 209 0.12986
203 -> 214 0.13127
203 -> 215 0.10378
204 -> 212 -0.13883
204 -> 216 0.11098
205 -> 213 0.14237
205 -> 217 0.23179
206 -> 211 -0.10743
206 -> 214 0.14851
206 -> 218 -0.17913
207 -> 213 -0.13993
207 -> 216 -0.21028
207 -> 217 0.18261
208 -> 215 0.13188
208 -> 218 -0.20237
208 -> 220 -0.11811

Excited state symmetry could not be determined.
Excited State 48: Singlet-?Sym 5.6117 eV 220.94 nm f=0.0226 <S**2>=0.000
203 -> 215 -0.10521
205 -> 213 0.22804
205 -> 216 0.13898

206 -> 214 0.23367
206 -> 218 -0.18623
207 -> 216 0.31932
207 -> 217 -0.24722
208 -> 215 -0.25175
208 -> 218 -0.16150

Excited state symmetry could not be determined.
Excited State 49: Singlet-?Sym 5.6139 eV 220.85 nm f=0.0000 <S**2>=0.000
203 -> 216 0.12338
204 -> 215 0.12436
205 -> 215 0.11621
205 -> 218 -0.26656
206 -> 216 -0.10100
206 -> 217 0.12402
207 -> 215 0.32723
208 -> 216 -0.23134
208 -> 217 0.26566

Excited state symmetry could not be determined.
Excited State 50: Singlet-?Sym 5.6195 eV 220.63 nm f=0.0003 <S**2>=0.000
201 -> 210 0.13200
203 -> 214 0.10230
204 -> 212 0.12064
205 -> 212 -0.10239
205 -> 217 0.20813
205 -> 219 0.18613
205 -> 222 0.17079
206 -> 210 0.10744
206 -> 215 -0.10902
206 -> 218 0.40948
207-> 213 0.12146

5.1c

Excitation energies and oscillator strengths:

Excited state symmetry could not be determined.
Excited State 1: Singlet-?Sym 4.5590 eV 271.95 nm f=0.0000 <S**2>=0.000
257 -> 262 -0.11481
257 -> 263 -0.13382
258 -> 261 -0.11469
259 -> 262 -0.18952

259 -> 263 -0.12955
260 -> 261 0.60083
This state for optimization and/or second-order correction.
Total Energy, E(TD-HF/TD-DFT) = -14866.1374461
Copying the excited state density for this state as the 1-particle RhoCI density.

Excited state symmetry could not be determined.
Excited State 2: Singlet-?Sym 4.5640 eV 271.66 nm f=0.4199 <S**2>=0.000
257 -> 261 -0.32422
258 -> 262 -0.10101
258 -> 263 -0.10588
259 -> 261 -0.18030
259 -> 264 0.10543
260 -> 262 0.52521
260 -> 263 0.11574

Excited state symmetry could not be determined.
Excited State 3: Singlet-?Sym 4.6295 eV 267.82 nm f=0.1382 <S**2>=0.000
258 -> 263 -0.11258
259 -> 261 0.54568
259 -> 264 0.17200
260 -> 262 0.14487
260 -> 263 -0.26841
260 -> 266 0.10654

Excited state symmetry could not be determined.
Excited State 4: Singlet-?Sym 4.6486 eV 266.71 nm f=0.0000 <S**2>=0.000
255 -> 261 -0.11433
256 -> 262 -0.10052
257 -> 262 0.38169
257 -> 263 0.11423
258 -> 261 0.39292
259 -> 263 -0.16755
260 -> 261 0.16152
260 -> 264 0.20020
260 -> 265 0.10381

Excited state symmetry could not be determined.
Excited State 5: Singlet-?Sym 4.6658 eV 265.73 nm f=0.0000 <S**2>=0.000
256 -> 262 0.14376
257 -> 262 -0.31098
258 -> 264 0.19495
259 -> 262 0.49543

259 -> 263 -0.12838
260 -> 264 0.17546

Excited state symmetry could not be determined.
Excited State 6: Singlet-?Sym 4.7089 eV 263.30 nm f=0.2476 <S**2>=0.000
255 -> 262 -0.15775
257 -> 261 0.24466
257 -> 264 -0.17615
258 -> 262 0.48909
259 -> 264 0.16045
260 -> 262 0.23671

Excited state symmetry could not be determined.
Excited State 7: Singlet-?Sym 4.7575 eV 260.61 nm f=0.0460 <S**2>=0.000
257 -> 261 0.41920
257 -> 264 0.20485
257 -> 265 0.11732
258 -> 262 -0.24877
258 -> 263 0.19206
258 -> 266 -0.10049
260 -> 262 0.22947
260 -> 263 -0.10157
260 -> 266 0.13780
260 -> 267 -0.11683

Excited state symmetry could not be determined.
Excited State 8: Singlet-?Sym 4.7714 eV 259.85 nm f=0.0000 <S**2>=0.000
257 -> 262 -0.26942
257 -> 263 0.14207
257 -> 266 -0.15920
258 -> 261 0.37954
258 -> 264 0.14623
258 -> 265 0.14341
259 -> 262 -0.24326
259 -> 267 0.14416
260 -> 264 -0.16124
260 -> 268 0.16105

Excited state symmetry could not be determined.
Excited State 9: Singlet-?Sym 4.8780 eV 254.17 nm f=0.0433 <S**2>=0.000
256 -> 261 -0.16317
257 -> 261 0.17442
257 -> 265 -0.14423

257 -> 269 0.11556
258 -> 266 0.18376
258 -> 267 0.15391
259 -> 261 -0.12490
259 -> 264 0.11966
259 -> 268 0.32429
260 -> 267 0.31838

Excited state symmetry could not be determined.
Excited State 10: Singlet-?Sym 4.8903 eV 253.53 nm f=0.0000 <S**2>=0.000
255 -> 261 0.15634
258 -> 261 -0.25440
258 -> 265 0.13132
258 -> 268 0.17051
258 -> 269 -0.14089
259 -> 263 -0.12075
259 -> 267 0.32450
260 -> 261 -0.10446
260 -> 264 0.18163
260 -> 268 0.26538

Excited state symmetry could not be determined.
Excited State 11: Singlet-?Sym 4.8966 eV 253.20 nm f=0.0000 <S**2>=0.000
256 -> 262 0.13411
257 -> 262 -0.14214
257 -> 266 0.16199
257 -> 267 -0.17080
257 -> 270 -0.10660
258 -> 268 0.18344
259 -> 262 -0.15545
259 -> 263 -0.12420
259 -> 266 0.22187
260 -> 261 -0.18167
260 -> 265 0.26659
260 -> 268 -0.19717
260 -> 269 -0.18417

Excited state symmetry could not be determined.
Excited State 12: Singlet-?Sym 4.9122 eV 252.40 nm f=0.0060 <S**2>=0.000
257 -> 261 -0.10421
257 -> 265 0.12248
257 -> 268 -0.19814
258 -> 267 0.19035

259 -> 261 -0.25668
259 -> 264 0.14977
259 -> 265 0.16426
259 -> 269 -0.19307
260 -> 262 -0.15697
260 -> 263 -0.14836
260 -> 266 0.29996

Excited state symmetry could not be determined.
Excited State 13: Singlet-?Sym 4.9956 eV 248.19 nm f=0.1965 <S**2>=0.000
258 -> 262 0.19182
258 -> 263 0.11609
258 -> 266 0.13863
258 -> 270 0.10880
259 -> 261 0.13679
259 -> 264 -0.18559
259 -> 265 0.32280
260 -> 263 0.35948
260 -> 266 0.24274

Excited state symmetry could not be determined.
Excited State 14: Singlet-?Sym 4.9979 eV 248.07 nm f=0.0000 <S**2>=0.000
254 -> 262 0.12844
256 -> 262 0.11696
257 -> 263 -0.12764
257 -> 266 -0.12683
257 -> 270 -0.11713
258 -> 264 -0.23230
258 -> 265 0.22146
259 -> 262 0.18485
259 -> 263 0.29345
259 -> 266 0.20952
259 -> 270 0.12299
260 -> 264 -0.11005
260 -> 265 0.22139

Excited state symmetry could not be determined.
Excited State 15: Singlet-?Sym 5.0390 eV 246.05 nm f=0.0000 <S**2>=0.000
254 -> 262 0.14805
256 -> 262 0.24477
257 -> 267 0.16425
258 -> 264 -0.20447
259 -> 262 -0.19595

260 -> 264 0.45583
260 -> 265 -0.10900
260 -> 269 0.13971

Excited state symmetry could not be determined.
Excited State 16: Singlet-?Sym 5.0501 eV 245.51 nm f=0.1280 <S**2>=0.000
256 -> 261 -0.21655
257 -> 261 0.10821
257 -> 265 0.27554
257 -> 269 0.14244
258 -> 263 -0.27781
258 -> 266 -0.17490
259 -> 261 0.10198
259 -> 264 0.17310
260 -> 263 0.34710

Excited state symmetry could not be determined.
Excited State 17: Singlet-?Sym 5.0770 eV 244.21 nm f=0.0000 <S**2>=0.000
255 -> 261 -0.12670
256 -> 263 -0.11641
257 -> 262 -0.10612
257 -> 263 0.32164
257 -> 266 0.16384
257 -> 267 0.13518
258 -> 261 -0.10276
258 -> 265 -0.20532
259 -> 263 0.12100
260 -> 265 0.30889
260 -> 268 0.20072
260 -> 271 0.11680

Excited state symmetry could not be determined.
Excited State 18: Singlet-?Sym 5.0988 eV 243.16 nm f=0.0560 <S**2>=0.000
255 -> 262 0.12072
256 -> 261 0.22415
257 -> 264 0.32618
257 -> 268 0.17285
258 -> 262 0.19056
258 -> 263 0.12575
258 -> 267 -0.21762
259 -> 264 0.14820
260 -> 267 0.27968

Excited state symmetry could not be determined.
Excited State 19: Singlet-?Sym 5.1503 eV 240.73 nm f=0.0000 <S**2>=0.000
254 -> 262 0.20238
256 -> 262 0.33770
257 -> 262 0.15107
257 -> 263 0.13651
258 -> 261 -0.10045
258 -> 264 -0.18341
258 -> 265 -0.11278
258 -> 269 -0.10687
259 -> 263 -0.20997
260 -> 264 -0.28606
260 -> 265 -0.15109
260 -> 269 -0.10055

Excited state symmetry could not be determined.
Excited State 20: Singlet-?Sym 5.1514 eV 240.68 nm f=0.0239 <S**2>=0.000
254 -> 261 0.11805
256 -> 261 0.46414
257 -> 261 0.11286
257 -> 264 -0.17540
257 -> 268 -0.12608
258 -> 266 -0.11994
258 -> 267 0.18865
259 -> 268 0.14047
260 -> 263 0.21356

Excited state symmetry could not be determined.
Excited State 21: Singlet-?Sym 5.1689 eV 239.86 nm f=0.0000 <S**2>=0.000
255 -> 261 0.32197
255 -> 265 0.11131
256 -> 263 0.17159
257 -> 266 0.19621
258 -> 261 0.15734
258 -> 265 -0.19897
258 -> 268 0.13600
259 -> 263 0.18301
259 -> 266 -0.11396
259 -> 267 0.11259
260 -> 264 -0.11838
260 -> 269 0.22231
260 -> 271 -0.12231

Excited state symmetry could not be determined.
Excited State 22: Singlet-?Sym 5.1773 eV 239.48 nm f=0.0000 <S**2>=0.000
255 -> 261 0.26027
256 -> 263 0.12608
257 -> 263 -0.22304
257 -> 266 0.11405
257 -> 267 0.22767
258 -> 261 0.13861
258 -> 264 -0.13095
258 -> 265 -0.12512
258 -> 268 -0.19251
259 -> 263 -0.20920
260 -> 268 0.18399
260 -> 269 -0.18464
260 -> 271 0.13995

Excited state symmetry could not be determined.
Excited State 23: Singlet-?Sym 5.1779 eV 239.45 nm f=0.1340 <S**2>=0.000
255 -> 262 -0.21747
256 -> 264 0.19537
257 -> 264 -0.24149
257 -> 268 0.26404
258 -> 262 -0.23527
258 -> 267 -0.21246
259 -> 264 0.16409
259 -> 265 0.17409
259 -> 268 -0.11867
260 -> 266 0.13333

Excited state symmetry could not be determined.
Excited State 24: Singlet-?Sym 5.1814 eV 239.29 nm f=0.0593 <S**2>=0.000
255 -> 262 0.19683
257 -> 265 -0.24520
258 -> 266 0.16517
259 -> 264 0.43584
259 -> 268 -0.15997
259 -> 269 0.10771
260 -> 263 0.14985
260 -> 267 -0.16183

Excited state symmetry could not be determined.
Excited State 25: Singlet-?Sym 5.1893 eV 238.92 nm f=0.0000 <S**2>=0.000
255 -> 261 0.24900

257 -> 262 0.11088
257 -> 263 0.22358
257 -> 266 -0.17202
257 -> 267 0.14697
258 -> 265 0.13356
258 -> 268 -0.18602
258 -> 269 -0.12144
259 -> 263 -0.21298
259 -> 266 0.16356
259 -> 267 -0.18121
260 -> 265 0.14112
260 -> 268 -0.15160
260 -> 269 0.17895

Excited state symmetry could not be determined.
Excited State 26: Singlet-?Sym 5.2183 eV 237.59 nm f=0.2312 <S**2>=0.000
254 -> 261 0.10315
255 -> 262 -0.23780
255 -> 263 -0.15781
256 -> 261 -0.24173
257 -> 261 -0.17253
257 -> 269 -0.18364
258 -> 263 0.35084
258 -> 266 -0.14938
259 -> 264 0.13386
259 -> 269 0.14315
260 -> 267 0.13321

Excited state symmetry could not be determined.
Excited State 27: Singlet-?Sym 5.2361 eV 236.79 nm f=0.0000 <S**2>=0.000
255 -> 261 0.19243
255 -> 264 -0.12789
256 -> 262 0.30590
257 -> 262 0.17939
258 -> 264 0.22125
259 -> 263 0.26394
259 -> 272 0.10345
260 -> 264 0.10231
260 -> 269 -0.20761
260 -> 271 0.17765

Excited state symmetry could not be determined.
Excited State 28: Singlet-?Sym 5.2539 eV 235.99 nm f=0.0036 <S**2>=0.000

255 -> 262 0.15919
256 -> 261 -0.10107
256 -> 274 -0.11826
257 -> 264 -0.12045
257 -> 269 -0.17906
257 -> 271 0.11754
257 -> 274 -0.11959
258 -> 263 0.14445
258 -> 273 -0.14565
259 -> 269 -0.20657
259 -> 271 0.29074
260 -> 272 0.31795

Excited state symmetry could not be determined.
Excited State 29: Singlet-?Sym 5.2579 eV 235.80 nm f=0.0000 <S**2>=0.000
255 -> 261 0.16915
255 -> 264 0.10240
256 -> 262 -0.16947
257 -> 262 -0.12723
257 -> 263 0.26714
258 -> 264 -0.19837
258 -> 268 0.10877
258 -> 269 -0.20485
258 -> 271 0.11647
259 -> 267 -0.10234
259 -> 272 0.14071
259 -> 273 -0.16862
260 -> 265 -0.16713
260 -> 269 -0.17900

Excited state symmetry could not be determined.
Excited State 30: Singlet-?Sym 5.2687 eV 235.32 nm f=0.0270 <S**2>=0.000
253 -> 262 -0.10750
255 -> 262 0.38127
257 -> 264 -0.26412
258 -> 270 -0.10658
259 -> 264 -0.10595
259 -> 269 0.21451
260 -> 266 0.20277
260 -> 270 0.10547

Excited state symmetry could not be determined.
Excited State 31: Singlet-?Sym 5.3017 eV 233.86 nm f=0.0085 <S**2>=0.000

254 -> 261 0.12817
255 -> 266 0.11580
256 -> 265 -0.11985
257 -> 261 -0.11349
257 -> 264 -0.13952
257 -> 269 0.17793
257 -> 271 -0.20057
258 -> 263 0.11148
258 -> 272 0.23576
258 -> 273 -0.13083
259 -> 274 0.25088
260 -> 273 -0.24021

Excited state symmetry could not be determined.
Excited State 32: Singlet-?Sym 5.3019 eV 233.85 nm f=0.0000 <S**2>=0.000
255 -> 261 0.17935
256 -> 262 -0.10363
257 -> 263 0.19628
257 -> 272 0.12712
258 -> 264 -0.20987
258 -> 269 0.14863
258 -> 271 -0.20612
258 -> 274 -0.13484
259 -> 266 0.10689
259 -> 272 -0.15631
259 -> 273 0.24401
260 -> 265 -0.11214
260 -> 274 -0.19450

Excited state symmetry could not be determined.
Excited State 33: Singlet-?Sym 5.3440 eV 232.01 nm f=0.0000 <S**2>=0.000
254 -> 262 0.10314
255 -> 268 -0.18998
256 -> 267 0.18277
257 -> 267 -0.22080
257 -> 272 0.10616
259 -> 263 -0.15904
259 -> 266 -0.17212
259 -> 272 0.13633
260 -> 265 0.17685
260 -> 269 0.17158
260 -> 271 0.25362

Excited state symmetry could not be determined.
Excited State 34: Singlet-?Sym 5.3457 eV 231.93 nm f=0.0822 <S**2>=0.000
252 -> 262 0.10828
253 -> 262 -0.22735
254 -> 261 0.43228
255 -> 263 -0.19316
256 -> 264 -0.14972
258 -> 263 -0.18714
259 -> 265 -0.12101
260 -> 266 0.15607

Excited state symmetry could not be determined.
Excited State 35: Singlet-?Sym 5.3605 eV 231.29 nm f=0.0092 <S**2>=0.000
254 -> 261 0.15048
257 -> 264 -0.10121
257 -> 265 0.14938
257 -> 269 0.11260
259 -> 265 0.36528
260 -> 266 -0.33094
260 -> 270 -0.31483

Excited state symmetry could not be determined.
Excited State 36: Singlet-?Sym 5.3654 eV 231.08 nm f=0.0000 <S**2>=0.000
254 -> 262 -0.20999
256 -> 267 0.10473
256 -> 272 -0.10228
257 -> 267 -0.14150
257 -> 272 -0.12549
258 -> 264 -0.20079
258 -> 271 0.11005
259 -> 266 -0.17367
259 -> 272 -0.11359
260 -> 265 0.20318
260 -> 268 0.22437
260 -> 271 -0.12935
260 -> 274 0.15078
260 -> 275 0.12228

Excited state symmetry could not be determined.
Excited State 37: Singlet-?Sym 5.3690 eV 230.93 nm f=0.0251 <S**2>=0.000
255 -> 262 -0.15285
255 -> 266 0.10701
255 -> 267 -0.13156

256 -> 268 0.15477
257 -> 264 0.14594
258 -> 263 -0.11713
259 -> 261 -0.10388
259 -> 265 0.15987
259 -> 268 0.11688
259 -> 269 0.24868
259 -> 271 0.12802
260 -> 267 -0.19984
260 -> 270 0.20370
260 -> 272 0.10099

Excited state symmetry could not be determined.
Excited State 38: Singlet-?Sym 5.3839 eV 230.29 nm f=0.0000 <S**2>=0.000
252 -> 261 -0.18681
253 -> 261 0.33617
254 -> 262 -0.33374
254 -> 263 -0.12286
255 -> 264 -0.10113
256 -> 262 0.16113
258 -> 264 -0.12471
260 -> 268 -0.13698
260 -> 269 0.10652

Excited state symmetry could not be determined.
Excited State 39: Singlet-?Sym 5.3867 eV 230.17 nm f=0.0364 <S**2>=0.000
255 -> 267 0.16893
256 -> 268 -0.20180
257 -> 265 0.16836
257 -> 268 0.26687
257 -> 269 -0.18443
257 -> 275 0.10011
259 -> 268 0.14742
259 -> 271 -0.10982
260 -> 266 -0.14305
260 -> 267 -0.22066
260 -> 270 0.15667
260 -> 272 -0.12657

Excited state symmetry could not be determined.
Excited State 40: Singlet-?Sym 5.4106 eV 229.15 nm f=0.0000 <S**2>=0.000
253 -> 261 0.15474
254 -> 263 -0.11666

255 -> 265 0.15627
255 -> 269 -0.14159
256 -> 266 -0.22498
256 -> 267 0.11249
257 -> 266 0.22082
258 -> 269 0.25139
259 -> 266 0.27848
259 -> 270 0.12440
260 -> 265 -0.11124

Excited state symmetry could not be determined.
Excited State 41: Singlet-?Sym 5.4160 eV 228.92 nm f=0.0398 <S**2>=0.000
253 -> 262 -0.15437
256 -> 265 0.17085
257 -> 264 0.11846
257 -> 269 -0.23766
258 -> 263 -0.16803
258 -> 266 -0.21410
258 -> 276 0.10945
259 -> 265 0.15180
259 -> 274 0.14230
260 -> 266 -0.14926
260 -> 267 0.24367
260 -> 273 -0.10086
260 -> 277 0.11629

Excited state symmetry could not be determined.
Excited State 42: Singlet-?Sym 5.4203 eV 228.74 nm f=0.0000 <S**2>=0.000
253 -> 261 -0.18126
255 -> 264 -0.14735
256 -> 263 -0.13149
256 -> 266 0.12862
258 -> 265 -0.16083
259 -> 266 0.33775
260 -> 265 -0.20291
260 -> 268 0.20498
260 -> 269 0.20314

Excited state symmetry could not be determined.
Excited State 43: Singlet-?Sym 5.4383 eV 227.98 nm f=0.0062 <S**2>=0.000
252 -> 262 -0.16769
253 -> 262 0.32090
254 -> 264 0.19908

255 -> 263 -0.10301
256 -> 269 0.10710
257 -> 269 -0.18420
259 -> 265 -0.15102
259 -> 268 -0.18221
259 -> 269 0.12735
259 -> 275 -0.11822
260 -> 270 -0.11577

Excited state symmetry could not be determined.
Excited State 44: Singlet-?Sym 5.4514 eV 227.43 nm f=0.0000 <S**2>=0.000
253 -> 261 -0.12411
256 -> 263 -0.13883
258 -> 268 -0.12710
258 -> 269 0.22289
258 -> 275 -0.11950
259 -> 267 0.40639
259 -> 277 0.10109
260 -> 268 -0.18533
260 -> 274 0.11221

Excited state symmetry could not be determined.
Excited State 45: Singlet-?Sym 5.4635 eV 226.93 nm f=0.0000 <S**2>=0.000
252 -> 261 -0.11406
253 -> 261 0.26360
254 -> 262 0.14759
254 -> 263 -0.18139
255 -> 264 0.13709
255 -> 265 -0.11566
256 -> 266 0.19057
256 -> 267 -0.13659
257 -> 266 -0.10447
258 -> 265 -0.15587
258 -> 269 0.13058
259 -> 267 -0.12801
260 -> 268 0.17828
260 -> 269 0.14383

Excited state symmetry could not be determined.
Excited State 46: Singlet-?Sym 5.4664 eV 226.81 nm f=0.0000 <S**2>=0.000
253 -> 261 -0.16510
255 -> 268 0.12601
256 -> 267 -0.20971

257 -> 266 0.21656
258 -> 265 0.21228
258 -> 268 0.19532
258 -> 269 0.17862
259 -> 266 -0.18120
259 -> 267 -0.15582
259 -> 270 0.22325
260 -> 269 0.17291

Excited state symmetry could not be determined.
Excited State 47: Singlet-?Sym 5.4692 eV 226.69 nm f=0.1453 <S**2>=0.000
252 -> 262 0.14185
253 -> 262 -0.21264
254 -> 261 -0.17976
254 -> 264 -0.17103
255 -> 263 0.13862
256 -> 265 -0.18826
257 -> 265 0.16690
258 -> 266 0.29513
258 -> 267 0.18195
259 -> 268 -0.14499
259 -> 275 -0.10559
260 -> 270 -0.12200

Excited state symmetry could not be determined.
Excited State 48: Singlet-?Sym 5.4808 eV 226.22 nm f=0.0000 <S**2>=0.000
252 -> 261 0.15318
254 -> 262 -0.20352
254 -> 263 0.10020
255 -> 261 -0.10308
255 -> 269 -0.11540
256 -> 263 0.33611
257 -> 266 -0.15307
258 -> 264 -0.11066
258 -> 265 -0.22384
258 -> 271 -0.12866
259 -> 270 0.22752
260 -> 268 -0.11203
260 -> 271 0.10016

Excited state symmetry could not be determined.
Excited State 49: Singlet-?Sym 5.4823 eV 226.16 nm f=0.0279 <S**2>=0.000
256 -> 264 0.16792

258 -> 266 0.11615
258 -> 267 -0.10299
259 -> 268 0.36569
259 -> 269 0.12997
260 -> 266 0.10538
260 -> 267 -0.16381
260 -> 270 -0.30978
260 -> 277 0.10501

Excited state symmetry could not be determined.
Excited State 50: Singlet-?Sym 5.4924 eV 225.74 nm f=0.0337 <S**2>=0.000
255 -> 266 -0.14676
255 -> 267 0.18451
256 -> 265 0.17119
256 -> 268 -0.24232
257 -> 269 0.20170
258 -> 267 0.11020
259 -> 265 -0.11120
259 -> 268 0.11951
259 -> 269 0.32589
260 -> 276 0.11793

chair-**4.2a**

Excitation energies and oscillator strengths:

Excited state symmetry could not be determined.
Excited State 1: Singlet-?Sym 4.2989 eV 288.41 nm f=0.1026 <S**2>=0.000
190 ->193 -0.11602
191 ->193 -0.13148
192 ->193 0.64910
This state for optimization and/or second-order correction.
Total Energy, E(TD-HF/TD-DFT) = -4573.24690426
Copying the excited state density for this state as the 1-particle RhoCI density.

Excited state symmetry could not be determined.
Excited State 2: Singlet-?Sym 4.3674 eV 283.89 nm f=0.0144 <S**2>=0.000
190 ->193 0.12068
191 ->193 0.64245
192 ->193 0.14211
192 ->196 -0.10707

Excited state symmetry could not be determined.

Excited State 3: Singlet-?Sym 4.4802 eV 276.74 nm f=0.1106 <S**2>=0.000
190 ->193 0.65718
191 ->193 -0.14041

Excited state symmetry could not be determined.
Excited State 4: Singlet-?Sym 4.5689 eV 271.37 nm f=0.0040 <S**2>=0.000
190 ->194 0.40687
190 ->195 0.11219
191 ->194 0.38166
192 ->194 -0.34316

Excited state symmetry could not be determined.
Excited State 5: Singlet-?Sym 4.6194 eV 268.40 nm f=0.0245 <S**2>=0.000
189 ->193 0.58467
191 ->196 -0.12255
192 ->194 0.18062
192 ->195 -0.16936
192 ->196 0.13384

Excited state symmetry could not be determined.
Excited State 6: Singlet-?Sym 4.6353 eV 267.48 nm f=0.0113 <S**2>=0.000
189 ->193 -0.10601
189 ->194 0.11496
189 ->195 -0.10097
190 ->194 -0.16626
191 ->194 0.40999
191 ->195 -0.30369
191 ->196 -0.14152
191 ->197 0.13611
192 ->194 0.28882

Excited state symmetry could not be determined.
Excited State 7: Singlet-?Sym 4.7650 eV 260.20 nm f=0.0036 <S**2>=0.000
189 ->193 -0.12989
190 ->194 0.42396
191 ->194 -0.10015
192 ->194 0.41466
192 ->196 -0.17199
192 ->198 -0.13607

Excited state symmetry could not be determined.
Excited State 8: Singlet-?Sym 4.8829 eV 253.92 nm f=0.0139 <S**2>=0.000
189 ->194 -0.12923

189 ->195 0.12470
189 ->196 0.11326
190 ->195 -0.17574
190 ->196 -0.13452
191 ->194 0.21507
191 ->195 0.18275
191 ->196 -0.13373
191 ->197 -0.19848
191 ->198 -0.20810
192 ->195 0.25881
192 ->196 0.14542
192 ->197 0.16288
192 ->198 -0.18098

Excited state symmetry could not be determined.
Excited State 9: Singlet-?Sym 4.8978 eV 253.14 nm f=0.0257 <S**2>=0.000
187 ->193 0.13755
188 ->193 -0.16068
189 ->194 0.23964
190 ->194 0.23857
190 ->196 -0.19760
190 ->197 -0.12762
191 ->194 -0.13097
191 ->195 -0.24771
191 ->196 -0.10503
192 ->195 0.15736
192 ->196 0.27055
192 ->198 0.12975

Excited state symmetry could not be determined.
Excited State 10: Singlet-?Sym 4.9313 eV 251.42 nm f=0.0203 <S**2>=0.000
187 ->193 -0.28388
188 ->193 0.20443
189 ->193 0.18023
189 ->194 0.12024
191 ->197 0.13896
192 ->195 0.39376
192 ->196 -0.20578

Excited state symmetry could not be determined.
Excited State 11: Singlet-?Sym 4.9678 eV 249.57 nm f=0.0441 <S**2>=0.000
188 ->193 -0.25322
189 ->196 -0.12063

189 ->197 -0.14489
191 ->194 0.17374
191 ->196 0.30713
191 ->198 -0.18180
191 ->202 0.10725
192 ->196 -0.11207
192 ->197 -0.28135

Excited state symmetry could not be determined.
Excited State 12: Singlet-?Sym 4.9906 eV 248.44 nm f=0.0370 <S**2>=0.000
187 ->193 0.20779
188 ->193 -0.22230
190 ->195 0.17857
190 ->196 0.24575
191 ->197 0.12033
192 ->195 0.29229
192 ->198 -0.26660

Excited state symmetry could not be determined.
Excited State 13: Singlet-?Sym 5.0175 eV 247.10 nm f=0.0195 <S**2>=0.000
189 ->194 0.25879
189 ->196 0.11634
189 ->198 -0.12844
190 ->195 0.10391
190 ->196 0.27521
190 ->197 0.12596
191 ->195 0.22375
191 ->196 -0.15226
192 ->197 -0.11134
192 ->198 0.20018
192 ->201 -0.11446
192 ->202 0.10950

Excited state symmetry could not be determined.
Excited State 14: Singlet-?Sym 5.0276 eV 246.60 nm f=0.0336 <S**2>=0.000
188 ->193 0.33165
189 ->193 -0.11967
189 ->194 0.21209
189 ->195 -0.10001
191 ->195 0.14963
191 ->197 0.13010
192 ->196 0.22776
192 ->197 -0.20719

192 ->198 -0.25530

Excited state symmetry could not be determined.
Excited State 15: Singlet-?Sym 5.0502 eV 245.50 nm f=0.0057 <S**2>=0.000
181 ->193 0.10510
187 ->193 0.14756
188 ->193 -0.12860
189 ->195 -0.10175
190 ->196 -0.22861
190 ->197 -0.19475
191 ->195 0.32958
191 ->196 -0.23224
191 ->197 0.15964
191 ->198 0.13776
192 ->196 -0.13618
192 ->203 0.10306

Excited state symmetry could not be determined.
Excited State 16: Singlet-?Sym 5.0914 eV 243.52 nm f=0.0329 <S**2>=0.000
187 ->193 0.47358
188 ->193 0.35378
188 ->195 0.10041
189 ->193 0.10059
192 ->196 -0.11541
192 ->198 0.20334

Excited state symmetry could not be determined.
Excited State 17: Singlet-?Sym 5.1117 eV 242.55 nm f=0.0597 <S**2>=0.000
186 ->193 -0.13482
187 ->193 -0.12480
189 ->194 0.11822
190 ->195 0.36412
190 ->196 -0.15637
190 ->197 -0.17134
190 ->198 0.16042
191 ->196 0.12392
191 ->197 -0.20712
191 ->198 -0.12022
192 ->197 0.21936

Excited state symmetry could not be determined.
Excited State 18: Singlet-?Sym 5.1507 eV 240.71 nm f=0.0372 <S**2>=0.000
184 ->193 0.10527

186 ->193 0.35379
189 ->195 0.12001
190 ->195 0.10345
190 ->199 -0.18107
191 ->196 -0.11771
191 ->197 -0.16801
191 ->199 -0.12626
191 ->201 -0.11258
192 ->197 -0.17276
192 ->198 -0.12186
192 ->199 0.10200
192 ->203 -0.20298

Excited state symmetry could not be determined.
Excited State 19: Singlet-?Sym 5.1570 eV 240.42 nm f=0.0130 <S**2>=0.000
186 ->193 -0.11656
189 ->194 -0.17390
189 ->198 0.13168
190 ->195 0.18534
191 ->194 0.14309
191 ->197 -0.10889
191 ->198 0.38031
191 ->200 -0.12114
192 ->194 0.14887
192 ->195 0.16792
192 ->196 0.14968
192 ->197 -0.20044
192 ->202 0.11062

Excited state symmetry could not be determined.
Excited State 20: Singlet-?Sym 5.1694 eV 239.84 nm f=0.0347 <S**2>=0.000
186 ->193 0.13826
187 ->193 0.10518
187 ->199 -0.14235
189 ->194 0.21087
190 ->195 -0.14723
190 ->196 0.10203
190 ->197 -0.13579
190 ->199 0.38620
191 ->197 -0.17900
191 ->199 0.13393
192 ->199 -0.14780

Excited state symmetry could not be determined.
Excited State 21: Singlet-?Sym 5.1804 eV 239.33 nm f=0.0025 <S**2>=0.000
189 ->194 0.24374
190 ->195 -0.19339
190 ->199 -0.17365
191 ->194 0.10565
191 ->195 0.12632
191 ->196 0.24585
191 ->198 0.15420
191 ->199 -0.12522
192 ->197 0.21103
192 ->198 0.10252
192 ->199 0.18084
192 ->200 -0.12795
192 ->201 0.18863

Excited state symmetry could not be determined.
Excited State 22: Singlet-?Sym 5.2083 eV 238.05 nm f=0.0232 <S**2>=0.000
186 ->193 0.35838
188 ->194 0.14879
189 ->194 -0.17261
190 ->197 -0.11485
191 ->196 0.14744
191 ->197 0.20263
192 ->194 0.10088
192 ->196 0.24126
192 ->203 0.14519

Excited state symmetry could not be determined.
Excited State 23: Singlet-?Sym 5.2150 eV 237.75 nm f=0.0121 <S**2>=0.000
185 ->195 0.12446
186 ->193 -0.15189
188 ->200 0.19863
189 ->200 -0.10776
190 ->195 -0.13013
191 ->198 0.11530
191 ->199 -0.12430
192 ->196 -0.10687
192 ->198 -0.11595
192 ->199 0.18082
192 ->200 0.29736
192 ->203 0.12241

Excited state symmetry could not be determined.
Excited State 24: Singlet-?Sym 5.2239 eV 237.34 nm f=0.0141 <S**2>=0.000
180 ->194 -0.10259
183 ->194 -0.13276
184 ->196 0.10558
186 ->199 -0.13072
187 ->194 -0.11419
187 ->199 -0.14842
189 ->194 -0.12441
189 ->195 0.11147
189 ->196 -0.11537
189 ->199 0.19232
190 ->199 0.10627
191 ->196 -0.17216
191 ->197 0.10108
191 ->199 -0.13742
191 ->201 -0.15409
192 ->199 0.21307
192 ->201 0.15507

Excited state symmetry could not be determined.
Excited State 25: Singlet-?Sym 5.2349 eV 236.84 nm f=0.0218 <S**2>=0.000
181 ->193 0.12319
183 ->193 -0.11494
186 ->197 -0.12011
189 ->195 0.14207
189 ->199 -0.15523
190 ->196 0.23884
190 ->197 -0.10730
191 ->196 -0.13012
191 ->197 -0.10156
191 ->199 0.11553
191 ->201 -0.19847
192 ->199 -0.18149
192 ->201 0.18030

Excited state symmetry could not be determined.
Excited State 26: Singlet-?Sym 5.2456 eV 236.36 nm f=0.0141 <S**2>=0.000
181 ->193 -0.11900
186 ->193 -0.13612
189 ->194 0.11019
189 ->195 0.29098
189 ->196 -0.11103

189 ->198 0.12952
191 ->195 0.13945
191 ->197 0.19374
191 ->200 -0.10622
191 ->203 0.14864
192 ->198 0.11480
192 ->202 -0.16622
192 ->203 -0.17291

Excited state symmetry could not be determined.
Excited State 27: Singlet-?Sym 5.2801 eV 234.81 nm f=0.0039 <S**2>=0.000
185 ->193 -0.11909
186 ->193 0.14966
189 ->197 -0.17898
190 ->195 0.20021
190 ->196 -0.12735
190 ->197 0.31526
190 ->199 0.12804
191 ->200 0.23287
192 ->198 0.10683
192 ->201 0.15548
192 ->202 -0.14802
192 ->204 -0.15743

Excited state symmetry could not be determined.
Excited State 28: Singlet-?Sym 5.2898 eV 234.38 nm f=0.1065 <S**2>=0.000
186 ->193 -0.11382
186 ->194 0.10055
187 ->194 -0.29946
188 ->194 0.39418
189 ->196 0.13229
189 ->197 -0.12986
190 ->197 0.13353
191 ->198 0.12158
191 ->203 -0.11000
192 ->200 -0.11498

Excited state symmetry could not be determined.
Excited State 29: Singlet-?Sym 5.2999 eV 233.94 nm f=0.0047 <S**2>=0.000
186 ->193 -0.12333
189 ->200 0.20040
189 ->202 -0.10642
190 ->200 -0.14441

191 ->198 0.11143
191 ->200 0.43607
191 ->202 -0.20335
191 ->203 0.10749
192 ->200 0.12066

Excited state symmetry could not be determined.
Excited State 30: Singlet-?Sym 5.3041 eV 233.75 nm f=0.0044 <S**2>=0.000
184 ->193 0.21605
185 ->193 0.28005
189 ->196 -0.10697
190 ->196 -0.14246
190 ->197 0.27284
191 ->197 0.11764
191 ->202 -0.11509
192 ->198 -0.16789
192 ->202 0.16998
192 ->203 0.13426

Excited state symmetry could not be determined.
Excited State 31: Singlet-?Sym 5.3397 eV 232.19 nm f=0.0098 <S**2>=0.000
183 ->193 0.14685
184 ->193 0.22992
185 ->193 0.35145
187 ->194 0.10335
189 ->197 -0.11581
190 ->196 0.14493
190 ->198 -0.15992
190 ->203 0.13746
191 ->202 0.16638
192 ->196 0.10154
192 ->202 -0.13675

Excited state symmetry could not be determined.
Excited State 32: Singlet-?Sym 5.3621 eV 231.22 nm f=0.0099 <S**2>=0.000
188 ->194 -0.11168
189 ->196 0.20835
189 ->197 0.18706
189 ->201 0.14103
189 ->203 0.13722
190 ->197 0.11489
190 ->198 -0.12711
190 ->199 0.10080

191 ->196 0.15096
191 ->201 -0.16538
192 ->204 0.25360

Excited state symmetry could not be determined.
Excited State 33: Singlet-?Sym 5.3698 eV 230.89 nm f=0.0154 <S**2>=0.000
183 ->193 0.16446
188 ->194 -0.19638
189 ->195 0.24404
189 ->196 0.25732
189 ->197 -0.13606
190 ->197 -0.10239
190 ->198 0.24583
190 ->202 -0.14177
191 ->197 0.13420
191 ->198 0.18191

Excited state symmetry could not be determined.
Excited State 34: Singlet-?Sym 5.3773 eV 230.57 nm f=0.0192 <S**2>=0.000
180 ->193 -0.16097
183 ->193 0.35276
184 ->193 -0.11266
185 ->193 0.14467
190 ->201 -0.12124
191 ->198 -0.10075
191 ->201 -0.10229
192 ->201 0.33071

Excited state symmetry could not be determined.
Excited State 35: Singlet-?Sym 5.4175 eV 228.86 nm f=0.0146 <S**2>=0.000
188 ->194 0.14235
189 ->195 0.25210
189 ->196 0.17015
189 ->197 0.13638
190 ->198 -0.14833
190 ->201 0.11115
190 ->202 0.12348
190 ->203 0.12276
191 ->201 0.24637
191 ->204 -0.12825
192 ->196 -0.12266
192 ->198 -0.13772
192 ->203 -0.10871

Excited state symmetry could not be determined.
Excited State 36: Singlet-?Sym 5.4271 eV 228.45 nm f=0.0155 <S**2>=0.000
181 ->193 -0.15727
183 ->193 -0.12670
184 ->193 0.13445
186 ->194 -0.12010
187 ->194 0.29223
188 ->194 0.12147
188 ->195 -0.10698
189 ->196 0.15986
190 ->197 -0.11990
190 ->201 -0.15704
191 ->202 -0.15011
191 ->203 -0.13683
192 ->200 -0.23159
192 ->205 0.12194

Excited state symmetry could not be determined.
Excited State 37: Singlet-?Sym 5.4409 eV 227.88 nm f=0.0990 <S**2>=0.000
181 ->193 0.13559
183 ->193 0.13299
184 ->193 -0.10990
186 ->194 0.12533
187 ->194 0.35688
188 ->194 0.11035
188 ->195 -0.14261
189 ->196 -0.17378
190 ->197 0.10964
190 ->198 0.22260
190 ->201 0.15764
192 ->203 -0.14450

Excited state symmetry could not be determined.
Excited State 38: Singlet-?Sym 5.4484 eV 227.56 nm f=0.0374 <S**2>=0.000
182 ->193 0.10542
184 ->193 0.17647
186 ->194 0.12921
189 ->195 -0.16854
189 ->196 0.17447
190 ->198 0.16154
190 ->202 -0.14260
191 ->201 0.26385

192 ->201 0.12711
192 ->204 -0.21446

Excited state symmetry could not be determined.
Excited State 39: Singlet-?Sym 5.4801 eV 226.24 nm f=0.0067 <S**2>=0.000
182 ->193 0.15727
188 ->194 0.15075
188 ->198 0.12472
190 ->198 -0.10490
190 ->199 0.10894
191 ->197 0.10221
191 ->200 0.10079
191 ->202 0.18339
191 ->203 0.12962
191 ->205 -0.16246
192 ->201 -0.10141
192 ->202 0.35349

Excited state symmetry could not be determined.
Excited State 40: Singlet-?Sym 5.4850 eV 226.04 nm f=0.0039 <S**2>=0.000
186 ->194 0.20531
186 ->199 0.15976
187 ->199 0.15533
190 ->198 0.13118
190 ->199 0.33400
191 ->199 -0.26420
192 ->199 0.13148
192 ->202 -0.17334

Excited state symmetry could not be determined.
Excited State 41: Singlet-?Sym 5.4958 eV 225.60 nm f=0.0333 <S**2>=0.000
184 ->193 0.10850
187 ->194 0.14053
189 ->195 -0.10677
189 ->196 0.15849
190 ->198 0.12919
190 ->201 -0.12933
190 ->202 0.10829
190 ->205 0.10892
191 ->198 0.10667
191 ->201 -0.10845
191 ->202 0.32994
192 ->200 0.18459

192 ->202 -0.12752
192 ->205 -0.11155

Excited state symmetry could not be determined.
Excited State 42: Singlet-?Sym 5.5170 eV 224.73 nm f=0.0105 <S**2>=0.000
186 ->194 0.29513
189 ->195 0.10485
189 ->197 0.15549
191 ->197 -0.10592
191 ->199 0.18752
191 ->203 0.22824
192 ->197 -0.15500
192 ->200 -0.24967
192 ->203 0.16860

Excited state symmetry could not be determined.
Excited State 43: Singlet-?Sym 5.5230 eV 224.49 nm f=0.0299 <S**2>=0.000
186 ->194 0.35869
187 ->195 0.11435
189 ->195 0.12461
189 ->197 -0.16704
190 ->198 -0.19411
190 ->199 -0.12445
191 ->203 -0.20670
192 ->200 0.18396

Excited state symmetry could not be determined.
Excited State 44: Singlet-?Sym 5.5281 eV 224.28 nm f=0.0008 <S**2>=0.000
189 ->197 -0.11788
189 ->198 0.12042
191 ->197 -0.11762
191 ->200 -0.22659
191 ->202 -0.13090
191 ->203 0.25419
192 ->197 -0.11206
192 ->200 0.20654
192 ->203 0.23058

Excited state symmetry could not be determined.
Excited State 45: Singlet-?Sym 5.5500 eV 223.40 nm f=0.0241 <S**2>=0.000
182 ->193 0.13392
186 ->194 -0.16412
188 ->195 -0.12429

188 ->198 0.13732
189 ->195 0.10722
189 ->196 -0.12759
189 ->197 0.15874
189 ->203 0.10984
190 ->198 0.14715
190 ->201 0.23139
190 ->202 0.15416
191 ->199 0.11739
192 ->202 -0.10000
192 ->203 0.23549

Excited state symmetry could not be determined.
Excited State 46: Singlet-?Sym 5.5665 eV 222.73 nm f=0.0085 <S**2>=0.000
189 ->198 0.10006
190 ->199 0.10464
190 ->201 -0.15895
190 ->203 -0.16702
191 ->199 0.35414
191 ->203 -0.15785
192 ->199 0.36967

Excited state symmetry could not be determined.
Excited State 47: Singlet-?Sym 5.5732 eV 222.46 nm f=0.0273 <S**2>=0.000
181 ->193 -0.10145
189 ->197 -0.17937
189 ->198 -0.17890
190 ->200 -0.18510
190 ->201 0.13694
190 ->203 0.28397
191 ->199 0.26332
191 ->202 -0.10944
192 ->199 0.20160
192 ->203 -0.13807
192 ->204 0.14358

Excited state symmetry could not be determined.
Excited State 48: Singlet-?Sym 5.5792 eV 222.23 nm f=0.0034 <S**2>=0.000
179 ->193 0.10828
182 ->193 0.18621
183 ->193 -0.27966
184 ->193 -0.36371
185 ->193 0.40053

188 ->195 -0.13274

Excited state symmetry could not be determined.
Excited State 49: Singlet-?Sym 5.5971 eV 221.51 nm f=0.0265 <S**2>=0.000
188 ->194 0.15835
188 ->195 0.24572
189 ->201 -0.15216
190 ->200 0.14193
190 ->201 0.14025
191 ->199 0.14923
191 ->201 -0.21094
191 ->204 0.27627
192 ->204 -0.20140

Excited state symmetry could not be determined.
Excited State 50: Singlet-?Sym 5.6100 eV 221.01 nm f=0.0292 <S**2>=0.000
182 ->193 0.10838
184 ->193 -0.10589
184 ->194 -0.11470
185 ->194 -0.12623
187 ->194 0.10511
187 ->195 -0.10297
188 ->194 0.17351
188 ->195 0.38484
189 ->196 -0.15012
189 ->203 0.11698
191 ->201 0.17554
191 ->204 -0.13042
192 ->202 -0.14952
192 ->204 0.10020

twist-**4.2a**

Excitation energies and oscillator strengths:

Excited state symmetry could not be determined.
Excited State 1: Singlet-?Sym 4.3867 eV 282.63 nm f=0.1551 <S**2>=0.000
192 ->193 0.67863
This state for optimization and/or second-order correction.
Total Energy, E(TD-HF/TD-DFT) = -4573.24900076
Copying the excited state density for this state as the 1-particle RhoCI density.

Excited state symmetry could not be determined.
Excited State 2: Singlet-?Sym 4.5264 eV 273.92 nm f=0.0563 <S**2>=0.000
189 ->193 -0.15647
191 ->193 0.24026
192 ->194 0.61046

Excited state symmetry could not be determined.
Excited State 3: Singlet-?Sym 4.6082 eV 269.05 nm f=0.0900 <S**2>=0.000
189 ->193 0.19344
191 ->193 0.60675
192 ->194 -0.19281
192 ->196 0.12708

Excited state symmetry could not be determined.
Excited State 4: Singlet-?Sym 4.6344 eV 267.53 nm f=0.0422 <S**2>=0.000
190 ->193 0.45442
190 ->195 0.13697
191 ->194 0.46464
191 ->196 0.10444

Excited state symmetry could not be determined.
Excited State 5: Singlet-?Sym 4.6839 eV 264.70 nm f=0.0026 <S**2>=0.000
189 ->193 0.46941
189 ->195 0.10013
190 ->194 -0.40146
191 ->193 -0.10559
191 ->195 -0.11771
192 ->194 0.13826
192 ->197 0.10653

Excited state symmetry could not be determined.
Excited State 6: Singlet-?Sym 4.6944 eV 264.11 nm f=0.0572 <S**2>=0.000
189 ->194 0.19298
190 ->193 0.45696
190 ->195 -0.13848
191 ->194 -0.43668

Excited state symmetry could not be determined.
Excited State 7: Singlet-?Sym 4.7472 eV 261.17 nm f=0.0355 <S**2>=0.000
189 ->193 0.36314
190 ->194 0.49020
191 ->193 -0.12333
191 ->195 0.17165

192 ->194 0.17316

Excited state symmetry could not be determined.
Excited State 8: Singlet-?Sym 4.8154 eV 257.47 nm f=0.0343 <S**2>=0.000
189 ->194 0.50046
190 ->193 -0.15638
190 ->195 -0.11097
191 ->194 0.12011
192 ->195 0.35075
192 ->199 0.17314

Excited state symmetry could not be determined.
Excited State 9: Singlet-?Sym 4.9941 eV 248.26 nm f=0.0015 <S**2>=0.000
187 ->193 0.13644
189 ->199 -0.10925
190 ->196 0.11460
190 ->197 0.20526
190 ->200 -0.17074
191 ->198 0.28679
191 ->199 -0.12990
192 ->196 0.34861
192 ->200 -0.17665

Excited state symmetry could not be determined.
Excited State 10: Singlet-?Sym 5.0041 eV 247.77 nm f=0.0176 <S**2>=0.000
182 ->195 0.11891
188 ->193 -0.18546
189 ->197 -0.12477
190 ->193 -0.12316
190 ->198 0.27436
190 ->201 -0.10638
191 ->196 0.25363
191 ->197 0.18813
191 ->200 -0.24489
192 ->198 0.17536
192 ->199 -0.16200

Excited state symmetry could not be determined.
Excited State 11: Singlet-?Sym 5.0129 eV 247.33 nm f=0.0020 <S**2>=0.000
185 ->194 0.10060
189 ->193 -0.13046
189 ->199 0.20070
190 ->196 0.14739

190 ->200 -0.11917
191 ->198 0.13763
191 ->201 -0.12218
192 ->197 0.42268
192 ->200 0.17442
192 ->202 -0.14227

Excited state symmetry could not be determined.
Excited State 12: Singlet-?Sym 5.0463 eV 245.69 nm f=0.0226 <S**2>=0.000
188 ->193 -0.16308
189 ->194 -0.18392
189 ->196 -0.11019
189 ->197 0.14760
189 ->200 0.19335
190 ->195 0.12336
190 ->199 -0.13171
191 ->194 -0.10842
191 ->196 0.14793
192 ->198 -0.17624
192 ->199 0.33975
192 ->201 -0.22351

Excited state symmetry could not be determined.
Excited State 13: Singlet-?Sym 5.0578 eV 245.14 nm f=0.0014 <S**2>=0.000
188 ->194 0.57587
188 ->202 0.11495
189 ->195 0.11039
190 ->196 -0.11346
190 ->197 0.11113
191 ->195 -0.21865
191 ->198 0.10493

Excited state symmetry could not be determined.
Excited State 14: Singlet-?Sym 5.0710 eV 244.49 nm f=0.0593 <S**2>=0.000
188 ->193 0.44284
190 ->198 0.13255
191 ->197 0.21999
192 ->195 -0.28855
192 ->198 0.15147
192 ->199 0.10093
192 ->201 -0.10113
192 ->203 0.13598

Excited state symmetry could not be determined.
Excited State 15: Singlet-?Sym 5.0849 eV 243.83 nm f=0.0260 <S**2>=0.000
189 ->193 -0.14867
189 ->201 -0.12531
190 ->196 -0.19681
191 ->198 -0.15569
192 ->196 0.51947
192 ->200 0.19781

Excited state symmetry could not be determined.
Excited State 16: Singlet-?Sym 5.0883 eV 243.66 nm f=0.0830 <S**2>=0.000
188 ->193 0.42866
189 ->194 -0.19733
190 ->195 0.13462
191 ->194 -0.10971
191 ->196 0.16431
191 ->197 -0.11114
192 ->195 0.38021

Excited state symmetry could not be determined.
Excited State 17: Singlet-?Sym 5.1183 eV 242.24 nm f=0.0254 <S**2>=0.000
189 ->194 0.28167
189 ->196 -0.10895
189 ->202 0.10657
190 ->195 0.26593
190 ->198 -0.10321
190 ->199 -0.16422
191 ->196 0.29109
191 ->197 -0.22895
192 ->195 -0.27122

Excited state symmetry could not be determined.
Excited State 18: Singlet-?Sym 5.1230 eV 242.01 nm f=0.0078 <S**2>=0.000
188 ->194 0.30029
190 ->194 -0.20158
190 ->196 0.24023
190 ->197 -0.18722
190 ->202 -0.11668
191 ->195 0.32524
191 ->198 -0.12500
191 ->199 -0.16525
192 ->197 -0.16309

Excited state symmetry could not be determined.
Excited State 19: Singlet-?Sym 5.1490 eV 240.79 nm f=0.0140 <S**2>=0.000
188 ->193 -0.16373
189 ->197 0.21712
189 ->200 -0.15969
190 ->198 -0.20630
192 ->198 0.47863
192 ->199 0.10639
192 ->203 0.20153

Excited state symmetry could not be determined.
Excited State 20: Singlet-?Sym 5.1703 eV 239.80 nm f=0.0437 <S**2>=0.000
189 ->198 -0.28850
190 ->197 0.17385
190 ->200 -0.14920
191 ->195 -0.10593
192 ->197 -0.28603
192 ->200 0.42449
192 ->205 -0.14591

Excited state symmetry could not be determined.
Excited State 21: Singlet-?Sym 5.2074 eV 238.09 nm f=0.0365 <S**2>=0.000
184 ->193 0.10527
187 ->193 0.63361
191 ->198 -0.10457

Excited state symmetry could not be determined.
Excited State 22: Singlet-?Sym 5.2379 eV 236.71 nm f=0.0155 <S**2>=0.000
189 ->196 0.33044
191 ->196 0.18968
191 ->200 0.13306
192 ->195 0.10139
192 ->199 -0.31786
192 ->201 -0.27289
192 ->203 0.20933

Excited state symmetry could not be determined.
Excited State 23: Singlet-?Sym 5.2622 eV 235.61 nm f=0.0492 <S**2>=0.000
185 ->194 0.15262
187 ->193 -0.11605
189 ->195 0.42188
190 ->197 0.12006
191 ->195 0.23731

191 ->199 0.14112
192 ->197 -0.22543
192 ->202 -0.20084

Excited state symmetry could not be determined.
Excited State 24: Singlet-?Sym 5.2896 eV 234.39 nm f=0.0099 <S**2>=0.000
187 ->194 0.10208
189 ->195 -0.16772
189 ->199 -0.13541
190 ->194 -0.11705
190 ->195 0.15004
190 ->196 -0.33160
191 ->195 0.36761
191 ->196 -0.11436
191 ->199 0.21926
192 ->197 0.10563

Excited state symmetry could not be determined.
Excited State 25: Singlet-?Sym 5.2899 eV 234.38 nm f=0.0526 <S**2>=0.000
184 ->194 0.11998
187 ->194 0.62082
188 ->195 -0.11943

Excited state symmetry could not be determined.
Excited State 26: Singlet-?Sym 5.3003 eV 233.92 nm f=0.0291 <S**2>=0.000
189 ->196 0.12928
190 ->195 0.44808
190 ->196 0.13799
190 ->199 0.15826
191 ->196 -0.31211
191 ->200 -0.11504

Excited state symmetry could not be determined.
Excited State 27: Singlet-?Sym 5.3775 eV 230.56 nm f=0.0055 <S**2>=0.000
189 ->197 -0.13188
189 ->200 -0.13752
190 ->195 0.16912
190 ->198 -0.15467
190 ->199 0.24829
190 ->201 -0.17698
191 ->196 0.17300
191 ->197 0.33826
191 ->200 0.26785

Excited state symmetry could not be determined.
Excited State 28: Singlet-?Sym 5.3903 eV 230.01 nm f=0.0155 <S**2>=0.000
189 ->195 -0.14364
189 ->201 0.11013
190 ->196 0.25253
190 ->197 0.26838
190 ->200 0.21406
191 ->198 -0.20591
191 ->199 0.24351
191 ->201 -0.25309
191 ->203 -0.11285

Excited state symmetry could not be determined.
Excited State 29: Singlet-?Sym 5.4107 eV 229.15 nm f=0.0102 <S**2>=0.000
180 ->193 -0.16306
185 ->193 0.30919
186 ->193 -0.30756
189 ->196 0.20655
190 ->201 0.13326
190 ->203 0.10177
191 ->197 0.13328
191 ->205 0.14322
192 ->199 0.10109
192 ->201 0.22351

Excited state symmetry could not be determined.
Excited State 30: Singlet-?Sym 5.4276 eV 228.43 nm f=0.0073 <S**2>=0.000
180 ->194 -0.10159
183 ->193 -0.10833
189 ->195 0.18536
189 ->203 -0.21071
192 ->197 0.21374
192 ->202 0.41563
192 ->204 -0.19298

Excited state symmetry could not be determined.
Excited State 31: Singlet-?Sym 5.4305 eV 228.31 nm f=0.0098 <S**2>=0.000
185 ->193 -0.19094
189 ->196 -0.26932
190 ->198 0.15256
190 ->199 -0.10637
191 ->196 -0.11321

191 ->197 0.11270
191 ->205 0.12840
192 ->198 -0.11934
192 ->199 -0.21504
192 ->201 0.18126
192 ->203 0.27517

Excited state symmetry could not be determined.
Excited State 32: Singlet-?Sym 5.4591 eV 227.11 nm f=0.0403 <S**2>=0.000
184 ->193 0.23532
186 ->197 -0.12308
187 ->198 -0.10522
188 ->197 0.12241
190 ->196 0.12525
190 ->197 0.20130
190 ->200 0.13993
190 ->204 -0.11910
190 ->205 0.13258
191 ->198 0.19950
191 ->201 0.19064
191 ->203 0.19903
191 ->206 0.15663
192 ->205 0.15814

Excited state symmetry could not be determined.
Excited State 33: Singlet-?Sym 5.4829 eV 226.13 nm f=0.0372 <S**2>=0.000
180 ->193 -0.20956
185 ->193 0.35780
186 ->193 0.31180
189 ->202 -0.10137
191 ->202 -0.10269
192 ->198 -0.18309
192 ->201 0.11967
192 ->203 0.25244
192 ->206 -0.14640

Excited state symmetry could not be determined.
Excited State 34: Singlet-?Sym 5.4967 eV 225.56 nm f=0.0251 <S**2>=0.000
185 ->193 -0.11760
186 ->193 0.42415
189 ->196 0.16778
190 ->201 0.18695
191 ->196 0.15557

191 ->200 0.10693
191 ->205 0.12349
192 ->199 0.19883

Excited state symmetry could not be determined.
Excited State 35: Singlet-?Sym 5.5008 eV 225.39 nm f=0.0066 <S**2>=0.000
181 ->193 0.16990
184 ->193 0.36911
185 ->194 0.23441
186 ->194 -0.13952
189 ->195 -0.12880
190 ->196 -0.11124
190 ->197 -0.17301
190 ->200 -0.10123
190 ->205 -0.11806
191 ->201 -0.14137
192 ->197 -0.12323
192 ->202 0.17000

Excited state symmetry could not be determined.
Excited State 36: Singlet-?Sym 5.5141 eV 224.85 nm f=0.0077 <S**2>=0.000
185 ->193 -0.18408
186 ->193 -0.14600
189 ->196 0.21678
189 ->197 -0.10742
189 ->205 0.12502
190 ->199 0.11899
190 ->203 -0.14234
191 ->196 0.10824
191 ->197 -0.15247
191 ->200 -0.22001
191 ->204 0.10066
192 ->198 -0.14703
192 ->199 0.20785
192 ->201 0.24171
192 ->203 0.21808

Excited state symmetry could not be determined.
Excited State 37: Singlet-?Sym 5.5214 eV 224.55 nm f=0.0014 <S**2>=0.000
180 ->194 -0.13312
184 ->193 -0.14040
185 ->194 0.17213
189 ->195 0.13550

189 ->198 0.14873
189 ->199 -0.18659
189 ->201 0.13260
189 ->203 0.14753
191 ->195 0.11535
191 ->199 -0.20565
192 ->200 0.32797
192 ->204 0.19708
192 ->205 0.14383

Excited state symmetry could not be determined.
Excited State 38: Singlet-?Sym 5.5529 eV 223.28 nm f=0.0017 <S**2>=0.000
180 ->194 0.14074
185 ->194 -0.23106
186 ->194 0.34694
187 ->195 0.10963
189 ->195 0.14974
189 ->198 0.14839
189 ->199 0.11071
190 ->197 -0.16011
191 ->198 0.22704
191 ->199 0.21006
192 ->197 -0.10879
192 ->202 0.10680

Excited state symmetry could not be determined.
Excited State 39: Singlet-?Sym 5.5605 eV 222.97 nm f=0.0136 <S**2>=0.000
184 ->193 0.11562
185 ->193 -0.10430
185 ->194 -0.13406
189 ->197 0.30593
190 ->198 -0.16041
190 ->199 -0.11433
191 ->197 0.26587
191 ->199 -0.14159
191 ->200 -0.22517
192 ->198 -0.11757
192 ->203 -0.13991

Excited state symmetry could not be determined.
Excited State 40: Singlet-?Sym 5.5626 eV 222.89 nm f=0.0187 <S**2>=0.000
180 ->194 -0.14133
184 ->193 -0.19759

185 ->194 0.22980
189 ->195 -0.10999
189 ->197 0.16298
190 ->196 0.15455
190 ->197 -0.19128
191 ->197 0.12096
191 ->199 0.32355
191 ->200 -0.11766
191 ->201 0.15405
191 ->203 -0.10302

Excited state symmetry could not be determined.
Excited State 41: Singlet-?Sym 5.5737 eV 222.44 nm f=0.0153 <S**2>=0.000
180 ->194 -0.13133
183 ->193 -0.13095
184 ->193 0.10899
185 ->194 0.10499
186 ->194 0.22609
188 ->196 0.32423
188 ->200 -0.11855
190 ->200 -0.30490
190 ->202 -0.12862
190 ->204 0.11193
191 ->206 -0.11677

Excited state symmetry could not be determined.
Excited State 42: Singlet-?Sym 5.5836 eV 222.05 nm f=0.0048 <S**2>=0.000
181 ->194 0.10816
187 ->196 0.10728
188 ->195 -0.17497
189 ->196 0.10473
189 ->197 0.21350
189 ->200 0.20411
190 ->203 -0.10677
191 ->200 0.25926
191 ->202 0.19777
192 ->201 0.30023

Excited state symmetry could not be determined.
Excited State 43: Singlet-?Sym 5.5930 eV 221.68 nm f=0.0173 <S**2>=0.000
184 ->194 -0.17893
187 ->194 0.11501
188 ->195 0.14703

189 ->197 0.12309
189 ->200 -0.23452
189 ->202 -0.17449
190 ->201 0.17263
190 ->203 -0.13240
190 ->206 0.17878
191 ->202 0.28041
191 ->204 -0.16829
192 ->198 -0.13144

Excited state symmetry could not be determined.
Excited State 44: Singlet-?Sym 5.6018 eV 221.33 nm f=0.0006 <S**2>=0.000
185 ->194 0.19592
186 ->194 0.38926
187 ->195 0.14571
188 ->196 -0.23890
188 ->200 0.10322
189 ->195 -0.15741
189 ->199 0.15067
190 ->197 0.13603
190 ->204 -0.10085
191 ->198 -0.20368

Excited state symmetry could not be determined.
Excited State 45: Singlet-?Sym 5.6054 eV 221.19 nm f=0.0046 <S**2>=0.000
187 ->194 0.11880
188 ->195 0.48364
189 ->196 0.14318
190 ->199 -0.29480
191 ->200 0.20003

Excited state symmetry could not be determined.
Excited State 46: Singlet-?Sym 5.6160 eV 220.77 nm f=0.0694 <S**2>=0.000
181 ->194 0.15825
182 ->193 0.12286
183 ->194 -0.10845
184 ->194 0.32055
186 ->193 0.13476
188 ->195 0.33940
189 ->197 0.10907
190 ->195 -0.12189
190 ->199 0.21260
191 ->196 0.10738

191 ->200 -0.12217

Excited state symmetry could not be determined.
Excited State 47: Singlet-?Sym 5.6197 eV 220.62 nm f=0.0277 <S**2>=0.000
181 ->193 -0.15495
183 ->193 0.13711
184 ->193 -0.16471
185 ->194 0.18643
188 ->197 0.10189
189 ->198 0.11077
189 ->199 0.23738
190 ->202 -0.23112
191 ->198 0.10575
191 ->201 -0.12680
191 ->203 0.20913
192 ->202 0.21422
192 ->204 0.10109

Excited state symmetry could not be determined.
Excited State 48: Singlet-?Sym 5.6312 eV 220.17 nm f=0.0057 <S**2>=0.000
189 ->195 0.15370
189 ->198 -0.11011
189 ->201 -0.26238
190 ->202 0.15274
190 ->204 -0.13008
191 ->198 -0.11743
192 ->200 -0.11525
192 ->202 0.22895
192 ->204 0.40839

Excited state symmetry could not be determined.
Excited State 49: Singlet-?Sym 5.6340 eV 220.06 nm f=0.0034 <S**2>=0.000
181 ->194 -0.15927
184 ->194 -0.21446
188 ->198 0.11122
189 ->196 -0.19216
189 ->197 0.20393
189 ->200 0.20118
190 ->198 0.18103
190 ->199 0.28039
191 ->204 0.21129

Excited state symmetry could not be determined.

Excited State 50: Singlet-?Sym 5.6448 eV 219.64 nm f=0.0302 <S**2>=0.000

180 ->193	0.11207
184 ->194	0.22454
185 ->195	-0.10798
186 ->194	0.10315
188 ->196	0.14516
189 ->201	-0.10362
190 ->199	-0.10986
190 ->200	0.19370
190 ->203	-0.13741
191 ->198	0.13245
191 ->202	0.28922
191 ->204	0.15357
192 ->205	-0.13395

7.6 Impact of stereoregularity on hybrid conjugated polymers

Isolation of *trans*-6.1 and *cis*-6.1

In a scintillation vial, 0.500 g of **6.1** (dr 63:37 *trans:cis*) was dissolved in 2 mL of DCM and layered with 18 mL of dry methanol. The solution was allowed to sit overnight in a glove box and colorless crystals were found at the bottom. The mixture was filtered through a fritted funnel, washed with 5 mL of dry methanol and dried under vacuum. *trans*-**6.1** (dr 90:10 *trans:cis*) (0.270 g) was collected as a colorless crystal. The filtrate was collected and dried under vacuum, yielding a white powder *cis*-**6.1** (dr 20:80 *trans:cis*) (0.178 g).

Synthesis of 6.2

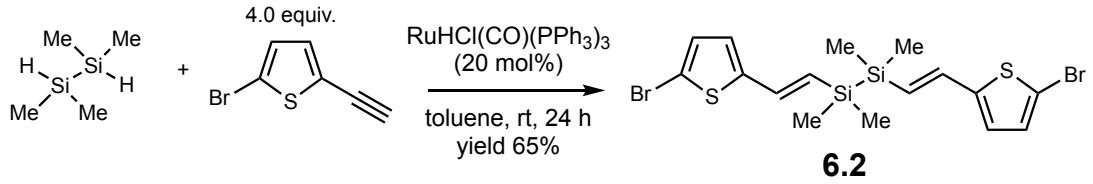

In a glove box, an oven-dried 2-dram vial with stir bar was charged with 1,1,2,2-tetramethyldisilane (1.0 equiv., 0.845 mmol, 0.100 g) and $RuHCl(CO)(PPh_3)_3$ (0.2 equiv., 0.1.69 mmol, 0.161 g). Toluene (2.5 mL) was added to dissolve the reagents. 2-bromo-5-ethynylthiophene (4 equiv., 3.38 mmol, 0.632 g) was diluted by 1 mL of toluene in a 1-dram vial and added dropwise into the reaction mixture by pipette. The vial was rinsed by 0.5 mL of toluene and the solution was added to the reaction as well. After the addition was complete, the reaction mixture turned dark red and was stirred for 24 hours at room temperature. The solution was concentrated under vacuum, transferred to a silica gel cartridge, and then dried on it under vacuum. The cartridge was subjected to automated

column chromatography with 100% hexanes to yield **6.2** as a pale-yellow oil (0.272 g, 65%).

Tabulated Characterization Data for ***6.2***

δ_H (400 MHz, $CDCl_3$)	6.93 (d, J = 3.8 Hz, 2H, thienyl), 6.78 (d, J = 18.7 Hz, 2H, vinyl), 6.68 (J = 3.8 Hz, 2H, thienyl), 6.14 (d, J = 18.7, 2H, vinyl), 0.22 (s, 12H, -CH_3).
δ_C (101 MHz, $CDCl_3$)	147.02 (vinyl), 136.01 (thienyl), 130.50 (thienyl), 128.67 (thienyl), 125.64 (thienyl), 111.92 (vinyl), -3.99 (-CH$_3$).
δ_{Si} (79 MHz, $CDCl_3$)	-23.80 (SiMe$_2$)

Synthesis of 6.3

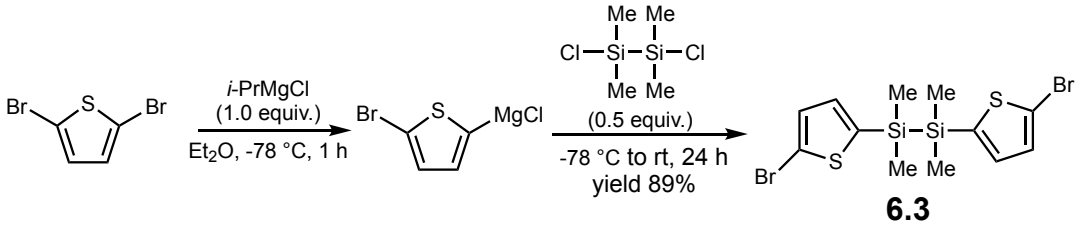

6.3

The procedure was adapted for literature.[7] On the Schlenk line, an oven-dried 100 mL Schlenk flask with a stir bar was charged with 2,5-dibromothiophene (1.0 equiv., 8.27 mmol, 2.00 g). Diethyl ether (50 mL) was added and the solution was cooled to -78 °C in an acetone/dry ice bath. With syringe pump, *i*-PrMgCl (2 M in THF, 4.13 mL) was slowly added in 30 minutes, and the reaction mixture was stirred for another 30 minutes. White precipitates were overserved during the addition. 1,2-dichloro-1,1,2,2-tetramethyldisilane (0.5 equiv., 4.13 mmol, 0.774 g) was then added through syringe. The reaction mixture was allowed to warm up to room temperature and stirred for 24 hours. The reaction was quenched with 50 mL of DI water. The aqueous layer was separated with the organic layer and washed with diethyl ether (50 mL x 3). All the organic layers were combined, dried over anhydrous magnesium sulfate, concentrated under vacuum and purified by silica column with 100 % hexanes. A white solid was isolated as **6.3** (3.25 g, 89%). NMR spectra were consistent with the literature.

General procedure of Kumada polycondensation using di(bromothienyl)silane and aryl dibromide building blocks

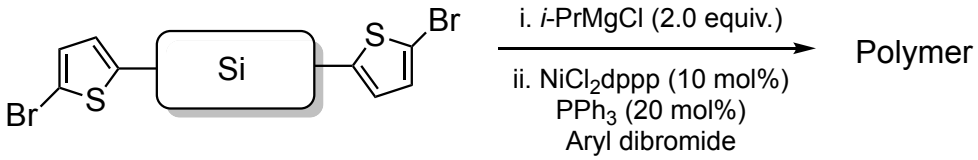

In a glove box, an oven-dried 2-dram vial with stir bar was charged with di(bromothienyl)silane (1.0 equiv) and THF (2 mL). *i*-PrMgCl (2.0 M in THF, 2.0 equiv.) was added by micro syringe. The solution was stirred at room temperature for 30 minutes, yielding a di-Grignard intermediate. NidpppCl_2 (0.1 equiv.), triphenylphosphine (0.2 equiv) and aryl dibromide (1.5 equiv.) were weighed in a 2-dram vial with stir bar and dissolved in THF. The di-Grignard solution was quickly added to the reaction mixture by pipette, yielding a dark red solution. 0.5 mL of THF was used to rinse the vial and combined with the reaction mixture. The reaction was heated to 40 ˚C and allowed to stir for 24 hours in a glove box.

After 24 hours, the reaction was quenched by adding the orange solution dropwise to 15 mL of dry methanol, which was stirred fast in a round bottom flask. Formation of precipitates was observed. The suspension was allowed to sit overnight, and the top clear yellow solution was removed. 10 mL of methanol were added, and precipitates were washed sufficiently by stirring vigorously for 30 minutes. The suspension was allowed to sit until the precipitates settled at the bottom. The above washing procedure was repeated 2 more times. Then the suspension was filtered through a Buchner funnel. The solid was washed with methanol and dried under vacuum, yielding hybrid polysilane products.

Synthesis of P6.2: The polycondensation was set up at the scale of 0.150 mmol with *cis*-**6.1** (dr 20:80 *trans:cis*) and 2,5-dibromothiophene. Yield: 67.2 mg, 73%.

Synthesis of P6.3: The polycondensation was set up at the scale of 0.150 mmol with **6.1** (dr 65:35 *trans:cis*) and 2,5-dibromothiophene. Yield: 57.9 mg, 63%.

Synthesis of P6.4: The polycondensation was set up at the scale of 0.203 mmol with **6.2** and 2,5-dibromothiophene. Yield: 50.5 mg, 61%.

Synthesis of P6.5: The polycondensation was set up at the scale of 0.227 mmol with **6.3** and 2,5-dibromothiophene. Yield: 59.2 mg, 70%.

Synthesis of P6.6: The polycondensation was set up at the scale of 0.150 mmol with *trans*-**6.1** (dr 90:10 *trans:cis*) and 1,4-dibromo-2,5-((2-ethylhexyl)oxy)benzene. Yield: 90.9 mg, 72%.

Synthesis of P6.7: The polycondensation was set up at the scale of 0.150 mmol with *cis*-**6.1** (dr 20:80 *trans:cis*) and 1,4-dibromo-2,5-((2-ethylhexyl)oxy)benzene. Yield: 85.8 mg, 68%.

Synthesis of P6.8: The polycondensation was set up at the scale of 0.510 mmol with **6.1** (dr 65:35 *trans:cis*) and 1,4-dibromo-2,5-((2-ethylhexyl)oxy)benzene. Yield: 70.7 mg, 56%.

Gel Permeation Chromatography

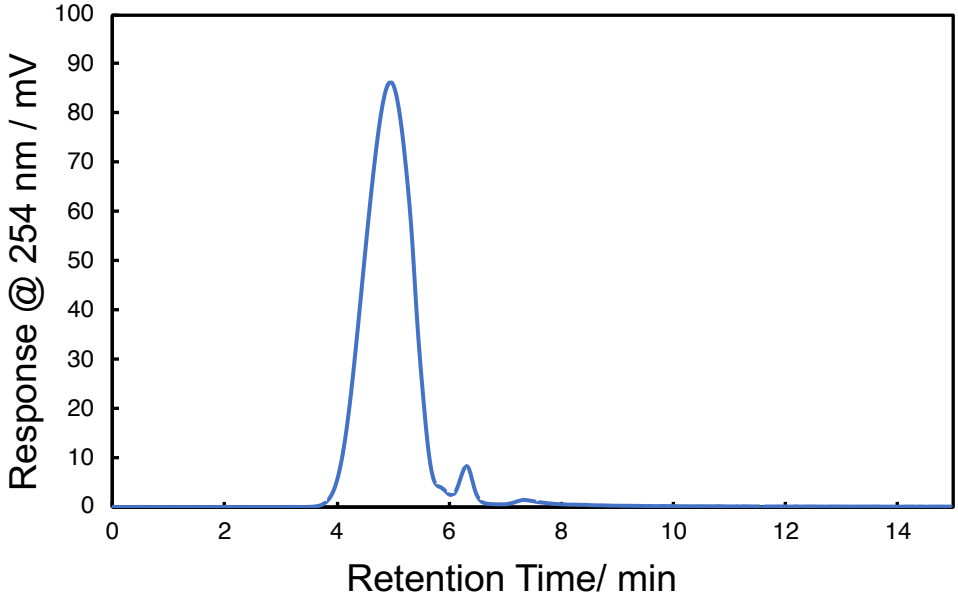

Polymer	M_n	M_w	M_w / M_n
P6.2	6382	16993	2.66

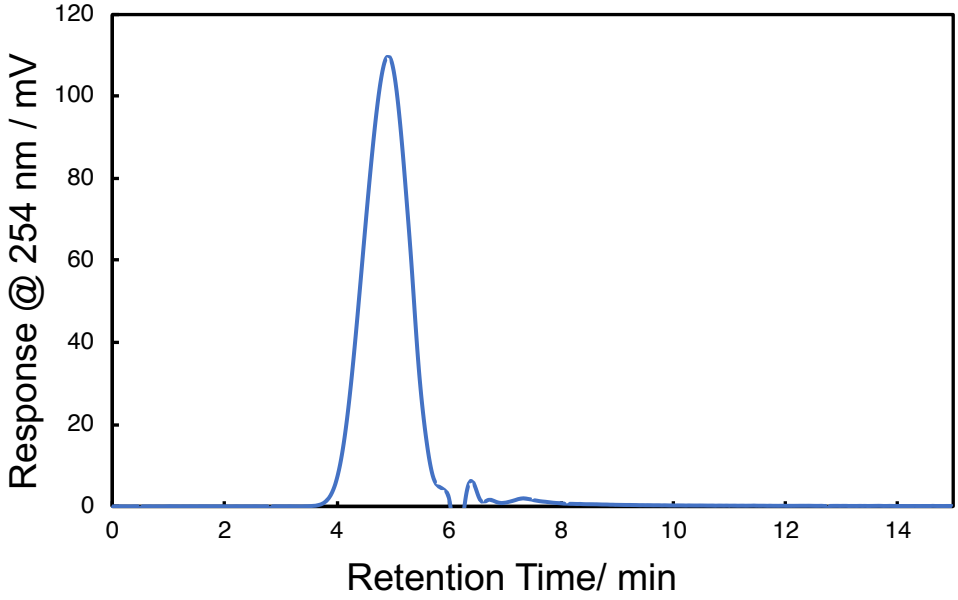

Polymer	M_n	M_w	M_w / M_n
P6.3	6883	17838	2.59

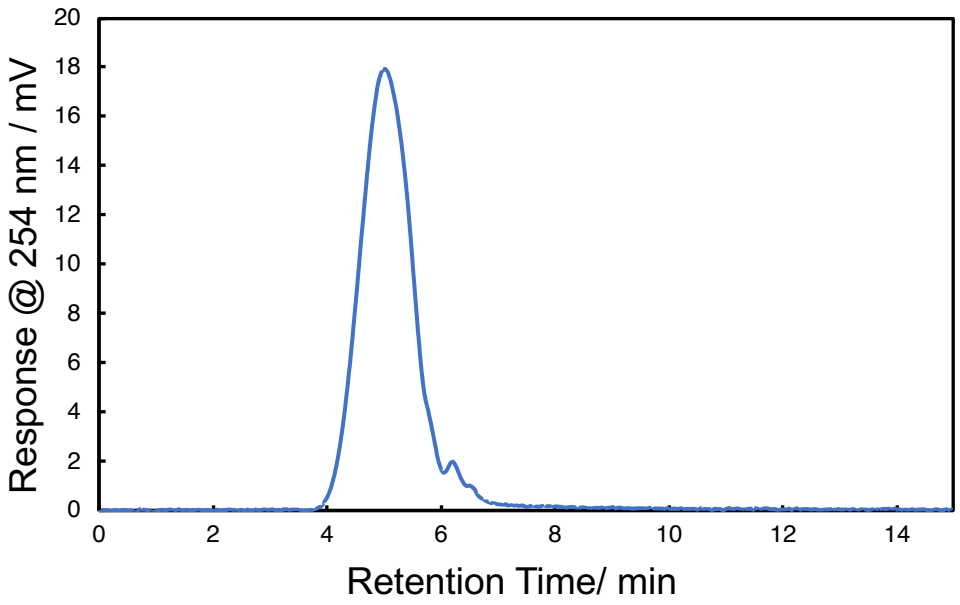

Polymer	M_n	M_w	M_w / M_n
P6.4	5051	10486	2.08

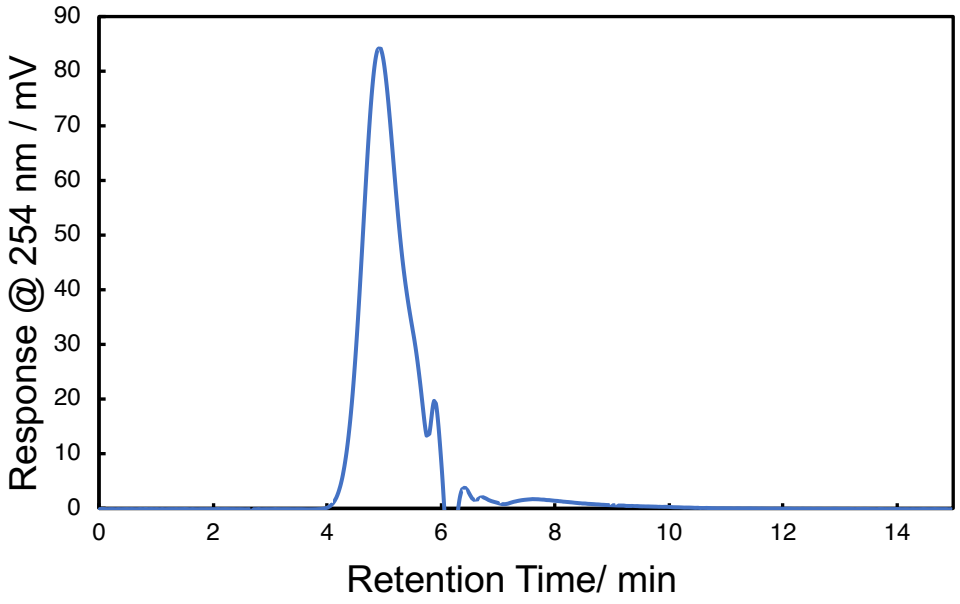

Polymer	M_n	M_w	M_w / M_n
P6.5	6528	10134	1.55

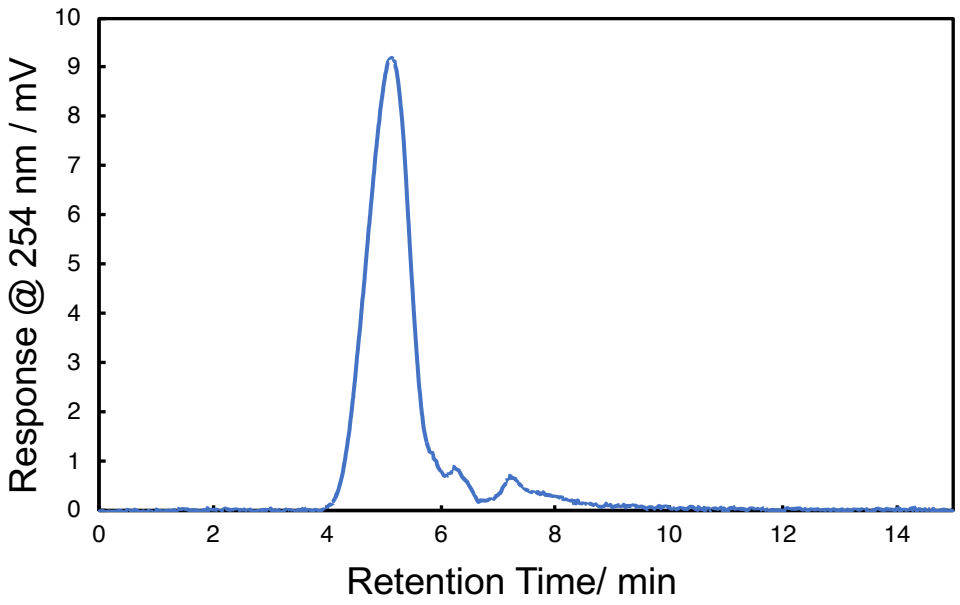

Polymer	M_n	M_w	M_w / M_n
P6.6	4163	10472	2.52

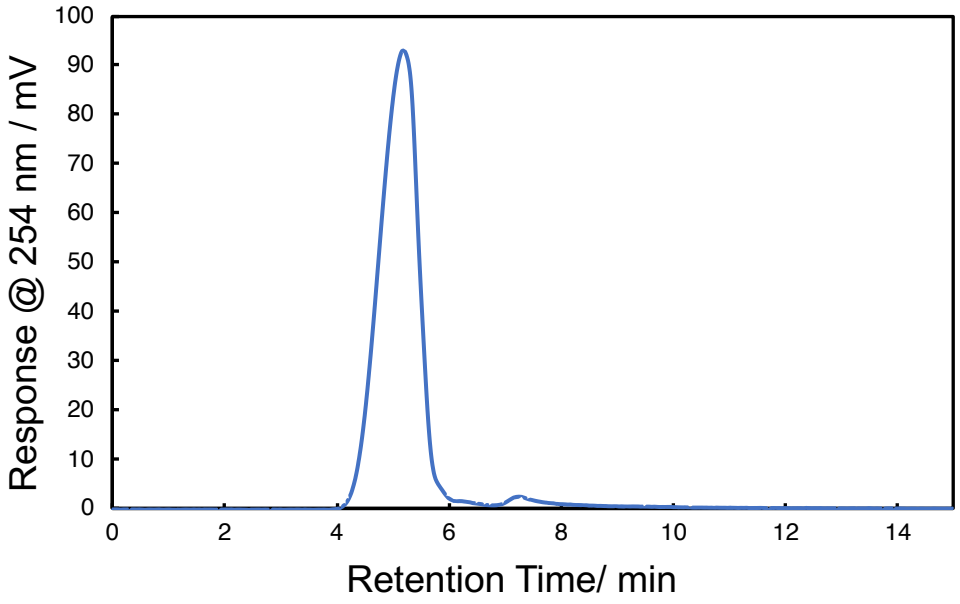

Polymer	M_n	M_w	M_w / M_n
P6.7	4051	9053	2.24

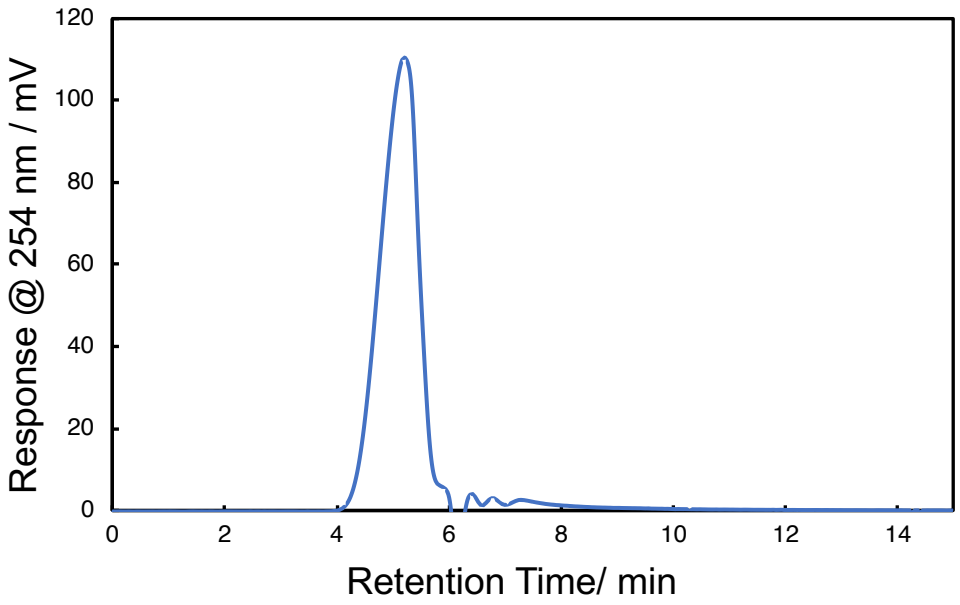

Polymer	M_n	M_w	M_w / M_n
P6.8	4468	9025	2.02

NMR Spectra

NMR Spectra of 6.2

^{1}H NMR Spectrum (400 MHz, $CDCl_3$)

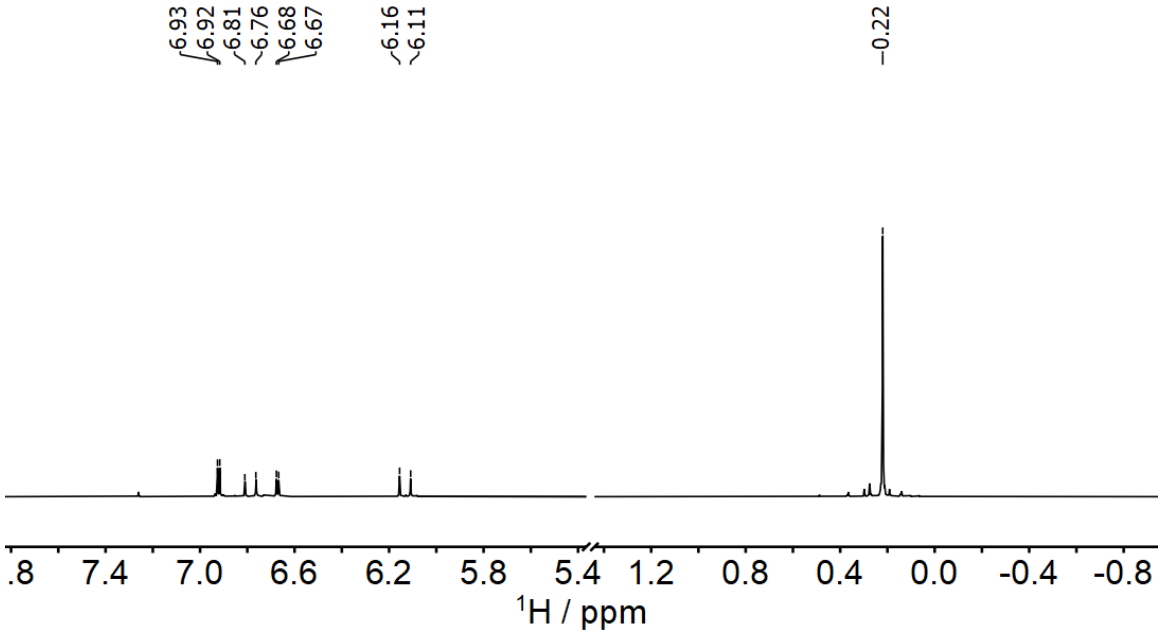

$^{13}C\{^{1}H\}$ NMR Spectrum (101 MHz, $CDCl_3$)

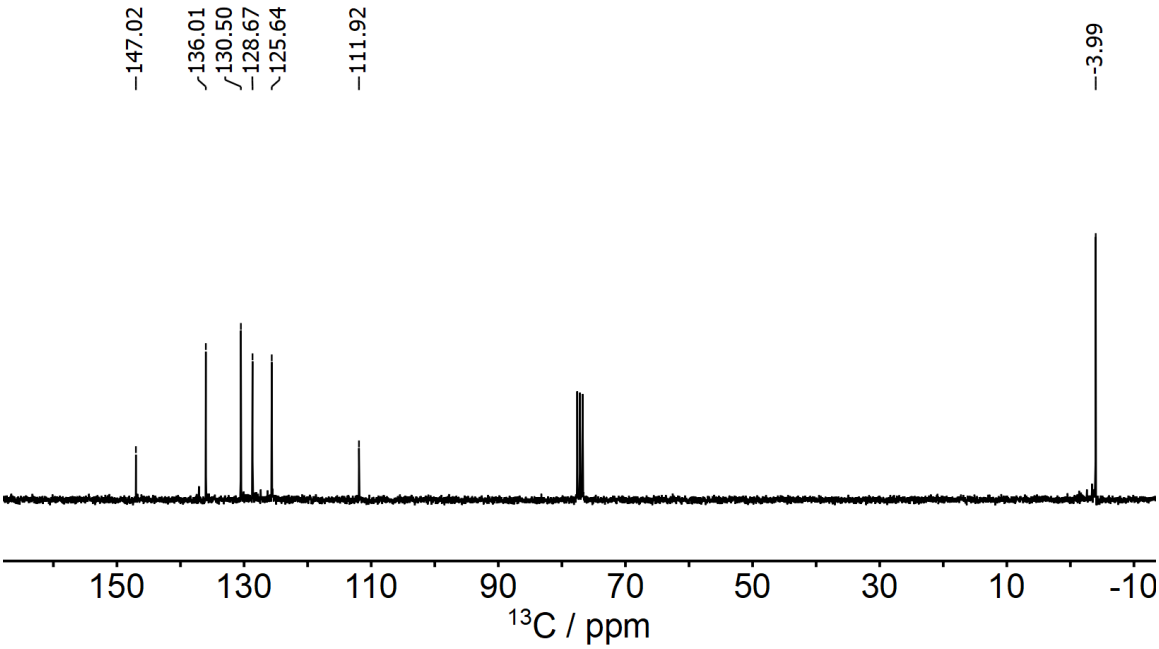

$^{29}Si\{^{1}H\}$ NMR Spectrum (79 MHz, $CDCl_3$). $^{1}J_{Si\text{-}H}$ = 7 Hz.

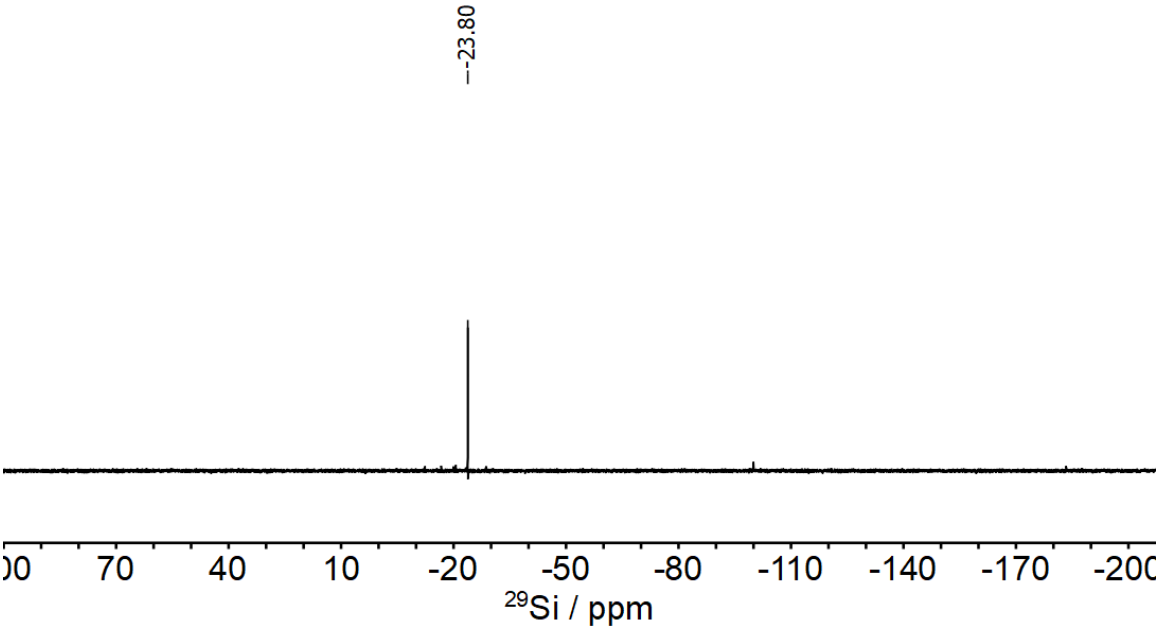

7.7 Reference

(1) Schmidt, M.; Wassy, D.; Hermann, M.; González, M. T.; Agräit, N.; Zotti, L. A.; Esser, B.; Leary, E. *Chem. Commun.* **2021**, *57*, 745–748.

(2) Sattler, L. E.; Hilt, G. *Chem. - A Eur. J.* **2021**, *27*, 605–608.

(3) Ho, P. Y.; Komber, H.; Horatz, K.; Tsuda, T.; Mannsfeld, S. C. B.; Dmitrieva, E.; Blacque, O.; Kraft, U.; Sirringhaus, H.; Lissel, F. *Polym. Chem.* **2020**, *11*, 472–479.

(4) Usta, H.; Alimli, D.; Ozdemir, R.; Tekin, E.; Alkan, F.; Kacar, R.; Altas, A. G.; Dabak, S.; Gürek, A. G.; Mutlugun, E.; Yazici, A. F.; Can, A. *J. Mater. Chem. C* **2020**, *8*, 8047–8060.

(5) Gaussian 09, Revision D.01, M. J. Frisch, G. W. Trucks, H. B. Schlegel, G. E. S.; M. A. Robb, J. R. Cheeseman, G. Scalmani, V. Barone, B. Mennucci, G. A. Petersson, H.; Nakatsuji, M. Caricato, X. Li, H. P. Hratchian, A. F. Izmaylov, J. Bloino, G. Zheng, J, 2013. .

(6) Gaussian 16, Revision C.01, M. J. Frisch, G. W. Trucks, H. B. Schlegel, G. E. Scuseria, M. A. Robb, J. R. Cheeseman, G. Scalmani, V. Barone, G. A. Petersson, H. Nakatsuji, X. Li, M. Caricato, A. V. Marenich, J. Bloino, B. G. Janesko, R. Gomperts, B. Mennu, 2016. .

(7) Wildeman, J.; Herrema, J. K.; Hadziioannou, G.; Schomaker, E. *J. Inorg. Organomet. Polym.* **1991**, *1*, 567–580.

Chapter 8: Curriculum vitae

Education

2017 to 2023	**Johns Hopkins University, Baltimore, MD** Department of Chemistry Ph.D. in Chemistry, with Prof. Rebekka S. Klausen
2013 to 2017	**Nanjing University, Nanjing, P.R. China** School of Chemistry & Chemical Engineering B.S. in Chemistry, research with Prof. Qun-dong Shen

Publications

1. **Jiang, Q.**; Melvin, S.; Klausen, R. S. "Impact of Stereoregularity on Hybrid Conjugated Polymers." *Manuscript in preparation.*
2. Guan, W.; Lu, L.; **Jiang, Q.**; Gittens, A.; Wang, Y.; Novaes, L. F. T.; Klausen, R. S.; Lin, S. "Electrochemical Logic to Synthesize Disilanes and Oligosilanes from Chlorosilanes" *Submitted.*
3. Gittens, A.; **Jiang, Q.**; Siegler, M. A; Klausen, R. S. "Conjugation in Isomeric Cyclosilane Thioethers." *Organometallics* **2022**, 41, 23, 3762–3769.
4. **Jiang, Q.**; Gittens, A.; Wong, S.; Siegler, M. A; Klausen, R. S. "Highly Regioselective and Diastereoselective Addition of Cyclosilanes to Alkynes Enabling New Conjugated Materials." *Chem. Sci.,* **2022**, *13*, 7587-7593.
5. Ji, Y.; Catazaro, J.; **Jiang, Q.**; Melvin, S.; Jiang J., Klausen, R. S. "Characterization of High Vinyl-Alcohol Content Polymers by Solid State CPMAS NMR Spectroscopy" *Macromolecules, **2022**, 55,* 7032–7038.
6. Fang, F.; **Jiang, Q.**; Klausen, R. S. "Poly(cyclosilane) Connectivity Tunes Optical Absorbance." *J. Am. Chem. Soc.,* **2022***, 144,* 7834–7843.
7. Wakefield, H. IV; **Jiang, Q.**; Klausen, R. S. "Azaborine Isomer Effects on Benzylic Ion Stability and Reactivity: Consequences for BN2VN Ionic Polymerization." *Org. Biomol. Chem.*, **2022**, *20*, 1407-1414.
8. **Jiang, Q.**; Wong, S.; Klausen, R. S. "Effect of Polycyclosilane Microstructure on Thermal Properties." *Polym. Chem.,* **2021**, ***12*,** 4785-4794.
9. Ferguson, J. T.; **Jiang, Q.**; Marro, E. A.; Siegler, M. A.; Klausen, R. S. "Long Range Coupling in Cyclic Silanes." *Dalton Trans*. **2020**, *49*, 14951-14961.

Presentations and Posters

- August 25, 2022, American Chemical Society Fall Meeting, Chicago

  Title: "Novel Cyclosilane Building Blocks for σ,π-Conjugated Polymer Synthesis via Kumada Polycondensation"

- June 9, 2022, Tosoh Polymer Conference (TPC2022), Hollywood (Poster session)

  Title: "Novel Cyclosilane Building Blocks for σ,π-Conjugated Polymer Synthesis via Kumada Polycondensation"
- August 22, 2021, American Chemical Society Fall Meeting, Virtual

  Title: "Cyclosilane Polymers" on behalf of Prof. Rebekka S. Klausen
- April 12, 2021, American Chemical Society Spring Meeting, Virtual

  Title: "Effect of Poly(cyclosilane) Microstructure on Thermal Properties"

Honors & Awards

- 2022, Outstanding Poster Award of TPC2022, Second Place.
- 2022, Harry and Cleio Greer Fellowship, awarded to an outstanding advanced-year graduate student.
- 2022, Dissertation Completion Fellowship of Johns Hopkins University.
- 2017, Excellent Undergraduate Thesis of Nanjing University, 3 awardees from School of Chemistry & Chemical Engineering per year.

  Thesis Title: New Bionic and Implantable Electronic Devices Based on Ferroelectric Polymer
- 2017, Chemistry Experiment Award in School of Chemistry & Chemical Engineering of Nanjing University, 3 awardees per year.

Teaching & Mentoring Experience

- *NMR Teaching Assistant*, Department of Chemistry, Johns Hopkins University, 2021 to 2023
- *Teaching Assistant*, Department of Chemistry, Johns Hopkins University
  - Advanced Organic Synthesis I (030.677), Fall 2019
  - Organic Chemistry II (030.206), Spring 2019
  - The Science of Color (030.118), Fall 2018
  - Introductory Chemistry (Lecture and Lab) II (030.102), Spring 2018
  - Introductory Chemistry (Lecture and Lab) I (030.101), Fall 2017
- *Mentoring Undergraduate Researchers*
  - First-generation Undergraduate Research Experience (FiGURE), Intersession 2022
  - Provost's Undergraduate Research Award (Summer PURA program), Summer 2021